

Mark D. Fairchild



# COLOR APPEARANCE MODELS

Third Edition

WILEY

WILEY-IS&T SERIES IN IMAGING SCIENCE AND TECHNOLOGY





# **Color Appearance Models**

**Wiley-IS&T Series in Imaging Science and Technology**

Reproduction of Colour (Sixth Edition)

**R. W. G. Hunt**

Colorimetry: Fundamentals and Applications

**Noburu Ohta and Alan R. Robertson**

Color Constancy

**Marc Ebner**

Color Gamut Mapping

**Ján Morovič**

Panoramic Imaging: Sensor-Line Cameras and Laser Range-Finders

**Fay Huang, Reinhard Klette and Karsten Scheibe**

Digital Color Management (Second Edition)

**Edward J. Giorgianni and Thomas E. Madden**

The JPEG 2000 Suite

**Peter Schelkens, Athanassios Skodras and Touradj Ebrahimi (Eds.)**

Color Management: Understanding and Using ICC Profiles

**Phil Green (Ed.)**

Fourier Methods in Imaging

**Roger L. Easton, Jr.**

Measuring Colour (Fourth Edition)

**R.W.G. Hunt and M.R. Pointer**

The Art and Science of HDR Imaging

**John McCann and Alessandro Rizzi**

Computational Colour Science Using MATLAB (Second Edition)

**Stephen Westland, Caterina Ripamonti and Vien Cheung**

Color in Computer Vision: Fundamentals and Applications

**Theo Gevers, Arjan Gijsenij, Joost van de Weijer and Jan-Mark Geusebroek**

Color Appearance Models (Third Edition)

**Mark D. Fairchild**

Published in Association with the Society for Imaging Science and  
Technology



# **Color Appearance Models**

Third Edition

**Mark D. Fairchild**

Rochester Institute of Technology, USA

**WILEY**

This edition first published 2013  
© 2013 John Wiley & Sons, Ltd

This book was previously published by Pearson Education, Inc.

*Registered Office*

John Wiley & Sons, Ltd, The Atrium, Southern Gate, Chichester, West Sussex, PO19 8SQ,  
United Kingdom

For details of our global editorial offices, for customer services and for information about how to apply for permission to reuse the copyright material in this book please see our website at [www.wiley.com](http://www.wiley.com).

The right of the author to be identified as the author of this work has been asserted in accordance with the Copyright, Designs and Patents Act 1988.

All rights reserved. No part of this publication may be reproduced, stored in a retrieval system, or transmitted, in any form or by any means, electronic, mechanical, photocopying, recording or otherwise, except as permitted by the UK Copyright, Designs and Patents Act 1988, without the prior permission of the publisher.

Wiley also publishes its books in a variety of electronic formats. Some content that appears in print may not be available in electronic books.

Designations used by companies to distinguish their products are often claimed as trademarks. All brand names and product names used in this book are trade names, service marks, trademarks or registered trademarks of their respective owners. The publisher is not associated with any product or vendor mentioned in this book.

**Limit of Liability/Disclaimer of Warranty:** While the publisher and author have used their best efforts in preparing this book, they make no representations or warranties with respect to the accuracy or completeness of the contents of this book and specifically disclaim any implied warranties of merchantability or fitness for a particular purpose. It is sold on the understanding that the publisher and the Society for Imaging Science and Technology are not engaged in rendering professional services and neither the publisher, the society nor the author shall be liable for damages arising herefrom. If professional advice or other expert assistance is required, the services of a competent professional should be sought.

*Library of Congress Cataloging-in-Publication Data*

Fairchild, Mark D.

Color appearance models / Mark D. Fairchild. – Third edition.

pages cm. – (The Wiley-IS&T series in imaging science and technology)

Includes bibliographical references and index.

ISBN 978-1-119-96703-3 (hardback)

1. Color vision. I. Title.

QP483.F35 2013

612.8'4–dc23

2013005445

A catalogue record for this book is available from the British Library.

ISBN: 9781119967033

Typeset in 10/12pt Bookman by SPi Publisher Services, Pondicherry, India

1 2013

To those that remind me that  
a journey of a thousand miles begins  
with a single step:

Lisa, Acadia, Ellie.

And to all the other animals that fill our lives.



*How much of beauty—of color  
as well as form—on which our eyes daily rest  
goes unperceived by us?*

Henry David Thoreau



# Contents

---

Series Preface	xiii
Preface	xv
Acknowledgments	xviii
Introduction	xix
<b>1 Human Color Vision</b>	<b>1</b>
1.1 Optics of the Eye	2
1.2 The Retina	7
1.3 Visual Signal Processing	14
1.4 Mechanisms of Color Vision	19
1.5 Spatial and Temporal Properties of Color Vision	27
1.6 Color Vision Deficiencies	32
1.7 Key Features for Color Appearance Modeling	36
<b>2 Psychophysics</b>	<b>38</b>
2.1 Psychophysics Defined	39
2.2 Historical Context	40
2.3 Hierarchy of Scales	43
2.4 Threshold Techniques	45
2.5 Matching Techniques	49
2.6 One-Dimensional Scaling	50
2.7 Multidimensional Scaling	52
2.8 Design of Psychophysical Experiments	54
2.9 Importance in Color Appearance Modeling	55
<b>3 Colorimetry</b>	<b>56</b>
3.1 Basic and Advanced Colorimetry	57
3.2 Why is Color?	57
3.3 Light Sources and Illuminants	59
3.4 Colored Materials	63
3.5 The Human Visual Response	68
3.6 Tristimulus Values and Color Matching Functions	70
3.7 Chromaticity Diagrams	77
3.8 CIE Color Spaces	79
3.9 Color Difference Specification	81
3.10 The Next Step	83

<b>4 Color Appearance Terminology</b>	<b>85</b>
4.1 Importance of Definitions	85
4.2 Color	86
4.3 Hue	88
4.4 Brightness and Lightness	88
4.5 Colorfulness and Chroma	90
4.6 Saturation	91
4.7 Unrelated and Related Colors	91
4.8 Definitions in Equations	92
4.9 Brightness–Colorfulness Vs Lightness–Chroma	94
<b>5 Color Order Systems</b>	<b>97</b>
5.1 Overview and Requirements	98
5.2 The Munsell Book of Color	99
5.3 The Swedish NCS	104
5.4 The Colorcurve System	106
5.5 Other Color Order Systems	107
5.6 Uses of Color Order Systems	109
5.7 Color Naming Systems	112
<b>6 Color Appearance Phenomena</b>	<b>115</b>
6.1 What are Color Appearance Phenomena?	115
6.2 Simultaneous Contrast, Crispening, and Spreading	116
6.3 Bezold–Brücke Hue Shift (Hue Changes with Luminance)	120
6.4 Abney Effect (Hue Changes with Colorimetric Purity)	121
6.5 Helmholtz–Kohlrausch Effect (Brightness Depends On Luminance and Chromaticity)	123
6.6 Hunt Effect (Colorfulness Increases with Luminance)	125
6.7 Stevens Effect (Contrast Increases with Luminance)	127
6.8 Helson–Judd Effect (Hue of Non-Selective Samples)	129
6.9 Bartleson–Breneman Equations (Image Contrast Changes with Surround)	131
6.10 Discounting-the-Illuminant	132
6.11 Other Context, Structural, and Psychological Effects	133
6.12 Color Constancy?	140
<b>7 Viewing Conditions</b>	<b>142</b>
7.1 Configuration of the Viewing Field	142
7.2 Colorimetric Specification of the Viewing Field	146
7.3 Modes of Viewing	149
7.4 Unrelated and Related Colors Revisited	154

<b>8 Chromatic Adaptation</b>	<b>156</b>
8.1 Light, Dark, and Chromatic Adaptation	157
8.2 Physiology	159
8.3 Sensory and Cognitive Mechanisms	170
8.4 Corresponding Colors Data	174
8.5 Models	177
8.6 Color Inconstancy Index	178
8.7 Computational Color Constancy	179
<b>9 Chromatic Adaptation Models</b>	<b>181</b>
9.1 Von Kries Model	182
9.2 Retinex Theory	186
9.3 Nayatani <i>et al.</i> Model	187
9.4 Guth's Model	190
9.5 Fairchild's 1990 Model	192
9.6 Herding CATs	196
9.7 CAT02	197
<b>10 Color Appearance Models</b>	<b>199</b>
10.1 Definition of Color Appearance Models	199
10.2 Construction of Color Appearance Models	200
10.3 CIELAB	201
10.4 Why Not Use Just CIELAB?	210
10.5 What About CIELUV?	210
<b>11 The Nayatani <i>et al.</i> Model</b>	<b>213</b>
11.1 Objectives and Approach	213
11.2 Input Data	214
11.3 Adaptation Model	215
11.4 Opponent Color Dimensions	217
11.5 Brightness	218
11.6 Lightness	219
11.7 Hue	219
11.8 Saturation	220
11.9 Chroma	221
11.10 Colorfulness	221
11.11 Inverse Model	222
11.12 Phenomena Predicted	222
11.13 Why Not Use Just the Nayatani <i>et al.</i> Model?	223
<b>12 The Hunt Model</b>	<b>225</b>
12.1 Objectives and Approach	225
12.2 Input Data	226
12.3 Adaptation Model	228
12.4 Opponent Color Dimensions	233
12.5 Hue	234
12.6 Saturation	235

12.7	Brightness	236
12.8	Lightness	238
12.9	Chroma	238
12.10	Colorfulness	238
12.11	Inverse Model	239
12.12	Phenomena Predicted	241
12.13	Why Not Use Just the Hunt Model?	242

## **13 The RLAB Model** **243**

13.1	Objectives and Approach	243
13.2	Input Data	245
13.3	Adaptation Model	246
13.4	Opponent Color Dimensions	248
13.5	Lightness	250
13.6	Hue	250
13.7	Chroma	252
13.8	Saturation	252
13.9	Inverse Model	252
13.10	Phenomena Predicted	254
13.11	Why Not Use Just the RLAB Model?	254

## **14 Other Models** **256**

14.1	Overview	256
14.2	ATD Model	257
14.3	LLAB Model	264
14.4	<i>IPT</i> Color Space	271

## **15 The CIE Color Appearance Model (1997), CIECAM97s** **273**

15.1	Historical Development, Objectives, and Approach	273
15.2	Input Data	276
15.3	Adaptation Model	277
15.4	Appearance Correlates	279
15.5	Inverse Model	280
15.6	Phenomena Predicted	281
15.7	The ZLAB Color Appearance Model	282
15.8	Why Not Use Just CIECAM97s?	285

## **16 CIECAM02** **287**

16.1	Objectives and Approach	287
16.2	Input Data	288
16.3	Adaptation Model	290
16.4	Opponent Color Dimensions	294
16.5	Hue	294
16.6	Lightness	295
16.7	Brightness	295
16.8	Chroma	295
16.9	Colorfulness	296

---

16.10 Saturation	296
16.11 Cartesian Coordinates	296
16.12 Inverse Model	297
16.13 Implementation Guidelines	297
16.14 Phenomena Predicted	298
16.15 Computational Issues	298
16.16 CAM02-UCS	300
16.17 Why Not Use Just CIECAM02?	301
16.18 Outlook	301
<b>17 Testing Color Appearance Models</b>	<b>303</b>
17.1 Overview	303
17.2 Qualitative Tests	304
17.3 Corresponding-Colors Data	308
17.4 Magnitude Estimation Experiments	310
17.5 Direct Model Tests	312
17.6 Colorfulness in Projected Images	316
17.7 Munsell in Color Appearance Spaces	317
17.8 CIE Activities	318
17.9 A Pictorial Review of Color Appearance Models	323
<b>18 Traditional Colorimetric Applications</b>	<b>328</b>
18.1 Color Rendering	328
18.2 Color Differences	333
18.3 Indices of Metamerism	335
18.4 A General System of Colorimetry?	337
18.5 What About Observer Metamerism?	338
<b>19 Device-Independent Color Imaging</b>	<b>341</b>
19.1 The Problem	342
19.2 Levels of Color Reproduction	343
19.3 A Revised Set of Objectives	345
19.4 General Solution	348
19.5 Device Calibration and Characterization	349
19.6 The Need for Color Appearance Models	354
19.7 Definition of Viewing Conditions	355
19.8 Viewing-Conditions-Independent Color Space	357
19.9 Gamut Mapping	357
19.10 Color Preferences	361
19.11 Inverse Process	362
19.12 Example System	363
19.13 ICC Implementation	364
<b>20 Image Appearance Modeling and the Future</b>	<b>369</b>
20.1 From Color Appearance to Image Appearance	370
20.2 S-CIELAB	375

20.3	The iCAM Framework	376
20.4	A Modular Image Difference Model	382
20.5	Image Appearance and Rendering Applications	385
20.6	Image Difference and Quality Applications	391
20.7	iCAM06	392
20.8	Orthogonal Color Space	393
20.9	Future Directions	396
<b>21</b>	<b>High-Dynamic-Range Color Space</b>	<b>399</b>
21.1	Luminance Dynamic Range	400
21.2	The HDR Photographic Survey	401
21.3	Lightness-Brightness Beyond Diffuse White	403
21.4	hdr-CIELAB	404
21.5	hdr-IPT	406
21.6	Evans, $G_0$ , and Brilliance	407
21.7	The Nayatani Theoretical Color Space	409
21.8	A New Kind of Appearance Space	409
21.9	Future Directions	416
References		418
Index		440

# Series Preface

---

Color is a subject that has fascinated scientists, philosophers and people in general for thousands of years. Virtually all people are familiar with the concepts of color and are fluent in its semantic description. However numerical descriptions of color and its manipulation using mathematical models is a field familiar to relatively few scientists and engineers. Indeed, color has only had a well defined mathematical basis for less than 100 years. The field of colorimetry was the first comprehensive mathematical description of color. The use of colorimetry, however, is limited to a description of whether colors appear to match one another under a defined set of viewing conditions. Colorimetry has enabled the precise control of color in many industrial applications including textile and paint manufacture, printing, photography, cinema, lighting and television and displays. Colorimetry however cannot provide us with a numerical description of the relative appearance of colors or how the appearance of colors will change in different viewing environments. This is the domain of color appearance modeling.

Scientific interest in color appearance modeling began with the observation that colors could change their appearance depending on the background they were seen against, the intensity and spectral properties of the illumination and many other factors. We have all experienced these phenomena, often realized when the fabric or paint that looked so perfect in the showroom doesn't quite look right when we bring it home. The first tentative steps towards a model of color appearance can be traced back to 1976 when the CIE introduced the CIELAB and CIELUV uniform color spaces. These color spaces allowed, for the first time, numerical correlates of lightness, hue, chroma and, in the case of CIELUV, saturation. Interest in color appearance modeling grew rapidly from this point. In the early 1980s leading color scientists including R.W.G. Hunt and Y. Nayatani developed the first versions of their color appearance models, designed to predict numerical correlates of all the perceptual attributes of color under a wide range of viewing conditions. Shortly after, Mark Fairchild developed the RLAB color appearance model. RLAB was a major advance in developing color appearance models for practical use in imaging applications. In 1997 the CIE proposed a simplified color appearance model, CIECAM97s, incorporating a number of features and approaches developed in the earlier models, as well as contributions by M.R. Luo and several others. Five years later CIECAM97s was succeeded by an improved, simpler and better model, CIECAM02. This model has now found widespread application in the imaging and printing industries, and an understanding of it is essential for scientists and engineers working in these areas.

The first two editions of *Color Appearance Models* are among the most significant and indispensable texts in the field of color science. This is because the author, Mark Fairchild, provides a technically detailed and comprehensive approach to the subject of color modeling. Mark's academic background, having postgraduate degrees in both imaging science and vision science, make him exceptionally qualified in this area. He has studied under, collaborated with and educated many of today's leading color scientists. Consequently, his treatment of the subject provides all the necessary context and background required for a full understanding of color appearance models. The book provides an explanation of how color phenomena arise from the anatomy and physiology of the human visual system. It summarizes the methodologies, from the field of psychophysics, that allow us to obtain numerical measures of perceptual phenomena such as color. Colorimetry – the foundation of all color appearance models – is explained clearly and thoroughly. Fairchild provides descriptions and explanations of a very broad range of color appearance phenomena that are addressed by color appearance models. The book also takes us on a historical and technical journey, visiting each of the major advances in color appearance modeling in turn, until finally arriving at today's most used model – CIECAM02. Fairchild provides a full technical explanation of all the major models as well as expert guidance on the strengths, weaknesses and uses of each model. The latter third of the book covers applications of color appearance modeling, with a strong focus on imaging science and technology. The third edition of *Color Appearance Models* extends the treatment of applications to the field of high dynamic-range (HDR) imaging. This is one of the important new challenges in imaging science and photography. Color appearance models provide the important scientific insights required for development and refinement of new HDR technologies.

Mark Fairchild is counted among the world's finest and most influential color imaging scientists and educators. His third edition of *Color Appearance Models* is destined to become a classic color science textbook. The Society for Imaging Science and Technology (IS&T) and John Wiley & Sons Ltd are proud to be able to make this outstanding book available to students, scientists and engineers working in color related fields.

Geoffrey J. Woolfe  
Canon Information Systems Research Australia  
Publications Vice President, Society for Imaging Science and Technology

# Preface

---

*The law of proportion according to which the several colors are formed, even if a man knew he would be foolish in telling, for he could not give any necessary reason, nor indeed any tolerable or probable explanation of them.*

Plato

Despite Plato's warning, this book is about one of the major unresolved issues in the field of color science, the efforts that have been made toward its resolution, and the techniques that can be used to address current technological problems. The issue is the prediction of the color appearance experienced by an observer when viewing stimuli in natural, complex settings. Useful solutions to this problem have impacts in a number of industries such as lighting, materials, and imaging. In lighting, color appearance models can be used to predict the color rendering properties of various light sources allowing specification of quality rather than just efficiency. In materials fields (coatings, plastics, textiles, etc.), color appearance models can be used to specify tolerances across a wider variety of viewing conditions than is currently possible and to more accurately evaluate metamerism. The imaging industries have produced the biggest demand for accurate and practical color appearance models. The rapid growth in color imaging technology, particularly the desktop publishing and digital photography markets, has led to the emergence of color management systems. It is widely acknowledged that such systems require color appearance models to allow images originating in one medium and viewed in a particular environment to be acceptably reproduced in a second medium and viewed under different conditions. While the need for color appearance models is recognized, their development has been at the forefront of color science and largely confined to the discourse of academic journals and conferences. This book brings the fundamental issues and current solutions in the area of color appearance modeling together in a single place for those needing to solve practical problems or looking for background for ongoing research projects.

Everyone knows what color is, but the accurate description and specification of colors is quite another story. In 1931, the Commission Internationale de l'Éclairage (CIE) recommended a system for color measurement establishing the basis for modern colorimetry. That system allows the specification of color matches through CIE XYZ tristimulus values. It was immediately recognized that more advanced techniques were required. The CIE

recommended the CIELAB and CIELUV color spaces in 1976 to enable uniform international practice for the measurement of color differences and establishment of color tolerances. While the CIE system of colorimetry has been applied successfully for over 80 years, it is limited to the comparison of stimuli that are identical in every spatial and temporal respect and viewed under matched viewing conditions. CIE XYZ values describe whether or not two stimuli match. CIELAB values can be used to describe the perceived differences between stimuli in a single set of viewing conditions. Color appearance models extend the current CIE systems to allow the description of what color stimuli would look like under a variety of viewing conditions. The application of such models opens up a world of possibilities for the accurate specification, control, and reproduction of color.

Understanding color-appearance phenomena and developing models to predict them have been the topics of a great deal of research — particularly in the last 20–30 years. Color appearance remains a topic of much active research that is often being driven by technological requirements. Despite the fact that the CIE is not yet able to recommend a single color appearance model as the best available for all applications, there are many who need to implement some form of a model to solve their research, development, and engineering needs. One such application is the development of color management systems based on the International Color Consortium (ICC) Profile Format that continues to be developed by the ICC and incorporated into essentially all modern computer operating systems. Implementation of color management using ICC profiles requires the application of color appearance models with no specific instructions on how to do so. Unfortunately, the fundamental concepts, phenomena, and models of color appearance are not recorded in a single source. Generally, one interested in the field must search out the primary references across a century of scientific journals and conference proceedings. This is due to the large amount of active research in the area. While searching for and keeping track of primary references is fine for those doing research on color appearance models, it should not be necessary for every scientist, engineer, and software developer interested in the field. The aim of this book is to provide the relevant information for an overview of color appearance and details of many of the most widely used models in a single source. The general approach has been to first provide an overview of the fundamentals of color measurement and the phenomena that necessitate the development of color appearance models. This eases the transition into the formulation of the various models and their applications that appear later in the book. This approach has proven quite useful in various university courses, short courses, and seminars in which the full range of material must be presented in a limited time.

Chapters 1 through 3 provide a review of the fundamental concepts of human color vision, psychophysics, and the CIE system of colorimetry that are prerequisite to understanding the development and implementation of color appearance models. Chapters 4 through 7 present the fundamental definitions, descriptions, and phenomena of color appearance. These

chapters provide a review of the historical literature that has led to modern research and development of color appearance models. Chapters 8 and 9 concentrate on one of the most important component mechanisms of color appearance, chromatic adaptation. The models of chromatic adaptation described in Chapter 9 are the foundation of the color appearance models described in later chapters. Chapter 10 presents the definition of color appearance models and outlines their construction using the CIELAB color space as an example. Chapters 11 through 13 provide detailed descriptions of the Nayatani *et al.*, Hunt, and RLAB color appearance models along with the advantages and disadvantages of each. Chapter 14 reviews the ATD and LLAB appearance models that are of increasing interest for some applications. Chapter 15 presents the CIECAM97s model established as a recommendation by the CIE just as the first edition of this book went to press (and included as an appendix in that edition). Also included is a description of the ZLAB simplification of CIECAM97s. Chapter 16 describes the recently formulated CIECAM02 model that represents a significant improvement of CIECAM97s and is the best possible model based on current knowledge. Chapters 17 and 18 describe tests of the various models through a variety of visual experiments and colorimetric applications of the models. Chapter 19 presents an overview of device-independent color imaging, the application that has provided the greatest technological push for the development of color appearance models. Finally, Chapters 20 and 21 introduce the concept of image appearance modeling as a potential future direction for color appearance modeling research, provide an overview of iCAM as one example of an image appearance model, and introduce new approaches to appearance prediction without color spaces and in high-dynamic-range environments.

While the field of color appearance modeling remains young and likely to continue developing in the near future, this book includes extensive material that will not change. Chapters 1 through 10 provide overviews of fundamental concepts, phenomena, and techniques that will change little, if at all, in the coming years. Thus, these chapters should serve as a steady reference. The models, tests, and applications described in the later chapters will continue to be subject to evolutionary changes as research progresses. However, these chapters do provide a useful snapshot of the current state of affairs and provide a basis from which it should be much easier to keep track of future developments. To assist readers in this task, a webpage has been set up ([www.cis.rit.edu/Fairchild/CAM.html](http://www.cis.rit.edu/Fairchild/CAM.html)), which lists important developments and publications related to the material in this book. A spreadsheet with example calculations can also be found there.

*'Yes,' I answered her last night;  
'No,' this morning sir, I say,  
Colors seen by candle-light  
Will not look the same by day.*

Elizabeth Barrett Browning

# Acknowledgments

---

A project like this book is never really completed by a single author. I particularly thank my family for the undying support that encouraged completion of this work. The research and learning that led to this book is directly attributable to my students. Much of the research would not have been completed without their tireless work, and I would not have learned about color appearance models were it not for their keen desire to learn more and more about them from me. I am deeply indebted to all of my students and friends — those that have done research with me, those working at various times at the Rochester Institute of Technology (RIT), and those that have participated in my university and short courses at all levels. There is no way to list all of them without making an omission, so I will take the easy way out and thank them as a group. I am also indebted to those that reviewed various chapters while the first edition of this book was being prepared and provided useful insights, suggestions, and criticisms as well as those who helped with revisions of the later editions. Thank you to Addison-Wesley for convincing me to write the first edition and then publishing it and to IS&T, the Society for Imaging Science and Technology, for having the vision to publish the second and third editions with Wiley. It has been a joy to work with all of the IS&T staff throughout my color imaging career. Thanks to all of the industrial and government sponsors of our research and education at RIT that lead to many of the results and analyses presented in this volume. I have been fortunate to work with a fascinating variety of students, staff, and faculty colleagues over the years; this edition would not have been possible without them.

M.D.F.  
*Honeoye Falls, NY*

*Ye'll come away from the links with a new hold on life,  
that is certain if ye play the game with all yer heart.*

Michael Murphy, *Golf in the Kingdom*

# Introduction

---

*Standing before it, it has no beginning;  
even when followed, it has no end.*

*In the now, it exists; to the present apply it,  
follow it well, and reach its beginning.*

Tao Te Ching, 300–600 BCE

Like beauty, color is in the eye of the beholder. For as long as human scientific inquiry has been recorded, the nature of color perception has been a topic of great interest. Despite tremendous evolution of technology, fundamental issues of color perception remain unanswered. Many scientific attempts to explain color rely purely on the physical nature of light and objects. However, without the human observer there is no color. It is often asked whether a tree falling in the forest makes a sound if no one is there to observe it. Perhaps equal philosophical energy should be spent wondering what color its leaves are.

*You can observe a lot by just watching.*

Yogi Bera

## WHAT IS A COLOR APPEARANCE MODEL?

It is common to say that certain wavelengths of light, or certain objects, are a given color. This is an attempt to relegate color to the purely physical domain. Instead it is proper to state that those stimuli are perceived to be of a certain color when viewed under specified conditions. Attempts to specify color as a purely physical phenomenon fall within the domain of spectrophotometry and spectroradiometry. When the lowest-level sensory responses of an average human observer are factored in, the domain of colorimetry has been entered. When the many other variables that influence color perception are considered, in order to better describe our perceptions of stimuli, one is within the domain of color appearance modeling — the subject of this book.

Consider the following observations:

- The headlights of an oncoming automobile are nearly blinding at night, but barely noticeable during the day.
- As light grows dim, colors fade from view while objects remain readily apparent.

- Stars disappear from sight during the daytime.
- The walls of a freshly painted room appear significantly different from the color of the sample that was used to select the paint in a hardware store.
- Artwork displayed in different color mat board takes on a significantly different appearance.
- Printouts of images do not match the originals on a self-luminous display (*e.g.*, computer monitor, tablet, smart phone, television).
- Scenes appear more colorful and of higher contrast on a sunny day than on an overcast day.
- Blue and green objects (*i.e.*, board-game pieces) become indistinguishable under dim incandescent illumination.
- It is nearly impossible to select appropriate socks (*e.g.*, black, brown, or blue) in the early morning light.
- There is no such thing as a gray, or brown, lightbulb.
- There are no colors described as reddish-green or yellowish-blue.

None of the above observations can be explained by physical measurements of materials and/or illumination alone. Rather, such physical measurements must be combined with other measurements of the prevailing viewing conditions and models of human visual perception in order to make reasonable predictions of these effects. This aggregate is precisely the task that color appearance models are designed to manage. Each of the observations outlined above, and many more like them, can be explained as instances of various color appearance phenomena and predicted by color appearance models. They cannot be explained by the established techniques of color measurement, sometimes referred to as basic colorimetry. Hutchings (1999), in the first chapter of his book on food color and appearance, provides a delightful review of the complexities of specifying the appearance of stimuli that all enjoy perceiving. This book details the differences between basic colorimetry and color appearance models, provides fundamental background on human visual perception and color appearance phenomena, and describes the application of color appearance models to current technological problems such as digital color reproduction. Upon completion of this book, a reader should be able to fairly easily explain the causes of, if not the physiological mechanisms for, each of the appearance phenomena listed above. Fairchild (2011a) and [whyiscolor.org](http://whyiscolor.org) provide an introductory and inquisitive look at the fundamental questions of color appearance and color science from the perspectives of students ranging from pre-school to graduate school.

Basic colorimetry provides the fundamental color measurement techniques that are used to specify stimuli in terms of their sensory impact for an average human observer. These techniques are absolutely necessary as the foundation for color appearance models. However, on their own, the techniques of basic colorimetry can only be used to specify whether or not two stimuli, viewed under identical conditions, match in color for an average observer. Advanced colorimetry aims to extend the techniques of basic colorimetry to enable the specification of color difference perceptions and ultimately color appearance. There are several established techniques for color difference specification

that have been formulated and refined over the past several decades. These techniques have also reached the point that a few, agreed upon, standards are used throughout the world while research continues to fine-tune, improve, and extend them. Color appearance models aim to go the final step. This would allow the mathematical description of the appearance of stimuli in a wide variety of viewing conditions. Such models have been the subject of much research in the late twentieth and early twenty-first centuries and have become required for practical applications. There are a variety of models that have been proposed. These models have found their way into color imaging systems through the refinement and extension of color management techniques. Techniques derived from color appearance models are even found in the image capture and display algorithms of popular smart phones. Such applications require an ever-broadening array of scientists, engineers, programmers, imaging specialists, and others to understand the fundamental philosophy, construction, and capabilities of color appearance models as described in the ensuing chapters.

Learning is best accomplished with positive feedback to assure that new ideas are assimilated and replace pre-existing misunderstandings. As such, and so as not to make the learning process too difficult, here are some clues to the explanations of the color appearance observations listed near the beginning of this introduction.

- The change of appearance of oncoming headlights can be largely explained by the processes of light adaptation and described by Weber's law.
- The fading of color in dim light while objects remain clearly visible is explained by the transition from trichromatic cone vision to monochromatic rod vision.
- The incremental illumination of a star on the daytime sky is not large enough to be detected, while the same physical increment on the darker nighttime sky is easily perceived, because the visual threshold to luminance increments has changed between the two viewing conditions.
- The paint chip does not match the wall due to changes in the size, surround, and illumination of the stimulus and due to inter-reflections among adjacent walls that serves to increase perceived saturation.
- Changes in the color of a surround or background profoundly influence the appearance of stimuli. This can be particularly striking for photographs and other artwork.
- Assuming the display and printer are accurately calibrated and characterized, differences in media, white point, luminance level, image size, and surround can still force the printed image to look significantly different from the original.
- The Hunt effect and Stevens effect describe the apparent increase in colorfulness and contrast of scenes with increases in illumination level.
- Low levels of incandescent illumination do not provide the energy required by the short-wavelength sensitive mechanisms of the human visual system (the least sensitive of the color mechanisms) to distinguish green objects from blue objects.

- In the dim early morning light, the ability to distinguish dark colors is diminished.
- The perceptions of gray and brown only occur as related colors, thus they cannot be observed as light sources that are normally the brightest element of a scene.
- The hue perceptions red and green (or yellow and blue) are encoded in a bipolar fashion by our visual system and thus cannot exist together.

Given those clues, it is time to read on and further unlock the mysteries of color appearance. All of the topics in these examples are explored in more detail, and from various perspectives, throughout the text.

# Human Color Vision

---

Color appearance models aim to extend basic colorimetry to specify the perceived color of stimuli in a wide variety of viewing conditions. To fully appreciate the formulation, implementation, and application of color appearance models, several fundamental topics in color science must first be understood. These are the topics of the first few chapters of this book. Since color appearance represents several of the dimensions of our visual experience, any system designed to predict correlates to these experiences must be based, to some degree, on the form and function of the human visual system. All of the color appearance models described in this book are derived with human visual function in mind, although most also include some empirical modeling of the visual system as a “black box.” It becomes much simpler to understand the formulations of the various models if basic visual anatomy, physiology, and performance of the visual system are understood. Thus, this book begins with a treatment of the human visual system.

As necessitated by the limited scope available in a single chapter, this treatment of the visual system is an overview of the topics most important for an appreciation of color appearance modeling. The field of vision science is immense, complex, and fascinating. Readers are encouraged to explore the literature and the many useful texts with differing perspectives on human vision in order to gain further insight and details. Of particular note are the review paper on the mechanisms of color vision by Lennie and D’Zmura (1988), the text on human color vision by Kaiser and Boynton (1996), the more general text on the foundations of vision by Wandell (1995), the comprehensive treatment by Palmer (1999), and edited collections on color vision by Backhaus *et al.* (1998) and Gegenfurtner and Sharpe (1999). Other interesting and more recent texts on vision include the extensive and complete volume by Chalupa and Werner (2004), the revision of Dowling’s (2012) classic on the retina, Livingstone’s (2002) interesting treatment of the relationships between art and biology of seeing, Mausfeld and Heyer’s (2003) book focused on perception,

Schwab's (2012) discussion of the evolution of vision, and Valberg's (2005) revised edition covering all of vision, but with some more focus on color. General texts on sensation and perception, such as Wolfe *et al.* (2012), are also excellent sources for learning fundamental aspects of the human visual system. Johnsen (2012) provides a slightly different perspective on visual systems and other optical phenomena in nature. The material that is briefly summarized in this chapter is treated in more detail in those references.

## 1.1 OPTICS OF THE EYE

Our visual perceptions are initiated and strongly influenced by the anatomical structure of the eye. Figure 1.1 shows a schematic representation of the optical structure of the human eye with some key features labeled. The human eye can be thought of as acting like a camera. The cornea and lens act together like

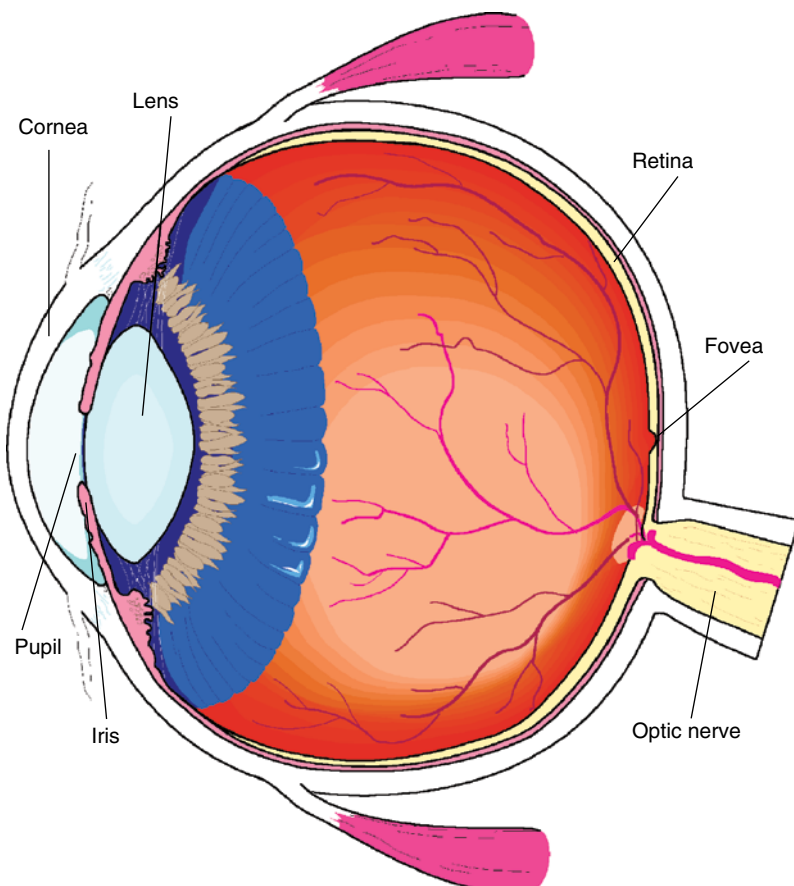


**Figure 1.1** Schematic diagram of the human eye with some key structures labeled

a camera lens to focus an image of the visual world on the retina at the back of the eye, which acts like the image sensor (e.g., CCD) of a camera. These and other structures have a significant impact on our perception of color.

## The Cornea

The *cornea* is the transparent outer surface of the front of the eye through which light passes. It serves as the most significant image-forming element of the eye since its curved surface at the interface with air represents the largest change in index of refraction within the eye's optical system. The cornea is avascular, receiving its nutrients from marginal blood vessels and the fluids surrounding it. Refractive errors, such as nearsightedness (myopia), farsightedness (hyperopia), or astigmatism, can be attributed to variations in the shape of the cornea with respect to the location and the shape of the retina. These refractive errors are sometimes corrected with laser surgery to reshape the cornea.

## The Lens

The *lens* serves the function of accommodation. It is a layered, flexible structure that varies in index of refraction. It is a naturally occurring gradient-index optical element with the index of refraction higher in the center of the lens than at the edges. This feature serves to reduce some of the aberrations that might normally be present in a simple optical system.

The shape of the lens is controlled by the ciliary muscles. When we gaze at a nearby object, the lens becomes “fatter” and thus has increased optical power to allow us to focus on the near object. When we gaze at a distant object, the lens becomes “flatter” resulting in the decreased optical power required to bring more distant objects into sharp focus. As we age, the internal structure of the lens changes, resulting in a loss of flexibility. Generally, when the age of about 45–50 years is reached, the lens has completely lost its flexibility and observers can no longer focus on near objects (this is called presbyopia, or “old eye”). It is at this point that most people must resort to reading glasses or bifocals.

Concurrent with the hardening of the lens is an increase in its optical density. The lens absorbs and scatters short-wavelength (blue and violet) energy. As it hardens, the level of this absorption and scattering increases. In other words, the lens becomes more and more yellow with age. Various mechanisms of chromatic adaptation generally make us unaware of these gradual changes. However, we are all looking at the world through a yellow filter that not only changes with age, but is significantly different from observer to observer. The effects are most noticeable when performing critical color matching or comparing metamerич color matches with other observers. The effect is particularly apparent with purple objects and nearly

monochromatic stimuli such as the primaries of wide-gamut displays. Since an older lens absorbs most of the blue energy reflected from a purple object but does not affect the reflected red energy, older observers will tend to report that the object is significantly more red than reported by younger observers. Important issues regarding the characteristics of lens aging and its influence on visual performance are discussed by Pokorny *et al.* (1987), Werner and Schefrin (1993), and Schefrin and Werner (1993) and in the Commission Internationale de l'Éclairage (CIE) (2006) report on physiological color matching functions.

## The Humors

The volume between the cornea and the lens is filled with *aqueous humor*, which is essentially water. The region between the lens and the retina is filled with *vitreous humor*, which is also a fluid, but with a higher viscosity similar to that of gelatin. Both humors exist in a state of slightly elevated pressure (relative to air pressure) to assure that the flexible eyeball retains its shape and dimensions in order to avoid the deleterious effects of wavering retinal images. The flexibility of the entire eyeball serves to increase its resistance to injury. It is much more difficult to break a structure that gives way under impact than one of equal "strength" that attempts to remain rigid. Since the indices of refraction of the humors are roughly equal to that of water, and those of the cornea and lens are only slightly higher, the rear surface of the cornea and the entire lens have relatively little optical power (in comparison with the front surface of the cornea).

## The Iris

The *iris* is the sphincter muscle that controls pupil size. The iris is pigmented, giving each of us our specific eye color. Eye color is determined by the concentration and distribution of melanin within the iris. The pupil, which is the hole in the middle of the iris through which light passes, defines the level of illumination on the retina. Pupil size is largely determined by the overall level of illumination, but it is important to note that it can also vary with nonvisual phenomena such as arousal. (This effect can be observed by enticingly shaking a toy in front of a cat and paying attention to its pupils.) Thus it is difficult to accurately predict pupil size from the prevailing illumination. In practical situations, pupil diameter varies from about 3 to 7 mm. This change in pupil diameter results in approximately a five-fold change in pupil area and therefore retinal illuminance. The visual sensitivity change with pupil area is further limited by the fact that marginal rays are less effective at stimulating visual response in the cones than central rays (the Stiles–Crawford effect). The change in pupil diameter alone is not sufficient

to explain excellent human visual function over prevailing illuminance levels that can vary over 10 orders of magnitude or more.

## The Retina

The optical image formed by the eye is projected onto the retina. The *retina* is a thin layer of cells, approximately the thickness of tissue paper, located at the back of the eye and incorporating the visual system's photosensitive cells and initial signal processing and transmission "circuitry." These cells are neurons, part of the central nervous system, and can appropriately be considered a part of the brain. The photoreceptors, rods and cones, serve to transduce the information present in the optical image into chemical and electrical signals that can be transmitted to the later stages of the visual system. These signals are then processed by a network of cells and transmitted to the brain through the optic nerve. More detail on the retina is presented in "The retina."

Behind the retina is a layer known as the *pigmented epithelium*. This dark pigment layer serves to absorb any light that happens to pass through the retina without being absorbed by the photoreceptors. The function of the pigmented epithelium is to prevent light from being scattered back through the retina, thus reducing the sharpness and contrast of the perceived image. Nocturnal animals give up this improved image quality in exchange for a highly reflective tapetum that reflects the light back in order to provide a second chance for the photoreceptors to absorb the energy. This is why the eyes of a deer, or other nocturnal animal, caught in the headlights of an oncoming automobile appear to glow. They are acting like very efficient retro-reflectors by focusing the light from the car they are looking at through the animal's eyes and right back to the car itself.

## The Fovea

Perhaps the most important structural area on the retina is the fovea. The *fovea* is the area on the retina where we have the best spatial and color vision. When we look at, or fixate, an object in our visual field, we move our head and eyes such that the image of the object falls on the fovea. As you are reading this text, you are moving your eyes to make the various words fall on your fovea as you read them. To illustrate how drastically spatial acuity falls off as the stimulus moves away from the fovea, try to read the preceding text in this paragraph while fixating on the period at the end of this sentence. It is probably difficult, if not impossible, to read the text that is only a few lines away from the point of fixation. The fovea covers an area that subtends about  $2^\circ$  of visual angle in the central field of vision. To visualize  $2^\circ$  of visual angle, a general rule is that the width of your thumbnail, held at arm's length, is approximately  $1^\circ$  of visual angle. (Also, the moon and

sun each subtend almost exactly  $0.5^\circ$  of visual angle in the sky, an interesting coincidence that enhances the possibility of the Earth having both complete lunar and solar eclipses.)

## The Macula

The fovea is also protected by a yellow filter known as the macula. The *macula* serves to protect this critical area of the retina from intense exposures to short-wavelength energy. It might also serve to reduce the effects of chromatic aberration that cause the short-wavelength image to be rather severely out of focus most of the time. Unlike the lens, the macula does not become more yellow with age. However, there are significant differences in the optical density of the macular pigment from observer to observer and in some cases between a single observer's left and right eyes. The yellow filters of the lens and macula, through which we all view the world, are the major source of variability in color vision between observers with normal color vision.

## The Optic Nerve

A last key structure of the eye is the optic nerve. The optic nerve is made up of the axons (outputs) of the ganglion cells, the last level of neural processing in the retina. It is interesting to note that the optic nerve is made up of approximately one million fibers carrying information generated by approximately 130 million photoreceptors. Thus there is a clear compression of the visual signal prior to transmission to higher levels of the visual system. A one-to-one "pixel map" of the visual stimulus is never available for processing by the brain's higher visual mechanisms. This processing is explored in greater detail below. Since the optic nerve takes up all of the space that would normally be populated by photoreceptors, there is a small area in each eye in which no visual stimulation can occur. This area is known as the *blind spot*.

The structures described above have a clear impact in shaping and defining the information available to the visual system that ultimately results in the perception of color appearance. The action of the pupil serves to define retinal illuminance levels that, in turn, have a dramatic impact on color appearance. The yellow-filtering effects of the lens and macula modulate the spectral responsivity of our visual system and introduce significant inter-observer variability. The spatial structure of the retina serves to help define the extent and nature of various visual fields that are critical for defining color appearance. The neural networks in the retina reiterate that visual perception in general, and specifically color appearance, cannot be treated as simple point-wise image processing problems. Several of these important features are discussed in more detail in the following sections on the retina, visual physiology, and visual performance.

## 1.2 THE RETINA

Figure 1.2 illustrates a cross-sectional representation of the retina. The retina includes several layers of neural cells beginning with the photoreceptors, the *rods* and *cones*. A vertical signal processing chain through the retina can be constructed by examining the connections of photoreceptors to bipolar cells, which are in turn connected to ganglion cells, which form the optic nerve. Even this simple pathway results in the signals from multiple photoreceptors being compared and combined. This is because multiple photoreceptors provide input to many of the bipolar cells, and

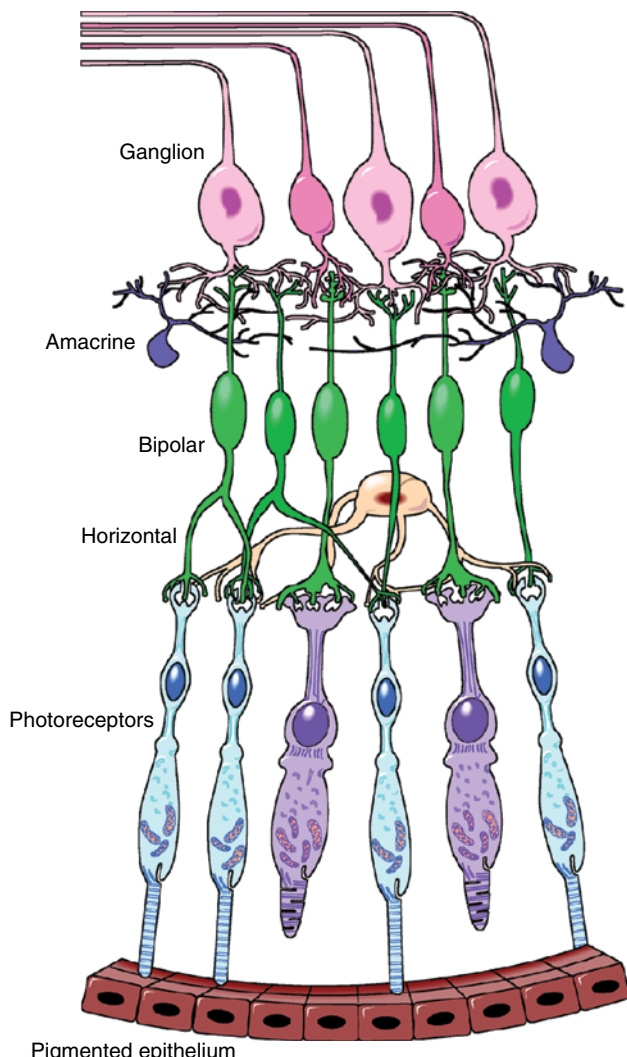


**Figure 1.2** Schematic diagram of the “wiring” of cells in the human retina

multiple bipolar cells provide input to many of the ganglion cells. More importantly, this simple concept of retinal signal processing ignores two other significant types of cells. These are the *horizontal cells*, which connect photoreceptors and bipolar cells laterally to one another, and the *amacrine cells*, which connect bipolar cells and ganglion cells laterally to one another. Figure 1.2 provides only a slight indication of the extent of these various interconnections.

The specific processing that occurs in each type of cell is not completely understood and is beyond the scope of this chapter. However, it is important to realize that the signals transmitted from the retina to the higher levels of the brain via the ganglion cells are not simple point-wise representations of the receptor signals, but rather consist of sophisticated combinations of the receptor signals. To envision the complexity of the retinal processing, keep in mind that each synapse between neural cells can effectively perform a mathematical operation (add, subtract, multiply, and divide) in addition to the amplification, gain control, and nonlinearities that can occur within the neural cells. Thus the network of cells within the retina can serve as a sophisticated image computer. This is how the information from 130 million photoreceptors can be reduced to signals in approximately one million ganglion cells without loss of visually meaningful data.

It is interesting to note that light passes through all of the neural machinery of the retina prior to reaching the photoreceptors. This has little impact on visual performance since these cells are largely transparent and in fixed position, thus not perceived. It also allows the significant amounts of nutrients required, and waste produced, by the photoreceptors to be processed through the back of the eye.

## Rods and Cones

Figure 1.3 provides a representation of the two classes of retinal photoreceptors: rods and cones. Rods and cones derive their respective names from their prototypical shape. Rods tend to be long and slender while peripheral cones are conical. This distinction is misleading since foveal cones, which are tightly packed due to their high density in the fovea, are long and slender, resembling peripheral rods.

The more important distinction between rods and cones is in visual function. Rods serve vision at low luminance levels (*e.g.*, less than  $1\text{ cd/m}^2$ ) while cones serve vision at higher luminance levels. Thus the transition from rod to cone vision is one mechanism that allows our visual system to function over a large range of luminance levels. At high luminance levels (*e.g.*, greater than  $100\text{ cd/m}^2$ ), the rods are effectively saturated and only the cones function. In the intermediate luminance levels, both rods and cones function and contribute to vision. Vision when only rods are active is referred to as *scotopic vision*. Vision served only by cones is referred to as *photopic vision*, and the term *mesopic vision* is used to refer to vision in which both rods and cones are active at intermediate luminance levels.

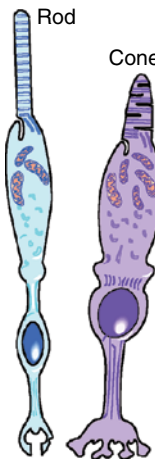


**Figure 1.3** Illustrations of prototypical rod and cone photoreceptors

Rods and cones also differ substantially in their spectral sensitivities as illustrated in Figure 1.4(a). There is only one type of rod receptor with a peak spectral responsivity at approximately 510 nm. There are three types of cone receptors with peak spectral responsivities spaced through the visual spectrum.

The three types of cones are most properly referred to as L, M, and S cones. These names refer to the long-wavelength, middle-wavelength, and short-wavelength sensitive cones, respectively. Sometimes the cones are denoted with other symbols such as RGB or  $\rho\beta$  suggestive of red, green, and blue sensitivities. As can be seen in Figure 1.4(a) this concept can be misleading, and the LMS names are more appropriately descriptive. Note that the spectral responsivities of the three cone types are broadly overlapping, a design that is significantly different from the “color separation” responsivities that are often built into physical imaging systems. Such non-overlapping sensitivities, often incorporated in imaging systems for practical reasons, are the fundamental reason that accurate color reproduction is often difficult, if not impossible, to achieve.

The three types of cones clearly serve color vision. Since there is only one type of rod, the rod system is incapable of color vision. This can easily be observed by viewing a normally colorful scene at very low luminance levels. Figure 1.4(b) illustrates the two CIE spectral luminous efficiency functions, the  $V'(\lambda)$  function for scotopic (rod) vision and the  $V(\lambda)$  function for photopic (cone) vision. These functions represent the overall sensitivity of the two systems with respect to the perceived brightness of the various wavelengths. Since there is only one type of rod, the  $V'(\lambda)$  function is identical to the spectral responsivity of the rods and depends on the spectral absorption of *rhodopsin*, the photosensitive pigment in rods. The  $V(\lambda)$  function, however, represents a combination of the three types of cone signals rather than the responsivity of any single cone type.

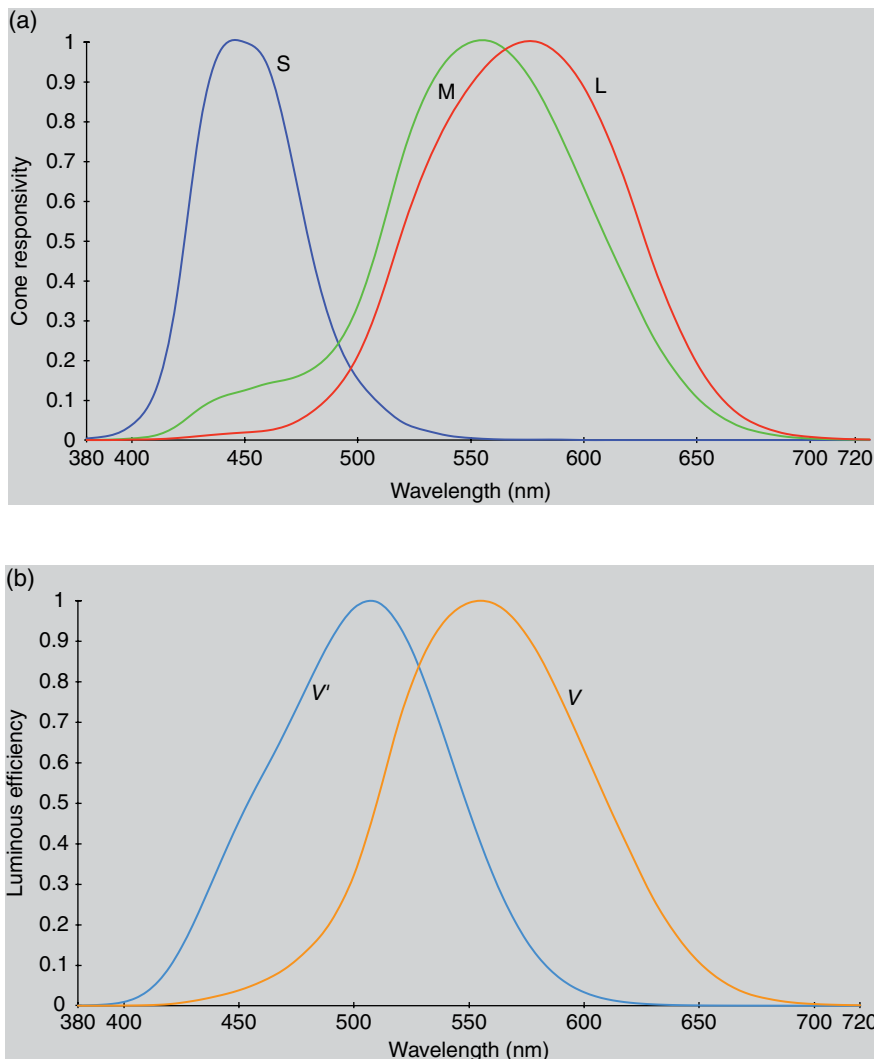


**Figure 1.4** (a) Spectral responsivities of the L, M, and S cones and (b) the CIE spectral luminous efficiency functions for scotopic,  $V'(\lambda)$ , and photopic,  $V(\lambda)$ , vision

Note the difference in peak spectral sensitivity between scotopic and photopic vision. With scotopic vision we are more sensitive to shorter wavelengths. This effect, known as the Purkinje shift, can be observed by finding two objects, one blue and the other red, that appear the same lightness when viewed in daylight. When the same two objects are viewed under very low luminance levels, the blue object will appear quite light while the red object will appear nearly black because of the scotopic spectral sensitivity function's sensitivity to blue energy and almost complete lack of sensitivity to red energy.

Another important feature about the three cone types is their relative distribution in the retina. It turns out that the S cones are relatively sparsely

populated throughout the retina and completely absent in the most central area of the fovea. There are far more L and M cones than S cones, and there are approximately twice as many L cones as M cones. The relative populations of the L : M : S cones are approximately 40 : 20 : 1. These relative populations must be considered when combining the cone responses (plotted with individual normalizations in Figure 1.4(a)) to predict higher-level visual responses. Figure 1.5 provides a schematic representation of the foveal photoreceptor mosaic with completely inaccurate and false coloring to represent a hypothetical distribution with the L cones in red, M cones in green, and S cones in blue. Figure 1.5 is presented simply as a convenient visual representation of the cone populations and should not be taken literally.

As illustrated in Figure 1.5, there are no rods present in the fovea. This feature of the visual system can also be observed when trying to look directly at a small dimly illuminated object, such as a faint star at night. It disappears since its image falls on the foveal area where there are no rods to detect the dim stimulus. Figure 1.6 shows the distribution of rods and cones across the retina. Several important features of the retina can be observed in Figure 1.6. First, note the extremely large numbers of photoreceptors. In some retinal regions, there are about 150 000 photoreceptors per square millimeter of retina! Also note that there are far more rods (around 120 million per retina) than cones (around 7 million per retina). This might seem somewhat counterintuitive since cones function at high luminance levels and produce high visual acuity while rods function at low luminance levels and produce significantly reduced visual acuity (analogous to low-speed fine-grain photographic film vs a high-speed coarse-grain film). The solution to this apparent mystery lies in the fact that single cones feed into ganglion cell signals while rods pool their responses over hundreds of receptors (feeding into a single ganglion cell) in order to produce increased sensitivity at the expense of acuity. This also partially explains how the information from so many receptors can be transmitted through one million ganglion cells. Figure 1.6 also illustrates that cone receptors are highly concentrated in the fovea and more sparsely populated throughout the peripheral retina while there are no rods in the central fovea. The lack of rods in the central fovea allows that valuable space to be used to produce the highest possible spatial acuity with the cone system. A final feature to be noted in Figure 1.6 is the blind spot. This is the area, 12–15° from the fovea, where the optic nerve is formed and there is no room for photoreceptors.

Figure 1.7 provides some stimuli that can be used to demonstrate the existence of the blind spot. One reason the blind spot generally goes unnoticed is that it is located on opposite sides of the visual field in each of the two eyes. However, even when one eye is closed, the blind spot is not generally visible. To observe your blind spot, close your left eye and fixate the cross in Figure 1.7(a) with your right eye. Then adjust the viewing distance of the book until the spot to the right of the cross disappears when it falls on the blind spot. Note that what you see when the spot disappears is not a black region. Rather it appears to be an area of blank paper. This is an example of a phenomenon known as filling-in. Since your brain no longer

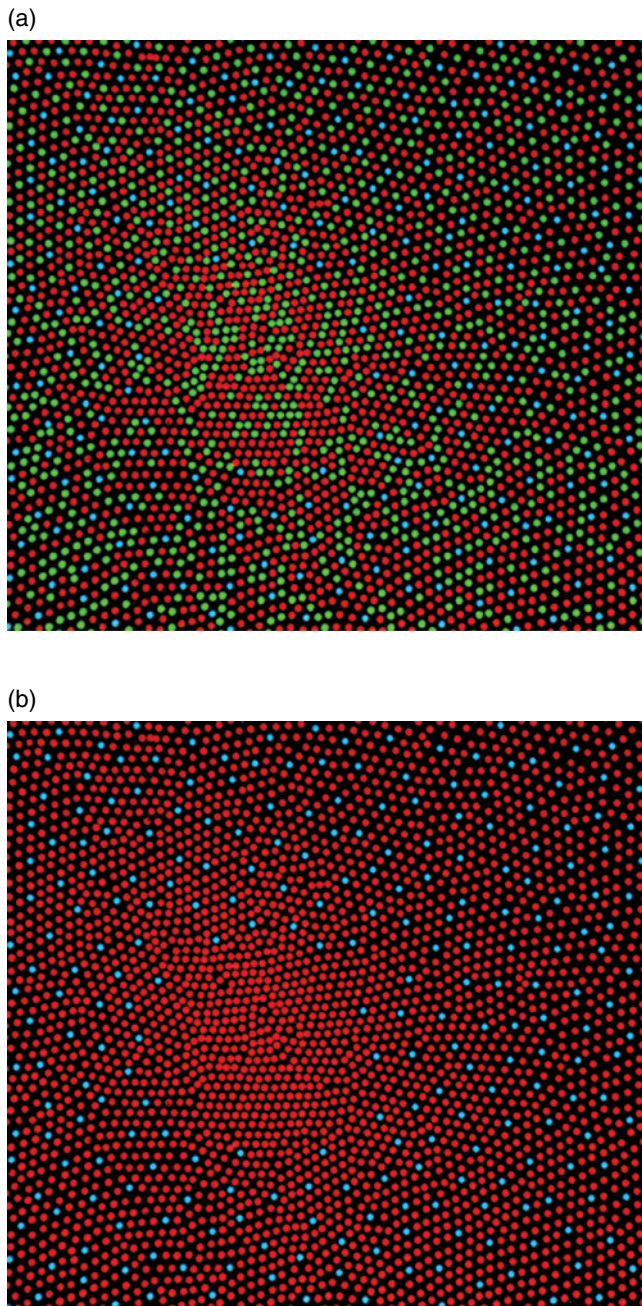


**Figure 1.5** (a) A representation of the retinal photoreceptor mosaic artificially colored to represent the relative proportions of L (colored red), M (green), and S (blue) cones in the human retina. Modeled after Williams *et al.* (1991). (b) The same representation for a hypothetical deuteranope whose M cones contain L-cone photopigments (or whose M cones have been replaced with L cones)

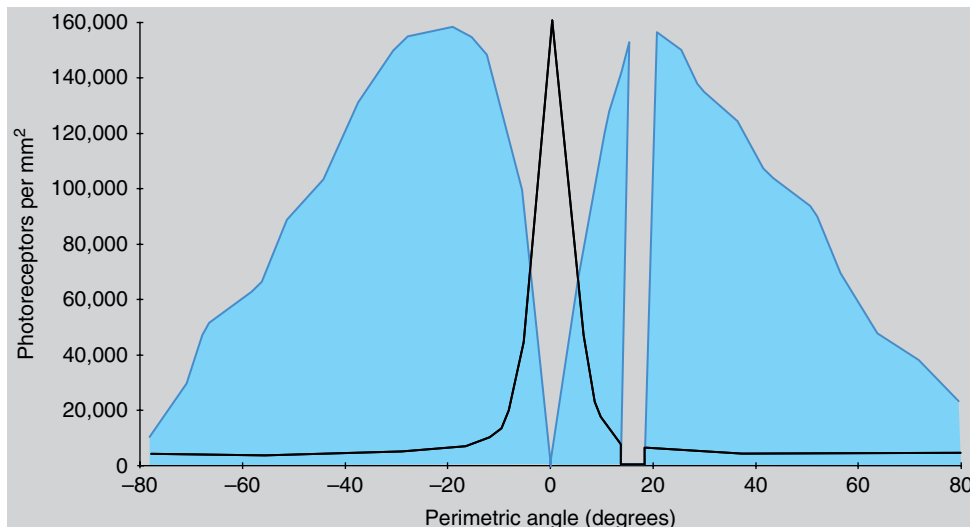


**Figure 1.6** Density (receptors per square millimeter) of rod and cone photoreceptors as a function of location on the human retina

(a)



(b)



**Figure 1.7** Stimuli used to illustrate the presence of the blind spot and “filling-in” phenomena. Close your left eye. Fixate the cross with your right eye and adjust the viewing distance until (a) the spot falls on your blind spot or (b) the gap in the line falls on your blind spot. Note the perception in that area in each case

has any signal indicating a change in the visual stimulus at that location, it simply fills in the most probable stimulus, in this case a uniform white of the paper. The strength of this filling-in can be illustrated by using Figure 1.7(b) to probe your blind spot. In this case, with your left eye closed, fixate the cross with your right eye and adjust the viewing distance until the gap in the line disappears when it falls on your blind spot. Amazingly the perception is that of a continuous line since that is now the most probable visual stimulus. If you prefer to perform these exercises using your left eye, simply turn the book upside down to find the blind spot on the other side of your visual field.

The filling-in phenomenon goes a long way to explain the function of the visual system. The signals present in the ganglion cells represent only local

changes in the visual stimulus. Effectively, only information about spatial or temporal transitions (*i.e.*, edges) is transmitted to the brain. Perceptually this code is sorted out by examining the nature of the changes and filling-in the appropriate uniform perception until a new transition is signaled. This coding provides tremendous savings in bandwidth to transmit the signal and can be thought of as somewhat similar to run-length encoding that is sometimes used in digital imaging.

## Intrinsically Photosensitive Retinal Ganglion Cells

Within the past decade, the properties and roles of intrinsically photosensitive retinal ganglion cells (ipGRC) are beginning to be understood. These are ganglion cells that are directly photosensitive due to a unique photopigment within their cellular structure, known as melanopsin. Thus, rather than simply transmitting the signals from rod and cone photoreceptors, these ganglion cells transmit photo-signals produced intrinsically. The spectral responsivity of ipRGCs is quite broad and peaks at roughly 480 nm, between the S-cones (approximately 440 nm) and rods (approximately 505 nm), with a width similar to the  $V(\lambda)$  function. Thus, ipRGCs represent a third class of photoreceptors in the retina and one that could have an interesting impact on how color appearance and chromatic adaptation are studied and modeled.

These cells have been implicated in a number of visual functions including modulation of circadian rhythms (Rea 2011), control of pupillary response, visual responses, and adaptation. The impacts of modification of these responses can include ailments such as seasonal affective disorder, obesity, cancer, and respiratory illness. Clearly ipRGCs are important to our welfare and visual performance and it remains to be seen how their understanding might improve our ability to predict color appearance.

### 1.3 VISUAL SIGNAL PROCESSING

The neural processing of visual information is quite complex within the retina and becomes significantly, if not infinitely, more complex at later stages. This section provides a very simplistic overview of the paths that some of this information takes. It is helpful to begin with a general map of the steps along the way. The optical image on the retina is first transduced into chemical and electrical signals in the photoreceptors. These signals are then processed through the network of retinal neurons (horizontal, bipolar, amacrine, and ganglion cells) described above. The ganglion cell axons gather to form the optic nerve, which projects to the lateral geniculate nucleus (LGN) in the thalamus. The LGN cells, after gathering input from the ganglion cells, project to visual area one (V1) in the occipital lobe of the cortex. Also note that there are more cells projecting from the cortex down to the LGN and vice versa. Therefore, the LGN clearly plays some role in modulating visual signals based on feedback from higher levels. At this

point, the information processing begins to become amazingly complex. At least 30 visual areas have been defined in the cortex with names such as V2, V3, V4, MT, etc. Signals from these areas project to several other areas and vice versa. The cortical processing includes many instances of feed-forward, feedback, and lateral processing. Somewhere in this network of information, our ultimate perceptions are formed. A few more details of these processes are described in the following paragraphs.

Light incident on the retina is absorbed by photopigments in the various photoreceptors (and ipRGCs). In rods, the photopigment is rhodopsin. Upon absorbing a photon, rhodopsin changes in structure, setting off a chemical chain reaction that ultimately results in the closing of ion channels in its cell walls which produce an electrical signal based on the relative concentrations of various ions (*e.g.*, sodium and potassium) inside and outside the cell wall. A similar process takes place in cones. Rhodopsin is made up of opsin and retinal. Cones have similar photopigment structures. However, in cones the “cone-opsins” have slightly different molecular structures resulting in the various spectral responsivities observed in the cones. Each type of cone (L, M, or S) contains a different form of “cone-opsin.” Figure 1.8 illustrates the relative responses of the photoreceptors as a function of retinal exposure.

It is interesting to note that these functions show characteristics similar to those found in all imaging systems. At the low end of the receptor responses there is a threshold, below which the receptors do not respond. There is then a fairly linear portion of the curves followed by response saturation at the high end. Such curves are representations of the photocurrent at the receptors and represent the very first stage of visual processing after optical absorption. These signals are then processed through

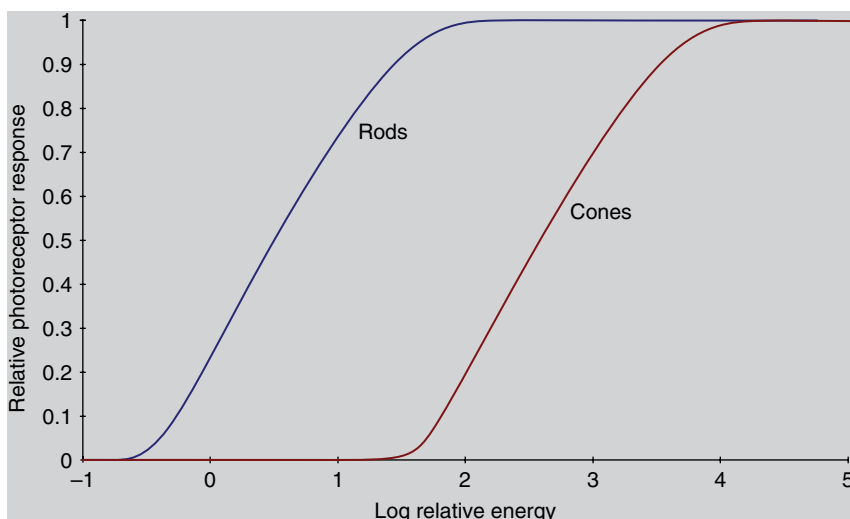


**Figure 1.8** Relative energy responses for the rod and cone photoreceptors

the retinal neurons and synapses until a transformed representation is generated in the ganglion cells for transmission through the optic nerve.

## Receptive Fields

For various reasons, including noise suppression and transmission speed, the amplitude-modulated signals in the photoreceptors are converted into frequency-modulated representations at the ganglion cell and higher levels. In these, and indeed most, neural cells the magnitude of the signal is represented in terms of the number of spikes of voltage per second fired by the cell rather than by the voltage difference across the cell wall. To represent the physiological properties of these cells, the concept of receptive fields becomes useful.

A *receptive field* is a graphical representation of the area in the visual field to which a given cell responds. In addition, the nature of the response (*e.g.*, positive, negative, spectral bias) is typically indicated for various regions in the receptive field. As a simple example, the receptive field of a photoreceptor is a small circular area representing the size and location of that particular receptor's sensitivity in the visual field. Figure 1.9 represents some prototypical receptive fields for ganglion cells. They illustrate center-surround antagonism, which is characteristic at this level of visual processing. The receptive field in Figure 1.9(a) illustrates a positive central response, typically generated by a positive input from a single cone, surrounded by a negative surround response, typically driven by negative inputs from several neighboring cones. Thus the response of this ganglion cell is made up of inputs from a number of cones with both positive and negative signs. The result is that the ganglion cell does not simply respond to points of light but serves as an edge detector (actually a “spot” detector). Those familiar with digital image processing can think of the ganglion cell responses as similar to the output of a convolution kernel designed for edge detection.

Figure 1.9(b) illustrates that a ganglion cell response of opposite polarity is equally possible. The response in Figure 1.9(a) is considered an on-center ganglion cell while that in Figure 1.9(b) is called an off-center ganglion cell. Often on-center and off-center cells will occur at the same spatial location, fed by the same photoreceptors, resulting in an enhancement of the system's dynamic range.

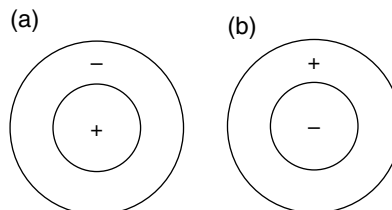


**Figure 1.9** Typical center-surround antagonistic receptive fields: (a) on-center and (b) off-center

Note that the ganglion cells represented in Figure 1.9 will have no response to uniform fields (given that the positive and negative areas are balanced). This illustrates one aspect of the image compression carried out in the retina. The brain is not bothered with redundant visual information; only information about changes in the visual world is transmitted. This spatial information processing in the visual system is the fundamental basis of the important impact of the background on color appearance. Figure 1.9 illustrates spatial opponency in ganglion cell responses. Figure 1.10 shows that in addition to spatial opponency, there is often spectral opponency in ganglion cell responses. Figure 1.10(a) shows a red-green opponent response with the center fed by positive input from an L cone and the surround fed by negative input from M cones (or combinations of cone types if wired randomly). Even random wiring of ganglion cells with a single cone in the center will result in some form of spectral opponency. Figure 1.10(b) illustrates the off-center version of this cell. Thus, before the visual information has even left the retina, processing has occurred with a profound effect on color appearance.

Figure 1.9 and Figure 1.10 illustrate typical ganglion cell receptive fields. There are other types and varieties of ganglion cell responses, but they all share these basic concepts. On their way to the primary visual cortex, visual signals pass through the LGN. While the ganglion cells do terminate at the LGN, making synapses with LGN cells, there appears to be a one-to-one correspondence between ganglion cells and LGN cells. Thus, the receptive fields of LGN cells are identical to those of the ganglion cells. The LGN appears to act as a relay station for the signals. However, it most certainly serves some visual function since there are numerous neural projections from the cortex back to the LGN that could serve as some type of switching or adaptation feedback mechanism. The axons of LGN cells project to visual area one (V1) in the visual cortex.

## Processing in Area V1

In area V1 of the cortex, the encoding of visual information becomes significantly more complex. Much as the outputs of various photoreceptors are combined and compared to produce ganglion cell responses, the outputs

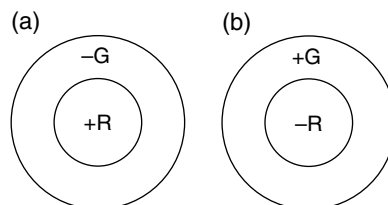


**Figure 1.10** Examples of (a) red–green and (b) green–red spectrally and spatially antagonistic receptive fields

of various LGN cells are compared and combined to produce cortical responses. As the signals move further up in the cortical processing chain, this process repeats itself with the level of complexity increasing very rapidly to the point that receptive fields begin to lose meaning. In V1, cells can be found that selectively respond to various types of stimuli, including

- Oriented edges or bars
- Input from one eye, the other, or both
- Various spatial frequencies
- Various temporal frequencies
- Particular spatial locations
- Various combinations of these features.

In addition, cells can be found that seem to linearly combine inputs from LGN cells and others with nonlinear summation. All of these various responses are necessary to support visual capabilities such as the perceptions of size, shape, location, motion, depth, and color. Given the complexity of cortical responses in V1 cells, it is not difficult to imagine how complex visual responses can become in an interwoven network of many visual areas.

Figure 1.11 schematically illustrates a small portion of the connectivity of the various cortical areas that had been identified around the turn of the century. Bear in mind that Figure 1.11 is showing connections of areas, not cells. There are on the order of  $10^9$  cortical neurons serving visual functions. At these stages it becomes exceedingly difficult to explain the function of single cortical cells in simple terms. In fact, the function of a single cell might not have meaning since the representation of various perceptions must be distributed across collections of cells throughout the cortex. Rather than attempting to explore the physiology further, the following sections will describe some of the overall perceptual and psychophysical properties of the visual system that help to specify its performance.

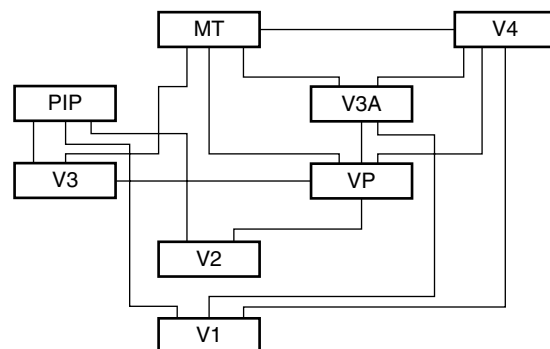


**Figure 1.11** Partial flow diagram to illustrate the many streams of visual information processing in the visual cortex. Information can flow in both directions along each connection

## 1.4 MECHANISMS OF COLOR VISION

Historically, there have been many theories that attempt to explain the function of color vision. A brief look at some of the more modern concepts provides useful insight into current concepts.

### Trichromatic Theory

In the later half of the nineteenth century, the trichromatic theory of color vision was developed based on the work of Maxwell, Young, and Helmholtz. They recognized that there must be three types of receptors, approximately sensitive to the red, green, and blue regions of the spectrum, respectively. The trichromatic theory simply assumed that three images of the world were formed by these three sets of receptors and then transmitted to the brain where the ratios of the signals in each of the images were compared in order to sort out color appearances. The trichromatic (three-receptor) nature of color vision was not in doubt, but the idea of three images being transmitted to the brain is both inefficient and fails to explain several visually observed phenomena.

### Hering's Opponent Colors Theory

At around the same time, Hering (1920) proposed and discussed an opponent colors theory of color vision based on many subjective observations of color appearance. These observations included appearance of hues, simultaneous contrast, afterimages, and color vision deficiencies. Hering noted that certain hues were never perceived to occur together. For example, a color perception is never described as reddish-green or yellowish blue, while combinations of red and yellow, red and blue, green and yellow, and green and blue are readily perceived. This suggested to Hering that there was something fundamental about the red-green and yellow-blue pairs causing them to oppose one another. Similar observations were made of simultaneous contrast in which objects placed on a red background appear greener, on a green background appear redder, on a yellow background appear bluer, and on a blue background appear yellower. Figure 1.12 demonstrates the opponent nature of visual afterimages. The afterimage of red is green, green is red, yellow is blue, and blue is yellow. (It is worth noting that afterimages can also be easily explained in terms of complementary colors due to adaptation in a trichromatic system. Hering only referred to light-dark afterimages in support of opponent theory, not chromatic afterimages.) Lastly, Hering observed that those with color vision deficiencies lose the ability to distinguish hues in red-green or yellow-blue pairs.

All of these observations provide clues regarding the processing of color information in the visual system. Hering proposed that there were three types of receptors, but Hering's receptors had bipolar responses to

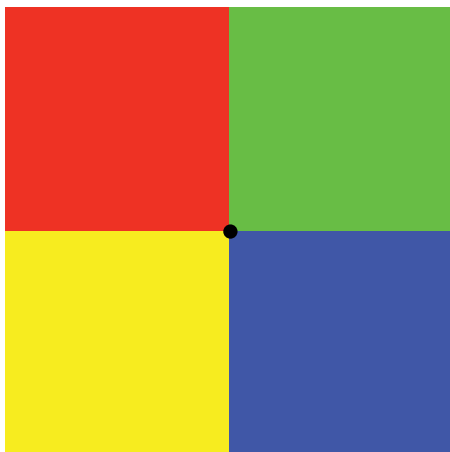


**Figure 1.12** Stimulus for the demonstration of opponent afterimages. Fixate upon the black spot in the center of the four-colored squares for about 30 seconds, and then move your gaze to fixate the black spot in the uniform white area. Note the colors of the afterimages relative to the colors of the original stimuli

light–dark, red–green, and yellow–blue. At the time, this was thought to be physiologically implausible, and Hering's opponent theory did not receive appropriate acceptance.

### Modern Opponent Colors Theory

In the middle of the twentieth century, Hering's opponent theory enjoyed a revival of sorts when quantitative data supporting it began to appear. For example, Svaetichin (1956) found opponent signals in electrophysiological measurements of responses in the retinas of goldfish (which happen to be trichromatic!). DeValois *et al.* (1958) found similar opponent physiological responses in the LGN cells of the macaque monkey. Jameson and Hurvich (1955) also added quantitative psychophysical data through their hue-cancellation experiments with human observers, which allowed measurement of the relative spectral sensitivities of opponent pathways. These data, combined with the overwhelming support of much additional research since that time, have led to the development of the modern opponent theory of color vision (sometimes called a stage theory) as illustrated in Figure 1.13.

Figure 1.13 illustrates that the first stage of color vision, the receptors, is indeed trichromatic as hypothesized by Maxwell, Young, and Helmholtz. However, contrary to simple trichromatic theory, the three “color-separation” images are not transmitted directly to the brain. Instead the neurons of the retina (and perhaps higher levels) encode the color into opponent signals. The outputs of all three cone types are summed ( $L + M + S$ ) to produce an

achromatic response that matches the CIE  $V(\lambda)$  curve as long as the summation is taken in proportion to the relative populations of the three cone types. Differencing of the cone signals allows construction of red-green ( $L - M + S$ ) and yellow-blue ( $L + M - S$ ) opponent signals. The transformation from LMS signals to the opponent signals serves to decorrelate the color information carried in the three channels, thus allowing more efficient signal transmission and reducing difficulties with noise. The three opponent pathways also have distinct spatial and temporal characteristics that are important for predicting color appearance. They are discussed further in Section 1.5.

The importance of the transformation from trichromatic to opponent signals for color appearance is reflected in the prominent place that it finds within the formulation of all color appearance models. Figure 1.13 includes not only a schematic diagram of the neural “wiring” that produces opponent responses, but also the relative spectral responsivities of these mechanisms both before and after opponent encoding.

## Adaptation Mechanisms

However, it is not enough to consider the processing of color signals in the human visual system as a static “wiring diagram.” The dynamic mechanisms of adaptation that serve to optimize the visual response to the particular viewing environment at hand must also be considered. Thus an overview of the various types of adaptation is in order. Of particular relevance to the study of color appearance are the mechanisms of dark, light, and chromatic adaptation.

### *Dark Adaptation*

*Dark adaptation* refers to the change in visual sensitivity that occurs when the prevailing level of illumination is decreased, such as when walking into a darkened theater on a sunny afternoon. At first the entire theater appears completely dark, but after a few minutes one is able to clearly see objects in the theater such as the aisles, seats, and other people. This happens because the visual system is responding to the lack of illumination by becoming more sensitive and therefore capable of producing a meaningful visual response at the lower illumination level.

Figure 1.14 shows the recovery of visual sensitivity (decrease in threshold) after transition from an extremely high illumination level to complete darkness. At first, the cones gradually become more sensitive until the curve levels off after a couple of minutes. Then, until about 10 minutes have passed, visual sensitivity is roughly constant. At that point, the rod system, with a longer recovery time, has recovered enough sensitivity to outperform the cones and thus the rods begin controlling overall sensitivity. The rod sensitivity continues to improve until it becomes asymptotic after about 30 minutes.

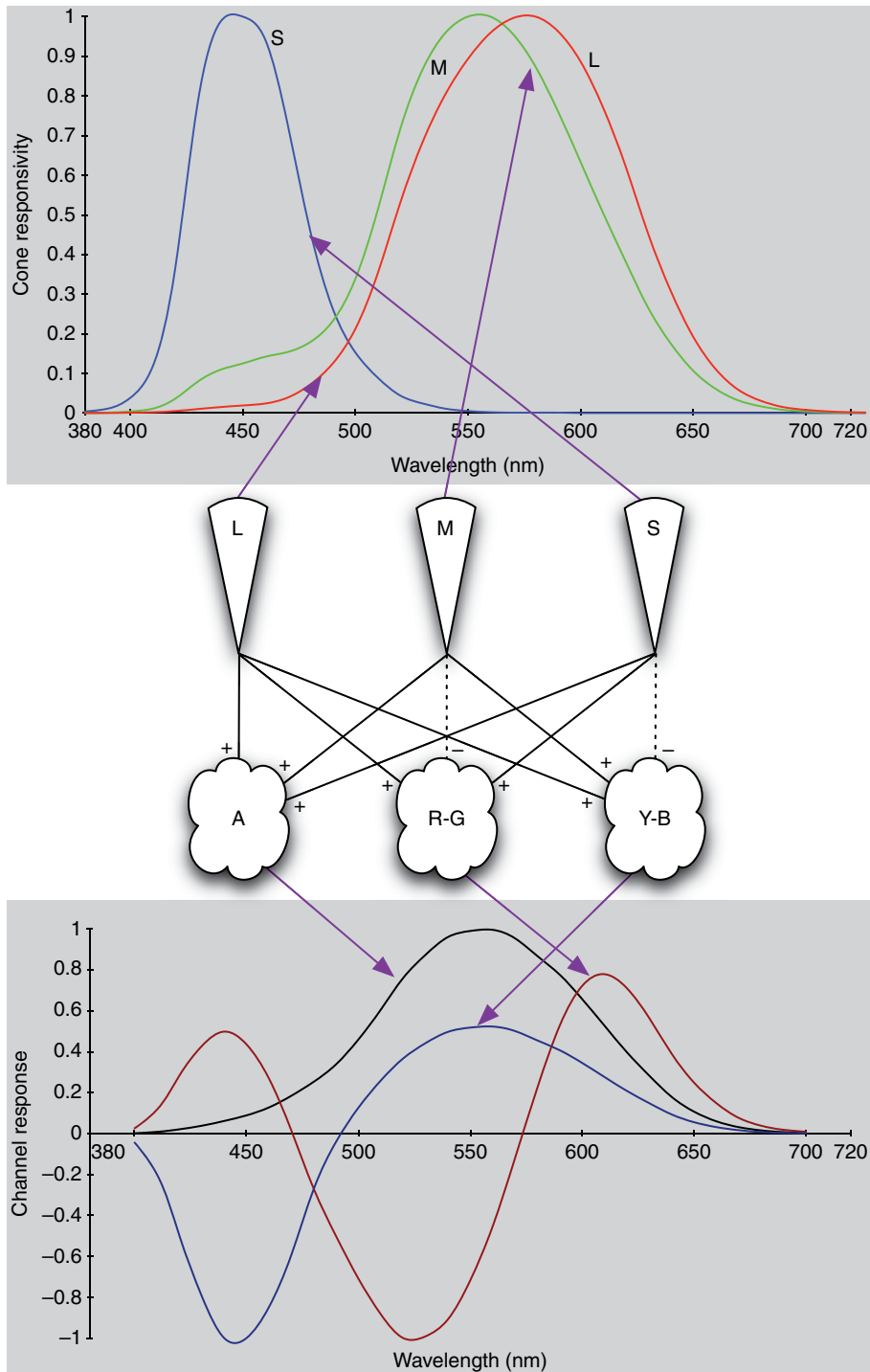


**Figure 1.13** Schematic illustration of the encoding of cone signals into opponent colors signals in the human visual system

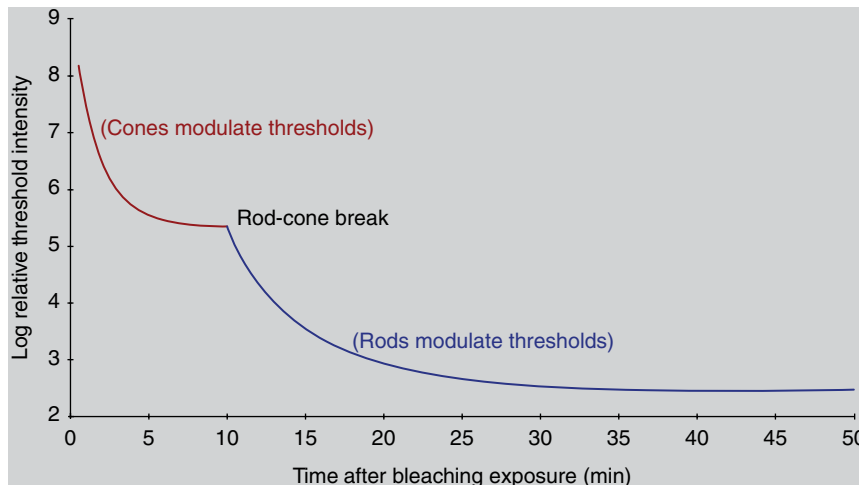


**Figure 1.14** Dark-adaptation curve showing the recovery of threshold after a bleaching exposure. The break in the curve illustrates the point at which the rods become more sensitive than the cones

Recall that the five-fold change in pupil diameter is not sufficient to serve vision over the large range of illumination levels typically encountered. Therefore, neural mechanisms must produce some adaptation. Mechanisms thought to be responsible for various types of adaptation include the following:

- Depletion and regeneration of photopigment
- The rod–cone transition
- Gain control in the receptors and other retinal cells
- Variation of pooling regions across photoreceptors
- Spatial and temporal opponency
- Gain control in opponent and other higher level mechanisms
- Neural feedback
- Response compression
- Cognitive interpretation.

### *Light Adaptation*

*Light adaptation* is essentially the inverse process of dark adaptation. However, it is important to consider it separately since its visual properties differ. Light adaptation occurs when leaving the darkened theater and returning outdoors on a sunny afternoon. In this case, the visual system must become less sensitive in order to produce useful perceptions since there is significantly more visible energy available.

The same physiological mechanisms serve light adaptation, but there is an asymmetry in the forward and reverse kinetics resulting in the time course of light adaptation being on the order of 5 minutes rather than

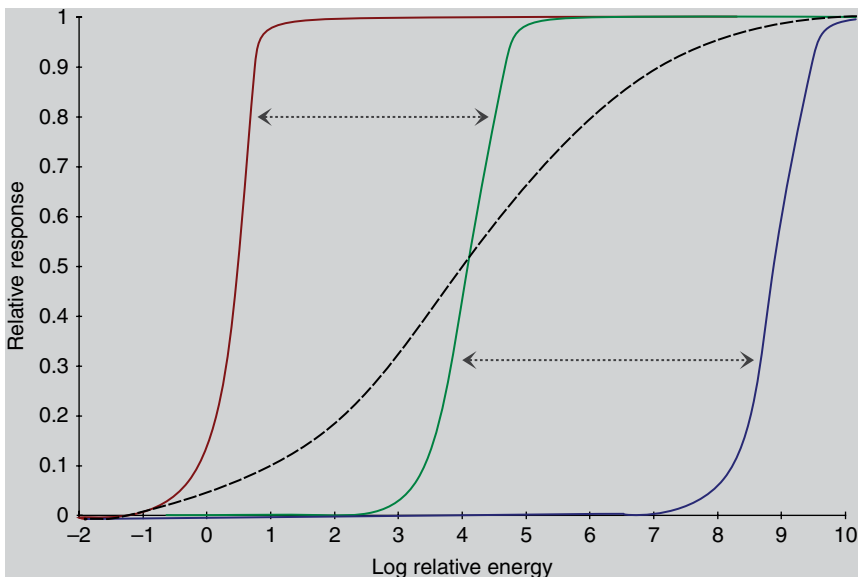


**Figure 1.15** Illustration of the process of light adaptation whereby a very large range of stimulus intensity levels can be mapped into a relatively limited response dynamic range. Solid curves show a family of adapted responses. Dashed curve shows a hypothetical response with no adaptation

30 minutes. Figure 1.15 illustrates the utility of light adaptation. The visual system has a limited output dynamic range, say 100 : 1, available for the signals that produce our perceptions. The world in which we function, however, includes illumination levels covering at least 10 orders of magnitude from a starlit night to a sunny afternoon. Fortunately, it is almost never important to view the entire range of illumination levels at the same time. If a single response function were used to map the large range of stimulus intensities into the visual system's output, then only a small range of the available output would be used for any given scene. Such a response is shown by the dashed line in Figure 1.15. Clearly, with such a response function, the perceived contrast of any given scene would be limited and visual sensitivity to changes would be severely degraded due to signal-to-noise issues.

On the other hand, light adaptation serves to produce a family of visual response curves as illustrated by the solid lines in Figure 1.15. These curves map the useful illumination range in any given scene into the full dynamic range of the visual output, thus resulting in the best possible visual perception for each situation. Light adaptation can be thought of as the process of sliding the visual response curve along the illumination level axis in Figure 1.15 until the optimum level for the given viewing conditions is reached. Light and dark adaptation can be thought of as analogous to an automatic exposure control in a photographic system.

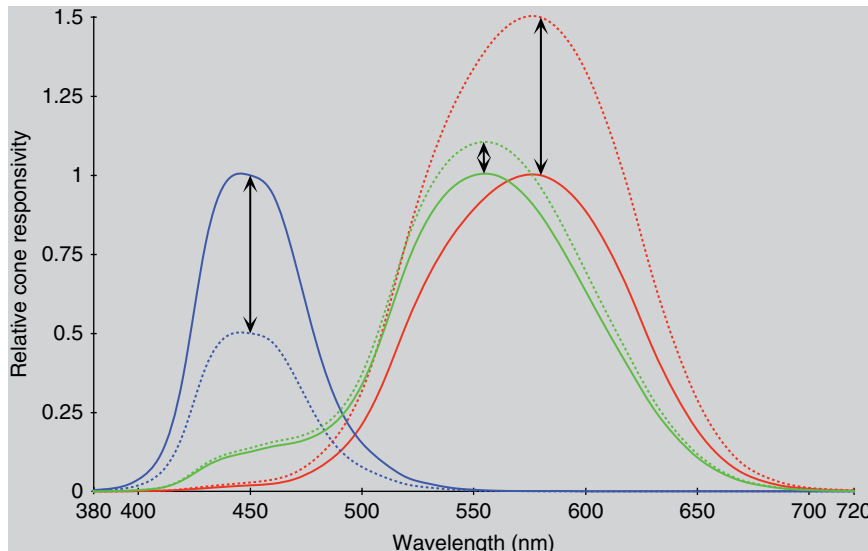


**Figure 1.16** Conceptual illustration of the process of chromatic adaptation as the independent sensitivity regulation of the three-cone responsivities

### Chromatic Adaptation

The third type of adaptation, closely related to light and dark adaptation, is chromatic adaptation. Again, similar physiological mechanisms are thought to produce chromatic adaptation. *Chromatic adaptation* is the largely independent sensitivity control of the three mechanisms of color vision. This is illustrated schematically in Figure 1.16, which shows that the overall height of the three-cone spectral responsivity curves can vary independently. While chromatic adaptation is often discussed and modeled as independent sensitivity control in the cones, there is no reason to believe that it does not occur in opponent and other color mechanisms as well.

Chromatic adaptation can be observed by examining a white object, such as a piece of paper, under various types of illumination (e.g., daylight, fluorescent, and incandescent). Daylight contains relatively far more short-wavelength energy than fluorescent light, and incandescent illumination contains relatively far more long-wavelength energy than fluorescent light. However, the paper approximately retains its white appearance under all three light sources. This is because the S-cone system becomes relatively less sensitive under daylight to compensate for the additional short-wavelength energy and the L-cone system becomes relatively less sensitive under incandescent illumination to compensate for the additional long-wavelength energy.

Chromatic adaptation can be thought of as analogous to an automatic white-balance in video cameras. Figure 1.17 provides a visual demonstration of chromatic adaptation in which the two halves of the visual field are

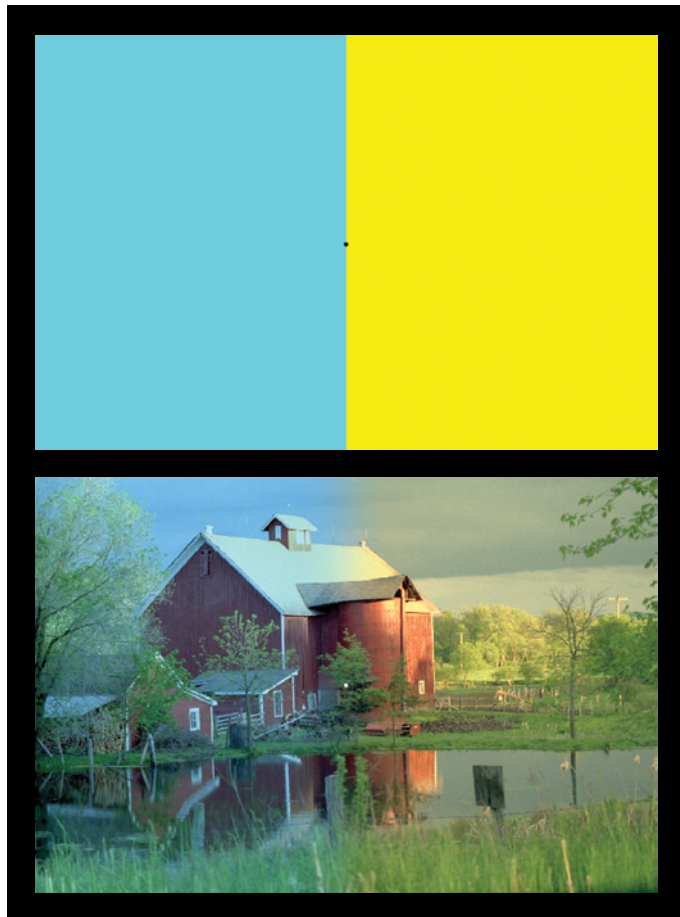


**Figure 1.17** A demonstration of retinally localized chromatic adaptation. Fixate the black spot in between the uniform blue and yellow areas for about 30 seconds, and then shift your gaze to the white spot in the center of the barn image. Note that the barn image appears approximately uniform after this adaptation. Original barn image from Kodak Photo Sampler PhotoCD

conditioned to produce disparate levels of chromatic adaptation. Given its fundamental importance in color appearance modeling, chromatic adaptation is covered in more detail in Chapter 8.

## Visual Mechanisms Impacting Color Appearance

There are many important cognitive visual mechanisms that impact color appearance. These are described in further detail in Chapters 6–8. They include memory color, color constancy, discounting-the-illuminant, and object recognition.

- *Memory color* refers to the phenomenon that recognizable objects often have a prototypical color that is associated with them. For example, most people have a memory for the typical color of green grass and can produce a stimulus of this color if requested to do so in an experiment. Interestingly, the memory color often is not found in the actual objects. For example, green grass and blue sky are typically remembered as being more saturated than the actual stimuli.
- *Color constancy* refers to the everyday perception that the colors of objects remain unchanged across significant changes in illumination color and luminance level. Color constancy is served by the mechanisms of chromatic adaptation and memory color and can easily be shown to be very poor when careful observations are made.
- *Discounting-the-illuminant* refers to an observer's ability to automatically interpret the illumination conditions and perceive the colors of objects after discounting the influences of illumination color.
- *Object recognition* is generally driven by the spatial, temporal, and light-dark properties of the objects rather than by chromatic properties (Davidoff 1991).

Thus once the objects are recognized, the mechanisms of memory color and discounting-the-illuminant can fill in the appropriate color. Such mechanisms have fascinating impacts on color appearance and become of critical importance when performing color comparisons across different media.

Clearly visual information processing is extremely complex and not yet fully understood (perhaps it never will be). It is of interest to consider the increasing complexity of cortical visual responses as the signal moves through the visual system. Single-cell electrophysiological studies have found cortical cells with extremely complex driving stimuli. For example, cells in monkeys that respond only to images of monkey paws or faces have been occasionally found in physiological experiments, and adaptation effects have been measured on stimuli as complex as the features of human faces. The existence of such cells begs the question of how complex a single-cell response can become. Clearly it is not possible for every perception to have its own cortical cell. Thus, at some point in the visual system, the representation of perceptions must be distributed with combinations of various signals producing various perceptions. Such distributed representations open up the possibilities for numerous permutations on a given perception, such as color appearance. It is clear from the large number of stimulus variables that impact color appearance that our visual system is often experimenting with these permutations.

## 1.5 SPATIAL AND TEMPORAL PROPERTIES OF COLOR VISION

No dimension of visual experience can be considered in isolation. The color appearance of a stimulus is not independent of its spatial and temporal characteristics. For example, a black and white stimulus flickering at

an appropriate temporal frequency can be perceived as quite colorful (Fechner–Benham colors). The spatial and temporal characteristics of the human visual system are typically explored through measurement of contrast sensitivity functions (CSFs). CSFs in vision science are analogous to modulation transfer functions (MTFs) in imaging science. However, CSFs cannot legitimately be considered MTFs since the human visual system is highly nonlinear and CSFs represent threshold sensitivity and not suprathreshold modulation. A CSF is defined by the threshold response to contrast (sensitivity is the inverse of threshold) as a function of spatial or temporal frequency. Contrast is typically defined as the difference between maximum and minimum luminance in a stimulus divided by the sum of the maximum and minimum luminances (called Michelson contrast), and CSFs are typically measured with stimuli that vary sinusoidally across space and/or time. Thus a uniform pattern has a contrast of 0 and sinusoidal patterns with troughs that reach a luminance of 0 have a contrast of 1.0 no matter what their mean luminance is.

Figure 1.18 conceptually illustrates typical spatial CSFs for luminance (black–white) and chromatic (red–green and yellow–blue at constant luminance) contrast. The luminance CSF is band-pass in nature, with peak sensitivity around five cycles per degree. This function approaches 0 at zero cycles per degree, illustrating the tendency for the visual system to be insensitive to uniform fields. It also approaches 0 at about 60 cycles per degree, the point at which detail can no longer be resolved by the optics of the eye or the photoreceptor mosaic. The band-pass CSF correlates with the concept of center-surround antagonistic receptive fields that would be most sensitive to an intermediate range of spatial frequency. The chromatic

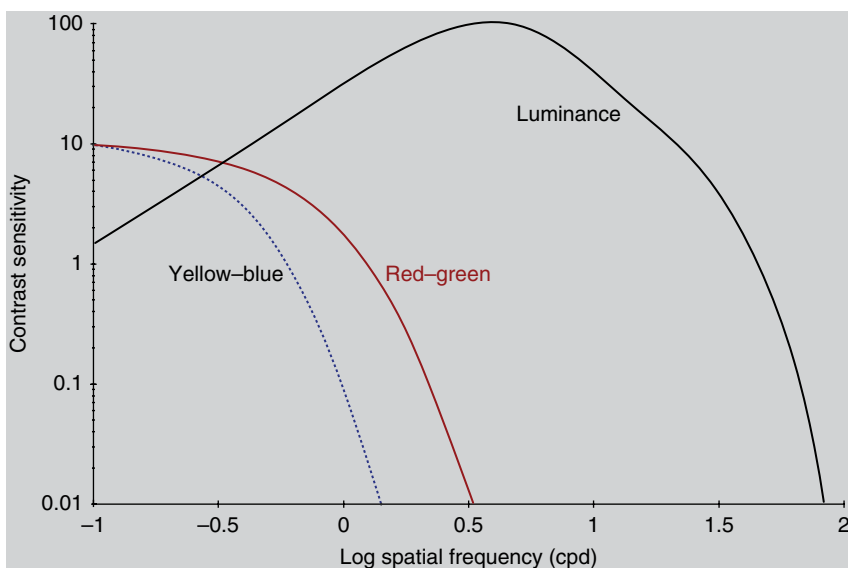


**Figure 1.18** Spatial CSFs for luminance and chromatic contrast

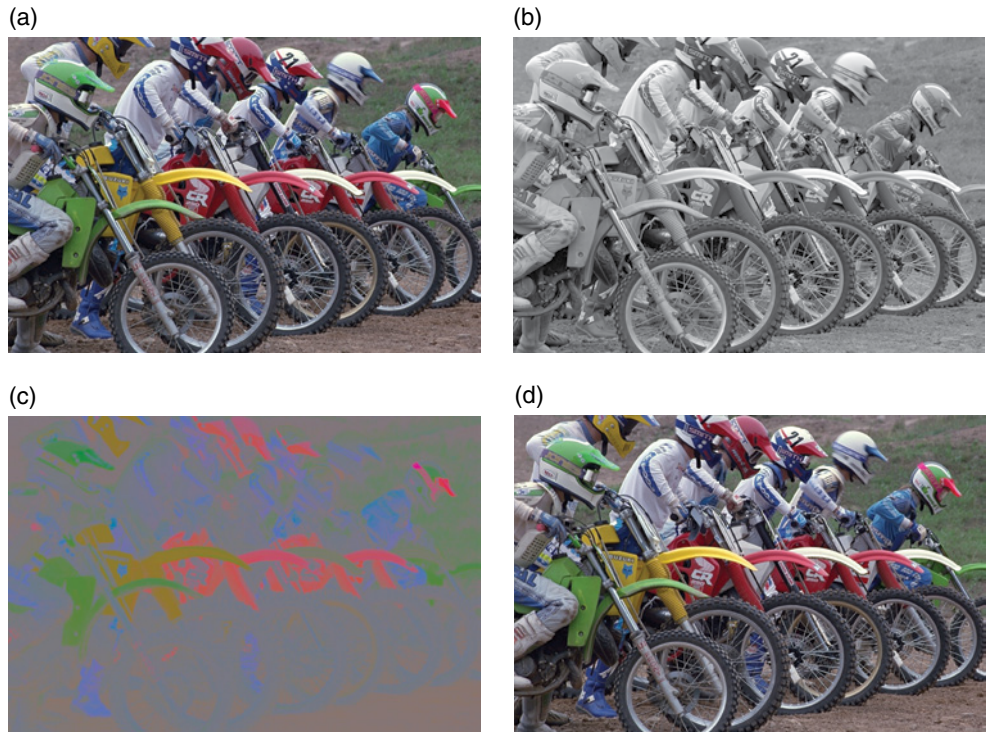
mechanisms are of a low-pass nature and have significantly lower cutoff frequencies (Mullen 1985). This indicates the reduced availability of chromatic information for fine details (high spatial frequencies) that is often taken advantage of in image coding and compression schemes (*e.g.*, MPEG, NTSC, or JPEG).

The low-pass characteristics of the chromatic mechanisms also illustrate that edge detection/enhancement does not occur along these dimensions. The blue–yellow chromatic CSF has a lower cutoff frequency than the red–green chromatic CSF due to the scarcity of S cones in the retina. It is also of note that the luminance CSF is significantly higher than the chromatic CSFs, indicating that the visual system is more sensitive to small changes in luminance contrast compared to chromatic contrast. However, this comparison is just conceptual as the dimensions of contrast in luminance are not easily related to chromatic contrast metrics. Changes in the measurement units, which can be made arbitrarily, can reverse the order of the CSF plots. The spatial CSFs for luminance and chromatic contrast are generally not directly incorporated in color appearance models although there is significant interest in doing so. Zhang and Wandell (1996) presented an interesting technique for incorporating these types of responses into the CIELAB color space calculations. Johnson and Fairchild (2003b) provide a more recent implementation of the model.

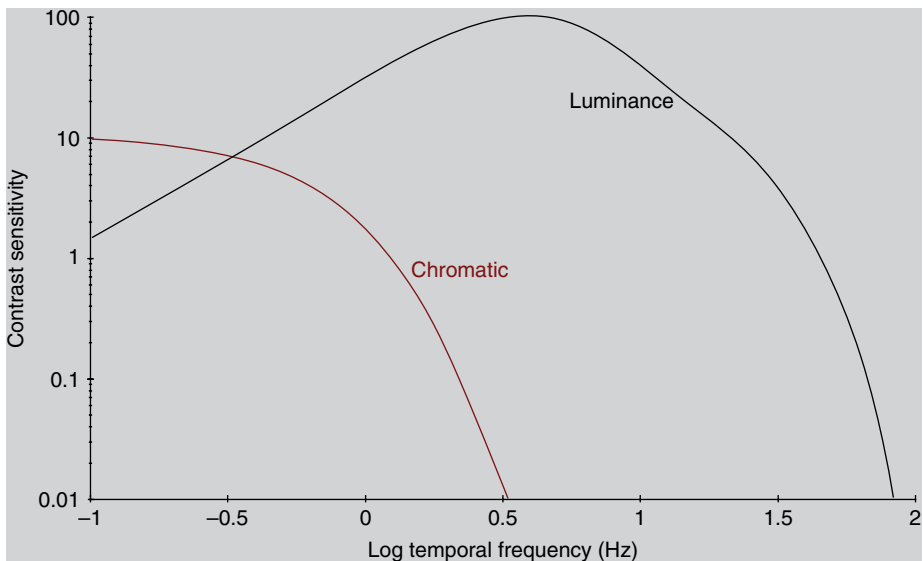
Figure 1.19 illustrates the spatial properties of color vision with a spatial analysis of a typical image. Figure 1.19(a) shows the original image. The luminance information is presented alone in Figure 1.19(b) and the residual chromatic information is presented alone in Figure 1.19(c). It is clear that far more spatial detail can be visually obtained from the luminance image than from the chromatic residual image. This is further illustrated in Figure 1.19(d), in which the image has been reconstructed using the full-resolution luminance image combined with the chromatic image after subsampling by a factor of four. This form of image compression produces no noticeable degradation in perceived resolution or color.

Figure 1.20 conceptually illustrates typical temporal CSFs for luminance and chromatic contrast. They share many characteristics with the spatial CSFs shown in Figure 1.18. Again, the luminance temporal CSF is higher in both sensitivity and cutoff frequency than the chromatic temporal CSFs, and it shows band-pass characteristics suggesting the enhancement of temporal transients in the human visual system. Again, temporal CSFs are not directly incorporated in color appearance models, but they might be of importance to consider when viewing time-varying images such as digital video clips that might be rendered at differing frame rates.

It is important to realize that the functions in Figure 1.18 and Figure 1.20 are typical and not universal. As stated earlier, the dimensions of human visual perception cannot be examined independently. The spatial and temporal CSFs interact with one another. A spatial CSF measured at different temporal frequencies will vary tremendously and the same is true for a temporal CSF measured at various spatial frequencies. These functions also depend on other variables such as



**Figure 1.19** Illustration of the spatial properties of color vision: (a) original image, (b) luminance information only, (c) chromatic information only, and (d) reconstruction with full resolution luminance information combined with chromatic information subsampled by a factor of four. Original motorcycles image from Kodak Photo Sampler PhotoCD



**Figure 1.20** Temporal CSFs for luminance and chromatic contrast

luminance level, stimulus size, retinal locus, etc. See Kelly (1994) for a detailed treatment of some of these interactions.

## The Oblique Effect

An interesting spatial vision phenomenon is the oblique effect. This refers to the fact that visual acuity is better for gratings oriented at  $0^\circ$  or  $90^\circ$  (relative to the line connecting the two eyes) than for gratings oriented at  $45^\circ$ . This phenomenon is considered in the design of rotated halftone screens that are set up such that the most visible pattern is oriented at  $45^\circ$ . The effect can be observed by taking a black-and-white halftone newspaper image and adjusting the viewing distance until the halftone dots are just barely imperceptible. If the image is kept at this viewing distance and then rotated  $45^\circ$ , the halftone dots will become clearly perceptible (since they will then be oriented at  $0^\circ$  or  $90^\circ$ ). Figure 1.21 illustrates this with a halftoned image with an enlarged dot structure that has been rotated  $45^\circ$ . Find the distance at which you can just barely perceive the dot pattern in the upright image and note how the pattern is significantly more visible in the rotated version of the image. The dot pattern is at  $45^\circ$  (oblique) in the upright image and  $0^\circ/90^\circ$  in the rotated image.

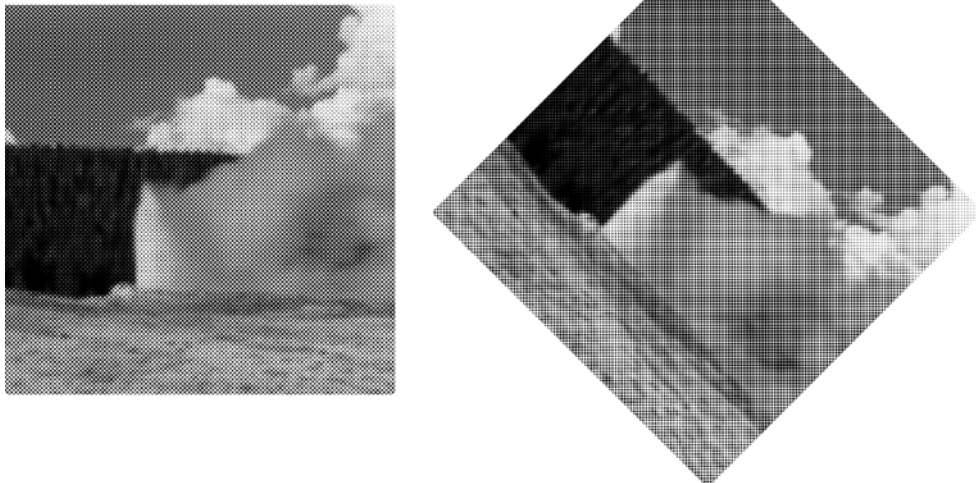


**Figure 1.21** Demonstration of the oblique effect. Find the distance at which you can just barely perceive the dot pattern in the upright image and note the visibility of the pattern in the rotated image. The dot pattern is oriented at  $45^\circ$  (oblique) in the upright image to be less visible and  $0^\circ/90^\circ$  in the rotated image, which makes it more visible

## CSFs and Eye Movements

The spatial and temporal CSFs are also closely linked to the study of eye movements. A static spatial pattern becomes a temporally varying pattern when observers move their eyes across the stimulus. Noting that both the spatial and temporal luminance CSFs approach 0 as either form of frequency variation approaches 0, it follows that a completely static stimulus is invisible. This is indeed the case. If the retinal image can be fixed using a video feedback system attached to an eye tracker, the stimulus does disappear after a few seconds (Kelly 1994). (Sometimes this can be observed by carefully fixating an object and noting that the perceptions of objects in the periphery begin to fade away after a few seconds. The centrally fixated object does not fade away since the ability to hold the eye completely still has variance greater than the high spatial resolution in the fovea. Peripheral objects fade away since the spatial resolution of the visual system is poor in the periphery. This phenomenon is known as Troxler fading.)

To avoid this rather unpleasant phenomenon in typical viewing, our eyes are constantly moving. Large eye movements take place to allow viewing of different areas of the visual field with the high-resolution fovea. Also, there are small constant eye movements that serve to keep the visual world nicely visible. This also explains why the shadows of retinal cells and blood vessels are generally not visible since they do not move *on* the retina, but rather move *with* the retina. The history of eye movements has significant impact on adaptation and appearance through integrated exposure of various retinal areas and the need for movements to preserve apparent contrast. Recent technological advances have allowed psychophysical investigation of these effects (Babcock *et al.* 2003).

## 1.6 COLOR VISION DEFICIENCIES

There are various types of inherited and acquired color vision deficiencies. Kaiser and Boynton (1996) provide a comprehensive overview of the topic while Rosenthal and Phillips (1997) provide some fascinating and useful insights. This section concentrates on the most common inherited deficiencies.

### Protanopia, Deutanopia, and Tritanopia

Some color vision deficiencies are caused by the lack of a particular type of cone photopigment. Since there are three types of cone photopigments, there are three general classes of these color vision deficiencies, namely protanopia, deutanopia, and tritanopia. An observer with protanopia, known as a protanope, is missing the L-cone photopigment and therefore is unable to discriminate reddish and greenish hues since the red-green

opponent mechanism cannot be constructed. A deutanope is missing the M-cone photopigment and therefore also cannot distinguish reddish and greenish hues due to the lack of a viable red-green opponent mechanism. Protanopes and deutanopes can be distinguished by their relative luminous sensitivity since it is constructed from the summation of different cone types. The protanopic luminous sensitivity function is shifted toward shorter wavelengths. A tritanope is missing the S-cone photopigment and therefore cannot discriminate yellowish and bluish hues due to the lack of a yellow-blue opponent mechanism.

## Anomalous Trichromacy

There are also anomalous trichromats who have trichromatic vision, but the ability to discriminate particular hues is reduced either due to shifts in the spectral sensitivities of the photopigments or contamination of photopigments (*e.g.*, some L-cone photopigment in the M-cones). Among the anomalous trichromats are those with any of the following:

- Protanomaly (weak in L-cone photopigment or L-cone absorption shifted toward shorter wavelengths)
- Deutanomaly (weak in M-cone photopigment or M-cone absorption shifted toward longer wavelengths)
- Tritanomaly (weak in S-cone photopigment or S-cone absorption shifted toward longer wavelengths).

There are also some cases of cone monochromatism (effectively only one cone type) and rod monochromatism (no cone responses).

While it is impossible for a person with normal color vision to experience what the visual world looks like to a person with a color vision deficiency, it is possible to illustrate the hues that become indistinguishable. Figure 1.22 provides such a demonstration. To produce Figure 1.22, the two color-normal images (Figure 1.22(a)) processed according to a simulation algorithm published by Brettel *et al.* (1997) as implemented at [www.vischeck.com](http://www.vischeck.com) to generate the images. More background on that model and the theory behind it can be found in Viénot *et al.* (1995). This allows an illustration of the various colors that would be confused by protanopes, deutanopes, and tritanopes. The study of color vision deficiencies is of more than academic interest in the field of color appearance modeling and color reproduction. This is illustrated in Table 1.1 showing the approximate percentages of the population (European descent) with various types of color vision deficiencies.

It is clear from Table 1.1 that color deficiencies are not extremely rare, particularly in the male population (about 8%), and that it might be important to account for the possibility of color-deficient observers in many applications.

(a)



(b)



(c)



(d)

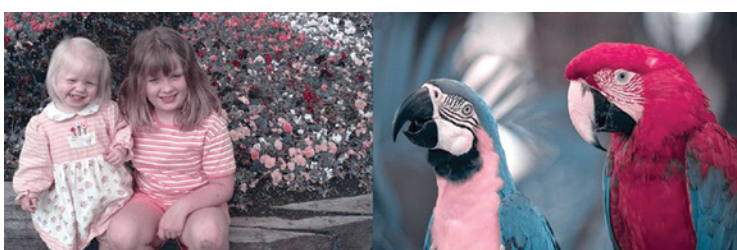


**Figure 1.22** Images illustrating the color discrimination capabilities that are missing from observers with various color vision deficiencies: (a) original images, (b) protanope, (c) deuteranope, and (d) tritanope. Original birds image from Kodak Photo Sampler PhotoCD. Original girls image from the author. Images were processed at [www.vischeck.com](http://www.vischeck.com)

**Table 1.1** Approximate percent occurrences of various color vision deficiencies in populations of European descent

Type	Male %	Female %
Protanopia	1.0	0.02
Deutanopia	1.1	0.01
Tritanopia	0.002	0.001
Cone monochromatism	~0	~0
Rod monochromatism	0.003	0.002
Protanomaly	1.0	0.02
Deutanomaly	4.9	0.38
Tritanomaly	~0	~0
Total	8.0	0.4

Based on data in Hunt (1991a).

## Color Vision Deficiencies and Gender

Why the disparity between the occurrence of color vision deficiencies in males and females? This can be traced back to the genetic basis of color vision deficiencies. It turns out that the most common forms of color vision deficiencies are sex-linked genetic traits.

The genes for photopigments are present on the X chromosome. Females inherit one X chromosome from their mother and one from their father. Only one of these need have the genes for the normal photopigments in order to produce normal color vision. On the other hand, males inherit an X chromosome from their mother and a Y chromosome from their father. If the single X chromosome does not include the genes for the photopigments, the son will have a color vision deficiency. If a female is color deficient, it means she has two deficient X chromosomes and all male children are destined to have a color vision deficiency. It is clear that the genetic “deck of cards” is stacked against males when it comes to inheriting deficient color vision. There are also multiple types of cones within classes (e.g., L cones), and it is possible for women to have X chromosomes that express two different types of L cones. Such heterozygous females can actually be tetrachromatic in terms of number of distinct cone types. However, it appears that tetrachromatic females are still behaviorally trichromats, so the four cone signals must be combined into three channels at some point (Jordon *et al.* 2010). Neitz and Neitz (2000) provide a nice review of the genetics of color vision that can lead to tetrachromatic females, and Mancuso *et al.* (2009) also introduce the possibility of gene therapy for one-day treating color vision deficiencies.

Knowledge regarding the genetic basis of color vision has grown tremendously in recent years. John Dalton was an early investigator of deficient color vision. He studied his own vision, which was historically thought to be protanopic based on his observations, and came up with a theory as to the cause of his deficiencies. Dalton hypothesized that his color vision deficiency was caused by a coloration of his vitreous humor causing it to act

like a filter. Upon his death, he donated his eyes to have them dissected to experimentally confirm his theory. Unfortunately Dalton's theory was incorrect. However, Dalton's eyes have been preserved to this day in a museum in Manchester, UK. Hunt *et al.* (1995) performed DNA tests on Dalton's preserved eyes and were able to show that Dalton was a deutanope rather than a protanope, but with an L-cone photopigment having a spectral responsivity shifted toward the shorter wavelengths. They were also able to complete a colorimetric analysis to show that their genetic results were consistent with the observations originally recorded by Dalton.

## Screening Observers Who Make Color Judgments

Given the fairly high rate of occurrence of color vision deficiencies, it is necessary to screen observers prior to allowing them to make critical color appearance or color matching judgments. There are a variety of tests available, but two types, pseudoisochromatic plates and the Farnsworth–Munsell 100-Hue test, are of practical importance.

Pseudoisochromatic plates (*e.g.*, Ishihara's Tests for Colour Blindness) are color plates made up of dots of random lightness that include a pattern or number in the dots formed out of an appropriately contrasting hue. The random lightness of the dots is a design feature to avoid discrimination of the patterns based on lightness difference only. The plates are presented to observers under properly controlled illumination and they are asked to respond by either tracing the pattern or reporting the number observed. Various plates are designed with color combinations that would be difficult to discriminate for observers with the different types of color vision deficiencies. These tests are commonly administered as part of a normal ophthalmological examination and can be obtained from optical suppliers and general scientific suppliers. Screening with a set of pseudoisochromatic plates should be considered as a minimum evaluation for anyone carrying out critical color judgments.

The Farnsworth–Munsell 100-Hue test, available through the Munsell Color company, consists of four sets of chips that must be arranged in an orderly progression of hue. Observers with various types of color vision deficiencies will make errors in the arrangement of the chips at various locations around the hue circle. The test can be used to distinguish between the different types of deficiencies and also to evaluate the severity of color discrimination problems. This test can also be used to identify observers with normal color vision, but poor color discrimination for all colors.

## 1.7 KEY FEATURES FOR COLOR APPEARANCE MODELING

This chapter provides a necessarily brief overview of the form and function of the human visual system concentrating on the features that are important in the study, modeling, and prediction of color appearance phenomena. What follows is a short review of the key features.

Important features in the optics of the eye include the lens, macula, and cone photoreceptors. The lens and macula impact color matching through their action as yellow filters. They impact inter-observer variability since their optical density varies significantly from person to person. The cones serve as the first stage of color vision, transforming the spectral power distribution on the retina into a three-dimensional signal that defines what is available for processing at higher levels in the visual system. This is the basis of metamerism, the fundamental governing principle of colorimetry.

The numerical distribution of the cones (L : M : S of about 40 : 20 : 1, but widely varying across observers) is important in constructing the opponent signals present in the visual system. Proper modeling of these steps requires the ratios to be accounted for appropriately. The spatial distribution of rods and cones and their lateral interactions are critical in the specification of stimulus size and retinal locus. A color appearance model for stimuli viewed in the fovea would be different from one for peripheral stimuli. The spatial interaction in the retina, represented by horizontal and amacrine cells, is critical for mechanisms that produce color appearance effects due to changes in background, surround, and level of adaptation.

The encoding of color information through the opponent channels along with the adaptation mechanisms before, during, and after this stage are perhaps the most important feature of the human visual system that must be incorporated into color appearance models. Each such model incorporates a chromatic adaptation stage, an opponent processing stage, and nonlinear response functions. Some models also incorporate light and dark adaptation effects and interactions between the rod and cone systems.

Lastly, the cognitive mechanisms of vision such as memory color and discounting-the-illuminant have a profound impact on color appearance. These and other color appearance phenomena are described in greater detail in Chapters 6–8.

# Psychophysics

Clearly an understanding of the basic function of the human visual system is necessary for appreciation of the formulation, implementation, and application of color appearance models. While the need for a basic understanding of the principles of psychophysics might not seem so clear, psychophysical techniques have produced most of our knowledge of human color vision and color appearance phenomena. These are the underpinnings of colorimetry and its extension through color appearance models. Also, psychophysical techniques are used to test, compare, and generate data for improving color appearance models. Thus to fully understand the use and evaluation of color appearance models, a basic appreciation of the field of psychophysics is essential. As an added bonus, psychophysical techniques such as those described in this chapter can help to prove that the implementation of a color appearance model truly improves a system.

This chapter provides an overview of experimental design and data analysis techniques for visual experiments. Carefully conducted visual experiments allow accurate quantitative evaluation of perceptual phenomena that are often thought of as being completely subjective. Such results can be of immense value in a wide variety of fields including color measurement and the evaluation of perceived image quality. Issues regarding the choice and design of viewing environments, an overview of various classes of visual experiments, and a review of experimental techniques for threshold, matching, and scaling experiments are also described. Data reduction and analysis procedures are also briefly discussed. The treatment of psychophysics presented in this chapter is based on the *ASTM Standard Guide for Designing and Conducting Visual Experiments* (ASTM 1996), which was based on materials from the RIT course work of this book's author. There are several excellent texts on psychophysics that provide additional details on the topics covered in this chapter. Of particular note are those of Gescheider (1985), Kingdom and Prins (2010), Bartleson and Grum (1984), Torgerson (1958), Thurstone (1959), and Stevens (1975). Unfortunately, the

last four references are out of print and can only be found in libraries or through used book dealers. An interesting overview of the application of psychophysics to image quality has been presented by Engeldrum (1995). Engeldrum's (2000) text on psychometric scaling provides an excellent, modern review of psychophysical techniques and their application.

## 2.1 PSYCHOPHYSICS DEFINED

*Psychophysics* is the scientific study of the relationships between the physical measurements of stimuli and the sensations and perceptions that those stimuli evoke. Psychophysics can be considered a discipline of science similar to the more traditional disciplines such as physics, chemistry, and biology.

The tools of psychophysics are used to derive quantitative measures of perceptual phenomena that are often considered subjective. It is important to note that the results of properly designed psychophysical experiments are just as objective and quantitative as the measurement of length with a ruler (or any other physical measurement). One important difference is that the uncertainties associated with psychophysical measurements tend to be significantly larger than those of most physical measurements. However, the results are equally useful and meaningful as long as those uncertainties are considered (as they always should be for physical measurements as well). Psychophysics is used to study all dimensions of human perception (and sometimes animal perception). Since the topic of this book is color appearance, visual psychophysics is specifically discussed.

### Two Classes of Visual Experiments

Visual experiments tend to fall into two broad classes:

1. threshold and matching experiments, designed to measure visual sensitivity to small changes in stimuli (or perceptual equality)
2. scaling experiments, intended to generate a relationship between the physical and perceptual magnitudes of stimuli.

It is critical to first determine which class of experiment is appropriate for a given application. Threshold experiments are appropriate for measuring sensitivity to changes and the detectability of stimuli. For example, threshold experiments could be used to determine whether an image compression algorithm was truly visually lossless or if the performance of two-color appearance models is perceptibly different in some practical applications.

Scaling experiments are appropriate when it is necessary to specify the relationships between stimuli. For example, a scaling experiment might be used to develop a quantitative relationship between the perceived quality of

a printed image and the spatial addressability of the printer (or pixel count of a display). In color appearance modeling, the results of scaling experiments are used to derive relationships between physically measurable colorimetric quantities (e.g., CIE XYZ tristimulus values) and perceptual attributes such as lightness, chroma, and hue.

## 2.2 HISTORICAL CONTEXT

As with any scientific discipline, a better appreciation of psychophysics can be obtained with a brief look at the historical development of the field. While scientists have been making and recording careful observations of their perceptions for centuries, the formal discipline of psychophysics is less than 200 years old. Important milestones in the history of psychophysics can be represented in the work of Weber, Fechner, and Stevens.

### Weber's Work

In the early part of the nineteenth century, E.H. Weber investigated the perception of the heaviness, or perceived weight, of lifted weights. Weber asked observers to lift a given weight and then he added to the weight (with all of the necessary experimental controls) until the observers could just distinguish the new weight from the original. This is a measurement of the threshold for perceived change in weight. Weber noted that as the initial weight increased, the change in weight required to reach the threshold increased proportionally. If the initial magnitude of the stimulus (weight in this case) is denoted as  $I$  and the change required to achieve a threshold is denoted as  $\Delta I$ , Weber's results can be expressed by stating that the ratio  $\Delta I/I$  is constant. In fact, this general relationship holds approximately true for many perceptual stimuli and has come to be known as *Weber's law*.

Weber's result is quite intuitive. For example, imagine carrying a few sheets of paper and then adding a 20-page document to the load. Clearly the difference between the two weights would be perceived. Now imagine carrying a briefcase or backpack full of books and papers and then adding another 20-page document. Most likely the added weight of 20 more pages would go unnoticed. That is because a greater change is required to reach a perceptual threshold when the initial stimulus intensity is higher. Weber's law can also be used to explain why stars cannot be seen during the daytime. At night, the stars represent a certain increment in intensity,  $\Delta I$ , over the background illumination of the sky,  $I$ , that exceeds the visual threshold and therefore they can be seen. During the day, the stars still produce the same increment in intensity,  $\Delta I$ , over the background illumination. However, the background intensity of the daytime sky,  $I$ , is much larger than at night. Therefore the ratio  $\Delta I/I$  is far lower during the day than at night. So low, in fact, that the stars cannot be perceived during the day.

## Fechner's Work

The next milestone is the work of Fechner. Fechner built on the work of Weber to derive a mathematical relationship between stimulus intensity and perceived magnitude. While Fechner's motivation was to solve the mind–body problem by proving that functions of the mind could be physically measured, he inadvertently became known as the father of psychophysics through his publication of *Elements of Psychophysics* in 1860 (Fechner 1966).

Fechner started with two basic assumptions:

1. Weber's law was indeed valid.
2. A just-noticeable difference (JND) can be considered a unit of perception.

Weber's results showed that the JNDs measured on the physical scale were not equal as the stimulus intensity increased, but rather increased in proportion to the stimulus intensity. Fechner strived to derive a transformation of the physical stimulus intensity scale to a perceptual magnitude scale on which the JNDs were of equal size for all perceptual magnitudes. This problem essentially becomes one of solving the differential equation posed by Weber's law. Since JNDs followed a geometric series on the stimulus intensity scale, the solution is straightforward that a logarithmic transformation will produce JNDs of equal incremental size on a perceptual scale. Thus the JNDs represented by equal ratios on the physical scale become transformed into equal increments on a perceptual scale according to what has come to be known as Fechner's law.

Simply put, *Fechner's law* states that the perceived magnitude of a stimulus is proportional to the logarithm of the physical stimulus intensity. This relationship is illustrated in Figure 2.1. Fechner's law results in a

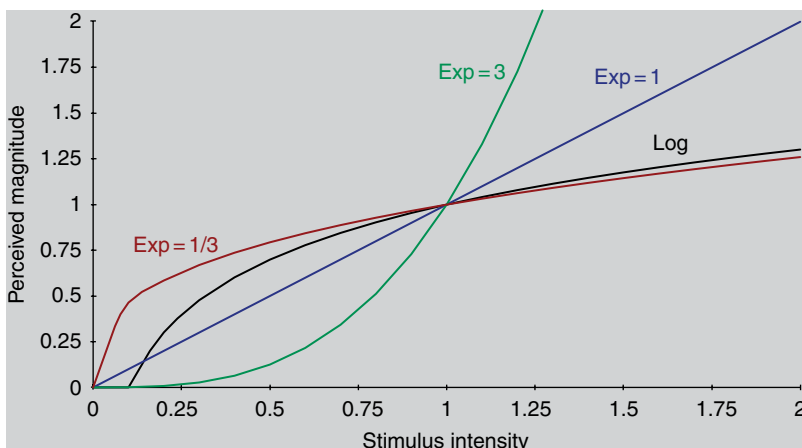


**Figure 2.1** Various psychophysical response functions including the logarithmic function suggested by Fechner and power law relationships with various exponents as suggested by Stevens

compressive nonlinear relationship between the physical measurement and perceived magnitude that illustrates a decreasing sensitivity (*i.e.*, slope of the curve in Figure 2.1) with increasing stimulus intensity. If Fechner's law were strictly valid, then the relationship would follow the same nonlinear form for all perceptions. While the general trend of a compressive nonlinearity is valid for most perceptions, various perceptions take on relationships with differently shaped functions. This means that Fechner's law is not completely accurate. However, there are numerous examples in the vision science literature of instances in which Fechner's law (or at least Weber's law) is obeyed. Carter and Silverstein (2012) have recently examined the relationships between threshold differences and larger perceptual steps on appearance scales. In general, a simple linear relationship between threshold and large color appearance differences is assumed to not exist.

## Stevens' Work

Addressing the lack of generality in Fechner's result, Stevens (1961) published an intriguing paper entitled "To honor Fechner and repeal his law." Stevens studied the relationship between physical stimulus intensity and perceptual magnitude for over 30 different types of perceptions using a magnitude estimation technique. Stevens found that his results produced straight lines when the logarithm of perceived magnitude was plotted as a function of the logarithm of stimulus intensity. However, the straight lines for various perceptions had different slopes. Straight lines on log-log coordinates are equivalent to power functions on linear coordinates with the slopes of the lines on the log-log coordinates equivalent to the exponents of the power functions on linear axes. Thus, Stevens hypothesized that the relationship between perceptual magnitude and stimulus intensity followed a power law with various exponents for different perceptions rather than Fechner's logarithmic function. This result is often referred to as the Stevens power law.

Figure 2.1 illustrates three power law relationships with differing exponents. When the exponent is less than unity, a power law follows a compressive nonlinearity typical of most perceptions. When the exponent is equal to unity, the power law becomes a linear relationship. While there are few examples of perceptions that are linearly related to physical stimulus intensity, one important one is the relationship between perceived and physical length over short distances. A power law with an exponent greater than unity predicts an expansive nonlinearity. Such perceptual relationships do exist in cases where the stimulus might be harmful and thus result in the perception of pain. A compressive function for the pain perception could be quite dangerous since the observer would become less and less sensitive to the stimulus as it became more and more dangerous.

The Stevens power law can be used to model many perceptual phenomena and can be found in fundamental aspects of color measurement such as the relationship between CIE XYZ tristimulus values and the

	Scale	Properties	Operations	Visualization
N	Nominal	Naming	Counting	
O	Ordinal	Order, unequal intervals	Ranking	
I	Interval	Equal intervals, arbitrary zero	Addition, subtraction	
R	Ratio	Natural zero, equal intervals	Multiplication, division	

**Figure 2.2** The hierarchy of scales. Mathematical operations are cumulative with each level of scaling allowing its operations and all of those from types of scales lower in the hierarchy

predictors of lightness and chroma in the CIELAB color space that are based on a cube-root compressive power-law nonlinearity.

## 2.3 HIERARCHY OF SCALES

When deriving perceived magnitude scales, it is critical to understand the properties of the resulting scales. Often a psychophysical technique will produce a scale with only limited mathematical utility. In such cases, it is critical that inappropriate mathematical manipulations are not applied to the scale. Four key types of scales have been defined. In order of increasing mathematical power and complexity, they are nominal, ordinal, interval, and ratio scales. The characteristics of these scales are illustrated in Figure 2.2.

### Nominal Scales

*Nominal scales* are relatively trivial in that they scale items simply by name; for color a nominal scale could consist of reds, yellows, greens, blues, and neutrals. Scaling in this case would simply require deciding which color belonged in which category. Only naming can be performed with nominal data.

### Ordinal Scales

*Ordinal scales* are scales in which elements are sorted in ascending or descending order based on greater or lesser amount of a particular attribute. A set of color swatches could be sorted by hue, and then in each

hue range the colors could be sorted from the lightest to the darkest. Since the swatch colors are not evenly spaced, there might be three dark, one medium, and two light green swatches. If these were numbered from one to six in order of increasing lightness, an ordinal scale would be created. There is no information on such a scale as to how much lighter one of the green swatches is than another, and it is clear that they are not evenly spaced. For an ordinal scale all that matters is that the samples be arranged in increasing or decreasing amounts of an attribute. The spacing between samples can be large or small and can change up and down the scale. Logical operations such as greater-than, less-than, or equal-to can be performed with ordinal scales.

## Interval Scales

*Interval scales* have equal intervals. On an interval scale if a pair of samples was separated by two units and a second pair at some other point on the scale was also separated by two units, the differences between the pairs would be perceptually equal. However, there is no meaningful zero point on an interval scale. In addition to the mathematical operations listed for the above scales, addition and subtraction can be performed with interval data. The Celsius and Fahrenheit temperature scales are interval scales.

## Ratio Scales

*Ratio scales* have all the properties of the above scales plus a meaningfully defined zero point. Thus it is possible to properly equate ratios of numbers on a ratio scale. Ratio scales in visual work are often difficult and sometimes impossible to obtain. This is sometimes the case since a meaningful zero point does not exist. For example, an interval scale of image quality is relatively easy to derive, but try to imagine an image with zero quality. Similarly, it is relatively straightforward to derive interval scales of hue, but there is no physically meaningful zero hue. All of the mathematical operations that can be performed on an interval scale can also be performed on a ratio scale. In addition, multiplication and division can be performed.

## Example of the Use of Scales

It is helpful to reinforce the concepts of the hierarchy of scales by example. Imagine that it is necessary to measure the height of all the people in a room. If only a nominal scale were available, you could choose a first subject and assign a name to his or her height, say Joe. Then you could examine the height of each additional subject relative to the height of Joe. If another person had the same height as Joe (assuming some reasonable tolerance),

their height would also be assigned the name Joe. If their height differed from Joe, they would be given a different name. This process could be completed by comparing the heights of everyone in the room until each unique height was assigned a unique name. Note that there is no information regarding who is taller or shorter than anyone else. The only information available is whether subjects share the same height (and therefore name) or not.

If, instead, an ordinal scale was used to measure height, Joe could arbitrarily be assigned a height of 0. If the next subject was taller than Joe, he or she would be assigned any number larger than Joe's, say 10. If a third subject was found to be taller than Joe, but shorter than the second subject, they would be assigned a number between 0 and 10. This would continue until everyone in the room was assigned a number to represent their height. Since the magnitude of the numbers was assigned arbitrarily, nothing can be said about how much shorter or taller one subject is than another. However, they could be put in order from shortest to tallest.

If an interval scale was available for measurement of height, Joe could again be arbitrarily assigned a height of 0. However, other subjects could then be assigned heights relative to Joe's in terms of meaningful increments such as +3 cm (taller than Joe) or -2 cm (shorter than Joe). If subjects A and B had heights of +3 cm and -2 cm, respectively, on this interval scale, it can be determined that subject A is 5 cm taller than subject B. Note, however, that there is still no information to indicate how tall either of the subjects is. The only information available with the interval scale are differences between subjects.

Finally, if a ratio scale is available to measure height (the normal situation), Joe might be measured and found to be 182 cm tall. Then subjects A and B would have heights of 185 and 180 cm, respectively. If another subject came along who was 91 cm tall, it could be concluded that Joe is twice as tall as this subject. Since 0 cm tall is a physically meaningful zero point, a true ratio scale is available for the measurement of height and thus multiplications and divisions of scale values can be performed.

## 2.4 THRESHOLD TECHNIQUES

Threshold experiments are designed to determine the just perceptible change in a stimulus, sometimes referred to as a JND. Threshold techniques are used to measure the observers' sensitivity to changes in a given stimulus. Absolute thresholds are defined as the just-perceptible difference for a change from no stimulus, while difference thresholds represent the just-perceptible difference from a particular stimulus level greater than 0. Thresholds are reported in terms of the physical units used to measure the stimulus. For example, a brightness threshold might be measured in luminance units of  $\text{cd}/\text{m}^2$ . Sensitivity is defined as the inverse of the threshold since a low threshold implies high sensitivity. Threshold techniques are useful for defining visual tolerances such as those for perceived color differences.

## Types of Threshold Experiments

There are several basic types of threshold experiments presented below in order of increasing complexity of experimental design and utility of the data generated. Many modifications of these techniques have been developed for particular applications. Experimenters strive to design experiments that remove as much control of the results from the observers as possible, thus minimizing the influence of variable observer judgment criteria. Generally, this comes at the cost of implementing more complicated experimental procedures. Threshold techniques include the following:

- Method of adjustment
- Method of limits
- Method of constant stimuli.

### Method of Adjustment

The *method of adjustment* is the simplest and most straightforward technique for deriving threshold data. In it, the observer controls the stimulus magnitude and adjusts it to a point that is just perceptible (absolute threshold) or just perceptibly different (difference threshold) from a starting level. The threshold is taken to be the average setting across a number of trials by one or more observers. The method of adjustment has the advantage that it is quick and easy to implement. However, a major disadvantage is that the observer is in control of the stimulus. This can bias the results due to variability in observers' criteria and adaptation effects. If an observer approaches the threshold from above, adaptation might result in a higher threshold than if it were approached from below. Often the method of adjustment is used to obtain a first estimate of the threshold to be used in the design of more sophisticated experiments. The method of adjustment is also commonly used in matching experiments, including asymmetric matching experiments used in color appearance studies.

### Method of Limits

The *method of limits* is only slightly more complex than the method of adjustment. In the method of limits, the experimenter presents the stimuli at predefined discrete intensity levels in either ascending or descending series. For an ascending series, the experimenter presents a stimulus, beginning with one that is certain to be imperceptible, and asks the observers to respond yes if they perceive it and no if they do not. If they respond no, the experimenter increases the stimulus intensity and presents another trial. This continues until the observer responds yes. A descending series begins with a stimulus intensity that is clearly perceptible and continues

until the observers respond no – that is, they cannot perceive the stimulus. The threshold is taken to be the average stimulus intensity at which the transition from no to yes (or yes to no) responses occurs for a number of ascending and descending series. Averaging over both types of series minimizes adaptation effects. However, the observers are still in control of their criteria since they can respond yes or no at their own discretion.

## Method of Constant Stimuli

In the *method of constant stimuli*, the experimenter chooses several stimulus intensity levels (typically about 5 or 7) around the level of the threshold. Then each of these stimuli is presented multiple times in random order. Over the trials, the frequency with which each stimulus level is perceived is determined. From such data, a frequency-of-seeing curve, or psychometric function, can be derived that allows determination of the threshold and its uncertainty. The threshold is generally taken to be the intensity at which the stimulus is perceived on 50% of the trials. Psychometric functions can be derived either for a single observer (through multiple trials) or for a population of observers (one or more trials per observer). Two types of response can be obtained:

- Yes–no (or pass–fail)
- Forced choice.

### Yes–No Method

In a *yes–no method* of constant stimuli procedure, the observers are asked to respond yes if they detect the stimulus (or stimulus change) and no if they do not. The psychometric function is then simply the percent of yes responses as a function of stimulus intensity. Fifty percent yes responses would be taken as the threshold level. Alternatively, this procedure can be used to measure visual tolerances above threshold by providing a reference stimulus intensity (*e.g.*, a color difference anchor pair) and asking observers to pass stimuli that fall below the intensity of the reference (*e.g.*, a smaller color difference) and fail those that fall above it (*e.g.*, a larger color difference). The psychometric function is then taken to be the percent of fail responses as a function of stimulus intensity, and the 50% fail level is deemed to be the point of visual equality.

### Forced-Choice Procedures

A *forced-choice procedure* eliminates the influence of varying observer criteria on the results. This is accomplished by presenting the stimulus in one of two intervals defined by either a spatial or temporal separation. The

observers are then asked to indicate in which of the two intervals the stimulus was presented. The observers are not allowed to respond that the stimulus was not present and are forced to guess one of the two intervals if they are unsure (hence the name forced choice). The psychometric function is then plotted as the percent of correct responses as a function of stimulus intensity. The function ranges from 50% correct when the observers are simply guessing to 100% correct for stimulus intensities at which they can always detect the stimulus. Thus the threshold is defined as the stimulus intensity at which the observers are correct 75% of the time and therefore detecting the stimulus 50% of the time. As long as the observers respond honestly, their criteria, whether liberal or conservative, cannot influence the results.

## Staircase Procedures

Staircase procedures are a modification of the forced-choice procedure designed to measure only the threshold point on the psychometric function. Staircase procedures are particularly applicable to situations in which the stimulus presentations can be fully automated. A stimulus is presented and the observer is asked to respond. If the response is correct, the same stimulus intensity is presented again. If the response is incorrect, the stimulus intensity is increased for the next trial. Generally, if the observer responds correctly on three consecutive trials, the stimulus intensity is decreased. The stimulus intensity steps are decreased until some desired precision in the threshold is reached. The sequence of three-correct or one-incorrect response prior to changing the stimulus intensity will result in a convergence to a stimulus intensity that is correctly identified on 79% of the trials ( $0.79^3 = 0.5$ ), very close to the nominal threshold level of 75%. Often several independent staircase procedures are run simultaneously to further randomize the experiment. Staircase procedure could also be run with yes–no responses. There are a variety of automated algorithms for seeking thresholds with staircase-like procedures. For example, the QUEST algorithm is readily available in the PsychToolBox routines for MATLAB.

## Probit Analysis of Threshold Data

Threshold data that generate a psychometric function can be most usefully analyzed using *Probit analysis*. Probit analysis is used to fit a cumulative normal distribution to the data (psychometric function). The threshold point and its uncertainty can then be easily determined from the fitted distribution. There are also several significance tests that can be performed to verify the suitability of the analyses. Finney (1971) provides details on the theory and application of Probit analysis. Several commercially available statistical software packages can be used to perform Probit analyses. An alternative to Probit analysis is to use a logistic function

(which, unlike the cumulative normal, is defined for frequencies of 0 and 1) and perform a similar analysis that is referred to as *Logit analysis*. At threshold, and with sound visual data, predictions of Probit and Logit analysis are essentially identical.

## 2.5 MATCHING TECHNIQUES

Matching techniques are similar to threshold techniques except that the goal is to determine when two stimuli are not perceptibly different. Measures of the variability in matching are sometimes used to estimate thresholds. Matching experiments provided the basis for CIE colorimetry through the metamerич matches used to derive color matching functions. For example, if a given color is perceptually matched by an additive mixture of red, green, and blue primary lights, that do not mix to produce a spectral energy distribution that is identical to the test color, then the match is considered *metamerич*. The physical properties of such matches can be used to derive the fundamental responsivities of the human visual system and ultimately be used to derive a system of tristimulus colorimetry as outlined in Chapter 3.

### Asymmetric Matching

Matching experiments are often used in the study of chromatic adaptation and color appearance as well. In such cases, asymmetric matches are made. An *asymmetric match* is a color match made across some change in viewing conditions. For example, a stimulus viewed in daylight illumination might be matched to another stimulus viewed under incandescent illumination to derive a pair of corresponding colors for this change in viewing conditions. Such data can then be used to formulate and test color appearance models designed to account for such changes in viewing condition. One special case of an asymmetric matching experiment is the *haploscopic experiment* in which one eye views a test stimulus in one set of viewing conditions and the other eye simultaneously views a matching stimulus in a different set of viewing conditions. The observer simultaneously views both stimuli and produces a match.

### Memory Matching

Another type of matching experiment that is sometimes used in the study of color appearance is called *memory matching*. In such experiments, observers produce a match to a previously memorized color. Typically such matches are asymmetric to study viewing condition dependencies. Occasionally, memory matches are made to mental stimuli such as an ideal achromatic (gray) color or a unique hue (*e.g.*, a unique red with no blue or yellow content).

## 2.6 ONE-DIMENSIONAL SCALING

Scaling experiments are intended to derive relationships between perceptual magnitudes and physical measures of stimulus intensity. Depending on the type and dimensionality of the scale required, several approaches are possible. Normally, the type of scale required and the scaling method to be used are decided upon before any visual data are collected. One-dimensional scaling requires the assumption that both the attribute to be scaled and the physical variation of the stimulus are one dimensional. Observers are asked to make their judgments on a single perceptual attribute (*e.g.*, how light is one sample compared to another, what is the quality of the difference between a pair of images). A variety of scaling techniques have been devised for the measurement of one-dimensional psychophysical scales, which are described in the following paragraphs:

- Rank order
- Graphical rating
- Category scaling
- Paired comparisons
- Partition scaling
- Magnitude estimation or production
- Ratio estimation or production.

In a *rank order* experiment, the observer is asked to arrange a given set of samples according to increasing or decreasing magnitudes of a particular perceptual attribute. With a large number of observers the data may be averaged and re-ranked to obtain an ordinal scale. To obtain an interval scale, certain assumptions about the data need to be made and additional analyses need to be performed. In general it is somewhat dubious to attempt to derive interval scales directly from rank order data. One of the more reasonable assumptions is to treat the data as if each pair of stimuli were compared, thereby deriving paired comparison data from the rank results.

*Graphical rating* allows direct determination of an interval scale. Observers are presented stimuli and asked to indicate the magnitude of their perception on a one-dimensional scale with defined endpoints. For example, in a lightness scaling experiment a line might be drawn with one end labeled white and the other end labeled black. When the observers are presented with a medium gray that is perceptually halfway between white and black, they would make a mark on the line at the midpoint. If the sample was closer to white than black, they would make a mark at the appropriate physical location along the line, closer to the end labeled white. The interval scale is taken to be the mean location on the graphical scale for each stimulus. This technique relies on the well-established fact that the perception of length over short distances is linear with respect to physically measured length.

*Category scaling* is a popular technique for deriving ordinal or interval scales for large numbers of stimuli. An observer is asked to separate a large number of samples into various categories. With several observers, the number of times each particular sample is placed in a category is recorded. For this to be an effective scaling method the samples need to be similar enough that they are not always placed in the distinct categories by different observers or by the same observer on different occasions. Interval scales may be obtained by this method by assuming that the perceptual magnitudes are normally distributed and by making use of the standard normal distribution according to the law of categorical judgments (Torgerson 1954).

When the number of different stimuli is smaller, a *paired comparison* experiment can be performed. In this method, all samples are presented to the observer in all the possible pairwise combinations, usually one pair at a time (sometimes with a third stimulus as a reference). The proportion of times a particular sample is judged greater in some attribute than each other sample is calculated and recorded. Interval scales can be obtained from such data by applying the law of comparative judgments (Thurstone 1927). Thurstone's law of comparative judgments and its extensions can be usefully applied to ordinal data (such as paired comparisons and category scaling) to derive meaningful interval scales. The perceptual magnitudes of the stimuli are normally distributed on the resulting scales. Thus, if it is safe to assume that the perceptual magnitudes are normally distributed on the true perceptual scale, these analyses derive the desired scale. They also allow useful evaluation of the statistical significance of differences between stimuli since the power of the normal distribution can be utilized. Torgerson (1958), Bartleson and Grum (1984), and Engeldrum (2000) describe these and other related analyses in detail. ASTM (1996) describes a simple method for deriving confidence limits on Thurstonian interval scales. That technique, while conservative, might be less than optimal and is difficult to derive with statistical rigor. Montag (2004) describes a Monte Carlo simulation of the problem and recommends a more appropriate method for deriving confidence intervals. Handley (2001) also describes some related techniques.

A rather direct method for deriving interval scales is through *partition scaling*. A common method is by equating intervals through bisection. The observer is given two different samples (A and B) and asked to select a third such that the difference between it and A appears equal to the difference between it and B. A full interval scale may be obtained by successive bisections.

Ratio scales can be directly obtained through the methods of *magnitude estimation or production*. In such experiments, the observer is asked to assign numbers to the stimuli according to the magnitude of the perception. Alternatively, observers are given a number and asked to produce a stimulus with that perceptual magnitude. This is one of the few techniques that can be used to generate a ratio scale. It can also be used to generate data for multidimensional scaling (MDS) by asking observers to scale the differences between pairs of stimuli.

A slightly more complicated technique involves *ratio estimation or production*. The observer is asked for judgments in one of two ways: (1) select or produce a sample that bears some prescribed ratio to a standard or (2) given two or more samples, to state the apparent ratios among them. A typical experiment is to give the observers a sample and ask them to find, select, or produce a test sample that is one-half or twice the standard in some attribute. For most practical visual work this method is too difficult to use either because of the sample preparation or the judgment by the observers. However, it can be also used to generate a ratio scale.

## 2.7 MULTIDIMENSIONAL SCALING

MDS is a method similar to one-dimensional scaling, but it does not require the assumption that the attribute to be scaled is one dimensional. The dimensionality is found as part of the analysis. In MDS, the data are interval or ordinal scales of the similarities or dissimilarities between each of the stimuli, and the resulting output is a multidimensional geometric configuration of the perceptual relationships between the stimuli, as on a map.

The dissimilarity data required for MDS can conveniently be obtained using paired comparison and triadic combination experiments. In a paired comparison experiment, all samples in all possible pairs are presented and the observer is asked to make a magnitude estimation of the perceived difference between each pair. The resulting estimates for each pairwise combination can then be subjected to MDS analyses. In the method of triadic combinations, observers are presented with each possible combination of the stimuli taken three at a time. They are then asked to judge which two of the stimuli in each triad are most similar to one another and which two are most different. The data can then be converted into frequencies of times each pair is judged most similar or most different. These frequency data can then be combined into either a similarity or dissimilarity matrix for use in MDS analyses.

MDS analysis techniques take such similarity or dissimilarity data as input and produce a multidimensional configuration of points representing the relationships and dimensionality of the data. It is necessary to use such techniques when either the perception in question is multidimensional (such as color – hue, lightness, and chroma) or the physical variation in the stimuli is multidimensional. Kruskal and Wish (1978) provide details of these techniques. There are several issues with respect to MDS analyses. There are two classes of MDS: metric, which requires interval data, and non-metric, which only requires ordinal data. Both classes of MDS techniques result in interval-scale output. Various MDS software packages process input data according to specific assumptions regarding the input data, treatment of individual cases, goodness-of-fit metrics (stress), distance metrics (*e.g.*, Euclidean or city-block), *etc.* Several commercial statistical software packages provide MDS capabilities.

**Table 2.1** Dissimilarity matrix consisting of distances between cities in the USA

	ATL	BOS	CHI	DAL	DEN	LA	SEA	NYC
ATL	—	—	—	—	—	—	—	—
BOS	1037	—	—	—	—	—	—	—
CHI	674	963	—	—	—	—	—	—
DAL	795	1748	917	—	—	—	—	—
DEN	1398	1949	996	781	—	—	—	—
LA	2182	2979	2054	1387	1059	—	—	—
SEA	2618	2976	2013	2078	1307	1131	—	—
NYC	841	206	802	1552	1771	2786	2815	—

**Table 2.2** Output two-dimensional coordinates for each city in the USA MDS example

City	Dimension 1	Dimension 2
Atlanta	-0.63	0.40
Boston	-1.19	-0.31
Chicago	-0.36	-0.15
Dallas	0.07	0.55
Denver	0.48	0.00
Los Angeles	1.30	0.36
Seattle	1.37	-0.66
New York City	-1.04	-0.21

A classic example of MDS analysis is the construction of a map from data representing the distances between cities (Kruskal and Wish 1978). In this example, a map of the USA is constructed from the dissimilarity matrix of distances between eight cities gathered from a road atlas as illustrated in Table 2.1.

The dissimilarity data are then analyzed via MDS. Stress (RMS error) is used as a measure of goodness-of-fit in order to determine the dimensionality of the data. In this example, the stress of a one-dimensional fit is about 0.12, while the stress in two or more dimensions is essentially 0. This indicates that a two-dimensional fit, as expected, is appropriate. The results output include the coordinates in each of the two dimensions for each of the cities as listed in Table 2.2.

Plotting the coordinates of each city in the two-output dimensions will result in a familiar map of the USA, as shown in Figure 2.3. However, it should be noted that dimension 1 goes from east to west and dimension 2 goes from north to south, resulting in a map that has the axes reversed from a traditional map. This illustrates a feature of MDS, namely that the definition of the output dimensions requires post hoc analysis by the experimenter. MDS experiments can be used to explore the dimensionality and structure of color appearance spaces (Indow 1988).

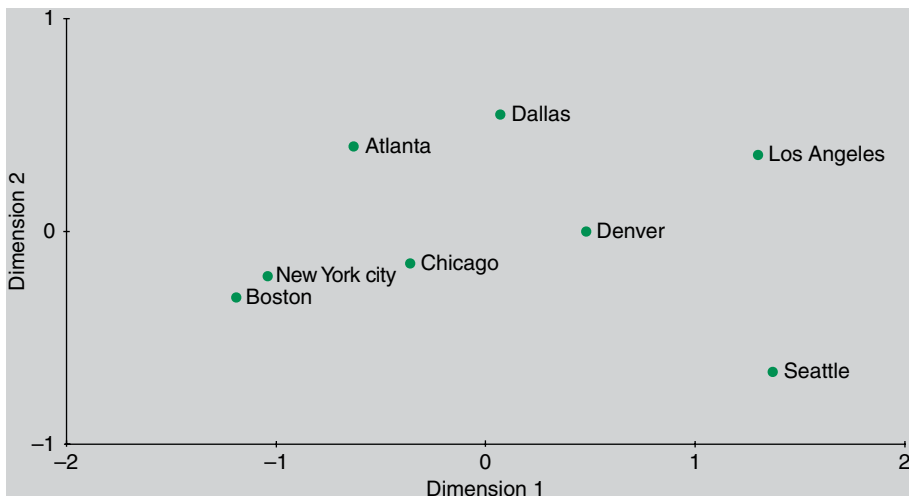


**Figure 2.3** The output of a MDS program used to generate a map of the USA from input data on the proximities of cities

## 2.8 DESIGN OF PSYCHOPHYSICAL EXPERIMENTS

The previous sections provide an overview of some of the techniques used to derive psychophysical thresholds and scales. However, there are many more issues that arise in the design of psychophysical experiments that have a significant impact on the experimental results, particularly when color appearance is concerned. Many of these experimental factors are the key variables that have illustrated the need to extend basic colorimetry with the development of color appearance models. A complete description of all of the variables involved in visual experiments could easily fill several books, and many of the critical issues for color appearance phenomena are described in more detail in later chapters. At this point a simple listing of some of the issues that require consideration should be sufficient to bring these issues to light. Important factors in visual experiments include (in no particular order):

Observer age	Illumination level
Observer experience	Illumination color
Number of observers	Illumination geometry
Screening for color vision deficiencies	Background condition
Observer acuity	Surround condition
Instructions	Control and history of eye movements
Context	Adaptation state
Feedback	Complexity of observer task
Rewards	Controls

Repetition rate	Duration of observation sessions
Range effects	Number of observation sessions
Regression effects	Observer motivation
Image content	Cognitive factors
Number of images	Statistical significance of results.

All of these items, and probably many more, can have a profound effect on psychophysical results and should be carefully specified and/or controlled. Such issues need to be addressed both by those performing experiments and those trying to interpret and utilize the results for various applications.

## 2.9 IMPORTANCE IN COLOR APPEARANCE MODELING

A fundamental understanding of the processes involved in psychophysical experiments provides useful insight for understanding the need for and development and evaluation of color appearance models. Psychophysical experiments provided much of the information reviewed in Chapter 1 on the human visual system. Psychophysics is the basis of colorimetry presented in Chapter 3. The results of psychophysical experiments are also presented in Chapters 6, 8, and 17 on color appearance phenomena, chromatic adaptation, and testing color appearance models. Simply put, without extensive psychophysical experimentation, none of the information required to create and use color appearance models would exist.

# Colorimetry

Colorimetry serves as the fundamental underpinning of color appearance specification. This chapter reviews the well-established practice of colorimetry according to the CIE (the International Commission on Illumination) system first established in 1931. This system allows the specification of color matches for an average observer and has amazingly withstood an onslaught of technological pressures and remained a useful international standard for over 65 years (Fairchild 1993b, Wright 1981b). However, CIE colorimetry provides only the starting point. Color appearance models enhance this system in an effort to predict the actual appearances of stimuli in various viewing conditions rather than simply whether or not two stimuli will match. This chapter provides a general review of the concepts of colorimetry to set the stage for development of various color appearance models. It is not intended to be a complete reference on colorimetry since there are a number of excellent texts available on the subject. For introductions to colorimetry, readers are referred to the texts of Hunt and Pointer (2011), Ohta and Robertson (2005), Berns (2000), Hunt (1991a), Berger-Schunn (1994), Kuehni (2005), and Hunter and Harold (1987). The precise definition of colorimetry can be found in the primary references: CIE Publication 15.2 (CIE 1986) and CIE Publication 15.3 (2004c). For complete details in an encyclopedic reference volume, the classic book by Wyszecki and Stiles (1982), *Color Science*, should be consulted. Despite being over three decades old, it is still the key reference in the field and poses many problems that remain unsolved. Fundamental insight into the mathematics and theory of visual color matching can be found in the work of Cohen (2001), and a fascinating and unique mathematical treatment of colorimetry is found in Koenderink (2010). Lastly, a look at the more physical aspects of color and materials is provided by Tilley (2011).

### 3.1 BASIC AND ADVANCED COLORIMETRY

Colorimetry is defined simply as the measurement of color. Wyszecki (1973) described an important distinction between basic and advanced colorimetry (see also Wyszecki (1986)). This distinction is the basis of this book and continues to warrant serious attention. It is perhaps most enlightening to quote Wyszecki's exact words in making the distinction. Wyszecki's (1973: 21) description of basic colorimetry is as follows.

*Colorimetry, in its strict sense, is a tool used to making a prediction on whether two lights (visual stimuli) of different spectral power distributions will match in colour for certain given conditions of observation. The prediction is made by determining the tristimulus values of the two visual stimuli. If the tristimulus values of a stimulus are identical to those of the other stimulus, a colour match will be observed by an average observer with normal color vision.*

Wyszecki (1973: 21) went on to describe the realm of advanced colorimetry.

*Colorimetry in its broader sense includes methods of assessing the appearance of colour stimuli presented to the observer in complicated surroundings as they may occur in everyday life. This is considered the ultimate goal of colorimetry, but because of its enormous complexity, this goal is far from being reached. On the other hand, certain more restricted aspects of the overall problem of predicting colour appearance of stimuli seem somewhat less elusive. The outstanding examples are the measurement of colour differences, whiteness, and chromatic adaptation. Though these problems are still essentially unresolved, the developments in these areas are of considerable interest and practical importance.*

This chapter describes the well-established techniques of basic colorimetry that form the foundation for color appearance modeling. It also describes some of the widely used methods for color difference measurement, one of the first objectives of advanced colorimetry. Wyszecki's distinction between basic and advanced colorimetry serves to highlight the purpose of this book, an account of the research and modeling aimed at the extension of basic colorimetry toward the ultimate goals of advanced colorimetry.

### 3.2 WHY IS COLOR?

To begin a discussion of the measurement of color, one must first consider the nature of color. Figure 3.1 illustrates the answer to the question – “Why is Color?” “Why” is a more appropriate question than the more typical “what” since color is not a simple thing that can be easily described to someone who has never experienced it. It is a process that exists in the environment and the mind of the observer rather than an object that can be



**Figure 3.1** The triangle of color. Color exists due to the interaction of light sources, objects, and the human visual system

defined independent from an observer. This question is also explored further at a children's science education website written by the author, [whyiscolor.org](http://whyiscolor.org). The word, color, cannot even be defined without resort to examples (Chapter 4). Color is an attribute of visual sensation, and the color appearance of objects depends on the three components making up the triangle denoted by red arrows in Figure 3.1. The first requirement is a source of visible electromagnetic energy necessary to initiate the sensory process of vision. This energy is then modulated by the physical and chemical properties of an object. The modulated energy is then imaged by the eye, detected by photoreceptors, and processed by the neural mechanisms of the human visual system to produce our perceptions of color. Note that the light source and visual system are also linked in Figure 3.1 to indicate the influence that the light source itself has on color appearance through chromatic adaptation, etc. The bidirectional arrow between the observer and objects is also deliberate to indicate that the observer's knowledge of the object and its environment can influence object appearance.

Since all three aspects of the triangle in Figure 3.1 are required to produce color, they must also be quantified in order to produce a reliable system of physical colorimetry. Light sources are quantified through their spectral power distribution and standardized as illuminants. Material objects are specified by the geometric and spectral distribution of the energy they reflect or transmit. The human visual system is quantified through its color

matching properties that represent the first stage response (photopigment absorption) in the system. Thus colorimetry, as a combination of all these areas, draws upon techniques and results from the fields of physics, chemistry, psychophysics, anatomy, physiology, and psychology.

### 3.3 LIGHT SOURCES AND ILLUMINANTS

The first component of the triangle of color in Figure 3.1 is the light source. Light sources provide the electromagnetic energy required to initiate visual responses. The specification of the color properties of light sources is performed in two ways for basic colorimetry: through measurement and through standardization. The distinction between these two techniques is clarified in the definition of light sources and illuminants. *Light sources* are actual physical emitters of visible energy. Incandescent lightbulbs, the sky at any given moment, and fluorescent tubes represent examples of light sources. *Illuminants*, on the other hand, are simply standardized tables of values that represent a spectral power distribution typical of some particular light source. CIE illuminants A, D65, and F2 are standardized representations of typical incandescent, daylight, and fluorescent sources. Some illuminants have corresponding sources that are physical embodiments of the standardized spectral power distributions. For example, CIE source A is a particular type of incandescent source that produces the relative spectral power distribution of CIE illuminant A. Other illuminants do not have corresponding sources. For example, CIE illuminant D65 is a statistical representation of an average daylight with a correlated color temperature (CCT) of approximately 6500 K, and thus there is no CIE source D65 capable of producing the illuminant D65 spectral power distribution. The importance of distinguishing between light sources and illuminants in color appearance specification is discussed in Chapter 7 (Table 7.1). Since there are likely to be significant differences between the spectral power distributions of a CIE illuminant and a light source designed to simulate it, the actual spectral power distribution of the light source must be used in colorimetric calculations of stimuli used in color appearance specification.

#### Spectroradiometry

The measurement of the spectral power distributions of light sources is the realm of spectroradiometry. *Spectroradiometry* is the measurement of radiometric quantities as a function of wavelength. In color measurement, the wavelength region of interest encompasses electromagnetic energy of wavelengths from approximately 400 (violet) to 700 nm (red). There are a variety of radiometric quantities that can be used to specify the properties of a light source. Of particular interest in color appearance measurement are irradiance and radiance. Both are measurements of the power of light sources with basic units of watts.

*Irradiance* is the radiant power per unit area incident onto a surface and has units of watts per square meter ( $\text{W}/\text{m}^2$ ). Spectral irradiance adds the wavelength dependency and has units of  $\text{W}/\text{m}^2\text{nm}$ , sometimes expressed as  $\text{W}/\text{m}^3$ . *Radiance* differs from irradiance in that it is a measure of the power emitted from a source (or surface), rather than incident upon a surface, per unit area per unit solid angle with units of watts per square meter per steradian ( $\text{W}/\text{m}^2\text{sr}$ ). Spectral radiance includes the wavelength dependency having units of  $\text{W}/\text{m}^2\text{sr nm}$  or  $\text{W}/\text{m}^3\text{sr}$ .

Radiance has the interesting properties that it is preserved through optical systems (neglecting absorption) and is independent of distance. Thus, the human visual system responds commensurably to radiance making it a key measurement in color appearance specification. The retina itself responds commensurably to the irradiance incident upon it, but in combination with the optics of the eyeball, retinal irradiance is proportional to the radiance of a surface. This can be demonstrated by viewing an illuminated surface from various distances and observing that the perceived brightness does not change (consistent with the radiance of the surface). The irradiance at the eye from a given surface falls off with the square of distance from the surface. Radiance does not fall off in this fashion since the decrease in power incident on the pupil is directly canceled by a proportional decrease in the solid angle subtended by the pupil with respect to the surface in question. The spectral radiance,  $L(\lambda)$ , of a surface with a spectral reflectance factor of  $R(\lambda)$  can be calculated from the spectral irradiance,  $E(\lambda)$ , falling upon the surface by using Equation 3.1 with the assumption that the surface is a Lambertian diffuser (i.e., equal radiance in all directions).

$$L(\lambda) = \frac{R(\lambda)E(\lambda)}{\pi} \quad (3.1)$$

A *spectral power distribution* (Figure 3.2) is simply a plot, or table, of a radiometric quantity as a function of wavelength. Since the overall power levels of light sources can vary over many orders of magnitude, spectral power distributions are often normalized to facilitate comparisons of color properties. The traditional approach is to normalize a spectral power distribution such that it has a value of 100 (or sometimes 1.0) at a wavelength of 560 nm (arbitrarily chosen as near the center of the visible spectrum). Such normalized spectral power distributions are referred to as *relative spectral power distributions* and are unitless.

## Black-Body Radiators

Another important radiometric quantity is the color temperature of a light source. A special type of theoretical light source, known as a *black-body radiator*, or *Planckian radiator*, emits energy due only to thermal excitation and is a perfect emitter of energy. The energy emitted by a black body increases in quantity and shifts toward shorter wavelengths as the

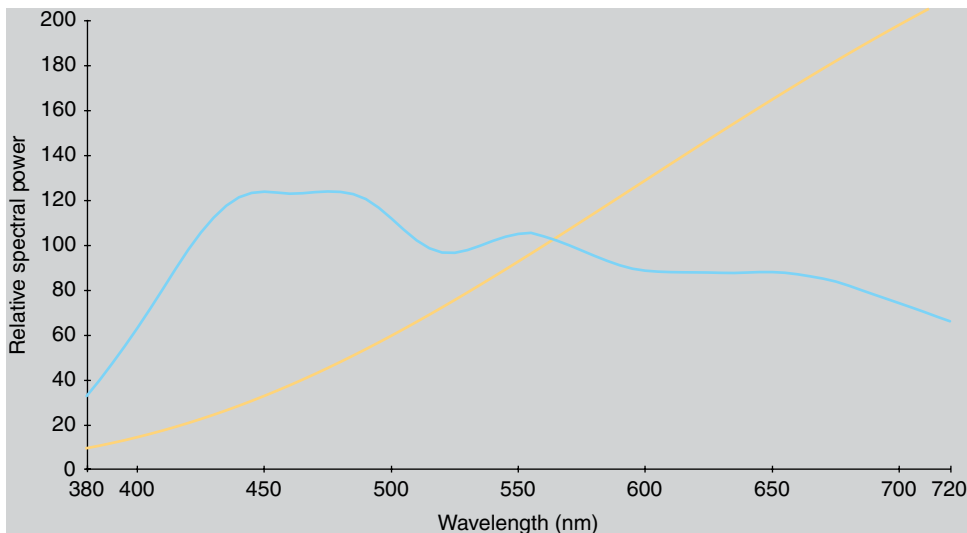


**Figure 3.2** Relative spectral power distributions of CIE illuminants A (yellow line) and C (blue line)

temperature of the black body increases. The spectral power distribution of a black-body radiator can be specified using Planck's equation as a function of a single variable, absolute temperature (in Kelvins). Thus, if the absolute temperature of a black body is known, so is its spectral power distribution. The temperature of a black body is referred to as its *color temperature* since it uniquely specifies the color (actually the spectral power distribution) of the source. Since black-body radiators seldom exist outside specialized laboratories, color temperature is not a generally useful quantity. A second quantity, *correlated color temperature*, is more generally useful. A light source need not be a black-body radiator in order to be assigned a CCT. The CCT of a light source is simply the color temperature of a black-body radiator that has most nearly the same color as the source in question. As examples, an incandescent source might have a CCT of 2800K, a typical fluorescent tube 4000K, an average daylight 6500K, and the white-point of a computer graphics display 9300K. As the CCT of a source increases, it becomes more blue, or less red.

## CIE Illuminants

The CIE has established a number of spectral power distributions as CIE illuminants for colorimetry. These include CIE illuminants A, C, D65, D50, F2, F8, and F11:

- CIE illuminant A represents a Planckian radiator with a color temperature of 2856K and is used for colorimetric calculations when incandescent illumination is of interest.

- CIE illuminant C is the spectral power distribution of illuminant A as modified by particular liquid filters defined by the CIE and represents a daylight simulator with a CCT of 6774 K.
- CIE illuminants D65 and D50 are part of the CIE D-series of illuminants that have been statistically defined based upon a large number of measurements of real daylight. Illuminant D65 represents an average daylight with a CCT of 6504 K and D50 represents an average daylight with a CCT of 5003 K. D65 is commonly used in colorimetric applications, while D50 is often used in graphic arts applications. CIE D illuminants with other CCTs can be easily obtained.
- CIE F illuminants (12 in all) represent typical spectral power distributions for various types of fluorescent sources. CIE illuminant F2 represents cool-white fluorescent with a CCT of 4230 K, F8 represents a fluorescent D50 simulator with a CCT of 5000 K, and F11 represents a triband fluorescent source with a CCT of 4000 K. Triband fluorescent sources are popular because of their efficiency, efficacy, and pleasing color-rendering properties.
- The equal-energy illuminant (sometimes called illuminant E) is often of mathematical utility. It is defined with a relative spectral power of 100.0 at all wavelengths.

Spectral power distributions for these illuminants can be found in various online sources and colorimetry textbooks. Colorimetric data, useful for color appearance computations, for these CIE illuminants is provided in Table 3.1. The relative spectral power distributions of these illuminants are plotted in Figure 3.2, Figure 3.3, and Figure 3.4.

While there are not yet CIE illuminants defined for solid state, or LED, lighting systems that are becoming readily available commercially, such lighting systems are quickly becoming important for colorimetry and color appearance. Figure 3.5 illustrates the spectral power distributions of a triband fluorescent lamp (similar CIE illuminant F11) and an LED lighting system that replaced it in the same fixture in early 2012. The LED illumination is a phosphor-type consisting of a blue (short wavelength) LED in combination with a yellow phosphor (excited by the LED) to produce white light. White LED illumination is also sometimes made with a combination of red, green, and blue LEDs.

**Table 3.1** Colorimetric data for some example CIE illuminants

Quantity	A	C	D65	D50	F2	F8	F11
X	109.85	98.07	95.05	96.42	99.20	96.43	100.96
Y	100.0	100.0	100.0	100.0	100.0	100.0	100.0
Z	35.58	118.23	108.88	82.49	67.40	82.46	64.37
x	0.4476	0.3101	0.3127	0.3457	0.3721	0.3458	0.3805
y	0.4074	0.3162	0.3290	0.3585	0.3751	0.3586	0.3769
CCT	2856 K	6800 K	6504 K	5003 K	4230 K	5000 K	4000 K

Colorimetric data are for the CIE 1931 standard colorimetric observer ( $2^\circ$ ).

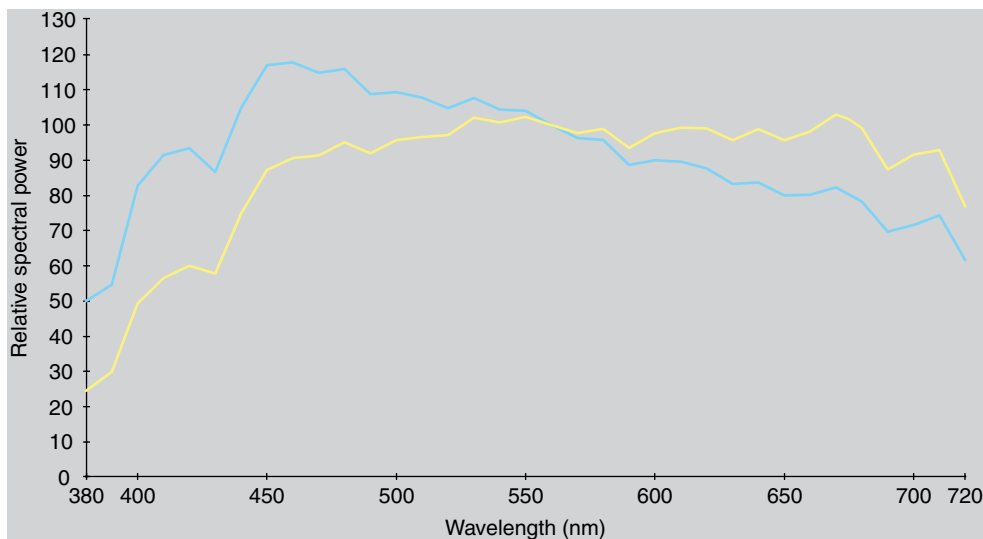


**Figure 3.3** Relative spectral power distributions of CIE illuminants D50 (yellow line) and D65 (blue line)

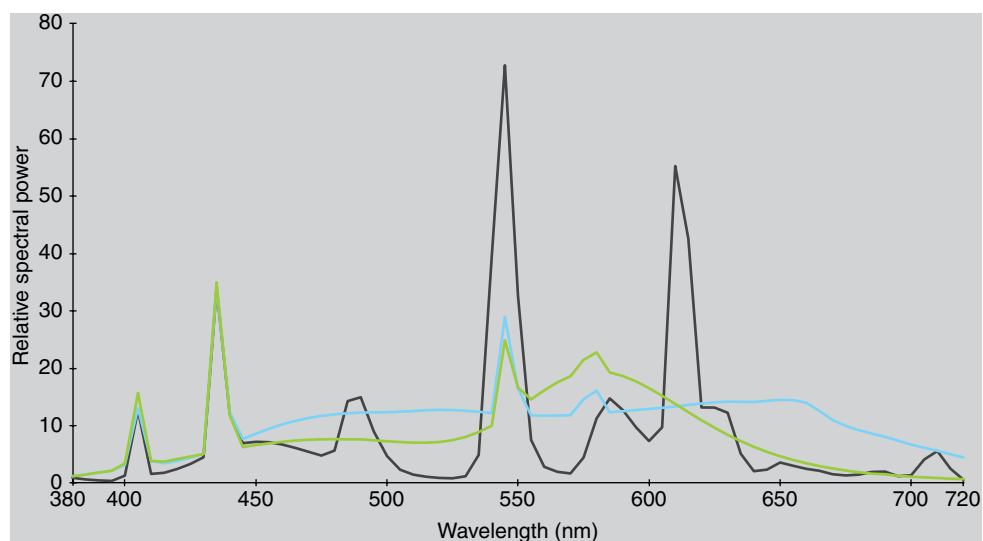


**Figure 3.4** Relative spectral power distributions of CIE illuminants F2 (green line), F8 (blue line), and F11 (black line)

### 3.4 COLORED MATERIALS

Once the light source or illuminant is specified, the next step in the colorimetry of material objects is the characterization of their interaction with visible radiant energy as illustrated in the second corner of the triangle in Figure 3.1. The interaction of radiant energy with materials obeys the law of conservation

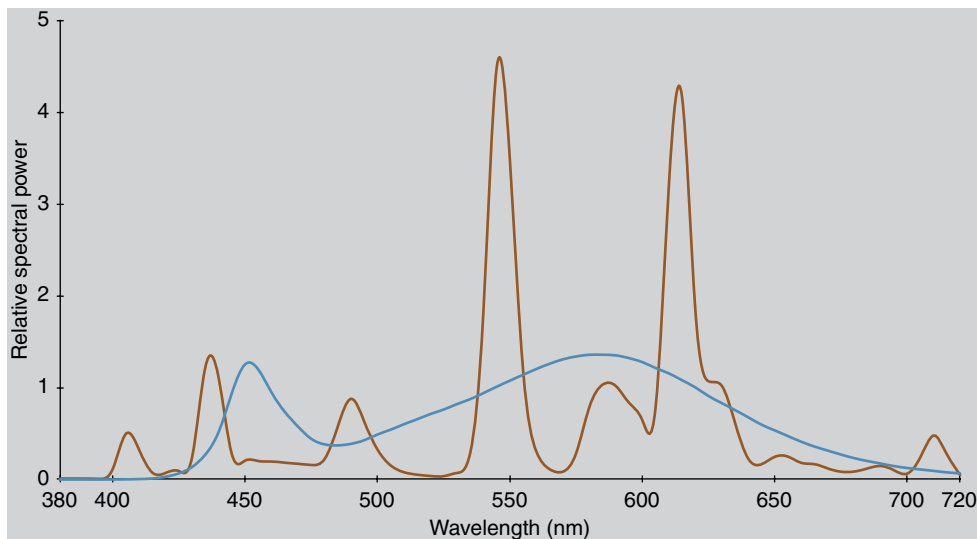


**Figure 3.5** Spectral power distributions for a new LED lighting system (blue line) and the triband fluorescent sources (brown line) replaced by it in a commercial setting in 2012

of energy. There are only three fates that can befall radiant energy incident on an object – absorption, reflection, and transmission. Thus the sum of the absorbed, reflected, and transmitted radiant power must sum to the incident radiant energy at each wavelength as illustrated in Equation 3.2 where  $\Phi(\lambda)$  is used as a generic term for incident radiant flux,  $R(\lambda)$  is the reflected flux,  $T(\lambda)$  is the transmitted flux, and  $A(\lambda)$  is the absorbed flux.

$$\Phi(\lambda) = R(\lambda) + T(\lambda) + A(\lambda) \quad (3.2)$$

Reflection, transmission, and absorption are the phenomena that take place when light interacts with matter, and reflectance, transmittance, and absorptance are the quantities measured to describe these phenomena. Since these quantities always must sum to the incident flux, they are typically measured in relative terms as percentages of the incident flux rather than as absolute radiometric quantities. Thus *reflectance* can be defined as the ratio of the reflected energy to the incident energy, *transmittance* as the ratio of transmitted energy to incident energy, and *absorptance* as the ratio of absorbed energy to incident energy. Note that all of these quantities are ratio measurements, the subject of *spectrophotometry*, which is defined as the measurement of ratios of radiometric quantities. Spectrophotometric quantities are expressed as either percentages (0–100%) or as factors (0.0–1.0). Figure 3.6 illustrates the spectral reflectance, transmittance, and absorptance of a red translucent object. Note that since the three quantities sum to 100%, it is typically unnecessary to measure all three. Generally either reflectance or transmittance is of particular interest in a given application.

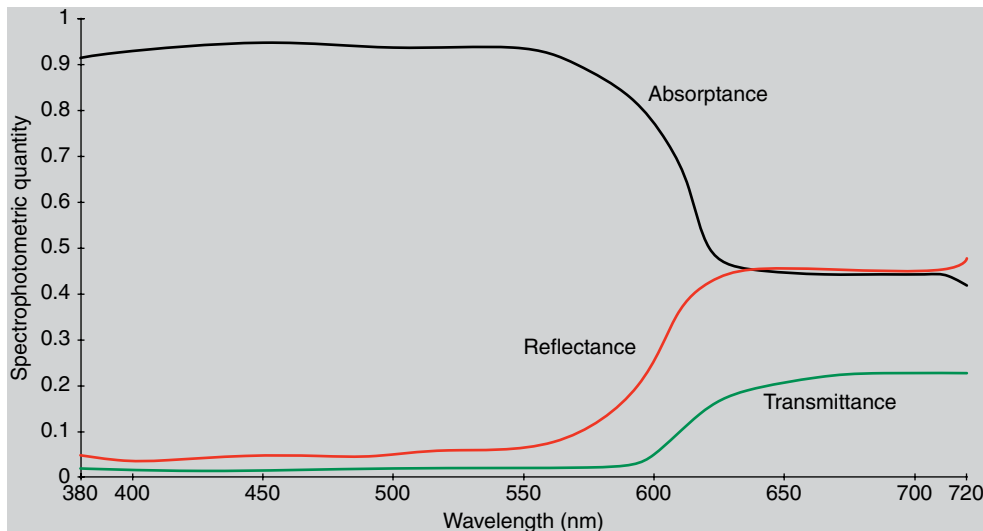


**Figure 3.6** Spectral absorptance, reflectance, and transmittance of a red translucent plastic material

Unfortunately (for colorimetrists), the interaction of radiant energy with objects is not just a simple spectral phenomenon. The reflectance or transmittance of an object is not just a function of wavelength but also a function of the illumination and viewing geometry. Such differences can be illustrated by the phenomenon of gloss. Imagine matte, semigloss, and glossy photographic paper or paint. The various gloss characteristics of these materials can be ascribed to the geometric distribution of the specular reflectance from the surface of the object. This is just one geometric appearance effect. Many others exist, such as interesting changes in the color of automotive finishes with illumination and viewing geometry (*e.g.*, metallic, pearlescent, and other “effect” coatings). To fully quantify such effects, complete bidirectional reflectance (or transmittance) distribution functions (BRDFs) must be obtained for each possible combination of illumination angle, viewing angle, and wavelength. Measurement of such functions is prohibitively difficult and expensive and produces massive quantities of data that are difficult to meaningfully utilize. To avoid this explosion of colorimetric data, a small number of standard illumination and viewing geometries have been established for colorimetry.

## CIE Illumination and Viewing Geometries

The CIE has historically defined four standard illumination and viewing geometries for spectrophotometric reflectance measurements. (More detailed designations and specifications are part of the recently published

CIE Publication 15.3 on Colorimetry (CIE 2004c.) These come as two pairs of optically reversible geometries:

1. Diffuse/normal ( $d/0$ ) and normal/diffuse ( $0/d$ )
2. 45/normal ( $45/0$ ) and normal/45 ( $0/45$ ).

The designations indicate first the illumination geometry and then the viewing geometry following the slash (/). Figure 3.7 illustrates the geometries as described below.

## Diffuse/Normal and Normal/Diffuse

In the diffuse/normal geometry, the sample is illuminated from all angles using an integrating sphere and viewed at an angle near the normal to the surface. In the normal/diffuse geometry, the sample is illuminated from an angle near to its normal, and the reflected energy is collected from all angles using an integrating sphere. These two geometries are optical reverses of one another and therefore produce the same measurement results (assuming all other instrumental variables are constant). The measurements made are of total reflectance. In many instruments, an area of the integrating sphere, corresponding to the angle of specular (regular)

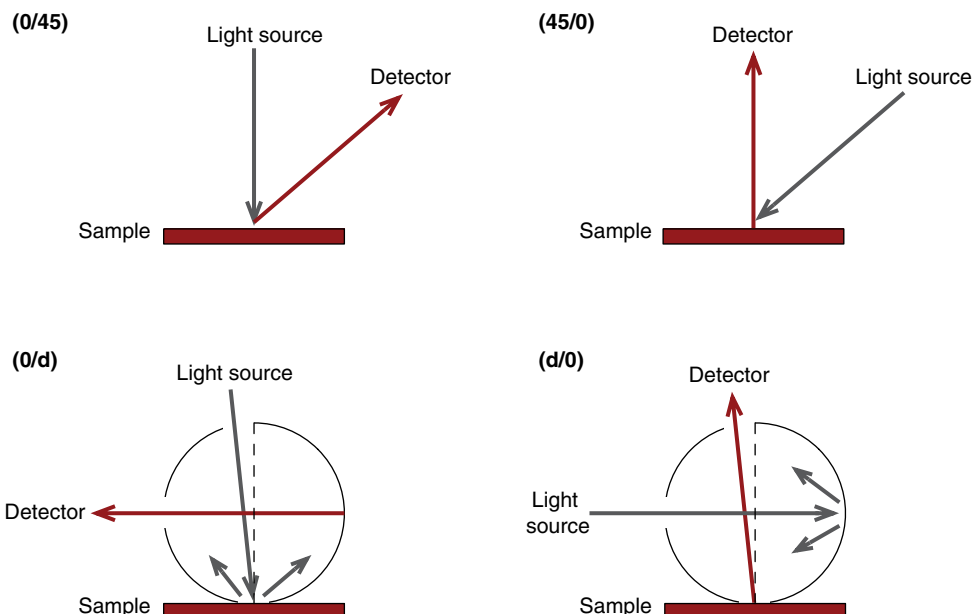


**Figure 3.7** Diagrams of the CIE illumination and detection geometries for spectrophotometry as described in the text

reflection of the illumination in a 0/d geometry or the angle from which specular reflection would be detected in a d/0 geometry, can be replaced with a black trap such that the specular component of reflection is excluded and only diffuse reflectance is measured. Such measurements are referred to as “specular component excluded” measurements as opposed to “specular component included” measurements made when the entire sphere is intact.

## 45/Normal and Normal/45

The second pair of geometries is the 45/normal (45/0) and normal/45 (0/45) measurement configurations. In a 45/0 geometry, the sample is illuminated with one or more beams of light incident at an angle of 45° from the normal and measurements are made along the normal. In the 0/45 geometry, the sample is illuminated normal to its surface and measurements are made using one or more beams at a 45° angle to the normal. Again, these two geometries are optical reverses of one another and produce identical results given equality of all other instrumental variables. Use of the 45/0 and 0/45 measurement geometries ensures that all components of gloss are excluded from the measurements. Thus these geometries are typically used in applications where it is necessary to compare the colors of materials having various levels of gloss (*e.g.*, graphic arts and photography). It is critical to note the instrumental geometry used whenever reporting colorimetric data for materials.

The definition of reflectance as the ratio of reflected energy to incident energy is perfectly appropriate for measurements of total reflectance (d/0 or 0/d). However, for bidirectional reflectance measurements (45/0 and 0/45), the ratio of reflected energy to incident energy is exceedingly small since only a small range of angles of the distribution of reflected energy is detected. Thus, to produce more practically useful values for any type of measurement geometry, reflectance factor measurements are made relative to a perfect reflecting diffuser (PRD). A *perfect reflecting diffuser* is a theoretical material that is both a perfect reflector (100% reflectance) and perfectly Lambertian (radiance equal in all directions). Thus, measurements of reflectance factor are defined as the ratio of the energy reflected by the sample to the energy that would be reflected by a PRD illuminated and viewed in the identical geometry. For the integrating sphere geometries, measuring total reflectance, this definition of reflectance factor is identical to the definition of reflectance. For the bidirectional geometries, measurement of reflectance factor relative to the PRD results in a zero-to-one scale similar to that obtained for total reflectance measurements. Since PRDs are not physically available, reference standards that are calibrated relative to the theoretical aim are provided by national standardizing laboratories (such as the National Institute of Standards and Technology (NIST), in the USA) and instrument manufacturers.

## Fluorescence

One last topic of importance in the colorimetric analysis of materials is fluorescence. Fluorescent materials absorb energy in a region of wavelengths and then emit this energy in a region of longer wavelengths. For example, a fluorescent orange material might absorb blue energy and emit it as orange energy. Fluorescent materials obey the law of conservation of energy as stated in Equation 3.2. However, their behavior is different in that some of the absorbed energy is emitted at (normally) longer wavelengths. A full treatment of the color measurement of fluorescent materials is complex and beyond the scope of this book. In general, a fluorescent material is characterized by its total radiance factor, which is the sum of the reflected and emitted energy at each wavelength relative to the energy that would be reflected by a PRD. This definition allows total radiance factors greater than 1.0, which is often the case. It is important to note that the total radiance factor will depend on the light source used in the measuring instrument since the amount of emitted energy is directly proportional to the amount of absorbed energy in the excitation wavelengths. Spectrophotometric measurements of reflectance or transmittance of nonfluorescent materials are insensitive to the light source in the instrument since its characteristics are normalized in the ratio calculations. This important difference highlights the major difficulty in measuring fluorescent materials. Unfortunately, many man-made materials (such as paper and inks) are fluorescent and thus significantly more difficult to measure accurately.

## 3.5 THE HUMAN VISUAL RESPONSE

Measurement or standardization of light sources and materials provides the necessary physical information for colorimetry. What remains to be defined is a quantitative technique to predict the response of the human visual system as illustrated by the third corner of the triangle in Figure 3.1. Following Wyszecki's (1973) definition of basic colorimetry, quantification of the human visual response focuses on the earliest level of vision, absorption of energy in the cone photoreceptors, through the psychophysics of color matching. The ability to predict when two stimuli match for an average observer, the basis of colorimetry, provides great utility in a variety of applications. While such a system does not specify color appearance, it provides the basis of color appearance specification and allows the prediction of matches for various applications and the tools required to set up tolerances on matches necessary for industry. The properties of human color matching are defined by the spectral responsivities of the three cone types. This is because, once the energy is absorbed by the three cone types, the spectral origin of the signals is lost, and if the signals from the three cone types are equal for two stimuli, they must match in color when seen in the same conditions since there is no further information introduced within the visual system to distinguish them.

Thus, if the spectral responsivities of the three cone types are known, two stimuli, denoted by their spectral power distributions  $\Phi_1(\lambda)$  and  $\Phi_2(\lambda)$ , will match in color if the product of their spectral power distributions and each of the three cone responsivities,  $L(\lambda)$ ,  $M(\lambda)$ , and  $S(\lambda)$ , integrated over wavelength are equal. This equality for a visual match is illustrated in Equations 3.3 through 3.5. Two stimuli match if all three of the equalities in Equations 3.3 through 3.5 hold true.

$$\int_{\lambda} \Phi_1(\lambda)L(\lambda)d\lambda = \int_{\lambda} \Phi_2(\lambda)L(\lambda)d\lambda \quad (3.3)$$

$$\int_{\lambda} \Phi_1(\lambda)M(\lambda)d\lambda = \int_{\lambda} \Phi_2(\lambda)M(\lambda)d\lambda \quad (3.4)$$

$$\int_{\lambda} \Phi_1(\lambda)S(\lambda)d\lambda = \int_{\lambda} \Phi_2(\lambda)S(\lambda)d\lambda \quad (3.5)$$

Equations 3.3 through 3.5 illustrate the definition of metamerism. Since only the three integrals need be equal for a color match, it is not necessary for the spectral power distributions of the two stimuli to be equal for every wavelength. The cone spectral responsivities are quite well known today as described in Chapter 1. With such knowledge, a system of basic colorimetry becomes nearly as simple to define as Equations 3.3 through 3.5. However, reasonable accurate knowledge of the cone spectral responsivities is a rather recent scientific development. The need for colorimetry predates this knowledge by several decades. Thus the CIE, in establishing the 1931 system of colorimetry, needed to take a less direct approach.

## The System of Photometry

To illustrate the indirect nature of the CIE system of colorimetry, it is useful to first explore the system of photometry, which was established in 1924. The aim for a system of photometry was the development of a spectral weighting function that could be used to describe the perception of brightness matches. (More correctly, the system describes the results of flicker photometry experiments rather than heterochromatic brightness matches as described further in Chapter 6. The historical data for, and inter-observer variability of, photometric visual experiments was thoroughly described by Gibson and Tyndall (1923).) In 1924, the CIE spectral luminous efficiency function,  $V(\lambda)$ , was established for photopic vision. This function, plotted in Figure 3.8, indicates that the visual system is more sensitive (with respect to the perception of brightness) to wavelengths in the middle of the spectrum and becomes less and less sensitive to wavelengths near the extremes of the visual spectrum. The  $V(\lambda)$  function is used as a spectral weighting function to convert radiometric quantities into photometric quantities via spectral integration as shown in Equation 3.6.

$$\Phi_V = \int_{\lambda} \Phi(\lambda)V(\lambda)d\lambda \quad (3.6)$$

The term  $\Phi_v$  in Equation 3.6 refers to the appropriate photometric quantity defined by the radiometric quantity,  $\Phi(\lambda)$ , used in the calculation. For example, the radiometric quantities of irradiance, radiance, and reflectance factor are used to derive the photometric quantities of illuminance (lumens/m<sup>2</sup> or lux), luminance (cd/m<sup>2</sup>), or luminance factor (unitless). All of the optical properties and relationships for irradiance and radiance are preserved for illuminance and luminance. To convert irradiance or radiance to illuminance or luminance, a normalization constant of 683 lumens/watt is required to preserve the appropriate units. For the calculation of luminance factor, a different type of normalization, described in section 3.6, is required.

The  $V(\lambda)$  function is clearly not one of the cone responsivities. In fact, according to the opponent theory of color vision, such a result would not be expected. Instead, as suggested by the opponent theory of color vision, the  $V(\lambda)$  function corresponds to a weighted sum of the three cone responsivity functions. When the cone functions are weighted roughly according to their relative population in the retina and summed, the overall responsivity matches the CIE 1924  $V(\lambda)$  function. Thus the photopic luminous response represents a combination of cone signals. This sort of combination is present in the entire system of colorimetry. The use of a spectral weighting function to predict luminance matches is the first step toward a system of colorimetry.

There is also a luminous efficiency function for scotopic vision (rods) known as the  $V'(\lambda)$  function. This function, used for photometry at very low luminance levels, is plotted in Figure 3.8 along with the  $V(\lambda)$  function. Since there is only one type of rod photoreceptor, the  $V'(\lambda)$  function corresponds exactly to the spectral responsivity of the rods after transmission through the ocular media. Figure 3.8 illustrates the shift in peak spectral sensitivity toward shorter wavelengths during the transition from photopic to scotopic vision. This shift, known as the *Purkinje shift*, explains why blue objects tend to look lighter than red objects at very low luminance levels. The  $V'(\lambda)$  function is used in a way similar to the  $V(\lambda)$  function.

It has long been recognized in vision research that the  $V(\lambda)$  function might underpredict observed responsivity in the short-wavelength region of the spectrum. To address this issue and standard practice in the vision community, an additional function, the CIE 1988 spectral luminous efficiency function,  $V_m(\lambda)$ , was established (CIE 1990) along with other similar functions that have been described in the literature. This work has culminated with a CIE recommendation for a supplemental system of photometry (CIE, 2011a).

### 3.6 TRISTIMULUS VALUES AND COLOR MATCHING FUNCTIONS

Following the establishment of the CIE 1924 luminous efficiency function,  $V(\lambda)$ , attention was turned to development of a system of colorimetry that could be used to specify when two metamerically stimuli match in color for an average observer. Since the cone responsivities were unavailable at that time, a system of colorimetry was constructed based on the principles of

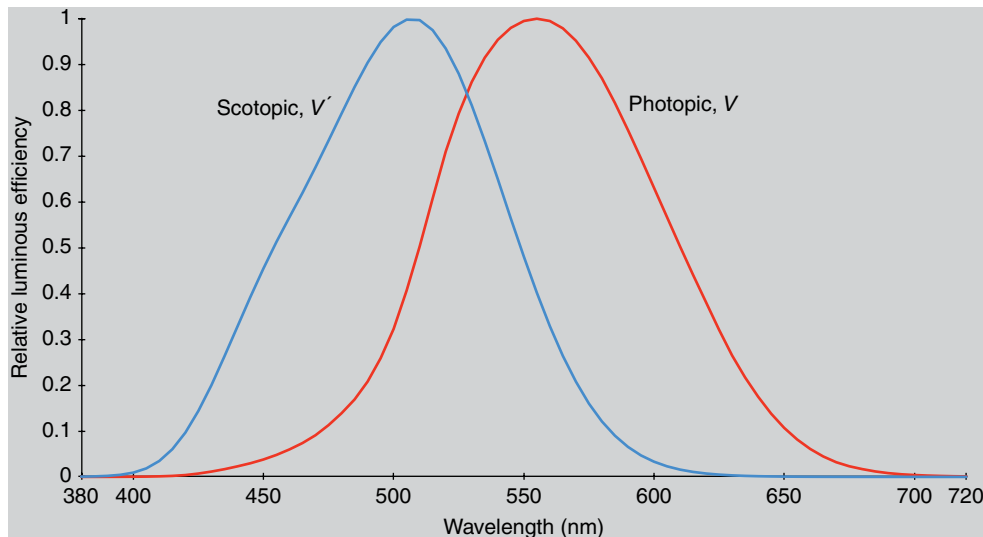


**Figure 3.8** CIE scotopic,  $V'(\lambda)$ , and photopic,  $V(\lambda)$ , luminous efficiency functions

trichromacy and Grassmann's laws of additive color mixture. The concept of this system is that color matches can be specified in terms of the amounts of three additive primaries required to visually match a stimulus. This is illustrated in the equivalence statement of Equation 3.7.

$$C \equiv R(\mathcal{R}) + G(\mathcal{G}) + B(\mathcal{B}) \quad (3.7)$$

The way Equation 3.7 reads is that a color  $C$  is matched by  $R$  units of the  $\mathcal{R}$  primary,  $G$  units of the  $\mathcal{G}$  primary, and  $B$  units of the  $\mathcal{B}$  primary. The script terms,  $\mathcal{RGB}$ , define the particular set of primaries and indicate that for different primary sets, different amounts of the primaries will be required to make a match. The terms,  $RGB$ , indicate the amounts of the primaries required to match the color and are known as tristimulus values. Since any color can be matched by certain amounts of three primaries, those amounts (tristimulus values), along with a definition of the primary set, allow the specification of a color. If two stimuli can be matched using the same amounts of the primaries (*i.e.*, they have equal tristimulus values), then they will also match each other when viewed in the same conditions.

### Tristimulus Values for Any Stimulus

The next step in the derivation of colorimetry is the extension of tristimulus values such that they can be obtained for any given stimulus, defined by a spectral power distribution. To accomplish this, two steps are required. The

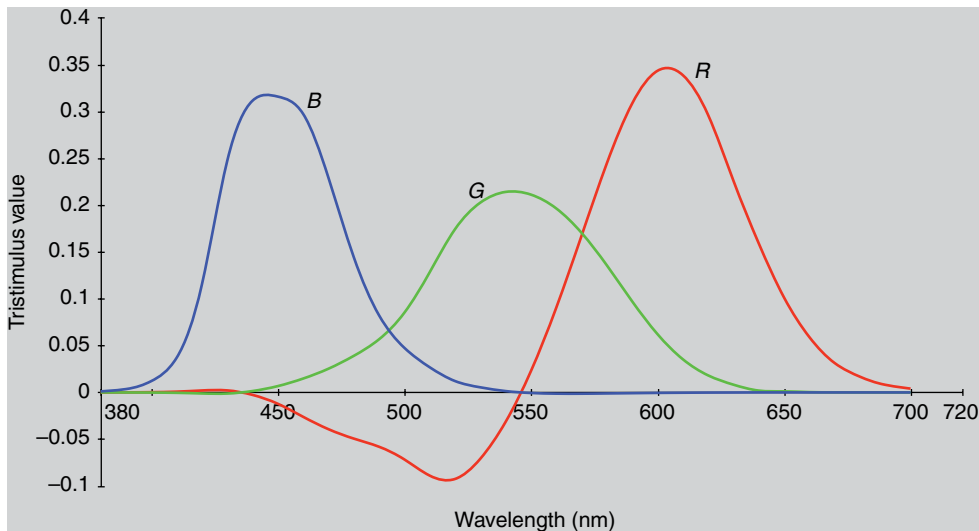


**Figure 3.9** Spectral tristimulus values for the CIE RGB system of colorimetry with monochromatic primaries at 435.8, 546.1, and 700.0nm

first is to obtain tristimulus values for matches to spectral colors. The second is to take advantage of Grassmann's laws of additivity and proportionality to sum tristimulus values for each spectral component of a stimulus spectral power distribution in order to obtain the integrated tristimulus values for the stimulus. Conceptually, the tristimulus values of the spectrum (*i.e.*, spectral tristimulus values) are obtained by matching a unit amount of power at each wavelength with an additive mixture of three primaries. Figure 3.9 illustrates a set of spectral tristimulus values for monochromatic primaries at 435.6 (**B**), 546.1 (**G**), and 700.0nm (**R**). Spectral tristimulus values for the complete spectrum are also known as *color matching functions*, or sometimes *color mixture functions*. Note that some of the spectral tristimulus values plotted in Figure 3.9 are negative. This implies the addition of a negative amount of power into the match. For example, a negative amount of the **R** primary is required to match a monochromatic 500nm stimulus. This is because that wavelength is too saturated to be matched by the particular primaries (*i.e.*, it is out of gamut). Clearly, a negative amount of light cannot be added to a match. Negative tristimulus values are obtained by adding the primary to the monochromatic light to desaturate it and bring it within the gamut of the primaries. Thus, a 500nm stimulus mixed with a given amount of the **R** primary is matched by an additive mixture of appropriate amounts of the **G** and **B** primaries.

The color matching functions illustrated in Figure 3.9 indicate the amounts of the primaries required to match unit amounts of power at each wavelength. By considering any given stimulus spectral power as an additive

mixture of various amounts of monochromatic stimuli, the tristimulus values for a stimulus can be obtained by multiplying the color matching functions by the amount of energy in the stimulus at each wavelength (Grassmann's proportionality) and integrating across the spectrum (Grassmann's additivity). Thus, the generalized equations for calculating the tristimulus values of a stimulus with spectral power distribution,  $\Phi(\lambda)$ , are given by Equations 3.8 through 3.10 where  $\bar{r}(\lambda)$ ,  $\bar{g}(\lambda)$ , and  $\bar{b}(\lambda)$  are the color matching functions.

$$R = \int_{\lambda} \Phi(\lambda) \bar{r}(\lambda) d\lambda \quad (3.8)$$

$$G = \int_{\lambda} \Phi(\lambda) \bar{g}(\lambda) d\lambda \quad (3.9)$$

$$B = \int_{\lambda} \Phi(\lambda) \bar{b}(\lambda) d\lambda \quad (3.10)$$

With the utility of tristimulus values and color matching functions established, it remains to derive a set of color matching functions that are representative of the population of observers with normal color vision. Color matching functions for individual observers, all with normal color vision, can be significantly different due to variations in lens transmittance; macula transmittance; and cone density, population, and spectral responsivities. Thus to establish a standardized system of colorimetry it is necessary to obtain a reliable estimate of the average color matching functions of the population of observers with normal color vision.

## Estimating Average Color Matching Functions

In the late 1920s, two sets of experiments were completed to estimate average color matching functions. These experiments were completed by Wright (1928–1929) using monochromatic primaries and by Guild (1931) using broadband primaries. Since the primaries from one experiment can be specified in terms of tristimulus values to match them using the other system, it is possible to derive a linear transform ( $3 \times 3$  matrix transformation) to convert tristimulus values from one set of primaries to another. This transformation also applies to the color matching functions since they are themselves tristimulus values. Thus, a transformation was derived to place the data from Wright's and Guild's experiments into a common set of primaries. When this was done, the agreement between the two experiments was extremely good, verifying the underlying theoretical assumptions in the derivation and use of color matching functions. Given this agreement, the CIE decided to establish a standard set of color matching functions based on the mean results of the Wright and Guild experiments. These mean functions were transformed to **RGB** primaries of 700.0, 546.1, and 435.8 nm, respectively, and are illustrated in Figure 3.9.

In addition, the CIE decided to transform to yet another set of primaries, the  $\text{XYZ}$  primaries. The main objectives in performing this transformation were to eliminate the negative values in the color matching functions and to force one of the color matching functions to equal the CIE 1924 photopic luminous efficiency function,  $V(\lambda)$ . The negative values were removed by selecting primaries that could be used to match all physically realizable color stimuli. This can only be accomplished with imaginary primaries that are more saturated than monochromatic lights. This is a straightforward mathematical construct and it should be noted that, although the primaries are imaginary, the color matching functions derived for those primaries are based on very real color matching results and the validity of Grassmann's laws. Forcing one of the color matching functions to equal the  $V(\lambda)$  function serves the purpose of incorporating the CIE system of photometry (established in 1924) into the CIE system of colorimetry (established in 1931). This is accomplished by choosing two of the imaginary primaries,  $X$  and  $Z$ , such that they produce no luminance response, leaving all of the luminance response in the third primary,  $Y$ . The color matching functions for the  $\text{XYZ}$  primaries,  $\bar{x}(\lambda)$ ,  $\bar{y}(\lambda)$ , and  $\bar{z}(\lambda)$ , respectively, known as the color matching functions of the CIE 1931 standard colorimetric observer, are plotted in Figure 3.10 for the practical wavelength range of 360–760 nm in 5-nm increments. (The CIE defines color matching functions from 360–830 nm in 1-nm increments and with more digits after the decimal point.)

$XYZ$  tristimulus values for colored stimuli are calculated in the same fashion as the  $RGB$  tristimulus values described above. The general

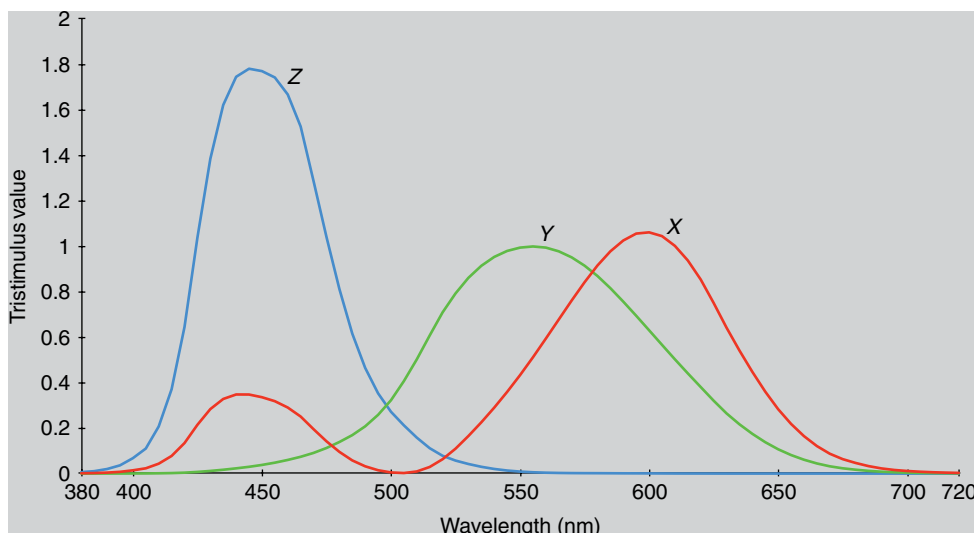


**Figure 3.10** Spectral tristimulus values of the CIE 1931 standard colorimetric observer

equations are given in Equations 3.11 through 3.13 where  $\Phi(\lambda)$  is the spectral power distribution of the stimulus,  $\bar{x}(\lambda)$ ,  $\bar{y}(\lambda)$ , and  $\bar{z}(\lambda)$  are the color matching functions, and  $k$  is a normalizing constant.

$$X = k \int_{\lambda} \Phi(\lambda) \bar{x}(\lambda) d\lambda \quad (3.11)$$

$$Y = k \int_{\lambda} \Phi(\lambda) \bar{y}(\lambda) d\lambda \quad (3.12)$$

$$Z = k \int_{\lambda} \Phi(\lambda) \bar{z}(\lambda) d\lambda \quad (3.13)$$

The spectral power distribution of the stimulus is defined in different ways for various types of stimuli. For self-luminous stimuli (e.g., light sources and CRT displays),  $\Phi(\lambda)$  is typically spectral radiance or a relative spectral power distribution. For reflective materials,  $\Phi(\lambda)$  is defined as the product of the spectral reflectance factor of the material,  $R(\lambda)$ , and the relative spectral power distribution of the light source or illuminant of interest,  $S(\lambda)$ , that is,  $R(\lambda)S(\lambda)$ . For transmitting materials,  $\Phi(\lambda)$  is defined as the product of the spectral transmittance of the material,  $T(\lambda)$ , and the relative spectral power distribution of the light source or illuminant of interest,  $S(\lambda)$ , that is  $T(\lambda)S(\lambda)$ .

The normalization constant,  $k$ , in Equations 3.11 through 3.13, is defined differently for relative and absolute colorimetry. In absolute colorimetry,  $k$  is set equal to 683 lumens/watt making the system of colorimetry compatible with the system of photometry. For relative colorimetry,  $k$  is defined by Equation 3.14.

$$k = \frac{100}{\int_{\lambda} S(\lambda) \bar{y}(\lambda) d\lambda} \quad (3.14)$$

The normalization for relative colorimetry in Equation 3.14 results in tristimulus values that are scaled from 0 to approximately 100 for various materials. It is useful to note that if relative colorimetry is used to calculate the tristimulus values of a light source, the  $Y$  tristimulus value is always equal to 100.

There is another, completely inappropriate, use of the term *relative colorimetry* in the graphic arts and other color reproduction industries. In some cases, tristimulus values are normalized to the paper white rather than a PRD. This results in a  $Y$  tristimulus value for the paper of 100 rather than its more typical value of about 85. The advantage of this is that it allows transformation between different paper types, preserving the paper white as the lightest color in an image, without having to keep track of the paper color. Such a practice might be useful, but it is actually a gamut mapping issue rather than a color measurement issue. A more appropriate terminology for this practice might be *normalized colorimetry* to avoid confusion with the long-established practice of relative colorimetry. It is also worth

noting that the practice of normalized colorimetry is not always consistent. In some cases, reflectance measurements are made relative to the paper white. This ensures that the  $Y$  tristimulus value is normalized between 0 for a perfect black and 1.0 (or 100.0) for the paper white, however, the  $X$  and  $Z$  tristimulus values might still range above 1.0 (or 100.0) depending on the particular illuminant used in the colorimetric calculations. Another approach is to normalize the tristimulus values for each stimulus color,  $XYZ$ , by the tristimulus values of the paper,  $X_p Y_p Z_p$ , individually ( $X/X_p$ ,  $Y/Y_p$ , and  $Z/Z_p$ ). This is analogous to the white-point normalization in CIELAB and is often used to adjust for white point changes and limited dynamic range in imaging systems. It is important to know which type of normalized colorimetry one is dealing with in various applications.

The relationship between CIE  $XYZ$  tristimulus values and cone responses (sometimes referred to as *fundamental tristimulus values*) is of great importance and interest in color appearance modeling. Like the  $V(\lambda)$  function, the CIE  $XYZ$  color matching functions each represent a linear combination of cone responsivities. Thus the relationship between the two is defined by a  $3 \times 3$  linear matrix transformation as described more fully in Chapter 9 (Figure 9.1). Cone spectral responsivities can be thought of as the color matching functions for a set of primaries that are constructed such that each primary stimulates only one cone type. It is possible to produce a real primary that stimulates only the S cones. However, no real primaries can be produced that stimulate only the M or L cones since their spectral responsivities overlap across the visible spectrum. Thus, the required primaries are also imaginary and produce all-positive color matching functions but do not incorporate the  $V(\lambda)$  function as a color matching function (since that requires a primary that stimulates all three cone types). The historical development of and recent progress in the development of colorimetric systems based on physiological cone responsivities has been reviewed by Boynton (1996) and new systems of colorimetry published by the CIE (2006).

## Two Sets of Color Matching Functions

It is important to be aware that there are two sets of color matching functions that have been established by the CIE. The CIE 1931 standard colorimetric observer was determined from experiments using a visual field that subtended  $2^\circ$ . Thus the matching stimuli were imaged onto the retina completely within the fovea. These color matching functions are used, almost exclusively, in color appearance modeling. Often they are referred to as the  $2^\circ$  *color matching functions* or the  $2^\circ$  *observer*. It is of historical interest to note that the 1931 standard colorimetric observer is based on data collected from fewer than 20 observers. In the 1950s, experiments were completed (Stiles and Burch 1959) to collect  $2^\circ$  color matching functions for more observers using more precise and accurate instrumentation. The results showed slight systematic discrepancies, but not of sufficient magnitude to warrant a change in the standard colorimetric observer. At the same

time, experiments were completed (Stiles and Burch 1959) to collect color matching function data for large visual fields. This was prompted by discrepancies between colorimetric and visual determination of the whiteness of paper. These experiments were completed using a 10° visual field that excluded the central fovea. Thus the color matching functions include no influence of the macular absorption. The results for large fields were deemed significantly different from the 2° standard to warrant the establishment of the CIE 1964 supplementary standard colorimetric observer, sometimes called the 10° *observer*. The difference between the two standard observers is significant, so care should be taken to report which observer is used with any colorimetric data. The differences are computationally significant, but certainly within the variability of color matching functions found for either 2° or 10° visual fields. Thus the two standard colorimetric observers can be thought of as representing the color matching functions of two individuals. Predictions of observer variability, and other sets of color matching functions, are facilitated by the CIE (2006) model of computing color matching functions as a function of observer age and field size.

### 3.7 CHROMATICITY DIAGRAMS

The color of a stimulus can be specified by a triplet of tristimulus values. To provide a convenient two-dimensional representation of colors, chromaticity diagrams were developed. This is based on the color triangle that was developed and expanded upon by James Clerk Maxwell in the nineteenth century. Maxwell's diagram puts each of the three fundamental primaries (lights that stimulate only one cone type) at the corner of the triangle as illustrated by R, G, and B in Figure 3.11. The spectrum locus drawn in Figure 3.11 shows two things, the relation to modern chromaticity diagrams and the facts that the cone spectral responses overlap and the B response is 0 beyond about 570 nm. Carefully studying the relationships between Maxwell's triangle and the modern CIE *xy* and *u'v'* diagrams provides great insight into the workings of colorimetry. The transformation from tristimulus values to chromaticity coordinates is accomplished through a normalization that removes luminance information. This transformation is a one-point perspective projection of data points in the three-dimensional tristimulus space onto the unit plane of that space (with a center of projection at the origin) as defined by Equations 3.15 through 3.17.

$$x = \frac{X}{X + Y + Z} \quad (3.15)$$

$$y = \frac{Y}{X + Y + Z} \quad (3.16)$$

$$z = \frac{Z}{X + Y + Z} \quad (3.17)$$

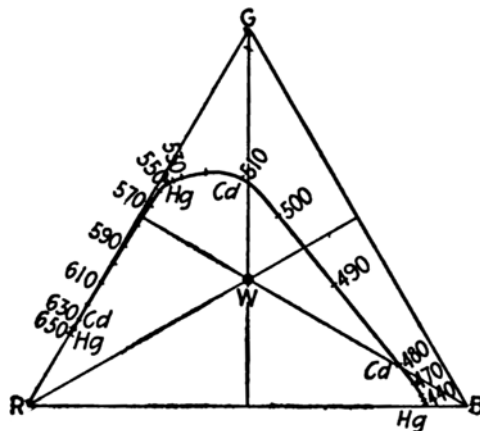


**Figure 3.11** Maxwell's triangle, an early form of a chromaticity diagram. R, G, and B represent primaries that uniquely stimulate a single cone type. A spectrum locus, illustrating properties of human color vision, and certain emission lines are drawn. A color is located on the diagram by the proportions of the three primaries required to match it. This diagram is adapted from Luckiesh (1915) that is in the public domain

Since there are only two dimensions of information in chromaticity coordinates, the third chromaticity coordinate can always be obtained from the other two by noting that the three always sum to unity. Thus  $z$  can be calculated from  $x$  and  $y$  using Equation 3.18.

$$z = 1.0 - x - y \quad (3.18)$$

Chromaticity coordinates should be used with great care since they attempt to represent a three-dimensional phenomenon with just two variables. To fully specify a colored stimulus, one of the tristimulus values must be reported in addition to two (or three) chromaticity coordinates. Usually the Y tristimulus value is reported since it represents the luminance information. The equations for obtaining the other two tristimulus values from chromaticity coordinates and the Y tristimulus value are often useful and therefore given in Equations 3.19 and 3.20.

$$X = \frac{xY}{y} \quad (3.19)$$

$$Z = \frac{(1.0 - x - y)Y}{y} \quad (3.20)$$

Chromaticity coordinates, alone, provide no information about the color appearance of stimuli since they include no luminance (or therefore lightness) information and do not account for chromatic adaptation. As an observer's state of adaptation changes, the color corresponding to a given

set of chromaticity coordinates can change in appearance dramatically (*e.g.*, a change from yellow to blue could occur with a change from daylight to incandescent-light adaptation).

Much effort has been expended in attempts to make chromaticity diagrams more perceptually uniform. While this is an intrinsically doomed effort (*i.e.*, an attempt to convert a nominal scale into an interval scale), it is worth mentioning one of the results, which is actually the chromaticity diagram currently recommended by the CIE for general use. It is the CIE 1976 Uniform Chromaticity Scales (UCS) diagram defined by Equations 3.21 and 3.22.

$$u' = \frac{4X}{X + 15Y + 3Z} \quad (3.21)$$

$$v' = \frac{9Y}{X + 15Y + 3Z} \quad (3.22)$$

The use of chromaticity diagrams should be avoided in most circumstances, particularly when the phenomena being investigated are highly dependent on the three-dimensional nature of color. For example, the display and comparison of the color gamuts of imaging devices in chromaticity diagrams is misleading to the point of being almost completely erroneous and should be performed in a three-dimensional color space such as CIELAB or CIECAM02. However, when chromaticity diagrams must be used (*e.g.*, for short-hand representations of additive display gamuts) then the  $u'v'$  diagram is strongly preferred and should be used in all cases rather than the  $xy$  diagram. That said, a chromaticity diagram such as CIE  $u' v'$  appears to be very useful for defining constant perceived saturation, which is equivalent to constant chromaticity. It might also be useful for predicting relative saturation, or scales of saturation perception.

### 3.8 CIE COLOR SPACES

The general use of chromaticity diagrams has been made largely obsolete by the advent of the CIE color spaces, CIELAB and CIELUV. These spaces extend tristimulus colorimetry to three-dimensional spaces with dimensions that approximately correlate with the perceived lightness, chroma, and hue of a stimulus. This is accomplished by incorporating features to account for chromatic adaptation and nonlinear visual responses. The main aim in the development of these spaces was to provide uniform practices for the measurement of color differences, something that cannot be done reliably in tristimulus or chromaticity spaces. In 1976, two spaces were recommended for use since there was no clear evidence to support one over the other at that time. The CIELAB and CIELUV color spaces are described in more detail in Chapter 10. Their equations are briefly summarized in this section. Wyszecki (1986) provides an overview of the development of the CIE color spaces.

## CIELAB

The CIE 1976 ( $L^*$   $a^*$   $b^*$ ) color space, abbreviated CIELAB, is defined by Equations 3.23 through 3.27 for tristimulus values normalized to the white that are greater than 0.008856.

$$L^* = 116 \left( \frac{Y}{Y_n} \right)^{1/3} - 16 \quad (3.23)$$

$$a^* = 500 \left[ \left( \frac{X}{X_n} \right)^{1/3} - \left( \frac{Y}{Y_n} \right)^{1/3} \right] \quad (3.24)$$

$$b^* = 200 \left[ \left( \frac{Y}{Y_n} \right)^{1/3} - \left( \frac{Z}{Z_n} \right)^{1/3} \right] \quad (3.25)$$

$$C_{ab}^* = \sqrt{a^{*2} + b^{*2}} \quad (3.26)$$

$$h_{ab} = \tan^{-1} \left( \frac{b^*}{a^*} \right) \quad (3.27)$$

In these equations  $X$ ,  $Y$ , and  $Z$  are the tristimulus values of the stimulus and  $X_n$ ,  $Y_n$ , and  $Z_n$  are the tristimulus values of the reference white.  $L^*$  represents lightness,  $a^*$  approximate redness-greenness,  $b^*$  approximate yellowness-blueness,  $C_{ab}^*$  chroma, and  $h_{ab}$  hue. The  $L^*$ ,  $a^*$ , and  $b^*$  coordinates are used to construct a Cartesian color space as illustrated in Figure 3.12. The  $L^*$ ,  $C_{ab}^*$ , and  $h_{ab}$  coordinates are the cylindrical representation of the same space. The CIELAB space, including the full set of equations for dark colors, is described in greater detail in Chapter 10.

## CIELUV

The CIE 1976 ( $L^*$   $u^*$   $v^*$ ) color space, abbreviated CIELUV, is defined by Equations 3.28 through 3.32. Equation 3.28 is also restricted to tristimulus values normalized to the white that are greater than 0.008856.

$$L^* = 116 \left( \frac{Y}{Y_n} \right)^{1/3} - 16 \quad (3.28)$$

$$u^* = 13L^* (u' - u'_{n}) \quad (3.29)$$

$$v^* = 13L^* (v' - v'_{n}) \quad (3.30)$$

$$C_{uv}^* = \sqrt{u^{*2} + v^{*2}} \quad (3.31)$$

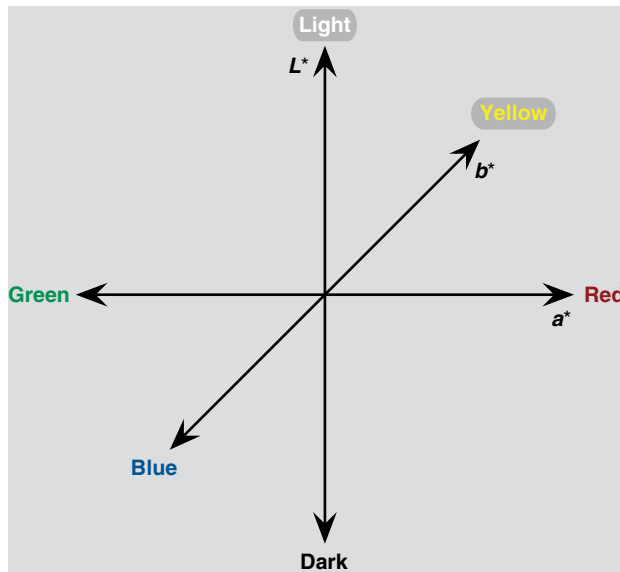


**Figure 3.12** Three-dimensional representation of the CIELAB  $L^*$ ,  $a^*$ , and  $b^*$  coordinates

$$h_{uv} = \tan^{-1} \left( \frac{v^*}{u^*} \right) \quad (3.32)$$

In these equations  $u'$  and  $v'$  are the chromaticity coordinates of the stimulus and  $u'_{nw}$  and  $v'_{nw}$  are the chromaticity coordinates of the reference white.  $L^*$  represents lightness,  $u^*$  redness–greenness,  $v^*$  yellowness–blueness,  $C_{nw}^*$  chroma, and  $h_{uw}$  hue. As in CIELAB, the  $L^*$ ,  $u^*$ , and  $v^*$  coordinates are used to construct a Cartesian color space and the  $L^*$ ,  $C_{nw}^*$ , and  $h_{uw}$  coordinates are the cylindrical representation of the same space.

The CIELAB and CIELUV spaces were both recommended as interim solutions to the problem of color difference specification of reflecting samples in 1976. Since that time, CIELAB has become almost universally used for color specification and particularly color difference measurement. At this time there appears to be no reason to use CIELUV over CIELAB.

### 3.9 COLOR DIFFERENCE SPECIFICATION

Color differences are measured in the CIELAB space as the Euclidean distance between the coordinates for the two stimuli. This is expressed in terms of a CIELAB  $\Delta E_{ab}^*$ , which can be calculated using Equation 3.33. It can also be expressed in terms of lightness, chroma, and hue differences as illustrated in Equation 3.34 by using the combination of Equations 3.33 and 3.35.

$$\Delta E_{ab}^* = (\Delta L^{*2} + \Delta a^{*2} + \Delta b^{*2})^{1/2} \quad (3.33)$$

$$\Delta E_{ab}^* = (\Delta L^{*2} + \Delta C_{ab}^{*2} + \Delta H_{ab}^{*2})^{1/2} \quad (3.34)$$

$$\Delta H_{ab}^* = (\Delta E_{ab}^{*2} - \Delta L^{*2} - \Delta C_{ab}^{*2})^{1/2} \quad (3.35)$$

While the CIELAB color space was designed with the goal of having color differences perceptually uniform throughout the space (*i.e.*, a  $\Delta E_{ab}^*$  of 1.0 for a pair of red stimuli is perceived to be equal in magnitude to a  $\Delta E_{ab}^*$  of 1.0 for a pair of gray stimuli), this goal was not strictly achieved.

To improve the uniformity of color difference measurements, modifications to the CIELAB  $\Delta E_{ab}^*$  equation have been made based upon various empirical data. One of the most widely used modifications is the CMC color difference equation (Clarke *et al.* 1984), which is based on a visual experiment on color difference perception in textiles. The CIE (1995b) has recently evaluated such equations, and the available visual data, recommending a new color difference equation for industrial use. This system for color difference measurement is called the CIE 1994 ( $\Delta L^*$   $\Delta C_{ab}^*$   $\Delta H_{ab}^*$ ) color difference model with the symbol  $\Delta E_{94}^*$  and abbreviation CIE94. Use of the CIE94 equation is preferred over a simple CIELAB  $\Delta E_{ab}^*$ . CIE94 color differences are calculated using Equations 3.36 through 3.39.

$$\Delta E_{94}^* = \left[ \left( \frac{\Delta L^*}{k_L S_L} \right)^2 + \left( \frac{\Delta C_{ab}^*}{k_C S_C} \right)^2 + \left( \frac{\Delta H_{ab}^*}{k_H S_H} \right)^2 \right]^{1/2} \quad (3.36)$$

$$S_L = 1 \quad (3.37)$$

$$S_C = 1 + 0.045 C_{ab}^* \quad (3.38)$$

$$S_H = 1 + 0.015 C_{ab}^* \quad (3.39)$$

The parametric factors,  $k_L$ ,  $k_C$ , and  $k_H$  are used to adjust the relative weighting of the lightness, chroma, and hue components, respectively, of color difference for various viewing conditions and applications that depart from the CIE94 reference conditions. It is also worth noting that, when averaged across the color space, CIE94 color differences are significantly smaller in magnitude than CIELAB color differences for the same stimuli pairs. Thus, use of CIE94 color differences to report overall performance in applications such as the colorimetric characterization of imaging devices results in the appearance of significantly improved performance if the numbers are mistakenly considered equivalent to CIELAB color differences. The same is true for CMC color differences.

The CIE (1995b) established a set of reference conditions for use of the CIE94 color difference equations. These are:

- *Illumination:* CIE illuminant D65 Simulator
- *Illuminance:* 1000 lux
- *Observer:* normal color vision
- *Background:* uniform, achromatic,  $L^*=50$
- *Viewing mode:* object
- *Sample size:* greater than  $4^\circ$  visual angle
- *Sample separation:* direct edge contact
- *Sample color difference magnitude:* 0 to 5 CIELAB Units
- *Sample structure:* no visually apparent pattern or nonuniformity.

The tight specification of reference conditions for the CIE94 equations highlights the vast amount of research that remains to be performed in order to generate a universally useful process for color difference specification. These issues are some of the same problems that must be tackled in the development of color appearance models. It should also be noted that for sample sizes greater than  $4^\circ$ , use of the CIE 1964 supplementary standard colorimetric observer is recommended.

More recently, the CIE has established the CIE DE2000 color difference equation (CIE 2001, Johnson and Fairchild 2003b) that extends the concept of CIE94 with further complexity. While the DE2000 equation certainly performs better than CIE94 for some data sets, its added complexity is probably not justified for most practical applications. The DE2000 equations are briefly summarized and presented in an alternative, somewhat simplified, form along with a numerical example in Hunt and Pointer (2011). While the statistical validity of the DE2000 computations for most real-world applications is questionable, the equation is gaining in popularity and most certainly represents an improvement over the simple CIELAB color difference equation for almost any application. In most color appearance applications, one will encounter one of three types of color difference computation most often, CIELAB color difference, DE2000, or a computation of differences in the appearance space itself.

### 3.10 THE NEXT STEP

This chapter has reviewed the fundamentals of basic colorimetry (and begun to touch on advanced colorimetry) as illustrated conceptually in Figure 3.1. While these techniques are well established and have been successfully used for decades, much more information needs to be added to the triangle of color in Figure 3.1 in order to extend basic colorimetry toward the specification of the color appearance of stimuli under a wide variety of viewing conditions. Some of the additional information that must be considered includes:

chromatic adaptation,  
light adaptation,  
luminance level,

background color,  
surround color,  
observer metamerism,  
dimensionality of color experience,  
*etc.*

These issues are explored further along the road to the development and use of color appearance models presented in the remaining chapters of this book.

# 4

# Color Appearance Terminology

---

In any scientific field a large portion of the knowledge is contained in the definitions of terms used by its practitioners. Newcomers to a field often realize that they understand the fundamental scientific concepts, but must first learn the language in order to communicate accurately, precisely, and effectively in the new discipline. Nowhere is this more true, or more important, than in the study of color appearance. Hunt (1978) showed concern that color scientists and technologists might be taking an attitude like Humpty-Dumpty from *Alice in Wonderland* who is quoted as saying “When I use a word it means just what I choose it to mean – neither more nor less.” We all know what happened to Humpty-Dumpty. The careful definition of color appearance terms presented in this chapter is intended to put everyone on a level playing field and help ensure that the concepts, data, and models discussed in this book are presented and interpreted in a consistent manner. As can be seen throughout this book, consistent use of terminology has not been the historical norm and continues to be one of the challenges of color appearance research and application.

## 4.1 IMPORTANCE OF DEFINITIONS

Why should it be particularly difficult to agree upon consistent terminology in the field of color appearance? Perhaps the answer lies in the very nature of the subject. Almost everyone *knows* what color is. After all, they have had firsthand experience of it since shortly after birth. However, very few can precisely describe their color experiences or even precisely define color. This innate knowledge, along with the imprecise use of color terms (*e.g.*, warmer, cooler, brighter, cleaner, fresher, *etc.*), leads to a subject that everyone

knows about, but few can discuss precisely. Clearly, if color appearance is to be described in a systematic, mathematical way, definitions of the phenomena being described need to be precise and universally agreed upon.

Since color appearance modeling remains an area of active research, the required definitions have not been set in stone for decades. The definitions presented in this chapter have been culled from three sources. The first, and authoritative, source is the *International Lighting Vocabulary* published by the Commission Internationale de l'Éclairage (CIE 1987) and updated in 2011 as CIE standard S 017/E:2011 (CIE 2011b). The *International Lighting Vocabulary* includes the definitions of approximately one thousand terms and quantities related to light and color "to promote international standardization in the use of quantities, units, symbols, and terminology." The other two sources, articles by Hunt (1977, 1978), provide descriptions of some of the work that led to the last two revisions of the *International Lighting Vocabulary*. It should be noted that there is also a relevant ASTM standard on appearance terminology (ASTM 1995).

Keep in mind that the definitions given below are of perceptual terms. These terms define our perceptions of colored stimuli. These are not definitions of specific colorimetric quantities. In the construction and use of color appearance models, the objective is to develop and use physically measurable quantities that correlate with the perceptual attributes of color appearance defined below.

## 4.2 COLOR

The definition of the word *color* itself provides some interesting challenges and difficulties. While most of us know what color is, it is an interesting challenge to try to write a definition of the word that does not contain an example. As can be seen below even the brightest and most dedicated color scientists who set out to write the 1987 edition of *International Lighting Vocabulary* could not meet this challenge.

### *Color*

*Attribute of visual perception consisting of any combination of chromatic and achromatic content. This attribute can be described by chromatic color names, such as yellow, orange, brown, red, pink, green, blue, purple, etc., or by achromatic color names, such as white, gray, black, etc., and qualified by bright, dim, light, dark, etc., or by combinations of such names.*

The authors of this definition were also well aware that the perception of color was not a simple matter and added a note that captures the essence of why color appearance models are needed.

### *Note*

*Perceived color depends on the spectral distribution of the color stimulus; on the size, shape, structure, and surround of the stimulus area; on the state of*

*adaptation of the observer's visual system; and on the observer's experience of the prevailing and similar situations of observations.*

The above note opens the door for the vast array of physical, physiological, psychological, and cognitive variables that influence color appearance – many of which are discussed in this book.

Since the very definition of color is so critical to this book, the 2011 *International Lighting Vocabulary* definition is included below for comparison.

**Colour (perceived)**

*Characteristic of a visual perception that can be described by attributes of hue, brightness (or lightness), and colorfulness (or saturation or chroma).*

**Note 1**

*When necessary, to avoid confusion between other meanings of the word, the term "perceived colour" may be used.*

**Note 2**

*Perceived colour depends on the spectral distribution of the color stimulus; on the size, shape, structure, and surround of the stimulus area; on the state of adaptation of the observer's visual system; and on the observer's experience of the prevailing and similar situations of observations.*

**Note 3**

*(A reference to an earlier definition, not important in this context.)*

**Note 4**

*Perceived colour may appear in several modes of colour appearance. The names for various modes of appearance are intended to distinguish among qualitative and geometric differences of colour perceptions. Some of the more important terms of the modes of colour appearance are given in "object colour," "surface colour," and "aperture colour." Other modes of colour appearance include film colour, volume colour, illuminant colour, body colour, and Ganzfeld colour. Each of these modes of colour appearance may be further qualified by adjectives to describe combinations of colour or their spatial and temporal relationships. Other terms that relate to qualitative differences among colours perceived in various modes of colour appearance are given in "luminous colour," "non-luminous colour," "related colour," and "unrelated colour."*

While many words were changed, there was no significant change in the definition of color. The importance of appearance remains in note 2 and is added to in note 4, which spells out modes of appearance discussed later in this book.

The above definitions might not be very satisfying due to their circularity, any definitions that avoid the circularity seem to be equally dissatisfying. One such example would be to define color as those attributes of a visual stimulus that are independent of spatial and temporal variations. Even this definition is flawed since in the absence of all temporal and spatial variation,

even the perception of color vanishes. Despite the difficulty in defining color, the various attributes of color can be defined much more precisely and those are the terms that are of utmost importance in color appearance modeling.

### 4.3 HUE

#### *Hue*

*Attribute of a visual perception according to which an area appears to be similar to one of the colours – red, yellow, green, and blue – or to a combination of adjacent pairs of these colours considered in a closed ring.*

#### *Achromatic Colour*

*Perceived color devoid of hue.*

#### *Chromatic Colour*

*Perceived colour possessing hue.*

Once again, it is difficult, if not impossible, to define hue without using examples. This is due, in part, to the nature of the hue perception. It is a natural interval scale as illustrated by the traditional description of a “hue circle.” There is no natural “zero” hue. Color without hue can be described, but there is no perception that corresponds to a meaningful hue of 0 units. Thus the color appearance models described in later chapters never aspire to describe hue with more than an interval scale.

The “circular” nature of hue can be observed in Figure 5.2, which illustrates the hue dimension in the *Munsell Book of Color*. The hue circle in Figure 5.2 also illustrates how all of the hues can be described using the terms red, yellow, green, blue, or combinations thereof as predicted by Hering’s opponent theory of color vision. Other examples of hue include the variation of color witnessed in a projected visible spectrum or a rainbow. Three of the rendered cubes in Figure 4.1 are of three different hues: red, green, and blue. The fourth is white and thus achromatic, possessing no hue.

### 4.4 BRIGHTNESS AND LIGHTNESS

#### *Brightness*

*Attribute of a visual perception according to which an area appears to emit, or reflect, more or less light.*

#### *Lightness*

*The brightness of an area judged relative to the brightness of a similarly illuminated area that appears to be white or highly transmitting.*

#### *Note*

*Only related colours exhibit lightness.*

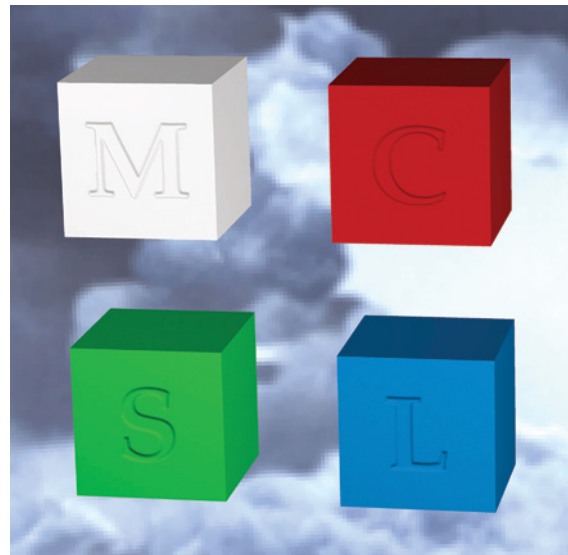


**Figure 4.1** A computer graphics rendering of four solid blocks illuminated by two light sources of differing intensities and angle of illumination to be used for demonstration of various color appearance attributes

The definitions of brightness and lightness are straightforward and rather intuitive. The important distinction is that brightness refers to the absolute level of the perception while lightness can be thought of as relative brightness – normalized for changes in the illumination and viewing conditions.

A classic example is to think about a piece of paper, such as this book page. If this page was viewed in a typical office environment, the paper would have some brightness and a fairly high lightness (perhaps it is the lightest stimulus in the field of vision and therefore white). If the book was viewed outside on a sunny summer day, there would be significantly more energy reflected from the page and the paper would appear brighter. However, the page would still likely be the lightest stimulus in the field of vision and retain its high lightness, approximately the same lightness it exhibited in office illumination. In other words, the paper still appears white, even though it is brighter outdoors. This is an example of approximate lightness constancy.

Figure 4.1 illustrates four rendered cubes that are illuminated by two light sources of different intensities, but the same color. Imagine that you are actually viewing the cubes in their illuminated environment. In this case, it would be clear that the different sides of the cubes are illuminated differently and exhibit different brightnesses. However, if you were asked to judge the lightness of the cubes, you could give one answer for all of the visible sides since you would interpret lightness as their brightness relative to the brightness of a similarly illuminated white object.

## 4.5 COLORFULNESS AND CHROMA

### *Colorfulness*

*Attribute of a visual perception according to which the perceived colour of an area appears to be more or less chromatic.*

#### *Note*

*For a color stimulus of a given chromaticity and, in the case of related colors, of a given luminance factor, this attribute usually increases as the luminance is raised, except when the brightness is very high.*

### *Chroma*

*Colorfulness of an area judged as a proportion of the brightness of a similarly illuminated area that appears white or highly transmitting.*

#### *Note*

*For given viewing conditions and at luminance levels within the range of photopic vision, a colour stimulus perceived as a related colour, of a given chromaticity, and from a surface having a given luminance factor exhibits approximately constant chroma for all levels of illuminance except when the brightness is very high. In the same circumstances, at a given level of illumination, if the luminance factor increases, the chroma usually increases.*

As was discussed in Chapters 1 and 3, color perception is generally thought of as being three dimensional. Two of those dimensions (hue and brightness/lightness) have already been defined. Colorfulness and chroma define the remaining dimension of color. Colorfulness is to chroma as brightness is to lightness. It is appropriate to think of chroma as relative colorfulness just as lightness can be thought of as relative brightness. Colorfulness describes the intensity of the hue in a given color stimulus. Thus, achromatic colors exhibit zero colorfulness and chroma, and as the amount of color content increases (with constant brightness/lightness and hue), colorfulness and chroma increase.

Like lightness, chroma is approximately constant across changes in luminance level. Note, however, that chroma is likely to change if the color of the illumination is varied. Colorfulness, on the other hand, increases for a given object as the luminance level increases since it is an absolute perceptual quantity. Figure 4.1 illustrates the difference between colorfulness and chroma. Again imagine you are in the illuminated environment with the cubes in Figure 4.1. Since different sides of each cube are illuminated with differing amounts of the same color energy, they vary in colorfulness. On the other hand, if you were to judge the chroma of the cubes, you could provide one answer for each of the cubes. This is because you would be judging each side relative to a similarly illuminated white object. The sides of the cubes with greater illumination exhibit greater colorfulness, but the chroma is roughly constant within each cube.

## 4.6 SATURATION

### Saturation

*Colorfulness of an area judged in proportion to its brightness.*

### Note

*For given viewing conditions and at luminance levels within the range of photopic vision, a colour stimulus of a given chromaticity exhibits approximately constant saturation for all luminance levels, except when brightness is very high.*

Saturation is a unique perceptual experience separate from chroma. Like chroma, saturation can be thought of as relative colorfulness. However, saturation is the colorfulness of a stimulus relative to its own brightness, while chroma is colorfulness relative to the brightness of a similarly illuminated area that appears white. In order for a stimulus to have chroma, it must be judged in relation to other colors, while a stimulus seen completely in isolation can have saturation. An example of a stimulus that exhibits saturation, but not chroma, is a traffic signal light viewed in isolation on a dark night. The lights, typically red, yellow, or green, are quite saturated and can be compared to the color appearance of oncoming headlights whose saturation is very nearly zero (since they typically appear white).

Saturation is sometimes described as a shadow series. This refers to the range of colors observed when a single object has a shadow cast upon it. As the object falls into deeper shadow, it becomes darker, but saturation remains constant. This can be observed in Figure 4.1 by assuming that the rendered environment is illuminated by a single light source. The various sides of the cubes will be of approximately constant saturation. Saturation seems to be a more fundamental perceptual attribute than chroma although chroma seems to be used more in object colorimetry. While one can be derived from the other (*i.e.*, both are derived from colorfulness), it does not seem possible to completely eliminate either of them. Saturation is more fundamental for the description of colour appearance while chroma is more fundamental for the measurement and specification of color differences.

## 4.7 UNRELATED AND RELATED COLORS

### Unrelated Colour

*Colour perceived to belong to an area seen in isolation from other colours.*

### Related Colour

*Colour perceived to belong to an area seen in relation to other colors.*

The distinction between related and unrelated colors is critical for a firm understanding of color appearance. The definitions are simple enough; related colors are viewed in relation to other color stimuli, while unrelated colors are viewed completely in isolation. Almost every color appearance

application of interest deals with the perception of related colors and they are the main focus of this book. However, it is important to keep in mind that many of the visual experiments that provide the foundations for understanding color vision and color appearance were performed with isolated stimuli – unrelated colors. It is important to keep the distinction in mind and not try to predict phenomena that only occur with related colors using models defined for unrelated colors and vice versa.

At times, related colors are thought of as object colors and unrelated colors are thought of as self-luminous colors. There is no correlation between the two concepts. An object color can be seen in isolation and thus be unrelated. Also, self-luminous stimuli (such as those presented on CRT displays) can be seen in relation to one another and thus be related colors.

There are various phenomena, discussed throughout this book, that only occur for related or unrelated colors. One interesting example is the perception of colors described by certain color names such as gray and brown. It is not possible to see unrelated colors that appear either gray or brown. Gray is an achromatic color with lightness significantly lower than white. Brown is an orange color with low lightness. Both of these color name definitions require specific lightness levels. Since lightness and chroma require judgments relative to other stimuli that are similarly illuminated, they cannot possibly be perceived as unrelated stimuli. To convince yourself, search for a light that can be viewed in isolation (*i.e.*, completely dark environment) and that appears either gray or brown. A nice demonstration of these related colors can be made by taking a spot of light that appears either white or orange and surrounding it with increasingly higher luminances of white light. As the luminance of the background light increases, the original stimuli will change in appearance from white and orange to gray and brown. If the background luminance is increased far enough, the original stimuli can be made to appear black. For interesting discussions on the color brown, see Bartleson (1976), Fuld *et al.* (1983), and Mausfeld and Niederée (1993).

The perceptual color terms defined previously are applied differently to related and unrelated colors. Unrelated colors only exhibit the perceptual attributes of hue, brightness, colorfulness, and saturation. The attributes that require judgment relative to a similarly illuminated white object cannot be perceived with unrelated colors. On the other hand, related colors exhibit all of the perceptual attributes of hue, brightness, lightness, colorfulness, chroma, and saturation.

## 4.8 DEFINITIONS IN EQUATIONS

The various terms used to carefully describe color appearance can be confusing at times. To keep the definitions straight, it is often helpful to think of them in terms of simple equations. These equations, while not strictly true in a mathematical sense, provide a first-order description of the relationships between the various color percepts. In fact, an understanding of the definitions

in terms of the following equations provides the first building block toward understanding the construction of the various color appearance models. In such models, it is usually possible to find the basic structure of the equations outlined below, but not the simple mathematical form. However, in some cases, a mathematical model can be formulated such that its correlates of appearance predictions come very close to these simple formulations.

Chroma can be thought of as colorfulness relative to the brightness of a similarly illuminated white as shown in Equation 4.1.

$$\text{Chroma} = \frac{\text{Colorfulness}}{\text{Brightness (white)}} \quad (4.1)$$

Saturation can be described as the colorfulness of a stimulus relative to its own brightness as illustrated in Equation 4.2.

$$\text{Saturation} = \frac{\text{Colorfulness}}{\text{Brightness}} \quad (4.2)$$

Finally, lightness can be expressed as the ratio of the brightness of a stimulus to the brightness of a similarly illuminated white stimulus as given in Equation 4.3.

$$\text{Lightness} = \frac{\text{Brightness}}{\text{Brightness (white)}} \quad (4.3)$$

The utility of these simple definitions in terms of equations is illustrated by a derivation of the fact that an alternative definition of saturation (used in some appearance models) is given by the ratio of chroma and lightness in Equation 4.4.

$$\text{Saturation} = \frac{\text{Chroma}}{\text{Lightness}} \quad (4.4)$$

This can be proven by first substituting the definitions of chroma and lightness from Equations 4.1 and 4.3 into Equation 4.4, arriving at Equation 4.5.

$$\text{Saturation} = \frac{\text{Colorfulness}}{\text{Brightness (white)}} \times \frac{\text{Brightness (white)}}{\text{Brightness}} \quad (4.5)$$

Completing the algebraic exercise by canceling out the brightness of the white terms in Equation 4.5 results in saturation being expressed as the ratio of colorfulness to brightness as shown in Equation 4.6, which is identical to the original definition in Equation 4.2.

$$\text{Saturation} = \frac{\text{Colorfulness}}{\text{Brightness}} \quad (4.6)$$

## 4.9 BRIGHTNESS–COLORFULNESS VS LIGHTNESS–CHROMA

While color is typically thought of as three dimensional and color matches can be specified by just three numbers, it turns out that three dimensions are not enough to completely specify color appearance. In fact, five perceptual dimensions are required for a complete specification of color appearance:

- Brightness
- Lightness
- Colorfulness
- Saturation
- Hue.

Chroma is redundant since it is known if the five attributes above are known. However, in many practical color appearance applications it is not necessary to know all five attributes. Typically, related colors are of most interest and only the relative appearance attributes are of significant importance. Thus it is often sufficient to be concerned with only the relative appearance attributes of lightness, chroma, and hue.

There might seem to be some redundancy in using all five appearance attributes to describe a color appearance. However, this is not the case as was elegantly described by Nayatani *et al.* (1990a). In that paper, Nayatani *et al.* illustrated both theoretically and experimentally the distinction between brightness–colorfulness appearance matches and lightness–chroma appearance matches and showed that in most viewing conditions the two types of matches are distinct. Imagine viewing a yellow school bus outside on a sunny day. The yellow bus will exhibit its typical appearance attributes of hue (yellow), brightness (high), lightness (high), colorfulness (high), and chroma (high). Now imagine viewing a printed photographic reproduction of the school bus in the relatively subdued lighting of an office or home. The image of the bus could be a perfect match to the original object in hue (yellow), lightness (high), and chroma (high). However, the brightness and colorfulness of the print viewed in subdued lighting could never equal that of the original school bus viewed in bright sunlight. This is simply because of the lack of energy reflecting off the print relative to the original object. If that same print were carried outside into the bright sunlight that the original bus was viewed under, it is then possible that the reproduction could match the original object in all five appearance attributes.

So which is more important, the matching (*i.e.*, reproduction) of brightness and colorfulness or the matching of lightness and chroma? (Note that hue is defined the same way in either circumstance.) The answer depends on the application, but it is safe to say that much more often it is lightness and chroma (or saturation) that are of greater importance. As illustrated by the above example, in color reproduction applications it is typically possible and desirable to aspire to lightness–chroma matching. Imagine trying to

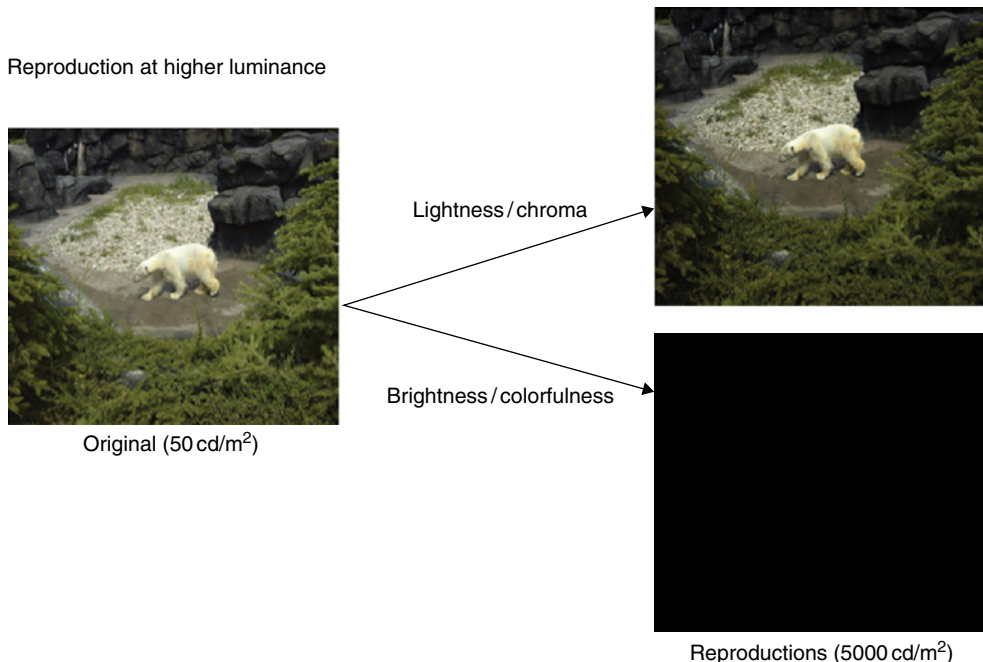


**Figure 4.2** Comparison of lightness–chroma(saturation) reproduction with brightness–colorfulness reproduction when the original is at a lower luminance than the reproduction. Brightness–colorfulness reproduction results in an image that is very dark to compensate for the increased level of illumination. Lightness–chroma(saturation) reproduction represents more complete adaptation since they are relative appearance attributes

make reproductions with a brightness–colorfulness matching objective. To reproduce the sunlight-illuminated school bus in office lighting, one would have to make a print that was literally glowing in order to reproduce brightness and colorfulness. This is not physically possible. Going in the other direction (subdued lighting to bright lighting) is possible, but is it desirable? Imagine taking a photograph of a person at a candlelight dinner and making a reproduction to be viewed under bright sunlight. It would be easy to reproduce the brightness and colorfulness of the original scene, but the print would be extremely dark (essentially black everywhere) and it would be considered a very poor print. Customers of such color reproductions expect lightness–chroma reproduction. Attempts to make such reproductions using a color appearance model across changes in luminance are given in Figure 4.2 and Figure 4.3.

There are a few situations in which brightness and colorfulness might be more important than lightness and chroma (or saturation). Nayatani *et al.* (1990a) suggest a few such situations. One of those is in the specification of the color rendering properties of light sources. In such an application it might be more important to know how bright and colorful objects appear under a given light source, rather than just lightness and chroma.

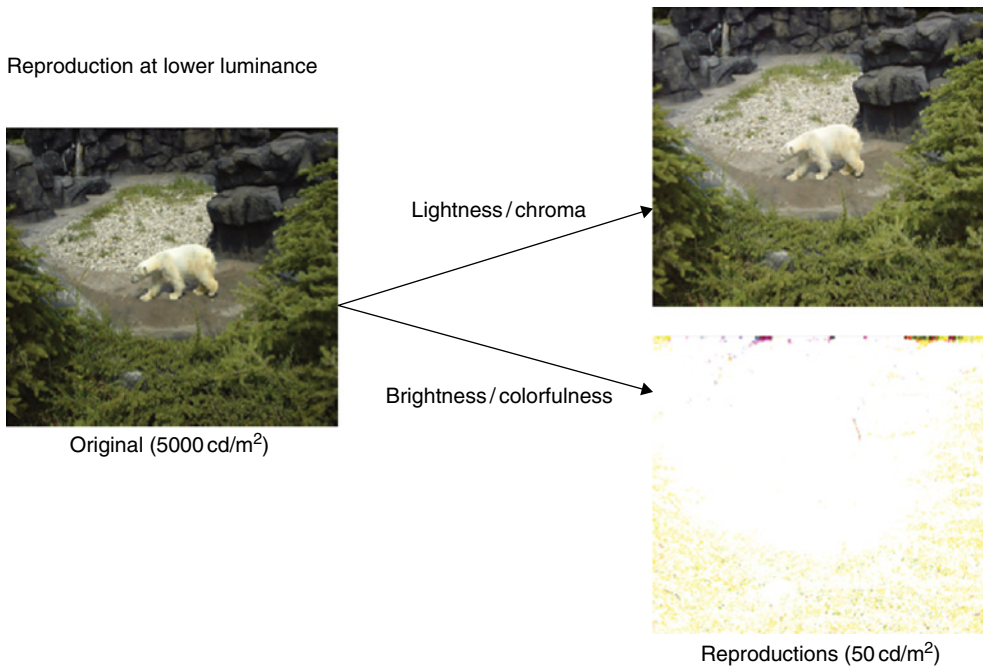


**Figure 4.3** Comparison of lightness-chroma(saturation) reproduction with brightness-colorfulness reproduction when the original is at a higher luminance than the reproduction. Brightness-colorfulness reproduction results in an image that is very bright to compensate for the decreased level of illumination. Lightness-chroma(saturation) reproduction represents more complete adaptation since they are relative appearance attributes

Another situation might be in the judgment of image quality for certain types of reproductions. For example, in comparing the quality of projected images in a darkened (or not so darkened) room, observers might be more interested in the brightness and colorfulness of an image than in the lightness and chroma. In fact, the lightness and chroma of image elements might remain nearly constant as the luminance of the projector is decreased while it is fairly intuitive that the perceived image quality would be decreasing. It is very rare for observers to comment that they wish the image from a projector was not so bright unless a bright projector image is displayed adjacent to a dim projector image!

# Color Order Systems

---

Since color appearance is a basic perception, the most direct method to measure it is through psychophysical techniques designed to elucidate perceptually uniform scales of the various color appearance attributes defined in Chapter 4. When such experiments are performed, it is possible to specify stimuli using basic colorimetry that embody the perceptual color appearance attributes. A collection of such stimuli, appropriately specified and denoted, forms a color order system. Such a color order system does allow a fairly unambiguous specification of color appearance. However, there is no reason to expect that the specified appearances will generalize to other viewing conditions or be mathematically related to physical measurements in any straightforward way. Thus, color order systems provide data and a technique for specifying color appearance but do not provide a mathematical framework to allow extension of that data to novel viewing conditions. Therefore color order systems are of significant interest in the development and testing of color appearance models, but cannot serve as a replacement for them.

*When asked an impression of a noted forest, a young traveler replied it had been impossible to see the forest because there were too many trees. That is somewhat the difficulty in discussing color. There are so many points of view, such diversity of aim, the very act of perceiving color is so complex, and the terms used to describe the sensation are so loose, that instead of reaching its essence we are lost in a tangle of externals.*

—Munsell (1907: 1)

This chapter provides an overview of some color order systems that are of particular interest in color appearance modeling and device-independent color imaging. Their importance and application will become self-evident in this and later chapters. Additional details on color order systems can be found in Hunt's text on color measurement (Hunt 1991a, 1998, Hunt and

Pointer 2011), Wyszecki and Stiles' (1982) reference volume on color science, Wyszecki's (1986) review chapter on color appearance, Derefeldt's (1991) review on color appearance systems, Kuehni's (2003) detailed historical review of color spaces, and the comprehensive and encyclopedic volume entitled *Color Ordered: A Survey of Color Order Systems from Antiquity to the Present* (Kuehni and Schwarz 2008).

## 5.1 OVERVIEW AND REQUIREMENTS

Many definitions of color order systems have been suggested, and it is probably most useful to adopt some combination of them. Wyszecki (1986) points out that color order systems fall into three broad groups:

- One based on the principles of additive mixtures of color stimuli. A well-known example is the Ostwald system.
- One consisting of systems based on the principles of colorant mixtures. The Lovibond Tintometer provides an example of a color specification system based on the subtractive mixture of colorants.
- One consisting of those based on the principles of color perception or color appearance.

In fact Derefeldt (1991) suggests that color appearance systems are the only systems appropriate for general use. She goes on to state that color appearance systems are defined by perceptual color coordinates or scales, and uniform or equal visual spacing of colors according to these scales.

This chapter focuses on color appearance systems such as the Natural Color System (NCS) and the Munsell system. Hunt (1991a) adds a useful constraint onto the definition of color order systems by stating that it must be possible to interpolate between samples in the system in an unambiguous way. Finally, a practical restriction on color order systems is that they be physically embodied with stable samples that are produced to tight tolerances. To summarize, color order systems are constrained in that they must:

- Be an orderly (and continuous) arrangement of colors
- Include a logical system of denotation
- Incorporate perceptually meaningful dimensions
- Be embodied with stable, accurate, and precise samples.

A further objective for a generally useful color order system is that the perceptual scales represent perceived magnitudes uniformly or that differences on the scales be of equal perceived magnitude.

The above definition excludes some color systems that have been found useful in practical applications. For example, the *PANTONE Color Formula Guide* is a useful color specification system for inks, but it is not a color order system since it does not include continuous scales or an appropriate

embodiment. It is more appropriately considered a color naming system. Swatches used to specify paint colors also fall into this category.

There are a variety of applications of color order systems in the study of color appearance. They provide independent data on the perceptual scaling of various appearance attributes such as lightness, hue, and chroma that can be used to evaluate mathematical models. Their embodiments provide reliable sample stimuli that can be used unambiguously in psychophysical experiments on color appearance. Their nomenclature provides a useful system for the specification and communication of color appearances. They also provide a useful educational tool for the explanation of various color appearance attributes and phenomena. The uses of color order systems in color appearance modeling are discussed in more detail in Section 5.6.

## 5.2 THE MUNSELL BOOK OF COLOR

One of the most widely used color order systems, particularly in the USA, is the Munsell system, embodied in the *Munsell Book of Color*. The history of the Munsell system has been reviewed by Nickerson (1940, 1976 a,b,c), and interesting insight can be obtained by reviewing the visual experiments leading to the renotation of the Munsell colors in the 1940s (Newhall 1940). An educational book with samples for an abridged version of the system is available as *The New Munsell Student Color Set* (Long and Luke, 2001) and is quite helpful in learning the system. The system was developed by an artist, Albert H. Munsell, in the early part of the twentieth century. Munsell was particularly interested in developing a system that would aid in the education of children. The basic premise of the system is to specify color appearance according to three attributes:

- Hue ( $H$ )
- Value ( $V$ )
- Chroma ( $C$ ).

The definitions of the three Munsell dimensions match the current definitions of the corresponding appearance attributes, with *Munsell value* referring to lightness. Munsell's objective was to specify colors (both psychophysically and physically) with equal visual increments along each of the three perceptual dimensions.

### Munsell Value

The Munsell value scale is the anchor of the system. There are ten main steps in the Munsell value scale with white given a notation of 10, black denoted 0, and intermediate grays given notations ranging between 0 and 10. The design of the Munsell value scale is such that an intermediate

gray with a Munsell value of 5 (denoted N5 for a neutral sample with value 5) is perceptually halfway between an ideal white (N10) and an ideal black (N0). Also, the perceived lightness difference between N3 and N4 samples is equivalent to the lightness difference between N6 and N7 samples or any other samples varying by one step in Munsell value. Lightness perceptions falling in between two Munsell value steps are denoted with decimals. For example, Munsell value 4.5 falls perceptually halfway between Munsell value 4 and 5. It is important to note that the relationship between Munsell value,  $V$ , and relative luminance,  $Y$ , is nonlinear. In fact, it is specified by the fifth-order polynomial given in Equation 5.1 and plotted in Figure 5.1.

$$Y = 1.2219V - 0.23111V^2 + 0.23951V^3 - 0.021009V^4 + 0.0008404V^5 \quad (5.1)$$

As can be seen in Figure 5.1, a sample that is perceived to be a middle gray (N5) has a relative luminance (or luminous reflectance factor) of about 20%. The Munsell value of any color (independent of hue or chroma) is defined by the same univariate relationship with relative luminance. Thus, if the Munsell value of a sample is known, so is its relative luminance, CIE  $Y$ , and vice versa. Unfortunately, the fifth-order polynomial in Equation 5.1 cannot be analytically inverted for practical application. Since the CIE lightness scale,  $L^*$ , was designed to model the Munsell system, it provides a very good computational approximation to Munsell value. As a very useful and accurate general rule, the Munsell value of a stimulus can be obtained from its CIE  $L^*$  (Ill. C, 2° Obs.) by simply dividing by 10. In fact, this approximation more accurately predicts some of the

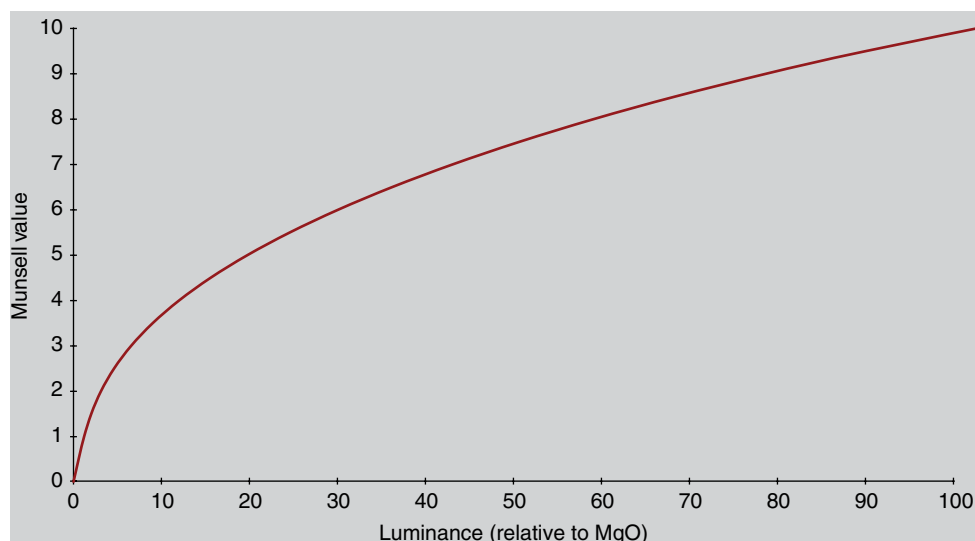


**Figure 5.1** Munsell value as a function of relative luminance

original Munsell lightness scaling data than the polynomial given in Equation 5.1 (Fairchild 1995b).

## Munsell Hue

The next dimension of the Munsell system is hue. The hue circle in the Munsell system is divided into five principle hues (purple, blue, green, yellow, and red, denoted 5P, 5B, 5G, 5Y, and 5R, respectively) and is designed to divide the complete hue circle into equal perceptual intervals. Five intermediate hues are also designated in the Munsell system as 5PB, 5BG, 5GY, 5YR, and 5RP for a total of 10 hue names. For each of the ten hues there are ten integral hues with notations as illustrated by the range between 5PB and 5P, which is 6PB, 7PB, 8PB, 9PB, 10PB, 1P, 2P, 3P, and 4P. This type of sequence continues around the entire hue circle resulting in 100 integer hue designations that are intended to be equal perceived hue intervals. Hues intermediate to the integer designations are denoted with decimal values (*e.g.*, 7.5PB).

## Munsell Chroma

The third dimension of the Munsell system is chroma. The chroma scale is designed to have equal visual increments from a chroma of 0 for neutral samples to increasing chromas for samples with stronger hue content. There is no set maximum for the chroma scale. The highest chromas achieved depend on the hue and value of the samples and the colorants used to produce them. For example, there are no high chroma samples with a yellow hue and low value, or a purple hue and high value. Such stimuli cannot be physically produced due to the nature of the human visual response. Figure 5.2 illustrates the three-dimensional arrangement of the Munsell system in terms of a constant value plane (Figure 5.2(a)) and a constant hue plane (Figure 5.2(b)). Figure 5.3 illustrates similar planes and a three-dimensional perspective of the Munsell system generated using a computer graphics model of the system. The Munsell system is used to denote a specific colored stimulus using its Munsell hue, value, and chroma designations in a triplet arranged with the hue designation followed by the value, a forward slash (/), and then the chroma. For example, a red stimulus of medium lightness and fairly high chroma would be designated 7.5R 5/10 (hue value/chroma).

## Munsell Book of Color

The Munsell system is embodied in the *Munsell Book of Color*. Figure 5.4 is a photograph of a number of historical and modern editions of the *Munsell Book of Color*. The *Munsell Book of Color* consists of about 1500 samples

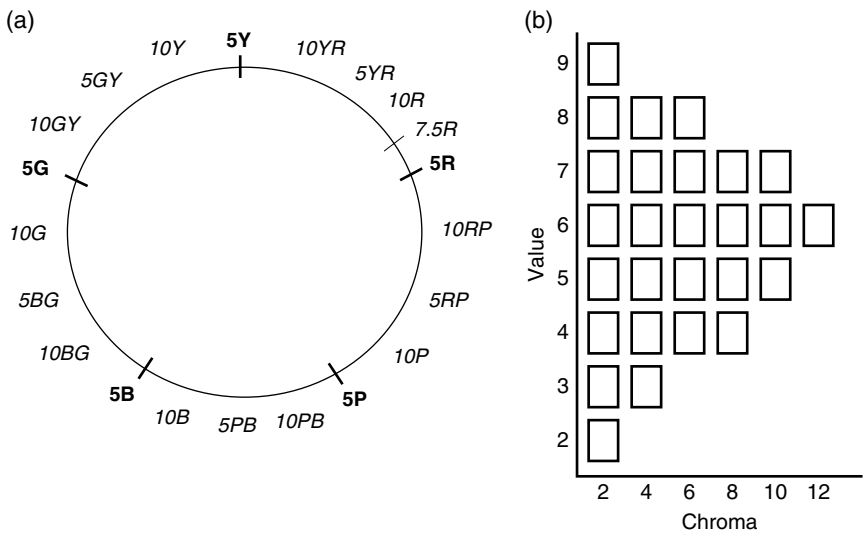


**Figure 5.2** A graphical representation of (a) the hue circle and (b) a value/chroma plane of constant hue in the Munsell system

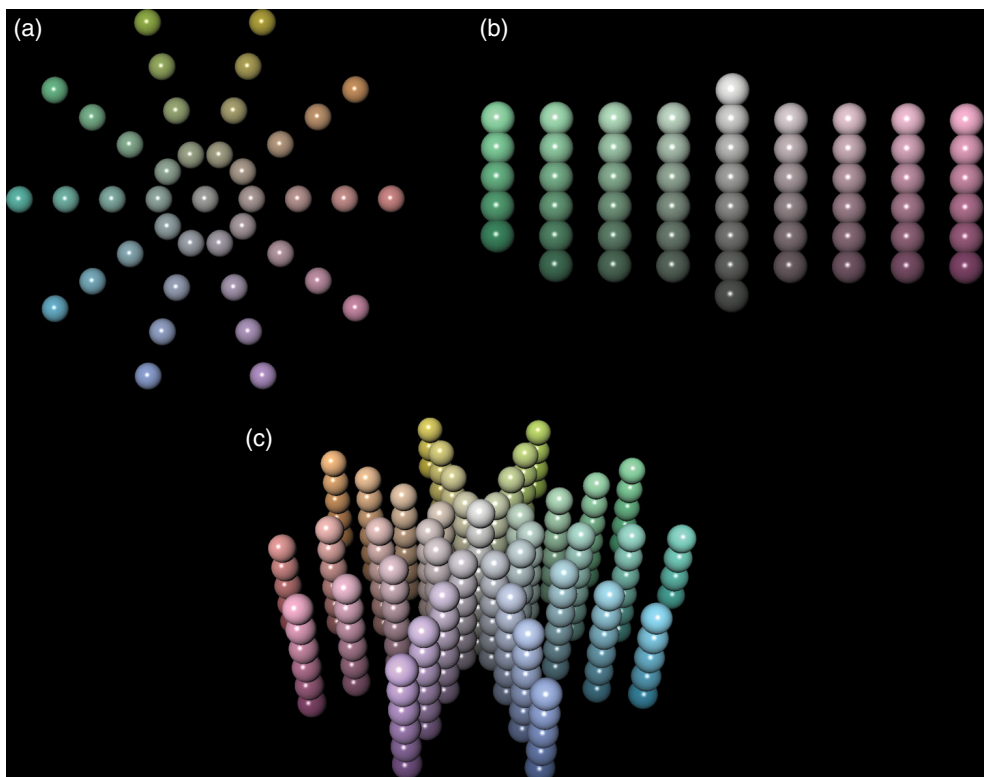


**Figure 5.3** A color rendering of samples from the Munsell system in (a) a constant value plane, (b) a pair of constant-hue planes, and (c) a three-dimensional perspective



**Figure 5.4** A variety of historical and modern editions of the *Munsell Book of Color* illustrating several constant-hue pages

arranged on 40 pages of constant hue. Each hue page is arranged in order of increasing lightness (bottom to top) and chroma (center of book to edge). The samples consist of painted paper and are available in both glossy and matte surfaces. Larger sized Munsell samples can also be purchased for special applications such as visual experiments or construction of test targets for imaging systems. Munsell samples are produced to colorimetric aim points that were specified by the experiments leading up to the Munsell renotation (Newhall 1940). The chromaticity coordinates and luminance factors for each Munsell sample (including many that cannot be easily produced) can be found in Wyszecki and Stiles (1982). The colorimetric specifications utilize CIE illuminant C and the CIE 1931 Standard Colorimetric Observer ( $2^\circ$ ). These specifications should be kept in mind when viewing any embodiment of the Munsell system. The perceptual uniformity of the system is only valid under source C, on a uniform middle gray (N5) background, with a sufficiently high illuminance level (e.g., greater than 500 lux). Viewing the samples in the *Munsell Book of Color* under any other viewing conditions does not represent an embodiment of the Munsell system.

It is worth noting that the Munsell system was scaled as three one-dimensional scales of color appearance, and the relationship between Munsell step size and perceived color difference is not constant across the three dimensions. It is generally accepted (see discussion of Nickerson Index of Fading in Berns (2000) or discussion of Munsell system in Hunt (1998)) that an increment of two Munsell chroma steps is perceptually equal to the color change of one step in Munsell value. Step size in Munsell hue is dependent on the chroma of the samples in question. The best practice is to simply keep the three dimensions independent from one another when computing differences or appearance.

### 5.3 THE SWEDISH NCS

More recently, the NCS has been developed in Sweden (Hard and Sivik 1981) and adopted as a national standard in Sweden (SS 01 91 02 and SS 01 91 03) and a few other European countries. The NCS is based on the opponent colors theory of Hering. The hue circle is broken up into four quadrants defined by the unique hues red, yellow, green, and blue as illustrated in Figure 5.5(a). The four unique hues are arranged orthogonally with equal numbers of steps between them. Thus, while the NCS hues are spaced with equal perceived intervals between each hue, the intervals are of different magnitude within each of the four quadrants. This is because there are more visually distinct hues between unique red and unique blue than between unique yellow and unique green. Perceived hues that fall between the unique hues are given notations representing the relative perceptual composition of the two neighboring unique hues. For example, an orange hue that is perceived to be midway between unique red and unique yellow would be given the notation Y50R.

Once the NCS hue notation is established, the remaining two dimensions of relative color appearance are specified on trilinear axes as illustrated in Figure 5.5(b). The three corners of the triangle represent colors of maximal blackness (S), whiteness (W), and chromaticness (C). For any stimulus, the whiteness, blackness, and chromaticness must sum to 100. Thus the sample of maximum blackness is denoted as  $s=100$ ,  $w=0$ , and  $c=0$ . The sample of maximum whiteness is denoted as  $s=0$ ,  $w=100$ , and  $c=0$ . The sample of maximum chromaticness is denoted  $s=0$ ,  $w=0$ , and  $c=100$ . Since the three numbers must sum to 100, only two are required for a complete specification (along with the hue notation). Typically, blackness and chromaticness are used. For example, an intermediate sample might be denoted  $s=20$  and  $c=70$ , implying a whiteness,  $w=10$ . The maximum chromaticness for each hue is defined using a mental anchor of the maximally chromatic sample

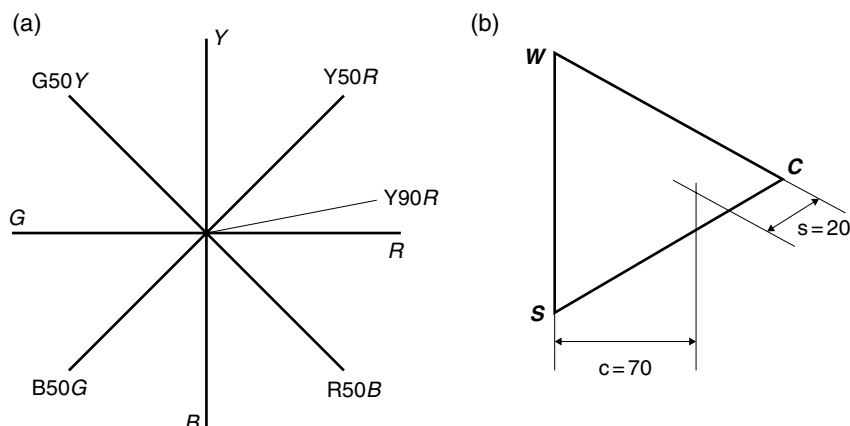


**Figure 5.5** A graphical representation of (a) the hue circle and (b) a blackness/chromaticness plane of constant hue in the NCS system

that could be perceived for that hue. Thus there is no direct relationship between Munsell chroma and NCS chromaticness. Likewise, there is no simple relationship between Munsell value and NCS blackness. It is also important to note that the samples of maximum chromaticness are of different relative luminance and lightness for the various hues. The Munsell and NCS systems represent two different ways to specify perceptual color appearance. It is not possible to say that one is better than the other; it can only be stated that the two are different. This was recently reaffirmed in the report of CIE TC1-31 (CIE 1996a), which was requested by ISO to recommend a single color order system as an international standard along with techniques to convert from one to another. This international committee of experts concluded that such a task is impossible.

A color is denoted in the NCS system by its blackness (s), chromaticness (c), and hue. For example, the stimulus described in the section “Munsell Value” with a Munsell designation of 7.5R 5/10 has an NCS designation of 2070-Y90R, where the blackness of 20 is followed immediately by the chromaticness of 70 with no space. Thus, the initial four-digit number represents blackness followed by chromaticness. The final part of the designation, following a dash, is the hue). This suggests that the sample is nearly a unique red, with only 10% yellow content. It is further described as being highly chromatic (70%) with only a small amount of blackness (20%). Note that even though this sample is of medium Munsell value, it is of substantially lower blackness (or higher whiteness) in the NCS system. This illustrates the fundamental difference between the Munsell value scale and the NCS whiteness–blackness–chromaticness scale.

Like the Munsell system, the NCS is embodied in an atlas, illustrated in Figure 5.6, and specified by CIE tristimulus values based on extensive visual observations. The NCS atlas includes 40 different hues and samples in steps of 10 along the blackness and chromaticness scales. Since it is not possible to produce all of the possible samples, due to limitations in pigments, there



**Figure 5.6** A photograph of a recent edition of the NCS Color Atlas

are approximately 1500 samples in the atlas. The NCS atlas should also be viewed under daylight illumination with appropriate luminance levels and background. NCS samples are also available in various sizes for different specialized applications. As a Swedish national standard, the NCS is taught at a young age and used widely in color communication in Sweden, providing an enviable level of precision in everyday color communication.

## 5.4 THE COLORCURVE SYSTEM

A recently developed color order system is the Colorcurve system (Stanziola 1992), designed as a color communication system representing a combination of a color appearance system and a color mixture system. The system is designed such that colors can be specified within the system and then spectral reflectance data for each sample can be used to formulate matching samples in various materials or media. Thus each sample in the system is specified not only by its colorimetric coordinates but also by its spectral reflectance properties.

The Colorcurve system uses the CIELAB color space as a starting point. Eighteen different  $L^*$  levels were chosen at which to construct constant lightness planes in the system. The  $L^*$  levels range from 30 to 95 in steps of five units with a few extra levels incorporated at the higher lightness levels that are particularly important in design (e.g., light colors are popular for wall paint). At each lightness level, nine starting points were selected. These consisted of one gray ( $a^*=0$ ,  $b^*=0$ ) and eight chromatic colors with chroma,  $C^*$ , of 60. The chromatic starting points were red (60, 0), orange (42.5, 42.5), yellow (0, 60), yellow/green (-42.5, 42.5), green (-60, 0), blue/green (-42.5, -42.5), blue (0, -60), and purple (42.5, -42.5). Thus the starting points were defined using principles of a color appearance space.

The remainder of the system was constructed using additive color mixing. Each quadrant of the CIELAB  $a^*b^*$  plane was filled with a rectangular sampling of additive mixtures of the gray and three chromatic starting points in that quadrant. Equal steps in the Colorcurve designations represent equal additive mixtures between the four starting points. These principles were used to define all of the aim points for the Colorcurve system. The samples were then formulated with real pigments such that the system could be embodied along with the desired spectral reflectance curve specifications. The system is embodied in two atlases made up of samples of nitrocellulose lacquer coated on paper. The Master Atlas is made up of about 1200 samples at 18 different lightness levels. There is also a Gray and Pastel Atlas made up of 956 additional samples that more finely sample the regions of color space that are near grays or pastels. Since the Colorcurve system is specified by the spectral reflectance characteristics of the samples, the viewing illumination is not critical as long as a spectral match is made to the color curve sample. If a spectral match is made, the sample produced will match the Colorcurve sample under all light sources. This is not possible with other color order systems. Like the other color order systems, Colorcurve samples can be obtained in a variety of forms and sizes for different applications.

One unique attribute of the Colorcurve system is of particular interest. The samples in the atlases are circular rather than square as found in most systems. The circular samples avoid two difficulties with color atlases. The first is the contrast illusion of dark spots that appear at the corners between square samples (the Hermann grid illusion). The second is that it is impossible to mount a circular sample crooked!

Unfortunately, the unique and interesting Colorcurve system is no longer commercially available.

## 5.5 OTHER COLOR ORDER SYSTEMS

The Munsell and NCS systems described above are the most important color order systems in the study of color appearance models. The Colorcurve system provides an interesting combination of color appearance and color mixture systems that could provide a useful source of samples for color appearance and reproduction research. However, there are many other color order systems that have been created for a variety of purposes. Derefeldt (1991), Wyszecki and Stiles (1982), and Kuehni and Schwarz (2008) provide more details, but there are a few systems that warrant mention here. These include the Optical Society of America (OSA) Uniform Color Scales, the Deutsches Institut für Normung (DIN) system, and the Ostwald system.

### OSA Uniform Color Scales

The OSA set up a committee on Uniform Color Scales in 1947. The ultimate results of this committee's work were described by MacAdam (1974, 1978) as the OSA Uniform Color Scales system, or OSA UCS. The OSA system is a color appearance system, but it is significantly different in nature than either the Munsell or NCS systems. The OSA system is designed such that a given sample is equal in perceptual color difference from each of its neighbors in three-dimensional color space (not simply one dimension at a time as in the Munsell system). The OSA space is designed in a three-dimensional Euclidean geometry with  $L$ ,  $j$ , and  $g$  axes representing lightness, yellowness-blueness, and redness-greenness, respectively. In order to make each sample equally spaced from each of its neighbors, a regular rhombohedral sampling of the three-dimensional space is required in which each sample has 12 nearest neighbors, all at an equal distance. If the 12 points of the nearest neighbors to a sample are connected, they form a polyhedron known as a cubo-octohedron. Such sampling allows rectangularly sampled planes of the color space to be viewed from a variety of directions. Figure 5.7(a) shows a computer graphics representation of two adjacent constant lightness planes in the OSA system illustrating the sampling scheme. Figure 5.7(b) illustrates a three-dimensional representation of the OSA system. It is clear that the objective of equal color differences in all directions results in a very different type of color order system. Perhaps due to its complex geometry (and the

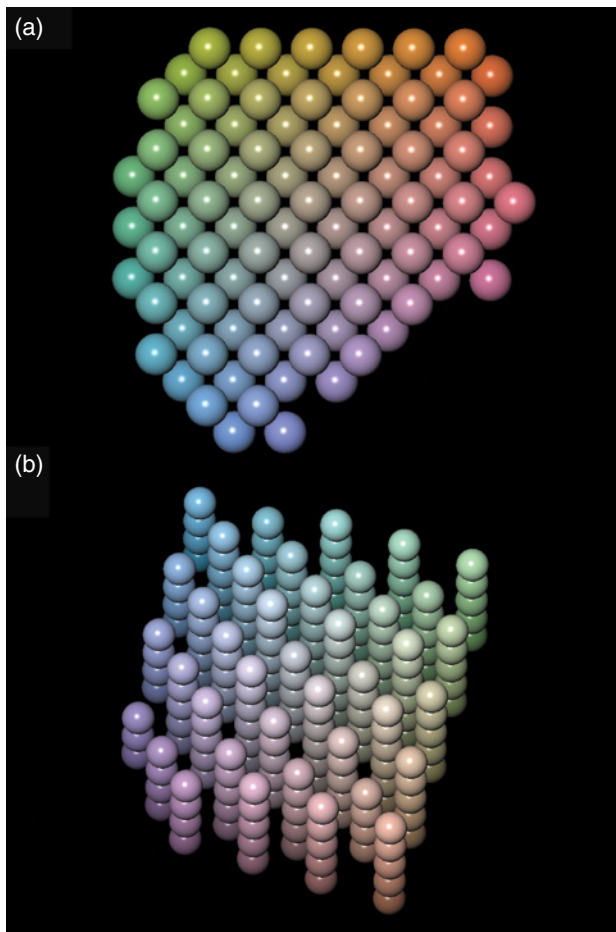


**Figure 5.7** A color rendering of samples from the OSA UCS system in (a) a pair of adjacent constant lightness planes and (b) a three-dimensional projection

lack of a useful embodiment), the OSA system is not very popular. It does provide another set of data that could be used in the evaluation of color appearance and color difference models. The OSA space was also specified in terms of equations to transform from CIE coordinates to the OSA system's  $L$ ,  $j$ , and  $g$  coordinates. Unfortunately, the equations are not invertible, limiting their practical utility. The equations and sample point specifications for the OSA system can be found in Wyszecki and Stiles (1982).

## DIN System

The DIN system was developed in Germany with the perceptual variables of hue, saturation, and darkness. An historical overview of the DIN system was presented by Richter and Witt (1986). The specification of colors in the

DIN system is closely related to colorimetric specification on a chromaticity diagram. Colors of equal hue in the DIN system fall on lines of constant dominant (or complementary) wavelength on the chromaticity diagram (i.e., straight lines radiating from the white point). Colors of constant DIN saturation represent constant chromaticities. The sampling of DIN hue and saturation is designed to be perceptually uniform. DIN darkness is related to the luminous reflectance of the sample relative to an ideal sample (a sample that either reflects all, or none, of the incident energy at each wavelength) of the same chromaticity resulting in a darkness scale that is similar to NCS blackness rather than Munsell value. The DIN system is embodied in the DIN Color Chart that includes constant hue pages with a rectangular sampling of darkness and saturation. Thus columns on a DIN page represent constant chromaticity (DIN saturation) and appear as a shadow series (a single object illuminated at various levels of the same illuminant). The DIN charts also illustrate that chromaticity differences become less distinguishable as darkness increases. The bottom row of any given DIN page appears uniformly black.

## Ostwald System

The Ostwald system has been widely used in art and design and is therefore of substantial historical interest (Derefeldt 1991). Like the NCS system, the Ostwald system is based on Hering's opponent colors theory. However, the Ostwald system, much like the Colorcurve system, represents a combination of a color appearance system and a color mixture system. Ostwald used Hering's four unique hues to set up a hue circle, but rather than placing the perceptually opponent hues opposite one another, he used colorimetric complements (chromaticities connected by a straight line through the white point on a chromaticity diagram) in the opposite positions on the hue circle. The Ostwald system also includes a trilinear representation of white content, black content, and full-color content on each constant-hue plane. In the NCS system, these planes are defined according to perceptual color scales. However, in the Ostwald system, these planes were defined by additive color mixtures of the three maxima located at the corners of the triangles. Thus the Ostwald system was set up with color appearance in mind, but the samples were filled in using additive color mixing. (This is exactly analogous to the much more recent formulation of the Colorcurve system based on CIELAB.)

## 5.6 USES OF COLOR ORDER SYSTEMS

Color order systems have a variety of applications in the study of color appearance and related areas. These include use as samples in experiments, color design, communication, education, model testing, test targets, and other applications where physical samples are helpful.

## Color Order Systems in Visual Experiments

Often in visual experiments aimed at studying color appearance it is necessary to view and/or match a variety of colored stimuli under different viewing conditions. Color order systems provide a useful source of samples for such experiments. For example, an experimenter might select a collection of Munsell, NCS, or Colorcurve samples to scale in a color appearance experiment. These samples will have well-known characteristics, and in publishing the notations of the samples used, the researchers provide a useful definition of the stimuli that can be used by others to replicate the experiments. Note that actually using samples from the color order systems, and not just their designations on arbitrary samples, has the advantage that the reflectance characteristics of the samples are also defined. A related use of color order systems in appearance experiments involves teaching the system to observers and then asking them to assign designations (Munsell and NCS are particularly useful in this type of experiment) to samples viewed under a variety of conditions. This allows a specification of the change in appearance caused by various changes in viewing conditions which can be used, together with the colorimetric specifications of each sample in each viewing condition, to formulate and test color appearance models.

## Color Order Systems in Art and Design

Color order systems are often used in art and design. Their very nature as an orderly arrangement of colors allows designers to easily select samples with various color relationships. For example, with the Munsell system it is simple to select a range of colors of constant lightness or hue or to select hues that complement one another in various ways. Color mixing systems provide this utility in addition to providing some insight for artists to help them actually produce the colors in various media. The color order systems not only provide a design tool, but also incorporate a communication tool in their designations allowing the chosen colors to be communicated to those producing the materials to be incorporated into a design.

## Color Order Systems in Communication

Clearly, precise communication of color appearance is an application for color order systems. This is effective as long as those on both ends of the communication link are viewing the systems in properly controlled environments. While colorimetric coordinates have the potential to provide much more precise, accurate, and useful specifications of colors, the perceptual meaning is not so readily apparent to various users. A color order system can provide a more readily accessible communication tool. It can also be

used to describe a color appearance to someone familiar with the system, but not necessarily in possession of an atlas. An interesting example of this type of communication can be found in the ANSI specifications for viewing of color images (ANSI 1989) in which the backgrounds are specified in terms of Munsell value when a reflectance factor alone is sufficient and potentially more precise.

## Color Order Systems in Education

Color order systems are immensely useful in education regarding color appearance (as well as many other aspects of color). For example, examination of the Munsell system allows a visual definition of the color appearance attributes of lightness, chroma, and hue. Moving pages from the *Munsell Book of Color* from a low luminance level to a high luminance level allows for a nice demonstration of how brightness and colorfulness increase substantially while lightness and chroma remain nearly constant. The DIN system is useful to illustrate the difference between chroma and saturation and how saturation is related to a shadow series (a single object illuminated by decreasing illuminance levels of the same spectral power distribution). Color order systems can also be educational in their limitations. For example, in the Munsell system, constant value is defined as constant relative luminance. However, it is well known (Helmholtz–Kohlrausch effect described in Chapter 6) that as samples increase in chroma at constant relative luminance they appear lighter. One need only examine a series of Munsell samples of constant value and varying chroma to see that indeed there is a large and systematic variation in lightness. Lastly, systems like the NCS systems can be a great aid in education regarding the opponent theory of color vision, particularly in their hue designations which closely follow the physiological encoding of color.

## Color Order Systems to Evaluate Mathematical Color Appearance Models

Since color order systems such as Munsell and NCS are based on perceptual scaling of color appearance, they provide readily available data that can be used to evaluate mathematical color appearance models. For example, the Munsell system includes planes of constant lightness and hue, and cylindrical surfaces of constant chroma. The tristimulus specifications of the Munsell system can be converted into the appropriate color appearance predictors for a given color appearance model in order to see how well it predicts the constant hue, lightness, and chroma contours. Such an evaluation provides a useful, widely understood, technique for the intercomparison of various color appearance models. Intercomparison of the predictions of Munsell and NCS contours in various models also allows further study to understand the fundamental differences between the two systems.

## Color Order Systems and Imaging Systems

Color order systems can also be used as sources for test targets for imaging systems or other measurement devices. For example, the Macbeth Color Checker Chart (McCamy *et al.* 1976) is a commonly used test target for imaging systems that are partially based on samples from the Munsell system. Despite its common use, the Macbeth Color Checker Chart incorporates only a small sample of colors (24) and an incomplete sampling of color space. Targets of greater practical utility could fairly easily be constructed. Samples from various color order systems can be used to develop custom test targets that can be reliably specified and replicated elsewhere.

## Limitations of Color Order Systems

While color order systems have a variety of useful applications in color appearance, they are not a substitute for a color appearance model. In general they suffer from two significant limitations in this regard. First, they are not specified mathematically in relationship to physically measurable values. While both the Munsell and NCS systems have colorimetric specifications for each sample in the system, there are no equations to relate the colorimetric coordinates to the perceptual coordinates of the color order systems. Approximate equations have been derived by statistical fitting and neural network modeling, but the only reliable technique for transformation from CIE colorimetry to color order system coordinates remains look-up table (LUT) interpolation. Clearly, the lack of mathematical definitions in the forward direction precludes the possibility of the analytical inverse models for the required reverse direction. Second, these color order systems have been established as perceptual scales of color appearance for a single viewing condition. They provide no data with respect to the changes in color appearance induced by changes in viewing conditions.

## 5.7 COLOR NAMING SYSTEMS

There are a variety of color specification systems available that do not meet the requirements for consideration as true color order systems, but are useful for some practical applications. Generally such systems, more properly considered color naming systems, are not arranged in a perceptually ordered manner (although some are arranged in order according to some imaging process) and are not presented or specified for controlled viewing conditions. In addition, the physical embodiments of these systems are not controlled with the colorimetric accuracy required for precise color communication. Examples of such systems include the PANTONE, Toyo, Focoltone, and Trumatch systems.

## The PANTONE System

The main component of the PANTONE system is the *PANTONE Color Formula Guide*. This guide is a swatch book containing 1012 PANTONE spot-color ink mixtures on coated and uncoated stock. Each swatch has a numerical identifier that can be used to communicate the desired color to a printer. The printer will then mix the spot-color ink using the prescribed PANTONE formula and the resulting printed color should be a reasonable approximation to the color in the swatch book. This system is the prevalent tool for the specification of spot color in the USA.

The *PANTONE Process Color Imaging Guide* includes 942 color swatches illustrating the PANTONE spot colors that can be reasonably well simulated with a four-color (CMYK) printing process. The swatch book includes a patch of the PANTONE spot color adjacent to the process-color simulation to indicate the variance that can be expected.

## The Trumatch System

The *Trumatch Colorfinder* is a swatch book including over 2000 process color samples. These samples are arranged in an order that is slightly more perceptually based than the PANTONE system. Such a system allows computer users to select CMYK color specifications according to the appearance of printed swatches rather than relying on the approximate color represented on a CRT display for a given CMYK specification. The user finds the desired color in the swatch book, sets the particular area in an image to those CMYK values, and then proceeds to ignore the often inappropriate appearance of the computer display with confidence that the final printed color will be a fairly close approximation to the color selected in the swatch book.

## Other Systems

In addition to the PANTONE and Trumatch process-color guides that can be used as shortcuts to specification of colors that are ultimately to be printed, there is the *PostScript Process Color Guide* published by Agfa that includes over 16 000 examples of process colors representing a complete sampling of CMY combinations from 0% to 100% (dot coverage) in 5% increments with additional samples incorporating four different levels of black ink coverage. The samples are presented on both coated and uncoated stock.

Given the variability in printing inks, papers, and processes, these systems can only be considered as approximate guides. They are known to not be very stable, and it is often recommended that swatch books be replaced every six months or so. However, their performance is far superior than working with no guides and uncalibrated/uncharacterized

imaging systems. However, a system in which all of the imaging devices have been carefully calibrated and characterized, and in which viewing conditions are carefully controlled, will be capable of easily producing superior color accuracy and precision for within-gamut colors. For out-of-gamut colors (such as metallic inks which cannot be simulated on a two-dimensional computer graphics display) a swatch-book system might still prove invaluable.

# 6

# Color Appearance Phenomena

---

Chapter 3 describes the fundamental concepts of basic colorimetry. While the CIE system of colorimetry has proven to be extremely useful, it is important to remember that it has limitations. Most of its limitations are inherent in the design of a system of tristimulus values based on color matching. Such a system can accurately predict color matches for an average observer, but it incorporates little of the information necessary for specifying the color appearance of those matching stimuli. Such is the realm of color appearance models. Tristimulus values can be considered as a nominal (or at best ordinal) scale of color. They can be used to state whether two stimuli match or not. The specification of color differences requires interval scales, and the description of color appearance requires interval scales (for hue) and ratio scales (for brightness, lightness, colorfulness, saturation, and chroma). Additional information is needed, in conjunction with tristimulus values, to derive these more sophisticated scales.

Where is this additional information found? Why is it necessary? What causes tristimulus colorimetry to “fail?” These questions can be answered through examination of various color appearance phenomena, several of which are described in this chapter. These phenomena represent instances in which one of the necessary requirements for the success of tristimulus colorimetry is violated. Understanding what causes these violations and the nature of the discrepancies is what allows the construction of color appearance models.

## 6.1 WHAT ARE COLOR APPEARANCE PHENOMENA?

Given two stimuli with identical CIE XYZ tristimulus values, they will match in color for an average observer as long as certain constraints are enforced.

These constraints include factors such as the retinal locus of stimulation, the angular subtense, and the luminance level. In addition, the two stimuli must be viewed with identical surrounds, backgrounds, size, shape, surface characteristics, illumination geometry, etc. If any of the above constraints are violated, it is likely that the color match will no longer hold. However, in many practical applications, the constraints necessary for successful color-match prediction using simple tristimulus colorimetry cannot be met. It is these applications that require colorimetry to be enhanced to include the influences of these variables. Such enhancements are color appearance models. The various phenomena that “break” the simple XYZ tristimulus system are the topics of the following sections of this chapter.

Figure 6.1 illustrates a simple example of one color appearance phenomenon: *simultaneous contrast* or *induction*. In Figure 6.1(a), the two gray patches with identical XYZ tristimulus values match in color since they are viewed under identical conditions (both on the same gray background). If one of the gray patches is placed on a white background and the other on a black background, as in Figure 6.1(b), the two patches no longer match in appearance, but their tristimulus values remain equal. Since the constraint that the stimuli are viewed in identical conditions is violated in Figure 6.1(b), tristimulus colorimetry can no longer predict a match. Instead, a model that includes the effect of background luminance factor on the appearance of the patches would be required.

Simultaneous contrast is just one of the many color appearance phenomena described in this chapter. Discussion of other phenomena addresses the effects of changes in surround, luminance level, illumination color, cognitive interpretation, and other viewing parameters. These phenomena justify the need to develop color appearance models and define the required input data and output predictions.

## 6.2 SIMULTANEOUS CONTRAST, CRISPENING, AND SPREADING

Simultaneous contrast, crispening, and spreading are three color appearance phenomena that are directly related to the spatial structure of the stimuli.

### Simultaneous Contrast

Figure 6.1 illustrates simultaneous contrast. The two identical gray patches presented on different backgrounds appear distinct. The black background causes the gray patch to appear lighter, while the white background causes the gray patch to appear darker. *Simultaneous contrast* causes stimuli to shift in color appearance when the color of their background is changed. These apparent color shifts follow the opponent theory of color vision in a contrasting sense along the opponent dimensions. In other words, a light background induces a stimulus to appear darker, a dark background

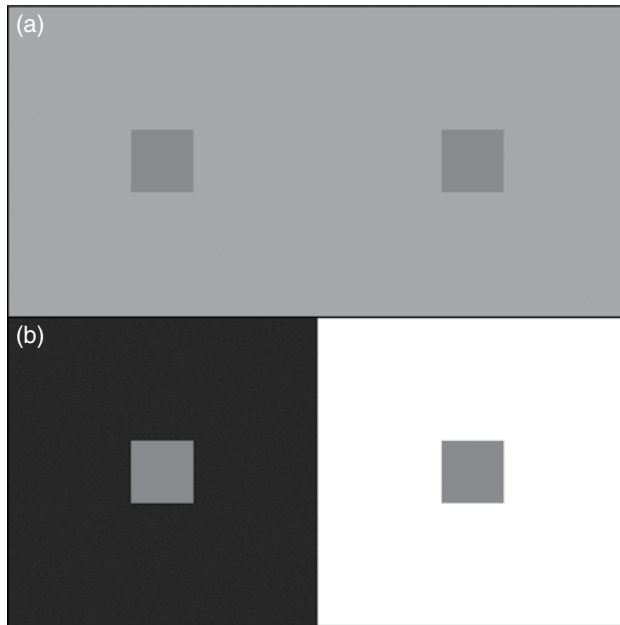


**Figure 6.1** An example of simultaneous contrast. The gray patches on the gray background (a) are physically identical to those on the white and black backgrounds (b)

induces a lighter appearance, red induces green, green induces red, yellow induces blue, and blue induces yellow. Josef Albers (1963), in his classic study, *Interaction of Color*, explores various aspects of simultaneous contrast and teaches artists and designers how to avoid pitfalls and take advantage of the effects. More complete explorations of the effect are available in classic color vision texts such as Hurvich (1981), Boynton (1979), and Evans (1948). Cornelissen and Brenner (1991) explore the relationship between adaptation and chromatic induction based on the concept that induction can be at least partially explained by localized chromatic adaptation. Blackwell and Buchsbaum (1988a) describe some of the spatial and chromatic factors that influence the degree of induction.

Robertson (1996) has presented an interesting example, reproduced in Figure 6.2, of chromatic induction that highlights the complex spatial nature of this phenomenon. The red squares in Figure 6.2(a) (or the cyan squares in Figure 6.2(b)) are all surrounded by the same chromatic edges (two yellow edges and two blue edges for each square). If chromatic induction were strictly determined by the colors at the edges, then all of the red squares and all of the cyan squares should appear similar. However, it is clear in Figure 6.2 that the squares that appear to be falling on the yellow stripes are subject to induction from the yellow and thus appear darker and bluer. On the other hand, the squares falling on the blue stripes appear lighter and yellower. Clearly, the simultaneous contrast for these stimuli is dependent on more of the spatial structure than

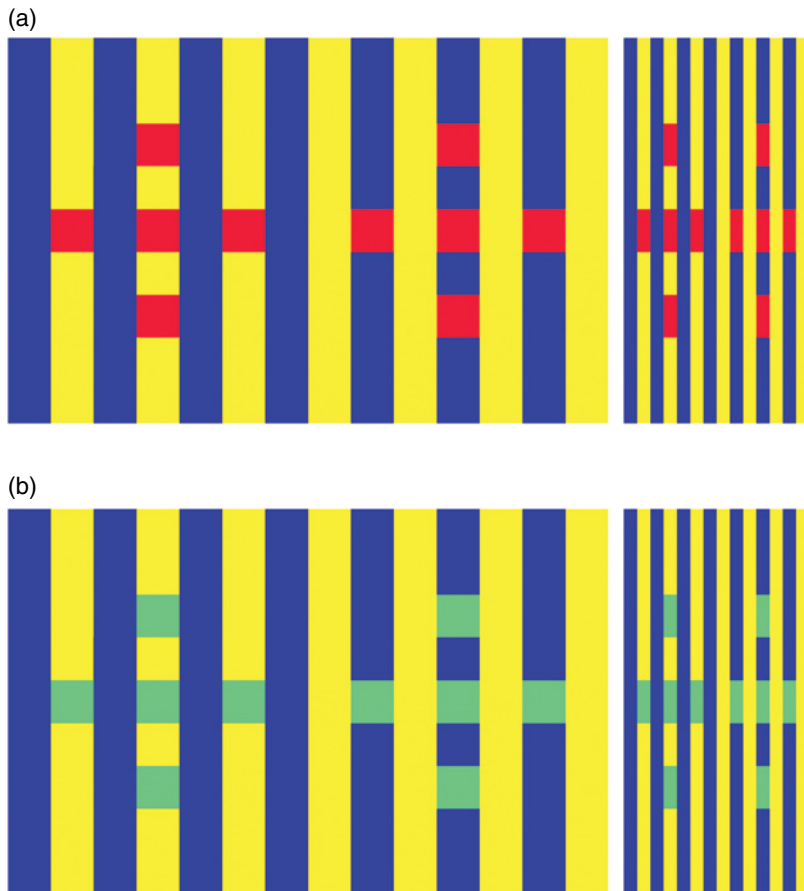


**Figure 6.2** Stimuli patterns that illustrate the complexity of simultaneous contrast. The local contrasts for the left and right sets of squares are identical. However, simultaneous contrast is apparently driven by the stripes on which the square patches appear to rest. The compressed panels to the right show the increased effect with smaller patch size (or higher spatial frequency). Tilt the page to one side and view the figure at a grazing angle to see an even larger effect

simply the local edges. The panels on the right side of Figure 6.2 have been compressed horizontally to illustrate the scale dependency of this effect. This phenomenon has been referred to as the *Chromatic White Effect*, but as White (2010) points out in a historical review of the gray-scale version of the effect (*White's Illusion*), it might be more properly referred to as the *Munker Illusion or Munker-White Illusion*. It has been the subject of various cognitive and computational explanations. While a Gestalt figure-ground explanation is common, Blakeslee and McCourt (1999) provide an interesting example of a computational vision model that can predict the effect.

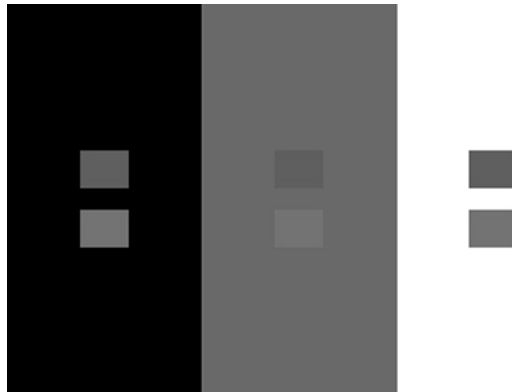


**Figure 6.3** An example of crispening. The pairs of gray patches are physically identical on all three backgrounds

## Crispening

A related phenomenon is crispening. *Crispening* is the increase in perceived magnitude of color differences when the background on which the two stimuli are compared is similar in color to the stimuli themselves. Figure 6.3 illustrates crispening for a pair of gray samples. The two gray stimuli appear to be of greater lightness difference on the gray background than on either the white or black backgrounds. Similar effects occur for color differences. Semmelroth (1970) published a comprehensive study on the crispening effect along with a model for its prediction. Whittle (1992) has published a more recent model in the context of perception of grayscale differences. The basis of crispening as a result of local adaptation was set in a classic paper by Craik (1939).

## Spreading

When the stimuli increase in spatial frequency, or become smaller, the simultaneous contrast effect disappears and is replaced with a spreading effect. Spreading refers to the apparent mixture of a color stimulus with its surround. This effect is complete at the point of spatial fusion when the stimuli are no longer viewed as discrete but fuse into a single stimulus (such as when a halftone image is viewed at a sufficient distance such that the individual dots cannot be resolved). Spreading, however, occurs at spatial frequencies below those at which fusion occurs (sometimes significantly so). Thus, the stimuli are still observed as distinct from the background, but their colors begin to blend.

Classic studies by Chevreul (1839) explored the importance of spreading and contrast in the design of tapestries where it was often desired to preserve the color appearance of design elements despite changes in spatial configuration and background color. Thus the tapestry designers were required to

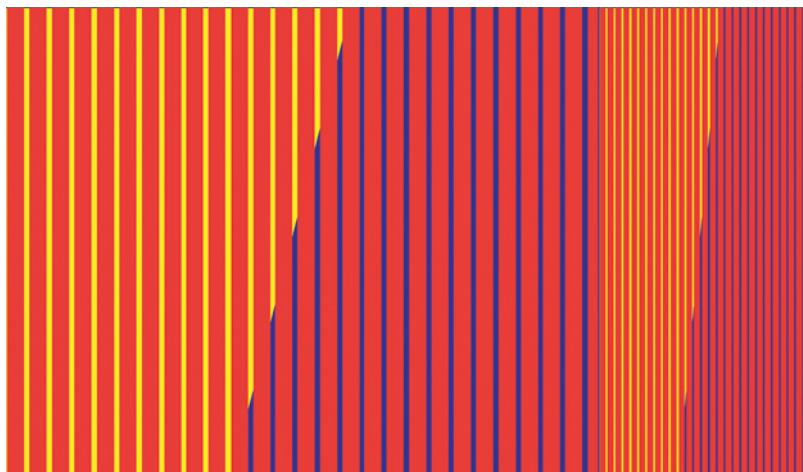


**Figure 6.4** An example of spreading. The red bars look bluer on the blue background and yellower on the yellow background. The magnitude of the effect depends on the relative spatial scale of all components in the pattern. The right side of the figure is a horizontally compressed version of the left side to increase spatial frequency of the red bars

physically change the colors used throughout the tapestry in order to preserve color appearance. A related, although more complex, phenomenon known as neon spreading is discussed by Bressan (1993). Neon spreading is an interesting combination of perceptions of spreading and transparency.

Figure 6.4 illustrates spreading along a color dimension. Colorimetrically identical red stimuli bars of various spatial frequency are presented on yellow or blue backgrounds. Depending on the spatial frequency of the overall pattern (rendered in a horizontal compression to the right; spatial frequency can also be increased by viewing the book from the side), various degrees of spreading can be observed. The general effect is for the red bars to appear more of a bluish-red when over the blue background and more of a yellowish-red over the yellow background. The dependency on spatial frequency can be explored by examining Figure 6.4 from various viewing distances and/or angles. Simultaneous contrast and spreading point to lateral interactions and adaptation effects in the human visual system.

### 6.3 BEZOLD–BRÜCKE HUE SHIFT (HUE CHANGES WITH LUMINANCE)

It is often assumed that hue can be specified by the wavelength of a monochromatic light. Unfortunately, this is not the case as illustrated by phenomena such as the Bezold–Brücke hue shift. This hue shift occurs when one observes the hue of a monochromatic stimulus while changing its luminance. The hue will not remain constant.

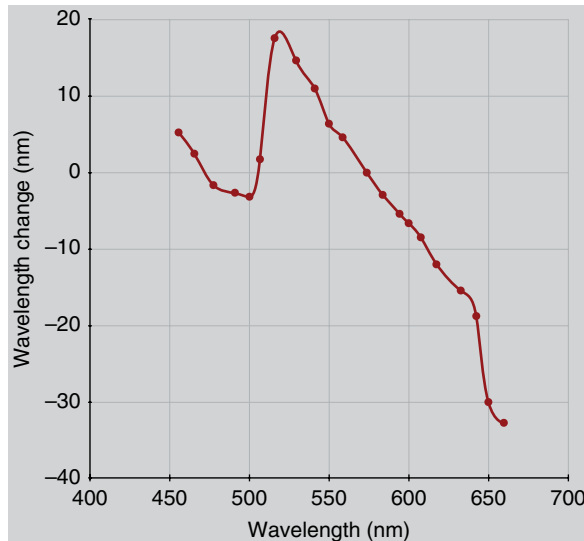


**Figure 6.5** Example data illustrating the Bezold–Brücke hue shift. Plot shows the wavelength shift required to maintain constant hue across a 10 $\times$  reduction in luminance

Some typical experimental results on the Bezold–Brücke hue shift have been reported by Purdy (1931). Figure 6.5 represents some of the results from the Purdy (1931) research. The data in Figure 6.5 indicate the change in wavelength required to preserve a constant hue appearance across a reduction in luminance by a factor of 10. For example, to match the hue of 650 nm light at a given luminance would require a light of 620 nm at one-tenth the luminance level (~30 nm shift). Recall that a given monochromatic light will have the same relative tristimulus values no matter what the luminance level (since absolute luminance level is usually not considered in tristimulus colorimetry). Thus, tristimulus values alone would predict that the color of a monochromatic light should remain constant at all luminance levels. Purdy's results clearly disprove that hypothesis and point to the need to consider the absolute luminance level in order to predict color appearance.

The Bezold–Brücke hue shift suggests that there are nonlinear processes in the visual system after the point of energy absorption in the cones, but prior to the point that judgments of hue are made. Savoie (1973) discusses some more modern data and modeling of the Bezold–Brücke hue shift. Hunt (1989) has shown that the Bezold–Brücke hue shift does not occur for related colors.

## 6.4 ABNEY EFFECT (HUE CHANGES WITH COLORIMETRIC PURITY)

If one were to additively mix white light with a monochromatic light of a given wavelength, the mixture would vary in colorimetric purity while retaining a constant dominant wavelength. Perhaps it is reasonable that a

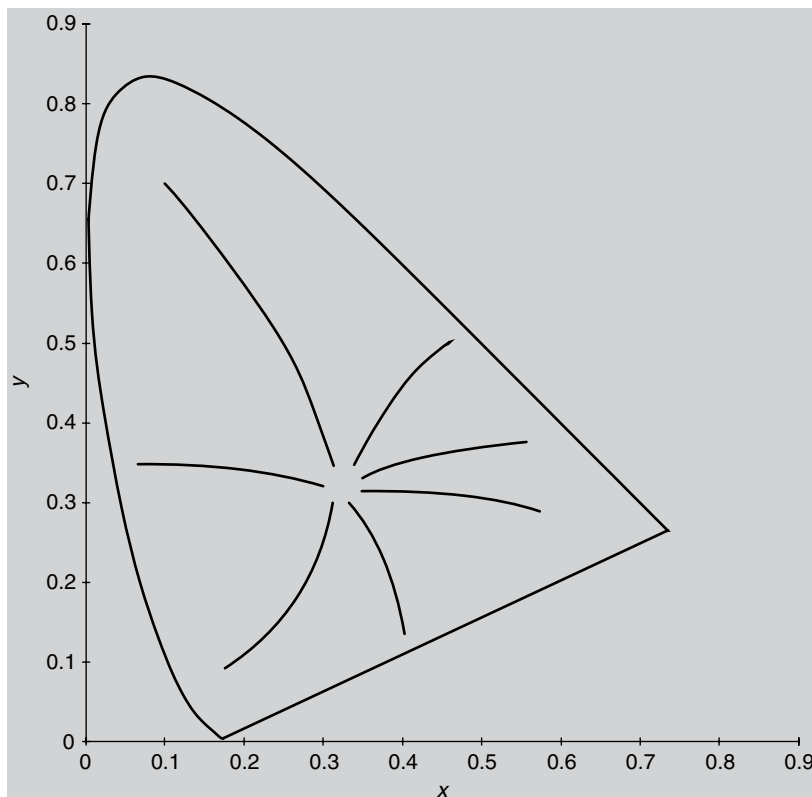


**Figure 6.6** Contours of constant hue in the CIE 1931 chromaticity diagram illustrating the Abney effect

collection of such mixtures, falling on a straight line between the white point and the monochromatic stimulus on a chromaticity diagram, would be of constant perceived hue. However, as the Bezold–Brücke hue shift illustrated, the wavelength of a monochromatic stimulus is not a good physical descriptor of perceived hue. Mixing a monochromatic light with white light also does not preserve constant hue. This phenomenon is known as the *Abney effect*.

The Abney effect can be illustrated by plotting lines of constant perceived hue for mixtures of monochromatic and white stimuli. Such results, from a study by Robertson (1970), are illustrated in Figure 6.6. Figure 6.6 shows several lines of constant perceived hue based on psychophysical results from three observers. The curvature of lines of constant perceived hue in chromaticity diagrams holds up for other types of stimuli as well. This can be illustrated for object color stimuli (related stimuli) by examining lines of constant Munsell hue from the Munsell renotation studies published by Newhall (1940), an example of which is illustrated in Figure 6.7.

To summarize, the Abney effect points out that straight lines radiating from the white point in a chromaticity diagram are not lines of constant

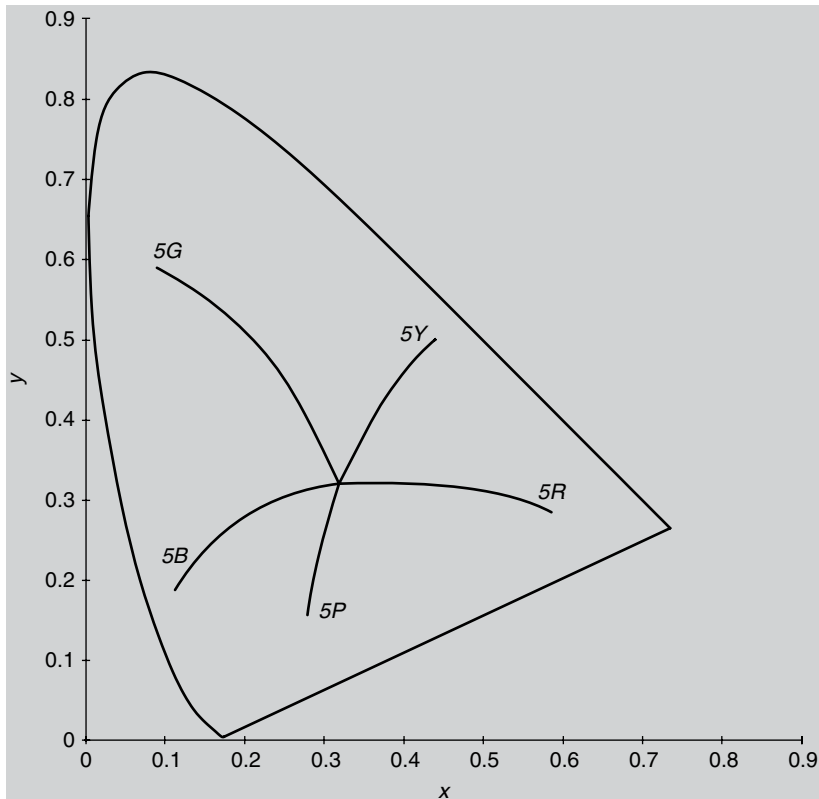


**Figure 6.7** Contours of constant Munsell hue at value 5 plotted in the CIE 1931 chromaticity diagram

hue. Like the Bezold–Brücke effect, the Abney effect suggests nonlinearities in the visual system between the stages of cone excitation and hue perception and was discussed by Purdy (1931). Recent experimental data on the Bezold–Brücke hue shift and Abney effect have been published by Ayama *et al.* (1987) and O’Neil *et al.* (2012).

## 6.5 HELMHOLTZ–KOHLRAUSCH EFFECT (BRIGHTNESS DEPENDS ON LUMINANCE AND CHROMATICITY)

In the CIE system of colorimetry, the Y tristimulus value defines the luminance, or luminance factor, of a stimulus. Since luminance is intended to represent the effectiveness of the various stimulus wavelengths in evoking the perception of brightness, it is often erroneously assumed that the Y tristimulus value produces a direct estimate of perceived brightness.

One phenomenon that confirms this error is known as the Helmholtz–Kohlrausch effect. This effect is best illustrated by examining contours of constant brightness-to-luminance ratio as shown in Figure 6.8 adapted

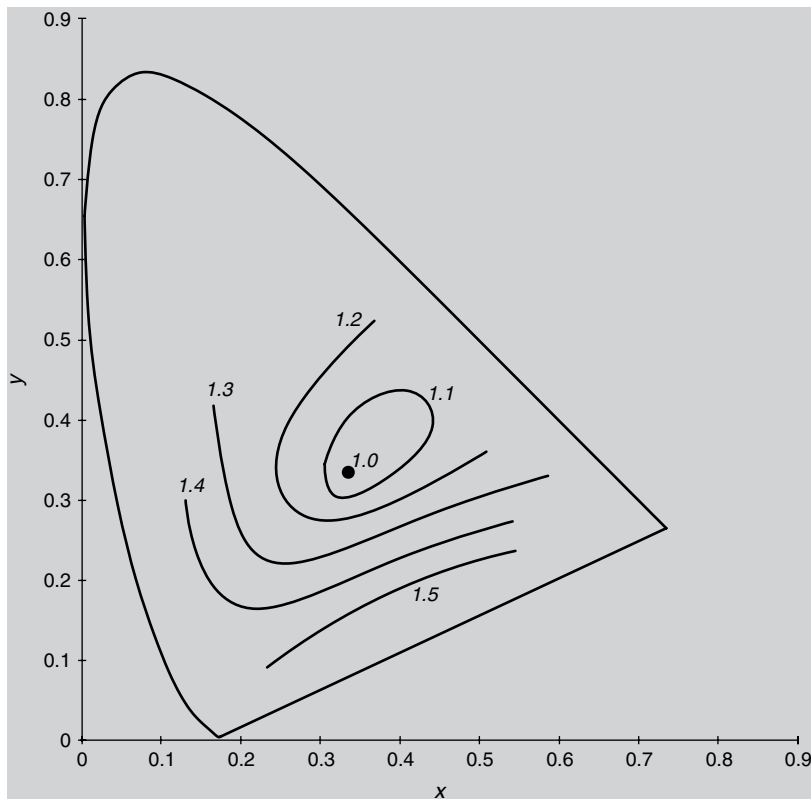


**Figure 6.8** Contours of constant brightness-to-luminance ratio illustrating the Helmholtz–Kohlrausch effect

from Wyszecki and Stiles (1982). The contours represent chromaticity loci of constant perceived brightness at a constant luminance. The labels on the contours represent the brightness of those chromaticities relative to the white point, again with constant luminance. These contours illustrate that, at constant luminance, perceived brightness increases with increasing saturation. They also illustrate that the effect depends upon hue.

Various approaches have been taken to model the Helmholtz–Kohlrausch effect. One such approach involves using the Ware and Cowan equations (Hunt 1991a). These equations rely on the calculation of a correction factor that depends on chromaticity as shown in Equation 6.1.

$$F = 0.256 - 0.184y - 2.527xy + 4.656x^3y + 4.657xy^4 \quad (6.1)$$

Correction factors are calculated for all of the stimuli in question and two stimuli are deemed to be equally bright if the equality in Equation 6.2 holds.

$$\log(L_1) + F_1 = \log(L_2) + F_2 \quad (6.2)$$

In Equation 6.2,  $L$  is luminance and  $F$  is the correction factor given by Equation 6.1.

The Ware and Cowan equations were derived for unrelated colors. Similar experiments have shown that the Helmholtz–Kohlrausch effect also holds for related colors. A review of some of this research and a derivation of a simple predictive equation was published by Fairchild and Pirrotta (1991). In this work, a correction to the CIELAB lightness predictor,  $L^*$ , was derived as a function of CIELAB chroma,  $C_{ab}^*$ , and hue angle,  $h_{ab}$ . The predictor of chromatic lightness,  $L^{**}$ , had the form of Equation 6.3.

$$L^{**} = L^* + f_2(L^*) f_1(h_{ab}) C_{ab}^* \quad (6.3)$$

Equation 6.3 describes the Helmholtz–Kohlrausch effect by adjusting the luminance-based predictor of lightness,  $L^*$ , with an additive factor of the chroma,  $C_{ab}^*$ , that is dependent upon the lightness and hue of the stimulus. Details of this predictor of lightness can be found in Fairchild and Pirrotta (1991).

An example of the Helmholtz–Kohlrausch effect can be witnessed by examining the samples of the *Munsell Book of Color*. Samples of constant Munsell value have been defined to also have constant luminance factor. Thus, as one examines Munsell chips of a given hue and value, the luminance factor is constant while chroma is changing. Examining such sets of chips illustrates that the higher chroma chips do appear brighter and that the magnitude of the effect depends on the particular hue and value being examined.

The Helmholtz–Kohlrausch effect illustrates that perceived brightness (and thus lightness) cannot be strictly considered a one-dimensional function of stimulus luminance (or relative luminance). As a stimulus becomes more chromatic, at constant luminance, it appears brighter. The differences between spectral luminous efficiency measured by flicker photometry (as in the  $V(\lambda)$  curve) and heterochromatic brightness matching (as described by the Helmholtz–Kohlrausch effect) as a function of observer age have been examined by Kraft and Werner (1994).

## 6.6 HUNT EFFECT (COLORFULNESS INCREASES WITH LUMINANCE)

Careful observation of the visual world shows that the color appearances of objects change significantly when the overall luminance level changes. Objects appear vivid and contrasty on a bright summer afternoon and more subdued at dusk. The Hunt effect and Stevens effect (Section 6.7) describe these attributes of appearance and are illustrated by the sequence of photographs simulating decreasing illumination levels shown in Figure 6.9.

The Hunt effect obtains its name from a study on the effects of light and dark adaptation on color perception published by Hunt (1952). In that



**Figure 6.9** A photographic simulation of the Hunt and Stevens effects in a scene. The leftmost image shows the appearance of a scene at high luminance levels (midday) with high levels of contrast and colorfulness. As luminance decreases moving to the right, the perceived contrast and colorfulness decreases until they reach the very low levels on the right that might represent illumination levels at dusk

study, Hunt collected corresponding colors data via haploscopic matching, in which each eye was adapted to different viewing conditions and matches were made between stimuli presented in each eye. Figure 6.10 shows a schematic representation of Hunt's results. The data points represent corresponding colorfulness perceptions for various levels of adaptation. What these results show is that a stimulus of low colorimetric purity viewed at  $10000\text{cd/m}^2$  is required to match a stimulus of high colorimetric purity viewed at  $1\text{cd/m}^2$ . Stated more directly, as the luminance of a given color stimulus is increased, its perceived colorfulness also increases.

The Hunt effect can be illustrated by viewing Figure 4.1 and imagining you are in the illuminated environment along with the rendered cubes. Note that the sides of the cubes with more illumination falling on them appear more colorful. The Hunt effect can also be witnessed by taking a color image, such as Figure 4.1, and changing the level of illumination under which it is viewed. When the image is viewed under a low level of illumination, the colorfulness of the various image elements will be quite low. If the image is then moved to a significantly brighter viewing environment (*e.g.*, a viewing booth or bright sunlight), the image elements will appear significantly more colorful. This effect is simulated in Figure 6.9.

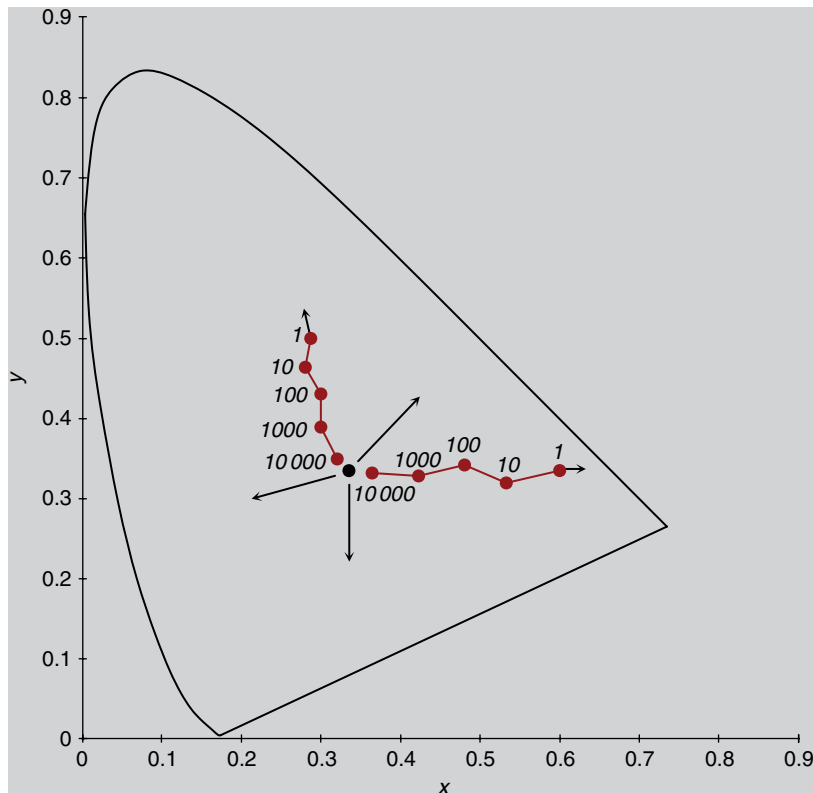


**Figure 6.10** A schematic representation of corresponding chromaticities across changes in luminance showing the Hunt effect. Points are labeled with luminance levels

The Hunt effect can be summarized by the statement that the colorfulness of a given stimulus increases with luminance level. This effect highlights the importance of considering the absolute luminance level in color appearance models – something that traditional colorimetry does not do.

## 6.7 STEVENS EFFECT (CONTRAST INCREASES WITH LUMINANCE)

The Stevens effect is a close relative of the Hunt effect. While the Hunt effect refers to an increase in chromatic contrast (colorfulness) with luminance, the Stevens effect refers to an increase in brightness (or lightness) contrast with increasing luminance. For the purposes of understanding these effects, contrast should be thought of as the rate of change of perceived brightness (or lightness) with respect to luminance. For a more complete discussion on contrast, refer to Fairchild (1995b).

Like the Hunt effect, the Stevens effect draws its name from a classic psychophysical study (Stevens and Stevens 1963). In this study, observers were asked to perform magnitude estimations on the brightness of stimuli across various adapting conditions. The results illustrated that the relationship between perceived brightness and measured luminance tended to follow a power function. This power function is sometimes referred to as Stevens power law in psychophysics. A relationship that follows a power function when plotted on linear coordinates becomes a straight line (with slope equal to the exponent of the power function) on log–log coordinates. Typical results from Stevens and Stevens (1963) experiments are plotted on logarithmic axes in Figure 6.11, which shows average relative brightness magnitude estimations as a function of relative luminance for four different adaptation levels. Figure 6.11 shows that the slope of this relationship (and thus the exponent of the power function) increases with increasing adapting luminance.

The Stevens effect indicates that, as the luminance level increases, dark colors will appear darker and light colors will appear lighter. While this prediction might seem somewhat counterintuitive, it is indeed the case. The Stevens effect can be demonstrated by viewing an image at high and low luminance levels. A black and white image is particularly effective for this demonstration. At a low luminance level, the image will appear of rather low contrast. White areas will not appear very bright and, perhaps surprisingly, dark areas will not appear very dark. If the image is then moved to a significantly higher level of illumination, white areas appear substantially

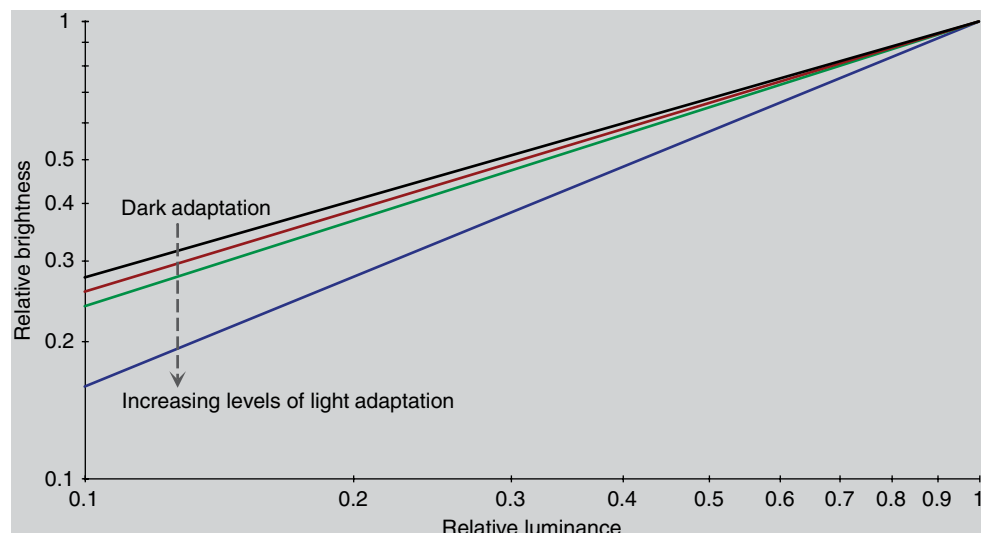


**Figure 6.11** Changes in lightness contrast as a function of adapting luminance according to the Stevens effect. Black curve is for dark adaptation while the red, green, and blue curves represent increasing levels of light adaptation, respectively

brighter and dark areas darker – the perceived contrast has increased. Figure 6.9 simulates this effect for a color image.

## 6.8 HELSON–JUDD EFFECT (HUE OF NON-SELECTIVE SAMPLES)

The Helson–Judd effect is elusive and perhaps cannot even be observed in normal viewing conditions. It is probably unimportant in practical situations. However, its description is included here since two color appearance models (Hunt and Nayatani *et al.*) make rather strong predictions of this effect. Thus it is important to understand its definition and consider its importance when implementing those models. The experimental data first describing the Helson–Judd effect were presented by Helson (1938).

In Helson's experiment, observers were placed in a light booth (effectively a closet) that was illuminated with nearly monochromatic light. They were then asked to assign Munsell designations (after a training period) to various non-selective (Neutral Munsell patches) samples. Typical results are illustrated in Figure 6.12 for a background of Munsell value 5/. Similar trends were observed on black and white backgrounds. Figure 6.12 shows the perceived chroma (in Munsell units) for non-selective samples of various Munsell values. The results indicate that these non-selective samples did not appear neutral under strongly chromatic illumination. Samples lighter than the background exhibited chroma of the same hue as the source

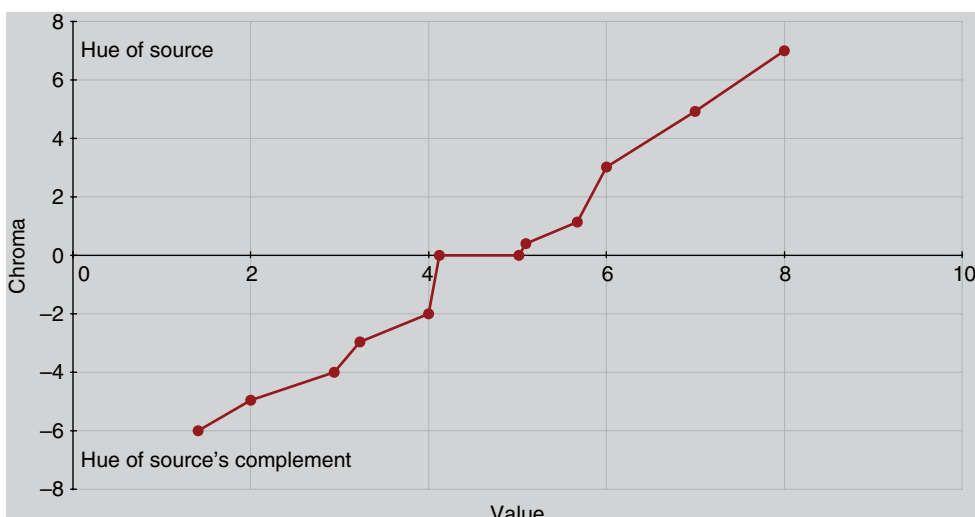


**Figure 6.12** A representation of some of the original Helson (1938) results illustrating the Helson–Judd effect. Munsell hue and chroma scaling of non-selective samples under a green source on a gray background

while samples darker than the background exhibited chroma of the hue of the source's complement. It is important to note that this effect only occurred for nearly monochromatic illumination. Helson (1938) stated that the effect completely disappeared if as little as 5% white light was added to the monochromatic light. Thus, the effect is of little practical importance since colored stimuli should never be evaluated under monochromatic illumination.

However, the effect is predicted by some color appearance models and has been observed in one recent experiment (Mori *et al.* 1991). The Mori *et al.* experiment was performed with haploscopic viewing (each eye adapted differently), which might increase the chance of observing the Helson–Judd effect. However, it is not possible to observe or demonstrate the Helson–Judd effect under normal viewing conditions. This raises an interesting question with respect to the original Helson (1938) study. Why was the effect so large? While this question cannot be directly answered, perhaps the effect was caused by incomplete chromatic adaptation (explaining the hue of the light samples) and chromatic induction (explaining the hue of the dark samples). In normal viewing situations, cognitive mechanisms are thought to “discount the illuminant” and thus result in the preservation of achromatic appearance of non-selective samples. Perhaps Helson's monochromatic chamber and more recent haploscopic viewing experiments did not allow these cognitive mechanisms to fully function. Another difficulty with the Helson results is that observers scaled chroma as high as 6–8 Munsell units for samples with values less than 2. Such perceptions are not possible in the object mode since value 2 is nearly black and an object cannot appear both that dark and highly chromatic at the same time. It seems that observers see a highly chromatic “glowing light” superimposed on the dark objects under these viewing conditions. This is consistent with an explanation through simultaneous contrast and incomplete adaptation.

Recent attempts to demonstrate the Helson–Judd effect in the author's laboratory have verified the unique nature of the percept. The effect cannot be observed with complex stimuli. It is only observed when individual non-selective patches are viewed on a uniform background. (Even a step tablet of non-selective stimuli of various reflectances is too complex to produce the effect.) Also, nearly monochromatic light is required as originally reported by Helson (1938). Under these conditions, observers do report a “glowing light” of the hue complementary to the light source superimposed on the samples darker than the background. Interestingly, only about 50% of observers report seeing any effect at all.

While the practical importance of the Helson–Judd effect might be questionable, it does raise some interesting questions and warrants consideration since it influences the predictions of some color appearance models. To review, the Helson–Judd effect suggests that non-selective samples, viewed under highly chromatic illumination, take on the hue of the light source if they are lighter than the background and take on the complementary hue if they are darker than the background.

## 6.9 BARTLESON–BRENEMAN EQUATIONS (IMAGE CONTRAST CHANGES WITH SURROUND)

While Stevens and Stevens (1963) showed that perceived contrast increased with increasing luminance level, Bartleson and Breneman (1967) were interested in the perceived contrast of elements in complex stimuli (images) and how it varied with luminance level and surround. They observed results similar to those described by the Stevens effect with respect to luminance changes, but they also observed some interesting results with respect to changes in the relative luminance of an image's surround.

Their experimental results, obtained through matching and scaling experiments, showed that the perceived contrast of images increased when the image surround was changed from dark to dim to light. This effect occurs because the dark surround of an image causes dark areas to appear lighter while having little effect on light areas (white areas still appear white despite changes in surround). Thus, since there is more of a perceived change in the dark areas of an image than in the light areas, there is a resultant change in perceived contrast.

These results are consistent with the historical requirements for optimum image tone reproduction. Photographic prints viewed in an average surround are reproduced with a one-to-one relationship between relative luminances in the original scene and the print. Photographic transparencies intended for projection in a dark surround are reproduced with a system transfer function that is a power function with an exponent of approximately 1.5 (roughly that is a photographic gamma of 1.5 for the complete system). This is one reason transparencies, or projected images, are produced with a physically higher contrast in order to counteract the reduction in perceived contrast caused by the dark surround. Similarly, television images, typically viewed in a dim surround, are reproduced using a power function with an exponent of about 1.25 (roughly the gamma for the complete television system). More details regarding the history and importance of surround compensation in image reproduction can be found in Hunt (1995) and Fairchild (1995b). It should also be noted that the magnitude of the surround effect is very dependent on individual observers, image size, and the viewing task. For example, if the observers are given a task that has them focus intently on the central parts of the image, then any surround effect can be completely eliminated (Fairchild and Johnson 1999, Liu and Fairchild 2007).

Bartleson and Breneman (1967) published equations that predict their experimental results quite well. Bartleson (1975), in a paper on optimum image tone reproduction, published a simplified set of equations that are of more practical value. Figure 6.13 illustrates predictions of perceived lightness as a function of relative luminance for various surround conditions according to results of the type described by Bartleson and Breneman. This plot is virtually identical to the results of Stevens and Stevens given in Figure 6.11 on logarithmic axes. The straight lines of various slopes on

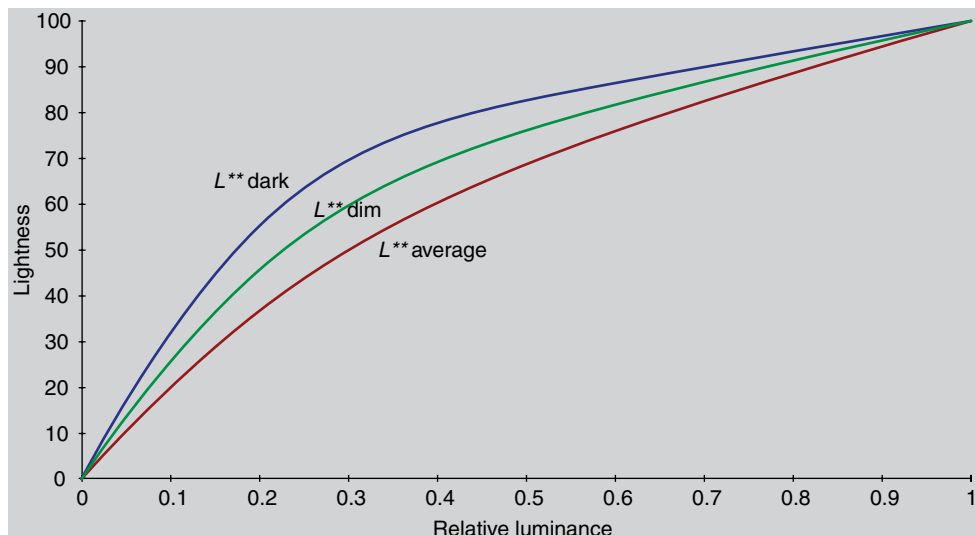


**Figure 6.13** Changes in lightness contrast as a function of surround relative luminance according to the results of Bartleson and Breneman (Bartleson 1975)

logarithmic axes transform into power functions with various exponents on linear axes such as those in Figure 6.13. Color appearance models such as Hunt's, RLAB, and the CIE models include predictions of the surround effects on perceived contrast of images.

Often, when working at a computer workstation, users turn off the room lights in order to make the CRT display appear of higher contrast. This produces a darker surround that should perceptually lower the contrast of the display. The predictions of Bartleson and Breneman are counter to everyday experience in this situation. The reason for this is that the room lights are usually introducing a significant amount of reflection off the face of the monitor and thus reducing the physical contrast of the displayed images. If the surround of the display can be illuminated without introducing reflection off the face of the display (*e.g.*, by placing a light source behind the monitor that illuminates the surrounding area), the perceived contrast of the display will actually be higher than when it is viewed in a completely darkened room.

## 6.10 DISCOUNTING-THE-ILLUMINANT

Mechanisms of chromatic adaptation can be classified as sensory or cognitive. It is well established (Fairchild 1992b, 1993a, Hunt and Winter 1975) that sensory mechanisms are not capable of complete chromatic adaptation. However, under most typical viewing conditions, observers perceive colored objects as if adaptation to the color of the illumination were complete (*i.e.*, a white object appears white under tungsten light, fluorescent

light, or daylight). Since the sensory mechanisms are incapable of mediating such perceptions, it can be shown that cognitive mechanisms (based on knowledge about objects, illumination, and the viewing environment) take over to complete the job. Further details of these different mechanisms of adaptation are presented in Chapter 8.

Discounting-the-illuminant refers to the cognitive ability of observers to interpret the colors of objects based on the illuminated environment in which they are viewed. This allows observers to perceive the colors of objects more independent of changes in the illumination and is consistent with the typical notion that color somehow “belongs” to an object. Discounting-the-illuminant is important to understand and has been allowed for in some color appearance models (*e.g.*, Hunt and RLAB). It is of importance in imaging applications where comparisons are made across various media. For example, when viewing prints, observers will be able to discount the illumination color. However, when viewing a computer display, there are no illuminated objects and discounting-the-illuminant does not occur. Thus in some situations it might be necessary to model this change in viewing mode.

There is a significant amount of recent research that addresses issues related to changes in color appearance induced by complex stimulus structure and observer interpretation. Examples of relevant references include Gilchrist (1980), Arend and Reeves (1986), Arend and Goldstein (1987, 1990), Schirillo *et al.* (1990), Arend *et al.* (1991), Arend (1993), Schirillo and Shevell (1993, 1996), Schirillo and Arend (1995), and Cornelissen and Brenner (1995). Recent work by Craven and Foster (1992) and Speigle and Brainard (1996) addresses the ability of observers to detect changes in illumination separate from changes in object colors. Lotto and Purves (2002), Purves *et al.* (2002), and Purves and Lotto (2003) have brought these concepts together nicely in an empirical theory of color perception.

## 6.11 OTHER CONTEXT, STRUCTURAL, AND PSYCHOLOGICAL EFFECTS

There are a wide variety of color appearance effects that depend on the structure and/or context of the stimuli. Some of these fall into the category of optical illusions and others present interesting challenges to traditional colorimetry and, at times, color appearance modeling.

There are many interesting optical illusions, and almost every good text on color or vision includes a number of interesting illusions (Barlow and Mollon 1982, Hurvich 1981, Wandell 1995). Thus, they will not be repeated here. However, a few examples do help to illustrate the importance of context and structural effects on color appearance. Figure 6.14 shows a structural illusion that has little to do with color, but does illustrate the importance of surround. The two central circles in Figure 6.14 are of physically identical diameter. However, the one surrounded by larger circles appears smaller than the other. While this effect does not specifically address color

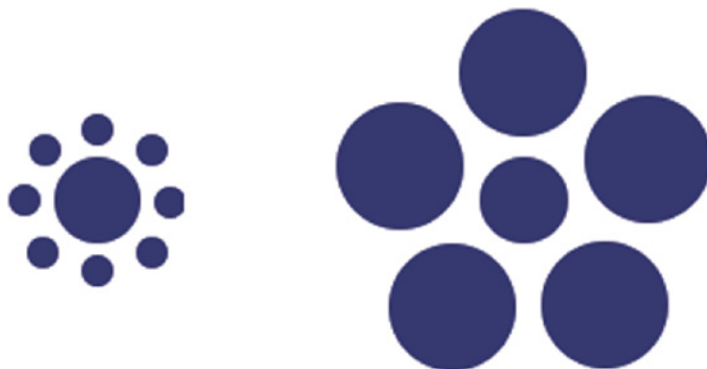


**Figure 6.14** An example of simultaneous contrast in shape. The central circles in the two patterns are identical in size

issues, it does show how spatial variables can influence appearance, and there is certainly an interaction between spatial and chromatic perceptions. In terms of color appearance, size, shape, and spatial structure can have important effects. In general, larger stimuli appear lighter and less chromatic, probably due to local adaptation to the stimulus itself. Xiao *et al.* (2009, 2010, 2011) have published some recent work on size and context effects in color appearance.

Various transparency effects help to illustrate the interaction of spatial and chromatic perceptions. One such demonstration has been constructed by Adelson (1993). Figure 6.15(a) shows two rows of identical gray diamonds. In Figure 6.15(b), tips of two different gray levels have been added to the diamonds with little or no effect on the appearance of the diamonds themselves. In Figure 6.15(c), the same diamonds have been partially placed on two different backgrounds. Since parts of the diamonds overlap the two backgrounds, the change in the appearance of the two rows is again minimal. However, in Figure 6.15(d), a more complete picture has been put together in which both the backgrounds and the tips have been added to the diamonds. Now there is a significant perceptual difference between the two rows of diamonds since the difference between them can be cognitively interpreted as either a transparency or shadow effect. The same demonstration can be completed in color by using, for example, yellow and blue backgrounds and tips. This demonstration illustrates that it is not just the spatial configuration of the stimuli, but their perceptual interpretation that influences appearance. Figure 6.16 illustrates a similar effect in a real scene where the darkening effect of the shadow on the side of the building is easily discounted (see also discounting-the-illuminant in Section 6.10 as Figure 6.16 provides an example). Additional recent psychophysical data related to stimulus structure and appearance can be found in the work of Logvinenko and Menshikova (1994) and Taya *et al.* (1995). Not completely unrelated are the various perceptual phenomena of “filling-in,” which are discussed in recent work by De Weerd *et al.* (1998).

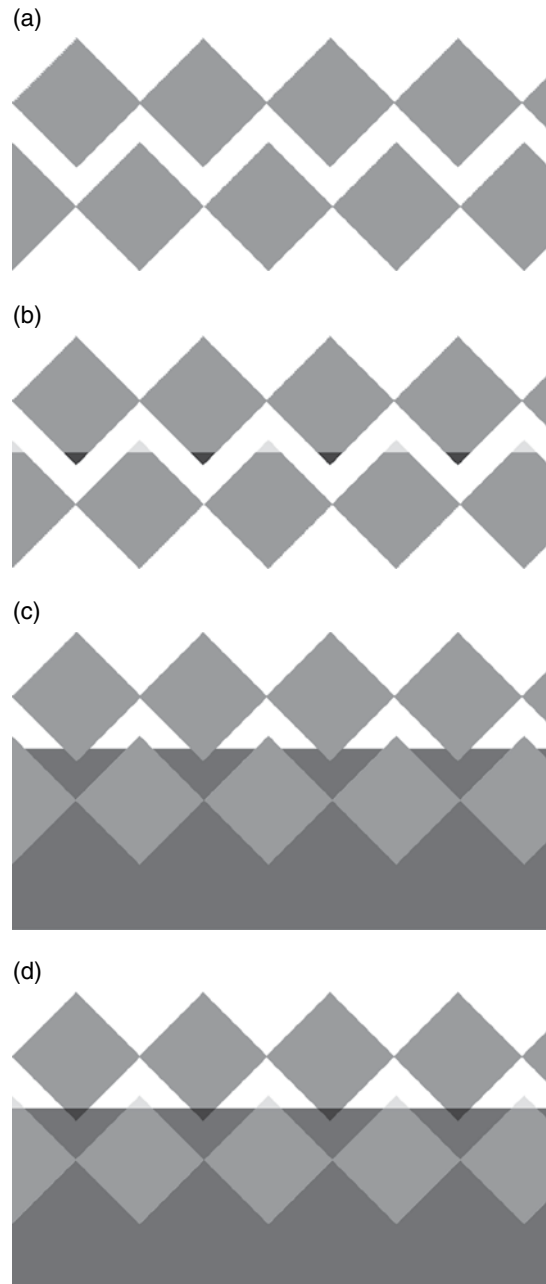


**Figure 6.15** An apparent contrast effect that depends on interpretation of spatial structure. (a) Two rows of identical gray diamonds. (b) The same diamonds with tips added that have little influence on their appearance. (c) The same diamonds on two backgrounds that have little influence on appearance since the diamonds overlap both backgrounds. (d) The combination of the tips and backgrounds on the same diamonds. In (d) there is a striking appearance change since the lower row of diamonds can be interpreted as light objects that are partially in a shadow or behind a filter



**Figure 6.16** Discounting-the-illuminant in the real world. We are able to easily see that the side of the shed is white paint in the shadow while the roof is made up of dark gray shingles in direct sunlight even though the absolute luminance levels of the two areas circled in yellow in the lower panel are identical. Even in the image, the white area looks brighter because we discount the differential illumination. (The effect is even larger in real-world scenes.)

Other evidence of important structural effects on color appearance has been reported by Shevell (1993, 2012). In the earlier experiments, simple spatial structures were added to the surrounds of colored stimuli with profound effects that could not be explained by the usual theories of simultaneous contrast and adaptation. Shevell (2012) reviews a collection of such works over several studies. Such results highlight the importance of considering spatial and color variables in conjunction with one another, not as separate entities. While various color appearance models do include spatial variables in a simple way, more complex approaches along the lines of those suggested by Poirson and Wandell (1993) need to be explored further.

Other interesting color demonstrations and effects rely to some degree on cognitive interpretation of the structure and context of the stimuli. Classic experiments on memory color that are often described in sensation and perception textbooks fall into this category. Memory color refers to the idea that observers remember prototypical colors for familiar objects. In image reproduction, objects such as sky, skin, and foliage are often mentioned (Bartleson 1960, Hunt 1995, Hunt *et al.* 1974). Other examples include simple experiments (which are quite repeatable!) in which, for example, cutouts in the shape of a tomato and a banana are made from orange construction paper, and observers are asked to scale the color appearance of the two objects. The orange cutout in the shape of the banana will typically be perceived as slightly more yellow than an arbitrary shape cut out of

the same paper and the cutout in the shape of a tomato will be perceived as more red. These effects are small, but consistent, and reiterate the importance of observers' interpretations of stimuli. Additional experimental results on the characteristics of color memory have been published by Nilsson and Nelson (1981) and Jin and Shevell (1996).

## Two-Color Projections

Partially related to memory color are the somewhat famous two-color projections that were demonstrated by Land (1959) and apparently included a full range of color appearances despite not having the three primaries required by conventional colorimetric theory. Figure 6.17 illustrates the process of the two-color projection. The original color image (Figure 6.17(a)) is separated into three black and white positive transparencies (Figure 6.17(b)), representing the red, green, and blue information, as done in Maxwell's (1858–1862) original color photographic process. Normally, the three transparencies would be projected through red, green, and blue filters and superimposed to produce an accurate reproduction of the original (as in Figure 6.17(a)). In the Land two-color projection, however, the red separation is projected through a red filter, the green separation is projected with white light, and the blue separation is not projected at all (Figure 6.17(c)). While one might expect such a projection could only produce a pinkish image, the result does indeed appear to be fairly colorful (although not nearly as colorful as a three-color projection to which Land apparently never made a direct comparison!). The quality of the two-color projection depends on the subject matter since the effect is strengthened if memory color can be applied. In fact, Kodak patented a two-color system, called Kodachrome (they went on to use that name on other products), in 1915, several decades before Land's accidental rediscovery (McCarthy 1987). There were also other commercial systems such as two-color Technicolor that was used in motion pictures and originated in 1916. Figure 6.18 shows an image from a two-color (orange/cyan) Kodachrome plate of George Eastman in 1914. As with Land's two-color projections, skin tones were a preferred subject. The remainder of the colors appearing in the two-color projection can be quite easily explained by simultaneous contrast and chromatic adaptation (Judd 1960, Valberg and Lange-Malecki 1990).

Cognitive aspects of color appearance and recognition are of significant interest, but largely outside the scope of this book. An interesting monograph on the subject has been published by Davidoff (1991). It is noteworthy that the cognitive model proposed by Davidoff is consistent with the various interpretations of color appearance necessary to explain the phenomena and models described in this book. The topic of cognitive aspects of color appearance cannot be fully considered without reference to the classic work of Katz (1935) that provides fascinating insight into the topic. The more recent work of Purves and Lotto (2003) on a so-called empirical theory of color vision also represents a cognitive-type model of color appearance.

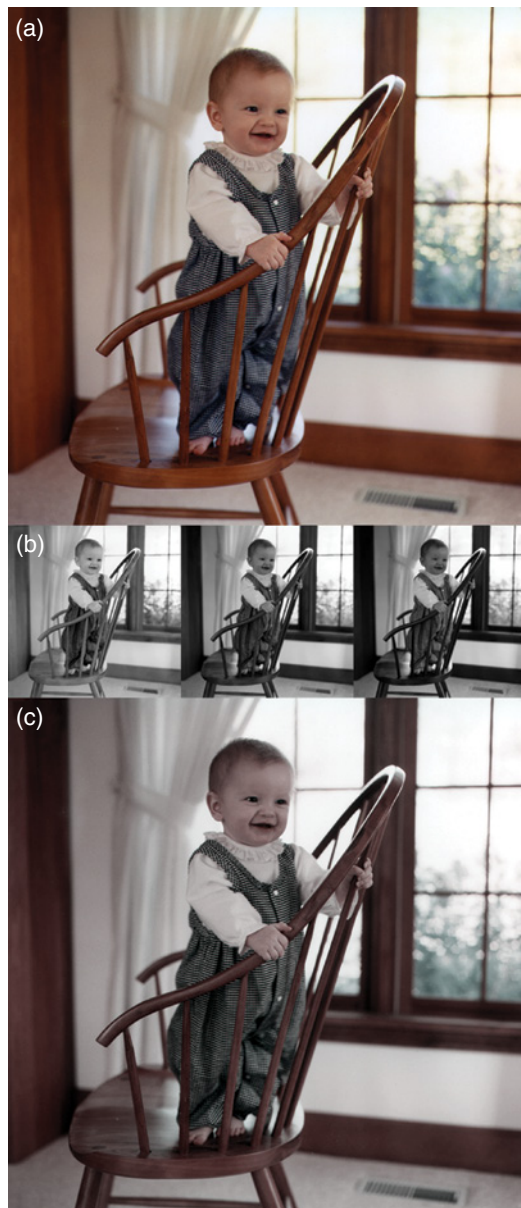


**Figure 6.17** Example of a two-color image reproduction. (a) Original full-color image. (b) Red, green, and blue separations of the image. (c) Combination of the red separation “projected” through a red filter and the green separation “projected” with white light



**Figure 6.18** Portrait of George Eastman circa 1914. Color plate, assembly process. This image was made with the early (patented in 1915) two-color Kodachrome process using a low-density greenish-cyan plate (from a green exposure) and a high-density orange plate (from a red exposure) sandwiched to create a single transparent plate. Courtesy of George Eastman House, International Museum of Photography and Film

Purely psychological effects, such as influence of color on mood, are also of significant interest (if not scientific elucidation) and can be related to color appearance effects. Overall treatments of color and human response can be found in Babbitt (1967), who focuses on the interplay between color and health, and Birren (1978), who provides a scientifically sound and appropriately skeptical treatment of the influence of color on humans. While color can, and certainly does, influence human emotion and sometimes performance, the effect is most often an individual one and the strength varies significantly from person to person. So decisions such as painting a room blue because it is calming cannot be made with any sort of universal certainty.

A few recent studies have, however, shown some fundamental psychological responses that are statistically significant (note that still does not make them universal). For example, Elliot and Niesta (2008) and Elliot *et al.* (2009) have shown that viewing the color red produces an avoidance response that

reduces performance on academic exams, but also, and somewhat counter to the first result, red clothing makes a woman appear more attractive than other colors. (The conclusion from the two studies that is just begging to be made is that seeing a woman dressed in red makes a man more attracted to her, but also makes him less able to perform.) The attraction to red was recently confirmed by Guéguen (2012) who found that women hitchhikers dressed in red were more attractive to drivers considering who to pick up. Another interesting color-psychology interaction was found in the study of aggression in professional ice hockey as influenced by uniform color (Webster *et al.* 2011).

## 6.12 COLOR CONSTANCY?

Color constancy is another phenomenon that is often discussed and often misunderstood. Typically, color constancy is defined as the apparent invariance in the color appearance of objects upon changes in illumination. This definition is somewhat misleading. The main reason for this is because color constancy does not exist in humans! The data presented in the previous sections of this chapter and the discussion of chromatic adaptation in Chapter 8 should make this point abundantly clear.

An interesting thought experiment also points out the difficulty with the term *color constancy*. If the colors of objects were indeed constant, then one would not have to include the light source in colorimetric calculations in order to predict color matches. In fact, color appearance models would not be necessary as CIE XYZ colorimetry would define color appearance for all viewing conditions. Clearly, this is not the case as demonstrated, sometimes painfully, by metamerically object color matches. Such objects match in color under one light source, but mismatch under others. Clearly, both objects in a metamerically pair cannot be color constant.

Then why does the term color constancy exist? Perhaps a quote from Evans (1943: 596) answers that question best;

*...in everyday life we are accustomed to thinking of most colors as not changing at all. This is due to the tendency to remember colors rather than to look at them closely.*

When colors are closely examined, the lack of color constancy becomes extremely clear. The study of color appearance and the derivation of color appearance models are, in fact, aiming to quantify and predict the failure of color constancy. Examples of recent data are presented in the research of Blackwell and Buchsbaum (1988b), Foster and Nascimento (1994), Kuriki and Uchikawa (1996), and Bäuml (1999).

Despite the lack of evidence that it exists (and the strong evidence that it does not), there still remains a great deal of interest in the concept of color constancy. At first this might seem strange, given the strength of the data. However, the study of color constancy can potentially lead to theories

describing how the human visual system might strive for approximate color constancy and the fundamental limitations preventing color constancy in the real world. Such studies take place in the arena of computational color constancy with potentially important and useful applications in machine vision (see, e.g., Drew and Finlayson 1994, Finlayson *et al.* 1994a,b, Maloney and Wandell, 1986). Xiao *et al.* (2012) and Brainard and Maloney (2011) present some of the more recent thinking on computational models of color constancy and experimental results on human limitations in separating the effects of object and illuminant on color appearance.

Jameson and Hurvich (1989) discussed some interesting concepts in regard to color constancy, the lack thereof in humans, and the utility in not being color constant that are suitable to end this chapter. They pointed out the value of having multiple mechanisms of chromatic adaptation, thus producing imperfect color constancy and retaining information about the illumination, to provide important information about changes, such as weather, light, and time of day, and the constant physical properties of objects in the scene.

# Viewing Conditions

---

Some of the various color appearance phenomena that produce the need for extensions to basic colorimetry were presented in Chapter 6. It is clear from these phenomena that various aspects of the visual field impact the color appearance of a stimulus. In this chapter, practical definitions and descriptions of the components of the viewing field that allow the development of reasonable color appearance models are given along with the required colorimetric measurements for these components. Accurate use of color appearance models requires accurate definition and measurement of the various components of the viewing field.

Different configurations of the viewing field will result in different cognitive interpretations of a stimulus and, in turn, different color perceptions. The last part of this chapter includes explanations of some of these phenomena and definitions of the various modes of viewing that can be observed for colored stimuli. Understanding these modes of viewing can help explain why seemingly physically identical stimuli can appear significantly different in color.

Related to the specification of viewing fields for color appearance models are the various definitions of standard viewing conditions used in different industries. These attempt to minimize difficulties with color appearance by defining appropriate viewing field configurations. One example of such a standard is the ANSI (1989) standard defining viewing conditions for prints and transparencies.

## 7.1 CONFIGURATION OF THE VIEWING FIELD

The color appearance of a stimulus depends on the stimulus itself as well as other stimuli that are nearby in either space or time. Temporal effects, while important, are generally not encountered in typical color appearance applications. They are dealt with by ensuring that observers have had adequate time to adapt to the viewing environment and by presenting

stimuli that do not vary in time. (Of course, there are several more recent applications, such as digital cinema, that will push color appearance studies toward the domain of temporal variation.) The spatial configuration of the viewing field is always of critical importance. (Since the eyes are constantly in motion it is impossible, in practical situations, to separate spatial and temporal effects.) The ideal spatial representation of the visual field would be to have a fully specified image of the scene. Such an image would have to have a spatial resolution greater than the visual acuity of the fovea, and each pixel would be represented by a complete spectral power distribution. With such a representation of the entire visual field, one would have almost all of the information necessary to specify the color appearance of any element of the scene from a specific location; however, cognitive experience of the observer and temporal information would still be missing. Some interesting recent data on the impact of the spatial configuration of stimulus and surround were published by Abramov *et al.* (1992).

Such a specification of the viewing field is not practical for several reasons. First, the extensive data required are difficult to obtain accurately, even in a laboratory setting. It is not plausible to require such data in practical applications. Second, even if the data could be obtained, the sheer volume would make its use quite difficult. Third, assuming these technical issues were overcome, one would then require a color appearance model capable of utilizing all of that data. Such a model does not exist and is not likely to be developed in the foreseeable future. When the inter-observer variability in color appearance judgments is considered, such a detailed model would certainly be unnecessarily complex.

Given all of the above limitations, the situation is simplified by defining a minimum number of important components of the viewing field. The various color appearance models use different subsets of these viewing field components. The most extensive set is the one presented by Hunt (1991b, 1995) for use with his color appearance model. Since Hunt's definition of the viewing field includes a superset of the components required by all other models, his definitions are presented below. The viewing field is divided into four components:

1. Stimulus
2. Proximal field
3. Background
4. Surround.

Figure 7.1 schematically represents these components of the visual field.

## Stimulus

The *stimulus* is defined as the color element for which a measure of color appearance is desired. Typically, the stimulus is taken to be a uniform patch of about  $2^\circ$  angular subtense. Figure 7.1 illustrates a  $2^\circ$  stimulus

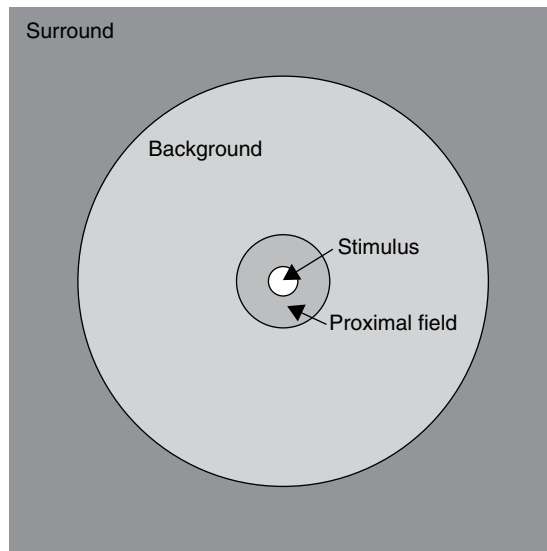


**Figure 7.1** Specification of components of the viewing field. When viewed from a distance of 20 cm, the angular subtenses are correct (*i.e.*, the 2° stimulus area will actually subtend a visual angle of 2°)

when viewed from 20 cm. (For additional references, the width of your thumbnail, viewed at arm's length, is approximately 1° of visual angle and the width of the full moon is about 0.5°.) A stimulus of approximately 2° subtense is assumed to correspond to the visual field appropriate for use of the CIE 1931 standard colorimetric observer. The 1931 observer is considered valid for stimuli ranging from 1° to 4° in angular subtense (CIE 1986). Trichromatic vision breaks down for substantially smaller stimuli and the CIE 1964 supplementary standard colorimetric observer should be considered for use with larger stimuli (10° or greater angular subtense).

The inhomogeneity of the retina with respect to color responsivity is a fundamental theoretical limitation to this definition of the stimulus. However, it is a practical necessity that has served basic colorimetry well since 1931. A more practical limitation, especially in imaging applications, is that the angular subtense of image elements is often substantially smaller than 2° and rarely as large as 10°. Fortunately, such limitations are often nulled, since in color reproduction, the objective is to reproduce a nearly identical spatial configuration of colors (*i.e.*, the image). Thus any assumptions that are not completely valid are equally violated for both the original and the reproduction. Care should be taken, however, when reproducing images with significant size changes or when trying to reproduce a color from one scene in a completely different visual context (*e.g.*, spot color or sampling color from an image).

When viewing real scenes, observers often consider an entire object as a “uniform” stimulus. For example, one might ask what color is that car? Even though different areas of the car will produce widely different color appearances, most observers would reply with a single answer. Thus, the

stimulus is not a  $2^\circ$  field, but the entire object. This occurs to a limited extent in images, but it is more conceivable for observers to break an image apart into smaller image elements.

## Proximal Field

The *proximal field* is defined as the immediate environment of the stimulus extending for about  $2^\circ$  from the edge of the stimulus in all, or most, directions. Definition of the proximal field is useful for modeling local contrast effects such as lightness or chromatic induction, crispening, or spreading. Of current models, only Hunt's model (1991b) distinguishes the proximal field from the background.

While knowledge of the proximal field is necessary for detailed appearance modeling, it is often impractical to specify it precisely. For example, in an image, the proximal field for any given element would be defined by its surrounding pixels. While these data are available (at least in digital imaging applications), utilizing them should require the parameters of the color appearance model to be recalculated for each spatial location within the image. Often, such computations are prohibitive and probably of little practical value. In cases where the proximal field is not known, it is normally specified to be equal to the background.

## Background

The *background* is defined as the environment of the stimulus, extending for about  $10^\circ$  from the edge of the stimulus (or proximal field, if defined) in all, or most, directions. Specification of the background is absolutely necessary for modeling simultaneous contrast. If the proximal field is different, its specification can be used for more complex modeling.

Like the proximal field, it becomes difficult to define the background in imaging applications. When considering a given image element, the background is usually made up of the surrounding image areas, the exact specification of which will change with image content and from location to location in the image. Thus, precise specification of the background in images would require point-wise recalculation of appearance model parameters. Since this is impractical in any typical applications, it is usually assumed that the background is constant and of some medium chromaticity and luminance factor (*e.g.*, a neutral gray with 20% luminance factor). Alternatively, the background can be defined as the area immediately adjacent to the image. However, such a definition tends to attribute more importance to this area than is warranted. The difficulty of such definitions of background and the impact on image reproduction are discussed by Braun and Fairchild (1995, 1997). Fortunately, the need for precise definition of the background is minimized in most imaging applications since the same spatial configuration of colors can be found in the original and in the reproduction. However, care-

ful consideration of the background is critical for spot color applications, in which it is desired to reproduce the same color appearance in various spatial configurations (e.g., application of the Pantone system).

## Surround

The *surround* is defined as the field outside the background. In practical situations, the surround can be considered to be the entire room or the environment in which the image (or other stimuli) is viewed. For example, printed images are usually viewed in an illuminated (average) surround, projected slides in a dark surround, and video displays in a dim surround. Thus, even in imaging applications, it is easy to specify the surround. It is the area outside the image display filling the rest of the visual field.

Specification of the surround is important for modeling long-range induction, flare (stimulus and within the eye), and overall image contrast effects (Bartleson and Breneman 1967, Fairchild 1995b). Practical difficulties arise in specifying the surround precisely when typical situations are encountered, particularly those involving a wide range of surround relative luminances and inhomogeneous spatial configurations.

## 7.2 COLORIMETRIC SPECIFICATION OF THE VIEWING FIELD

Various color appearance models utilize more or less colorimetric information on each component of the visual field. Essentially, it is necessary to know absolute (luminance or illuminance units) tristimulus values for each component of the field of view. However, some models require or utilize more or less data. In addition to the above components of the visual field, a specification of the “adapting stimulus” is often required to implement color appearance models. The adapting stimulus is sometimes considered to be the background and at other times (or in other models) it is considered to be a measure of the light source itself. Thus it becomes necessary to specify absolute tristimulus values for the illumination or a white object under the given illumination.

When measuring the absolute tristimulus values for each of the visual fields, it is important to consider the standard observer used [usually the CIE 1931 (2°) standard colorimetric observer] and the geometry of measurement and viewing. It is ideal to make colorimetric measurements using the precise geometry under which the images will be viewed. Often this is not possible, and a compromise must be made. It is important to remember that this compromise, if necessary, has been made and can influence the correlation between model predictions and visual evaluation.

When dealing with self-luminous displays (such as CRT and LCD monitors), the determination of absolute tristimulus values can be accomplished in a straightforward manner by measuring the display with a colorimeter or spectroradiometer. However, when dealing with reflective or transmissive

**Table 7.1** CIELAB coordinates and  $\Delta E_{ab}^*$  values for photographic samples evaluated using CIE illuminants D50 and F8

Sample	D50			F8			$\Delta E_{ab}^*$
	$L^*$	$a^*$	$b^*$	$L^*$	$a^*$	$b^*$	
Gray	53.7	-2.6	-9.7	53.6	-3.2	-9.8	0.6
Red	39.1	41.0	20.4	39.4	41.5	21.0	0.8
Green	43.2	-41.4	22.8	42.9	-40.6	22.0	1.2
Blue	26.5	11.2	-28.8	26.4	9.2	-28.5	2.0
Cyan	64.2	-38.7	-29.4	63.7	-40.8	-30.6	2.5
Magenta	54.7	57.3	-24.8	55.0	56.3	-23.6	1.6
Yellow	85.3	0.5	63.2	85.5	2.2	63.0	1.7
Average							1.49

media, the situation becomes more complex. Normally, such materials are characterized by their spectral reflectance, or transmittance, distributions as measured with a spectrophotometer. Colorimetric coordinates (such as CIE tristimulus values) are then calculated using a standard colorimetric observer and, normally, one of the defined illuminants (*e.g.*, CIE illuminant D65, D50, A, F2). Such measurements and calculations are usually adequate in basic colorimetric applications. However, it is an extremely rare case in which images, or other colored objects, are actually viewed under light sources that closely approximate one of the CIE illuminants (Hunt 1992). The difference in color between that calculated using a CIE illuminant and that observed under a real source intended to simulate such an illuminant can be quite significant. A conservative example of the differences encountered is given in Table 7.1. The spectral reflectances for seven different colors produced on a digital photographic printer were measured and used to calculate CIELAB coordinates using CIE illuminants D50 and F8. Illuminant F8 is specified as a typical fluorescent illuminant with a CCT of 5000 K and can be thought of as an extremely high-quality illuminant D50 simulator. A real fluorescent lamp, intended to simulate illuminant D50 as found in typical viewing booths, would most likely have a spectral power distribution that deviates more from illuminant D50 than F8. The spectral power distributions of illuminants D50 and F8 are illustrated (for 10 nm increments) in Figure 7.2.

The color differences in Table 7.1 are as large as 2.5, a magnitude that would be perceptible in an image and easily perceptible in simple patches. While perceptible, the differences in this example are probably small enough to not be of significant concern. However, more typical light sources will produce substantially larger errors.

A common example is encountered when colorimetric values (*e.g.*, CIELAB coordinates) are used to color balance an imaging system. When the colorimetric coordinates indicate that printed samples should be neutral

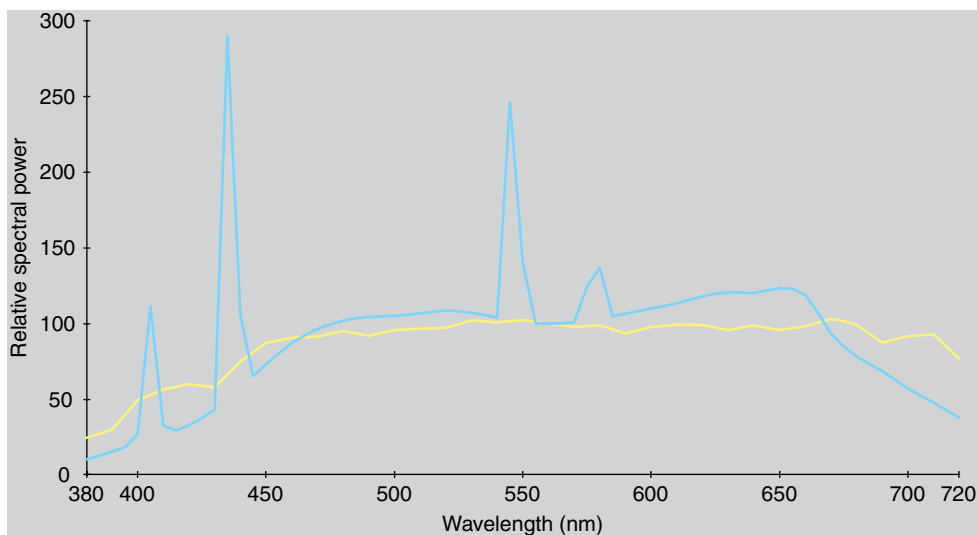


**Figure 7.2** The relative spectral power distributions of CIE illuminants D50 and F8 (each normalized to 100.0 at 560 nm)

(i.e.,  $a^* = b^* = 0.0$ ), significant chromatic content is often observed. This result can be traced to two causes. The first cause is differences between the standard illuminant used in the calculation and the light source used for observation, and the second cause is differences between the CIE standard observer and the particular human observer making the evaluation. Differences between individual observers can be significant. For color reproduction stimuli, the average CIELAB  $\Delta E_{ab}^*$  between colors deemed to be matches by an individual observer is approximately 2.5 with maxima ranging up to 20 units (Alfvín and Fairchild, 1997, Fairchild and Alfvín 1995). The former cause can be corrected by using the actual spectral power distribution of the observing condition in the colorimetric calculation. The latter is a fundamental limitation of colorimetry (indeed a limitation of any mean value) that cannot be corrected but can only be understood. Fairchild and Wyble (2007) also address this issue for modern display technology and using a variety of color matching functions recommended by the CIE (2006).

To summarize, it is critical to use the actual spectral power distribution of illuminating sources, rather than CIE standard illuminants, when precise estimates of color appearance are required. When this is not feasible, viewing booths with light sources that are close approximations of the CIE illuminants should be used.

While it would be ideal to have absolute spectral power distributions (and thus absolute tristimulus values) for each component of the viewing field, it is not necessary to have such detailed information for each model. The minimum data required for each subfield are described below. Some models require even less data as they do not consider each of the components of the visual field. The adapting field must be specified by at least its absolute

tristimulus values (an alternative and equivalent specification is to have relative tristimulus values and the absolute luminance or illuminance). The stimulus must also be specified by absolute tristimulus values (preferably calculated with the actual light source). Similar data are also required for the proximal field and the background although often the background is assumed to be achromatic and can then be specified using only its luminance factor.

The color of the surround is not considered in any appearance model; it is sufficient to know the relative luminance of the surround with respect to the image (or stimulus) areas. Often, this is even more detail on the surround than is necessary, and the surround can be specified sufficiently with an adjective such as dark, dim, and average. As a practical definition of surround relative luminance, dark can be taken to be 0%, dim between 0% and 20%, and average between 20% and 100% of the luminance of the scene, or image, white.

### 7.3 MODES OF VIEWING

While it is often hard to accept, especially by those with an affinity for physical sciences and engineering, it has been clearly shown that the mode of appearance, and thus apparent color, depends upon the stimulus configuration and cognitive interpretation. This is most clearly illustrated by example and most clearly understood (and believed!) upon personal experience.

One example, which has been observed by the author (and others), was when viewing a familiar house that was painted a light yellow color and had a front door of the same yellow color. On one occasion in the late evening it appeared that the door of this yellow house had been painted blue. A blue door on a yellow house is a noteworthy perception! However, upon closer examination, it was determined that the door was still its normal yellow color. The illumination was such that the house was illuminated directly by the sunlight from the setting sun (quite yellow), while a small brick wall (at first unnoticed) cast a shadow that just covered the door. Thus the door was illuminated only by skylight (and no direct sunlight) and therefore appeared substantially bluer than the rest of the house. On first sight, the scene was interpreted as a yellow house and blue door under uniform illumination. However, once it was understood that the illumination was not uniform (and the door was actually illuminated with blue light), the door actually changed in appearance from blue to yellow. The change in color appearance of the door was based completely on cognitive information about the illumination and could not be reversed once the illumination was known. A simulation of this effect is illustrated in Figure 7.3, which is an ambiguous figure that can be geometrically interpreted in two ways. In one interpretation, the darker area looks like a shadow and the entire object seems to be of one yellowish color. In the other geometric interpretation, the darker area cannot be a shadow and is interpreted as a piece of the object “painted” a different color. Turning the figure upside down can sometimes enhance the

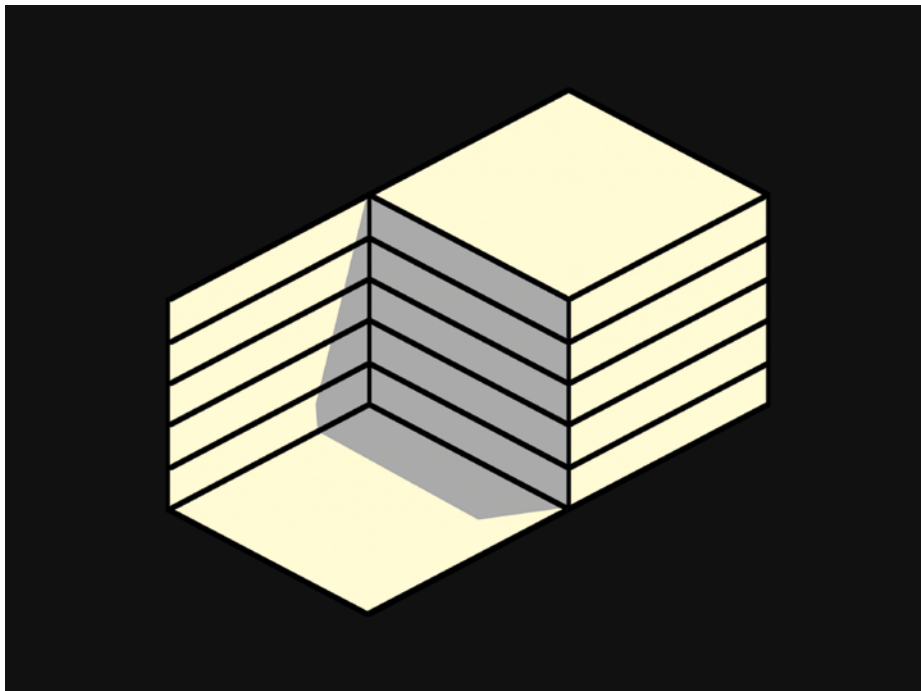


**Figure 7.3** An ambiguous figure illustrating the concept of discounting-the-illuminant. In one spatial interpretation the gray area looks like a shadow, while in the other it appears to be paint on the object

effect or help the transition from one interpretation to the other. This effect is similar to the transparency effect observed in Figure 6.15.

Another experience was related to the author in which a young child was watching black and white photographic prints being developed in a darkroom under an amber safelight. Of course, the prints were completely achromatic and the illumination was of a single, highly chromatic color. However, the child insisted she could recognize the colors of familiar objects in a print as it was being developed. Only when the parent took the black and white print out into an illuminated room did the child believe that the “known” colors of the familiar objects were not present on the print. This is another example where knowledge of the object produced a color perception. This phenomenon is completely compatible with the cognitive model of color recognition proposed by Davidoff (1991). An interesting discussion of the apparent brightness of snow, in the context of viewing modes, can be found in Koenderink and Richards (1992).

Other similar phenomena and a systematic description of the modes of viewing that produce them have been described nicely in Chapter 5 of the OSA (1963) publication, *The Science of Color*. (Note that, sadly, no equivalent

**Table 7.2** Color appearance attributes most commonly associated with the various modes of appearance. Those in parentheses are possible, although less likely

Attribute	Illuminant (glow)	Illumination (fills space)	Surface (object)	Volume (object)	Film (aperture)
Brightness	***	***			***
Lightness			***	***	(***)
Colorfulness	***	***			***
Saturation	***	***	***	***	***
Chroma			***	***	(***)
Hue	***	***	***	***	***

chapter exists in the more recent second edition of the OSA book.) Following are the five modes of viewing defined in the OSA chapter:

1. Illuminant
2. Illumination
3. Surface
4. Volume
5. Film.

These are defined and described in the following sections. Table 7.2 summarizes the color appearance attributes (see also Chapter 4) that are most commonly associated with each mode of viewing. It is noteworthy that hue and saturation are the only perceptual attributes that play a prominent role in all modes of appearance. Brightness and colorfulness also are possible in all modes, but are largely ignored in surface and volume mode. Lightness and chroma are not possible in illuminant and illumination modes. Figure 7.4 provides examples of each of the five modes of viewing.

In addition to the normal color appearance attributes, other attributes such as duration, size, shape, location, texture, gloss, transparency, fluctuation, insistence, and pronouncedness (as defined by OSA (1963)) can be considered. The modes of viewing described with respect to the interpretation of color appearance are strikingly similar to the types of “objects” that efforts are made to produce realistic renderings of in the field of computer graphics (Foley *et al.* 1990, Chapter 16). This similarity points to a fundamental link between the perception and interpretation of stimuli and their synthesis.

## Illuminant

The *illuminant mode* of appearance is defined as color perceived as belonging to a source of light. Illuminant color perceptions are likely to involve the brightest perceived colors in the field of view. Thus objects much lighter than the surroundings can sometimes give rise to the illuminant mode

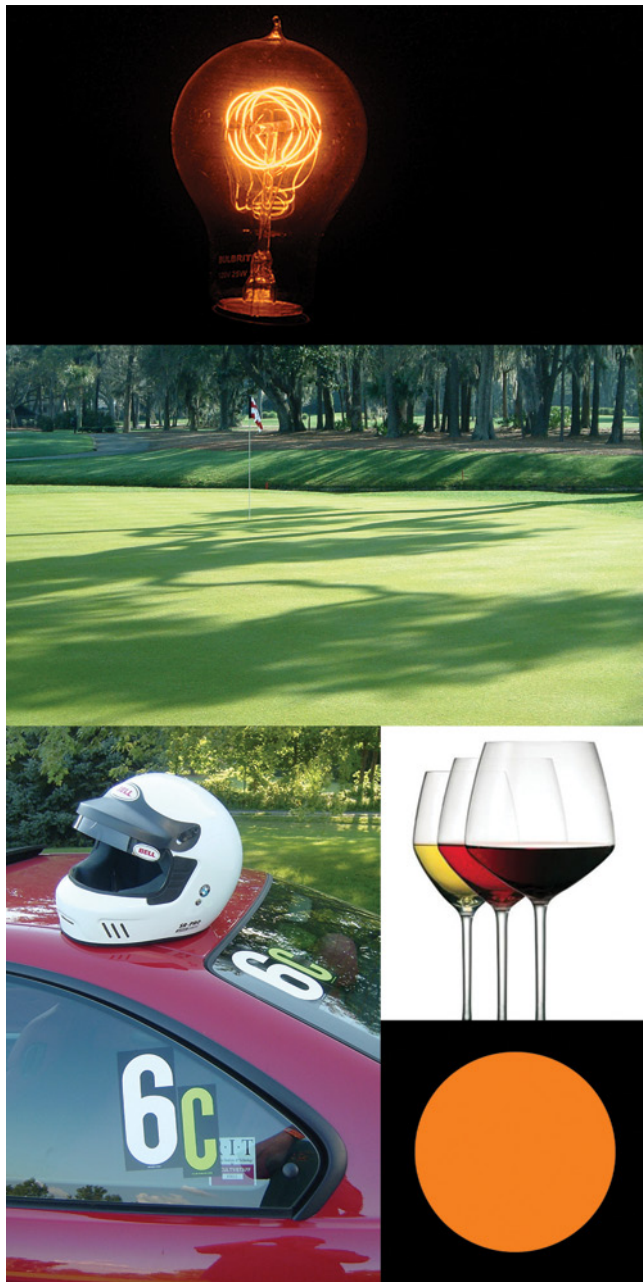


**Figure 7.4** Examples of the five modes of viewing. The lightbulb represents illuminant mode. The shadows on the putting green represent illumination mode as they are properly interpreted as caused by the lighting and not a pattern in the grass. The car, helmet, foliage, and other objects represent surface mode. The wine represents color attributed to three-dimensional extent of the material, volume mode. And finally the orange spot with no structure or content represents film (or aperture) mode

perception. The illuminant mode of perception is an “object mode” (i.e., the color belongs to an object) and can be typified as “glow.”

## Illumination

The *illumination* mode of appearance is defined as color attributed to properties of the prevailing illumination rather than to objects. The “blue door” example described earlier is an example of a mode change between illuminant and surface. OSA (1963) gave an example of a perception of irregular splotches of highly chromatic yellow paint (surface mode) on the dark shadowed side of a railroad coach. When the observer came closer, noticed the angle of the setting sun, and could see penumbral gradations, he realized that the yellow patches were due to sunlight masked off by obstructions (illumination mode). The illumination mode of perception is a “non-object” mode and is mediated by the presence of illuminated objects that reflect light and cast shadows (sometimes particles in the atmosphere).

## Surface

The *surface mode* of appearance is defined as color perceived as belonging to a surface. Any recognizable, illuminated object provides an example of the surface mode. This mode requires the presence of a physical surface and light being reflected from the surface. It is an “object mode.”

## Volume

The *volume mode* of appearance is defined as color perceived as belonging to the bulk of a more or less uniform and transparent substance. For example, as the number of air bubbles in a block of ice increases, the lightness of the block increases toward white, while the transparency decreases toward 0. Thus a volume color transforms into a surface color. The volume mode of perception is an “object mode” and requires transparency and a three-dimensional structure.

## Film

The *film mode* of appearance (also referred to as aperture mode) is defined as color perceived in an aperture with no connection to an object. For example, failure to focus on a surface can cause a mode shift from surface to film. An aperture screen accomplishes this since the observer tends to focus on the plane of the aperture. The film mode of perception is a “non-object” mode. All other modes of appearance can be reduced to film mode.

## 7.4 UNRELATED AND RELATED COLORS REVISITED

Unrelated and related colors were defined in Chapter 4. However, their fundamental importance in color appearance specification, their simplifying and unifying theme with respect to modes of appearance, and their important relation to the specification of brightness-colorfulness or lightness-chroma appearance matches warrant a revisit. The distinction between related and unrelated colors is the single most important viewing-mode concept to understand.

### *Unrelated Color*

*Color perceived to belong to an area or object seen in isolation from other colors.*

### *Related Color*

*Color perceived to belong to an area or object seen in relation to other colors.*

Unrelated colors only exhibit the perceptual attributes of hue, brightness, colorfulness, and saturation. The attributes that require judgment relative to a similarly illuminated white object cannot be perceived with unrelated colors. On the other hand, related colors exhibit all of the perceptual attributes of hue, brightness, lightness, colorfulness, chroma, and saturation. Recall that gray and brown do not exist as unrelated colors. Both of those perceptions rely on a low lightness (requiring a relative judgment) and brown also relies on a low chroma (another relative judgment). Thus, brown and gray only exist as related colors. This point was made in an amusing fashion when an attempt was made to make a rendering of Guinness (dark brown) beer as a neon sign (Figure 7.5). In the first attempt, the part of the sign representing the dark beer was made with a yellow neon



**Figure 7.5** A neon Guinness sign representing one attempt to create brown as an unrelated color. See text for an explanation of why that is not possible

tube. While this was colorimetrically correct relative to the white areas of the sign, when illuminated in a dark area, one could only perceive the unrelated yellow color (nothing like the dark color of Guinness). An attempt was made to correct this by painting the yellow tubes a dark brown on later versions of the sign. This looks better in daylight, but again at night those “brown” lights appear to glow orange (unrelated colors). It simply is not possible to make a dark brown light! That is why you cannot purchase gray and brown lights (related colors) but rather can purchase white and orange lights (unrelated colors with the same tristimulus values).

Recall that five perceptual dimensions are required for a complete specification of the color appearance of related colors. These are brightness, lightness, colorfulness, chroma (or saturation), and hue. However, in most practical color appearance applications it is not necessary to know all five of these attributes. Typically, for related colors, only the three relative appearance attributes are of significant importance. Thus it is often sufficient to be concerned with only the relative appearance attributes of lightness, chroma (or saturation), and hue. See Chapter 4 for a discussion of the distinction between brightness–colorfulness matching and lightness–chroma matching and their relative importance.

# 8

# Chromatic Adaptation

---

Various color appearance phenomena were discussed in Chapter 6. These phenomena illustrated cases in which simple tristimulus colorimetry was not capable of adequately describing appearance. Many of those phenomena could be considered second-order effects. The topic of this chapter, chromatic adaptation, is clearly the most important first-order color appearance phenomenon. Tristimulus colorimetry tells us when two stimuli match for an average observer when viewed under identical conditions. Interestingly enough, such visual matches persist when the stimuli are viewed (as a pair) under an extremely wide range of viewing conditions (as long as the changes in viewing conditions do not change the spectral power distributions of the two stimuli). While the match persists, the color appearance of the two stimuli might be changing drastically. Changes in chromatic adaptation are one instance in which matches persist, but appearance changes. It is this change in appearance that must be understood to construct a color appearance model.

The term *chromatic adaptation* refers to the human visual system's capability to adjust to widely varying colors of illumination in order to approximately preserve the appearance of object colors. Perhaps it is best illustrated by considering a system that does not have the capacity for chromatic adaptation – photographic transparency film. Most transparency film was designed for exposure under daylight sources. If such film was used to make photographs of objects under incandescent illumination, the resulting transparencies have an unacceptable yellow-orange cast. This is because the film cannot adjust the relative responsivities of its red, green, and blue imaging layers in the way the human visual system adjusts the responsivities of its color mechanisms. Humans perceive relatively little change in the colors of objects when the illumination is changed from daylight to incandescent.

This chapter reviews some of the basic concepts of chromatic adaptation. Issues related to chromatic adaptation have been studied for much of modern history. The topic is even discussed by Aristotle (Wandell 1995: 65).

*In woven and embroidered stuffs the appearance of colors is profoundly affected by their juxtaposition with one another (purple, for instance, appears different on white than on black wool), and also by differences of illumination. Thus embroiderers say that they often make mistakes in their colors when they work by lamplight, and use the wrong ones.*

Aristotle, *Meteorologica*

There are many excellent discussions of chromatic adaptation available in books (Barlow and Mollon 1982, Spillman and Werner 1990, Wandell 1995, Wyszecki and Stiles 1982) and journals (Bartleson 1978, Hunt 1976, Lennie and D'Zmura 1988, Terstiege 1972, Wright 1981). The interested reader is encouraged to explore this extensive and fascinating literature.

## 8.1 LIGHT, DARK, AND CHROMATIC ADAPTATION

*Adaptation* is the ability of an organism to change its sensitivity to a stimulus in response to changes in the conditions of stimulation. The general concept of adaptation applies to all domains of perception. The various mechanisms of adaptation can act over extremely short durations (on the order of milliseconds) or very long durations (weeks, months, or years!). In general, the mechanisms of adaptation serve to make the observer less sensitive to a stimulus when the physical intensity of the stimulus is greater. For example, one might be keenly aware of the ticking of a clock in the middle of a quiet night, but completely unable to perceive the same ticking during a busy cocktail party. In the realm of vision, three types of adaptation become most important: light, dark, and chromatic.

### Light Adaptation

*Light adaptation* is the decrease in visual sensitivity upon increases in the overall level of illumination. For example, it is easy to see millions of stars on a clear night. An equivalent number and variety of stars are present in the sky on a clear day; however, we are unable to perceive them. This is because the overall luminance level of the sky is several orders of magnitude higher in the daytime than at night. This causes visual sensitivity to changes in luminance to be reduced in the daytime relative to night. Thus the luminance change that served to produce the perception of millions of stars at night is inadequate to allow their perception during the day.

As another example, imagine waking up in the middle of the night and switching on a bright room light. At first your visual system is dazzled, you are unable to see much of anything, and you might even feel a little pain.

Then, after tens of seconds, you begin to be able to view objects normally in the illuminated room. What has happened is that the mechanisms of vision were at their most sensitive in the dark room. When the light was first switched on, they were overloaded due to their high sensitivity. After a short period, they adapted to the light, thus decreasing their sensitivity and allowing normal vision.

## Dark Adaptation

*Dark adaptation* is similar to light adaptation, with the exception that dark adaptation refers to sensitivity changes in the opposite direction. Thus dark adaptation is the increase in visual sensitivity experienced upon decreases in luminance level. While the phenomena associated with light and dark adaptation are similar, it is useful to distinguish the two since they are mediated by different mechanisms and exhibit different visual performance.

For example, light adaptation takes place much more quickly than dark adaptation (Kalloniatis and Luu 2012). One can experience dark adaptation when entering a dark movie theater after being outdoors in bright sunlight. At first the theater will seem completely dark. Often people stop walking immediately upon entering a darkened room because they cannot see anything. However, after a short period objects in the room (theater seats, other people, etc.) begin to become visible. After several minutes, objects will become quite visible and there is little difficulty identifying other people, finding better seats, etc. All of this happens because the mechanisms of dark adaptation are gradually increasing the overall sensitivity of the visual system. Light and dark adaptation in the visual system can be thought of as analogous to automatic exposure controls in cameras.

## Chromatic Adaptation

The processes of light and dark adaptation do have profound impacts on the color appearance of stimuli. Thus they are considered in various color appearance models. However, a third type of visual adaptation, chromatic adaptation, is far more important and must be included in all color appearance models. *Chromatic adaptation* is the largely independent sensitivity regulation of the mechanisms of color vision. Often it is considered to be only the independent changes in responsivity of the three types of cone photoreceptors (while light and dark adaptation refer to overall responsivity changes in all of the receptors). However, it is important to keep in mind that there are other mechanisms of color vision (e.g., at the opponent level and even at the object recognition level) that are capable of changes in sensitivity that can be considered mechanisms of chromatic adaptation.

As an example of chromatic adaptation, consider a piece of white paper illuminated by daylight. When such a piece of paper is moved to a room with incandescent light, it still appears white despite the fact that the energy reflected from the paper has changed from predominantly blue to predominantly yellow (this is the change in illumination that the transparency film discussed in the introduction to this chapter could not adjust to). Figure 8.1 illustrates such a change in illumination. Figure 8.1(a) illustrates a typical scene under daylight illumination. Figure 8.1(b) shows what the scene would look like under incandescent illumination when viewed by a visual system that is incapable of chromatic adaptation. Figure 8.1(c) illustrates the same scene viewed under incandescent illumination by a visual system capable of adaptation similar to that observed in the human visual system.

*Afterimages* provide a second illustrative example of chromatic adaptation. These can be observed by viewing Figure 8.2. Stare at the black dot in the center of Figure 8.2 and memorize the positions of the various colors. After approximately 30 seconds, move your gaze to an illuminated white area such as a wall or blank piece of paper. Note the various colors and their locations. These afterimages are the result of independent sensitivity changes of the color mechanisms. For example, the retinal areas exposed to the red area in Figure 8.2 became less sensitive to red energy during the adapting exposure, resulting in the cyan appearance of the afterimage when viewing a white area. This is caused by the lack of red response in this area that would normally be expected when viewing a white stimulus. Similar explanations hold for the other colors observed in the afterimage. While light adaptation can be thought of as analogous to an automatic exposure control, chromatic adaptation can be thought of as analogous to an automatic white-balance feature on a video camera or digital still camera.

## 8.2 PHYSIOLOGY

While the various phenomena of adaptation are interesting in their own right, it becomes necessary to understand something of the physiological mechanisms of adaptation in order to model them properly. There are a variety of mechanisms of adaptation ranging from strictly sensory, reflex-like responses, to purely cognitive. While all of these mechanisms are not fully understood, it is instructive to examine their variety in order to later understand how they are incorporated into various models. The mechanisms discussed here are the following:

- Pupil dilation/constriction
- Rod-cone transition
- Receptor gain control
- Subtractive mechanisms
- High-level adaptation.



**Figure 8.1** Illustration of (a) a scene illuminated by daylight, (b) the same scene illuminated by tungsten light as perceived by a visual system incapable of chromatic adaptation, and (c) the scene illuminated by tungsten light as perceived by a visual system with typical von Kries-type chromatic adaptation (similar to the human visual system). Original lighthouse image from Kodak Photo Sampler PhotoCD

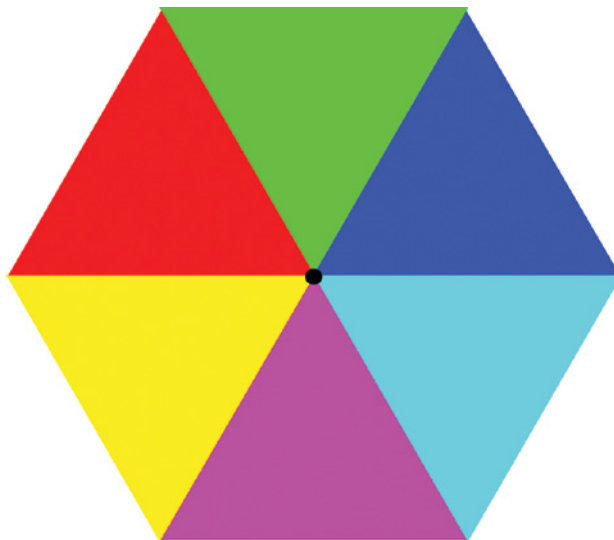


**Figure 8.2** An example of afterimages produced by local retinal adaptation. Fixate the black spot in the colored pattern for about 30 seconds and then move your gaze to a uniform white area. Note the colors of the afterimages with respect to the original colors of the pattern

## Pupil Dilation/Constriction

The most apparent mechanism of light and dark adaptation is dilation and constriction of the pupil. In ordinary viewing situations, the pupil diameter can typically range from about 3 to 7 mm (2–8 mm in the extreme). This represents a change in pupil area of approximately a factor of 5. Thus, the change in pupil size could explain light and dark adaptation over a 5 $\times$  range of luminances. While this might seem significant, the range of luminance levels over which the human visual system can comfortably operate spans at least 10 orders of magnitude. Clearly, while the pupil provides one mechanism of adaptation, it is insufficient to explain observed visual capabilities. Thus there must be additional adaptational mechanisms embedded in the physiological mechanisms of the retina and beyond.

## Role of the Rods and Cones

There are two classes of photoreceptors in the human retina: rods and cones. The cones are less sensitive and respond to higher levels of illumination while the rods are more sensitive, responding to lower levels of illumination. Thus the transition from cone vision to rod vision (which occurs at luminances on the order of 0.1–1.0 cd/m<sup>2</sup>) provides an additional mechanism for light and dark adaptation.

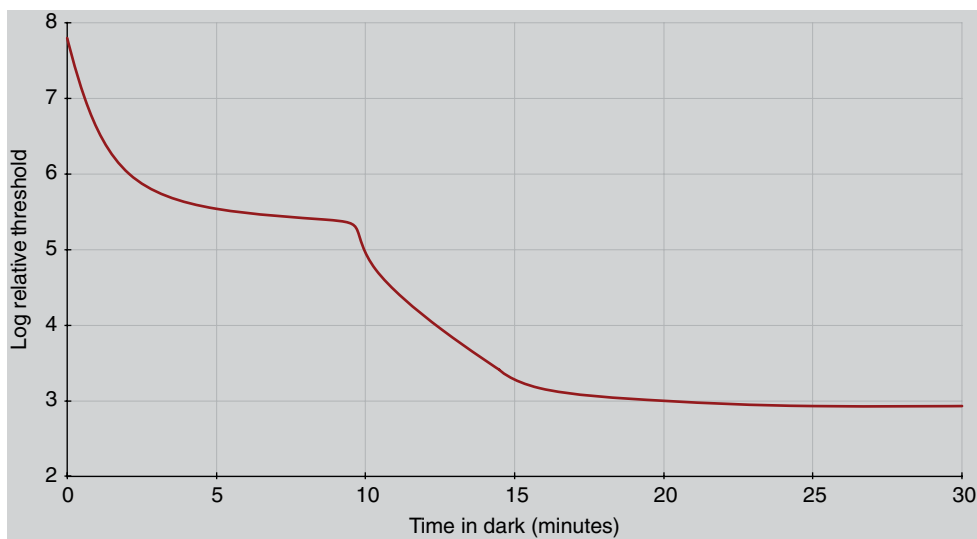


**Figure 8.3** A typical dark adaptation curve showing the recovery of threshold after a strong exposure

The decrease in responsivity of the cones upon exposure to increased luminance levels (light adaptation) takes place fairly rapidly, requiring a few minutes at most. The increase in sensitivity of the rods upon exposure to decreased luminance levels requires more time. This can be illustrated with a classic dark-adaptation curve showing the recovery of threshold after exposure to an extremely bright adapting stimulus as illustrated in Figure 8.3. The first phase of the curve shows the recovery of sensitivity of the cones, which levels off after a couple of minutes. Then, after about 10 minutes, the rods have recovered enough sensitivity to become more sensitive than the cones and the curve takes another drop. After about 20 minutes, the rods have reached their maximal sensitivity and the dark-adaptation curve levels off. This curve explains the perceptions observed over time after entering a darkened movie theater.

In addition to providing a mechanism for light and dark adaptation, the rod-cone transition has a profound impact on color appearance. Recall that there are three types of cones to serve the requirements of color vision, but only one type of rod. Thus when luminance is reduced to levels at which only the rods are active, humans become effectively color blind, seeing the world only in shades of gray. Thus the rod-cone transition is of limited interest in color appearance and chromatic adaptation models, and other mechanisms must be considered. (Note: The influence of rods on color appearance can be important at low luminance levels and it is incorporated in Hunt's color appearance model.)

## Receptor Gain Control

Perhaps the most important mechanism of chromatic adaptation is independent sensitivity changes in the photoreceptors, sometimes referred to as *receptor gain control*. It is possible to imagine a gain control that varies the relationship between the number of photons incident on a photoreceptor and the electrochemical signal it produces in response to those photons. Chromatic adaptation would be served by turning down the gain when there are many photons (high levels of excitation for the particular cone type) and turning up the gain when photons are less readily available. The key to chromatic adaptation is that these gain controls are independent in each of the three cone types. (Gain control is certainly a mechanism of light adaptation as well, but light adaptation could be served by a single gain control for all three cone types. It is overly well served by independent mechanisms of chromatic adaptation.)

Physiologically, changes in photoreceptor gain can be explained by pigment depletion at higher luminance levels. Light breaks down molecules of visual pigment (part of the process of phototransduction) and thus decreases the number of molecules available to produce further visual response. Therefore, at higher stimulus intensities there is less photopigment available and the photoreceptors exhibit a decreased responsivity. While pigment depletion provides a nice explanation, there is evidence that the visual system adapts in a similar way at lower luminance levels for which there is insignificant pigment depletion. This adaptation is thought to be caused by gain-control mechanisms at the level of the horizontal, bipolar, and ganglion cells in the retina. Gain control in retinal cells beyond the photoreceptors helps to explain some of the spatially low-pass characteristics of chromatic adaptation. Delahunt and Brainard (2000) also discuss the interaction of various cone types in the control of chromatic adaptation. Recent research suggests a likely role for ipRGC mediated by melanopsin absorption in retinal sensitivity control and adaptation. This additional photosensitive element in the retina might well explain some limitations to adaptation models that are based solely on cone responses.

## Subtractive Mechanisms

There is also psychophysical evidence for subtractive mechanisms of chromatic adaptation in addition to gain control mechanisms (Shevell 1978, Walraven 1976). Physiological mechanisms for such subtractive adaptation can be found by examining the temporal impulse response of the cone photoreceptors, which is biphasic and thus enhances transients and suppresses steady signals. Similar processes are found in lateral inhibitory mechanisms in the retina that produce its spatially antagonistic impulse response

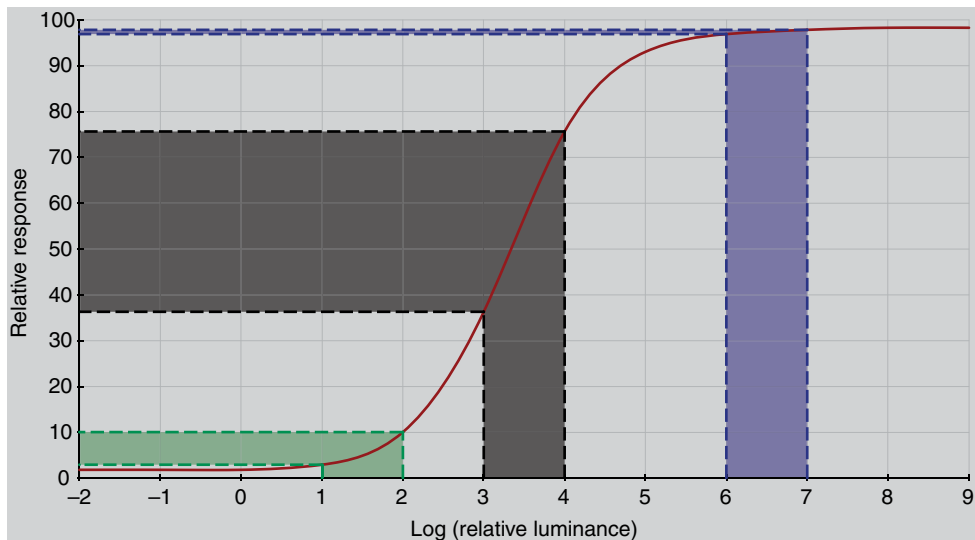


**Figure 8.4** A prototypical response function for the human visual system illustrating response compression at low and high levels of the input signal

that enhances spatial transients and suppresses spatially uniform stimuli. Physiological models of adaptation that require both multiplicative (gain) and subtractive mechanisms (Hayhoe *et al.* 1987, 1989) can be made completely compatible with models typically proposed in the field of color appearance (Chapter 9) that include only gain controls by assuming that the subtractive mechanism takes place after a compressive nonlinearity. If the nonlinearity is taken to be logarithmic, then a subtractive change after a logarithmic transformation is identical to a multiplicative change before the nonlinearity. This bit of mathematical manipulation serves to provide consistency between the results of threshold psychophysics, physiology, and color appearance. It also highlights the importance of compressive nonlinearities as mechanisms of adaptation.

Figure 8.4 illustrates a nonlinear response function typical of the human visual system (or any imaging system). The function exhibits a threshold level below which the response is constant and a saturation level above which the response is also constant. The three sets of inputs with 10:1 ratios at different adapting levels are illustrated. It can be seen in Figure 8.4 that a 10:1 range of input stimuli produces a small output range at low and high adapting luminance levels and a large output range at intermediate levels. The decrease in response at low levels has to do with the fundamental limitation of the mechanism's sensitivity, while the response compression at high levels can be considered a form of adaptation (decreased responsiveness with increased input signal). Nonlinear response functions such as the one illustrated in Figure 8.4 are required in color appearance models to predict phenomena such as the Stevens and Hunt effects described in Chapter 6.

## High-Level Adaptation Mechanisms

Thus far, the mechanisms discussed have been at the front end of the visual system. These are low-level mechanisms that respond and adapt to very simple stimulus configurations. Webster and Mollon (1994) present interesting results that illustrate the relationship between spatial contrast, color appearance, and higher level visual mechanisms. There are also numerous examples of visual adaptation that must take place at higher levels in the system (*i.e.*, in the visual cortex). Examples of such cortical adaptation include

- The McCollough effect
- Spatial frequency adaptation
- Motion adaptation
- Blur adaptation
- Noise adaptation
- Face adaptation.

It is useful to consider these examples as illustrations of the potential for other types of high-level adaptation not yet considered.

A nice example of the McCollough effect can be found in Barlow and Mollon (1982). To experience the McCollough effect, one must intermittently view a pattern of red and black strips in one orientation, say horizontal, and another pattern of green and black strips of a second orientation, say vertical. By viewing each pattern for several seconds and then switching to the other, it is ensured that no simple afterimages are formed. After continuing this adaptation process for about four minutes, the observers can then turn their attention to patterns of black and white strips of spatial frequency similar to the adapting patterns. What will be observed is that black and white patterns of a vertical orientation will appear black and pink and black and white patterns in a horizontal pattern will appear black and pale green. The effect is contingent upon the color and orientation of the adapting stimuli and cannot be explained as a simple afterimage. It suggests adaptation at a cortical level in the visual system, where neurons that respond to particular orientations and spatial frequencies are first observed. The effect is also very persistent, sometimes lasting for several days or longer! Neitz *et al.* (2002) describe fascinating experiments that showed chromatic adaptation over a period of weeks and effectively long-term resetting (or recalibration) of the observer white point.

Spatial frequency adaptation can be observed by examining Figure 8.5. Adapt to Figure 8.5(a) by gazing at the black bar in the center for one to two minutes. In order to avoid producing simple afterimages, do not fixate a single point, but rather let your gaze move back and forth along the black bar. After the adaptation period, fixate on the black dot in the middle of Figure 8.5(b). The pattern on the right in Figure 8.5(b) should look like it is of a higher spatial frequency than the pattern on the left. The two patterns in Figure 8.5(b) are identical. The difference in appearance after adaptation to Figure 8.5(a) is

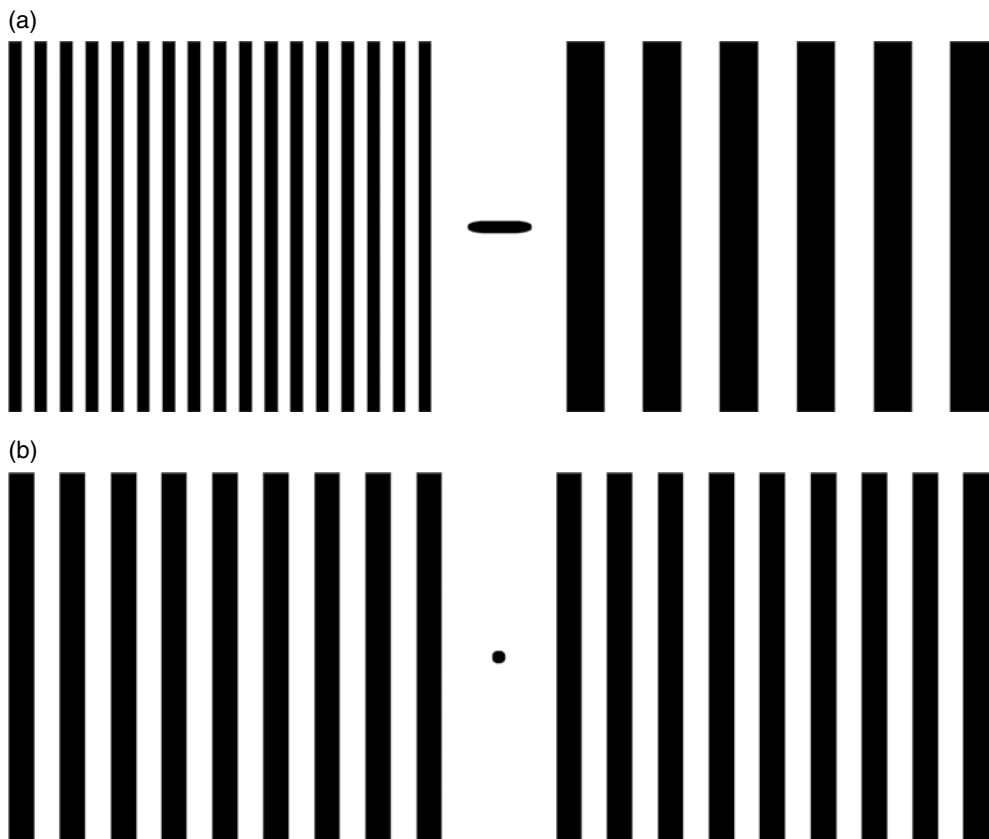


**Figure 8.5** A stimulus configuration to illustrate spatial frequency adaptation. Gaze at the black bar in the middle of (a) for about 60 seconds and then fixate on the black point in the middle of (b). Note the perceived relative spatial frequencies of the two patterns in (b) after this adaptation period

caused by the adaptation of mechanisms sensitive to various spatial frequencies. When adapting to a high spatial frequency, other patterns appear to be of lower spatial frequency and vice versa. Once again, this adaptation is attributed to cortical cells that selectively respond to various spatial frequencies.

A more complex form of spatial frequency adaptation is blur adaptation as demonstrated in Figure 8.6. In Figure 8.6(a), there are two images with the one on the left being sharpened and the one on the right blurred. These can be adapted to by gazing at the ellipse between them. Strict fixation is not required. After about 30 seconds of adaptation, move your gaze to the pair of images in Figure 8.6(b) and look at the ellipse between them. These two images are identical, but the image on the left will look blurred after adaptation to the sharpened image above it and the image on the right will look sharper after adaptation to the blurred image above it. Again this is a compelling illustration of higher level adaptational mechanisms in our visual systems.

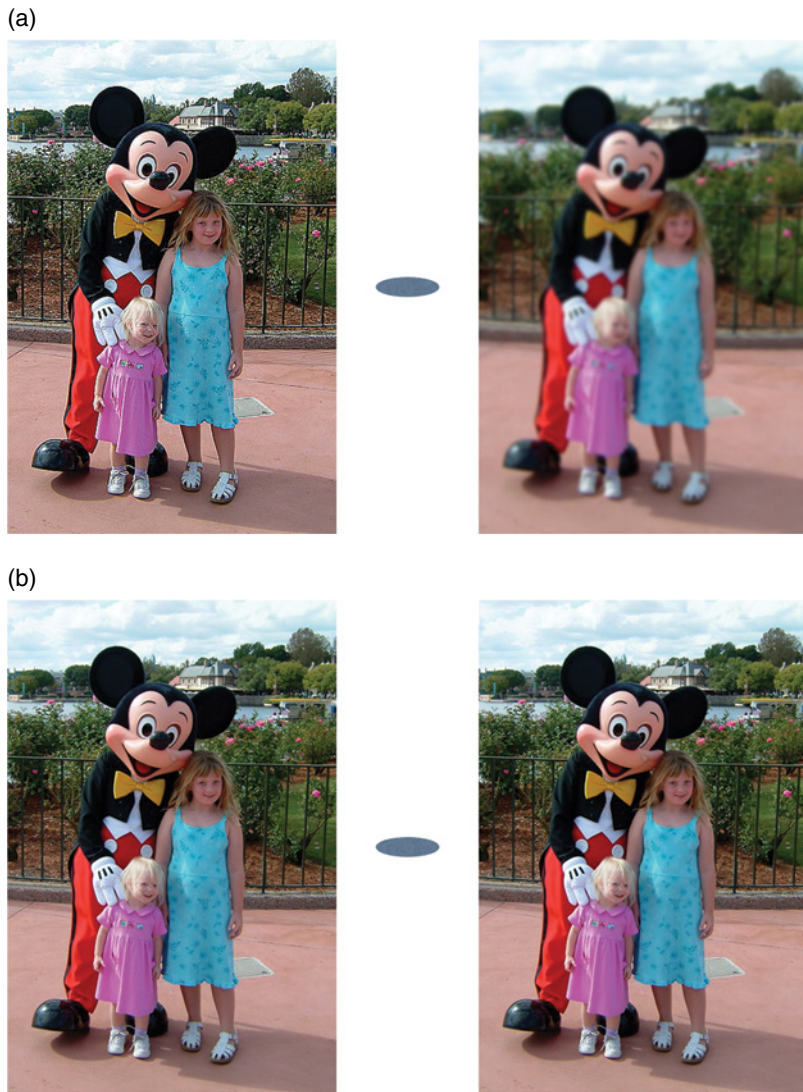


**Figure 8.6** A demonstration of blur adaptation. Fixate the ellipse between the images in (a) for about 30 seconds and then gaze at the ellipse between the physically identical images in (b) and note their relative appearance. This is a more complex example of spatial frequency adaptation

To add another layer of complexity to the story, humans also adapt to noise in images (Fairchild and Johnson 2005, 2007). Figure 8.7 is similar to Figure 8.6 except that the adapting stimuli, Figure 8.7(a), have two disparate levels of noise added to the image. After adaptation, again for about 30 seconds, when one observes the identical images in Figure 8.7(b) with intermediate noise levels, it can be seen that adaptation to higher levels of noise suppresses the noise perception and vice versa for lower

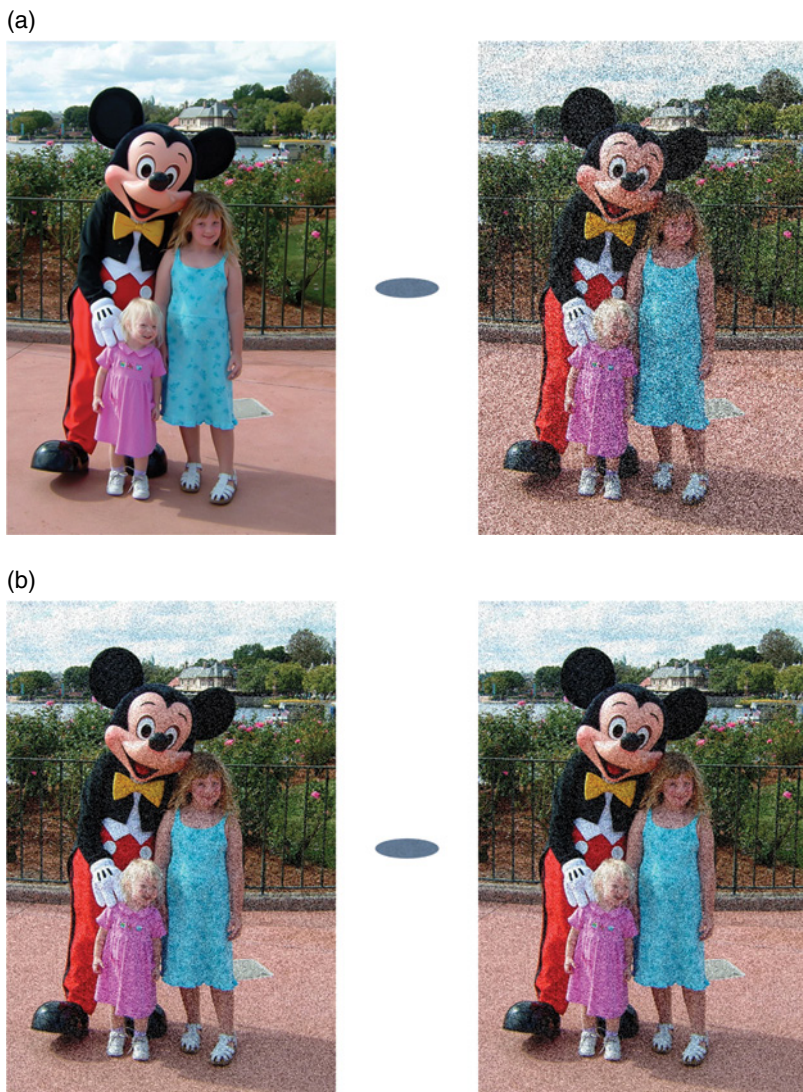


**Figure 8.7** A demonstration of noise adaptation. Fixate the ellipse between the images in (a) for about 30 seconds and then gaze at the ellipse between the physically identical images in (b) and note their relative appearance. This is an extremely complex example of spatial frequency adaptation

levels of noise in the adapting stimulus. The complexity here is that this adaptation cannot be explained as simple spatial frequency adaptation since the noise pattern is made up of white noise (energy at all frequencies). Interestingly, this type of adaptation makes it more difficult for observers to detect constant sources of artifacts in imaging systems.

Webster (2011) has explored visual adaptation to a variety of highly complex stimuli. For example, he has illustrated that human observers adapt to certain

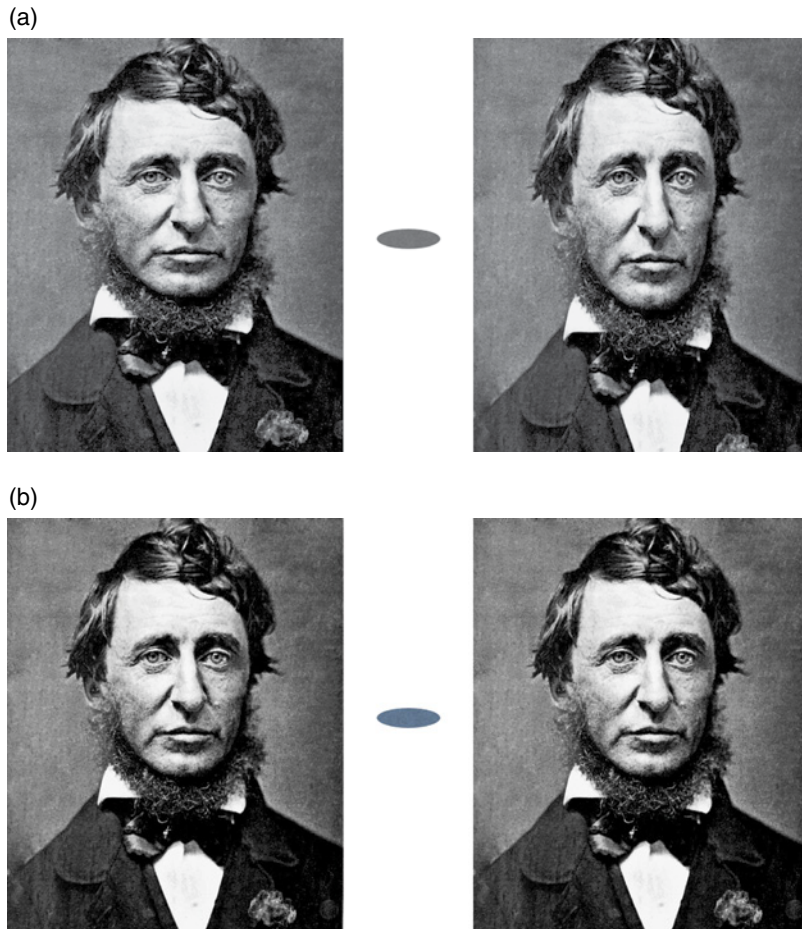


**Figure 8.8** A demonstration of face shape adaptation. Fixate the ellipse between the faces in (a) for about 30 seconds and then gaze at the ellipse between the physically identical faces in (b) and note their relative appearance. This is a high level adaptation effect on mechanisms sensitive to components of face appearance

characteristics in faces (separation of eyes, length-to-width ratio, hairline, nose size, smile, etc.) in such a way that adaptational aftereffects such as those illustrated in Figure 8.6 and Figure 8.7 can be created on facial images. For example, if adapted to a face with a big smile, then look at one with a neutral expression, you might see a bit of a frown. This type of result indicates that there are adaptation mechanisms acting on very high-level processes in the visual system. Figure 8.8 illustrates a very simple example of face adaptation. The two images in Figure 8.8(a) show a face distorted to be fat and short and another distorted to be tall and thin. After adapting for about 30 seconds by gazing at the ellipse between them, move your gaze to the ellipse between the two identical images in Figure 8.8(b) and note which face appears fatter.

Motion adaptation provides similar evidence in the temporal domain. An example of motion adaptation can be observed when viewing the credits at the end of a motion picture (or text scrolling up a computer terminal). If the credits are scrolling up the screen (and being observed) for several minutes, it can be noticed that when the final credit is stationary on the screen it appears to be moving downward (and going nowhere at the same time!). This occurs because the cortical mechanisms selective for upward motion have become adapted while viewing the moving credits. Once the motion stops, the response of the upward and downward selective mechanisms should be nulled out, but the adapted (*i.e.*, fatigued) upward mechanisms are not responding as strongly as they should and the stationary text appears to be moving downward. Motion adaptation can also be observed sometimes after driving a car on a highway for long periods of time. The visual system adapts to the motion toward the observer and then when the car is stopped, it can sometimes appear as if the outside world is moving away from the observer even though there is no real motion.

The examples of cortical adaptation discussed above lead to the next logical step. If there are adaptive mechanisms at such a high level in the visual system, is it possible that there are also cognitive mechanisms of adaptation that require our knowledge and interpretation of the scene? This issue is discussed in Section 8.3.

### 8.3 SENSORY AND COGNITIVE MECHANISMS

It is tempting to assume that chromatic adaptation can be considered a sensory mechanism that is some sort of automatic response to changes in the stimulus configuration. However, there is clear evidence for mechanisms of chromatic adaptation that depend on knowledge of the objects and their illuminated environment (Fairchild, 1992a,b, 1993a). These are cognitive mechanisms of adaptation.

Chromatic adaptation mechanisms can be classified into two groups:

- Sensory – those that respond automatically to the stimulus energy.
- Cognitive – those that respond based upon observers' knowledge of scene content.

#### Sensory Mechanisms

Sensory chromatic adaptation mechanisms are well known and have been widely discussed in the vision and color science literature. The physiological locus of such mechanisms is generally believed to be sensitivity control in the photoreceptors and neurons in the first few stages of the visual system as discussed previously. Most modern theories and models of sensory chromatic adaptation trace their roots to the work of von Kries (1902) who wrote:

*... the individual components present in the organ of vision are completely independent of one another and each is fatigued or adapted exclusively according to its own function [trans. MacAdam 1970: 118].*

These words of von Kries' are known to be not precisely correct today, but the concept is accurate and provides useful insight. To this day, the idea that chromatic adaptation takes place through normalization of cone signals is known as the *von Kries coefficient law* and serves as the basis of all modern models of chromatic adaptation and color appearance.

## Cognitive Mechanisms

Cognitive mechanisms have also been long recognized in the literature. However, perhaps because of the difficulty of quantifying cognitive effects, they are usually discussed briefly and are not as widely recognized or understood. To help understand the idea of cognitive chromatic adaptation mechanisms it might be best to quote some of those that have mentioned them in the past two centuries. Helmholtz (1866) in his treatise on physiological optics discussed object color appearance:

*We learn to judge how such an object would look in white light, and since our interest lies entirely in the object color, we become unconscious of the sensations on which the judgement rests [trans. Woodworth 1938].*

Hering (1920), who is known for hypothesizing the opponent colors theory of color vision, discussed the concept of memory color:

*All objects that are already known to us from experience, or that we regard as familiar by their color, we see through the spectacles of memory color [trans. Hurvich and Jameson 1964: 89].*

Judd (1940: 2) who made innumerable contributions to the field of color science referred to two types of chromatic adaptation mechanisms:

*The processes by means of which the observer adapts to the illuminant or discounts most of the effect of a nondaylight illuminant are complicated; they are known to be partly retinal and partly cortical.*

Lastly, Evans (1943: 596) who wrote and lectured on many aspects of color photography and color perception discussed reasons why the colors in photographs look acceptable:

*... in everyday life we are accustomed to thinking of most colors as not changing at all. This is in large part due to the tendency to remember colors rather than to look at them closely.*

Jameson and Hurvich (1989) discussed the value of having multiple mechanisms of chromatic adaptation to provide important information both about changes such as weather, light, and time of day and constant physical properties of objects in the scene. Finally, Davidoff (1991) published a monograph on the cognitive aspects of color and object recognition, and Purves and Lotto (2003) have described an empirical theory of vision that relies on cognitive mechanisms.

## Hard-Copy Vs Soft-Copy Output

While it is clear that chromatic adaptation is complicated and relies on both sensory and cognitive mechanisms, it is less clear how important it is to distinguish between the two types of mechanisms when viewing image displays. If an image is being reproduced in the same medium as the original and is viewed under similar conditions, it is safe to assume that the same chromatic-adaptation mechanisms are active when viewing both the original and the reproduction. But, what happens when the original is presented in one medium, such as a soft-copy display, and the reproduction is viewed in a second medium, such as a hard-copy output? A series of experiments have been described (Fairchild 1992b, 1993a) that quantify some of the characteristics of chromatic adaptation mechanisms and indicate that the same mechanisms are not active when soft-copy displays are viewed as are active when hard-copy displays or original scenes are viewed.

When hard-copy images are being viewed, an image is perceived as an object that is illuminated by the prevailing illumination. Thus both sensory mechanisms, that respond to the spectral energy distribution of the stimulus, and cognitive mechanisms, that discount the “known” color of the light source, are active. When a soft-copy display is being viewed, it cannot easily be interpreted as an illuminated object. Therefore, there is no “known” illuminant color and only sensory mechanisms are active. This can be demonstrated by viewing a white piece of paper under incandescent illumination and comparing the appearance to that of a self-luminous display of a uniform field with exactly the same chromaticity and luminance viewed in a darkened room. The paper will appear white or just slightly yellowish. The display will appear relatively high-chroma yellowish-orange. In fact, a white piece of paper illuminated by that display will appear white while the display itself retains a yellowish appearance! Color appearance models such as RLAB, the Hunt model, and CIECAM02 include provisions for various degrees of cognitive “discounting-the-illuminant” as described here.

## The Time-Course of Adaptation

Another important feature of chromatic adaptation mechanisms is their time course. The time course of chromatic adaptation for color appearance judgments has been explored in detail (Fairchild and Lennie 1992,

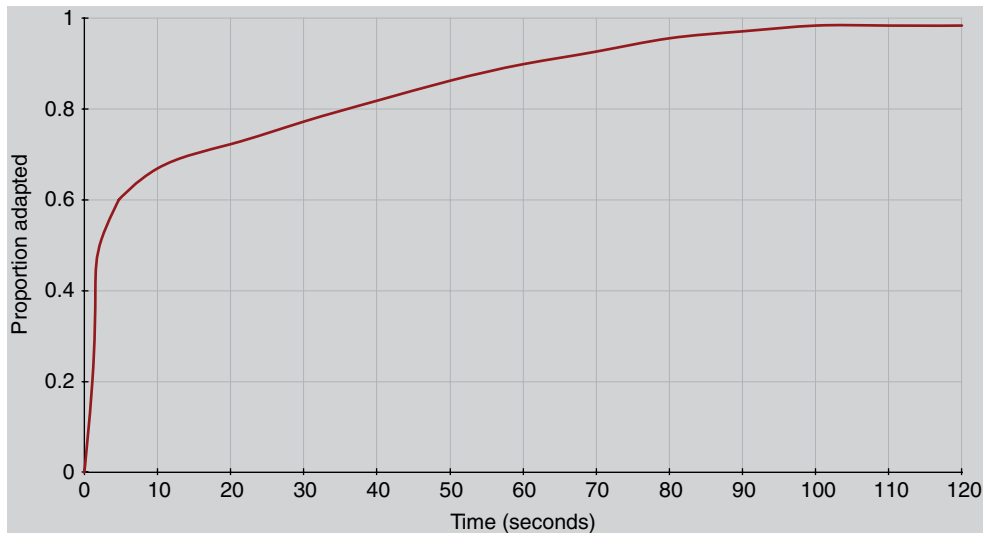


**Figure 8.9** The time course of chromatic adaptation with no luminance-level changes as measured by Fairchild and Reniff (1995)

Fairchild and Reniff 1995). The results of these studies suggest that the sensory mechanisms of chromatic adaptation are about 90% complete after 60 seconds for changes in adapting chromaticity at constant luminance. Results from Fairchild and Reniff (1995) illustrating the degree of adaptation as a function of time after a change in chromaticity of the adapting stimulus are shown in Figure 8.9. Sixty seconds can be considered a good general rule for the minimum duration observers should adapt to a given viewing environment prior to making critical judgments. Adaptation is slightly slower when significant luminance changes are also involved (Hunt 1950). As far as luminance adaptation (light and dark adaptation), it is reasonable to assume that both can be modeled with exponential decay functions. The time constant for light adaptation is in the order of 5–10 seconds while the time constant for dark adaptation of the cones is more like 2–3 minutes (and approximately 10 minutes for rods). Remember that the time constants will depend on stimulus details such as size, luminance level, and retinal locus (Kalloniatis and Luu 2012). Cognitive mechanisms of adaptation rely on knowledge and interpretation of the stimulus configuration. Thus they can be thought of as effectively instantaneous once such knowledge is obtained. However, in some unusual viewing situations, the time required to interpret the scene can be quite lengthy, if not indefinite. Ferwerda *et al.* (1996) and Pattanaik *et al.* (2000) illustrate mathematical models for modifying the appearance of images based on changes in visual perception and adaptation.

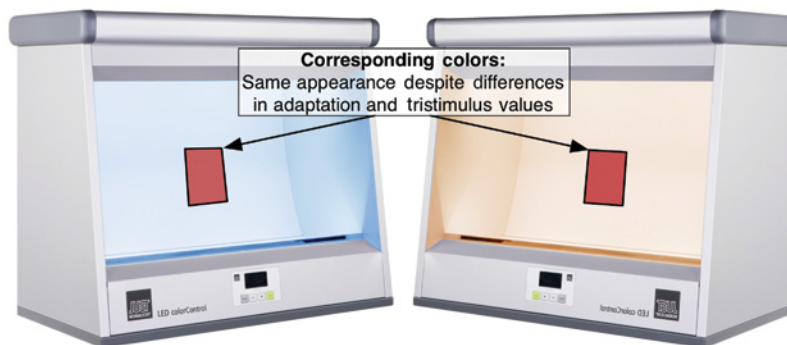


**Figure 8.10** A schematic diagram of a corresponding colors experiment. A stimulus in one viewing condition (left) is matched in appearance by a second stimulus in a second viewing condition (right), but will normally have different tristimulus values due to the change in viewing environment

## 8.4 CORRESPONDING COLORS DATA

The most extensively available visual data on chromatic adaptation are corresponding colors data. *Corresponding colors* are defined as two stimuli, viewed under differing viewing conditions, that match in color appearance, see Figure 8.10. For example, a stimulus specified by the tristimulus values,  $XYZ_1$ , viewed in one set of viewing conditions, might appear the same as a second stimulus specified by the tristimulus values,  $XYZ_2$ , viewed in a second set of viewing conditions.  $XYZ_1$  and  $XYZ_2$ , together with specifications of their respective viewing conditions, represent a pair of corresponding colors. It is important to note, however, that  $XYZ_1$  and  $XYZ_2$  are rarely numerically identical.

Corresponding colors data have been obtained through a wide variety of experimental techniques. Wright (1981a) provides an historical review of how and why chromatic adaptation has been studied. Some of the techniques, along with studies that have used them, are briefly described here.

### Asymmetric Matching

Since the collection of corresponding colors data requires a visual match to be determined across a change in viewing conditions, the experiments are sometimes referred to as *asymmetric matching experiments*. Ideally, color matches are made by direct, side-by-side comparison of the two stimuli. This is technically impossible to accomplish with two sets of viewing conditions unless some simplifying assumptions are made. Perhaps the most fascinating example is an experiment reported by MacAdam (1961) in which differential retinal conditioning was used. In this experiment, two different areas of the retina (left and right halves) were exposed to different adapting stimuli and then test and matching stimuli were presented in the two halves of the visual field for color matching. This technique requires the assumption that differential adaptation of

the two halves of the retina is similar to adaptation in normal viewing. This assumption is likely false and the differential retinal conditioning technique is only of historical interest.

## Haploscopic Matching

The next type of experiment is *haploscopic matching* in which one eye is adapted to one viewing condition and the other eye is adapted to a second viewing condition. Then a test stimulus presented in one eye is compared and matched with a stimulus presented to the other eye. Haploscopic experiments require the assumption that adaptation takes place independently in the two eyes. This assumption might be valid for sensory mechanisms, but it is certainly not valid for cognitive mechanisms. Some of the advantages and disadvantages of haploscopic experiments in color appearance research have been described by Fairchild *et al.* (1994). Hunt (1952) provides an example of a classic study using haploscopic viewing. Breneman (1987) described a clever device for haploscopic matching. An extensive study completed by the Color Science Association of Japan (CSAJ) (Mori *et al.* 1991) used haploscopic viewing with object–color stimuli.

## Memory Matching

To avoid the assumptions of differential retinal conditioning or haploscopic viewing, one must give up the precision of direct color matches in exchange for more realistic viewing conditions. One technique that allows more natural viewing is *memory matching*. In memory matching, observers generate a match in one viewing condition to the remembered color of a stimulus in a different viewing condition. Nelson *et al.* (1952) used a variation of memory matching in which observers assigned Munsell coordinates to various color stimuli. In effect, the observers were matching the stimuli to remembered Munsell samples under standard viewing conditions. Wright (1981a) suggested that achromatic memory matching (matching a gray appearance) would be an extremely useful technique for studying chromatic adaptation. Such a technique has been used to derive a variety of corresponding colors data (Fairchild 1990, 1991b, 1992b, 1993a).

## Magnitude Estimation

Another technique that allows natural viewing is magnitude estimation. In *magnitude estimation*, observers assign scale values to various attributes of appearance such as lightness, chroma, and hue, or brightness, colorfulness, and hue. Such experiments can provide color appearance data as well as corresponding colors data. An extensive series of magnitude estimation experiments has been reported by Luo *et al.* (1991a,b) and summarized by Hunt and Luo (1994).

## Cross-Media Comparisons

Braun *et al.* (1996) published an extensive series of experiments aimed at comparing various viewing techniques for cross-media image comparisons. They concluded that a short-term memory matching technique produced the most reliable results. It is also worthwhile to note that the Braun *et al.* (1996) study showed that the common practice of comparing self-luminous displays and reflection prints side-by-side produces unpredictable color appearances (or, alternatively, predicted matching images that are unacceptable when viewed individually).

Given all of these experimental techniques for deriving corresponding colors data, what can be learned from the results? Figure 8.11 illustrates corresponding colors data from the study of Breneman (1987). The circles represent chromaticities under illuminant D65 adaptation that match the corresponding chromaticities under illuminant A adaptation plotted using triangles. Given these data, it can safely be assumed that the pairs of corresponding colors represent lightness–chroma matches in color appearance across the change in viewing conditions. This is the case since lightness and chroma are the appearance parameters most intuitively judged for related colors. With this assumption, the corresponding colors data can be used to test a color appearance model by taking the set of values for the first viewing condition, using the model to predict lightness chroma matches for the second viewing condition, and comparing the predictions with the visual results.

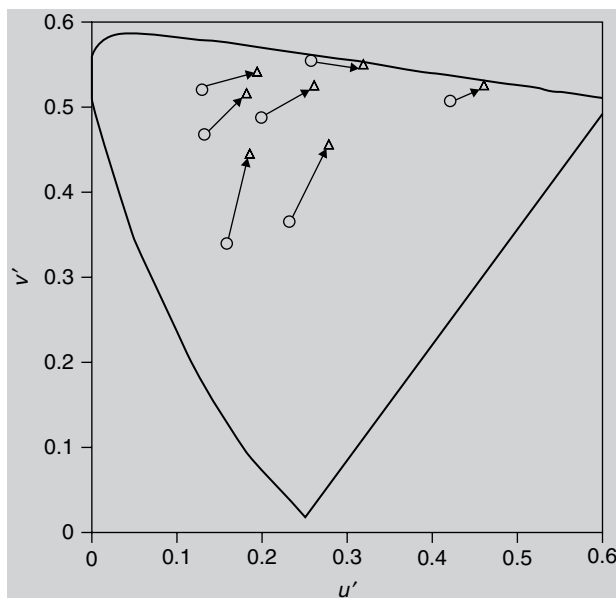


**Figure 8.11** An example of corresponding colors data for a change in chromatic adaptation from the chromaticity of illuminant D65 to that of illuminant A plotted in the  $u'v'$  chromaticity diagram

This same sort of test can be completed with a simpler form of model, known as a *chromatic adaptation transform* (or chromatic adaptation model). A chromatic adaptation model does not include correlates of appearance attributes such as lightness, chroma, and hue. Instead, a chromatic adaptation model simply provides a transformation from tristimulus values in one viewing condition to matching tristimulus values in a second set of viewing conditions, or in some pre-defined reference viewing condition.

## 8.5 MODELS

As described in Section 8.4, a chromatic adaptation model allows prediction of corresponding colors data. A general form of a chromatic adaptation model can be expressed as shown in Equations 8.1 through 8.3.

$$L_a = f(L, L_{\text{white}}, \dots) \quad (8.1)$$

$$M_a = f(M, M_{\text{white}}, \dots) \quad (8.2)$$

$$S_a = f(S, S_{\text{white}}, \dots) \quad (8.3)$$

This generic chromatic adaptation model is designed to predict three cone signals,  $L_a$ ,  $M_a$ , and  $S_a$ , after all of the effects of adaptation have acted upon the initial cone signals,  $L$ ,  $M$ , and  $S$ . Such a model requires, as a minimum, the cone excitations for the adapting stimulus,  $L_{\text{white}}$ ,  $M_{\text{white}}$ , and  $S_{\text{white}}$ . It is quite likely that an accurate model would require additional information as well (represented by the ellipses). A chromatic adaptation model can be converted into a chromatic adaptation transform by combining the forward model for one set of viewing conditions with the inverse model for a second set. Often such a transform is expressed in terms of CIE tristimulus values as shown in Equation 8.4.

$$XYZ_2 = f(XYZ_1, XYZ_{\text{white}1}, XYZ_{\text{white}2}, \dots) \quad (8.4)$$

In order to accurately model the physiological mechanisms of chromatic adaptation, it is necessary to express stimuli in terms of cone excitations, LMS, rather than CIE tristimulus values, XYZ. Fortunately, cone excitations (sometimes called cone fundamentals) can be reasonably approximated by a linear transformation ( $3 \times 3$  matrix) of CIE tristimulus values. Thus a generic chromatic adaptation transform can be described as shown in the flow chart in Figure 8.12. The complete process is as follows:

1. Begin with CIE tristimulus values ( $X_1 Y_1 Z_1$ ) for the first viewing condition.
2. Transform them to cone excitations ( $L_1 M_1 S_1$ ).
3. Incorporate information about the first set of viewing conditions ( $VC_1$ ) using the chromatic adaptation model to predict adapted cone signals ( $L_a M_a S_a$ ).
4. Reverse the process for the second set of viewing conditions ( $VC_2$ ) to determine the corresponding color in terms of cone excitations ( $L_2 M_2 S_2$ ) and ultimately CIE tristimulus values ( $X_2 Y_2 Z_2$ ).

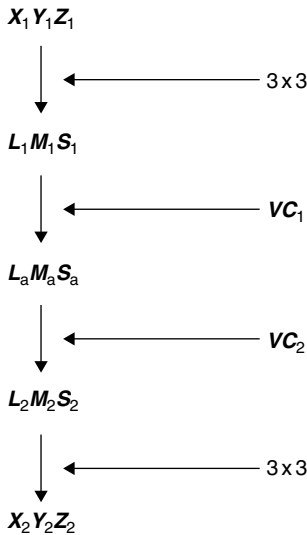


**Figure 8.12** A flow chart of the application of a chromatic adaptation model to the calculation of corresponding colors

Examples of specific chromatic adaptation models are given in Chapter 9. The CIE (2004c) has published a technical report reviewing the status of chromatic adaptation transforms. Further details on derivation of modern measures of the LMS cone responsivities and their relationship with CIE tristimulus values can be found in the work of Hunt *et al.* (1998), Logvinenko (1998), and Stockman *et al.* (1999, 2000).

Chromatic adaptation models provide predictions of corresponding colors and thus can be used to predict required color reproductions for changes in viewing conditions. If this is the only requirement for a given application, then a chromatic adaptation model might provide a simpler alternative to a complete color appearance model. Chromatic adaptation models are also the basic building blocks of all color appearance models. However, they do have some disadvantages. A chromatic adaptation model does not provide any predictors of appearance attributes such as lightness, chroma, and hue. These attributes might be necessary for some applications, such as image editing and gamut mapping. In these circumstances, a more complete color appearance model is required.

## 8.6 COLOR INCONSTANCY INDEX

One application in which a chromatic adaptation model is both necessary and useful is in the computation of a color inconstancy index. As explained in Chapter 6, the apparent color of objects tends to remain somewhat constant across changes in illumination, but it is not perfectly constant and any change in appearance depends on the spectral reflectance properties

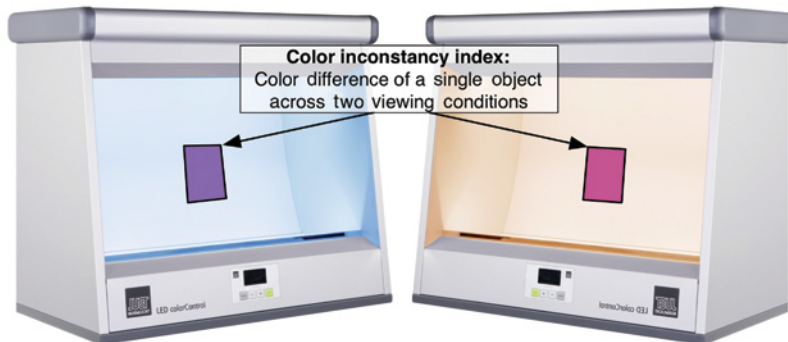


**Figure 8.13** A schematic diagram of a color inconstancy index measurement. A color difference is computed between the object in one viewing condition (left) and the same object (but different appearance) in a second viewing condition (right). A perfectly color constant object (extremely rare) would have the same appearance in both conditions and therefore a color inconstancy index of 0

of the object and the spectral power distributions of the illumination in question. A measure of color inconstancy is like a simple color difference measurement (*e.g.*,  $\Delta E_{ab}^*$ ) except that the two stimuli are each viewed in different viewing conditions as opposed to the normal situation where they are viewed side-by-side (Figure 8.13). One could simply compute the CIELAB values of the sample in each of its respective viewing conditions and then compute a color difference between the resulting coordinates. This procedure, however, assumes that CIELAB is a perfect appearance space and has an accurate chromatic adaptation transform/model. Neither of these assumptions is valid. Instead, a better color inconstancy index can be computed by using a more accurate chromatic adaptation transformation (*e.g.*, a von Kries model applied on LMS responsivities or the CAT02 model embedded in CIECAM02) to compute corresponding colors for both stimuli (the single object under both illuminations) under a single reference viewing condition (*e.g.*, CIE illuminant D65). Then those corresponding colors could be used to compute a color difference in CIELAB using whichever equation is desired. Thus the steps in a good color inconstancy index are to first use a good chromatic adaptation transform to compute corresponding colors under a single reference viewing condition and then use a selected color difference equation.

## 8.7 COMPUTATIONAL COLOR CONSTANCY

There is another field of study that produces mathematical models that are, at times, closely related to chromatic adaptation models. This is the field of *computational color constancy*. The objective in this approach is to take limited color information available in a typically trichromatic representation of a scene and produce color-constant estimates of the objects.

Essentially this reduces to an attempt to estimate signals that depend only on the spectral reflectances of objects and not on the illumination. On the other hand, chromatic adaptation models aim to predict the failure of color constancy actually observed in humans.

It is simple to prove that precise color constancy is not possible, or desirable, for the human visual system. The examples of metamerically object color pairs that cannot both be color constant and the need to include illuminants in practical colorimetry suffice to make this point. All this means is that striving for the most color-constant model is not necessarily a good way to model the human visual system. There are, however, applications in machine vision that could benefit greatly from having the most color-constant sensors possible.

The results in the field of computational color constancy provide some interesting constraints and techniques that could help in modeling human performance. For example, the results of Maloney and Wandell (1986) illustrate limits to the accuracy with which a trichromatic system could possibly estimate surface reflectances in a natural scene. D'Zmura and Lennie (1986) show how a trichromatic visual system can provide color-constant responses for one dimension of color appearance, hue, while sacrificing constancy for the other dimensions. The work of Finlayson *et al.* (1994a,b) illustrates how optimum sensory spectral responsivities can be derived to utilize the von Kries coefficient rule to obtain near color constancy.

These studies, and many more in the field, provide interesting insights into what the visual system could possibly do at the limits. Such insights can help in the construction, implementation, and testing of color appearance models. The techniques also provide definitive answers to questions pertaining to requirements for the collection of color images (digital still cameras, computer vision systems, and other image scanners), the synthesis of realistic images (computer graphics), and the design of colorimetric instrumentation (imaging colorimeters). Brill and West (1986) provide a useful review of the similarities and differences in the studies of chromatic adaptation and color constancy. Fairchild (2006, 2007a) illustrated how the lessons learned in human chromatic adaptation could be applied in spectral imaging systems to create a spectral adaptation model. Surprisingly, such a model could have a small amount of physiological plausibility as humans do have access to spectral information in scenes as long as they are three dimensional and include inter-reflections.

# Chromatic Adaptation Models

---

Chromatic adaptation is the single most important property of the human visual system with respect to understanding and modeling color appearance. Given this importance in vision science, there is significant literature available on various aspects of the topic. Chapter 8 reviewed some of the important properties of adaptation phenomena and mechanisms. It also provided the generic outline of a chromatic adaptation model for predicting corresponding colors. This chapter builds upon that information by including more detailed descriptions of a few specific chromatic adaptation transformations. It is impossible to cover all of the models that have been published. An attempt has been made to cover a variety of models and show their fundamental relationships to each other. Readers interested in more detail on the models or historical developments should delve into the available literature and also explore the review conducted by the CIE (2004b).

There are several other good places to start, including the review papers cited in Chapter 8 (Bartleson 1978, Lennie and D'Zmura Lennie and D'Zmura, 1988, Terstiege 1972, Wright 1981a). Further details on the early history of chromatic adaptation models can be found in an interesting overview study by Helson *et al.* (1952). Another excellent review of the entire field of color appearance with significant treatment of chromatic adaptation was written by Wyszecki (1986). Many of the classic papers in the field can be found in the collection edited by MacAdam (1993).

The models described in this chapter do allow the computation of corresponding colors, but they are not color appearance models. They include no predictors of appearance attributes such as lightness, chroma, and hue. They are, however, quite useful in predicting color matches across changes in viewing conditions. This is a significant extension of tristimulus colorimetry, all that is necessary in some applications, and the fundamental basis upon which all color appearance models are constructed.

Any physiologically plausible model of chromatic adaptation must act on signals representing the cone responses (or at least relative cone responses) or simple combinations thereof. Thus, in applications for which the use of CIE colorimetry is important, it is necessary to first transform from CIE tristimulus values ( $XYZ$ ) to cone responses (denoted  $LMS$ ,  $RGB$ , or  $\rho\gamma\beta$  depending on the model). Fortunately, cone responsivities can be accurately represented using a linear transformation of CIE tristimulus values. An example of such a transformation is graphically illustrated in Figure 9.1. This transformation, or a similar one, is common to all chromatic adaptation and color appearance models that are compatible with CIE colorimetry. Thus it is not explicitly included in every case in this book. Where the particular transformation is of importance to a particular model, it is explicitly stated in this and the following chapters.

## 9.1 VON KRIES MODEL

All viable modern chromatic adaptation models can trace their roots, both conceptually and mathematically, to the hypotheses of Johannes von Kries (1902). von Kries laid down some ideas about chromatic adaptation that, to this day, are being “rediscovered.” His idea was to propose a simple model of chromatic adaptation that would serve as a “straw man” for future research. He had fairly low expectations of his ideas as can be illustrated by the following quote from MacAdam’s translation of the 1902 paper:

*If some day it becomes possible to distinguish in an objective way the various effects of light by direct observation of the retina, people will perhaps recall with pitying smiles the efforts of previous decades which undertook to seek an understanding of the same phenomena by such lengthy detours [trans. MacAdam 1970: 119].*

Over eleven decades later, there is no one looking back at von Kries’ work with a “pitying smile.” Rather, many are looking back at his work with astonishment at how well it has withstood the test of time.

Von Kries (1902) did not outline a specific set of equations as representative of what is today referred to as the von Kries model, the von Kries proportionality law, the von Kries coefficient law, and other similar names. He simply outlined his hypothesis in words and described the potential impact of his ideas. In MacAdam’s translation of von Kries’ words:

*This can be conceived in the sense that the individual components present in the organ of vision are completely independent of one another and each is fatigued or adapted exclusively according to its own function [trans. MacAdam 1970: 118].*

The ideas that von Kries outlined were considered by him to be an extension of Grassmann’s laws of additive color mixture to comparisons across two viewing conditions.

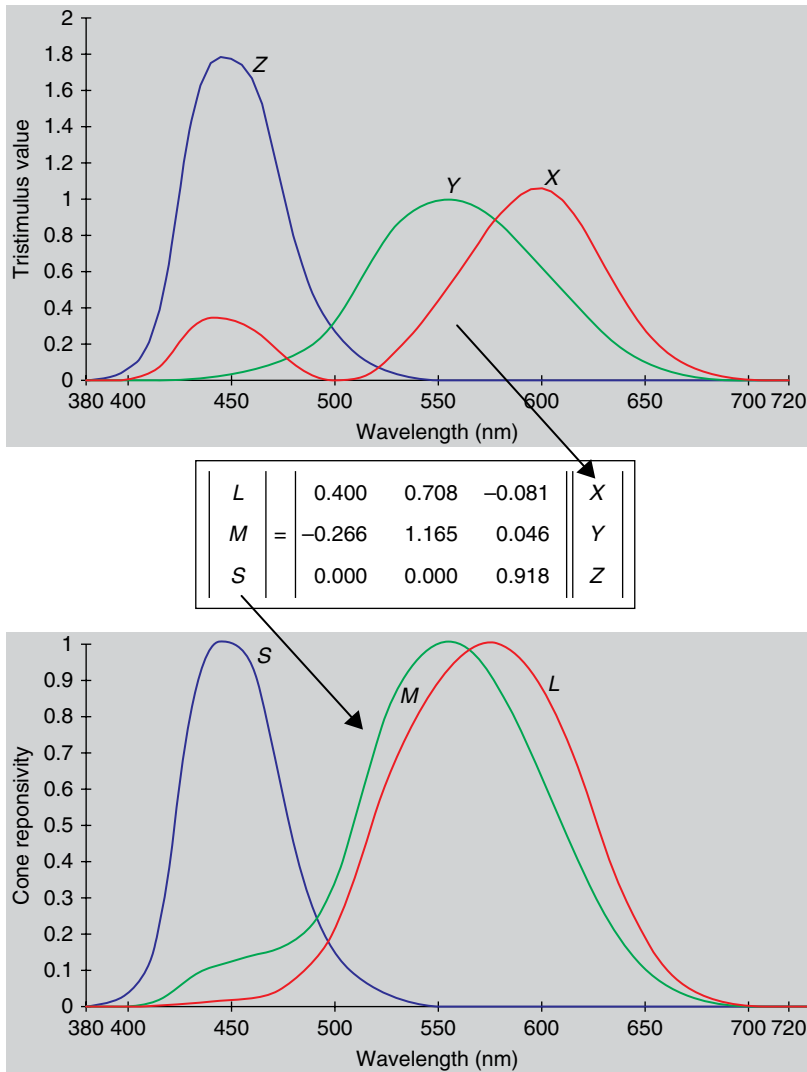


**Figure 9.1** The process of transformation from XYZ tristimulus values to LMS cone responsivities using an example linear matrix multiplication

The modern interpretation of the von Kries hypothesis in terms of a chromatic adaptation model is expressed in Equations 9.1 through 9.3.

$$L_a = k_L L \quad (9.1)$$

$$M_a = k_M M \quad (9.2)$$

$$S_a = k_S S \quad (9.3)$$

$L$ ,  $M$ , and  $S$  represent the initial cone responses;  $k_L$ ,  $k_M$ , and  $k_S$  are the coefficients used to scale the initial cone signals (*i.e.*, gain control); and  $L_a$ ,  $M_a$ , and  $S_a$  are the post-adaptation cone signals. Equations 9.1 through 9.3 represent a simple gain-control model of chromatic adaptation in which each of the three cone types has a separate gain coefficient. A key aspect of any model is how the particular values of  $k_L$ ,  $k_M$ , and  $k_S$  are obtained. In most modern instantiations of the von Kries model, the coefficients are taken to be the inverse of the  $L$ ,  $M$ , and  $S$  cone responses for the scene white or maximum stimulus as illustrated in Equations 9.4 through 9.6.

$$k_L = \frac{1}{L_{\max}} \quad \text{or} \quad k_L = \frac{1}{L_{\text{white}}} \quad (9.4)$$

$$k_M = \frac{1}{M_{\max}} \quad \text{or} \quad k_M = \frac{1}{M_{\text{white}}} \quad (9.5)$$

$$k_S = \frac{1}{S_{\max}} \quad \text{or} \quad k_S = \frac{1}{S_{\text{white}}} \quad (9.6)$$

Equations 9.4 through 9.6 are a mathematical representation of von Kries' statement that "each is fatigued or adapted exclusively according to its own function." Given the above interpretations of the gain coefficients, the von Kries model can be used to calculate corresponding colors between two viewing conditions by calculating the post-adaptation signals for the first condition, setting them equal to the post-adaptation signals for the second condition, and then reversing the model for the second condition. Performing these steps and completing the algebra results in the transformations given in Equations 9.7 through 9.9 that can be used to calculate corresponding colors.

$$L_2 = \left( \frac{L_1}{L_{\max 1}} \right) L_{\max 2} \quad (9.7)$$

$$M_2 = \left( \frac{M_1}{M_{\max 1}} \right) M_{\max 2} \quad (9.8)$$

$$S_2 = \left( \frac{S_1}{S_{\max 1}} \right) S_{\max 2} \quad (9.9)$$

In some cases, it becomes more convenient to express chromatic adaptation models in terms of matrix transformations. The interpretation of the von Kries model as described above is expressed in matrix notation in Equation 9.10.

$$\begin{vmatrix} L_a \\ M_a \\ S_a \end{vmatrix} = \begin{vmatrix} 1/L_{\max} & 0.0 & 0.0 \\ 0.0 & 1/M_{\max} & 0.0 \\ 0.0 & 0.0 & 1/S_{\max} \end{vmatrix} \begin{vmatrix} L \\ M \\ S \end{vmatrix} \quad (9.10)$$

The matrix notation can be extended to the calculation of corresponding colors across two viewing conditions and to explicitly include the transformation (matrix  $\mathbf{M}$ ) from CIE tristimulus values ( $XYZ$ ) to relative cone responses ( $LMS$ ). This is illustrated in Equation 9.11.

$$\begin{vmatrix} X_2 \\ Y_2 \\ Z_2 \end{vmatrix} = \mathbf{M}^{-1} \begin{vmatrix} L_{\max 2} & 0.0 & 0.0 \\ 0.0 & M_{\max 2} & 0.0 \\ 0.0 & 0.0 & S_{\max 2} \end{vmatrix} \begin{vmatrix} 1/L_{\max 1} & 0.0 & 0.0 \\ 0.0 & 1/M_{\max 1} & 0.0 \\ 0.0 & 0.0 & 1/S_{\max 1} \end{vmatrix} \begin{vmatrix} X_1 \\ Y_1 \\ Z_1 \end{vmatrix} \quad (9.11)$$

The von Kries transformation was used to predict the visual data of Breneman (1987) that were described in Chapter 8. The results are illustrated in a  $u'u'$  chromaticity diagram in Figure 9.2. The open symbols represent Breneman's corresponding colors data and the filled symbols represent the predictions using a von Kries model. Perfect model predictions would result in the filled triangles completely coinciding with the open triangles. In this calculation, the

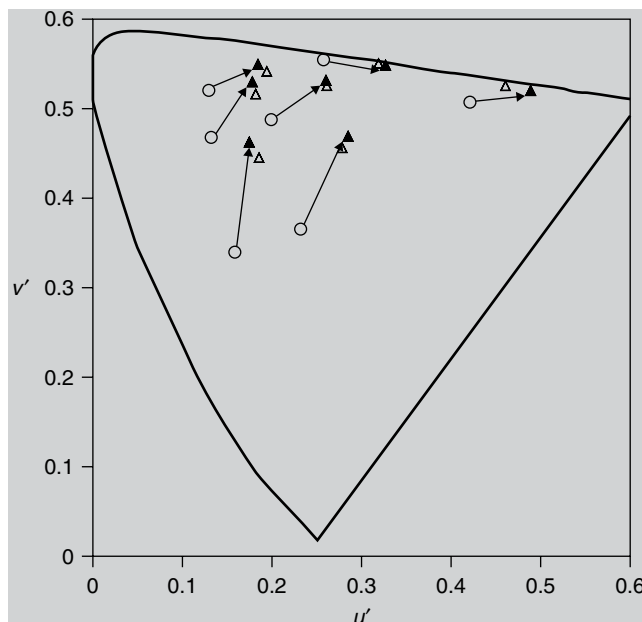


**Figure 9.2** Prediction of some example corresponding colors data using the von Kries model. Open triangles represent visual data and filled triangles represent model predictions

chromaticities under daylight adaptation (open circles in Figure 9.2) were used to predict the corresponding chromaticities under incandescent adaptation (triangles in Figure 9.2). It is clear in Figure 9.2 that the von Kries hypothesis was indeed a good one and that the modern interpretation as a chromatic adaptation transformation predicts the data surprisingly well.

Helson *et al.* (1952) presented an early study in which corresponding colors were derived by memory matching and the von Kries hypothesis was tested and performed quite well. Examples of more recent experimental data and analyses that address the utility and limitations of the von Kries hypothesis can be found in the work of Brainard and Wandell (1992) and Chichilnisky and Wandell (1995). There are some discrepancies between these, and other, visual data and the predictions of the von Kries model. Such discrepancies have led investigators down many paths that are described in the remaining sections of this chapter and throughout this book. Perhaps it should not be too surprising to realize that von Kries (1902) himself foresaw this. The next line after his description of what is now referred to as the von Kries model reads:

*But if the real physiological equipment is considered, on which the processes are based, it is permissible to doubt whether things are so simple* [trans. MacAdam 1970: 118].

Indeed things are not so simple, but it is amazing how close such a simple hypothesis comes to explaining the majority of the chromatic adaptation phenomena.

## 9.2 RETINEX THEORY

An often discussed account of the mechanisms of chromatic adaptation under the rubric of color constancy is the retinex theory developed by Edwin Land and his colleagues (Land 1977, 1986, Land and McCann 1971). The *retinex theory* can be considered an enhanced version of the von Kries model. Various enhancements have been proposed, but the key feature is that the retinex algorithm explicitly treats the spatial distribution of colors in a scene in order to better model the visual perceptions that can be observed in complex scenes.

Land's theory was formulated to explain demonstrations of the independence of color appearance on the spectral distribution of reflected light (tristimulus values). Land suggested that color appearance is controlled by surface reflectances rather than the distribution of reflected light. The retinex algorithm, in Land's (1986) most recent form, is quite simple. Land proposed three color mechanisms with the spectral responsivities of the cone photoreceptors. He called these mechanisms *retinexes* since they are thought to be some combination of retinal and cortical mechanisms. Land hypothesized a three-dimensional color appearance space with the output of the long-, middle-, and short-wavelength sensitive retinexes as

the dimensions. The output of a retinex is determined by taking the ratio of the signal at any given point in the scene and normalizing it with an average of the signals in that retinex throughout the scene. The most interesting feature of this algorithm is that it acknowledges variations in color due to changes in the background of the stimulus. The influence of the background can be varied by changing the spatial distribution of the retinex signals that are used to normalize a given point in the scene. If one takes the normalizing signal to be the scene average for a given retinex, then the retinex algorithm reduces to a typical instantiation of a von Kries-type transformation. There are some flaws in the physiological implementation of the retinex model (Brainard and Wandell 1986, Lennie and D'Zmura Lennie and D'Zmura, 1988), but if one is more interested in the algorithm output than having a strict physiological model of the visual system (which is also the case for most color appearance models), then the concepts in the retinex theory might prove useful. For example, the retinex algorithm has recently been applied in the development of a digital image processing algorithm for dynamic range compression and color correction (Jobson *et al.* 1997). Other applications, challenges, and successes for such a theory have been reviewed by McCann (1993).

The need to consider spatial as well as spectral dimensions in high-level color appearance models is undeniable. Concepts embedded in the retinex theory provide some insight on how this might be accomplished. Other approaches are also under development (Poirson and Wandell 1993, Zhang and Wandell 1996). The retinex theory sets the stage for other developments in chromatic adaptation models. The general theme is that the von Kries model provides a good foundation but needs enhancement to address certain adaptation phenomena. Spatial models of chromatic adaptation and image appearance are discussed more fully in Chapter 20.

### 9.3 NAYATANI ET AL. MODEL

One important enhancement to the von Kries hypothesis is the nonlinear chromatic adaptation model developed by Nayatani and coworkers. This nonlinear model was developed from a colorimetric background (enhancement to CIE tristimulus colorimetry) within the field of illumination engineering. The early roots of this model can be traced to the work of MacAdam (1961).

#### MacAdam's Model

MacAdam (1961) described a nonlinear model of chromatic adaptation in which the output of the cones was expressed as a constant plus a multiplicative factor of the cone excitation raised to some power. This nonlinear model represented an empirical fit to MacAdam's (1956) earlier chromatic adaptation data. Interestingly enough, MacAdam required a visual system with five types of cones in order to explain his data with a linear model! (This is probably because MacAdam used a rather unusual experimental

technique in which two halves of the same retina were differentially adapted.) MacAdam's nonlinear model provided a good fit to the data and was the precursor of later nonlinear models.

## Nayatani's Model

The nonlinear model of Nayatani *et al.* (1980, 1981) begins with a gain adjustment followed by a power function with a variable exponent. In this model, the von Kries coefficients are proportional to the maximum long-, middle-, and short-wavelength cone responses and the exponents of the power functions depend on the luminance of the adapting field. The power function nonlinearity was suggested in the classic brightness study by Stevens and Stevens (1963). Another interesting and important feature of the nonlinear model is that noise terms are added to the cone responses. This helps to model threshold behavior and avoid any possibility of division by 0. Equations 9.12 through 9.14 are generalized expressions of the nonlinear model.

$$L_a = \alpha_L \left( \frac{L + L_n}{L_0 + L_n} \right)^{\beta_L} \quad (9.12)$$

$$M_a = \alpha_M \left( \frac{M + M_n}{M_0 + M_n} \right)^{\beta_M} \quad (9.13)$$

$$S_a = \alpha_S \left( \frac{S + S_n}{S_0 + S_n} \right)^{\beta_S} \quad (9.14)$$

$L_a$ ,  $M_a$ , and  $S_a$  are the cone signals after adaptation;  $L$ ,  $M$ , and  $S$  are the cone excitations;  $L_n$ ,  $M_n$ , and  $S_n$  are the noise terms;  $L_0$ ,  $M_0$ , and  $S_0$  are the cone excitations for the adapting field;  $\beta_L$ ,  $\beta_M$ , and  $\beta_S$  are the exponents and are monotonically increasing functions of the respective cone excitations for the adapting field; and  $\alpha_L$ ,  $\alpha_M$ , and  $\alpha_S$  are coefficients determined by the principle that exact color constancy holds for a non-selective sample of the same luminance factor as the adapting background.

The formulations for the exponents can be found in Nayatani *et al.* (1982). Takahama *et al.* (1984) extended the model to predict corresponding colors for backgrounds of various luminance factors. A version of the model (Nayatani *et al.* 1987) was accepted for field trial by the CIE. This meant that the CIE, through its technical committee activities, wanted to collect additional data to test the model, possibly improve it, and determine whether it or some other model should be recommended for general use. The results of the field trials were inconclusive, so the CIE did not make a recommendation on this model. Refinements of the model were made during the course of field trials and these have been summarized in a CIE technical

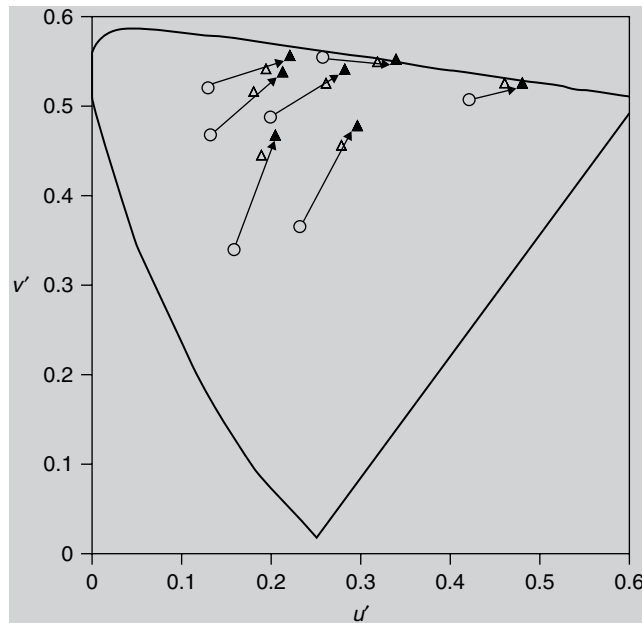


**Figure 9.3** Prediction of some example corresponding colors data using the nonlinear model of Nayatani *et al.* Open triangles represent visual data and filled triangles represent model predictions

report (CIE 1994), which provides full details of the current formulation of the model.

The nonlinear model was used to predict Breneman's (1987) corresponding colors. The results, analogous to those presented in Figure 9.2 for the von Kries model, are illustrated in Figure 9.3. The predictions are quite good, but not as good as those of the simple von Kries model (for these particular data). One reason for this is that Breneman's data were collected under viewing conditions for which discounting-the-illuminant could not occur and thus chromatic adaptation was less complete. This is illustrated by the predictions of the Nayatani model, which are all shifted toward the yellow side of the visual data. This indicates that the incandescent adapting field in Breneman's experiment retained some yellowish appearance. Recent enhancements (Nayatani 1997) have provided techniques to estimate and account for the degree of chromatic adaptation in various experiments.

This nonlinear model is capable of predicting the Hunt (1952) effect (increase in colorfulness with adapting luminance), the Stevens effect (increase in lightness contrast with luminance), and the Helson–Judd effect (hue of non-selective samples under chromatic illumination). It is worth noting that the von Kries adaptation transform is luminance-independent and therefore cannot be used to predict appearance phenomena that are functions of luminance. Also, the linear nature of the simple von Kries transform precludes it from predicting the Helson–Judd effect.

Nayatani's nonlinear model is important for several reasons. It provides a relatively simple extension of the von Kries hypothesis that is capable of predicting several additional effects, it has had a significant historical impact on the CIE work in chromatic adaptation and color appearance modeling, and it provides the basis for one of just two comprehensive color appearance models. The full Nayatani color appearance model is described in Chapter 11.

## 9.4 GUTH'S MODEL

There are many variations of the von Kries hypothesis. One significant variation that is in some ways similar to the Nayatani model, from the field of vision science (rather than colorimetry), is the model described by Guth (1991, 1995). Guth's model is not directly related to CIE tristimulus colorimetry since the cone responsivities used are not linear transformations of the CIE color matching functions. This produces some practical difficulties in implementing the model, but for practical situations it is advisable and certainly not harmful to the predictions to use a set of cone responsivities that can be derived directly from CIE tristimulus values, along with the remainder of Guth's formulation. This model, part of the ATD vision model described in Chapter 14, has been developed over many years to predict the results of various vision experiments. Most of these experiments involve classical threshold psychophysics rather than scaling of the various dimensions of color appearance as defined in Chapter 4.

The general form of Guth's chromatic adaptation model is given in Equations 9.15 through 9.20.

$$L_a = L_r \left[ 1 - \left( \frac{L_{r0}}{\sigma + L_{r0}} \right) \right] \quad (9.15)$$

$$L_r = 0.66L^{0.7} + 0.002 \quad (9.16)$$

$$M_a = M_r \left[ 1 - \left( \frac{M_{r0}}{(\sigma + M_{r0})} \right) \right] \quad (9.17)$$

$$M_r = 1.0M^{0.7} + 0.003 \quad (9.18)$$

$$S_a = S_r \left[ 1 - \left( \frac{S_{r0}}{\sigma + S_{r0}} \right) \right] \quad (9.19)$$

$$S_r = 0.45S^{0.7} + 0.00135 \quad (9.20)$$

$L_a$ ,  $M_a$ , and  $S_a$  are the cone signals after adaptation;  $L$ ,  $M$ , and  $S$ , are the cone excitations;  $L_{r0}$ ,  $M_{r0}$ , and  $S_{r0}$  are the cone excitations for the adapting field

after the nonlinear function; and  $\sigma$  is a constant (nominally 300) that can be thought of as representing a noise term. It is also important to note that the cone responses in this model must be expressed in absolute units since the luminance level does not enter the model elsewhere.

Some algebraic manipulation of the adaptation model as expressed above helps to illustrate its relationship with the von Kries model. Ignoring the initial nonlinearity, a von Kries-type gain control coefficient for the Guth model can be pulled out of Equation 9.15 as shown in Equation 9.21.

$$k_L = 1 - \left( \frac{L_{r0}}{\sigma + L_{r0}} \right) \quad (9.21)$$

Using the algebraic substitutions illustrated in Equations 9.22 through 9.24, the relationship to the traditional von Kries coefficient becomes clear. The difference lies in the  $\sigma$  term, which can be thought of as a noise factor that is more important at low stimulus intensities than at high intensities. Thus, as luminance level increases, the Guth model becomes more and more similar to the nominal von Kries model.

$$k_L = \left( \frac{\sigma + L_{r0}}{\sigma + L_{r0}} \right) - \left( \frac{L_{r0}}{\sigma + L_{r0}} \right) \quad (9.22)$$

$$k_L = \frac{\sigma + L_{r0} - L_{r0}}{\sigma + L_{r0}} \quad (9.23)$$

$$k_L = \frac{\sigma}{\sigma + L_{r0}} \quad (9.24)$$

Figure 9.4 shows the Guth model prediction of Breneman's (1987) corresponding colors data. The calculations were carried out using the nominal, published form of the Guth model. It is clear that there is a systematic deviation between the observed and predicted results. This discrepancy can be traced to the  $\sigma$  parameter. The Breneman data are fairly well predicted using a simple von Kries model. Thus if the  $\sigma$  parameter were made smaller, the prediction of the Guth model would improve. This highlights a feature (or a drawback) of the Guth model. As a framework for a vision model, it is capable of making impressive predictions of available data. However, the model often requires a small amount of adjustment in its parameters for any given viewing condition or experiment. This is acceptable when trying to predict various observed phenomena, but is not practical in many applications such as cross-media color reproduction where the viewing conditions are often not known until it is time to calculate a predicted image and there is no chance for iterations. Thus to apply the Guth adaptation model (and the full ATD model described in Chapter 14) to such situations, some interpretation of how to implement the model is necessary.

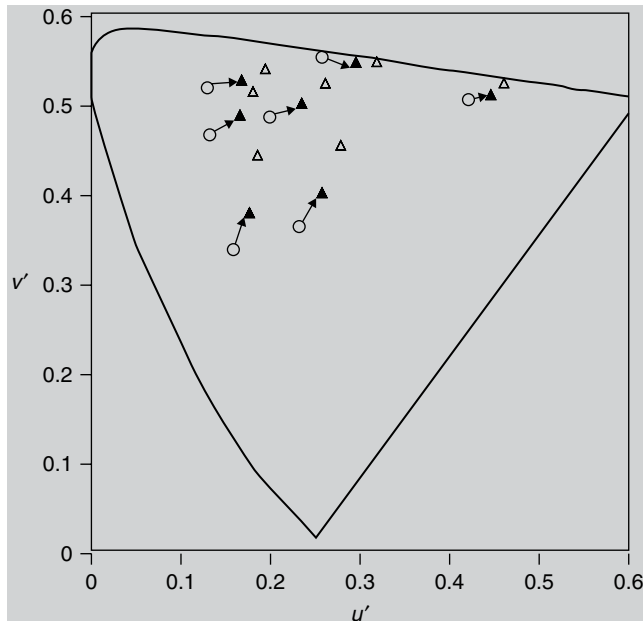


**Figure 9.4** Prediction of some example corresponding colors data using the Guth model. Open triangles represent visual data and filled triangles represent model predictions

## 9.5 FAIRCHILD'S 1990 MODEL

The Breneman (1987) results showing incomplete chromatic adaptation inspired a series of experiments (Fairchild 1990) aimed at measuring the degree of chromatic adaptation to various forms of adapting stimuli. This work led to the development of yet another modification of the von Kries hypothesis that included the ability to predict the degree of adaptation based on the adapting stimulus itself (Fairchild 1991a,b). This model, like Nayatani's model, is designed to be fully compatible with CIE colorimetry; however, it is more rooted in the field of imaging science rather than in illumination engineering. It was designed to be a relatively simple model and to include discounting-the-illuminant and the Hunt effect, in addition to incomplete chromatic adaptation.

The model is most clearly formulated as a series of matrix multiplications. The first step is a transformation from CIE tristimulus values,  $XYZ$ , to fundamental tristimulus values,  $LMS$ , for the first viewing condition as shown in Equations 9.25 and 9.26. The Hunt–Pointer–Estevez transformation with illuminant D65 normalization is used.

$$\begin{vmatrix} L_1 \\ M_1 \\ S_1 \end{vmatrix} = \mathbf{M} \begin{vmatrix} X_1 \\ Y_1 \\ Z_1 \end{vmatrix} \quad (9.25)$$

$$\mathbf{M} = \begin{vmatrix} 0.4002 & 0.7076 & -0.0808 \\ -0.2263 & 1.1653 & 0.0457 \\ 0.0 & 0.0 & 0.9182 \end{vmatrix} \quad (9.26)$$

The next step is to apply a modified form of the von Kries chromatic adaptation transform that takes incomplete chromatic adaptation into account as illustrated in Equations 9.27 through 9.31.

$$\begin{vmatrix} L'_1 \\ M'_1 \\ S'_1 \end{vmatrix} = \mathbf{A}_1 \begin{vmatrix} L_1 \\ M_1 \\ S_1 \end{vmatrix} \quad (9.27)$$

$$\mathbf{A} = \begin{vmatrix} a_L & 0.0 & 0.0 \\ 0.0 & a_M & 0.0 \\ 0.0 & 0.0 & a_S \end{vmatrix} \quad (9.28)$$

$$a_M = \frac{p_M}{M_n} \quad (9.29)$$

$$p_M = \frac{1 + Y_n^\nu + m_E}{1 + Y_n^\nu + 1/m_E} \quad (9.30)$$

$$m_E = \frac{3(M_n/M_E)}{L_n/L_E + M_n/M_E + S_n/S_E} \quad (9.31)$$

The  $p$  and  $a$  terms for the short- (S) and long-wavelength (L) sensitive cones are derived in a similar fashion.  $Y_n$  is the luminance of the adapting stimulus in  $\text{cd}/\text{m}^2$ , and terms with  $n$  subscripts refer to the adapting stimulus while terms with  $E$  subscripts refer to the equal-energy illuminant. The exponent,  $\nu$ , is set equal to 1/3. The form of these equations for incomplete adaptation is based on those used in the Hunt (1991b) color appearance model, which is described in more detail in Chapter 12. (A separate chromatic adaptation transformation was never published by Hunt; thus Hunt's model is treated in full in Chapter 12.) When cognitive discounting-the-illuminant occurs, the  $p_L$ ,  $p_M$  and  $p_S$  terms are all set equal to 1.0. The  $a$  terms are modified von Kries coefficients. The  $p$  terms represent the proportion of complete von Kries adaptation. They depart from 1.0 as adaptation becomes incomplete. The  $p$  values depend on the adapting luminance and color. As the luminance increases, the level of adaptation becomes more complete. As the adapting chromaticity moves farther and farther from a normalizing point (the equal-energy illuminant), adaptation becomes less complete. Equations 9.30 and 9.31 serve to ensure this behavior in the model. These predictions are consistent with the available experimental data (Breneman 1987, Fairchild 1992b, Hunt and Winter 1975). Related results of interest are those of Hurvich and Jameson (1951) where they showed that the perception of

white arises for the lowest luminance levels when the chromaticity is near that of D65 and the recent work of Rea and Freyssinier (2013) illustrating that lighting appears white for chromaticities above the Planckian locus for high CCTs and below the Planckian locus for low CCTs.

The final step in the calculation of post-adaptation signals is a transformation that allows luminance-dependent interaction between the three cone types as shown in Equations 9.32 through 9.34.

$$\begin{vmatrix} L_a \\ M_a \\ S_a \end{vmatrix} = \mathbf{C}_1 \begin{vmatrix} L'_1 \\ M'_1 \\ S'_1 \end{vmatrix} \quad (9.32)$$

$$\mathbf{C} = \begin{vmatrix} 1.0 & c & c \\ c & 1.0 & c \\ c & c & 1.0 \end{vmatrix} \quad (9.33)$$

$$c = 0.219 - 0.0784 \log_{10}(Y_n) \quad (9.34)$$

The  $c$  term was derived from the work of Takahama *et al.* (1977) known as the *linkage model*. In that model, which the authors later gave up, citing a preference for the nonlinear model (Nayatani *et al.* 1981), the interaction terms were introduced to predict luminance-dependent effects. This is the same reason the  $\mathbf{C}$  matrix was included in this model.

To determine corresponding chromaticities for a second adapting condition, the  $\mathbf{A}$  and  $\mathbf{C}$  matrices must be derived for that condition, inverted, and applied as shown in Equations 9.35 through 9.37.

$$\begin{vmatrix} L'_2 \\ M'_2 \\ S'_2 \end{vmatrix} = \mathbf{C}_2^{-1} \begin{vmatrix} L_a \\ M_a \\ S_a \end{vmatrix} \quad (9.35)$$

$$\begin{vmatrix} L_2 \\ M_2 \\ S_2 \end{vmatrix} = \mathbf{A}_2^{-1} \begin{vmatrix} L'_2 \\ M'_2 \\ S'_2 \end{vmatrix} \quad (9.36)$$

$$\begin{vmatrix} X_2 \\ Y_2 \\ Z_2 \end{vmatrix} = \mathbf{M}^{-1} \begin{vmatrix} L_2 \\ M_2 \\ S_2 \end{vmatrix} \quad (9.37)$$

The entire model can be expressed as the single matrix Equation 9.38.

$$\begin{vmatrix} X_2 \\ Y_2 \\ Z_2 \end{vmatrix} = \mathbf{M}^{-1} \mathbf{A}_2^{-1} \mathbf{C}_2^{-1} \mathbf{C}_1 \mathbf{A}_1 \mathbf{M} \begin{vmatrix} X_1 \\ Y_1 \\ Z_1 \end{vmatrix} \quad (9.38)$$

Subsequent experiments (Pirrotta and Fairchild 1995) showed that the **C** matrix introduced an unwanted luminance dependency that resulted in an overall shift in lightness with luminance level. This shift did not impact the quality of image reproductions since the whole image shifted. However, it did introduce significant systematic error in predictions for simple object colors. Thus the model was revised (Fairchild 1994b) by eliminating the **C** matrix. This improved the predictions for simple colors, while having no impact on the results for images. It did remove the model's capability to predict the Hunt effect. However, in imaging applications, this turns out to be unimportant since any predictions of the Hunt effect would be counteracted by the process of gamut mapping. These changes, along with some further simplifications in the equations (different normalizations) were compiled and used as the basis for the latest version of the RLAB (Fairchild 1996) color appearance model presented in Chapter 13.

Figure 9.5 shows predictions of the Breneman (1987) corresponding colors data using the Fairchild chromatic adaptation transformation. The predictions are identical for either version (original or simplified) of the model described above. The predictions are as good as, or better than, each of the models presented thus far. Quantitative analyses of all of Breneman's (1987) data confirms this result (Fairchild 1991a,b).

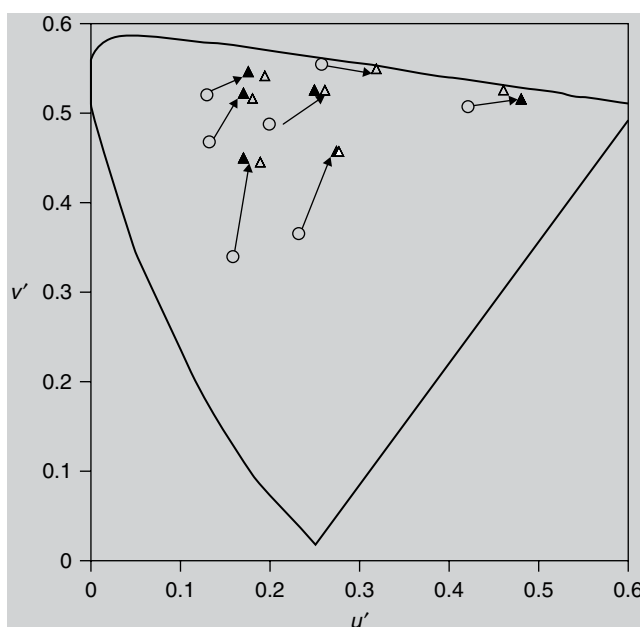


**Figure 9.5** Prediction of some example corresponding colors data using the Fairchild (1991b) model. Open triangles represent visual data and filled triangles represent model predictions

## 9.6 HERDING CATS

The CIE (1998) established the CIECAM97s color appearance model as described in Chapter 15. That model used a modified form of a chromatic adaptation transform known as the Bradford transformation. The Bradford transformation is essentially a von Kries transformation with an additional exponential nonlinearity on the blue channel only and optimized cone responsivities. The nonlinearity on the blue channel introduced some practical issues with respect to inversion of the CIECAM97s model, so a new emphasis was placed on simple linear chromatic adaptation transforms (or CATs as they have come to be called) through optimization of the matrix transformation from *XYZ* to *RGB* values prior to the von Kries normalization.

Fairchild (2001) published a review of various linear CATs for consideration in a revised version of CIECAM97s ultimately to become CIECAM02 (Chapter 16). A variety of techniques for deriving optimal matrix transformations were explored and each produced slightly different results with various advantages or disadvantages. The common result was that, with an optimized matrix transformation, a linear CAT could be derived that would perform as well as the nonlinear CAT incorporated in CIECAM97s for all available data sets. This encouraging result led to the ultimate derivation of CIECAM02 by CIE TC8-01 with a linear CAT.

The decision by TC8-01 to use a linear CAT was an easy one. The more difficult decision was which optimized matrix transformation to select. The candidate matrices were quite similar and all shared the characteristic that the responsivities they defined were more spectrally sharp (narrower, more spectrally distinct, and including negative values) than cone responsivities. While the physiological plausibility of a simple von Kries transformation on such optimized responsivities is questionable, the models might well represent a more accurate simple black-box prediction of the output of the combined mechanisms of chromatic adaptation in the human visual system. The von Kries predictions obtained using sharpened responsivities tend to be more color constant than von Kries predictions obtained using cone responsivities. This prediction of improved color constancy likely mimics the enhancements produced by higher level adaptation mechanisms.

Calabria and Fairchild (2001) performed a practical intercomparison of the various linear CATs that had been proposed. Their results indicated that images computed with the various optimized matrices were indistinguishable for any practical applications. The only linear CAT that produced significantly different results was that based on cone responsivities. Thus, the Calabria and Fairchild (2001) work confirmed that significant gains were made by using optimized transformation matrices as opposed to simple cone responsivities. This result was consistent with the tests completed by CIE TC8-01 on various corresponding colors data sets. Since the various optimized matrices performed identically within practical limits, TC8-01 then moved on to secondary criteria to select the transformation ultimately used in CIECAM02, known as CAT02.

## 9.7 CAT02

As described in the preceding Section 9.6, CIE TC8-01 (CIE 2004a) selected a linear CAT based on a matrix optimized to a wide variety of corresponding colors data while maintaining approximate compatibility with the non-linear transformation in CIECAM97s. The chromatic adaptation transform thus specified is known as CAT02 and is presented in Equations 9.39 and 9.40.

$$\begin{vmatrix} X_2 \\ Y_2 \\ Z_2 \end{vmatrix} = \mathbf{M}_{\text{CAT02}}^{-1} \begin{vmatrix} R_{\text{adapt2}} & 0.0 & 0.0 \\ 0.0 & G_{\text{adapt2}} & 0.0 \\ 0.0 & 0.0 & B_{\text{adapt2}} \end{vmatrix} \begin{vmatrix} 1/R_{\text{adapt1}} & 0.0 & 0.0 \\ 0.0 & 1/G_{\text{adapt1}} & 0.0 \\ 0.0 & 0.0 & 1/B_{\text{adapt1}} \end{vmatrix} \mathbf{M}_{\text{CAT02}} \begin{vmatrix} X_1 \\ Y_1 \\ Z_1 \end{vmatrix} \quad (9.39)$$

$$\mathbf{M}_{\text{CAT02}} = \begin{vmatrix} 0.7328 & 0.4296 & -0.1624 \\ -0.7036 & 1.6975 & 0.0061 \\ 0.0030 & 0.0136 & 0.9834 \end{vmatrix} \quad (9.40)$$

The process follows the normal von Kries transformation with a conversion from CIE tristimulus values ( $XYZ$ ) to sharpened cone responsivities ( $RGB$ )

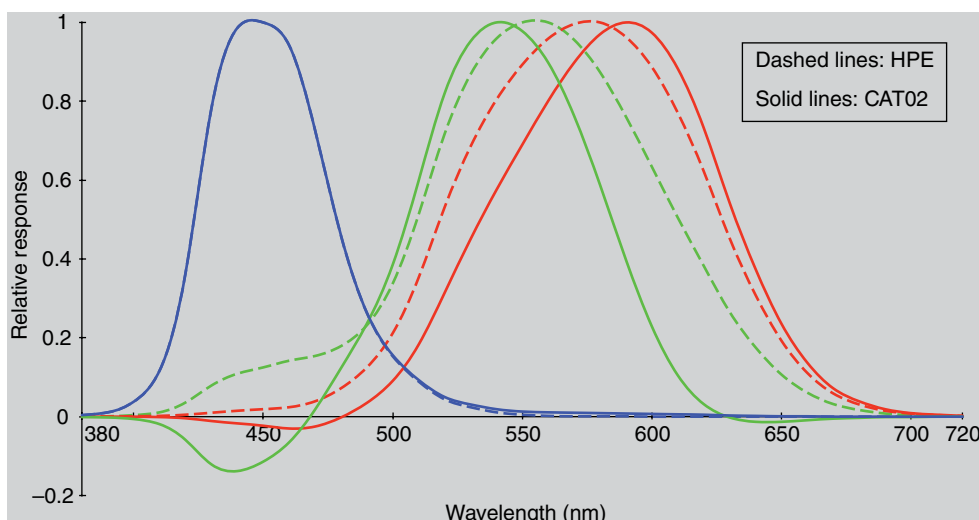


**Figure 9.6** Comparison of the Hunt–Pointer–Estevez cone responsivities (thin lines, labeled HPE) with the “sharpened” responsivities used in the CAT02 chromatic adaptation transform (thick lines, labeled CAT02). Note how the “sharpened” responsivities are more spectrally distinct, narrower, and include some negative values. All responsivities have been normalized to set their maximum value to 1.0

using the  $\mathbf{M}_{\text{CAT02}}$  matrix transformation. The *RGB* values are then divided by the adapting *RGB* values for the first viewing condition and multiplied by the adapting *RGB* values for the second viewing condition prior to a linear transformation back to corresponding CIE tristimulus values. In Figure 9.6, the spectral responsivities represented by  $\mathbf{M}_{\text{CAT02}}$  are contrasted with the Hunt–Pointer–Estevez cone responsivities used in many chromatic adaptation transformations and color appearance models.

It should also be noted that Equations 9.39 and 9.40 represent CAT02 in its simplest form under the assumption of complete chromatic adaptation. Simple enhancements to the transformation to allow for the prediction of incomplete chromatic adaptation and discounting-the-illuminant are presented in the full description of CIECAM02 in Chapter 16.

# 10

# Color Appearance Models

---

The chromatic adaptation transforms discussed in Chapter 9 go a long way toward extending tristimulus colorimetry toward the prediction of color appearance. However, they are still limited in that they can only predict matches across disparate viewing conditions (*i.e.*, corresponding colors). A chromatic adaptation transform alone cannot be used to describe the actual color appearance of stimuli. To do this, one must use the appearance parameters defined in Chapter 4 – the absolute color appearance attributes of brightness, colorfulness, and hue and the relative color appearance attributes of lightness, chroma, saturation, and, again, hue. These terms are used to describe the color appearance of stimuli. Chromatic adaptation transforms provide no measure of correlates to these perceptual attributes. This is the domain of color appearance models.

## 10.1 DEFINITION OF COLOR APPEARANCE MODELS

The world of color measurement is full of various descriptors of color such as tristimulus values, chromaticity coordinates, UCS, uniform color spaces, and “just plain-old” color spaces. Sometimes it is difficult to keep all the names and distinctions straight. So just what is it that sets a color appearance model apart from all of these other types of color specification? CIE Technical Committee 1-34, *Testing Colour Appearance Models*, was given the task of evaluating the performance of various color appearance models and recommending a model for general use. Thus, one of the first tasks of this committee became the definition of just what constitutes a color appearance model in order to be included in the tests (Fairchild 1995a).

TC1-34 agreed on the following definition: A color appearance model is any model that includes predictors of at least the relative color appearance attributes of lightness, chroma, and hue. For a model to include reasonable predictors of these attributes, it must include at least some form of a chromatic adaptation transform. Models must be more complex to include predictors of brightness and colorfulness or to model other luminance-dependent effects such as the Stevens effect or the Hunt effect.

Given the above definition, some fairly simple uniform color spaces, such as the CIE 1976  $L^*a^*b^*$  color space (CIELAB) and the CIE 1976  $L^*u^*v^*$  color space (CIELUV), can be considered color appearance models. These color spaces include simple chromatic adaptation transforms and predictors of lightness, chroma, and hue. The general construction of a color appearance model and then a discussion of CIELAB as a specific example are presented in the following sections.

## 10.2 CONSTRUCTION OF COLOR APPEARANCE MODELS

Some general concepts that apply to the construction of all color appearance models are described in this section. All color appearance models for practical applications begin with the specification of the stimulus and viewing conditions in terms of CIE XYZ tristimulus values (along with certain absolute luminances for some models). The first process applied to these data is generally a linear transformation from XYZ tristimulus values to cone responses in order to more accurately model the physiological processes in the human visual system. The importance of beginning with CIE tristimulus values is a matter of practicality. There is a great deal of color measurement instrumentation that is available to quickly and accurately measure stimuli in terms of CIE tristimulus values. The CIE system is also a well-established, international standard for color specification and communication. Whether the model begins with CIE 1931 ( $2^\circ$ ) or CIE 1964 ( $10^\circ$ ) tristimulus values is of little practical importance as the uncertainty in scaling color appearance is much larger than the difference in color match predictions due to the selection of standard observer.

Occasionally, vision-science-based models of color vision and appearance are based upon cone responsivities that are not linear transformations of CIE color matching functions (Guth 1995). The small advantage in performance that such an approach provides is far outweighed by the inconvenience in practical applications.

Given tristimulus values for the stimulus, other data regarding the viewing environment must also be considered in order to predict color appearance. This is illustrated by all of the color appearance phenomena described in Chapters 6 and 7. As a minimum, the tristimulus values of the adapting stimulus (usually taken to be the light source) are also required. Additional data that might be utilized include the absolute luminance level, colorimetric data on the proximal field, background, and surround, and perhaps other spatial or temporal information.

Given some or all of the above data, the first step in a color appearance model is generally a chromatic adaptation transform such as those described in Chapter 9. The post-adaptation signals are then combined into higher level signals usually modeled after the opponent theory of color vision and including threshold and/or compressive nonlinearities. These signals are then combined in various ways to produce predictors of the various appearance attributes. Data on the adapting stimulus, background, surround, etc. are incorporated into the model at the chromatic adaptation stage and later stages as necessary.

This general process can be witnessed within all of the color appearance models described in this book. However, each model has been derived with a different approach and various of the previously given aspects are stressed to a greater or lesser degree. A simple example of a color appearance model that follows most of the construction steps outlined above is CIELAB. The interpretation of the CIELAB color space as a color appearance model is described in Section 10.3.

### 10.3 CIELAB

Those historically trained in traditional colorimetry usually have a negative reaction when they hear CIELAB described as a color appearance model. This is because the CIE (1986) went to great care to make sure that it was called a uniform color space and not an appearance space. CIELAB was developed as a color space to be used for the specification of color differences. In the early 1970s, there were as many as 20 different formulas being used to calculate color differences. To promote uniformity of practice pending the development of a better formula, the CIE recommended two color spaces, CIELAB and CIELUV, for use in 1976 (Robertson 1977, 1990). The Euclidean distance between two points in these spaces is taken to be a measure of their color difference ( $\Delta E_{ab}^*$  or  $\Delta E_{uv}^*$ ). As an historical note, in 1994 the CIE recommended a single better formula for color difference measurement, based on the CIELAB space, known as  $\Delta E_{94}^*$  (Berns 1993a, CIE 1995b). This was later followed by the CIE DE2000 color difference formula, also based on CIELAB (CIE 2001). In the process of creating a color difference formula, the CIE happened to construct a color space with some predictors of color appearance attributes. Perhaps it is not surprising that the best way to describe the difference in color of two stimuli is to first describe the appearance of each. Thus, with appropriate care, CIELAB can be considered a color appearance model.

#### Calculating CIELAB Coordinates

To calculate CIELAB coordinates, one must begin with two sets of CIE XYZ tristimulus values, those of the stimulus,  $XYZ$ , and those of the reference white,  $X_n Y_n Z_n$ . These data are utilized in a modified form of the von Kries

chromatic adaptation transform by normalizing the stimulus tristimulus values by those of the white (*i.e.*,  $X/X_n$ ,  $Y/Y_n$ , and  $Z/Z_n$ ). Note that the CIE tristimulus values are not first transformed to cone responses as would be necessary for a true von Kries adaptation model. These adapted signals are then subject to a compressive nonlinearity represented by a cube root in the CIELAB equations. This nonlinearity is designed to model the compressive response typically found between physical energy measurements and perceptual responses (Stevens 1961). These signals are then combined into three response dimensions corresponding to the light–dark, red–green, and yellow–blue responses of the opponent theory of color vision. Finally, appropriate multiplicative constants are incorporated into the equations to provide the required uniform perceptual spacing and proper relationship between the three dimensions. The full CIELAB equations are given in Equations 10.1 through 10.4.

$$L^* = 116 f\left(\frac{Y}{Y_n}\right) - 16 \quad (10.1)$$

$$a^* = 500 \left[ f\left(\frac{X}{X_n}\right) - f\left(\frac{Y}{Y_n}\right) \right] \quad (10.2)$$

$$b^* = 200 \left[ f\left(\frac{Y}{Y_n}\right) - f\left(\frac{Z}{Z_n}\right) \right] \quad (10.3)$$

$$f(\omega) = \begin{cases} (\omega)^{1/3} & \omega > 0.008856 \\ 7.787(\omega) + 16 / 116 & \omega \leq 0.008856 \end{cases} \quad (10.4)$$

The alternative forms for low tristimulus values were introduced by Pauli (1976) to overcome limitations in the original CIELAB equations that limited their application to values of  $X/X_n$ ,  $Y/Y_n$ , and  $Z/Z_n$  greater than 0.01. Such low values are not often encountered in color materials, but sometimes are found in flare-free specifications of imaging systems. It is critical to use the full set of Equations 10.1 through 10.4 in cases for which low values might be encountered.

The  $L^*$  measure given in Equation 10.1 is a correlate to perceived lightness ranging from 0.0 for black to 100.0 for a diffuse white ( $L^*$  can sometimes exceed 100.0 for stimuli such as specular highlights in images). The  $a^*$  and  $b^*$  dimensions correlate approximately with red–green and yellow–blue chroma perceptions. They take on both negative and positive values. Both  $a^*$  and  $b^*$  have values of 0.0 for achromatic stimuli (*i.e.*, white, gray, black). Their maximum values are limited by the physical properties of materials rather than the equations themselves.

The CIELAB  $L^*$ ,  $a^*$ , and  $b^*$  dimensions are combined as Cartesian coordinates to form a three-dimensional color space as illustrated in Figure 10.1. This color space can also be represented in terms of cylindrical coordinates as shown in Figure 10.2. The cylindrical coordinate system

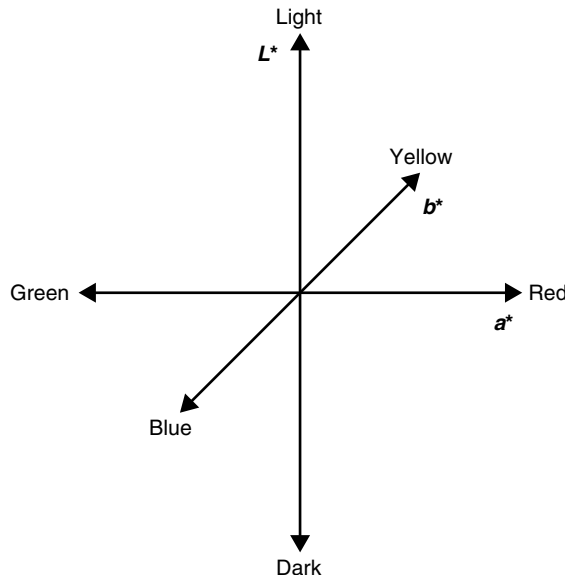


**Figure 10.1** Cartesian representation of the CIELAB color space

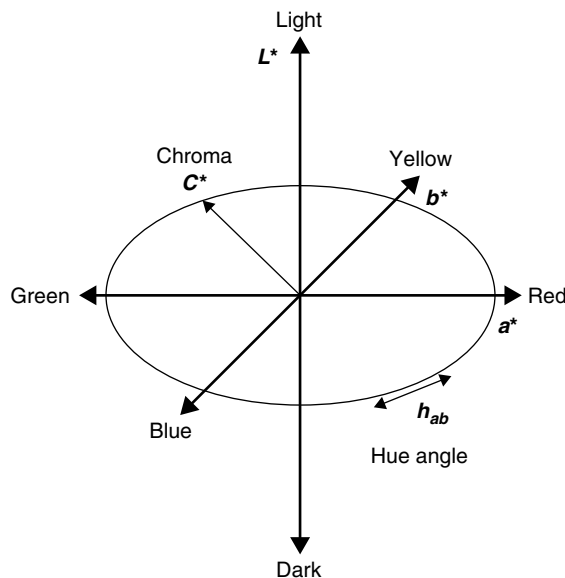


**Figure 10.2** Cylindrical representation of the CIELAB color space

provides predictors of chroma,  $C_{ab}^*$ , and hue,  $h_{ab}$  (hue angle in degrees) as expressed in Equations 10.5 and 10.6.

$$C_{ab}^* = \sqrt{a^{*2} + b^{*2}} \quad (10.5)$$

$$h_{ab} = \tan^{-1} \left( \frac{b^*}{a^*} \right) \quad (10.6)$$

$C^*$  has the same units as  $a^*$  and  $b^*$ . Achromatic stimuli have  $C^*$  values of 0.0 (i.e., no chroma). Hue angle,  $h_{ab}$ , is expressed in positive degrees starting from 0° at the positive  $a^*$  axis and progressing in a counter-clockwise direction. Figure 10.3 is a full-color three-dimensional representation of the CIELAB color space sampled along the lightness, chroma, and hue angle dimensions. While saturation is not officially defined in CIELAB by the CIE, a good approximation to perceived saturation can be computed by dividing  $C_{ab}^*$  by  $L^*$ .

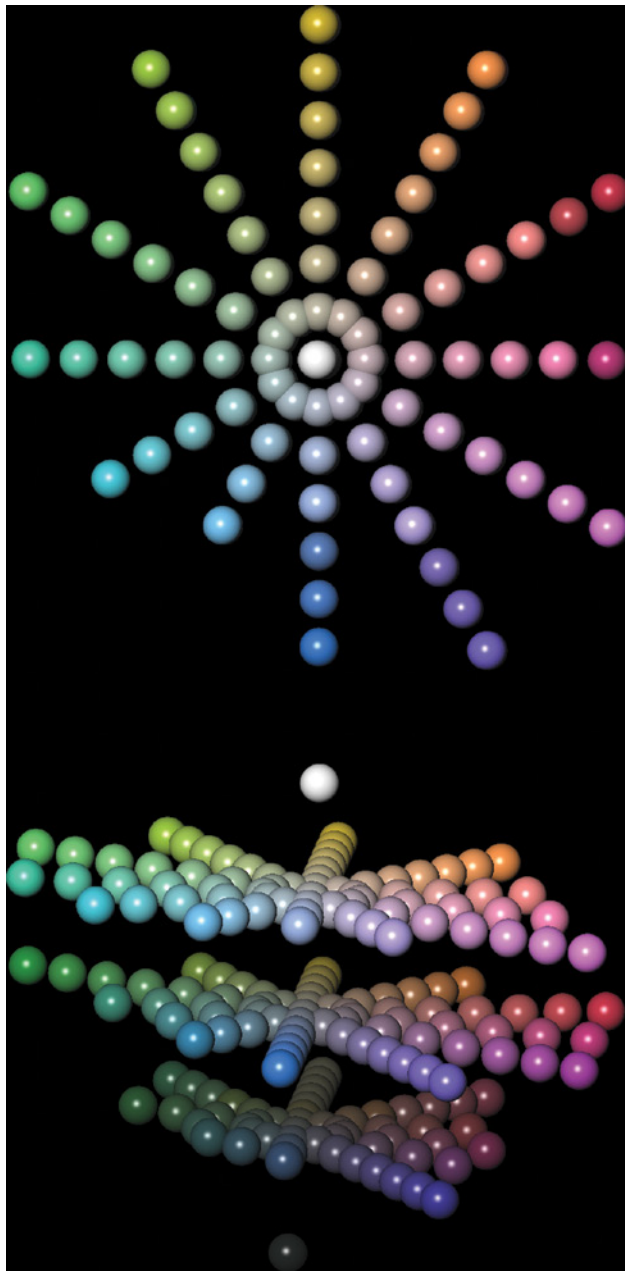
The CIELAB formulae takes the XYZ tristimulus values of a stimulus and the reference white as input and produces correlates to lightness,  $L^*$ , chroma,  $C_{ab}^*$ , and hue,  $h_{ab}$ , as output. Thus CIELAB is a simple form of a color appearance model. Table 10.1 provides worked examples of CIELAB calculations.

While the CIELAB space provides a simple example of a color appearance model, there are some known limitations. The perceptual uniformity of the CIELAB space can be evaluated by examining plots of constant hue and chroma contours from the *Munsell Book of Color*. Such a plot is illustrated in Figure 10.4. Since the Munsell system is designed to be perceptually uniform in terms of hue and chroma, to the extent that it realizes this objective, Figure 10.4 should ideally be a set of concentric circles representing the constant chroma contours with straight lines radiating from the center representing constant hue. As can be seen in Figure 10.4, the CIELAB space does a respectable job of representing the Munsell system uniformly. However, further examination of constant hue contours using a CRT system (capable of achieving higher chroma than generally available in the *Munsell Book of Color*) have illustrated discrepancies between observed and predicted results (Hung and Berns 1995). Figure 10.5 shows constant perceived hue lines from Hung and Berns (1995). It is clear that these lines are curved in the CIELAB space, particularly for red and blue hues.

A similar examination of the CIELAB lightness scale can be made by plotting Munsell value as a function of  $L^*$  as shown in Figure 10.6. Clearly, the  $L^*$  function predicts lightness, as defined by Munsell value, quite well. In fact, the  $L^*$  function predicts the original Munsell lightness scaling data better than the fifth-order polynomial used to define Munsell value (Fairchild 1995b). The result in Figure 10.6 is not surprising given the historical derivation of the  $L^*$  scale to be a close approximation to the Munsell value scale (Robertson 1990).

It is also worth noting that the perceptual unique hues (red, green, yellow and blue) do not align directly with the CIELAB  $a^*b^*$  axes. The unique hues under daylight illumination lie approximately at hue angles of 24° (red), 90° (yellow), 162° (green), and 246° (blue) (Fairchild 1996).

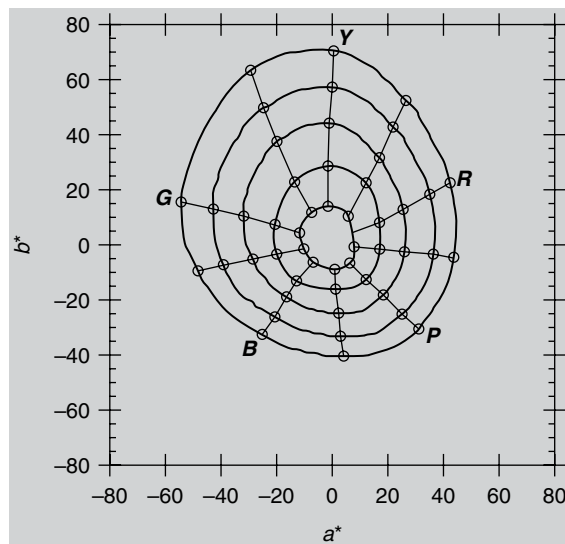
Other limitations of CIELAB are caused by the implementation of a von Kries-type chromatic adaptation transform using CIE XYZ tristimulus values rather than cone responsivities. This has been called a *wrong von Kries transform* (Terstiege 1972) as described in “Wrong von Kries Transform”.



**Figure 10.3** Two views of a three-dimensional computer graphics rendering of a sampling of the CIELAB color space along the lightness, chroma, and hue dimensions

**Table 10.1** Example CIELAB calculations

Quantity	Case 1	Case 2	Case 3	Case 4
$X$	19.01	57.06	3.53	19.01
$Y$	20.00	43.06	6.56	20.00
$Z$	21.78	31.96	2.14	21.78
$X_n$	95.05	95.05	109.85	109.85
$Y_n$	100.00	100.00	100.00	100.00
$Z_n$	108.88	108.88	35.58	35.58
$L^*$	51.84	71.60	30.78	51.84
$a^*$	0.00	44.22	-42.69	-13.77
$b^*$	-0.01	18.11	2.30	-52.86
$C_{ab}^*$	0.01	47.79	42.75	54.62
$h_{ab}$	270.0	22.3	176.9	255.4

**Figure 10.4** Contours of constant Munsell chroma and hue at value 5 plotted in the CIELAB  $a^*b^*$  plane

## Wrong von Kries Transform

Terstiege (1972) has referred to von Kries-type adaptation transforms applied to values other than cone responses (sometimes called fundamental tristimulus values) as *wrong von Kries transforms*. Thus, CIELAB incorporates a wrong von Kries transform through its normalization of CIE XYZ tristimulus values to those of the source. It is important to realize that the normalization of XYZ tristimulus values is not equivalent to the process of first transforming (linearly) to cone responses and then performing the

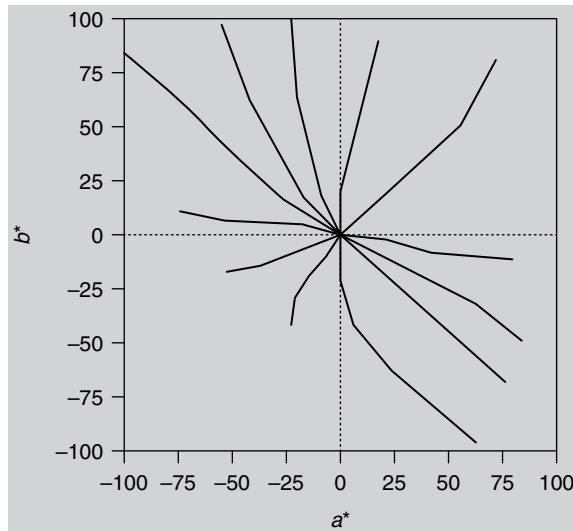


**Figure 10.5** Contours of constant perceived hue from Hung and Berns (1995) plotted in the CIELAB  $a^*b^*$  plane

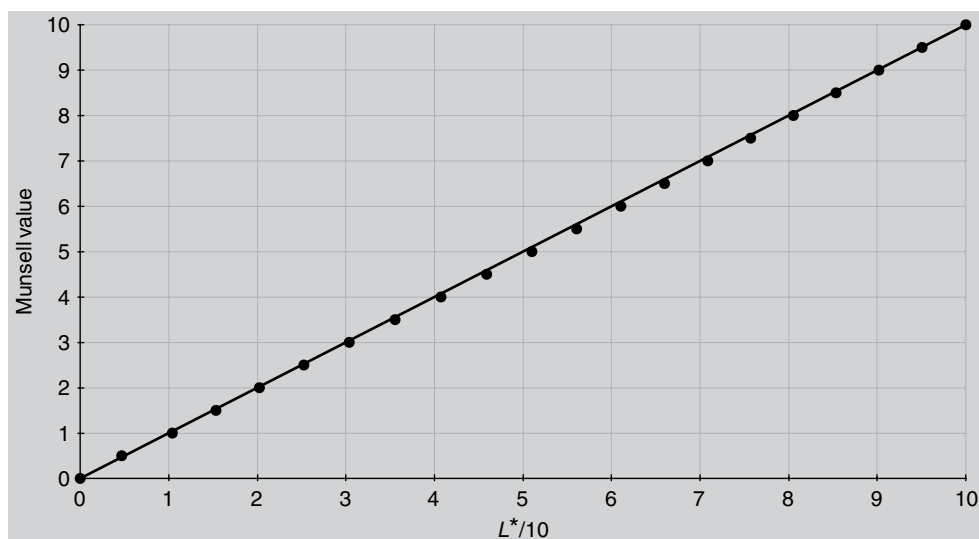


**Figure 10.6** Munsell value plotted as a function of CIELAB  $L^*$ . The red line represents a slope of 1.0 and is not fitted to the data

normalization. This inequality is illustrated in Equations 10.7 through 10.11, which take a correct von Kries transformation in matrix form and convert it into an operation on CIE tristimulus values.

The wrong von Kries transformation incorporated in CIELAB can be expressed as a diagonal matrix transformation on CIE XYZ tristimulus

values. A “right” von Kries transformation is a diagonal matrix transformation of LMS cone responses as shown in Equation 10.7.

$$\begin{vmatrix} L_a \\ M_a \\ S_a \end{vmatrix} = \begin{vmatrix} k_l & 0 & 0 \\ 0 & k_M & 0 \\ 0 & 0 & k_S \end{vmatrix} \begin{vmatrix} L \\ M \\ S \end{vmatrix} \quad (10.7)$$

Since LMS cone responses can be expressed as linear transformations of CIE XYZ tristimulus values, Equation 10.8 can be derived from Equation 10.7 through a simple substitution and then Equation 10.9 follows through algebraic substitution.

$$\mathbf{M} \begin{vmatrix} X_a \\ Y_a \\ Z_a \end{vmatrix} = \begin{vmatrix} k_l & 0 & 0 \\ 0 & k_M & 0 \\ 0 & 0 & k_S \end{vmatrix} \mathbf{M} \begin{vmatrix} X \\ Y \\ Z \end{vmatrix} \quad (10.8)$$

$$\begin{vmatrix} X_a \\ Y_a \\ Z_a \end{vmatrix} = \mathbf{M}^{-1} \begin{vmatrix} k_l & 0 & 0 \\ 0 & k_M & 0 \\ 0 & 0 & k_S \end{vmatrix} \mathbf{M} \begin{vmatrix} X \\ Y \\ Z \end{vmatrix} \quad (10.9)$$

The nature of the matrix transformation,  $\mathbf{M}$ , is critical.  $\mathbf{M}$  is never a diagonal matrix. A typical  $\mathbf{M}$  matrix is given in Equation 10.10.

$$\mathbf{M} = \begin{vmatrix} 0.390 & 0.689 & -0.079 \\ -0.230 & 1.183 & 0.046 \\ 0 & 0 & 1.000 \end{vmatrix} \quad (10.10)$$

Evaluating Equation 10.9 using the  $\mathbf{M}$  matrix of Equation 10.10 results in Equation 10.11. Since the matrix transformation relating the tristimulus values of the stimulus before and after adaptation is not a diagonal matrix, the wrong von Kries transformation cannot be equal to a correct von Kries transformation applied on cone responses.

$$\begin{vmatrix} X_a \\ Y_a \\ Z_a \end{vmatrix} = \begin{vmatrix} 0.74k_l + 0.26k_M & 1.32k_l - 1.32k_M & -0.15k_l - 0.05k_M + 0.20k_S \\ 0.14k_l - 0.14k_M & 0.26k_l + 0.74k_M & -0.03k_l + 0.03k_M \\ 0 & 0 & k_S \end{vmatrix} \begin{vmatrix} X \\ Y \\ Z \end{vmatrix} \quad (10.11)$$

An interesting experimental example of the shortcoming of the wrong von Kries transformation embedded in the CIELAB equations has been described by Liu *et al.* (1995). They studied the perceived hue shift in the color of the gemstone tanzanite upon changes from daylight to incandescent

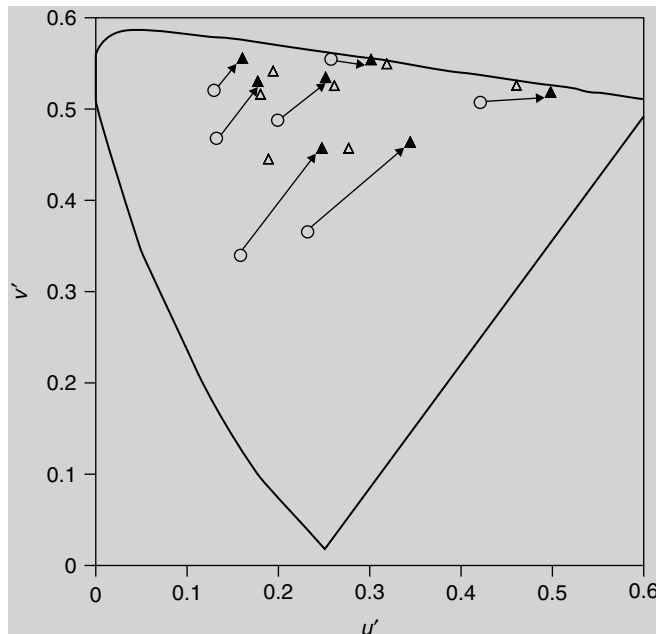


**Figure 10.7** Prediction of some example corresponding colors data using the CIELAB model. Open triangles represent visual data and filled triangles represent model predictions

illumination. Some rare examples of tanzanite appear blue under daylight and purple under incandescent light. However, the CIELAB equations predict that the change in hue for these gemstones would be from blue toward blue-green upon changing from daylight to incandescent. This prediction is in the opposite direction of the perceived hue change. If the same calculations are performed using a correct von Kries transformation acting on cone responsivities, the correct hue shift is predicted (Liu *et al.* 1995). Moroney (2003) explores the poor blue constancy of CIELAB in detail and expands on the above explanation. Li and Melgosa (2013) also explore the hue abnormalities of CIELAB.

The Breneman (1987) corresponding colors data that were used to compare chromatic adaptation models in Chapter 9 were also evaluated using the chromatic adaptation transform of the CIELAB equations. The predicted and observed results are illustrated using  $u'v'$  chromaticity coordinates in Figure 10.7. The errors in the predictions are significantly larger than those found with a normal von Kries transformation (Figure 9.2). The results indicate particularly large errors in the hue predictions for blue stimuli for this change in adaptation from daylight to incandescent. This is consistent with the errors observed by Liu *et al.* (1995) for tanzanite.

## 10.4 WHY NOT USE JUST CIELAB?

Given that CIELAB is a well-established, *de facto* international-standard, color space that has been widely used for two decades and that it is capable of color appearance predictions, why are any other color appearance models necessary? As can be seen in Chapter 15, CIELAB performs quite well as a color appearance model in some applications. So why not just quit there and work with CIELAB?

The limitations of CIELAB discussed previously provide much of the answer to these questions. The modified von Kries adaptation transformation incorporated into the CIELAB equations is clearly less accurate than transformations that more closely follow known visual physiology. Also, there are limitations in CIELAB's ability to predict hue that prompt further work on appearance models.

There are also several aspects of color appearance that CIELAB is incapable of predicting. CIELAB incorporates no luminance-level dependency. Thus it is completely incapable of predicting luminance-dependent effects such as the Hunt effect and the Stevens effect. CIELAB also incorporates no background or surround dependency. Therefore it cannot be used to predict simultaneous contrast or the Bartleson-Breneman results showing a change in image contrast with surround relative luminance. CIELAB also has no mechanism for modeling cognitive effects, such as discounting-the-illuminant, that can become important in cross-media color reproduction applications. Lastly, CIELAB does not provide correlates for the absolute appearance attributes of brightness and colorfulness. As a reminder, it is useful to recall note 6 on the CIELAB space from CIE publication 15.2 (CIE 1986: 32) which states:

*These spaces are intended to apply to comparisons of differences between object colours of the same size and shape, viewed in identical white to middle-grey surroundings, by an observer photopically adapted to a field of chromaticity not too different from that of average daylight.*

This long list of limitations seems to indicate that it should be possible to significantly improve upon CIELAB in the development of a color appearance model. Such models are described in the next few chapters. The CIELAB space should be kept in mind as a simple model that can be used as a benchmark to measure whether more sophisticated models are indeed improvements.

## 10.5 WHAT ABOUT CIELUV?

Since CIELAB can be considered a color appearance model, what about the other color space that the CIE recommended in 1976, CIELUV? CIELUV has many of the same properties as CIELAB (*e.g.*, stimulus and source

chromaticities as input and lightness, chroma, and hue predictors as output), so it might deserve equal attention.

CIELUV incorporates a different form of chromatic adaptation transform than CIELAB. It uses a subtractive shift in chromaticity coordinates ( $u' - u'_n$ ,  $v' - v'_n$ ) rather than a multiplicative normalization of tristimulus values ( $X/X_n$ ,  $Y/Y_n$ ,  $Z/Z_n$ ). The formulae for CIELUV are given in Equations 10.12 through 10.20.

$$L^* = 116f\left(\frac{Y}{Y_n}\right) - 16 \quad (10.12)$$

$$u^* = 13L^*(u' - u'_n) \quad (10.13)$$

$$v^* = 13L^*(v' - v'_n) \quad (10.14)$$

$$f(\omega) = \begin{cases} (\omega)^{1/3} & \omega > 0.008856 \\ 7.787(\omega) + 16 / 116 & \omega \leq 0.008856 \end{cases} \quad (10.15)$$

$$u' = \frac{4X}{X + 15Y + 3Z} \quad (10.16)$$

$$v' = \frac{9Y}{X + 15Y + 3Z} \quad (10.17)$$

$$C^*_{uv} = \sqrt{u^{*2} + v^{*2}} \quad (10.18)$$

$$h_{uv} = \tan^{-1}\left(\frac{v^*}{u^*}\right) \quad (10.19)$$

$$s_{uv} = \frac{C^*_{uv}}{L^*} \quad (10.20)$$

The structure of CIELUV is generally similar to CIELAB with the exceptions of the subtractive adaptation transformation on  $u'v'$  (Equations 10.13 and 10.14) and the formal definition of saturation given in Equation 10.20.

The subtractive adaptation transform incorporated in CIELUV is even farther from physiological reality than the wrong von Kries transform of CIELAB. This subtractive shift can result in predicted corresponding colors being shifted right out of the gamut of realizable colors. (This produces predicted tristimulus values less than 0, which cannot happen with the CIELAB transformation. Note that predicting corresponding colors outside the spectrum locus is not necessarily incorrect since some perceptions simply cannot be replicated under other viewing conditions. However, the extent of the predictions in CIELUV is excessive beyond plausibility.) Even if this does not occur, the transform is likely to shift predicted colors outside the gamut of colors producible by any given device. In addition to this

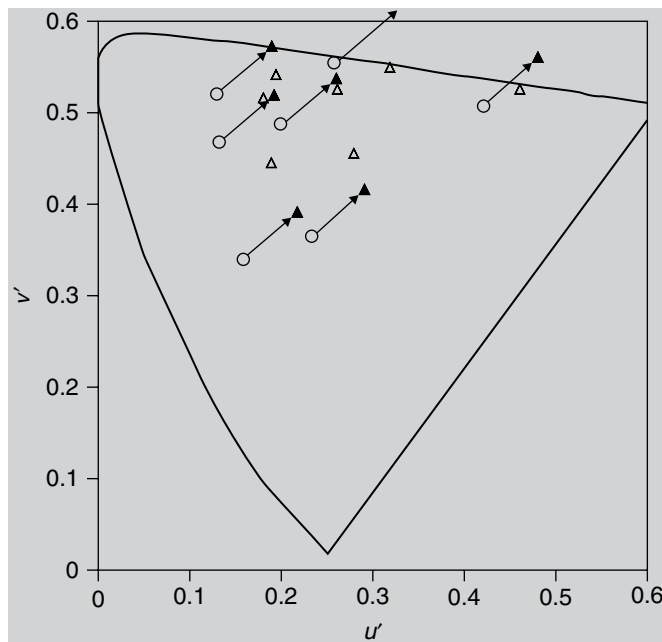


**Figure 10.8** Prediction of some example corresponding colors data using the CIELUV model. Open triangles represent visual data and filled triangles represent model predictions

problem, the CIELUV adaptation transform is extremely inaccurate with respect to predicting visual data. This is illustrated nicely in Figure 10.8, which shows the CIELUV predictions of the Breneman (1987) corresponding colors data. Figure 10.8 illustrates how some colors are shifted outside the gamut of realizable colors (outside the spectrum locus on the  $u'u'$  chromaticity diagram) and the inaccuracy of all the predictions.

The difficulties with the CIELUV adaptation transform are reason enough to eliminate it from serious consideration as an appearance model. However, additional evidence is provided by its poor performance for predicting color differences. The current CIE recommendation for color difference specification, CIE94 (CIE 1995b), is based on the CIELAB color space. So are the more recent CIE DE2000 (CIE 2001) color difference equations. While the DE2000 equations are more recent, their added complexity over the CIE94 specification is probably unwarranted in most applications. Alman *et al.* (1989) provide experimental evidence for the poor performance of CIELUV as a color difference equation. Additional comparisons between CIELUV and CIELAB have been made by Robertson (1990).

The most significant benefit of CIELUV is the formal definition of saturation (Equation 10.20) that is not present in CIELAB. However, if one is willing to approximate saturation in CIELAB as  $C_{ab}^*/L^*$  without the formal sanction of the CIE, then a saturation metric can be used in CIELAB along with all its other advantages.

# 11

# The Nayatani *et al.* Model

---

The next few chapters describe details of the most widely discussed and used historical and current color appearance models. This chapter discusses the color appearance model developed by Nayatani and his coworkers that evolved as one of the more important early colorimetry-based models. This model, along with Hunt's model (described in Chapter 12), is a complete color appearance model capable of predicting the full array of color appearance parameters defined in Chapter 4 for a fairly wide range of viewing conditions.

## 11.1 OBJECTIVES AND APPROACH

The Nayatani *et al.* color appearance model evolved as a natural extension of their chromatic adaptation model described in Chapter 9 (Nayatani *et al.* 1981) in conjunction with the attributes of a color appearance model first outlined by Hunt (1982, 1985). The Nayatani *et al.* color appearance model was first described in Nayatani *et al.* (1986, 1987) and most recently revised and summarized in Nayatani *et al.* (1995). The latter version of the model is described in this chapter.

As with any color appearance model, it is important to note the context in which the Nayatani *et al.* model was formulated. The researchers who developed this model came from the field of illumination engineering, in which the critical application of color appearance models is the specification of the color rendering properties of light sources. This application provides significantly different challenges than those encountered in the field of image reproduction. Thus, those interested in image reproduction might find some aspects of the Nayatani *et al.* model inappropriate for their needs. The reverse is also true. Models derived strictly for imaging applications might

not fulfill the requirements for illumination engineering applications. Despite the different pedigrees of the various models, it is worthwhile to stretch them to applications for which they were not designed. The best possible result will be that they work well (indicating good generality) and the worst outcome is that something more is learned about the important differences in applications. Thus, while the Nayatani *et al.* model was not designed for imaging applications, it is certainly worthy of evaluation in any application that might require a color appearance model.

The model attempts to predict a wide range of color appearance phenomena including the Stevens effect, the Hunt effect, and the Helson-Judd effect in addition to the effects of chromatic adaptation. It is designed to predict the color appearance of simple patches on uniform mid-to-light-gray backgrounds. It is not designed for complex stimuli or changes in background or surround. The model includes output values designed to correlate with all of the important color appearance attributes including brightness, lightness, colorfulness, chroma, and hue. The model's design for simple stimuli on uniform backgrounds highlights the distinction between it and models such as Hunt's, RLAB, and CIECAM02 that were designed with specific attributes for imaging applications. These apparent limitations of the model are not limitations at all for lighting and illumination color rendering applications.

## 11.2 INPUT DATA

The input data for the model include the colorimetric and photometric specification of the stimulus, the adapting illuminant, and the luminance factor of the background. Specifically, the required data include the following:

- The luminance factor of the achromatic background is expressed as a percentage,  $Y_o$ .  $Y_o$  is limited to values equal to or greater than 18% (0.18).
- The color of the illumination,  $x_o$ ,  $y_o$ , is expressed in terms of its chromaticity coordinates for the CIE 1931 standard colorimetric observer.
- The test stimulus is specified in terms of its chromaticity coordinates,  $x$ ,  $y$ , and its luminance factor,  $Y$ .
- The absolute luminance of the stimulus and adapting field is defined by the illuminance of the viewing field,  $E_o$ , expressed in lux.

In addition, two other parameters must also be specified to define the model's required input:

- The normalizing illuminance,  $E_{or}$ , which is expressed in lux and usually in the range of 1000–3000 lux.
- The noise term,  $n$ , used in the nonlinear chromatic adaptation model which is usually taken to be 1.

From these input data, a variety of intermediate and final output values are calculated according to the model. The equations necessary for determining

these values are presented in the following sections. A few preliminary calculations are required before proceeding with the main features of the model. The first is the calculation of the adapting luminance and the normalizing luminance in cd/m<sup>2</sup> according to Equations 11.1 and 11.2.

$$L_o = \frac{Y_o E_o}{100\pi} \quad (11.1)$$

$$L_{or} = \frac{Y_o E_{or}}{100\pi} \quad (11.2)$$

Equations 11.1 and 11.2 are valid given the assumption that the background is a Lambertian diffuser.

Second, in the Nayatani *et al.* model, the transformation from CIE tristimulus values to cone responsivities for the adapting field is expressed in terms of chromaticity coordinates rather than tristimulus values. This necessitates the calculation of the intermediate values of  $\xi$  (xi),  $\eta$  (eta), and  $\zeta$  (zeta) as illustrated in Equations 11.3 through 11.5.

$$\xi = \frac{0.48105x_o + 0.78841y_o - 0.08081}{y_o} \quad (11.3)$$

$$\eta = \frac{-0.27200x_o + 1.11962y_o + 0.04570}{y_o} \quad (11.4)$$

$$\zeta = \frac{0.91822(1 - x_o - y_o)}{y_o} \quad (11.5)$$

### 11.3 ADAPTATION MODEL

As with all color appearance models, the first stage of the Nayatani *et al.* color appearance model is a chromatic adaptation transformation. The adaptation model used is a refined form of the nonlinear model of chromatic adaptation described in Chapter 9 (CIE 1994, Nayatani *et al.* 1981). In the formulation of the color appearance model, the chromatic adaptation model is embedded in other equations. Rather than separate the two, the treatment in Nayatani *et al.* (1995) will be followed and the important features of the chromatic adaptation model that are embedded in other equations will be pointed out to clarify the formulation of the color appearance model.

First, the cone responses for the adapting field must be calculated in terms of the absolute luminance level. This relies on the chromaticity transform described in Equations 11.3 through 11.5, the illuminance level,  $E_o$ , and the luminance factor of the adapting background,  $Y_o$ , as formulated in Equation 11.6.

$$\begin{vmatrix} R_o \\ G_o \\ B_o \end{vmatrix} = \frac{Y_o E_o}{100\pi} \begin{vmatrix} \xi \\ \eta \\ \zeta \end{vmatrix} \quad (11.6)$$

Given the adapting-level cone responses from Equation 11.6, the exponents of the nonlinear model of chromatic adaptation are calculated as described by Equations 11.7 through 11.9. Note that, in this formulation, the exponent for the short-wavelength sensitive cones ( $B$  in Nayatani's notation) differs from the exponents for the middle- and long-wavelength sensitive cones ( $R$  and  $G$  in Nayatani's notation).

$$\beta_1(R_o) = \frac{6.469 + 6.362R_o^{0.4495}}{6.469 + R_o^{0.4495}} \quad (11.7)$$

$$\beta_1(G_o) = \frac{6.469 + 6.362G_o^{0.4495}}{6.469 + G_o^{0.4495}} \quad (11.8)$$

$$\beta_2(B_o) = \frac{8.414 + 8.091B_o^{0.5128}}{8.414 + B_o^{0.5128}} \times 0.7844 \quad (11.9)$$

An additional exponential factor that depends on the normalizing luminance must also be calculated using the same functional form as the exponents for the middle- and long-wavelength sensitive cones as shown in Equation 11.10.

$$\beta_1(L_{or}) = \frac{6.469 + 6.362L_{or}^{0.4495}}{6.469 + L_{or}^{0.4495}} \quad (11.10)$$

The cone responses for the test stimulus are calculated from their tristimulus values using a more traditional linear transformation given in Equation 11.11.

$$\begin{vmatrix} R \\ G \\ B \end{vmatrix} = \begin{vmatrix} 0.40024 & 0.70760 & -0.08081 \\ -0.22630 & 1.16532 & 0.04570 \\ 0.0 & 0.0 & 0.91822 \end{vmatrix} \begin{vmatrix} X \\ Y \\ Z \end{vmatrix} \quad (11.11)$$

Finally, two scaling coefficients,  $e(R)$  and  $e(G)$ , are calculated according to Equations 11.12 and 11.13.

$$e(R) = \begin{cases} 1.758 & R \geq 20\xi \\ 1.0 & R < 20\xi \end{cases} \quad (11.12)$$

$$e(G) = \begin{cases} 1.758 & G \geq 20\eta \\ 1.0 & G < 20\eta \end{cases} \quad (11.13)$$

The above calculations provide all of the intermediate data necessary to implement the nonlinear chromatic adaptation model within the color appearance model. The precise use of these values is described within the appearance equations as they come into play.

## 11.4 OPPONENT COLOR DIMENSIONS

The cone responses are transformed directly into intermediate values representing classical opponent dimensions of visual response: an achromatic channel and two chromatic channels. These equations, used to model these opponent processes, also incorporate the nonlinear chromatic adaptation model.

First, the achromatic response,  $Q$ , is calculated using Equation 11.14.

$$Q = \frac{41.69}{\beta_1(L_{\text{or}})} \left[ \frac{2}{3} \beta_1(R_o) e(R) \log \frac{R+n}{20\xi+n} + \frac{1}{3} \beta_1(G_o) e(G) \log \frac{G+n}{20\eta+n} \right] \quad (11.14)$$

At first, Equation 11.14 looks fairly complex, but its components can be readily teased apart and understood. First, the general structure of Equation 11.14 is such that the achromatic response is calculated as a weighted sum of the outputs of the long- and middle-wavelength cone responses ( $R$  and  $G$ ) as is often postulated in color vision theory. The outputs are summed with relative weights of  $2/3$  and  $1/3$ , which correspond to their relative population in the human retina. They are first normalized after addition of noise,  $n$ , by the cone responses for the adapting stimulus represented by  $\xi$  and  $\eta$  according to a von Kries-type transformation. The value of  $n$  is typically taken to be 1.0 although it can vary. A logarithmic transform is then taken to model the compressive nonlinearity that is known to occur in the human visual system. Given the logarithmic transformation, the exponents ( $\beta$  terms) of the nonlinear chromatic adaptation model become multiplicative factors along with the scaling factors [ $e(R)$  and  $e(G)$ ] as shown in Equation 11.14. All that remains is one more scaling factor, 41.69, and the luminance-dependent exponential adjustment,  $\beta_1(L_{\text{or}})$ , to complete the equation. Thus the achromatic response can be simply expressed as a weighted sum of the post-adaptation signals from the long- and middle-wavelength sensitive cones.

Next, preliminary chromatic channel responses,  $t$  (red-green) and  $p$  (yellow-blue), are calculated in a similar manner using Equations 11.15 and 11.16.

$$t = \beta_1(R_o) \log \frac{R+n}{20\xi+n} - \frac{12}{11} \beta_1(G_o) \log \frac{G+n}{20\eta+n} + \frac{1}{11} \beta_2(B_o) \log \frac{B+n}{20\xi+n} \quad (11.15)$$

$$p = \frac{1}{9} \beta_1(R_o) \log \frac{R+n}{20\xi+n} + \frac{1}{9} \beta_1(G_o) \log \frac{G+n}{20\eta+n} - \frac{2}{9} \beta_2(B_o) \log \frac{B+n}{20\xi+n} \quad (11.16)$$

The explanation of Equations 11.15 and 11.16 follow the same logic as that for the achromatic response, Equation 11.14. Beginning with the  $t$  response, it is a weighted combination of the post-adaptation signals from each of the three cone types. The combination is the difference between the long- and middle-wavelength sensitive cones with a small input from the short-wavelength sensitive cones that adds with the long-wavelength response. This results in a red minus green response that also includes some reddish input from the short wavelength end of the spectrum that is often used to explain the violet (rather than blue) appearance of those wavelengths. It is also required for correct prediction of unique yellow. The  $p$  response is calculated in a similar manner by adding the long- and middle-wavelength sensitive cone outputs to produce a yellow response and then subtracting the short-wavelength cone output to produce the opposing blue response. The weighting factors were those of the original Hunt model.

It is of interest to note that the  $t$  and  $p$  notation is derived from the terms tritanopic and protanopic response. A tritanope has only the red-green response ( $t$ ) and a protanope has only the yellow-blue response ( $p$ ). The  $Q$ ,  $t$ , and  $p$  responses are used in further equations to calculate correlates of brightness, lightness, saturation, colorfulness, and hue.

One aspect of the hue correlate, hue angle,  $\theta$ , is calculated directly from  $t$  and  $p$  as shown in Equation 11.17.

$$\theta = \tan^{-1}\left(\frac{p}{t}\right) \quad (11.17)$$

Hue angle is calculated as a positive angle from  $0^\circ$  to  $360^\circ$  beginning from the positive  $t$  axis, just as is done in the CIELAB color space (CIE 1986). The hue angle is required to calculate some of the other appearance correlates since a hue-dependent adjustment factor is required in some cases.

## 11.5 BRIGHTNESS

The brightness,  $B_r$ , of the test sample is calculated using Equation 11.18.

$$B_r = Q + \frac{50}{\beta_1(L_{or})} \left[ \frac{2}{3} \beta_1(R_o) + \frac{1}{3} \beta_1(G_o) \right] \quad (11.18)$$

$Q$  is the achromatic response, given by Equation 11.14, which is adjusted using the adaptation exponents in order to include the dependency upon absolute luminance level that is required for brightness, as opposed to lightness.

It is also necessary to calculate the brightness of an ideal white,  $B_{rw}$ , according to Equation 11.19. Equation 11.19 is derived by substituting Equation 11.14 evaluated for a perfect reflector into Equation 11.18.

$$B_{rw} = \frac{41.69}{\beta_1(L_{or})} \left[ \frac{2}{3} \beta_1(R_o)(1.758) \log \frac{100\xi + n}{20\xi + n} + \frac{1}{3} \beta_1(G_o)(1.758) \log \frac{100\eta + n}{20\eta + n} \right] \\ + \frac{50}{\beta_1(L_{or})} \left[ \frac{2}{3} \beta_1(R_o) + \frac{1}{3} \beta_1(G_o) \right] \quad (11.19)$$

## 11.6 LIGHTNESS

The achromatic lightness,  $L_p^*$ , of the test sample is calculated directly from the achromatic response,  $Q$ , by simply adding 50 as shown in Equation 11.20. This is the case since the achromatic response can take on both negative and positive values with a middle gray having  $Q = 0.0$  while lightness is scaled from 0 for a black to 100 for a white.

$$L_p^* = Q + 50 \quad (11.20)$$

A second lightness correlate, known as normalized achromatic lightness,  $L_N^*$ , is calculated according to the CIE definition that lightness is the brightness of the test sample relative to the brightness of a white as shown in Equation 11.21.

$$L_N^* = 100 \left( \frac{B_r}{B_{rw}} \right) \quad (11.21)$$

The differences between the two lightness correlates,  $L_p^*$  and  $L_N^*$ , are generally negligible. Neither of the lightness values correlate with the perceived lightness of chromatic object colors since the model does not include the Helmholtz–Kohlrausch effect (Fairchild and Pirrotta 1991, Nayatani *et al.* 1992). An additional model is necessary to include the Helmholtz–Kohlrausch effect, which is necessary for the comparison of the lightness or brightness of stimuli with differing hue and/or chroma.

## 11.7 HUE

Hue angle,  $\theta$ , is calculated as shown previously in Equation 11.17, which is identical to the technique used in the CIELAB color space. More descriptive hue correlates can be obtained by determining the hue quadrature,  $H$ , and the hue composition,  $H_c$ .

Hue quadrature,  $H$ , is a 400-step hue scale on which the unique hues take on values of 0 (red), 100 (yellow), 200 (green), and 300 (blue). The hue quadrature is computed via linear interpolation using the hue angle,  $\theta$ , of the test sample and the hue angles for the four unique hues, which are defined as 20.14° (red), 90.00° (yellow), 164.25° (green), and 231.00° (blue).

The hue composition,  $H_c$ , describes perceived hue in terms of percentages of two of the unique hues from which the test hue is composed. For example, an orange color might be expressed as 50Y50R indicating that the hue is perceived to be halfway between unique red and unique yellow. Hue composition is computed by simply converting the hue quadrature into percent components between the unique hues falling on either side of the test color (again by a linear process). For example, a color stimulus with a hue angle of 43.19° will have a hue quadrature of 32.98 and a hue composition of 33Y 67R.

## 11.8 SATURATION

In the Nayatani *et al.* color appearance model, saturation is derived most directly, and then the measures of colorfulness and chroma are derived from it. Saturation is expressed in terms of a red-green component,  $S_{RG}$ , derived from the  $t$  response as shown in Equation 11.22 and a yellow-blue component,  $S_{YB}$ , derived from the  $p$  response as shown in Equation 11.23.

$$S_{RG} = \frac{488.93}{\beta_1(L_{or})} E_s(\theta) t \quad (11.22)$$

$$S_{YB} = \frac{488.93}{\beta_1(L_{or})} E_s(\theta) p \quad (11.23)$$

The saturation predictors include a scaling factor, 488.93, for convenience; the luminance-dependent  $\beta$  terms required to predict the Hunt effect; and a chromatic strength function,  $E_s(\theta)$ , that was introduced to correct the saturation scale as a function of hue angle (Nayatani 1995). It takes on the empirically derived form expressed in Equation 11.24.

$$\begin{aligned} E_s(\theta) = & 0.9394 - 0.2478 \sin \theta - 0.0743 \sin 2\theta + 0.0666 \sin 3\theta \\ & - 0.0186 \sin 4\theta - 0.0055 \cos \theta - 0.0521 \cos 2\theta \\ & - 0.0573 \cos 3\theta - 0.0061 \cos 4\theta \end{aligned} \quad (11.24)$$

Finally, an overall saturation correlate,  $S$ , is calculated using Equation 11.25. This is precisely the same functional form as the chroma calculation in CIELAB (Euclidean distance from the origin).

$$S = \left( S_{RG}^2 + S_{YB}^2 \right)^{1/2} \quad (11.25)$$

## 11.9 CHROMA

Given the correlates for saturation described above, correlates of chroma can be easily derived by considering their definitions. As was illustrated in Chapter 4, saturation can be expressed as chroma divided by lightness. Thus chroma can be described as saturation multiplied by lightness. This is almost exactly the functional form for chroma in the Nayatani *et al.* model. The correlates for the red-green, yellow-blue, and overall chroma of the test sample are given in Equations 11.26 through 11.28.

$$C_{RG} = \left( \frac{L_P^*}{50} \right)^{0.7} S_{RG} \quad (11.26)$$

$$C_{YB} = \left( \frac{L_P^*}{50} \right)^{0.7} S_{YB} \quad (11.27)$$

$$C = \left( \frac{L_P^*}{50} \right)^{0.7} S \quad (11.28)$$

The only differences between the nominal definition of chroma and Equations 11.26 through 11.28 are the scaling factor of 50 and the slight nonlinearity introduced by the power function of lightness with an exponent of 0.7. This nonlinearity was introduced to better model constant chroma contours from the *Munsell Book of Color* (Nayatani *et al.* 1995).

## 11.10 COLORFULNESS

The predictors of colorfulness in the Nayatani *et al.* model can also be derived directly from the CIE definitions of the appearance attributes. Recall that chroma is defined as colorfulness of the sample relative to the brightness of a white object under similar illumination. Thus colorfulness is simply the chroma of the sample multiplied by the brightness of an ideal white as illustrated in Equations 11.29 through 11.31.

$$M_{RG} = C_{RG} \frac{B_{rw}}{100} \quad (11.29)$$

$$M_{YB} = C_{YB} \frac{B_{rw}}{100} \quad (11.30)$$

$$M = C \frac{B_{rw}}{100} \quad (11.31)$$

The normalizing value of 100 is derived as the brightness of an ideal white under illuminant D65 at the normalizing illuminance. It provides a convenient place to tie down the scale.

### 11.11 INVERSE MODEL

In many applications, and particularly image reproduction, it is necessary to use a color appearance model in both forward and reverse directions. Thus it is important, or at least highly convenient, that the equations can be analytically inverted. Fortunately, the Nayatani *et al.* color appearance model can be inverted analytically. Nayatani *et al.* (1990a) published a paper that introduces the process for inverting the model for both brightness–colorfulness and lightness–chroma matches. While the model has changed slightly, the same general procedure can be followed.

In applying the model, it is often useful to consider its implementation as a simple step-by-step process. Thus the steps required to implement the model (and in reverse order to invert it) are given below.

1. Obtain physical data.
2. Calculate  $Q$ ,  $t$ , and  $p$ .
3. Calculate  $\theta$ ,  $E_s(\theta)$ ,  $H$ , and  $H_C$ .
4. Calculate  $B_r$ ,  $B_{rw}$ ,  $L_p^*$ ,  $L_N^*$ , and  $S$ .
5. Calculate  $C$ .
6. Calculate  $M$ .

### 11.12 PHENOMENA PREDICTED

The Nayatani *et al.* color appearance model accounts for changes in color appearance due to chromatic adaptation and luminance level (Stevens effect and Hunt effect). It also predicts the Helson–Judd effect. The model can be used for different background luminance factors (greater than 18%), but the model's authors caution against using it for comparisons between different luminance levels (Nayatani *et al.* 1990b). It cannot be used to predict the effects of changes in background color (simultaneous contrast) or surround relative luminance (e.g., Bartleson–Breneman equations).

The Nayatani *et al.* color appearance model also does not incorporate mechanisms for predicting incomplete chromatic adaptation or cognitive discounting-the-illuminant. Nayatani (1997) has outlined a procedure to estimate the level of chromatic adaptation from experimental data. This is useful to allow the model to be used to predict the results of visual experiments in which chromatic adaptation is incomplete. However, this technique is of little value in practical applications in which a prediction of the level of chromatic adaptation must be made for a set of viewing conditions for which prior visual data are not available.

Example calculations using the Nayatani *et al.* color appearance model as described in this chapter are given for four samples in Table 11.1.

**Table 11.1** Example Nayatani *et al.* color appearance model calculations

Quantity	Case 1	Case 2	Case 3	Case 4
X	19.01	57.06	3.53	19.01
Y	20.00	43.06	6.56	20.00
Z	21.78	31.96	2.14	21.78
X <sub>n</sub>	95.05	95.05	109.85	109.85
Y <sub>n</sub>	100.00	100.00	100.00	100.00
Z <sub>n</sub>	108.88	108.88	35.58	35.58
E <sub>o</sub>	5000	500	5000	500
E <sub>or</sub>	1000	1000	1000	1000
B <sub>r</sub>	62.6	67.3	37.5	44.2
L <sub>p</sub> *	50.0	73.0	24.5	49.4
L <sub>N</sub> *	50.0	75.9	29.7	49.4
θ	257.5	21.6	190.6	236.3
H	317.8	2.1	239.4	303.6
H <sub>c</sub>	82B 18R	98R 2Y	61G 39B	96B 4R
S	0.0	37.1	81.3	40.2
C	0.0	48.3	49.3	39.9
M	0.0	42.9	62.1	35.8

## 11.13 WHY NOT USE JUST THE NAYATANI ET AL. MODEL?

Given the extensive nature of the Nayatani *et al.* color appearance model and its inclusion of correlates for all of the important color appearance attributes, it is reasonable to wonder why the CIE did not simply adopt this model as a recommended color appearance model. There are several reasons this did not happen.

First it is worth reiterating the positive features of the Nayatani *et al.* model. It is a complete model in terms of output correlates. It is fairly straightforward (although the equations could be presented in a more simplified way) and it is analytically invertible.

However, there are some negative aspects of the model that prevent it from becoming the single best answer. It cannot account for changes in background, surround, or cognitive effects. Surround and cognitive factors are critical in image reproduction applications. It also does not predict adaptation level, which is also important in cross-media reproduction applications. It has been derived and tested mainly for simple patches, which might limit its usefulness in more complex viewing situations. The model also significantly over-predicts the Helson–Judd effect by predicting strong effects for illuminants that are not very chromatic (such as illuminant A). It is clear that the Helson–Judd effect does not occur under such conditions as was originally pointed out by Helson (1938) himself. Lastly, in various tests of color appearance models described in later chapters, the Nayatani *et al.* model has been generally shown to be not particularly accurate. The

Nayatani *et al.* model also does not incorporate rod contributions to color appearance as can be found in the Hunt model.

Given all of the above limitations, it is clear that this model cannot provide the ultimate answer for a single color appearance model. This does not lessen its significance and contributions to the development of color appearance models. It is almost certain that some aspects of the Nayatani *et al.* model will find their way into whatever model is agreed upon for general use in the future as illustrated by the evolution of CIECAM97s and CIECAM02.

While the Nayatani *et al.* model essentially stopped evolving with the development of CIECAM97s, Nayatani himself pursued some very interesting avenues in the development of the “Nayatani Theoretical” color space (Nayatani 2004) which incorporated concepts and phenomena such as Evans’ “brilliance” (or fluorescence), the NCS concept of whiteness–blackness and chromaticness, and the all-important Helmholtz–Kohlrausch effect. The space and the concept of brilliance have been put to good practical use in applications such as enhancing color images to fill extended color gamuts of displays (Heckaman and Fairchild 2008, 2009, 2011).

# The Hunt Model

---

## The Hunt Model

This chapter continues the review of some of the most widely discussed and used color appearance models with a description of the model developed by Robert William Gainer Hunt. This model is the most extensive, complete, and complex color appearance model that has been developed. Its roots can be traced to some of Hunt's early chromatic adaptation studies (Hunt 1952) up through its rigorous development in the 1980s and 1990s (Hunt 1982, 1987, 1991b, 1994, 1995, Hunt and Pointer 1985), and it had a very significant impact on the development and design of CIECAM02.

The Hunt color appearance model is not simple, but it is designed to predict a wide range of visual phenomena, and as Hunt himself has stated in regard to the model's complexity, the human visual system is not simple either. While there are applications in which simpler models such as those described in later chapters are adequate, it is certainly of great value to have a complete model that can be adapted to a wider range of viewing conditions for more well-defined or unusual circumstances. The Hunt model serves this purpose well and most of the other color appearance models discussed in this book can trace many of their features back to ideas that originally appeared in Hunt's model.

### 12.1 OBJECTIVES AND APPROACH

Hunt spent 36 years of his career in the Kodak Research Laboratories. Thus, the Hunt model has been developed in the context of the requirements for color image reproduction. This is a significantly different point of view than found in the field of illumination engineering from which the Nayatani *et al.* model discussed in Chapter 11 was developed. The imaging science influence on the Hunt model can be easily witnessed by examining its input param-

ters. For example, the surround relative luminance is an important factor that is not present in the Nayatani *et al.* model. Other examples can be found in parameters that are set to certain values for “transparencies projected in a dark room” or “television displays in a dim surround” or “normal scenes.” Such capabilities clearly indicate that the model was intended to be applied to imaging situations. However, this is not the limit of the model’s applicability. For example, it has also been extended for unrelated colors such as those found in traditional vision-science experiments.

The Hunt model is designed to predict a wide range of visual phenomena including the appearance of related and unrelated colors in various backgrounds, surrounds, illumination colors, and luminance levels ranging from low scotopic to bleaching levels. In this sense, it is a complete model of color appearance for static stimuli. Hunt’s model, like most of the others described in this book, does not attempt to incorporate complex spatial or temporal characteristics of appearance.

To make reasonable predictions of appearance over such a wide range of conditions, the Hunt model requires more rigorous definition of the viewing field. Thus, Hunt (1991b) defined the components of the viewing field as described in Chapter 7. These components include the stimulus, the proximal field, the background, and the surround. The Hunt model is the only available model that treats each of these components of the viewing field separately.

While Hunt’s model has been continuously evolving over the past two decades (see Hunt 1982, 1985, 1987, 1991b, and 1994 for major milestones), a comprehensive review of the model’s current formulation can be found in Chapter 31 of the 5th Edition of Hunt’s book, *The Reproduction of Colour* (Hunt 1995). The treatment that follows is adapted from that chapter. Those desiring more detail on Hunt’s model should refer to Chapter 31 of Hunt’s book.

## 12.2 INPUT DATA

The Hunt model requires an extensive list of input data. All colorimetric coordinates are typically calculated using the CIE 1931 standard colorimetric observer ( $2^\circ$ ). The chromaticity coordinates ( $x, y$ ) of the illuminant and the adapting field are required. Typically, the adapting field is taken to be the integrated chromaticity of the scene, which is assumed to be identical to that of the illuminant (or source). Next, the chromaticities ( $x, y$ ) and luminance factors ( $Y$ ) of the background, proximal field, reference white, and test sample are required. If separate data are not available for the proximal field, it is generally assumed to be identical to the background. Also, the reference white is often taken to have the same chromaticities as the illuminant with a luminance factor of 100 if specific data are not available.

All of these data are relative colorimetric values. Absolute luminance levels are required to predict several luminance-dependent appearance phenomena. Thus the absolute luminance levels, in  $\text{cd}/\text{m}^2$ , are required

for the reference white and the adapting field. If the specific luminance of the adapting field is not available, it is taken to be 20% of the luminance of the reference white under the assumption that scenes integrate to a gray with a reflectance factor of 0.2. Additionally, scotopic luminance data are required in order to incorporate rod responses into the model (another feature unique to the Hunt model). Thus, the scotopic luminance of the adapting field in scotopic cd/m<sup>2</sup> is required. Since scotopic data are rarely available, the scotopic luminance of the illuminant,  $L_{AS}$ , can be approximated from its photopic luminance,  $L_A$ , and CCT,  $T$ , using Equation 12.1.

$$L_{AS} = 2.26L_A \left[ \left( \frac{T}{4000} \right) - 0.4 \right]^{1/3} \quad (12.1)$$

The scotopic luminance of the test stimulus relative to the scotopic luminance of the reference white is also required. Again, since such data are rarely available, an approximation is often used by substituting the photopic luminance of the sample relative to the reference white for the scotopic values.

Lastly, there are several input variables that are decided based on the viewing configuration. Two of these are the chromatic ( $N_c$ ) and brightness ( $N_b$ ) surround induction factors. Hunt (1995) suggests using values optimized for the particular viewing situation. Since this is often not possible, the nominal values listed in Table 12.1 are recommended.

The last two input parameters are the chromatic ( $N_{cb}$ ) and brightness ( $N_{bb}$ ) background induction factors. Again, Hunt recommends optimized values. Assuming these are not available, the background induction factors are calculated from the luminances of the reference white,  $Y_w$ , and background,  $Y_b$ , using Equations 12.2 and 12.3.

$$N_{cb} = 0.725 \left( \frac{Y_w}{Y_b} \right)^{0.2} \quad (12.2)$$

$$N_{bb} = 0.725 \left( \frac{Y_w}{Y_b} \right)^{0.2} \quad (12.3)$$

**Table 12.1** Values of the chromatic and brightness surround induction factors

Situation	$N_c$	$N_b$
Small areas in uniform backgrounds and surrounds	1.0	300
Normal scenes	1.0	75
Television and CRT displays in dim surrounds	1.0	25
Large transparencies on light boxes	0.7	25
Projected transparencies in dark surrounds	0.7	10

A final decision must be made regarding discounting-the-illuminant. Certain parameters in the model are assigned different values for situations in which discounting-the-illuminant occurs. Given all of the above data one can then continue with the calculations of the Hunt model parameters.

### 12.3 ADAPTATION MODEL

As with all of the models described in this book, the first step is a transformation from CIE tristimulus values to cone responses. In Hunt's model the cone responses are denoted  $\rho\gamma\beta$  rather than LMS. The transformation used (referred to as the *Hunt, Pointer, Estevez transformation* also used in the Nayatani *et al.*, RLAB, and CIECAM models) is given in Equation 12.4. For the Hunt model, this transformation is normalized such that the equal-energy illuminant has equal  $\rho\gamma\beta$  values. In some models, different normalizations are used.

$$\begin{vmatrix} \rho \\ \gamma \\ \beta \end{vmatrix} = \begin{vmatrix} 0.38971 & 0.68898 & -0.07868 \\ -0.22981 & 1.18340 & 0.04641 \\ 0.0 & 0.0 & 1.0 \end{vmatrix} \begin{vmatrix} X \\ Y \\ Z \end{vmatrix} \quad (12.4)$$

The transformation from XYZ to  $\rho\gamma\beta$  values must be completed for the reference white, background, proximal field, and test stimulus.

The chromatic adaptation model embedded in Hunt's color appearance model is a significantly modified form of the von Kries hypothesis. The adapted cone signals,  $\rho_a\gamma_a\beta_a$ , are determined from the cone responses for the stimulus,  $\rho\gamma\beta$ , and those for the reference white,  $\rho_w\gamma_w\beta_w$ , using Equations 12.5 through 12.7.

$$\rho_a = B_\rho \left[ f_n \left( \frac{F_L F_\rho \rho}{\rho_w} \right) + \rho_D \right] + 1 \quad (12.5)$$

$$\gamma_a = B_\gamma \left[ f_n \left( \frac{F_L F_\gamma \gamma}{\gamma_w} \right) + \gamma_D \right] + 1 \quad (12.6)$$

$$\beta_a = B_\beta \left[ f_n \left( \frac{F_L F_\beta \beta}{\beta_w} \right) + \beta_D \right] + 1 \quad (12.7)$$

The von Kries hypothesis can be recognized in Equations 12.5 through 12.7 by noting the ratios  $\rho/\rho_w$ ,  $\gamma/\gamma_w$ ,  $\beta/\beta_w$  at the heart of the equations. Clearly, there are many other parameters in Equations 12.5 through 12.7 that require definition and explanation; these are given below. First,  $f_n()$  is a general hyperbolic function given in Equation 12.8 that is used to model the nonlinear behavior of various visual responses.

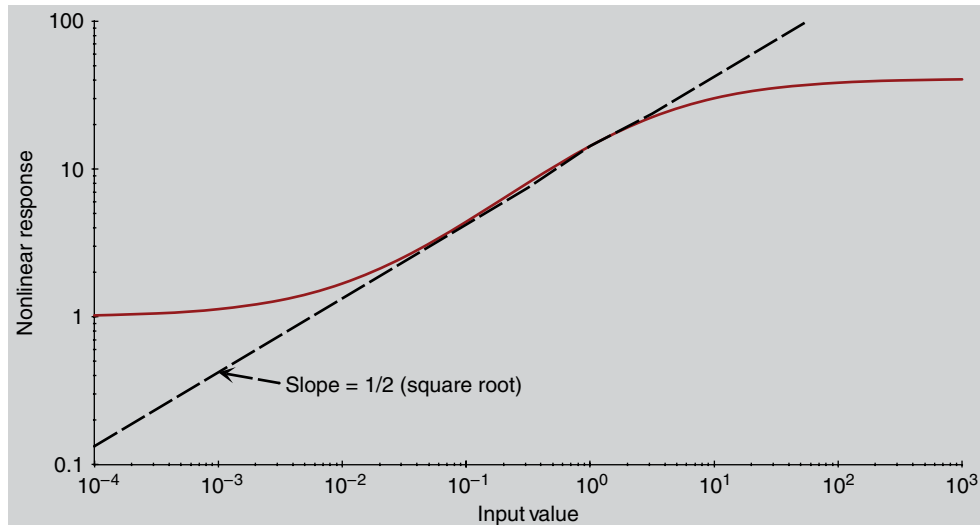


**Figure 12.1** The nonlinear response function,  $f_n()$ , of the Hunt color appearance model

$$f_n(I) = 40 \left( \frac{I^{0.73}}{I^{0.73} + 2} \right) \quad (12.8)$$

Figure 12.1 illustrates the form of Hunt's nonlinear function on log-log axes. In the central operating range, the function is linear and therefore equivalent to a simple power function (in this case with an exponent of about 1/2). However, this function has the advantage that it models threshold behavior at low levels (the gradual increase in slope) and saturation behavior at high levels (the decrease in slope back to 0). Such a nonlinearity is required to model the visual system over the large range in luminance levels that the Hunt model addresses.

$F_L$  is a luminance-level adaptation factor incorporated into the adaptation model to predict the general behavior of light adaptation over a wide range of luminance levels. It also reintroduces the absolute luminance level prior to the nonlinearity, allowing appearance phenomena such as the Stevens effect and Hunt effect to be predicted.  $F_L$  is calculated using Equations 12.9 and 12.10.

$$F_L = 0.2k^4 (5L_A) + 0.1(1 - k^4)^2 (5L_A)^{1/3} \quad (12.9)$$

$$k = \frac{1}{5L_A + 1} \quad (12.10)$$

$F_p$ ,  $F_\gamma$ , and  $F_\beta$  are chromatic adaptation factors that are introduced to model the fact that chromatic adaptation is often incomplete. These factors are designed such that chromatic adaptation is always complete for the equal-

energy illuminant (sometimes referred to as illuminant E). This means that the chromaticity of illuminant E always appears achromatic according to the model and thus  $F_\rho$ ,  $F_\gamma$ , and  $F_\beta$  are all equal to one. Such a prediction is supported by experimental results of Hurvich and Jameson (1951), Hunt and Winter (1975), and Fairchild (1991b). As  $F_\rho$ ,  $F_\gamma$ , and  $F_\beta$  depart from one (in either direction depending on the adapting field color), chromatic adaptation is predicted to be less complete. The formulation of  $F_\rho$ ,  $F_\gamma$ , and  $F_\beta$  is given in Equations 12.11 through 12.16, and the behavior of these functions is illustrated in Figure 12.2 for  $F_\rho$  as an example.

$$F_\rho = \frac{1 + L_A^{1/3} + h_\rho}{1 + L_A^{1/3} + 1/h_\rho} \quad (12.11)$$

$$F_\gamma = \frac{1 + L_A^{1/3} + h_\gamma}{1 + L_A^{1/3} + 1/h_\gamma} \quad (12.12)$$

$$F_\beta = \frac{1 + L_A^{1/3} + h_\beta}{1 + L_A^{1/3} + 1/h_\beta} \quad (12.13)$$

$$h_\rho = \frac{3\rho_w}{\rho_w + \gamma_w + \beta_w} \quad (12.14)$$

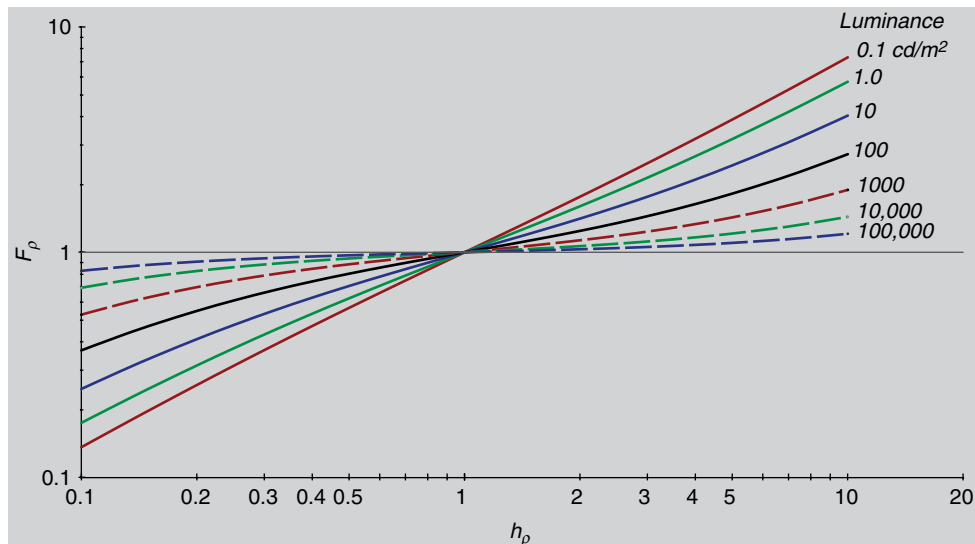


**Figure 12.2** One of the chromatic adaptation factors,  $F_\rho$ , plotted as a function of the adapting chromaticity for a variety of adapting luminance levels. This function illustrates how adaptation becomes less complete ( $F_\rho$  departs from 1.0) as the purity of the adapting stimulus increases ( $h_\rho$  departs from 1.0) and the luminance level decreases

$$h_\gamma = \frac{3\gamma_w}{\rho_w + \gamma_w + \beta_w} \quad (12.15)$$

$$h_\beta = \frac{3\beta_w}{\rho_w + \gamma_w + \beta_w} \quad (12.16)$$

The parameters  $h_\rho$ ,  $h_\gamma$ , and  $h_\beta$  can be thought of as chromaticity coordinates scaled relative to illuminant E (since  $\rho\gamma\beta$  themselves are normalized to illuminant E). They take on values of 1.0 for illuminant E and depart further from 1.0 as the reference white becomes more saturated. These parameters, taken together with the luminance level dependency ( $L_A$ ) in Equations 12.11 through 12.13, produce values that depart from 1.0 by increasing amounts as the color of the reference white moves away from illuminant E (becoming more saturated) and the adapting luminance increases. The feature that chromatic adaptation becomes more complete with increasing adapting luminance is also consistent with the visual experiments cited above. This general behavior is illustrated in Figure 12.2 with a family of curves for various adapting luminance levels.

If discounting-the-illuminant occurs, then chromatic adaptation is taken to be complete, and  $F_\rho$ ,  $F_\gamma$ , and  $F_\beta$  are set equal to values of 1.0.

The parameters  $\rho_D$ ,  $\gamma_D$ , and  $\beta_D$  are included to allow prediction of the Helson–Judd effect. This is accomplished by additive adjustments to the cone signals that are dependent upon the relationship between the luminance of the background,  $Y_b$ , the reference white,  $Y_w$ , and the test stimulus as given in Equations 12.17 through 12.19.

$$\rho_D = f_n \left[ \left( \frac{Y_b}{Y_w} \right) F_L F_\gamma \right] - f_n \left[ \left( \frac{Y_b}{Y_w} \right) F_L F_\rho \right] \quad (12.17)$$

$$\gamma_D = 0.0 \quad (12.18)$$

$$\beta_D = f_n \left[ \left( \frac{Y_b}{Y_w} \right) F_L F_\gamma \right] - f_n \left[ \left( \frac{Y_b}{Y_w} \right) F_L F_\beta \right] \quad (12.19)$$

The Helson–Judd effect does not occur in most typical viewing situations (Helson 1938). In such cases  $\rho_D$ ,  $\gamma_D$ , and  $\beta_D$  should be set equal to 0.0. In cases for which discounting-the-illuminant occurs, there is no Helson–Judd effect and  $\rho_D$ ,  $\gamma_D$ , and  $\beta_D$  are forced to 0.0 since  $F_\rho$ ,  $F_\gamma$ , and  $F_\beta$  are set equal to 1.0. There are some situations in which it is desirable to have  $F_\rho$ ,  $F_\gamma$ , and  $F_\beta$  take on their normal values while  $\rho_D$ ,  $\gamma_D$ , and  $\beta_D$  are set to 0.0. These include the viewing of images projected in a darkened surround or viewed on CRT displays.

The last factors in the chromatic adaptation formulas (Equations 12.5 through 12.7) are the cone bleach factors  $B_\rho$ ,  $B_\gamma$ , and  $B_\beta$ . Once again, these factors are only necessary to model visual responses over extremely large

ranges in luminance level. They are formulated to model photopigment depletion (*i.e.*, bleaching) that occurs at high luminance levels resulting in decreased photoreceptor output as shown in Equations 12.20 through 12.22.

$$B_\rho = \frac{10^7}{10^7 + 5L_A (\rho_w / 100)} \quad (12.20)$$

$$B_\gamma = \frac{10^7}{10^7 + 5L_A (\gamma_w / 100)} \quad (12.21)$$

$$B_\beta = \frac{10^7}{10^7 + 5L_A (\beta_w / 100)} \quad (12.22)$$

The cone bleaching factors are essentially 1.0 for most normal luminance levels. As the adapting luminance,  $L_A$ , reaches extremely high levels, the bleaching factors begin to decrease, resulting in decreased adapted cone output. In the limit, the bleaching factors will approach 0 as the adapting luminance approaches infinity. This would result in no cone output when the receptors are fully bleached (sometimes referred to as a retinal burn). Such adapting levels are truly dangerous to the observer and would cause permanent damage. However, the influence of the cone bleaching factors does begin to take effect at high luminance levels that are below the threshold for retinal damage such as outdoors on a sunny day. In such situations, one can observe the decreased range of visual response due to “too much light,” and a typical response is to put on sunglasses. These high luminance levels are not found in typical image reproduction applications (except, perhaps, in some original scenes).

The adaptation formulas (Equations 12.5 through 12.7) are completed with the addition of 1.0 designed to represent noise in the visual system.

If the proximal field and background differ from a gray, chromatic induction is modeled by adjusting the cone signals for the reference white used in the adaptation equations. This suggests that the state of adaptation is being influenced by the local color of the proximal field and background in addition to the color of the reference white. This type of modeling is completely consistent with observed visual phenomena. Hunt (1991b) has suggested one algorithm for calculating adjusted reference white signals  $\rho'_w$ ,  $\gamma'_w$ , and  $\beta'_w$  from the cone responses for the background,  $\rho_b$ ,  $\gamma_b$ , and  $\beta_b$ , and proximal field,  $\rho_p$ ,  $\gamma_p$ , and  $\beta_p$ , given in Equations 12.23 through 12.28.

$$\rho'_w = \frac{\rho_w [(1-p)\rho_p + (1+p)/p_\rho]^{1/2}}{[(1+p)\rho_p + (1-p)/p_\rho]^{1/2}} \quad (12.23)$$

$$\gamma'_w = \frac{\gamma_w [(1-p)\gamma_p + (1+p)/p_\gamma]^{1/2}}{[(1+p)\gamma_p + (1-p)/p_\gamma]^{1/2}} \quad (12.24)$$

$$\beta'_w = \frac{\beta_w [(1-p)p_\beta + (1+p)/p_\beta]^{1/2}}{[(1+p)p_\beta + (1-p)/p_\beta]^{1/2}} \quad (12.25)$$

$$p_\rho = \frac{\rho_p}{\rho_b} \quad (12.26)$$

$$p_\gamma = \frac{\gamma_p}{\gamma_b} \quad (12.27)$$

$$p_\beta = \frac{\beta_p}{\beta_b} \quad (12.28)$$

Values of  $p$  in Equations 12.23 through 12.25 are taken to be between 0 and -1 when simultaneous contrast occurs and between 0 and +1 when assimilation occurs. In most practical applications, the background and proximal field are assumed to be achromatic and adjustments such as those given in Equations 12.23 through 12.25 are not used.

Now that the adapted cone signals,  $\rho_a$ ,  $\gamma_a$ , and  $\beta_a$  are available, it is possible to move onward to the opponent responses and color appearance correlates. The rod signals and their adaptation will be treated at the point they are incorporated in the achromatic response.

## 12.4 OPPONENT COLOR DIMENSIONS

Given the adapted cone signals,  $\rho_a$ ,  $\gamma_a$ , and  $\beta_a$ , opponent-type visual responses are calculated in a very simple manner as shown in Equations 12.29 through 12.32.

$$A_a = 2\rho_a + \gamma_a + \left(\frac{1}{20}\right)\beta_a - 3.05 + 1 \quad (12.29)$$

$$C_1 = \rho_a - \gamma_a \quad (12.30)$$

$$C_2 = \gamma_a - \beta_a \quad (12.31)$$

$$C_3 = \beta_a - \rho_a \quad (12.32)$$

The achromatic post-adaptation signal,  $A_a$ , is calculated by summing the cone responses with weights that represent their relative population in the retina. The subtraction of 3.05 and the addition of 1.0 represents removal of the earlier noise components followed by the addition of new noise. The three color difference signals,  $C_1$ ,  $C_2$ , and  $C_3$ , represent all of the possible chromatic opponent signals that could be produced in the retina. These may or may not have direct physiological correlates, but they are

convenient formulations and used to construct more traditional opponent responses as described below.

## 12.5 HUE

Hue angle in the Hunt color appearance model is calculated just as it is in other models once red-green and yellow-blue opponent dimensions are specified as appropriate combinations of the color difference signals described in Equations 12.30 through 12.32. Hue angle,  $h_s$ , is calculated using Equation 12.33.

$$h_s = \tan^{-1} \left[ \frac{(1/2)(C_2 - C_3) / 4.5}{C_1 - (C_2 / 11)} \right] \quad (12.33)$$

Given the hue angle,  $h_s$ , the hue quadrature value,  $H$ , is calculated by interpolation between specified hue angles for the unique hues with adjustment of an eccentricity factor,  $e_s$ . The interpolating function is given by Equation 12.34.

$$H = H_1 + \frac{100[(h_s - h_1) / e_1]}{[(h_s - h_1) / e_1 + (h_2 - h_s) / e_2]} \quad (12.34)$$

$H_1$  is defined as 0, 100, 200, or 300 based on whether red, yellow, green, or blue, respectively, is the unique hue with the hue angle nearest to and less than that of the test sample. The values of  $h_1$  and  $e_1$  are taken from Table 12.2 as the values for the unique hue having the nearest lower value of  $h_s$  while  $h_2$  and  $e_2$  are taken as the values of the unique hue with the nearest higher value of  $h_s$ .

Hue composition,  $H_c$ , is calculated directly from the hue quadrature just as it was in the Nayatani *et al.* model described in Chapter 11. Hue composition is expressed as percentages of two unique hues that describe the composition of the test stimulus hue.

Finally, an eccentricity factor,  $e_s$ , must be calculated for the test stimulus to be used in further calculations of appearance correlates. This is accomplished through linear interpolation using the hue angle,  $h_s$ , of the test stimulus and the data in Table 12.2.

**Table 12.2** Hue angles,  $h_s$ , and eccentricity factors,  $e_s$ , for the unique hues

Hue	$h_s$	$e_s$
Red	20.14	0.8
Yellow	90.00	0.7
Green	164.25	1.0
Blue	237.53	1.2

## 12.6 SATURATION

As a step toward calculating a correlate of saturation, yellowness–blueness and redness–greenness responses must be calculated from the color difference signals according to Equations 12.35 and 12.36.

$$M_{\text{YB}} = 100 \left[ \frac{(1/2)(C_2 - C_3)}{4.5} \right] \left[ e_s \left( \frac{10}{13} \right) N_c N_{\text{cb}} F_t \right] \quad (12.35)$$

$$M_{\text{RG}} = 100 \left[ C_1 - \left( \frac{C_2}{11} \right) \right] \left[ e_s \left( \frac{10}{13} \right) N_c N_{\text{cb}} \right] \quad (12.36)$$

The constant values in Equations 12.35 and 12.36 are simply scaling factors.  $N_c$  and  $N_{\text{cb}}$  are the chromatic surround and background induction factors determined at the outset.  $F_t$  is a low-luminance tritanopia factor calculated using Equation 12.37.

$$F_t = \frac{L_A}{L_A + 0.1} \quad (12.37)$$

Low-luminance tritanopia is a phenomenon whereby observers with normal color vision become more and more tritanopic (yellow–blue deficient) as luminance decreases since the luminance threshold for short-wavelength sensitive cones is higher than that for the other two cone types. As can be seen in Equation 12.37,  $F_t$  is essentially 1.0 for all typical luminance levels. It approaches 0 as the adapting luminance,  $L_A$ , approaches 0, forcing the yellowness–blueness response to decrease at low luminance levels. This factor is also of little importance in most practical situations, but necessary to model appearance over an extremely wide range of luminance levels. For most applications, it is better to avoid this situation by viewing samples at sufficiently high luminance levels.

Given the yellowness–blueness and redness–greenness responses defined above, an overall chromatic response,  $M$ , is calculated as their quadrature sum as shown in Equation 12.38.

$$M = \left( M_{\text{YB}}^2 + M_{\text{RG}}^2 \right)^{1/2} \quad (12.38)$$

Finally, saturation,  $s$ , is calculated from  $M$  and the adapted cone signals using Equation 12.39. This calculation follows the definition of saturation (colorfulness of stimulus relative to its own brightness) if one takes the overall chromatic response,  $M$ , to approximate colorfulness, and the sum of the adapted cone signals in the denominator of Equation 12.39 to approximate the stimulus brightness.

$$s = \frac{50M}{\rho_a + \gamma_a + \beta_a} \quad (12.39)$$

## 12.7 BRIGHTNESS

Further development of the achromatic signals is required to derive correlates of brightness and lightness. Recall that the Hunt color appearance model is designed to function over the full range of luminance levels. In so doing, it must also incorporate the response of the rod photoreceptors, which are active at low luminance levels. The rod response is incorporated into the achromatic signal (which in turn impacts the predictors of chroma and colorfulness). The rod response after adaptation,  $A_s$ , is given by Equation 12.40. The S subscript is derived from the word scotopic, which is used to describe vision at the low luminance levels for which the rod response dominates.

$$A_s = 3.05B_s \left[ f_n \left( \frac{F_{LS}S}{S_w} \right) \right] + 0.3 \quad (12.40)$$

The formulation of the adapted rod signal is analogous to the formulation of the adapted cone signals described previously (Equations 12.5 through 12.7). At its heart is a von Kries-type scaling of the scotopic response for the stimulus,  $S$ , by that for the reference white,  $S_w$ .  $F_{LS}$  is a scotopic luminance level adaptation factor given by Equations 12.41 and 12.42 that is similar to the cone luminance adaptation factor.

$$F_{LS} = 3800j^2 \left( \frac{5L_{AS}}{2.26} \right) + 0.2(1-j^2)^4 \left( \frac{5L_{AS}}{2.26} \right)^{1/6} \quad (12.41)$$

$$j = \frac{0.00001}{(5L_{AS}/2.26) + 0.00001} \quad (12.42)$$

The same nonlinear photoreceptor response function,  $f_n()$ , is also used for the scotopic response (Equation 12.8). The value 3.05 is simply a scaling factor and the noise level of 0.3 (rather than 1.0) is chosen since the rods are more sensitive than cones. Finally, a rod bleaching factor,  $B_s$ , is added to reduce the rod contribution to the overall color appearance as luminance level increases and the rods become less active. This factor is calculated using Equation 12.43. Examination of the rod bleaching factor in comparison with the cone bleaching factors given in Equation 12.20 through 12.22 shows that the rods will become saturated and their response will become significantly decreased at much lower luminance levels.

$$B_s = \frac{0.5}{\left\{ 1 + 0.3 \left[ (5L_{AS}/2.26)(S/S_w) \right]^{0.3} \right\} + 0.5 / \{ 1 + 5[5L_{AS}/2.26] \}} \quad (12.43)$$

Given the achromatic cone signal,  $A_a$  (Equation 12.29), the adapted scotopic signal,  $A_s$  (Equation 12.40), and the brightness background induction factor

determined at the outset, an overall achromatic signal,  $A$ , is calculated using Equation 12.42.

$$A = N_{bb} \left[ A_a - 1 + A_s - 0.3 + (1^2 + 0.3^2)^{1/2} \right] \quad (12.44)$$

All of the constant values in Equation 12.44 represent removal of the earlier noise terms and then their reintroduction through quadrature summation.

The achromatic signal,  $A$ , is then combined with the overall chromatic signal,  $M$ , to calculate a correlate of brightness,  $Q$ , using Equation 12.45.

$$Q = \left\{ 7 \left[ A + \left( \frac{M}{100} \right) \right] \right\}^{0.6} N_1 - N_2 \quad (12.45)$$

The correlate of brightness,  $Q$ , depends on both the achromatic,  $A$ , and chromatic,  $M$ , responses in order to appropriately model the Helmholtz–Kohlrausch effect. Equation 12.45 also includes two terms,  $N_1$  and  $N_2$ , that account for the effects of surround on perceived brightness (e.g., Stevens effect and Bartleson–Breneman results discussed in Chapter 6). These terms are calculated from the achromatic signal for the reference white,  $A_w$ , and the brightness surround induction factor,  $N_b$  (also determined at the outset), through Equations 12.46 and 12.47.

$$N_1 = \frac{(7A_w)^{0.5}}{5.33N_b^{0.13}} \quad (12.46)$$

$$N_2 = \frac{7A_w N_b^{0.362}}{200} \quad (12.47)$$

Note that since the achromatic signal for the reference white,  $A_w$ , is required, it is necessary to carry through all of the model calculations described above for the reference white in addition to the test stimulus. The brightness of the reference white,  $Q_w$ , must also be calculated for use in later equations.

Another form of brightness, referred to as whiteness–blackness,  $Q_{WB}$ , can be calculated in the Hunt model. This is a bipolar value similar to the  $Q$  value in the Nayatani *et al.* model that illustrates that black objects look darker and white objects look brighter as the adapting luminance level increases (another way to state the Stevens effect).  $Q_{WB}$  is calculated according to Equation 12.48 using the brightness of the background (which also must be calculated through the model).

$$Q_{WB} = 20(Q^{0.7} - Q_b^{0.7}) \quad (12.48)$$

## 12.8 LIGHTNESS

Given the brightness of the test stimulus,  $Q$ , and the brightness of the reference white,  $Q_w$ , the Hunt color appearance model correlate of lightness,  $J$ , is calculated as shown in Equation 12.49.

$$J = 100 \left( \frac{Q}{Q_w} \right)^z \quad (12.49)$$

This formulation for lightness follows the CIE definition that lightness is the brightness of the test stimulus relative to the brightness of a white. This ratio is raised to a power,  $z$ , that models the influence of the background relative luminance on perceived lightness according to Equation 12.50. The exponent,  $z$ , increases as the background becomes lighter, indicating that dark test stimuli will appear relatively more dark on a light background than they would on a dark background. This follows the commonly observed phenomenon of simultaneous lightness contrast.

$$z = 1 + \left( \frac{Y_b}{Y_w} \right)^{1/2} \quad (12.50)$$

## 12.9 CHROMA

The Hunt color appearance model correlate of chroma,  $C_{94}$ , is determined from saturation,  $s$ , and the relative brightness (approximately lightness) following the general definitions given in Chapter 4 that indicate chroma can be represented as saturation multiplied by lightness. The precise formulation is given in Equation 12.51.

$$C_{94} = 2.44s^{0.69} \left( \frac{Q}{Q_w} \right)^{Y_b/Y_w} (1.64 - 0.29^{Y_b/Y_w}) \quad (12.51)$$

Equation 12.51 illustrates that chroma depends on the relative brightness of the stimulus,  $Q/Q_w$ , and on the relative luminance of the background,  $Y_b/Y_w$ . The formulation for chroma given by Equation 12.51 was derived empirically based upon the results of a series of appearance scaling experiments (Hunt 1994, Hunt and Luo 1994).

## 12.10 COLORFULNESS

Given chroma, colorfulness can be determined by factoring in the brightness (or at least the luminance level). This is accomplished in the Hunt color appearance model by multiplying chroma,  $C_{94}$ , by the luminance level

adaptation factor  $F_L$  (Equation 12.9) raised to a power of 0.15 as shown in Equation 12.52.

$$M_{94} = F_L^{0.15} C_{94} \quad (12.52)$$

Thus  $M_{94}$  is the colorfulness correlate for the Hunt color appearance model. It was also derived empirically through analysis of visual scaling results.

## 12.11 INVERSE MODEL

Unfortunately, because of its complexity, the complete Hunt color appearance model cannot be analytically inverted. It is an even more severe problem if one has only lightness, chroma, and hue correlates to start from, which is often the case. Many applications, particularly image reproduction, require a color appearance model to be used in both forward and reverse directions. Thus the lack of an analytical inverse introduces some difficulty in using the Hunt model for these applications. Hunt (1995) provides some suggestions on how to deal with this difficulty.

In all cases, it is easier to reverse the model if all of the appearance correlates are available rather than just three. One alternative is to use the model without the scotopic response. This simplifies the inversion process since the introduction of the scotopic terms into higher level equations is one feature that prevents analytical inversion. The predictions of the model are slightly changed when the scotopic response is ignored, but this difference might be negligible for many applications. Hunt (1995) suggests that this technique is appropriate for reference white luminances greater than  $10 \text{ cd/m}^2$ . Most situations in which careful judgments of color reproduction are made are at luminance levels above  $10 \text{ cd/m}^2$ .

Other techniques suggested by Hunt (1995) require successive approximation for some parts of the reverse model. In most applications, it is simpler to use successive approximation for the whole model, iterating until appropriate output tristimulus values are obtained that produce the appearance correlates that are available at the outset. This technique can be accomplished with a technique such as a Newton-Raphson optimization, and it can be applied when only lightness, chroma, and hue are available (in fact it is the only option). While a successive approximation technique can be very time consuming for large data sets, such as images, this drawback is overcome by using the forward and reverse models to build three-dimensional lookup tables, which are then used with an interpolation technique to convert image data. Then, the time-consuming model inversion process need only be performed once for each viewing condition in order to build the lookup table. This approach helps, but if users want to vary the viewing conditions, they must wait a long time for the lookup table to be recalculated.

before an image can be processed. The delay might be significant enough to render the full Hunt model impractical for some applications.

In applying the model, it is often useful to consider its implementation as a simple step-by-step process. Thus the steps required to implement the model (and in reverse, as possible, to invert it) are given below.

1. Obtain physical data and decide on other parameters.
2. Calculate cone excitations,  $\rho\gamma\beta$ , for the various stimulus fields.
3. Calculate relative cone excitations.
4. Calculate the luminance-level adaptation factor,  $F_L$ .
5. Calculate chromatic adaptation factors,  $F_\rho$ ,  $F_\gamma$ ,  $F_\beta$ .
6. Calculate Helson-Judd effect parameters,  $\rho_D$ ,  $\gamma_D$ ,  $\beta_D$ .
7. Calculate adapted cone signals,  $\rho_a$ ,  $\gamma_a$ ,  $\beta_a$ .
8. Calculate achromatic,  $A_a$ , and color difference,  $C_1$ ,  $C_2$ ,  $C_3$ , signals.
9. Calculate hue angle,  $h_s$ .
10. Calculate hue quadrature,  $H$ .
11. Calculate hue composition,  $H_c$ .
12. Calculate eccentricity factor,  $e_s$ .
13. Calculate low-luminance tritanopia factor,  $F_t$ .
14. Calculate chromatic responses,  $M$ , and saturation,  $s$ .
15. Calculate scotopic luminance adaptation factor,  $F_{LS}$ .
16. Calculate scotopic response,  $A_s$ .
17. Calculate complete achromatic response,  $A$ .
18. Calculate brightness,  $Q$ .
19. Calculate lightness,  $J$ .
20. Calculate chroma,  $C_{94}$ .
21. Calculate colorfulness,  $M_{94}$ .
22. Calculate whiteness–blackness,  $Q_{WB}$ .

The Hunt color appearance model is the most complex to implement of the traditional color appearance models described in this book. There are a couple of implementation techniques that can simplify program development and greatly improve computational speed. One is to go through the model and calculate all of the parameters that are constant for a given set of viewing conditions first in a pre-calculation routine. This can be applied to all of the adaptation factors, correlates for the reference white, etc. Then, these precalculated data can be used for the remaining data calculations rather than recalculating the values for each stimulus (or pixel in an image). This can be particularly useful when transforming image data (or lookup tables) that might require the model calculations to be completed millions of times. Secondly, many of the equations, for example the achromatic response,  $A$  (Equation 12.44), include operations on constants. The number of computations can be reduced by combining all of these constants into a single number first (some compilers will do this for you). For example, the  $-1 - 0.3 + (1^2 + 0.3^2)^{1/2}$  can be converted into simply 1.044.

## 12.12 PHENOMENA PREDICTED

As stated previously, the Hunt color appearance model is the most extensive and complete color appearance model available. It has the following features:

- It is designed to predict the appearance of stimuli in a variety of backgrounds and surrounds at luminance levels ranging from the absolute threshold of human vision to cone bleaching.
- It can be used for related or unrelated stimuli (see Hunt 1991b for an explanation of how the model is applied to unrelated colors).
- It predicts a wide range of color appearance phenomena including the Bezold–Brücke hue shift, Abney effect, Helmholtz–Kohlrausch effect, Hunt effect, simultaneous contrast, Helson–Judd effect, Stevens effect, and Bartleson–Breneman observations.
- It predicts changes in color appearance due to light and chromatic adaptation and cognitive discounting-the-illuminant.
- It is unique in that it includes the contributions of rod photoreceptors.

While the list of appearance phenomena that the Hunt model addresses is extensive, this comes at the price of complexity (with no apologies required, the visual system is complex) that makes the model difficult to use in some applications.

Example calculations using the Hunt color appearance model as described in this chapter are given for four samples in Table 12.3. These results were

**Table 12.3** Example Hunt color appearance model calculations

Quantity	Case 1	Case 2	Case 3	Case 4
X	19.01	57.06	3.53	19.01
Y	20.00	43.06	6.56	20.00
Z	21.78	31.96	2.14	21.78
X <sub>w</sub>	95.05	95.05	109.85	109.85
Y <sub>w</sub>	100.00	100.00	100.00	100.00
Z <sub>w</sub>	108.88	108.88	35.58	35.58
L <sub>A</sub>	318.31	31.83	318.31	31.83
N <sub>c</sub>	1.0	1.0	1.0	1.0
N <sub>b</sub>	75	75	75	75
Discounting?	Y	Y	Y	Y
h <sub>s</sub>	269.3	18.6	178.3	262.8
H	317.2	398.8	222.2	313.4
H <sub>c</sub>	83B 17R	99R 1B	78G 22B	87B 13R
s	0.03	153.36	245.40	209.29
Q	31.92	31.22	18.90	22.15
J	42.12	66.76	19.56	40.27
C <sub>94</sub>	0.16	63.89	74.58	73.84
M <sub>94</sub>	0.16	58.28	76.33	67.35

calculated with the assumptions that the proximal field and background were both achromatic (same chromaticity as the source) with luminance factors of 20% and that the reference white also had the same chromaticity as the source with a luminance factor of 100%. Scotopic input was calculated using the approximate equations described in this chapter. The Helson–Judd parameters were always set to 0.0.

### 12.13 WHY NOT USE JUST THE HUNT MODEL?

Given that the Hunt color appearance model seems to be able to do everything that anyone could ever want a color appearance model to do, why is it not adopted as the single standard color appearance model for all applications? The main reason could be the very fact that it is so complete. In its completeness also lies its complexity. Its complexity makes application of the Hunt model to practical situations range from difficult to impossible. However, the complexity of the Hunt model also allows it to be extremely flexible. As will be seen in Chapter 15, the Hunt model is generally capable of making accurate predictions for a wide range of visual experiments. This is because the model is flexible enough to be adjusted to the required situations. Clearly, this flexibility and general accuracy are great features of the Hunt model. However, often it is not possible to know just how to apply the Hunt model (*i.e.*, decide on the appropriate parameter values) until after the visual data have been obtained. In other cases, the parameters actually need to be optimized, not just chosen, for the particular viewing situation. This is not a problem if the resources are available to derive the optimized parameters. However, when such resources are not available and the Hunt model must be used “as is” with the recommended parameters, the model can perform extremely poorly (Chapter 15). This is because the nominal parameters used for a given viewing condition are being used to make specific predictions of phenomena that may or may not be important in that situation. After the fact, adjustments can be made, but that might be too late. Thus, if it is not possible to optimize (or optimally choose) the implementation of the Hunt model, its precision might result in predictions that are worse than much simpler models for some applications.

Other negative aspects that counteract the positive features of the Hunt color appearance model are that it cannot be easily inverted and that it is computationally expensive, difficult to implement, and requires significant user knowledge to use consistently. The Hunt model also uses functions with additive offsets to predict contrast changes due to variation in surround relative luminance. These functions can result in predicted corresponding colors with negative tristimulus values for some changes in surround.

# The RLAB Model

---

This chapter completes the discussion of some of the most widely used historical (pre-CIE models) color appearance models with a description of the RLAB model. While the Hunt and Nayatani *et al.* models discussed in the preceding chapters are designed to predict all of the perceptual attributes of color appearance for a wide range of viewing conditions, the RLAB model was designed with other considerations. RLAB was developed with the intent of producing a simple color appearance model capable of predicting the most significant appearance phenomena in practical applications. RLAB was developed with cross-media image reproduction as its target application, and it has been effectively applied to such situations.

## 13.1 OBJECTIVES AND APPROACH

The RLAB color appearance model evolved from studies of chromatic adaptation (Fairchild 1990), chromatic adaptation modeling (Fairchild 1991a,b), fundamental CIE colorimetry (CIE 1986), and practical implications in cross-media image reproduction (Fairchild 1994b, Fairchild and Berns 1993). The starting point for RLAB is the CIELAB color space. While CIELAB can be used as an approximate color appearance model, it does have significant limitations. These include an inaccurate chromatic adaptation transform, no luminance-level dependency, no surround dependency, and no distinction for when discounting-the-illuminant occurs. While CIELAB has other limitations as a color appearance model, these are most important for many practical applications. Thus, RLAB was designed to build on the positive aspects of CIELAB and, by making additions, to address its limitations. It is worth noting that Richter (1980) took a similar approach to modifying and improving the CIELAB and CIELUV color spaces to create a simple appearance model.

CIELAB provides good perceptual uniformity with respect to color appearance for average daylight illuminants. This is illustrated by the

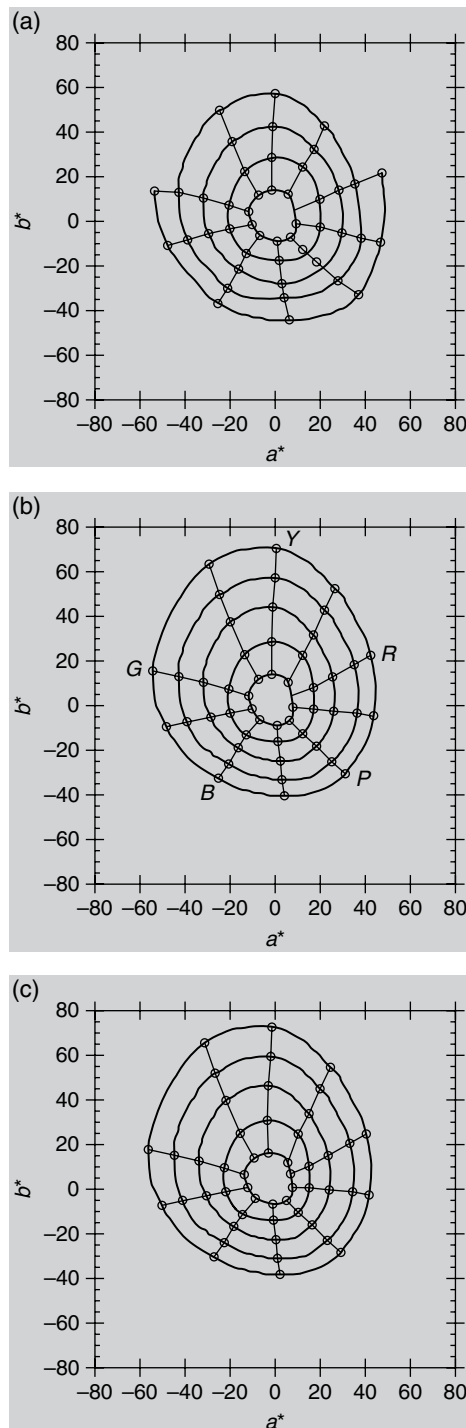


**Figure 13.1** Contours of constant Munsell hue and chroma plotted in the CIELAB/RLAB color space at (a) value 3, (b) value 5, and (c) value 7

spacing of constant hue and chroma contours from the *Munsell Book of Color* shown in Figure 13.1. The contours plotted in Figure 13.1 are as good as, and in some cases better than, those produced using any other color appearance model. However, due to CIELAB's "wrong von Kries" chromatic adaptation transform, the good perceptual spacing of CIELAB quickly degrades as the illuminant moves away from average daylight. The concept of RLAB is to take advantage of the good spacing under daylight and familiarity of the CIELAB space while improving its applicability to non-daylight illuminants. This was accomplished by defining a reference set of viewing conditions (illuminant D65, 318 cd/m<sup>2</sup>, average surround, discounting-the-illuminant) for which the CIELAB space is used, and then using a more accurate chromatic adaptation transform (Fairchild 1991b, 1994b, 1996) to determine corresponding colors between the test viewing conditions and the reference viewing conditions. Thus, test tristimulus values are first transformed into corresponding colors under the reference viewing condition, and then a modified CIELAB space is used to describe appearance correlates. This concept could be applied with any desired chromatic adaptation transform such as the CAT02 transform based on CIECAM02.

In addition, the compressive nonlinearity (cube root) of the CIELAB space is adapted to become a function of the surround relative luminance. This allows the prediction of decreases in perceived image contrast as the surround becomes darker as suggested in the work of Bartleson (1975). The improved chromatic adaptation transform and the surround dependence enhance CIELAB in the two areas that are most critical in image reproduction.

RLAB was designed to include predictors of only relative color appearance attributes. Thus it can be used to calculate correlates of lightness, chroma, saturation, and hue, but it cannot be used to predict brightness or colorfulness. This limitation was imposed to keep the model as simple as possible and because the prediction of brightness and colorfulness have little importance in most image reproduction applications.

The fact that RLAB is based on the CIELAB space has benefit in addition to familiarity. Since the RLAB spacing is essentially identical to CIELAB spacing, color difference formulas such as CIELAB  $\Delta E_{ab}^*$  (CIE 1986), CMC (Clark *et al.* 1984), and CIE94 (CIE 1995b) can be used with results that are similar to those obtained when using CIELAB alone under average daylight illuminants.

A more detailed description of the RLAB model, as presented in this chapter, can be found in Fairchild (1996).

## 13.2 INPUT DATA

Input data for the RLAB model include the relative tristimulus values of the test stimulus ( $XYZ$ ) and the white point ( $X_n Y_n Z_n$ ), the absolute luminance of a white object in the scene in cd/m<sup>2</sup>, the relative luminance of the surround (dark, dim, average), and a decision on whether discounting-the-illuminant

is taking place. The surround relative luminance is generally taken to be average for reflection prints, dim for self-luminous displays or televisions, and dark for projected transparencies under the assumption that these media are being viewed in their typical environments. The surround is not directly tied to the medium. Thus it is certainly possible to have reflection prints viewed in a dark surround and projected transparencies viewed in an average surround. Discounting-the-illuminant is assumed to occur for object color stimuli such as prints and not to occur for emissive displays such as CRTs. Intermediate levels of discounting-the-illuminant are likely to occur in some situations such as the viewing of projected transparencies.

### 13.3 ADAPTATION MODEL

The following equations describe the chromatic adaptation model built into RLAB. It is based on the model of incomplete chromatic adaptation described by Fairchild (1991b) and later modified (Fairchild 1994b, 1996). This transformation is also discussed in Chapter 9. One begins with a conversion from CIE tristimulus values ( $Y = 100$  for white) to fundamental tristimulus values as illustrated in Equations 13.1 and 13.2. All CIE tristimulus values are normally calculated using the CIE 1931 Standard Colorimetric Observer ( $2^\circ$ ). The transformation must also be completed for the tristimulus values of the adapting stimulus.

$$\begin{vmatrix} L \\ M \\ S \end{vmatrix} = \mathbf{M} \begin{vmatrix} X \\ Y \\ Z \end{vmatrix} \quad (13.1)$$

$$\mathbf{M} = \begin{vmatrix} 0.3897 & 0.6890 & -0.0787 \\ -0.2298 & 1.1834 & 0.0464 \\ 0.0 & 0.0 & 1.0000 \end{vmatrix} \quad (13.2)$$

The transformation to cone responses is the same as that used in the Hunt model. Matrix  $\mathbf{M}$  is normalized such that the tristimulus values for the equal-energy illuminant ( $X = Y = Z = 100$ ) produce equal cone responses ( $L = M = S = 100$ ). The next step is calculation of the  $\mathbf{A}$  matrix that is used to model the chromatic adaptation transformation.

$$\mathbf{A} = \begin{vmatrix} a_L & 0.0 & 0.0 \\ 0.0 & a_M & 0.0 \\ 0.0 & 0.0 & a_S \end{vmatrix} \quad (13.3)$$

The  $\mathbf{A}$  matrix represents von Kries adaptation coefficients that are applied to the cone responses for the test stimulus (LMS). The von Kries-type coefficients are calculated using Equations 13.4 through 13.12.

$$a_L = \frac{p_L + D(1.0 - p_L)}{L_n} \quad (13.4)$$

$$a_M = \frac{p_M + D(1.0 - p_M)}{M_n} \quad (13.5)$$

$$a_S = \frac{p_S + D(1.0 - p_S)}{S_n} \quad (13.6)$$

The  $p$  terms describe the proportion of complete von Kries adaptation that is occurring. They are calculated using formulas that predict chromatic adaptation to be more complete as the luminance level increases and less complete as the color of the adapting stimulus departs from that of the equal-energy illuminant. These terms are equivalent to the chromatic adaptation factors in the Hunt model and are calculated using the same equations given in Equations 13.7 through 13.12.

$$p_L = \frac{(1.0 + Y_n^{1/3} + \ell_E)}{(1.0 + Y_n^{1/3} + 1.0 / \ell_E)} \quad (13.7)$$

$$p_M = \frac{(1.0 + Y_n^{1/3} + m_E)}{(1.0 + Y_n^{1/3} + 1.0 / m_E)} \quad (13.8)$$

$$p_S = \frac{(1.0 + Y_n^{1/3} + s_E)}{(1.0 + Y_n^{1/3} + 1.0 / s_E)} \quad (13.9)$$

$$\ell_E = \frac{3.0L_n}{L_n + M_n + S_n} \quad (13.10)$$

$$m_E = \frac{3.0M_n}{L_n + M_n + S_n} \quad (13.11)$$

$$s_E = \frac{3.0S_n}{L_n + M_n + S_n} \quad (13.12)$$

$Y_n$  in Equations 13.7 through 13.9 is the absolute adapting luminance in  $\text{cd/m}^2$ . The cone response terms with  $n$  subscripts ( $L_n, M_n, S_n$ ) refer to values for the adapting stimulus derived from relative tristimulus values. The  $D$  factor in Equations 13.4 through 13.6 allows various proportions of cognitive discounting-the-illuminant.  $D$  should be set equal to 1.0 for hard-copy images, 0.0 for soft-copy displays, and an intermediate value for situations such as projected transparencies in completely darkened rooms. The exact value of the  $D$  factor can be used to account for the various levels of chromatic adaptation found in the infinite variety of practical viewing situations. The exact choice of intermediate values will depend upon the specific viewing conditions. Katoh (1994) has illustrated an example of

intermediate adaptation in direct comparison between soft- and hard-copy displays, and Fairchild (1992a) has reported a case of intermediate discounting-the-illuminant for a soft-copy display. When no visual data are available and an intermediate value is necessary, a value of 0.5 should be chosen and refined with experience.

Note that if discounting-the-illuminant occurs and  $D$  is set equal to 1.0, then the adaptation coefficients described in Equations 13.4 through 13.6 reduce to the reciprocals of the adapting cone excitations exactly as would be implemented in a simple von Kries model.

After the **A** matrix is calculated, the tristimulus values for a stimulus color are converted to corresponding tristimulus values under the reference viewing conditions using Equations 13.13 and 13.14.

$$\begin{vmatrix} X_{\text{ref}} \\ Y_{\text{ref}} \\ Z_{\text{ref}} \end{vmatrix} = \mathbf{RAM} \begin{vmatrix} X \\ Y \\ Z \end{vmatrix} \quad (13.13)$$

$$\mathbf{R} = \begin{vmatrix} 1.9569 & -1.1882 & 0.2313 \\ 0.3612 & 0.6388 & 0.0 \\ 0.0 & 0.0 & 1.0000 \end{vmatrix} \quad (13.14)$$

The **R** matrix represents the inverse of the **M** and **A** matrices for the reference viewing conditions ( $\mathbf{M}^{-1}\mathbf{A}^{-1}$ ) plus a normalization, discussed below, that is always constant and can therefore be precalculated. Thus Equation 13.13 represents a modified von Kries chromatic adaptation transform that converts test stimulus tristimulus values to corresponding colors under the RLAB reference viewing conditions (illuminant D65, 318 cd/m<sup>2</sup>, discounting-the-illuminant). The next step is to use these reference tristimulus values to calculate modified CIELAB appearance correlates as shown in the following sections.

## 13.4 OPPONENT COLOR DIMENSIONS

Opponent type responses in RLAB are calculated using Equations 13.15 through 13.17.

$$L^R = 100(Y_{\text{ref}})^\sigma \quad (13.15)$$

$$a^R = 430 \left[ (X_{\text{ref}})^\sigma - (Y_{\text{ref}})^\sigma \right] \quad (13.16)$$

$$b^R = 170 \left[ (Y_{\text{ref}})^\sigma - (Z_{\text{ref}})^\sigma \right] \quad (13.17)$$

$L^R$  represents an achromatic response analogous to CIELAB  $L^*$ . The red-green chromatic response is given by  $a^R$  (analogous to CIELAB  $a^*$ ) and the yellow-blue chromatic response is given by  $b^R$  (analogous to CIELAB  $b^*$ ). Recall that, for the reference viewing conditions, the RLAB coordinates are nearly identical to CIELAB coordinates. They are not identical because Equations 13.15 through 13.17 have been simplified from the CIELAB equations for computational efficiency. The conditional compressive nonlinearities (*i.e.*, different functions for low tristimulus values) of CIELAB have been replaced with simple power functions. This results in the exponents and the scaling factors being slightly different than the CIELAB equations. Fairchild (1996) provides more details on these differences. It is also worth noting that the divisions by the tristimulus values of the white point that are incorporated in the CIELAB equations are missing from Equations 13.15 through 13.17. This is because these normalizations are constant in the RLAB model and they have been built into the **R** matrix given in Equation 13.14.

The exponents in Equations 13.15 through 13.17 vary depending on the relative luminance of the surround. For an average surround  $\sigma = 1/2.3$ , for a dim surround  $\sigma = 1/2.9$ , and for a dark surround  $\sigma = 1/3.5$ . The ratios of these exponents are precisely in line with the contrast changes suggested by Bartleson (1975) and Hunt (1995) for image reproduction. More detail on the exponents can be found in Fairchild (1995b). As a nominal definition, a dark surround is considered essentially zero luminance, a dim surround is considered a relative luminance less than 20% of white in the image, and an average surround is considered a relative luminance equal to or greater than 20% of the image white. The precise nature and magnitude of the contrast changes required for various changes in image viewing conditions is still a topic of research and debate. Thus it is best to use these parameters with some flexibility. In some applications, it might be desired to use intermediate values for the exponents in order to model less severe changes in surround relative luminance. This requires no more than a substitution in the RLAB equations since they do not include the conditional functions that are found in the CIELAB equations. In addition, it might be desirable to use different exponents on the lightness,  $L^R$ , dimension than on the chromatic,  $a^R$  and  $b^R$ , dimensions. This can also be easily accommodated. The equations have been formulated as simple power functions to encourage the use of different exponents, which might be more appropriate than the nominal exponents for particular, practical viewing conditions.

Figure 13.2 illustrates the effect of changing the exponents. The left image (a) is a typical printed reproduction. The other two images (b and c) show the change in contrast necessary to reproduce the same appearance if the image were viewed in a dark surround. Note the increase in contrast required for viewing in a dark surround. In the middle image (b), the adjustment has been made on lightness contrast only. In the right image (c), the surround compensation has been applied to the chromatic dimensions, as well as to lightness. The right image (c) is similar to the reproduction that would be produced in a simple photographic system (since the contrast of all three

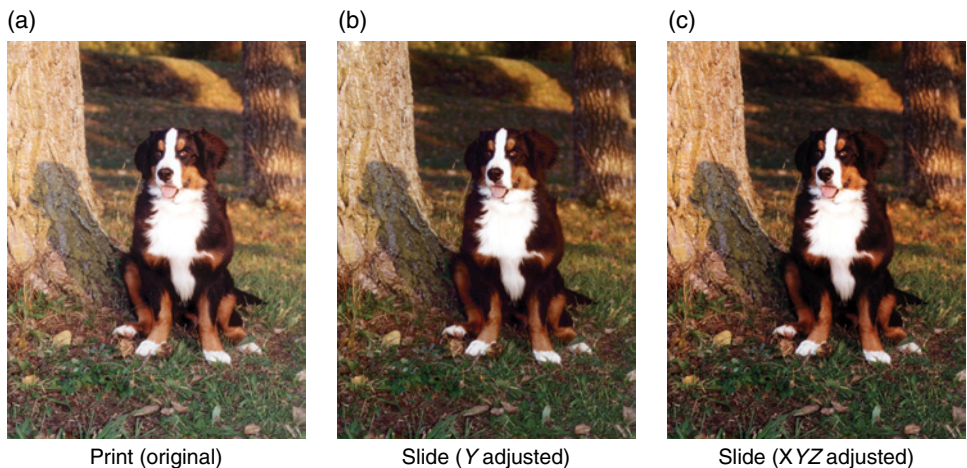


**Figure 13.2** Images illustrating the change in image contrast necessary to account for appearance differences due to change in surround relative luminance. (a) Original print image. (b) Image for viewing in a dark surround, adjusted only in lightness contrast. (c) Image for viewing in a dark surround, adjusted in both lightness and chromatic contrast

film layers must be changed together) and is generally preferable. Note, however, that inter-image effects in real film could be used to compensate for some of the increase in saturation with contrast (as could matrixing operations in digital systems). The images in Figure 13.2 should only be used to judge the relative impact of the adjustments since they are not being viewed in the appropriate viewing conditions.

## 13.5 LIGHTNESS

The RLAB correlate of lightness is  $L^R$ , given in Equation 13.15. No further calculations are required.

## 13.6 HUE

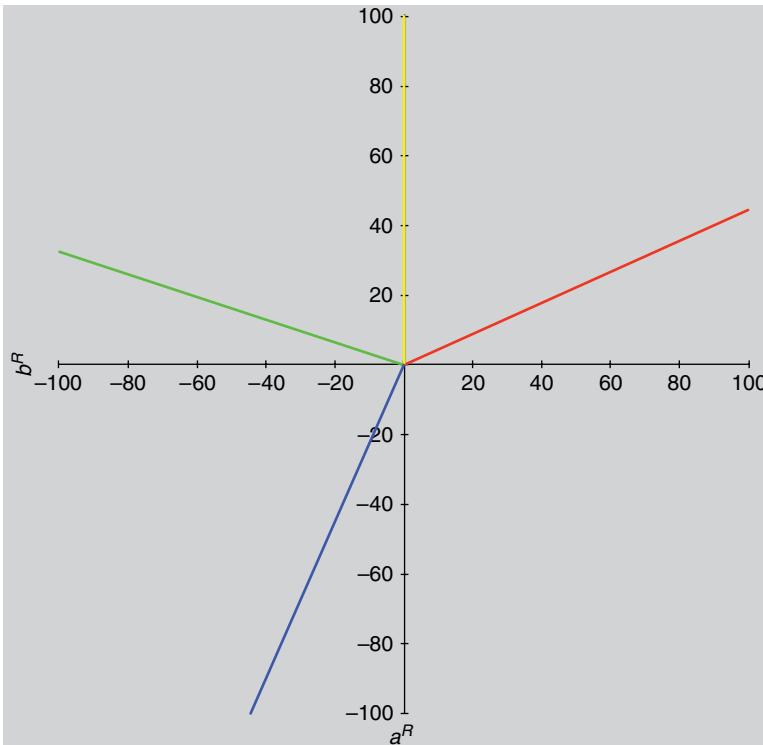
Hue angle,  $h^R$ , is calculated in the RLAB space using the same procedure as CIELAB. As in CIELAB,  $h^R$  is expressed in degrees ranging from 0 to 360 measured from the positive  $a^R$  axis calculated according to Equation 13.18.

$$h^R = \tan^{-1} \left( \frac{b^R}{a^R} \right) \quad (13.18)$$

Hue composition can be determined in RLAB using a procedure similar to that of the Hunt model and Nayatani *et al.* model. This is useful when

**Table 13.1** Data for conversion from hue angle to hue composition

$h^R$	$R$	$B$	$G$	$Y$	$H^R$
24	100	0	0	0	R
90	0	0	0	100	Y
162	0	0	100	0	G
180	0	21.4	78.6	0	B79G
246	0	100	0	0	B
270	17.4	82.6	0	0	R83B
0	82.6	17.4	0	0	R17B
24	100	0	0	0	R

**Figure 13.3** Illustration of the hue angles of the perceptually unique hues in the RLAB color space

testing a color appearance model against magnitude estimation data and when it is desired to reproduce a named hue. Hue composition,  $H^R$ , can be calculated via linear interpolation of the values in Table 13.1. These were derived based on the notation of the Swedish NCS and are illustrated in Figure 13.3. Figure 13.3 is a useful visualization of the loci of the unique hues since they do not correspond to the principal axes of the color space. The unique hue locations are the same as those in the CIELAB

space under only the reference conditions. Example hue composition values are listed in Table 13.1 in italics.

## 13.7 CHROMA

RLAB chroma,  $C^R$ , is calculated in the same way as CIELAB chroma, as shown in Equation 13.19.

$$C^R = \sqrt{(a^R)^2 + (b^R)^2} \quad (13.19)$$

## 13.8 SATURATION

In some applications, such as the image color manipulation required for gamut mapping, it might be desirable to change colors along lines of constant saturation rather than constant chroma. Wolski *et al.* (1994) have proposed such a technique, and Montag and Fairchild (1996, 1997) also describe such situations. *Saturation* is defined as colorfulness relative to brightness, *chroma* is defined as colorfulness relative to the brightness of a white, and *lightness* is defined as brightness relative to the brightness of a white. Therefore, saturation can be defined as chroma relative to lightness. Chroma,  $C^R$ , and lightness,  $L^R$ , are already defined in RLAB; thus saturation,  $s^R$ , is defined as shown in Equation 13.20.

$$s^R = \frac{C^R}{L^R} \quad (13.20)$$

It is of interest to note that a progression along a line of constant saturation is the series of colors that can be observed when an object is viewed in ever deepening shadows. This could be why transformations along lines of constant saturation, rather than chroma, are sometimes useful in gamut mapping applications.

## 13.9 INVERSE MODEL

Since the RLAB model was designed with image reproduction applications in mind, computational efficiency and simple inversion were considered of significant importance. Thus the RLAB model is very easy to invert and requires a minimum of calculations. A step-by-step procedure for implementing the RLAB model is given below.

*Step 1.* Obtain the colorimetric data for the test and adapting stimuli and the absolute luminance of the adapting stimulus. Decide on the discounting-the-illuminant factor and the exponent (based on surround relative luminance).

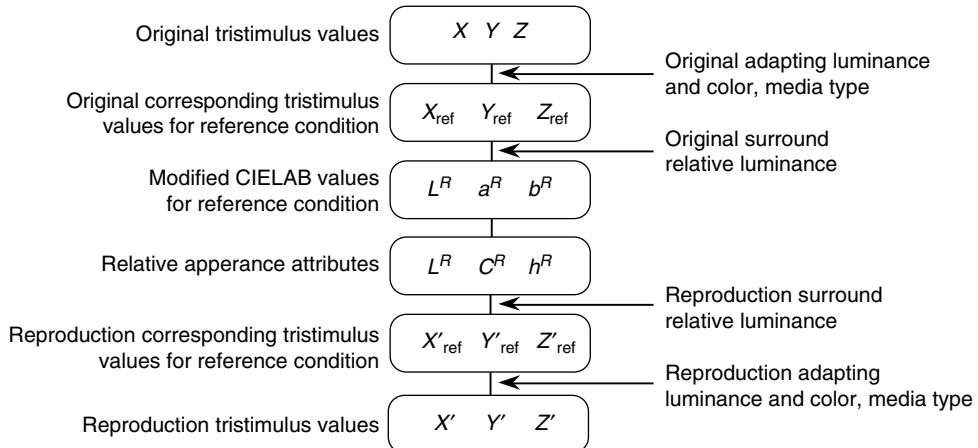


**Figure 13.4** A flow chart of the application of the RLAB model to image reproduction applications

*Step 2.* Calculate the chromatic adaptation matrix, **A**.

*Step 3.* Calculate the reference tristimulus values.

*Step 4.* Calculate the RLAB parameters,  $L^R$ ,  $a^R$ , and  $b^R$ .

*Step 5.* Use  $a^R$  and  $b^R$  to calculate  $C^R$  and  $h^R$ .

*Step 6.* Use  $h^R$  to determine  $H^R$ .

*Step 7.* Calculate  $s^R$  using  $C^R$  and  $L^R$ .

In typical color reproduction applications, it is not enough to know the appearance of image elements; it is necessary to reproduce those appearances in a second set of viewing conditions as illustrated in Figure 13.4. To accomplish this, one must be able to calculate CIE tristimulus values,  $XYZ$ , from the appearance parameters,  $L^R a^R b^R$ , and the definition of the new viewing conditions. These tristimulus values are then used, along with the imaging-device characterization, to determine device color signals such as RGB or CMYK. The following equations outline how to calculate CIE tristimulus values from RLAB  $L^R a^R b^R$ . If starting with  $L^R C^R h^R$ , one must first transform back to  $L^R a^R b^R$  using the usual transformation from cylindrical to rectangular coordinates.

The reference tristimulus values are calculated from the RLAB parameters using Equations 13.21 through 13.23 with an exponent,  $\sigma$ , appropriate for the second viewing condition.

$$Y_{\text{ref}} = \left( \frac{L^R}{100} \right)^{1/\sigma} \quad (13.21)$$

$$X_{\text{ref}} = \left[ \left( \frac{a^R}{430} \right) + (Y_{\text{ref}})^{\sigma} \right]^{1/\sigma} \quad (13.22)$$

$$Z_{\text{ref}} = \left[ (Y_{\text{ref}})^\sigma - \left( \frac{b^R}{170} \right) \right]^{1/\sigma} \quad (13.23)$$

The reference tristimulus values are then transformed to tristimulus values for the second viewing condition using Equation 13.24 with an **A** matrix calculated for the second viewing conditions.

$$\begin{vmatrix} X \\ Y \\ Z \end{vmatrix} = (\mathbf{RAM})^{-1} \begin{vmatrix} X_{\text{ref}} \\ Y_{\text{ref}} \\ Z_{\text{ref}} \end{vmatrix} \quad (13.24)$$

## 13.10 PHENOMENA PREDICTED

The RLAB model provides correlates for relative color appearance attributes only (lightness, chroma, saturation, and hue). It cannot be used to predict brightness and colorfulness. This limitation is of little practical importance for image reproduction since there are few applications in which brightness and colorfulness are required. RLAB includes a chromatic adaptation transform with a parameter for discounting-the-illuminant, and predicts incomplete chromatic adaptation to certain stimuli (*e.g.*, RLAB correctly predicts that a CRT display with a D50 white point will retain a yellowish appearance). It also includes variable exponents,  $\sigma$ , that modulate image contrast as a function of the surround relative luminance. These are the most important color appearance phenomena for cross-media image reproduction applications. If it is necessary to predict absolute appearance attributes (*i.e.*, brightness and colorfulness) or more unusual appearance phenomena, then more extensive appearance models such as the Nayatani *et al.* and Hunt models described in preceding chapters should be considered.

Example calculations for the RLAB color appearance model are given in Table 13.2.

## 13.11 WHY NOT USE JUST THE RLAB MODEL?

The RLAB model is simple, straightforward, easily invertible, and has been found to be as accurate as, or better than, more complicated color appearance models for many practical applications. Given all of these features, why would not RLAB be considered as a recommendation for a single, universal color appearance model?

**Table 13.2** Example RLAB color appearance model calculations

Quantity	Case 1	Case 2	Case 3	Case 4
X	19.01	57.06	3.53	19.01
Y	20.00	43.06	6.56	20.00
Z	21.78	31.96	2.14	21.78
X <sub>n</sub>	95.05	95.05	109.85	109.85
Y <sub>n</sub>	100.00	100.00	100.00	100.00
Z <sub>n</sub>	108.88	108.88	35.58	35.58
Y <sub>n</sub> (cd/m <sup>2</sup> )	318.31	31.83	318.31	31.83
σ	0.43	0.43	0.43	0.43
D	1.0	1.0	1.0	1.0
L <sup>R</sup>	49.67	69.33	30.78	49.83
a <sup>R</sup>	0.00	46.33	-40.96	15.57
b <sup>R</sup>	-0.01	18.09	2.25	-52.61
h <sup>R</sup>	270.0	21.3	176.9	286.5
H <sup>R</sup>	R83B	R2B	B74G	R71B
C <sup>R</sup>	0.01	49.74	41.02	54.87
s <sup>R</sup>	0.00	0.72	1.33	1.10

RLAB's weaknesses are the same as its strengths. Since it is such a simple model, it is not exhaustive in its prediction of color appearance phenomena. It does not include correlates of brightness and colorfulness. It cannot be applied over a wide range of luminance levels. It does not predict some color appearance phenomena such as the Hunt effect, the Stevens effect (although these could be simulated by making σ change with adapting luminance rather than surround relative luminance), and the Helson–Judd effect. In practical imaging applications, these limitations are of little consequence due to device-gamut limitations. In other applications, where these phenomena might be important, a different color appearance model is required. In summary, RLAB performs well for the image reproduction applications for which it was designed, but is not comprehensive enough for all color appearance situations that might be encountered.

# Other Models

---

The preceding chapters have reviewed four of the most widely used and general color appearance models representing the evolution toward the CIECAM models presented in the following chapters. These and other models have been continually modified and introduced over the years. This chapter provides overviews of three more color appearance models – one that has been evolving for many years, a second that is relatively new, and a third with a very specific aim in the prediction of constant hue. For various reasons discussed herein, these models are not as well suited for general application as those described in earlier chapters or the more refined CIECAM models. However, various aspects of their formulation are of interest both historically and for development of future models or applications. Thus, they have been included to appropriately cover their potential impact on the field.

## 14.1 OVERVIEW

The formulation of color appearance models remains an area of active, ongoing research. That explains why this book can only provide an overview of the associated problems and several approaches to solving them. It is not possible to present a single model of color appearance that will solve all problems if followed in a “cookbook” manner. This is the “holy grail” for researchers in the field, but not likely to be achieved in short order. Chapters 10 through 13 presented some of the best historically available approaches to problems of color appearance specification and reproduction. Chapters 15 and 16 present more recent CIE color appearance models: CIECAM97s and CIECAM02. One of those models is likely to be the most appropriate solution for any given application. However, one model is not likely to be the best solution for all applications. Since the development of color appearance models remains an ongoing endeavor,

it is important to describe other models that have had, or are likely to have, significant impact on the field.

Three such models are described in this chapter:

1. The ATD model formulated by Guth (1995), which has a history of development dating back over 20 years (Guth 1994a).
2. A more recent model derived by Luo *et al.* (1996) known as LLAB.
3. A color space for constant hue predictions by Ebner and Fairchild (1998) known as IPT.

A fourth model was under development by CIE Technical Committee 1-34 as an attempt to promote uniformity of practice in color appearance specification for industry when the first edition of this book was published. The then current status of this CIE color appearance model was described in an appendix. In the intervening years, that model, CIECAM97s, was published and widely used and revised. It is discussed in Chapter 15. The results of further research on CIECAM97s (within CIE TC8-01) resulted in further improvements being adopted by the CIE in the CIECAM02 model, described in Chapter 16.

## 14.2 ATD MODEL

The ATD model, developed by Guth, is a different type of model than those described in earlier (and later) chapters. In fact, according to the CIE TC1-34 definition of what makes a color appearance model, it cannot be considered a color appearance model. This is because the model was developed with different aims. It is described as a model of color vision, or more appropriately the first few stages of color vision.

Guth (1994a,b) has given a good overview of the development and performance of the model. The model's history dates back as far as 1972. The ATD model was developed to predict a wide range of vision science data on phenomena such as chromatic discrimination, absolute thresholds, the Bezold-Brücke hue shift, the Abney effect, heterochromatic brightness matching, light adaptation, and chromatic adaptation. The ATD model is capable of making remarkable predictions of vision data for these phenomena. However, most such experiments have been performed using unrelated stimuli. Thus the model is designed for unrelated stimuli and only by somewhat arbitrary modification of the model can it be applied to related colors. This background explains why the model incorporates measures of color discrimination, brightness, saturation, and hue, but does not distinguish other important appearance attributes such as lightness, colorfulness, and chroma. This limits the model's applicability somewhat, but its general structure and chromatic adaptation transformation are certainly worthy of further study and attention.

The ATD model has been modified and used in practical imaging applications. Such applications have been described by Granger (1994, 1995). Granger (1994, 1995) took advantage of the opponent colors encoding

of the ATD model to develop a space that is useful for describing color appearance and doing color manipulations in desktop publishing. However, Granger (1994, 1995) did not incorporate any chromatic adaptation transformation in his modified ATD model; thus the utility of the model is limited to a single illumination white point unless a user is willing to make the erroneous assumption that printed color images represent color-constant stimuli.

## Objectives and Approach

As stated above, the ATD model has a long history of development aimed at the prediction of various color vision data. Guth (1995) refers to it as a “model for color perception and visual adaptation,” and that is certainly an appropriate description. Regarding what the model is intended for, Guth (1995) states that it “should now be seriously considered by the vision community as a replacement for all models that are currently used to make predictions (or to establish standards) that concern human color perception.” This is an ambitious goal that clearly overlaps the objectives of some of the other models described in this book. As discussed below it is also an extreme overstatement of the capabilities of the model.

One revision of the ATD model referred to as “ATD95” is described in the following sections. The treatment in Guth (1995) has been followed. Earlier papers such as Guth (1991) should also be referred to in order to obtain a more global understanding of the model’s derivation and capabilities. Interested readers are encouraged to look for more recent literature on modifications of the model.

The model begins with nonlinear cone responses followed by a nonlinear von Kries-type receptor gain control and two stages of opponent responses necessary for the prediction of various discrimination and appearance phenomena. Finally the model includes a neural compression of the opponent signals. The letters *A*, *T*, and *D* are abbreviations for achromatic, tritanopic, and deuteranopic mechanisms. The *A* system signals brightness, the *T* system redness–greenness, and the *D* system yellowness–blueness.

## Input Data

The input data for the ATD model operating on unrelated colors are the  $X'Y'Z'$  tristimulus values (Judd’s modified tristimulus values, not CIE XYZ tristimulus values) expressed in absolute luminance units. The  $X'Y'Z'$  tristimulus values are scaled such that  $Y'$  is set equal to  $Y$  (photopic luminance) expressed in trolands. Trolands are a measure of retinal illuminance that factors in the eye’s pupil diameter. Since the pupil diameter is controlled by the scene luminance (to some degree), Guth (1995) suggests converting from luminance in  $\text{cd}/\text{m}^2$  to retinal illuminance in trolands by raising the luminance to the power of 0.8 and multiplying by 18 as a reasonable approximation.

Strictly, the ATD model is incompatible with CIE colorimetry since it is based on Judd-modified  $X'Y'Z'$  tristimulus values rather than CIE  $XYZ$  tristimulus values. However, Guth (1995) states that “it is probably true that  $XYZ$ s rather than  $X'Y'Z'$ s can be used in most situations.” For the remainder of this chapter, it will be assumed that CIE  $XYZ$  tristimulus values are used.

For predictions involving related colors, the absolute tristimulus values expressed in trolands must also be available for the adapting stimulus,  $X_0Y_0Z_0$ . Guth (1995) is equivocal on how to obtain these values, so it will be assumed that they are the tristimulus values for a perfect white under illumination similar to the test stimulus.

No other input data are required, or used, in the ATD model. Thus it is clear that it cannot be used to account for background, surround, or cognitive effects.

## Adaptation Model

As with all of the models presented in this book, the first step of the ATD model is a transformation from CIE (or Judd) tristimulus values to cone responses. However, a significant difference in the ATD model is that the cone responses are nonlinear and additive noise signals are incorporated at this stage. The transformations are given in Equations 14.1 through 14.3.

$$L = [0.66(0.2435X + 0.8524Y - 0.0516Z)]^{0.70} + 0.024 \quad (14.1)$$

$$M = [1.0(-0.3954X + 1.1642Y + 0.0837Z)]^{0.70} + 0.036 \quad (14.2)$$

$$S = [0.43(0.04Y + 0.6225Z)]^{0.70} + 0.31 \quad (14.3)$$

Chromatic adaptation is then modeled using a modified form of the von Kries transformation as illustrated in Equations 14.4 through 14.6.

$$L_g = L \left( \frac{\sigma}{\sigma + L_a} \right) \quad (14.4)$$

$$M_g = M \left( \frac{\sigma}{\sigma + M_a} \right) \quad (14.5)$$

$$S_g = S \left( \frac{\sigma}{\sigma + S_a} \right) \quad (14.6)$$

$L_g$ ,  $M_g$ , and  $S_g$  are the post-adaptation cone signals. The constant,  $\sigma$ , is varied to predict different types of data, but is nominally set equal to 300. The cone signals for the adapting light,  $L_a$ ,  $M_a$ , and  $S_a$ , are determined from a weighted sum of the tristimulus values for the stimulus itself and for a perfect white (or other adapting stimulus), as shown in Equations 14.7

through 14.9, which are then transformed to cone signals using Equations 14.1 through 14.3.

$$X_a = k_1 X + k_2 X_0 \quad (14.7)$$

$$Y_a = k_1 Y + k_2 Y_0 \quad (14.8)$$

$$Z_a = k_1 Z + k_2 Z_0 \quad (14.9)$$

For unrelated colors, there is only self-adaptation, and  $k_1$  is set to 1.0 while  $k_2$  is set to 0.0. For related colors such as typical colorimetric applications,  $k_1$  is set to 0.0 and  $k_2$  is set to a value between 15 and 50 (Guth 1995). In some cases, the observer might adapt to both the test stimulus and the white point to some degree, and some other combination of values, such as  $k_1 = 1.0$  and  $k_2 = 5.0$ , would be used (Guth 1995). Guth (1995) makes no specific recommendation on how to calculate cone signals for the adapting light. It is left open for interpretation. However, it is worth noting that as the value of  $k_2$  increases, the adaptation transform of Equations 14.4 through 14.6 becomes more and more like the nominal von Kries transformation. This is also true as  $\sigma$  is decreased. Thus it is not difficult to make the ATD model perform almost the same as a simple von Kries model for color reproduction applications. It is therefore recommended that Guth's maximum value of  $k_2$  equal to 50 be used with  $k_1$  set to 0.0.

## Opponent Color Dimensions

The adapted cone signals are then transformed into two sets of initial opponent signals. The first stage initial signals are denoted  $A_{1i}$ ,  $T_{1i}$ , and  $D_{1i}$  and calculated according to Equations 14.10 through 14.12. The second stage initial signals, calculated using Equations 14.13 through 14.15, are denoted as  $A_{2i}$ ,  $T_{2i}$ , and  $D_{2i}$ .

$$A_{1i} = 3.57L_g + 2.64M_g \quad (14.10)$$

$$T_{1i} = 7.18L_g - 6.21M_g \quad (14.11)$$

$$D_{1i} = -0.70L_g + 0.085M_g + 1.00S_g \quad (14.12)$$

$$A_{2i} = 0.09A_{1i} \quad (14.13)$$

$$T_{2i} = 0.43T_{1i} + 0.76D_{1i} \quad (14.14)$$

$$D_{2i} = D_{1i} \quad (14.15)$$

The final ATD responses after compression are calculated for both the first and second stages according to Equations 14.16 through 14.21.

$$A_1 = \frac{A_{1i}}{200 + |A_{1i}|} \quad (14.16)$$

$$T_1 = \frac{T_{1i}}{200 + |T_{1i}|} \quad (14.17)$$

$$D_1 = \frac{D_{1i}}{200 + |D_{1i}|} \quad (14.18)$$

$$A_2 = \frac{A_{2i}}{200 + |A_{2i}|} \quad (14.19)$$

$$T_2 = \frac{T_{2i}}{200 + |T_{2i}|} \quad (14.20)$$

$$D_2 = \frac{D_{2i}}{200 + |D_{2i}|} \quad (14.21)$$

The first-stage opponent responses are used to model apparent brightness and discriminations (absolute and difference thresholds). Discriminations are modeled using Euclidean distance in the  $A_1 T_1 D_1$  three-space with a visual threshold set to approximately 0.005 units. The second-stage mechanisms are used to model large color differences, hue, and saturation.

## Perceptual Correlates

The ATD model incorporates measures to predict brightness, saturation, and hue. The brightness correlate is the quadrature summation of the  $A_1$ ,  $T_1$ , and  $D_1$  responses as illustrated in Equation 14.22.

$$Br = (A_1^2 + T_1^2 + D_1^2)^{1/2} \quad (14.22)$$

Saturation is calculated as the quadrature sum of the second-stage chromatic responses,  $T_2$  and  $D_2$ , divided by the achromatic response,  $A_2$ , as shown in Equation 14.23.

$$C = \frac{(T_2^2 + D_2^2)^{0.5}}{A_2} \quad (14.23)$$

Guth (1995) incorrectly uses the terms *saturation* and *chroma* interchangeably. However, it is clear that the formulation of Equation 14.23

is a measure of saturation rather than chroma since it is measured relative to the achromatic response for the stimulus rather than that of a similarly illuminated white.

Guth (1995) indicates that hue is directly related to  $H$  as defined in Equation 14.24. However, the ratio in Equation 14.24 is equivocal (giving equal values for complementary hues, infinite values for some, and undefined values for others), and it is therefore necessary to add an inverse tangent function as is typical practice.

$$H = \frac{T_2}{D_2} \quad (14.24)$$

There are no correlates of lightness, colorfulness, chroma, or hue composition in the ATD model.

## Phenomena Predicted

The ATD model accounts for chromatic adaptation, heterochromatic brightness matching (Helmholtz–Kohlrausch effect), the Bezold–Brücke hue shift, the Abney effect, and various color discrimination experiments. It includes correlates for brightness and saturation. A correlate for hue can also be easily calculated although hue composition has not been specifically defined. The model is also inadequately defined for related stimuli since it does not include correlates for lightness and chroma. There is no way to distinguish between brightness–colorfulness matching and lightness–chroma matching using the ATD model. It is unclear which type of matching is predicted by the adaptation transform, but it is likely to be more similar to brightness–colorfulness matching due to the way absolute units are used in the ATD model. The ATD model cannot be used (without modification) to predict background or surround effects or effects based on medium changes, such as discounting-the-illuminant. Examples of calculated values using the ATD model as described in this chapter are given in Table 14.1.

## Why Not Use Just the ATD Model?

The ATD model provides a simple, elegant framework for the early stages of signal processing in the human color vision system. While the framework is clearly sound given the wide range of data the model can be used to predict, it is not well defined for particular applications. There are several aspects of the model that require further definition or specification for practical application. Thus, the flexibility of the ATD model that allows it to predict a wide range of data also precludes it from being practically useful. The model can be applied to practical applications with some modification as has been done by Granger (1994, 1995). However, even this formulation is incomplete as a color appearance model since it neglects chromatic adaptation.

**Table 14.1** Example ATD color vision model calculations

Quantity	Case 1	Case 2	Case 3	Case 4
X	19.01	57.06	3.53	19.01
Y	20.00	43.06	6.56	20.00
Z	21.78	31.96	2.14	21.78
$X_0$	95.05	95.05	109.85	109.85
$Y_0$	100.00	100.00	100.00	100.00
$Z_0$	108.88	108.88	35.58	35.58
$Y_0$ (cd/m <sup>2</sup> )	318.31	31.83	318.31	31.83
$\sigma$	300	300	300	300
$k_1$	0.0	0.0	0.0	0.0
$k_2$	50.0	50.0	50.0	50.0
$A_1$	0.1788	0.2031	0.1068	0.1460
$T_1$	0.0287	0.0680	-0.0110	0.0007
$D_1$	0.0108	0.0005	0.0044	0.0130
$A_2$	0.0192	0.0224	0.0106	0.0152
$T_2$	0.0205	0.0308	-0.0014	0.0102
$D_2$	0.0108	0.0005	0.0044	0.0130
$Br$	0.1814	0.2142	0.1075	0.1466
C	1.206	1.371	0.436	1.091
H	1.91	63.96	-0.31	0.79

The ATD model has the advantages that it is fairly simply and generally easily invertible (for  $k_1 = 0.0$ ). Its disadvantages include the lack of a strict definition of its implementation, inadequate treatment of related colors (necessary for most applications), and lack of cognitive factors. Strictly speaking, the ATD model is also not directly relatable to CIE tristimulus values. Since it does not incorporate distinct predictors for lightness and chroma, it actually cannot be considered a color appearance model. However, as a framework for visual processing and discrimination, it certainly warrants some attention.

## ATD04 Model

It should be noted that Guth (1998) published a short note discussing errors that he felt were made in the description of the ATD model in the first edition of this book. Interested readers are welcome to review that publication and judge for themselves. Since the publication of the first two editions of this book, the ATD model has continued to go through some further evolution, with the most recent version appearing to be the ATD04 model published by Guth (2004) in the proceedings of the *SPIE-IS&T Electronic Imaging Conference*. That paper presents some updates to the details of the model, but it still follows the basic structure outlined in this chapter. The paper also describes why “color constancy” is a myth. That is a nice analysis to see and something well understood by those studying actual color

appearance and chromatic adaptation who seldom fall into the trap of believing in precise “color constancy” (Chapter 6). However, Guth’s agreement with traditional observational science in color appearance and color perception ends there. Unfortunately, Guth (2004) continues to deny the need for definitions of related and unrelated colors as well as the distinctions between lightness and brightness and colorfulness and chroma. These are fundamental attributes of visual perception. Otherwise, for example, brown and gray would not be such important color names. However, if one is interested in arguments to the contrary, Guth (2004) might be a place to start.

### 14.3 LLAB MODEL

The LLAB model is a more recent entry into the field of color appearance models. It is similar in structure to the RLAB model described in Chapter 13. However, the LLAB model does incorporate a different range of effects than the RLAB model. The LLAB color appearance model was developed by Luo *et al* (1996). However, prior to the Luo *et al* (1996) article’s publication, the LLAB model was revised by Luo and Morovic (1996) in a conference proceedings. The treatment in this chapter follows the revised model, but includes some comments on the original formulation presented in Luo *et al* (1996). LLAB is designed as a colorimetric model and is clearly an extension of CIE colorimetry (as opposed to a vision model). It was synthesized from the results of a series of experiments on color appearance and color difference scaling.

The LLAB model is designed to be a universal model for color matching, color appearance specification, and color difference measurement. It therefore incorporates features from previous work in both areas of study. Like RLAB, it is designed to be relatively simple and not inclusive of all visual phenomena. It is not as simple as the RLAB model. It does, however, predict some effects that RLAB cannot (the converse is also true).

### Objectives and Approach

The LLAB model, as described by Luo *et al.* (1996), is derived from an extensive series of data derived by Luo and his coworkers on color appearance scaling and color discrimination. This work has resulted in tests of color appearance models and the development of color difference equations as summarized by Luo *et al* (1996). The LLAB model is an attempt to synthesize this work into a single coherent model. A similar effort has been made to combine the CIECAM02 color appearance model with color difference results to create what is known as CAM02-UCS (Luo *et al.* 2006).

The formulation of the LLAB model is similar to RLAB in concept, but differs markedly in detail. It begins with a chromatic adaptation transform known as the BFD transform (developed at the University of

Bradford and previously unpublished) from the test viewing conditions to defined reference conditions. Then, modified CIELAB coordinates are calculated under the reference conditions and appearance correlates are specified. The surround relative luminance is accounted for using variable exponents as in RLAB. The colorfulness scale is adjusted based on the nonlinear chroma functions incorporated into the CMC color difference equation (Clarke *et al.* 1984). LLAB also incorporates a factor for lightness contrast due to the relative luminance of the background. Hue angle is defined the same way as in CIELAB, and hue composition is specified according to techniques similar to those used by Nayatani *et al.*, Hunt, and RLAB. Lastly, lightness and chroma weighting factors can be applied for the calculation of color differences in a manner identical to that used in the CMC and CIE94 color difference equations. Thus the full designation of the model is LLAB(*l:c*).

## Input Data

The LLAB model requires the relative tristimulus values of the stimulus,  $XYZ$ , the reference white,  $X_0Y_0Z_0$ , the luminance (in  $\text{cd}/\text{m}^2$ ) of the reference white,  $L$ , and the luminance factor of the background,  $Y_b$ . It also requires choices regarding the discounting-the-illuminant factor,  $D$ , the surround induction factor,  $F_s$ , the lightness induction factor,  $F_L$ , and the chroma induction factor,  $F_C$ . Values for specified viewing conditions are given in Table 14.2.

## Adaptation Model

In the LLAB model, the BFD adaptation transform is used to calculate corresponding colors under a reference viewing condition. The BFD transform is a modified von Kries transform in which the short-wavelength sensitive cone signals are subjected to an adaptation-dependent nonlinearity, while the middle- and long-wavelength sensitive cone signals are subject to a simple von Kries transform. The first step is a transform from CIE  $XYZ$  tristimulus values to normalized cone responses, denoted  $RGB$ , as shown in Equations 14.25 and 14.26.

**Table 14.2** Values of induction factors for the LLAB model

	$D$	$F_s$	$F_L$	$F_C$
Reflection samples and images in average surround				
Subtending $>4^\circ$	1.0	3.0	0.0	1.00
Subtending $<4^\circ$	1.0	3.0	1.0	1.00
Television and VDU displays in dim surround				
Cut-sheet transparency in dim surround	0.7	3.5	1.0	1.00
35 mm projection transparency in dark surround	1.0	5.0	1.0	1.10
	0.7	4.0	1.0	1.00

$$\begin{vmatrix} R \\ G \\ B \end{vmatrix} = \mathbf{M} \begin{vmatrix} X / Y \\ Y / Y \\ Z / Y \end{vmatrix} \quad (14.25)$$

$$\mathbf{M} = \begin{vmatrix} 0.8951 & 0.2664 & -0.1614 \\ -0.7502 & 1.7135 & 0.0367 \\ 0.0389 & -0.0685 & 1.0296 \end{vmatrix} \quad (14.26)$$

It should be noted that the transform in Equations 14.25 and 14.26 is atypical in two ways. First, the CIE tristimulus values are always normalized to  $Y$  prior to the transform. This results in all stimuli with identical chromaticity coordinates having the same cone signals (a luminance normalization). This normalization is required to preserve achromatic scales through the nonlinear chromatic adaptation transform described below. Second, the transform itself does not represent plausible cone responses, but rather “spectrally sharpened” cone responses with negative responsivity at some wavelengths. These responsivities tend to preserve saturation across changes in adaptation and impact predicted hue changes across adaptation. Despite the fact that the BFD transformation results in RGB signals that cannot be considered physiologically plausible cone responses, they will be referred to as cone responses for simplicity. The cone responses are then transformed to the corresponding cone responses for adaptation to the reference illuminant. The reference illuminant is defined to be CIE illuminant D65 using the 1931 standard colorimetric observer ( $X_{0r} = 95.05$ ,  $Y_{0r} = 100.0$ ,  $Z_{0r} = 108.88$ ). The transformation is performed using Equations 14.27 through 14.30.

$$R_r = \left[ D \left( \frac{R_{0r}}{R_0} \right) + 1 - D \right] R \quad (14.27)$$

$$G_r = \left[ D \left( \frac{G_{0r}}{G_0} \right) + 1 - D \right] G \quad (14.28)$$

$$B_r = \left[ D \left( \frac{B_{0r}}{B_0^\beta} \right) + 1 - D \right] B^\beta \quad (14.29)$$

$$\beta = \left( \frac{B_0}{B_{0r}} \right)^{0.0834} \quad (14.30)$$

In the event that the  $B$  response is negative, Equation 14.29 is replaced with Equation 14.31 to avoid taking a root of a negative number.

$$B_r = - \left[ D \left( \frac{B_{0r}}{B_0^\beta} \right) + 1 - D \right] |B|^\beta \quad (14.31)$$

The  $D$  factors in Equations 14.27 through 14.31 allow for discounting-the-illuminant. When discounting occurs,  $D = 1.0$  and observers completely adapt to the color of the light source. If there is no adaptation,  $D = 0.0$  and observers are always adapted to the reference illuminant. For intermediate values of  $D$ , observers are adapted to chromaticities intermediate to the light source and the reference illuminant (with  $D$  specifying the proportional level of adaption to the source). This is different from the  $D$  value in RLAB, which allows for various levels of incomplete adaptation that depend on the color and luminance of the source. ( $D = 0.0$  in RLAB does not mean no adaptation, rather it means incomplete adaptation to that particular source.)

The final step of the chromatic adaptation transformation is the conversion from the cone signals for the reference viewing condition to CIE tristimulus values,  $X_r Y_r Z_r$ , using Equation 14.32.

$$\begin{vmatrix} X_r \\ Y_r \\ Z_r \end{vmatrix} = \mathbf{M}^{-1} \begin{vmatrix} R_r Y \\ G_r Y \\ B_r Y \end{vmatrix} \quad (14.32)$$

## Opponent Color Dimensions

The corresponding tristimulus values under the reference illuminant (D65) are then transformed to preliminary opponent dimensions using modified CIELAB formulae as illustrated in Equations 14.33 through 14.36.

$$L_L = 116f\left(\frac{Y_r}{100}\right)^z - 16 \quad (14.33)$$

$$z = 1 + F_L \left(\frac{Y_b}{100}\right)^{1/2} \quad (14.34)$$

$$A = 500 \left[ f\left(\frac{X_r}{95.05}\right) - f\left(\frac{Y_r}{100}\right) \right] \quad (14.35)$$

$$B = 200 \left[ f\left(\frac{Y_r}{100}\right) - f\left(\frac{Z_r}{108.88}\right) \right] \quad (14.36)$$

The  $z$  exponent is incorporated to account for lightness contrast from the background. It is similar to the form used in the Hunt model. Since the  $L_L$ ,  $A$ , and  $B$  dimensions follow the definitions of the CIELAB equations, the non-linearity is dependent on the relative tristimulus values as shown in Equations 14.37 and 14.38. For values of  $\omega > 0.008856$ , Equation 14.37 is used.

$$f(\omega) = (\omega)^{1/F_s} \quad (14.37)$$

For values of  $\omega \leq 0.008856$ , Equation 14.38 is used.

$$f(\omega) = [(0.008856^{1/F_s} - 16/116) / 0.008856] \omega + 16/116 \quad (14.38)$$

The value of  $F_s$  depends on the surround relative luminance as specified in Table 14.2. This is similar to the surround dependency incorporated in the RLAB model.

## Perceptual Correlates

The LLAB model includes predictors for lightness, chroma, colorfulness, saturation, hue angle, and hue composition. The lightness predictor,  $L_L$ , is defined in Equation 14.33. The chroma predictor,  $Ch_L$ , and colorfulness predictor,  $C_L$ , are derived using a nonlinear function similar to that incorporated in the CMC color difference equation as a chroma weighting function. This incorporates the behavior of the CMC color difference equation into the LLAB color space as shown in Equations 14.39 through 14.43.

$$C = (A^2 + B^2)^{1/2} \quad (14.39)$$

$$Ch_L = 25 \ln(1 + 0.05C) \quad (14.40)$$

$$C_L = Ch_L S_M S_C F_C \quad (14.41)$$

$$S_C = 1.0 + 0.47 \log(L) - 0.057 [\log(L)]^2 \quad (14.42)$$

$$S_M = 0.7 + 0.02L_L - 0.0002L_L^2 \quad (14.43)$$

$F_C$  is the chroma induction factor defined in Table 14.2.  $S_C$  provides the luminance dependency necessary to predict an increase in colorfulness with luminance. Thus  $C_L$  is truly a colorfulness predictor.  $S_M$  provides a similar lightness dependency.

Saturation is defined in LLAB as the ratio of chroma to lightness as shown in Equation 14.44.

$$s_L = \frac{Ch_L}{L_L} \quad (14.44)$$

LLAB hue angle,  $h_L$ , is calculated in the usual way according to Equation 14.45.

$$h_L = \tan^{-1} \left( \frac{B}{A} \right) \quad (14.45)$$

Hue composition in NCS notation is calculated via linear interpolation between the hue angles for the unique hues, which are defined as 25° (red), 93° (yellow), 165° (green), and 254° (blue).

The final opponent signals are calculated using the colorfulness scale,  $C_L$ , and the hue angle,  $h_L$ , as shown in Equations 14.46 and 14.47.

$$A_L = C_L \cos(h_L) \quad (14.46)$$

$$B_L = C_L \sin(h_L) \quad (14.47)$$

There were no predictors of brightness, chroma, or saturation defined in the LLAB model as initially published by Luo *et al* (1996). In the revised version (Luo and Morovic 1996), the predictors of chroma and saturation were added.

## Color Differences

The LLAB model incorporates the chroma weighting function from the CMC color difference equation. This chroma dependency is the most important factor that produces the improved performance of the CMC color difference equation over the simple CIELAB  $\Delta E_{ab}^*$  equation. Thus LLAB( $l:c$ ) color differences are defined by Equation 14.48.

$$\Delta E_L = \left[ \left( \frac{\Delta L_L}{l} \right)^2 + \Delta A_L^2 + \Delta B_L^2 \right]^{0.5} \quad (14.48)$$

The lightness weight,  $l$ , is defined to be 1.0, 1.5, and 0.67 for perceptibility, acceptability, and large color differences, respectively. The chroma weight,  $c$  (not present in this formulation), is always set equal to 1.0.

## Phenomena Predicted

The revised LLAB model accounts for chromatic adaptation, lightness induction, surround relative luminance, discounting-the-illuminant, and the Hunt effect. It cannot predict the Stevens effect, incomplete chromatic adaptation, or the Helmholtz–Kohlrausch effect. It also cannot predict the Nelson–Judd effect.

LLAB includes predictors for lightness, chroma, saturation, colorfulness, and hue in its latest revision (Luo and Morovic 1996). This corrected the unnatural combination of appearance attributes (lightness, colorfulness, hue) in the original version (Luo *et al* 1996). The natural sets are lightness, chroma, and hue or brightness, colorfulness, and hue. The original LLAB formulation could not be used to calculate either brightness–colorfulness matches or lightness–chroma matches. It could be used to predict lightness–colorfulness matches, which probably have little practical utility. If corresponding colors are predicted at constant luminance, then the lightness–colorfulness matches become equivalent to lightness–chroma matches. Interestingly, the original LLAB formulation did not meet the CIE TC1-34

**Table 14.3** Example LLAB color appearance model calculations

Quantity	Case 1	Case 2	Case 3	Case 4
X	19.01	57.06	3.53	19.01
Y	20.00	43.06	6.56	20.00
Z	21.78	31.96	2.14	21.78
$X_0$	95.05	95.05	109.85	109.85
$Y_0$	100.00	100.00	100.00	100.00
$Z_0$	108.88	108.88	35.58	35.58
$L$ (cd/m <sup>2</sup> )	318.31	31.83	318.31	31.83
$Y_b$	20.0	20.0	20.0	20.0
$F_s$	3.0	3.0	3.0	3.0
$F_L$	1.0	1.0	1.0	1.0
$F_c$	1.0	1.0	1.0	1.0
$L_L$	37.37	61.26	16.25	39.82
$Ch_L$	0.01	30.51	30.43	29.34
$C_L$	0.02	56.55	53.83	54.59
$s_L$	0.00	0.50	1.87	0.74
$h_L$	229.5	22.3	173.8	271.9
$H_L$	72B 28G	98R 2B	90G 10B	86B 14R
$A_L$	-0.01	52.33	-53.51	1.76
$B_L$	-0.01	21.43	5.83	-54.56

requirements of a color appearance model that it include predictors of at least lightness, chroma, and hue. These limitations were corrected in the Luo and Morovic (1996) formulation presented in this chapter.

Table 14.3 includes example calculations of LLAB appearance attributes for a few stimuli.

### Why Not Use Just the LLAB Model?

The LLAB model has the advantages that it is fairly simple, incorporates a potentially accurate adaptation model, includes surround effects, and has a reliable built-in measure of color differences. However, its original formulation could not be considered a complete appearance model since it had predictors for the unusual combination of lightness, colorfulness, and hue with no predictor of chroma. The revised formulation includes both chroma and saturation predictors. LLAB has a serious drawback in that it is not analytically invertible. LLAB is also not capable of predicting incomplete chromatic adaptation. The revised formulation does include the  $D$  factor that can be used to model cognitive effects that occur upon changes in media. Lastly, it was not tested with data independent of those from which it was derived (mainly since the CIE models were derived soon after LLAB's publication). It is possible that some of the parameters in the model have been too tightly fit to one collection of visual data and might not generalize well to other data. However, its good performance on the Loughborough

University of Technology Computer Human Interface (LUTCHI) data from which it was derived suggests that it has potential to be quite useful for some applications.

## 14.4 IPT COLOR SPACE

The *IPT* color space was published by Ebner and Fairchild (1998) and derived specifically for image processing applications to have a simple formulation and a hue-angle component with good prediction of constant perceived hue (important in gamut-mapping applications). More recent work on perceived hue has validated the applicability of the *IPT* space for constant hue predictions. The transformation from *RGB* to the *IPT* opponent space is far simpler than the transformations used in most color appearance models. The process, expressed in Equations 14.49 through 14.53, involves a linear transformation to an optimized cone-response space, application of power-function nonlinearities, and then a final linear transformation to the *IPT* opponent space (*I*, light-dark; *P*, red-green; *T*, yellow-blue). Note that the input tristimulus values are for CIE illuminant D65. Thus, the viewing conditions must either incorporate a D65 white point or a selected chromatic adaptation transform must first be used to convert to corresponding colors predictions for illuminant D65 adaptation.

$$\begin{bmatrix} L \\ M \\ S \end{bmatrix} = \begin{bmatrix} 0.4002 & 0.7075 & -0.0807 \\ -0.2280 & 1.1500 & 0.0612 \\ 0.0 & 0.0 & 0.9184 \end{bmatrix} \begin{bmatrix} X_{D65} \\ Y_{D65} \\ Z_{D65} \end{bmatrix} \quad (14.49)$$

$$\begin{aligned} L' &= L^{0.43}; & L \geq 0 \\ L' &= -|L|^{0.43}; & L \leq 0 \end{aligned} \quad (14.50)$$

$$\begin{aligned} M' &= M^{0.43}; & M \geq 0 \\ M' &= -|M|^{0.43}; & M \leq 0 \end{aligned} \quad (14.51)$$

$$\begin{aligned} S' &= S^{0.43}; & S \geq 0 \\ S' &= -|S|^{0.43}; & S \leq 0 \end{aligned} \quad (14.52)$$

$$\begin{bmatrix} I \\ P \\ T \end{bmatrix} = \begin{bmatrix} 0.4000 & 0.4000 & 0.2000 \\ 4.4550 & -4.8510 & 0.3960 \\ 0.8056 & 0.3572 & -1.1628 \end{bmatrix} \begin{bmatrix} L' \\ M' \\ S' \end{bmatrix} \quad (14.53)$$

Hue angle can then be computed in the normal way through the inverse tangent of the ratio of *T* to *P*.

$$h_{IPT} = \tan^{-1} \left( \frac{T}{P} \right) \quad (14.54)$$

## Why Not Use Just the IPT Model?

Since its initial formulation as a color space with optimal predictions of constant hue perceptions, the IPT color space has been implemented in a number of color critical gamut-mapping applications such as in digital cinema workflows and projection systems, television production workflows, and digital photography systems. It has also been the foundation of an image-based color appearance model (Fairchild and Johnson 2002, 2003), the appearance of complex visual stimuli (Fairchild 2008b, 2010), the extension to color specifications for high-dynamic-range (HDR) images and scenes (Fairchild and Chen 2011, Fairchild and Wyble, 2010 ), and the development of space-free color appearance scales (Fairchild 2011b, Fairchild and Heckaman 2012). Despite all those successes, *IPT* does not do it all. The model includes no method to account for chromatic adaptation, therefore an adaptation transform must be applied prior to computing *IPT* coordinates. There are also no luminance, background, or surround dependencies in the model, so it cannot account for such effects. Lastly, the dimensions were never really intended to predict lightness and chroma, but rather to be good opponent representations. In that regard, it should also be noted that the *IPT* coordinates are not mathematically orthogonal to one another. That means that spatial filtering differentially applied to the three dimensions might result in unexpected artifacts. This is true of most color spaces as discussed by Johnson *et al.* (2010), who also derived an orthogonal opponent colors transformation.

# The CIE Color Appearance Model (1997), CIECAM97s

---

Publication of the first edition of this book coincided with the creation and publication of the first CIE color appearance model, CIECAM97s. At that time it was clear there was a significant amount of interest in the establishment and use of a single, standardized, color appearance model, but it was uncertain how effective a single CIE model could be. The industrial demand for such a model led the CIE to step up its efforts to establish a model to be put into use, tested, and perhaps recommended as a standard later on. CIECAM97s represents such a model and also represents a significant accomplishment in the field of color appearance modeling. This chapter provides an overview of the development and formulation of CIECAM97s. It is not an extensive treatment, since an improved model, the subject of the next chapter, has been developed by the CIE. As will be seen in the following chapter, the CIE experiment of CIECAM97s was a great success and led to real progress in color appearance models. It also continues to do so as witnessed by proposed enhancements to CIECAM02 and ideas for new types of appearance models.

## 15.1 HISTORICAL DEVELOPMENT, OBJECTIVES, AND APPROACH

In March of 1996 the CIE held an expert symposium on *Colour Standards for Image Technology* in Vienna (CIE 1996b). While the symposium covered many aspects of image technology for which the CIE could provide guidance

or standards to assist industry, one of the most critical issues was the establishment of a color appearance model for general use. Industrial participants in the symposium recognized the need to apply a color appearance model, but requested guidance from the CIE in establishing a single model that could be used throughout the industry to promote uniformity of practice and compatibility between various components in modern open imaging systems.

The push toward a single model was highlighted and summarized in a presentation by Hunt made at that symposium (CIE 1996b) entitled *The Function, Evolution, and Future of Colour Appearance Models*. In that presentation, Hunt reviewed the current status and historical development of various models and presented 12 principles for consideration in establishing a single model. These principles are reproduced here verbatim (CIE 1996b).

1. *The model should be as comprehensive as possible, so that it can be used in a variety of applications; but at this stage, only static states of adaptation should be included, because of the great complexity of dynamic effects.*
2. *The model should cover a wide range of stimulus intensities, from very dark object colours to very bright self-luminous colour. This means that the dynamic response function must have a maximum, and cannot be a simple logarithmic or power function.*
3. *The model should cover a wide range of adapting intensities, from very low scotopic levels, such as occur in starlight, to very high photopic levels, such as occur in sunlight. This means that rod vision should be included in the model; but because many applications will be such that rod vision is negligible, the model should be usable in a mode that does not include rod vision.*
4. *The model should cover a wide range of viewing conditions, including backgrounds of different luminance factors, and dark, dim, and average surrounds. It is necessary to cover the different surrounds because of their widespread use in projected and self-luminous displays.*
5. *For ease of use, the spectral sensitivities of the cones should be a linear transformation of the CIE  $\bar{X}$ ,  $\bar{Y}$ ,  $\bar{Z}$  or  $\bar{X}_{10}$ ,  $\bar{Y}_{10}$ ,  $\bar{Z}_{10}$  functions, and the  $V'(\lambda)$  function should be used for the spectral sensitivity of the rods. Because scotopic photometric data is often unknown, methods of providing approximate scotopic values should be provided.*
6. *The model should be able to provide for any degree of adaptation between complete and none, for cognitive factors, and for the Helson-Judd effect, as options.*
7. *The model should give predictions of hue (both as hue-angle and as hue-quadrature), brightness, lightness, saturation, chroma, and colourfulness.*
8. *The model should be capable of being operated in a reverse mode.*
9. *The model should be no more complicated than is necessary to meet the above requirements.*

10. Any simplified version of the model, intended for particular applications, should give the same predictions as the complete model for some specified set of conditions.
11. The model should give predictions of colour appearance that are not appreciably worse than those given by the model that is best in each application.
12. A version of the model should be available for application to unrelated colours (those seen in dark surrounds in isolation from other colours).

The conclusion drawn at the symposium was that the CIE should immediately begin work on the formulation of such a model with the goal that it be completed prior to the AIC (International Colour Association) quadrennial meeting to be held in Kyoto in May 1997. The CIE decided that TC1-34 was the most appropriate committee to complete this work and expanded its terms of reference at the 1996 meeting of CIE Division 1 in Gothenburg to include:

*To recommend one colour appearance model. This model should give due consideration to the findings of other relevant Technical Committees.*

TC1-34 immediately began work on the formulation of a CIE model (both simple and comprehensive versions). A technical report on the simple version, CIECAM97s, was published by the CIE in 1998 (CIE 1998). The comprehensive version was never formulated due to an apparent lack of interest and demand.

TC1-34 members R.W.G. Hunt and M.R. Luo agreed to develop the first set of equations for consideration of the committee. The working philosophy of TC1-34 was to essentially follow the 12 principles outlined by Hunt in the development of a comprehensive CIE model and a simplified version for practical applications. The general concept was to develop a comprehensive model (like the Hunt model) that can be applied to a wide range of color appearance phenomena and a simplified version (like the RLAB model) that is sufficient for applications such as device-independent color imaging with the additional constraint that the two versions of the model be compatible for some defined set of conditions.

In preparing these models, revised versions of the Hunt color appearance model were developed. These are referred to as the Bradford-Hunt 96S (simple) model and the Bradford-Hunt 96C (comprehensive) model. These models represented one intermediate step in the formulation of CIECAM97s and were included in the first edition of this book (Fairchild 1998a), courtesy of the authors (Hunt 1996, Personal Communication, October 14). These models were not approved by TC1-34 as the CIE model; however, they served as the starting point for the committee and provide good illustrations of how the 12 principles above could be fulfilled. As expected these models underwent some significant revision prior to consideration of the full committee. R.W.G. Hunt and M.R. Luo provided two revised models for TC1-34 consideration prior to the Kyoto

meeting. In addition M. Fairchild provided a third alternative and K. Richter provided a fourth. These four alternatives were considered at the May 1997 meeting of TC1-34 in Kyoto and an agreement was reached to adopt one of the Hunt and Luo alternatives as the simple form of the CIE Color Appearance Model 1997, designated CIECAM97s. This model is presented in the following sections. The model was formally approved and published by the CIE (1998). A comprehensive version of the model that extends upon CIECAM97s, to be designated CIECAM97c, was never formulated. A significantly simpler alternative with similar performance over a limited range of viewing conditions was prepared by Fairchild, but not recommended by the committee since it was not as extensible to a comprehensive form as the model selected to become CIECAM97s. (In hindsight, this should not have been a concern.) This model has been designated as the ZLAB color appearance model and is presented in Section 15.7 since it has proven useful in some simple image reproduction applications.

## 15.2 INPUT DATA

Some slight, but important, revisions were made to the Bradford–Hunt 96S model to derive the model agreed upon by TC1-34 to become the CIECAM97s model (*i.e.*, the simple version of the CIE Color Appearance Model (1997)). These include a reformulation of the surround compensation to use power functions in order to avoid predictions of corresponding colors with negative CIE tristimulus values and a clear definition of the adaptation level factor,  $D$ . It is important to note that the formulation of CIECAM97s builds upon the work of many researchers in the field of color appearance. This was a key issue in TC1-34's establishment of this model as the best of what is currently available. Various aspects of the model can be traced to the works of (in alphabetical order) Bartleson, Breneman, Fairchild, Estevez, Hunt, Lam, Luo, Nayatani, Rigg, Seim, and Valberg among others. Since a comprehensive model was never formulated, those interested in color appearance predictions for more extreme viewing conditions (such as high luminance levels when bleaching occurs or low luminance levels when the rods become active) or more esoteric appearance phenomena (such as the Helson–Judd effect) should explore use of the Hunt model described in Chapter 12.

The input data to the model are the luminance of the adapting field (normally taken to be 20% of the luminance of white in the adapting field),  $L_A$ , the tristimulus values of the sample in the source conditions,  $XYZ$ , the tristimulus values of the source white in the source conditions,  $X_w Y_w Z_w$ , the relative luminance of the source background in the source conditions,  $Y_b$ . Additionally, the constants  $c$ , for the impact of surround,  $N_c$ , a chromatic induction factor,  $F_{Lc}$ , a lightness contrast factor, and  $F$ , a factor for degree of adaptation, must be selected according to the guidelines in Table 15.1.

**Table 15.1** Input parameters for the CIECAM97s model

Viewing condition	<i>c</i>	<i>N<sub>c</sub></i>	<i>F<sub>LL</sub></i>	<i>F</i>
Average surround, samples subtending >4°	0.69	1.0	0.0	1.0
Average surround	0.69	1.0	1.0	1.0
Dim surround	0.59	1.1	1.0	0.9
Dark surround	0.525	0.8	1.0	0.9
Cut-sheet transparencies	0.41	0.8	1.0	0.9

### 15.3 ADAPTATION MODEL

An initial chromatic adaptation transform is used to go from the source viewing conditions to the equal-energy-illuminant reference viewing conditions (although tristimulus values need never be expressed in the reference conditions). First, tristimulus values for both the sample and white are normalized and transformed to spectrally sharpened cone responses using the transformation given in Equations 15.1 and 15.2.

$$\begin{bmatrix} R \\ G \\ B \end{bmatrix} = \mathbf{M}_B \begin{bmatrix} X / Y \\ Y / Y \\ Z / Y \end{bmatrix} \quad (15.1)$$

$$\mathbf{M} = \begin{bmatrix} 0.8951 & 0.2664 & -0.1614 \\ -0.7502 & 1.7135 & 0.0367 \\ 0.0389 & -0.0685 & 1.0296 \end{bmatrix} \quad (15.2)$$

The chromatic adaptation transform is a modified von Kries transformation (performed on a type of chromaticity coordinates) with an exponential non-linearity added to the short-wavelength sensitive channel as given in Equations 15.3 through 15.6. In addition, the variable *D* is used to specify the degree of adaptation. *D* is set to 1.0 for complete adaptation or discounting-the-illuminant. *D* is set to 0.0 for no adaptation. *D* takes on intermediate values for various degrees of incomplete chromatic adaptation. Equation 15.7 allows calculation of *D* for various luminance levels and surround conditions.

$$R_c = \left[ D \left( \frac{1.0}{R_w} \right) + 1 - D \right] R \quad (15.3)$$

$$G_c = \left[ D \left( \frac{1.0}{G_w} \right) + 1 - D \right] G \quad (15.4)$$

$$B_c = \left[ D \left( \frac{1.0}{B_w^p} \right) + 1 - D \right] |B|^p \quad (15.5)$$

$$p = \left( \frac{B_w}{1.0} \right)^{0.0834} \quad (15.6)$$

$$D = F - F / \left[ 1 + 2(L_A^{1/4}) + (L_A^2 / 300) \right] \quad (15.7)$$

If  $B$  happens to be negative, then  $B_c$  is also set to be negative. Similar transformations are also made for the source white since they are required in later calculations. Various factors must be calculated prior to further calculations as shown in Equations 15.8 through 15.12. These include a background induction factor,  $n$ , the background and chromatic brightness induction factors,  $N_{bb}$  and  $N_{cb}$ , and the base exponential nonlinearity,  $z$ .

$$k = \frac{1}{5L_A + 1} \quad (15.8)$$

$$F_L = 0.2k^4 (5L_A) + 0.1(1 - k^4)^2 (5L_A)^{1/3} \quad (15.9)$$

$$n = \frac{Y_b}{Y_w} \quad (15.10)$$

$$N_{bb} = N_{cb} = 0.725(1/n)^{0.2} \quad (15.11)$$

$$z = 1 + F_{LL} n^{1/2} \quad (15.12)$$

The post-adaptation signals for both the sample and the source white are then transformed from the sharpened cone responses to the Hunt–Pointer–Estevez cone responses as shown in Equations 15.13 and 15.14 prior to the application of a nonlinear response compression.

$$\begin{bmatrix} R' \\ G' \\ B' \end{bmatrix} = \mathbf{M}_H \mathbf{M}_B^{-1} \begin{bmatrix} R_c Y \\ G_c Y \\ B_c Y \end{bmatrix} \quad (15.13)$$

$$\mathbf{M}_H = \begin{bmatrix} 0.38971 & 0.68898 & -0.07868 \\ -0.22981 & 1.18340 & 0.04641 \\ 0.00 & 0.00 & 1.00 \end{bmatrix} \quad (15.14)$$

The post-adaptation cone responses (for both the sample and the white) are then calculated using Equations 15.15 through 15.17.

$$R'_a = \frac{40(F_L R' / 100)^{0.73}}{(F_L R' / 100)^{0.73} + 2} + 1 \quad (15.15)$$

$$G'_a = \frac{40(F_L G' / 100)^{0.73}}{(F_L G' / 100)^{0.73} + 2} + 1 \quad (15.16)$$

$$B'_a = \frac{40(F_L B' / 100)^{0.73}}{(F_L B' / 100)^{0.73} + 2} + 1 \quad (15.17)$$

## 15.4 APPEARANCE CORRELATES

Preliminary red–green and yellow–blue opponent dimensions are calculated using Equations 15.18 and 15.19.

$$a = R'_a - 12G'_a / 11 + B'_a / 11 \quad (15.18)$$

$$b = \frac{1}{9}(R'_a + G'_a - 2B'_a) \quad (15.19)$$

The hue angle,  $h$ , is then calculated from  $a$  and  $b$  using Equation 15.20.

$$h = \tan^{-1}\left(\frac{b}{a}\right) \quad (15.20)$$

Hue quadrature,  $H$ , and eccentricity factor,  $e$ , are calculated from the following unique hue data in the usual way (linear interpolation):

Red:  $h = 20.14$ ,  $e = 0.8$ ,  $H = 0$  or  $400$ ,

Yellow:  $h = 90.00$ ,  $e = 0.7$ ,  $H = 100$ ,

Green:  $h = 164.25$ ,  $e = 1.0$ ,  $H = 200$ ,

Blue:  $h = 237.53$ ,  $e = 1.2$ ,  $H = 300$ .

Equations 15.21 and 15.22 illustrate calculation of  $e$  and  $H$  for arbitrary hue angles where the quantities subscripted 1 and 2 refer to the unique hues with hue angles just below and just above the hue angle of interest.

$$e = e_1 + (e_2 - e_1)(h - h_1) / (h_2 - h_1) \quad (15.21)$$

$$H = H_1 + \frac{100(h - h_1) / e_1}{(h - h_1) / e_1 + (h_2 - h) / e_2} \quad (15.22)$$

The achromatic response is calculated as shown in Equation 15.23 for both the sample and the white.

$$A = \left[ 2R'_a + G'_a + \left( \frac{1}{20} \right) B'_a - 2.05 \right] N_{bb} \quad (15.23)$$

Lightness,  $J$ , is calculated from the achromatic signals of the sample and white using Equation 15.24.

$$J = 100 \left( \frac{A}{A_w} \right)^{cz} \quad (15.24)$$

Brightness,  $Q$ , is calculated from lightness and the achromatic for the white using Equation 15.25.

$$Q = \frac{1.24}{c} \cdot \left( \frac{J}{100} \right)^{0.67} (A_w + 3)^{0.9} \quad (15.25)$$

Finally, saturation,  $s$ , chroma,  $C$ , and colorfulness,  $M$ , are calculated using Equations 15.26 through 15.28, respectively.

$$s = \frac{50(a^2 + b^2)^{1/2} 100e(10 / 13) N_c N_{cb}}{R_a + G_a + (21 / 20) B_a} \quad (15.26)$$

$$C = 2.44 s^{0.69} \left( \frac{J}{100} \right)^{0.67n} (1.64 - 0.29^n) \quad (15.27)$$

$$M = CF_L^{0.15} \quad (15.28)$$

## 15.5 INVERSE MODEL

The CIECAM97s Model can be nearly analytically inverted, but requires one approximation since the  $Y$  value on inversion is not easily computed (step 8). Beginning with lightness,  $J$ , chroma,  $C$ , and hue angle,  $h$ , the process is as follows:

1. From  $J$  obtain  $A$ .
2. From  $h$  obtain  $e$ .
3. Calculate  $s$  using  $C$  and  $J$ .
4. Calculate  $a$  and  $b$  using  $s$ ,  $h$ , and  $e$ .
5. Calculate  $R'_a$ ,  $G'_a$ , and  $B'_a$  from  $A$ ,  $a$ , and  $b$ .
6. Calculate  $R'$ ,  $G'$ , and  $B'$  from  $R'_a$ ,  $G'_a$ , and  $B'_a$ .
7. Calculate  $R_c Y$ ,  $G_c Y$ , and  $B_c Y$  from  $R'$ ,  $G'$ , and  $B'$ .
8. Calculate  $Y$  from  $R_c Y$ ,  $G_c Y$ , and  $B_c Y$  using  $M_B^{-1}$  (approximation).
9. Calculate  $R_c$ ,  $G_c$ , and  $B_c$  from  $R_c Y$ ,  $G_c Y$ , and  $B_c Y$  and  $Y$ .
10. Calculate  $R$ ,  $G$ , and  $B$  from  $R_c$ ,  $G_c$ , and  $B_c$ .
11. Calculate  $X$ ,  $Y$ , and  $Z$ , from  $R$ ,  $G$ ,  $B$ , and  $Y$ .

While CIECAM97s cannot be simply inverted in an analytical form, its inversion is far simpler and more accurate than some previous models. Thus CIECAM97s has been of far more practical utility. A detailed explanation of the inversion process can be found at <http://www.cis.rit.edu/fairchild/CAM.html>.

## 15.6 PHENOMENA PREDICTED

Although CIECAM97s is a fairly simple model, it is also quite complete in the variety of phenomena predicted. It includes correlates of all the important appearance dimensions (lightness, brightness, chroma, colorfulness, saturation, and hue) and it can predict a wide range of adaptation-, surround-, and luminance-dependent effects. It is not applicable to extremely high or low luminance levels, which are atypical of careful color judgments. Example calculations using the CIECAM97s color appearance model as described in this chapter are given for four samples in Table 15.2. A spreadsheet with these example calculations can be found at <http://www.cis.rit.edu/fairchild/CAM.html>.

**Table 15.2** Example CIECAM97s calculations

Quantity	Case 1	Case 2	Case 3	Case 4
X	19.01	57.06	3.53	19.01
Y	20.00	43.06	6.56	20.00
Z	21.78	31.96	2.14	21.78
X <sub>w</sub>	95.05	95.05	109.85	109.85
Y <sub>w</sub>	100.00	100.00	100.00	100.00
Z <sub>w</sub>	108.88	108.88	35.58	35.58
L <sub>A</sub>	318.31	31.83	318.31	31.83
F	1.0	1.0	1.0	1.0
D	0.997	0.890	0.997	0.890
Y <sub>b</sub>	20.0	20.0	20.0	20.0
N <sub>c</sub>	1.0	1.0	1.0	1.0
F <sub>LL</sub>	1.0	1.0	1.0	1.0
F <sub>L</sub>	1.17	0.54	1.17	0.54
N <sub>bb</sub> , N <sub>cb</sub>	1.0	1.0	1.0	1.0
H	212.3	19.3	175.4	250.8
H	269.5	399.4	217.7	306.9
H <sub>C</sub>	70B 30G	99R 1B	82G 18B	93B 7R
J	42.44	65.27	21.04	39.88
Q	32.86	31.88	20.54	22.96
S	0.15	146.98	232.18	180.56
C	0.50	61.96	72.99	66.85
M	0.51	56.52	74.70	60.98

## 15.7 THE ZLAB COLOR APPEARANCE MODEL

A simple model was derived from the various models submitted to TC1-34 for consideration of the committee. Ultimately the committee determined that a more extensible model was required for recommendation as CIECAM97s. Thus, the simpler model was abandoned by the committee and has been rennotated by the author as the ZLAB color appearance model (Fairchild 1998b). It was derived from the CIECAM97s, LLAB, and RLAB models with significant input from the work of Luo and Hunt submitted to TC1-34. The ZLAB model was designed to perform nearly as well as the CIECAM97s model for a limited set of viewing conditions. These limitations include a restriction to intermediate values of adapting luminance since the hyperbolic nonlinearity has been replaced with a square-root function that describes the hyperbolic function well for intermediate luminance levels. Additionally, the ZLAB model is limited to medium gray backgrounds in order to further simplify computation. Lastly, ZLAB is limited to the prediction of the relative appearance attributes of lightness, chroma, saturation, and hue. It cannot be used to predict colorfulness or brightness. This is due to the removal of most of the luminance dependencies resulting in significantly simplified equations. The ZLAB model performs identically to CIECAM97s for most corresponding colors calculations since it utilizes the same chromatic adaptation transform. It also performs very nearly as well for the prediction of appearance scaling data. The ZLAB model has found some useful application in image reproduction where gamut mapping and lack of viewing conditions control are major limiting factors obviating the need for a more complex model.

### Input Data

The input data to the model are the luminance of the adapting field,  $L_A$  (taken to be 0.2 times the luminance of a reference white), the tristimulus values of the sample in the source conditions,  $XYZ$ , the tristimulus values of the source white in the source conditions,  $X_w Y_w Z_w$ .

### Chromatic Adaptation

As with CIECAM97s the Bradford chromatic adaptation transform is used to go from the source viewing conditions to corresponding colors under the reference (equal-energy illuminant) viewing conditions. First, all three sets of tristimulus values are normalized and transformed to sharpened cone responses using the Bradford transformation as given in Equations 15.29 and 15.30.

$$\begin{bmatrix} R \\ G \\ B \end{bmatrix} = \mathbf{M} \begin{bmatrix} X / Y \\ Y / Y \\ Z / Y \end{bmatrix} \quad (15.29)$$

$$\mathbf{M} = \begin{bmatrix} 0.8951 & 0.2664 & -0.1614 \\ -0.7502 & 1.7135 & 0.0367 \\ 0.0389 & -0.0685 & 1.0296 \end{bmatrix} \quad (15.30)$$

The chromatic adaptation transform is a modified von Kries transformation (performed on a type of chromaticity coordinates) with an exponential nonlinearity added to the short-wavelength sensitive channel as given in Equations 15.31 through 15.34. In addition, the variable  $D$  is used to specify the degree of adaptation.  $D$  is set to 1.0 for complete adaptation or discounting-the-illuminant.  $D$  is set to 0.0 for no adaptation.  $D$  is set to intermediate values for various degrees of incomplete chromatic adaptation. The  $D$  variable could be left as an empirical parameter, or calculated using Equation 15.35, as in CIECAM97s, with  $F = 1.0$  for average surrounds and  $F = 0.9$  for dim or dark surrounds. If Equation 15.35 is used, it is the only place absolute luminance is required in the ZLAB model.

$$R_c = \left[ D \left( \frac{1.0}{R_w} \right) + 1 - D \right] R \quad (15.31)$$

$$G_c = \left[ D \left( \frac{1.0}{G_w} \right) + 1 - D \right] G \quad (15.32)$$

$$B_c = \left[ D \left( \frac{1.0}{B_w^p} \right) + 1 - D \right] |B|^p \quad (15.33)$$

$$p = \left( \frac{B_w}{1.0} \right)^{0.0834} \quad (15.34)$$

$$D = F - F / \left[ 1 + 2 \left( L_A^{1/4} \right) + \left( L_A^2 \right) / 300 \right] \quad (15.35)$$

If  $B$  happens to be negative, then  $B_c$  is also set to be negative.  $R_c$ ,  $G_c$ , and  $B_c$  represent the corresponding colors of the test stimulus under the reference condition (*i.e.*, illuminant E). The final step in the adaptation transform is to convert from the sharpened cone responses back to CIE XYZ tristimulus values for the reference condition as illustrated in Equation 15.36.

$$\begin{bmatrix} X_c \\ Y_c \\ Z_c \end{bmatrix} = \mathbf{M}^{-1} \begin{bmatrix} R_c Y \\ G_c Y \\ B_c Y \end{bmatrix} \quad (15.36)$$

## Apearance Correlates

Opponent responses are calculated using modified CIELAB-type equations with the power-function nonlinearity defined by the surround relative luminances. These were derived from a simplification of the CIECAM97s model by recalling that the hyperbolic nonlinear function in CIECAM97s can be approximated by a square-root function for intermediate luminances. Thus the opponent responses reduce to the forms given in Equations 15.37 and 15.38.

$$A = 500 \left[ \left( \frac{X_c}{100} \right)^{1/2\sigma} - \left( \frac{Y_c}{100} \right)^{1/2\sigma} \right] \quad (15.37)$$

$$B = 200 \left[ \left( \frac{Y_c}{100} \right)^{1/2\sigma} - \left( \frac{Z_c}{100} \right)^{1/2\sigma} \right] \quad (15.38)$$

The exponents are directly related to those used in CIECAM97s as illustrated in Table 15.3. The values of  $1/\sigma$  (called  $c$ ) in CIECAM97s are modified to  $1/2\sigma$  in ZLAB in order to incorporate the square-root approximation to the hyperbolic nonlinearity of CIECAM97s.

Hue angle is calculated in the typical manner as illustrated in Equation 15.39.

$$h^z = \tan^{-1} \left( \frac{B}{A} \right) \quad (15.39)$$

Hue composition is also determined in the usual way via linear interpolation between the defined angles for the unique hues. These are  $h_r^z = 25^\circ$ ,  $h_y^z = 93^\circ$ ,  $h_g^z = 165^\circ$ , and  $h_b^z = 254^\circ$ .

ZLAB is only specified for a background of medium (20%) luminance factor. Thus the  $z$  parameter in the CIECAM97s model takes on a constant value of 1.45 and lightness,  $L^z$ , is expressed as shown in Equation 15.40.

$$L^z = 100 \left( \frac{Y_c}{100} \right)^{1.45/2\sigma} \quad (15.40)$$

**Table 15.3** ZLAB surround parameters

	Surround		
	Average	Dim	Dark
$1/\sigma$	0.69	0.59	0.525
$1/2\sigma$	0.345	0.295	0.2625

Chroma,  $C^z$ , is given by Equation 15.41 as originally defined in the LLAB model to predict magnitude estimation data well. Saturation,  $s^z$ , is simply the ratio of chroma to lightness as illustrated in Equation 15.42.

$$C^z = 25 \log_e \left[ 1 + 0.05 (A^2 + B^2)^{1/2} \right] \quad (15.41)$$

$$s^z = \frac{C^z}{L^z} \quad (15.42)$$

If rectangular coordinates are required for color space representations, they can easily be obtained from  $C^z$  and  $h^z$  using Equations 15.43 and 15.44.

$$a^z = C^z \cos(h^z) \quad (15.43)$$

$$b^z = C^z \sin(h^z) \quad (15.44)$$

## Inverse Model

The ZLAB model is extremely simple to operate in the inverse direction. Starting with lightness, chroma, and hue angle the following steps are followed.

1. Calculate  $(A^2+B^2)^{1/2}$  from  $C^z$ .
2. Calculate  $A$  and  $B$  from  $(A^2+B^2)^{1/2}$  and  $h^z$ .
3. Calculate  $X_c$ ,  $Y_c$ , and  $Z_c$  from  $L^z$ ,  $A$ , and  $B$ .
4. Calculate  $R_c$ ,  $G_c$ , and  $B_c$  from  $X_c$ ,  $Y_c$ , and  $Z_c$ .
5. Calculate  $R$ ,  $G$ , and  $B$  from  $R_c$ ,  $G_c$ , and  $B_c$ .
6. Calculate  $X$ ,  $Y$ , and  $Z$  from  $R$ ,  $G$ , and  $B$ .

## 15.8 WHY NOT USE JUST CIECAM97s?

It was a truly unprecedented event that CIE TC1-34 was able to agree upon the derivation of the CIECAM97s model within a one-year time frame as was its goal. As anticipated in the first edition of this book, the CIE approval procedures did not introduce any changes of significance to the model. It is important to note that CIECAM97s was considered an interim model with the expectation that it would be revised as more data and theoretical understanding became available. Industrial response to the CIECAM97s model was strong, and it was quickly brought to bear on commercial applications, particularly in the imaging industry. Application of CIECAM97s, and further scientific research, quickly led to understanding of limitations in its formulation and performance as well as the creation of additional data for improvements. The great success of CIECAM97s was in the focus it provided

to researchers and engineers in the field. With so many focusing on a single model for testing and improvement, it became possible to make rapid, significant improvement. The fruits of that work are the CIECAM02 color appearance model that is the topic of Chapter 16.

The existence of CIECAM02 is one reason to not use just CIECAM97s. CIECAM02 is a simpler formulation with better performance. Also, CIECAM97s might be too complex for some applications. In such cases, models like ZLAB, RLAB, or the combination of a chromatic adaptation transform with CIELAB might be adequate.

# 16

# CIECAM02

---

CIECAM97s was a great success. If that is so, then why is there a CIECAM02 model? The answer is that the natural evolution of color appearance models was anticipated and encouraged with the publication of CIECAM97s. That is exactly why the year (97) is in the name. The success of CIECAM97s is that it allowed a variety of researchers and practitioners in color appearance to focus their efforts on a single model. This focus quickly lead to suggested improvements in CIECAM97s that ultimately led to the formulation of a simpler and more effective model called CIECAM02 (CIE 2004a). This chapter discusses the derivation and formulation of CIECAM02, the current CIE color appearance model – a model likely to remain the current CIE recommendation for some time. Luo (2012) has provided a brief overview of the development of CIECAM97s, CIECAM02, and recent suggested improvements that echoes the treatment in this chapter. There is also an excellent overview of CIECAM02 and possible extensions in Chapters 15 through 17 of Hunt and Pointer (2011).

## 16.1 OBJECTIVES AND APPROACH

As soon as CIECAM97s was published, the intense scrutiny it was subjected to resulted in suggestions for its improvement and in some cases for simple corrections to certain elements. With the creation of CIE Division 8, *Image Technology*, came the formation of its first technical committee. This was CIE TC8-01, *Colour Appearance Modeling for Colour Management Systems*, chaired by Nathan Moroney and charged with suggesting revisions to CIECAM97s and perhaps a new CIE model. The ultimate result of TC8-01's work to collect and test suggested revisions of CIECAM97s has been the formulation and publication of a revised color appearance model, CIECAM02 (CIE 2004a, Moroney *et al.* 2002). Note that CIECAM02 has no "s" notation at the end of its name. This is because there is no intention

to create a comprehensive version (especially since CIECAM97c was never created), and even if one were created, a “c” could be added at the end of its name.

A number of potential improvements to CIECAM97s were suggested, and these were compiled into a single publication on behalf of TC8-01 by Fairchild (2001). The adjustments considered and ultimately included in CIECAM02 in some form included:

- Linearization of the chromatic adaptation transform to simplify the model and facilitate analytical inversion (Finlayson and Drew 1999, Finlayson and Süsstrunk 2000, Li *et al.* 2000a,b)
- Correction of anomalous surround compensation (Li *et al.* 1999, 2000a, Moroney 1998)
- Correction of the lightness scale for perfect black stimuli (Li *et al.* 1999, 2000a, Moroney 1998)
- Correction of chroma-scale expansion for color of low chroma (Newman and Pirrotta 2000, Wyble and Fairchild 2000)
- Inclusion of a continuously variable surround compensation (Fairchild 1995b, 1996)
- Improved response compression function to facilitate an improved saturation correlate (Hunt *et al.* 2003).

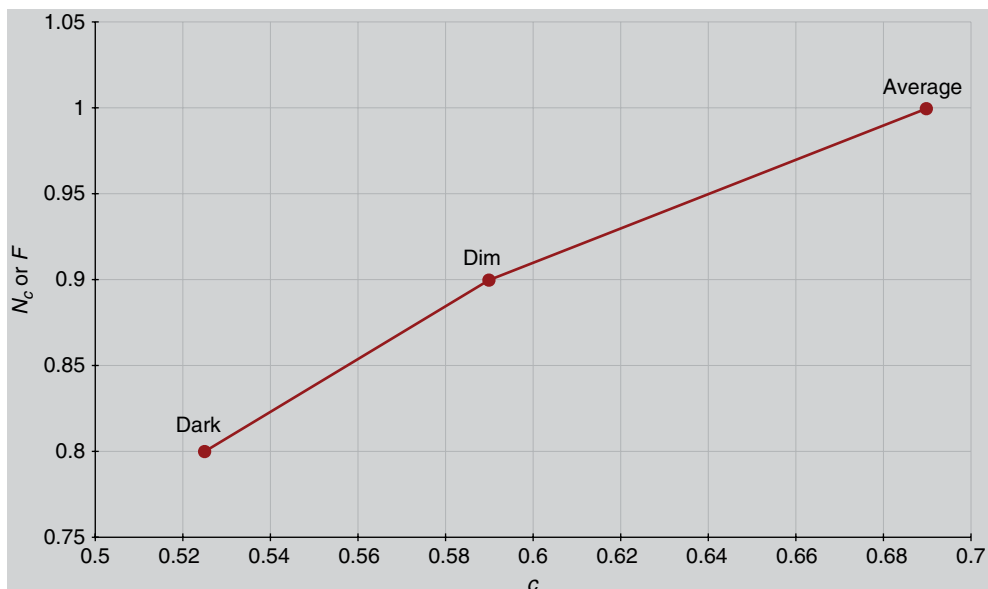
After significant consideration of all the suggested revisions, TC8-01 converged on a single set of new equations and formulated a revised model designated CIECAM02 (CIE 2004a, Moroney *et al.* 2002). The year remains in the name as acknowledgment, that much remains to be learned about color appearance psychophysics and modeling. Simply put, CIECAM02 is simpler in formulation, easier to invert, and performs as well as, if not better, than CIECAM97s for all available data sets. CIECAM02 should be considered for any applications that were previously served well by CIECAM97s and, in fact, it is safe to say that CIECAM02 is widely used at this time while CIECAM97s is rarely mentioned. The following sections describe the formulation and use of CIECAM02.

## 16.2 INPUT DATA

Input data for the CIECAM02 include the relative tristimulus values of the test stimulus ( $XYZ$ ) and the white point ( $X_w Y_w Z_w$ ), the adapting luminance (often taken to be 20% of the luminance of a white object in the scene),  $L_A$ , in  $\text{cd}/\text{m}^2$ , the relative luminance of the surround (dark, dim, average), and a decision on whether discounting-the-illuminant is taking place. The surround relative luminance is generally taken to be average for reflection prints, dim for CRT displays or televisions, and dark for projected transparencies under the assumption that these media are being viewed in their typical environments. The surround is not directly tied to the medium. Thus it is certainly possible to have reflection prints viewed in a dark

**Table 16.1** Input parameters for the CIECAM02 model

Viewing condition	$c$	$N_c$	$F$
Average surround	0.69	1.0	1.0
Dim surround	0.59	0.9	0.9
Dark surround	0.525	0.8	0.8

**Figure 16.1** Linear relationship between surround parameters used for the computation of intermediate, continuously variable, surround settings in CIECAM02

surround and projected transparencies viewed in an average surround. Discounting-the-illuminant is generally assumed to occur for object color stimuli such as prints and not to occur for emissive displays such as CRTs. When discounting-the-illuminant occurs, the  $D$  factor in the chromatic adaptation model is set to 1.0. Otherwise it is computed as described in Section 16.3.

Once the surround relative luminance is established, Table 16.1 is used to set the values of  $c$ , an exponential nonlinearity,  $N_c$ , the chromatic induction factor, and  $F$ , the maximum degree of adaptation. In CIECAM02, intermediate values for these parameters are allowed. If intermediate values are desired, the proper procedure is to choose the intermediate value for  $c$  and then compute the corresponding intermediate values for  $N_c$  and  $F$  via linear interpolation as shown in the relationship plotted in Figure 16.1. These values have been corrected slightly from those in CIECAM97s and the number of conditions has been reduced to a more meaningful, and simpler, set.

### 16.3 ADAPTATION MODEL

One of the most important changes in CIECAM02 is the use of a linear, von Kries-type chromatic adaptation transform (as described in more detail in Chapter 9). This results in a simpler model with equivalent performance (Calabria and Fairchild 2001) and allows for a simple analytical inversion of CIECAM02 (another significant improvement over CIECAM97s). One begins with a conversion from CIE tristimulus values (scaled approximately between 0 and 100, rather than 0 and 1.0) to RGB responses based on the optimized transform matrix,  $\mathbf{M}_{\text{CAT02}}$ , as illustrated in Equations 16.1 and 16.2. All CIE tristimulus values are normally calculated using the CIE 1931 Standard Colorimetric Observer ( $2^\circ$ ). The transformation must also be completed for the tristimulus values of the adapting stimulus.

$$\begin{vmatrix} R \\ G \\ B \end{vmatrix} = \mathbf{M}_{\text{CAT02}} \begin{vmatrix} X \\ Y \\ Z \end{vmatrix} \quad (16.1)$$

$$\mathbf{M}_{\text{CAT02}} = \begin{vmatrix} 0.7328 & 0.4296 & -0.1624 \\ -0.7036 & 1.6975 & 0.0061 \\ 0.0030 & 0.0136 & 0.9834 \end{vmatrix} \quad (16.2)$$

The transformation to cone responses is the same as that used in the Hunt model. Matrix  $\mathbf{M}_{\text{CAT02}}$  is normalized such that the tristimulus values for the equal-energy illuminant ( $X = Y = Z = 100$ ) produce equal cone responses ( $L = M = S = 100$ ).

The  $D$  factor for degree of adaptation is computed as a function of the adapting luminance,  $L_A$ , and surround,  $F$ , according to Equation 16.3. If complete discounting-the-illuminant is assumed, then  $D$  is simply set to 1.0. Theoretically,  $D$  ranges from 1.0 for complete adaptation to 0.0 for no adaptation. As a practical limitation, it will rarely go below 0.6.

$$D = F \left[ 1 - \left( \frac{1}{3.6} \right) e^{-(L_A + 42)/92} \right] \quad (16.3)$$

Once  $D$  is established, the tristimulus responses for the stimulus color are converted to adapted tristimulus responses,  $R_c G_c B_c$ , representing corresponding colors for an implied equal-energy illuminant reference condition using Equations 16.4 through 16.6.  $R_w G_w B_w$  are the tristimulus responses for the adapting white.

$$R_c = \left[ \left( 100 \frac{D}{R_w} \right) + (1 - D) \right] R \quad (16.4)$$

$$G_C = \left[ \left( 100 \frac{D}{G_w} \right) + (1 - D) \right] G \quad (16.5)$$

$$B_C = \left[ \left( 100 \frac{D}{B_w} \right) + (1 - D) \right] B \quad (16.6)$$

## A Note on the CIECAM02 Chromatic Adaptation Transform

Equations 16.4 through 16.6 represent the most general form of the CIECAM02 chromatic adaptation transform as a simple von Kries transform to implicit equal-energy reference conditions with incomplete adaptation. This transformation can be used consistently independent of the remainder of the CIECAM02 model. It can also be applied regardless of the scaling of initial tristimulus values (0 to approximately 100 as normal in CIECAM02, or 0 to approximately 1.0 as sometimes used). It is recommended that equations 16.4 through 16.6 be used in all applications of CIECAM02 to maximize generality and minimize confusion in the function of the adaptation transform. However, the CIE (2004a) technical report on CIECAM02 provides slightly different default equations as given in Equations 16.4a through 16.6a.

$$R_C = \left[ \left( Y_w \frac{D}{R_w} \right) + (1 - D) \right] R \quad (16.4a)$$

$$G_C = \left[ \left( Y_w \frac{D}{G_w} \right) + (1 - D) \right] G \quad (16.5a)$$

$$B_C = \left[ \left( Y_w \frac{D}{B_w} \right) + (1 - D) \right] B \quad (16.6a)$$

Since  $Y_w$ , the  $Y$  tristimulus value of white, is normally 100, the two sets of equations are normally indistinguishable. However, there are times when  $Y_w$  values different from 100 are used such as when one considers paper, rather than the PRD, to be white in a printing application. While it appears that the  $Y_w$  factor in Equations 16.4a through 16.6a might account for the change in adopted white, it does not. Such normalization is already built into the equations with  $R_w$ ,  $G_w$ , and  $B_w$ . The  $Y_w$  terms serve no meaningful purpose and is a remnant of an earlier model formulation (similar to that in CIECAM97s) that was not corrected prior to the publication of the CIE technical report. There will be little effect of the difference in equations on final computed appearance correlates since the scaling of appearance relative to the white point is accomplished in later equations (such as that

for lightness,  $J$ ) in CIECAM02. However, the transform in Equations 16.4a through 16.6a cannot be used without the remainder of the CIECAM02 model. Doing so will produce inconsistent results (e.g., white from one viewing condition might not map to white in a second viewing condition). If the adaptation transform is to be used separately from the full CIECAM02 model, the form in Equations 16.4 through 16.6 must be used for consistent predictions. Also, it should be noted that the  $Y_w$  factor in Equations 16.4a through 16.6a does not normalize the scaling of tristimulus values (it actually has the opposite effect) and values scaled from 0 to approximately 100 should be used as input to CIECAM02.

## Remainder of CIECAM02 Adaptation Model

Next a number of viewing-condition-dependent components are computed as intermediate values required for further computations. These include a luminance-level adaptation factor,  $F_L$ , and induction factors,  $N_{bb}$  and  $N_{cb}$ , and the base exponential nonlinearity,  $z$ , that each depend on the background relative luminance,  $Y_b$ . These factors are computed using Equations 16.7 through 16.11.

$$k = \frac{1}{5L_A + 1} \quad (16.7)$$

$$F_L = 0.2k^4 (5L_A) + 0.1(1 - k^4)^2 (5L_A)^{1/3} \quad (16.8)$$

$$n = \frac{Y_b}{Y_w} \quad (16.9)$$

$$N_{bb} = N_{cb} = 0.725 \left( \frac{1}{n} \right)^{0.2} \quad (16.10)$$

$$z = 1.48 + \sqrt{n} \quad (16.11)$$

In order to apply post-adaptation nonlinear compression, the adapted RGB responses must first be converted from the  $\mathbf{M}_{CAT02}$  specification to Hunt–Pointer–Estevez fundamentals that more closely represent cone responsivities. This transformation is represented by Equations 16.12 through 16.14 and can be thought of as a conversion from the CAT02 RGB system back to CIE tristimulus values then to cone responsivities. The relative spectral responsivities of the CAT02 system and the Hunt–Pointer–Estevez fundamentals are illustrated in Figure 16.2.

$$\begin{vmatrix} R' \\ G' \\ B' \end{vmatrix} = \mathbf{M}_{HPE} \mathbf{M}_{CAT02}^{-1} \begin{vmatrix} R_C \\ G_C \\ B_C \end{vmatrix} \quad (16.12)$$

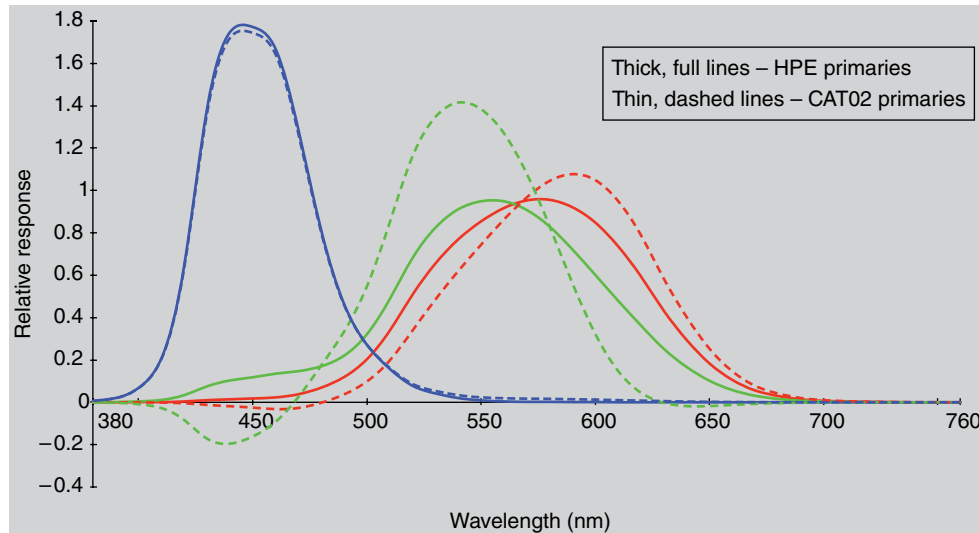


**Figure 16.2** The relative spectral responsivities for the  $\mathbf{M}_{\text{CAT02}}$  primaries (thin, dashed lines) and the Hunt–Pointer–Estevez cone fundamentals (thick, solid lines). Note that both are simple linear transformations of the CIE two-degree color matching functions

$$\mathbf{M}_{\text{HPE}} = \begin{vmatrix} 0.38971 & 0.68898 & -0.07868 \\ -0.22981 & 1.18340 & 0.04641 \\ 0.00000 & 0.00000 & 1.00000 \end{vmatrix} \quad (16.13)$$

$$\mathbf{M}_{\text{CAT02}}^{-1} = \begin{vmatrix} 1.096124 & -0.278869 & 0.182745 \\ 0.454369 & 0.473533 & 0.072098 \\ -0.009628 & -0.005698 & 1.015326 \end{vmatrix} \quad (16.14)$$

The post-adaptation nonlinearities are similar in form to those in CIECAM97s but slightly modified to produce a simple power-function response over a larger dynamic range. This facilitates a simple definition of saturation later in the model. For much of the normal operating range of these functions, these are similar to simple square-root functions. These nonlinearities are given in Equations 16.15 through 16.17.

$$R'_a = \frac{400(F_L R' / 100)^{0.42}}{27.13 + (F_L R' / 100)^{0.42}} + 0.1 \quad (16.15)$$

$$G'_a = \frac{400(F_L G' / 100)^{0.42}}{27.13 + (F_L G' / 100)^{0.42}} + 0.1 \quad (16.16)$$

$$B'_a = \frac{400(F_L B' / 100)^{0.42}}{27.13 + (F_L B' / 100)^{0.42}} + 0.1 \quad (16.17)$$

These values are then used to create opponent color responses and formulate correlates of color appearance.

## 16.4 OPPONENT COLOR DIMENSIONS

Initial opponent-type responses in CIECAM02 are calculated using Equations 16.18 and 16.9.

$$a = R'_a - 12G'_a / 11 + B'_a / 11 \quad (16.18)$$

$$b = \frac{1}{9} (R'_a + G'_a - 2B'_a) \quad (16.19)$$

## 16.5 HUE

Hue angle,  $h$ , is calculated in CIECAM02 space using the same procedure as CIELAB. As in CIELAB,  $h$  is expressed in degrees ranging from 0 to 360 measured from the positive  $a$  axis calculated according to Equation 16.20.

$$h = \tan^{-1} \frac{b}{a} \quad (16.20)$$

Next an eccentricity factor,  $e_t$ , is computed. This factor is similar to that in CIECAM97s but has been formulated analytically as given in Equation 16.21.

$$e_t = \frac{1}{4} \left[ \cos \left( h \frac{\pi}{180} + 2 \right) + 3.8 \right] \quad (16.21)$$

Hue quadrature and hue composition can be determined through linear interpolation of the data given in Table 16.2 using Equation 16.22.

$$H = H_i + \frac{100(h - h_i) / e_i}{(h - h_i) / e_i + (h_{i+1} - h) / e_{i+1}} \quad (16.22)$$

**Table 16.2** Data for conversion from hue angle to hue quadrature

	Red	Yellow	Green	Blue	Red
$i$	1	2	3	4	5
$h_i$	20.14	90.00	164.25	237.53	380.14
$e_i$	0.8	0.7	1.0	1.2	0.8
$H_i$	0	100	200	300	400

## 16.6 LIGHTNESS

An initial achromatic response is computed by weighted summation of the nonlinear adapted cone responses modified with the brightness induction factor as illustrated in Equation 16.23. A similar quantity must also be computed for the white in order to facilitate computation of lightness and brightness.

$$A = \left[ 2R'_a + G'_a + \left( \frac{1}{20} \right) B'_a - 0.305 \right] N_{bb} \quad (16.23)$$

Lightness,  $J$ , is then simply computed from the achromatic response,  $A$ , achromatic response for white,  $A_w$ , the surround factor,  $c$ , and the base exponent,  $z$ , according to Equation 16.24.

$$J = 100 \left( \frac{A}{A_w} \right)^{cz} \quad (16.24)$$

## 16.7 BRIGHTNESS

The CIECAM02 correlate to brightness,  $Q$ , is computed from lightness,  $J$ , the achromatic response for white,  $A_w$ , the surround factor,  $c$ , and the luminance-level adaptation factor,  $F_L$ , as shown in Equation 16.25.

$$Q = \left( \frac{4}{c} \right) \sqrt{J / 100} (A_w + 4) F_L^{0.25} \quad (16.25)$$

## 16.8 CHROMA

A temporary quantity,  $t$ , that is related to saturation and incorporates the chromatic induction factors for surround and background ( $N_c$  and  $N_{cb}$ ) as well as the eccentricity adjustment,  $e_t$ , is computed as the basis for chroma, colorfulness, and saturation correlates. The formula for  $t$  is given in Equation 16.26.

$$t = \frac{(50000 / 13) N_c N_{cb} e_t \sqrt{a^2 + b^2}}{R'_a + G'_a + (21 / 20) B'_a} \quad (16.26)$$

CIECAM02 chroma,  $C$ , is then computed by multiplying a slightly non-linear form of  $t$  by the square root of lightness,  $J$ , with some adjustment for

background,  $n$ , as shown in Equation 16.27. This formulation, as with most of the model, is based on empirical fitting to various color appearance scaling data.

$$C = t^{0.9} \sqrt{J / 100} (1.64 - 0.29^n)^{0.73} \quad (16.27)$$

## 16.9 COLORFULNESS

The colorfulness correlate in CIECAM02 is calculated by scaling the chroma predictor,  $C$ , by the fourth root of the luminance-level adaptation factor,  $F_L$ , as illustrated in Equation 16.28. This makes sense since colorfulness is related to chroma, but increases with adapting luminance while chroma is relatively constant across changes in luminance.

$$M = CF_L^{0.25} \quad (16.28)$$

## 16.10 SATURATION

Lastly, a simple and logically defined predictor of saturation,  $s$ , is defined in CIECAM02 as the square root of colorfulness relative to brightness in Equation 16.29. This is analogous to the CIE definition of saturation as the colorfulness of a stimulus relative to its brightness.

$$s = 100 \sqrt{\frac{M}{Q}} \quad (16.29)$$

## 16.11 CARTESIAN COORDINATES

Color spaces related to appearance models are normally specified in terms of cylindrical coordinates of lightness, chroma, and hue ( $JCh$ ) or brightness, colorfulness, and hue ( $QMh$ ). However, in some applications it is useful to have the equivalent Cartesian coordinates. While this computation is a simple coordinate transformation, it was never explicitly defined in CEICAM97s. Thus Cartesian coordinates for chroma, colorfulness, and saturation dimensions are defined in Equations 16.30 through 16.35.

$$a_c = C \cos(h) \quad (16.30)$$

$$b_c = C \sin(h) \quad (16.31)$$

$$a_M = M \cos(h) \quad (16.32)$$

$$b_M = M \sin(h) \quad (16.33)$$

$$a_s = s \cos(h) \quad (16.34)$$

$$b_s = s \sin(h) \quad (16.35)$$

## 16.12 INVERSE MODEL

Particularly for color reproduction applications, an inverse color appearance model is of practical importance. CIECAM02 is a significant improvement over CIECAM97s in terms of simplicity of inversion. This is largely due to the adoption of a simple linear chromatic adaptation transform. In addition, the CIE technical report on CIECAM02 includes a detailed explanation of the model inversion and worked examples (CIE 2004a). A step-by-step procedure for implementing the CIECAM02 model in reverse is given below (starting from  $JCh$ ).

- Step 1. Calculate  $t$  from  $C$  and  $J$ .
- Step 2. Calculate  $e_t$  from  $h$ .
- Step 3. Calculate  $A$  from  $A_w$  and  $J$ .
- Step 4. Calculate  $a$  and  $b$  from  $t$ ,  $e_t$ ,  $h$ , and  $A$ .
- Step 5. Calculate  $R'_a$ ,  $G'_a$ , and  $B'_a$  from  $A$ ,  $a$ , and  $b$ .
- Step 6. Use the inverse nonlinearity to compute  $R'$ ,  $G'$ , and  $B'$ .
- Step 7. Convert to  $R_c$ ,  $G_c$ , and  $B_c$  via linear transform.
- Step 8. Invert the chromatic adaptation transform to compute  $R$ ,  $G$ , and  $B$  and then  $X$ ,  $Y$ , and  $Z$ .

## 16.13 IMPLEMENTATION GUIDELINES

Another improved feature of the CIECAM02 technical report (CIE 2004a) are more detailed guidelines for implementation of the model. Several worked examples are provided along with examples of parameter settings. This information is valuable to those interested in implementing the model in forward and reverse directions rather than simply understanding the concepts of its formulation. Table 16.3 illustrates some of the example parameter settings included in the report. The surround is considered average when the luminance of the surround white is greater than 20% of the scene, or image, white and dim when the surround luminance is less than 20%. A dark surround setting is used when the surround has essentially no luminance.

**Table 16.3** Example CIECAM02 parameter settings for typical applications

Example	Ambient lighting in lux (cd/m <sup>2</sup> )	Scene or device white luminance	$L_A$ in cd/m <sup>2</sup>	Adopted white point	Surround
Surface color evaluation in a light booth	1000 (318.3)	318.30	63.66	Light booth WP	Average
Viewing self-luminous display at home	38 (12)	80	16	Between display and ambient WPs	Dim
Viewing slides in dark room	0 (0)	150	30	Between projector WP and E	Dark
Viewing self-luminous display in office	500 (159.2)	80	16	Between display WP and office illumination	Average

## 16.14 PHENOMENA PREDICTED

CIECAM02 can predict all the phenomena that can be predicted by CIECAM97s. It includes correlates of all the typical appearance attributes (relative and absolute) and can be applied over a large range of luminance levels and states of chromatic adaptation. Like CIECAM97s, CIECAM02 is not applicable to situations in which there is significant rod contribution to vision or at extremely high luminances in which cone bleaching might occur. It is appropriate to think of CIECAM02 as a simpler and better version on CIECAM97s. Example calculations for CIECAM02 are given in Table 16.4.

## 16.15 COMPUTATIONAL ISSUES

It has been recognized for some time that there are computational difficulties with the CIECAM02 model for certain applications and other unusual viewing conditions or stimuli. The applications include the computation of profiles for color management systems that sometimes require the calculation of color appearance for a uniform grid of input colorimetric coordinates that spans the gamut of all physically realizable colors and also goes beyond that to include physically impossible stimuli (*i.e.*, stimuli with negative CIE tristimulus values). In other cases, computational issues might arise simply by choosing adaptation illumination that is very saturated and/or physically real stimuli that are very near the spectrum locus and thus rarely encountered in typical situations.

**Table 16.4** Example CIECAM02 calculations

Quantity	Case 1	Case 2	Case 3	Case 4
X	19.01	57.06	3.53	19.01
Y	20.00	43.06	6.56	20.00
Z	21.78	31.96	2.14	21.78
X <sub>w</sub>	95.05	95.05	109.85	109.85
Y <sub>w</sub>	100.00	100.00	100.00	100.00
Z <sub>w</sub>	108.88	108.88	35.58	35.58
L <sub>A</sub>	318.31	31.83	318.31	31.83
F	1.0	1.0	1.0	1.0
D	0.994	0.875	0.994	0.875
Y <sub>b</sub>	20.0	20.0	20.0	20.0
N <sub>c</sub>	1.0	1.0	1.0	1.0
F <sub>L</sub>	1.17	0.54	1.17	0.54
N <sub>bb</sub> , N <sub>cb</sub>	1.0	1.0	1.0	1.0
H	219.0	19.6	177.1	248.9
H	278.1	399.6	220.4	305.8
H <sub>c</sub>	78B 22G	100R	80G 20B	94B 6R
J	41.73	65.96	21.79	42.53
Q	195.37	152.67	141.17	122.83
S	2.36	52.25	58.79	60.22
C	0.10	48.57	46.94	51.92
M	0.11	41.67	48.80	44.54
a <sub>c</sub>	-0.08	45.77	-46.89	-18.69
b <sub>c</sub>	-0.07	16.26	2.43	-48.44
a <sub>M</sub>	-0.08	39.27	-48.74	-16.03
b <sub>M</sub>	-0.07	13.95	2.43	-41.56
a <sub>s</sub>	-1.83	49.23	-58.72	-21.67
b <sub>s</sub>	-1.49	17.49	2.93	-56.18

The various challenges have been more recently summarized by Hunt (2009) and Luo (2012) and despite a significant history of various intricacies in various aspects of the model, the ultimate focus narrowed in on the use of two matrices, one for the adaptation transform and a second for the color space construction, and on the form of the response nonlinearity as it approaches 0. For those interested in the details of problems that arise in various chromatic adaptation transforms and other aspects of the model, there is a significant collection of literature (Brill 2006, Brill and Mahy 2013, Brill and Süsstrunk 2008, Li and Luo 2005, Li *et al.* 2009, 2012a-d, 2013). The largest problem arises in the CAT02 matrix that, with its sharpened responses, makes possible negative RGB values that cause problems when propagated through the adaptation transform and remainder of the model. When such negative values occur, there can also be problems with model inversion, division by 0, and the compressive nonlinearity has an infinite slope as it passes through zero (which is a computational problem, but should not ever happen with real stimuli).

This problem has been undertaken by CIE TC8-11, chaired by Li. The committee has not yet published a final solution but it appears likely that it will suggest a modified form of CIECAM02 for those desiring a model that is computationally more robust, but perhaps slightly less accurate. This modified model will likely be put forth as an alternative to CIECAM02, not a replacement for it. The committee's objective is to fit one matrix that can replace both CAT02 adaptation matrix and Hunt-Pointer-Estevez color space (post-adaptation matrix) and encompass the spectrum locus thus eliminating most problems while maximizing accuracy. Simply using the Hunt-Pointer-Estevez matrix for adaptation as well as the color space is not as accurate. The planned optimization would be a compromise between accuracy and mathematical simplicity. While this would eliminate most of the problems with the infinite slope of the nonlinear function at 0, it does not completely do that since some users require processing of non-real stimulus values in order to populate three-dimensional lookup tables. This remaining problem can, and likely will, be addressed with a small linear segment for the function around 0. It is also worth noting that some advances in color appearance predictions such as hue naming and cancellation can be obtained with modification of the sharpened sensor responses rather than reverting to cone responses (Vazquez-Corral *et al.* 2012).

## 16.16 CAM02-UCS

There has been an interesting effort to combine the appearance scales of a color appearance model with the desired predictions of uniform color differences typified by formulae such as the CIE DE2000 equations. This is a difficult task since it is generally recognized that scales of color appearance (large interval changes in attributes) do not linearly relate to small interval changes near, and slightly above, threshold changes in perception. One outcome of such efforts is known as CAM02-UCS (Luo *et al.* 2006). In essence, the concept is to adjust the appearance dimensions of the color space, in this case CIECAM02, in such a way that they included the weight functions that are usually required in a color difference equation.

Equations 16.36 and 16.37 show modified forms of CIECAM02 lightness and colorfulness. Equations 16.38 and 16.39 are simply the coordinate transformation to a rectangular space to facilitate the simple color difference computation given in Equation 16.40. This is the essence of CAM02-UCS.

$$J' = \frac{1.7J}{1 + 0.007J} \quad (16.36)$$

$$M' = \frac{1}{0.0228} \log_{10} (1 + 0.0228M) \quad (16.37)$$

$$a'_M = M' \cos(h) \quad (16.38)$$

$$b'_M = M' \sin(h) \quad (16.39)$$

$$\Delta E' = \sqrt{(\Delta J')^2 + (\Delta a'_M)^2 + (\Delta b'_M)^2} \quad (16.40)$$

CIE TC1-75, chaired by Luo, is examining the possibility of proposing a CIE model that incorporates color appearance and color difference. It is still too early in that work to predict the outcome. CAM02-UCS is certainly a useful approach and has been applied in a number of situations. However, it is questionable in its use of colorfulness rather than the chroma attribute that is the normal judgment in color difference experiments (perhaps an easy modification), and it should be noted that the adjustment of the appearance scales to accommodate color differences makes them inaccurate for color appearance. So, while the CAM02-UCS approach incorporates both in a single model, it does not do so with one set of scales.

## 16.17 WHY NOT USE JUST CIECAM02?

If one is looking for an internationally agreed upon color appearance model with a relatively simple formulation that performs as well as, if not better, than any similar model as of 2004, then CIECAM02 is the answer. There is no scientific reason to prefer CIECAM97s over CIECAM02, and CIECAM02 is simpler to implement and use in practical settings. In some situations, the detailed knowledge and control of viewing conditions required to best take advantage of CIECAM02 might not be available. In such situations, simpler models might well suffice. In general the logical progression of color appearance models is to begin by simply using CIELAB. If CIELAB is found to be inadequate for the application, then a combination of CIELAB with a better chromatic adaptation model (like the CAT02 linear chromatic adaptation transform) would be the next logical step. If additional flexibility was required, a slightly more complex model like RLAB, or RLAB with the adaptation transform replaced with the CAT02 transform, would be most appropriate. Then, if further sophistication is required, CIECAM02 would be the best choice. Lastly, if CIECAM02 is not adequate for the given situation (such as when rod contributions are to be predicted), then the Hunt model would be the most comprehensive choice.

## 16.18 OUTLOOK

CIECAM02 represents a significant advance in color appearance models over the six years between its publication and the initial formulation of CIECAM97s. Immediately upon the publication of CIECAM97s, limitations were noted, suggestions for improvements were made, and a new CIE committee was formed to suggest improvements. Currently, no similar situations are arising with respect to a complete replacement for CIECAM02.

It appears that the time between CIECAM02 and the next CIE color appearance model will be significantly longer than six years. One reason for this is that this type of model seems to be predicting the available visual data to within experimental uncertainty. Thus there is no room for significant improvement until more precise (and accurate) experimental data become available or until vastly larger volumes of data are produced to allow improved prediction of the mean response. The cost and difficulty of collecting such data as well as inherent inter-observer variability make it unlikely that significant improvements in the available data will be obtained in the foreseeable future. Instead it is likely that only the slight modifications, or alternative models to be used in addition to CIECAM02, might find CIE approval in the near term.

That said, there certainly has been interest in improvements, enhancements, modifications, or alternatives to CIECAM02. One example is the work of Luo *et al.* (2006) and CIE TC1-75 in the CAM02-UCS that aims to combine color difference and color appearance predictions into a single model and is fairly often used. Kunkel and Reinhard (2009) published a fascinating alternative to CIECAM02 that is significantly more physiologically plausible and somewhat simpler mathematically while making appearance predictions that are virtually identical. It is certainly an approach that should be noted in the development of any future CIE models. Fu *et al.* (2012) published visual data and an extension to CIECAM02 to facilitate treatment of the appearance of unrelated colors. And as a final example, Park *et al.* (2013) have proposed an extension for incorporating visual glare seen with mobile displays. The crystal-ball prediction for the future of color appearance models appears to be a movement to two versions (CIE TC8-11) plus a generalized model (CIE TC1-75).

Instead, many researchers in the field of color appearance are turning to more complex viewing situations and deriving models with new and different capabilities. Such capabilities include computational prediction of spatial and temporal effects. These types of models were only just being considered when the first edition of this book was published, but are becoming more of a practical reality as the second edition is being produced. The concepts of such models and one example are described in Chapter 20. Perhaps such models are the direction color appearance modeling will move in the future. Meanwhile, it is likely that CIECAM02 will see significant practical adoption and use. It will be interesting to see the degree to which it is considered a practical success.

# 17

# Testing Color Appearance Models

---

Chapters 10 through 16 described several color appearance models with little reference to data on the visual phenomena they are intended to predict. In contemplating the existence of this variety of color appearance models, it is logical to wonder just how well they work. Quantitative tests of the models are certainly required (as with any scientific theory, they must be supported by data); unfortunately far more has been published on the formulation of the models than their actual performance. There are several reasons for this. The first is the paucity of reliable data measuring observers' perceptions of color appearance. The second is that the models themselves have evolved at a rate that outpaced researchers' abilities to evaluate their performance. Fortunately, both of these situations continue to change. This chapter reviews some of the experimental work to test color appearance models and collect additional color appearance data for future model testing. This remains an area of research and it is to be expected that additional tests (and model revisions) will continue to be published provided there remain some interested enough in the results to fund the needed research.

## 17.1 OVERVIEW

One might expect that the derivation of color appearance models of the sophistication presented in Chapters 10 through 16 would require extensive data. This is true; however, the data used to derive the models come from a long history of vision experiments, each aimed at one particular aspect of color appearance. These include the experiments described in Chapter 6 on color appearance phenomena. The models were then formulated to simultaneously predict a wide variety of these phenomena. In so doing, quite sophisticated models can be derived with little or no data that

simultaneously probe the wide variety of predictions. To truly test the models, visual data scaling the appearance attributes of brightness, lightness, colorfulness, saturation, chroma, and hue are required. Alternately, visual evaluations of the performance can be made for existent models.

A variety of tests of color appearance models have been performed. Unfortunately, none of these tests are completely satisfactory and the question of which model is best cannot be unequivocally answered for all situations. The various tests that have been performed can be classified into four general groups as described in the following sections:

- Qualitative tests of various phenomena
- Prediction of corresponding colors data
- Magnitude estimation of appearance attributes
- Direct psychophysical comparison of the predictions of various models.

Each of these types of tests contributes to the evaluation of models in a unique way and none is adequate, on its own, to completely specify the best color appearance model. There are also organized activities within the CIE technical committee structure aimed at the evaluation of color appearance models. These activities draw upon evaluations in each of the four groups described above with the ultimate aim to recommend models and procedures for color appearance specification.

## 17.2 QUALITATIVE TESTS

There are a variety of model tests that can be considered qualitative for one reason or another. A test is qualitative if the results show general trends in the predictions rather than providing numerical comparisons of various models. Such tests include

- Calculations showing that a particular appearance phenomenon can be predicted (*e.g.*, colorfulness increases with luminance)
- Prediction of trends from historical data
- Comparisons with color order systems
- Abridged visual experiments on model features.

Nayatani *et al.* (1988) published an early example of qualitative evaluation of their color appearance model. They looked at two sets of data. The first was the predicted color appearance of Munsell samples under CIE illuminant A and the second was the evaluation of results from a color rendering experiment of Mori and Fuchida (1982). Their predictions for the Munsell samples showed that their model predicted the Helson–Judd effect under illuminant A while a von Kries transformation would not. Nayatani *et al.* followed this up with a brief visual experiment in which three observers (including the authors) observed a small Helson–Judd effect for samples viewed under an incandescent lamp. They also examined some color discrimination observations that correlated better with results from their

model than predictions made using a von Kries transformation. They also showed that the Nayatani *et al.* color appearance model made reasonable predictions of the Mori and Fuchida corresponding colors data. However, they did not compare these results with other models.

As illustrated in the Nayatani *et al.* (1988) study cited above, color order systems are often used to evaluate the performance of appearance models. The systems used are those based on color appearance (Munsell and NCS) as described in Chapter 5. In many cases when formulating a model, its authors will plot contours of Munsell hue, value, and chroma in order to evaluate the perceptual uniformity of the model. Alternatively, contours of constant NCS hue, whiteness–blackness, and chromaticness can be examined. The assumption is that the color order systems have been constructed with accurate appearance scales. Thus, for example, a model should be able to predict that samples with constant Munsell hue have the same predicted hue and make analogous predictions for value (lightness) and chroma. Many authors have included plots of Munsell or NCS contours along with the formulation of their models. Examples include Nayatani *et al.* (1987, 1990b), Guth (1991), Hunt (1995), and Fairchild and Berns (1993). In fact, the latest revision of the Nayatani *et al.* (1995) model was formulated to correct discrepancies in plots of Munsell hue and chroma contours at various value levels. Seim and Valberg (1986) provide a more quantitative analysis of the Munsell system in the CIELAB color space and propose alternative equations similar to those found in the Hunt model. Wyble and Fairchild (2000) performed quantitative analyses of the Munsell system, described in Section 17.7, in various color appearance models that helped lead to some of the improvements in CIECAM02.

Nayatani *et al.* (1990b) published an interesting comparison of the Hunt and Nayatani *et al.* models. This included plots of Munsell contours in the color spaces of each model as well as flow charts comparing the computational procedure for each model. While this work is interesting, at this point it is largely historical since both models have been revised significantly since it was published. Plots of Munsell and NCS contours do provide some insight into the performance and properties of various color appearance models; however, none of the published results include a quantitative comparison between the color order systems and color appearance models. For example, constant hue contours should plot as straight radial lines and constant chroma contours as concentric, evenly spaced circles. It would be possible to derive measures of how close the models come to producing these results. See Wyble and Fairchild (2000) for an example. Perhaps this has not often been done because the results would not be terribly impressive. Another reason is that the perceptual uncertainty of the color order systems is not well defined, making it difficult to know how good the predictions should be. Examination of the published results suggests that the models perform about equally well in these qualitative comparisons. This conclusion is confirmed by a study of constant-hue contours completed by Hung and Berns (1995) in which extensive visual evaluations were made. Quantitative analysis by Hung and Berns (1995) showed that the observed constant hue contours were not adequately predicted by any color appearance model and that no single model was clearly superior. Moroney

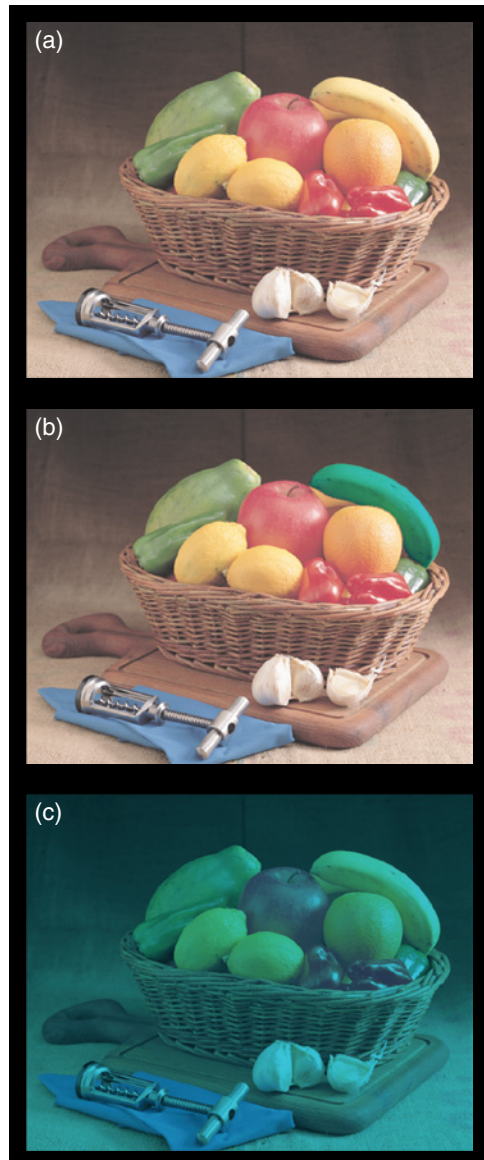


**Figure 17.1** An illustration of chromatic adaptation. (a) Original image. (b) Simulation of a cyan filter placed over the yellow banana resulting in the appearance of a green banana. (c) Simulation of the same cyan filter placed over the entire image. Note how the banana in (c) returns to a yellowish appearance despite being physically identical to the banana in (b). Original image part of the ISO SCID set

(2000a) and others have shown that more recent color spaces such as IPT, CIECAM97s, and CIECAM02 perform better for constant-hue predictions.

Hunt (1991b) provides an excellent example of qualitative evaluation of his appearance model. For example, Hunt (1991b) shows how the model

predicts cone and rod saturation, the Stevens effect, the Hunt effect, and the effect of surround relative luminance on image contrast, as well as other effects. One fascinating demonstration that Hunt (1991b) predicts is the appearance of objects in a filtered slide. In a classic demonstration (Hunt 1995), a cyan filter is superimposed over a yellow cushion in a slide resulting in the cushion appearing green. However, if the same filter is placed over the entire slide, the cushion retains much of its yellow appearance due to chromatic adaptation. This effect is strongest for projected slides but can be observed in printed images as well (Hunt 1995). The effect is also simulated in Figure 17.1 with the filter being added over the banana. Hunt (1991b) shows that his model is capable of predicting this effect. It is worth noting that simpler models, including CIELAB and RLAB, are also capable of predicting this effect (Fairchild and Berns 1993).

Perhaps the most useful result of qualitative analysis of color appearance models is a summary of the various effects that can be predicted by each model. Table 17.1 provides such a summary. While Table 17.1 is useful to gauge the capabilities of each model, it is important to remember that it includes no information on how accurately each model can predict the various phenomena. This lack of information on accuracy is the most significant drawback of qualitative model tests and necessitates the additional tests described in the following sections.

**Table 17.1** Color appearance phenomena predicted by various color appearance models. Check marks indicate that the model is capable of directly making the prediction

	ATD	CIELAB	LLAB	RLAB	Nayatani	Hunt	CIECAM
Lightness		✓	✓	✓	✓	✓	✓
Brightness	✓				✓	✓	✓
Chroma		✓	✓	✓	✓	✓	✓
Saturation	✓	?	✓	✓	✓	✓	✓
Colorfulness			✓		✓	✓	✓
Hue angle	✓	✓	✓	✓	✓	✓	✓
Hue			✓	✓	✓	✓	✓
Helson–Judd effect					✓	✓	
Stevens effect					✓	✓	✓
Hunt effect	✓		✓		✓	✓	✓
Helmholtz–	✓				✓	✓	
Kohlrausch effect							
Bartleson–			✓	✓		✓	✓
Breneman results							
Discounting-the-illuminant			✓	✓		✓	✓
Incomplete adaptation				✓		✓	✓
Color difference		✓	✓	✓			?
Others	✓				✓	✓	

### 17.3 CORRESPONDING-COLORS DATA

Corresponding colors data were described in Chapter 8 with respect to the study of chromatic adaptation. In addition, corresponding colors data can be collected and analyzed for a wide range of color appearance phenomena in addition to simple chromatic adaptation. Corresponding colors are defined by two sets of tristimulus values specifying stimuli that match in color appearance for two disparate sets of viewing conditions. Recall that if the change in viewing conditions has an impact on color appearance, then the corresponding tristimulus values of the stimuli will be different in absolute value.

Corresponding colors data are used to test color appearance models by taking the tristimulus values for the first viewing condition and transforming them to the matching tristimulus values under the second viewing condition. The predicted corresponding colors can then be compared with visually observed corresponding colors to determine how well the model performs. The results are often analyzed in terms of RMS deviations between predicted and observed colors in either a uniform chromaticity space (*e.g.*,  $u'v'$ ) or a uniform color space, (*e.g.*, CIELAB). Recall that Nayatani *et al.* (1990a) illustrated the important distinction between lightness–chroma and brightness–colorfulness matches. Complete color appearance models can be used to predict either type of match. The two types of matches will be different if there is a change in luminance level between the two viewing conditions in question.

One of the most extensive series of experiments measuring corresponding colors data for color appearance analysis was completed by the CSAJ and reported by Mori *et al.* (1991). Data from four experiments performed by CSAJ were summarized by Mori *et al.* (1991).

1. An experiment on chromatic adaptation from illuminant D65 to illuminant A simulators at an illuminance of 1000 lux. Judgments were made by 104 observers on 87 samples using a modified haploscopic matching technique.
2. An experiment that collected data consisting of measurements of the Hunt effect using five colored samples judged under illuminant D65 simulators at five different illuminance levels by 40 observers.
3. An experiment that collected data representing measurements of the Stevens effect using five neutral samples viewed under five different illuminance levels by 31 observers.
4. An experiment that examined the Helson–Judd effect for achromatic samples viewed under highly chromatic fluorescent light sources.

These data represent one of the most extensive studies, with the largest numbers of observers, completed in the area of color appearance to date.

Unfortunately, Mori *et al.* (1991) reported only qualitative analyses of the experimental results. They showed plots of predicted and observed corresponding colors for the chromatic adaptation experiment and the Nayatani, von Kries, and Hunt models. Mori *et al.* (1991) concluded that the Nayatani

model made the best predictions. However, examination of their plots suggests that Hunt's model provides similar performance to it and the von Kries transform perhaps works better than both of them. They illustrated that the Nayatani *et al.* model could predict the Hunt effect data well, but they did not compare the results with predictions of the Hunt model. Similar analyses were performed for the Stevens effect and Helson–Judd effect data. The results showed a fairly small Stevens effect that was over-predicted by the Nayatani *et al.* model. The Helson–Judd effect, while observed in this experiment, was also over-predicted by the Nayatani *et al.* model. Further, quantitative analyses of these data have been carried out through CIE TC1-34 and are described later in the chapter.

Breneman (1987) collected a fairly extensive set of corresponding colors data for changes in chromatic adaptation and luminance level. These data were used to evaluate various chromatic adaptation transforms and color appearance models by Fairchild (1991a,b). The models were compared in terms of RMS deviations between observed and predicted results in the CIE 1976  $u'v'$  chromaticity diagram. The chromatic adaptation data were best predicted by the Hunt and RLAB models followed by the Nayatani and von Kries models. The CIELAB and CIELUV models performed the worst for these data. Breneman's data showed a small Hunt effect that was over-predicted by the Hunt and Nayatani *et al.* models and not predicted at all by the other models. The RMS deviations produced by both sets of models are similar in magnitude, suggesting that making no prediction is as accurate as an over-prediction for these particular data.

Luo *et al.* (1991b) converted some of their magnitude scaling data (described in Section 17.4) to sets of corresponding colors for various changes in viewing conditions. They generated three sets of corresponding colors data for changes in chromatic adaptation from CIE illuminant D65 to D50, D65 to A, and D65 to white fluorescent, and then evaluated six different chromatic adaptation transforms using mean and RMS color differences in the CIELAB space. The results showed that the Bradford model, the basis of LLAB and CIECAM97s, performed best. The Hunt, Nayatani *et al.*, and CIELAB models performed similarly and almost as well. These were followed by the simple von Kries transformation and a transformation proposed by Bartleson. Additional results can be found in Kuo *et al.* (1995).

Braun and Fairchild (1997) performed an experiment in which observers were asked to adjust CRT-displayed images to match printed images viewed under a different white point. Matching images were obtained for five observers using two different images for white point changes from 3000K to 6500K and 9300K to 6500K. The data were analyzed by segmenting the images into meaningful object regions to avoid overly weighting large image areas. The corresponding colors were analyzed in terms of average and RMS CIELAB color differences. The results showed that RLAB, LLAB, and CIELAB best predicted the observed corresponding colors. The Hunt and Nayatani *et al.* models did not perform as well.

The above-mentioned studies illustrate the variety of corresponding colors experiments that have been completed. Unfortunately, a clear pic-

ture of relative model performance does not emerge from the analysis of these results. This is partly due to the fact that the models have changed, and new ones have emerged, since some of the results were published.

## 17.4 MAGNITUDE ESTIMATION EXPERIMENTS

Magnitude estimation experiments involve asking observers to directly assign numerical values to the magnitude of their perceptions. The utility of such experimental techniques was brought into focus by the classic study of Stevens (1961). Magnitude estimation experiments allow the rather direct measurement of the magnitudes of color appearance attributes such as lightness, chroma, and hue for various stimuli and viewing conditions. These data can then be used to evaluate various color appearance models and derive new models.

The most extensive series of experiments on the magnitude scaling of color appearance has been carried out through the Loughborough University of Technology Computer Human Interface (LUTCHI) Research Centre as published in a series of papers by Luo *et al.* (1991a,b, 1993a,b, 1995), the results of which have been summarized by Hunt and Luo (1994).

### Luo *et al.* (1991a)

Six or seven observers were each asked to scale the lightness, colorfulness, and hue of between 61 and 105 stimuli presented in a series of 21 different viewing conditions. The viewing conditions varied in white point, medium, luminance level, and background. The results showed that the most significant influences on color appearance were background and white point. Other effects were not clearly present in the data. One reason for this is the intrinsically high uncertainty in magnitude estimation experiments. The uncertainty in the data was expressed in terms of coefficients of variation (CV), which can be thought of as percent standard deviations. The overall CV values for intra-observer variability were about 13 for lightness, 18 for colorfulness, and 9 for hue. No color appearance models were evaluated in part I.

One problem with the LUTCHI studies is the rather unusual choice of appearance attributes that were scaled – lightness, colorfulness, and hue. The authors claim that colorfulness is more natural than chroma. However, chroma is the more appropriate attribute to scale with lightness. It is the attribute that observers normally associate with objects, and it does not require that the observers be taught its definition. At a single luminance level it is probably reasonable to assume that chroma and colorfulness are related by a simple scaling factor. However, there is no reason to believe that chroma and colorfulness are linearly related across changes in luminance.

### Luo et al. (1991b)

The part one data were used to evaluate various color appearance and chromatic adaptation models. The models were analyzed by calculating CV values between the observed results and the model predictions. As an overall summary, the Hunt model performed best for lightness, followed by CIELAB and then Nayatani. For colorfulness, no model performed particularly well, but Hunt's model (and a version of Hunt's modified with respect to these data) performed slightly better than others. For hue, the Hunt model performed significantly better than the Nayatani *et al.* model. Other models were not tested for hue. These data were also used to formulate later versions of the Hunt model.

### Luo et al. (1993a)

Additional data were collected to check previous results, extend the range of conditions, and include the scaling of brightness, and then used to test various models. Four observers took part in the scaling for collection of new data for a CIE illuminant D50 simulator at six different luminance levels. Analyses of the results showed that the Hunt model performed best overall. For lightness scaling, CIELAB performed nearly as well when the lowest luminance level was ignored. For colorfulness and hue scaling, the Hunt model performed substantially better than the Nayatani *et al.* model.

### Luo et al. (1993b)

In this part, they extended their experimental technique to the evaluation of transmissive media including both projected transparencies and transparencies viewed on light boxes. Between five and eight observers took part in these experiments, scaling lightness, colorfulness, and hue for a total of 16 different sets of viewing conditions. They found that the Hunt model did not perform as well as in previous experiments and proposed some changes that have been incorporated in the latest version of the model. CIELAB performed very well for these data, in fact better than the unmodified Hunt model. The Nayatani *et al.* model performed worse than both CIELAB and the unmodified Hunt model. The Hunt model with modifications based on the experimental data performed best overall.

### Luo et al. (1995)

The phenomenon of simultaneous contrast was specifically examined. Five or six observers scaled lightness, colorfulness, and hue of samples in systematically varied proximal fields presented on a CRT display. The

results showed that all three dimensions of color appearance are influenced by induction (as expected). Evaluation of the Hunt model (the only model capable of directly accounting for simultaneous contrast) showed that it did not perform well and required further modification.

Hunt and Luo (1994) summarize the first four parts of the LUTCHI experiments and how the results were used to refine the Hunt color appearance model. Overall, they show that the Hunt model predicts the hue results with CVs between 7 and 8 while the inter-observer variability CV is 8. For lightness, the model CVs range from 10 to 14 with the inter-observer variability of 13. For colorfulness, the model CVs are around 18 with inter-observer variability of 17. Thus they conclude that the Hunt model is capable of predicting the experimental results as well as the results from one observer would predict the mean. This is impressive, and certainly a good result, but it should be kept in mind that these data are not independent of the model formulation.

Many of the results of the LUTCHI experiments were also contributed to the efforts of CIE TC1-34 in order to allow the evaluation of more recent color appearance models and the formulation of CIECAM97s. The results of these analyses are described in Section 17.6. Unfortunately, the data themselves were deemed proprietary by the research sponsors and were not released for a number of years. Ultimately these data were made publicly available and used as one of the data sets for development of CIECAM02.

## 17.5 DIRECT MODEL TESTS

One way to overcome the limited precision of magnitude estimation experiments is to take advantage of more refined psychophysical techniques to evaluate model performance. One such technique involves paired comparison experiments in which observers view two stimuli at a time and simply choose which is better. The results are then analyzed using the law of comparative judgments to derive an interval scale and associated uncertainties. To evaluate color appearance models in this fashion, one must begin with an original stimulus (or image) in one set of viewing conditions and then calculate the corresponding stimulus (or image) for the second set of viewing conditions using each model to be tested. The observers then look at each possible pair of stimuli and choose which is a better reproduction of the original in its viewing condition. The interval scale results are then used to measure the relative performance of each model. The significant drawback of this approach is that the results cannot be used to derive new models and are limited to the models available and included at the time of the experiment. An extensive series of these experiments has been conducted at the Munsell Color Science Laboratory at Rochester Institute of Technology and summarized by Fairchild (1996). The results of these and other experiments are described below.

Fairchild and Berns (1993) described an early and simplified form of these experiments to confirm the utility of color appearance models in

cross-media image reproduction applications. They examined the transformation from prints viewed under either illuminant A or D50 simulators to CRT displays with a D65 white point and various backgrounds using a simple successive binocular viewing technique. Six different images were used and 14 observers took part in the experiment. Comparisons were made between no model (CIE XYZ reproduction), CIELAB, and RLAB. The results indicated that observers chose the RLAB reproduction as the best nearly 70% of the time, the CIELAB image about 30% of the time, and the XYZ image almost never. This result showed that a color appearance transformation was indeed required for these viewing conditions and that the RLAB model outperformed CIELAB.

Kim *et al.* (1993) examined the performance of eight color-appearance transformations for printed images viewed under different viewing conditions. Original prints were viewed under a CIE illuminant A simulator and reproductions calculated using the various appearance transformations were viewed under CIE illuminant D65 simulators at three different luminance levels. A paired-comparison experiment was completed and an interval scale was derived using the law of comparative judgments. A successive *Ganzfeld* haploscopic viewing technique (Fairchild *et al.* 1994) was used with 30 observers. The results showed that the Hunt, RLAB, CIELAB, and von Kries models performed similarly to one another and significantly better than the other models. The Nayatani *et al.* model performed worse than each of the above models. Three models performed significantly worse and were not included in further experiments. These included CIELUV, LABHNU2, and a proprietary model. The Nayatani *et al.* model performed poorly due to its prediction of the Helson–Judd effect resulting in yellowish highlights and bluish shadows in the reproductions. The Helson–Judd effect cannot be observed for complex stimuli under these viewing conditions. CIELUV and the others performed poorly due to their intrinsically flawed chromatic adaptation transformations.

Pirrotta and Fairchild (1995) performed a similar experiment using simple stimuli on gray backgrounds rather than images. The first phase of this study was a computational comparison of the various models in order to find the stimuli and viewing conditions for which the models differed the most such that the visual experiments could concentrate on these differences. It is useful to examine a few of these results. Figure 17.2 shows the CIELAB coordinates of corresponding colors under CIE illuminant A at 1000 lux for neutral Munsell samples of values 3, 5, and 7 viewed under CIE illuminant D65 at either 1000 or 10 000 lux. The points labeled F illustrate the incomplete adaptation predicted by the Fairchild (1991b) model used in RLAB. The points labeled N show the prediction of the Helson–Judd and Stevens effects incorporated in the Nayatani *et al.* model. The points labeled H show the prediction of the Stevens effect for the condition with a luminance change according to the Hunt model. Figure 17.2 illustrates the extreme prediction of the Helson–Judd effect for illuminant A according to the Nayatani *et al.* model. Figure 17.3 illustrates the wide range of corresponding color predictions for a 5PB 5/12 Munsell sample under the same viewing

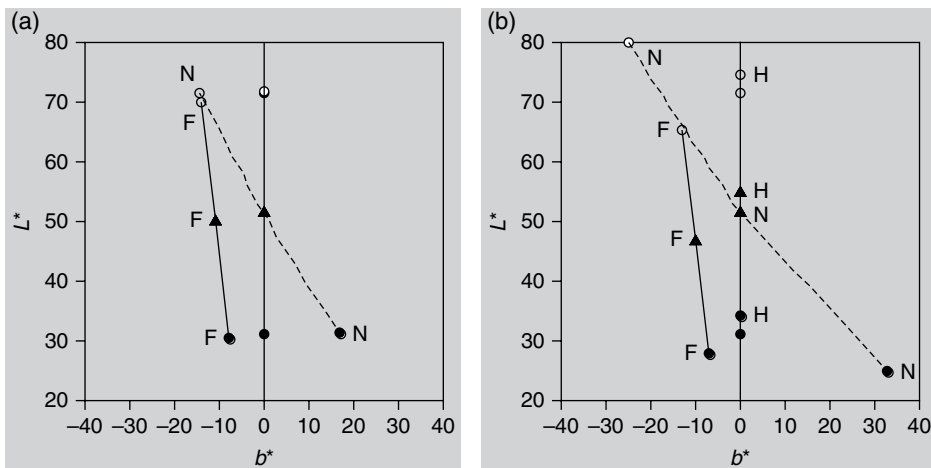


**Figure 17.2** Illustration of differences between predictions of various appearance models represented in the CIELAB  $L^*-b^*$  plane. Neutrals at (a) 1000 lux and (b) 10000 lux

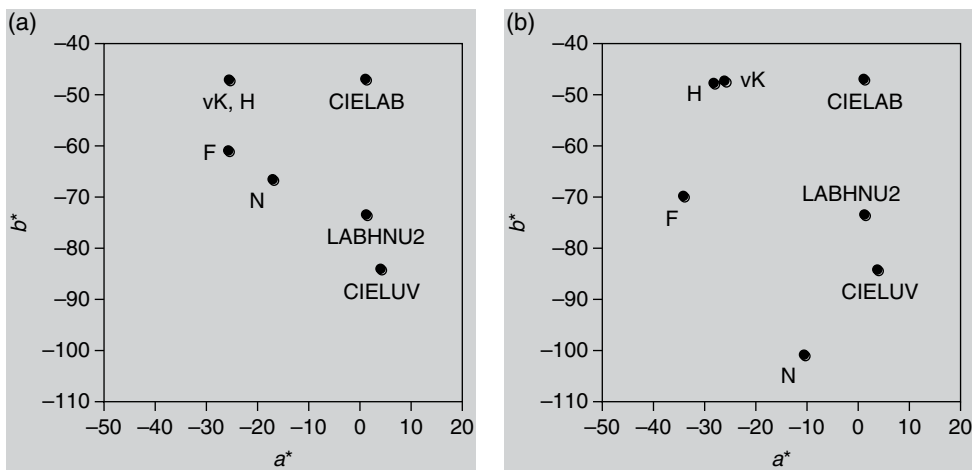


**Figure 17.3** Illustration of differences between predictions of various appearance models represented in the CIELAB  $a^*-b^*$  plane. 5PB 5/12 at (a) 1000 lux and (b) 10000 lux

conditions. One should note the extreme differences in the predictions of the various models as the scales of the plots in Figure 15.3 encompass 50 CIELAB units. The Pirrotta *et al.* (1995) visual experiment used a paired-comparison technique with 26 observers, 10 stimulus colors, and a change in viewing conditions from an illuminant A simulator at  $76 \text{ cd/m}^2$  to

an illuminant D65 simulator at 763 cd/m<sup>2</sup>. The results showed that the Hunt model performed best. Von Kries, CIELAB, and the Nayatani *et al.* model performed similarly to one another, but not as well as the Hunt model. CIELUV and the Fairchild (1991b) model performed significantly worse. These results led to the revision of the adaptation model incorporated in RLAB (Fairchild 1996).

Braun *et al.* (1996) investigated viewing techniques and the performance of color appearance models for changes in image medium and viewing conditions. They examined the reproduction of printed images viewed under CIE illuminant D50 and A simulators on a CRT display with a CIE illuminant D65 white point. Fifteen observers took part in this experiment using five different viewing techniques. It was concluded that a successive binocular viewing technique with a 60 second adaptation period provided the most reliable results. Interestingly, a simultaneous binocular viewing technique, common in many practical situations, produced completely unreliable results. The experiment utilized five different pictorial images with a variety of content. The result showed significant differences in the performance of each model tested. The order of performance from best to worst was RLAB, CIELAB, von Kries, Hunt, and Nayatani *et al.*

Fairchild *et al.* (1996) performed a similar experiment on the reproduction of CRT displayed images as projected 35 mm slides. The CRT display was set up with both illuminant D65 and D93 white points at 60 cd/m<sup>2</sup> and viewed in dim surround. The projected image had a 3900 K white point at 109 cd/m<sup>2</sup> with a dark surround. Fifteen observers completed the experiment with three different pictorial images. The RLAB model performed best, followed by CIELAB and von Kries with similar performance and then the Hunt model. The Nayatani *et al.* model was not included in the final visual experiments since it produced clearly inferior images due to its prediction of the Helson–Judd effect and the limited number of images that could be included in the experiment.

Braun and Fairchild (1997) extended the experiments of Braun *et al.* (1996) to a wide variety of viewing conditions. Ten different sets of viewing conditions were investigated using between 14 and 24 observers. The viewing conditions varied in white point, luminance level, background, and surround. Overall, the RLAB model performed best. For changes in white point, CIELAB and a von Kries transformation also performed well. The Hunt and Nayatani *et al.* models did not perform as well as those three. Similar results were obtained for changes in luminance level. For changes in background, the Hunt model performed poorly, apparently because it over-predicted the effect for complex images. The models that did not account for changes in background performed better. This result was as expected since the background of an image does not coincide with what is normally considered the background of a stimulus (*i.e.*, an image element). For changes in surround, RLAB performed worst with the Hunt model performing poorly as well. These were the only two models that accounted for the surround change and, while they were predicting the correct trend, both models over-predicted the effect for these viewing conditions.

Braun and Fairchild (1997) extended the corresponding colors experiment described in Section 17.3 by including the results of the image matching technique in a paired comparison experiment with other color appearance models. In this research, a paired comparison experiment was carried out that included model predictions as well as the matching images generated by the observers, and statistical linear transformations between white points derived from the match data. Five observers took part in the image matching experiment and 32 were used in the paired-comparison experiment. The results showed that the RLAB model produced a matching image that was as good as the image produced by observers and the statistical models. The CIELAB, von Kries, and Hunt models did not perform as well as RLAB.

Lo *et al.* (1996) and Luo *et al.* (1996) presented the results of paired comparison experiments for the reproduction of printed images on CRT displays. They evaluated five different changes in white point at constant luminance using 9–18 observers. The results show that the CIELUV model performs significantly worse than all of the other models tested. The other models performed similarly to one another, with the LLAB model performing slightly better for adaptation from illuminant A to illuminant D65.

There are other similar experiments that have been more recently completed or are underway in a variety of laboratories. The results of these ongoing experiments and those described above have been used by various CIE committees in the formulation, testing, and revision of color appearance models. To date this type of research has validated the CIE models as consistently among the best, if not the best, for various applications.

## 17.6 COLORFULNESS IN PROJECTED IMAGES

Based on the theory and implementation of color appearance models, manipulation of the white point luminance relative to other stimuli in a projected image (perceived as a uniform scene in terms of adaptation) should have very significant effects on color appearance. This theory can be rather easily tested using DLP-based digital video projectors with four-segment (red, green, blue, and white) filter wheels. These projectors are designed with the fourth, white, channel to provide additional luminance in applications such as business presentations where the room lighting might be on. Unfortunately, that additional white luminance comes with no increase in the luminance of the RGB primaries, and this change in relative luminance would suggest, according to color appearance models, that the display colorfulness is reduced despite the increase in luminance.

Heckaman *et al.* (2005) and Heckaman and Fairchild (2006a,b) tested this theory through psychophysical scaling of display colorfulness, and other appearance attributes, for various relationships between the luminance of display white and the luminance of the display color primaries. Their results confirmed both the theory that an increase in adapting white luminance relative to a color stimulus luminance decreases perceived colorfulness (thus a brighter display with a fourth white channel might well look less colorful

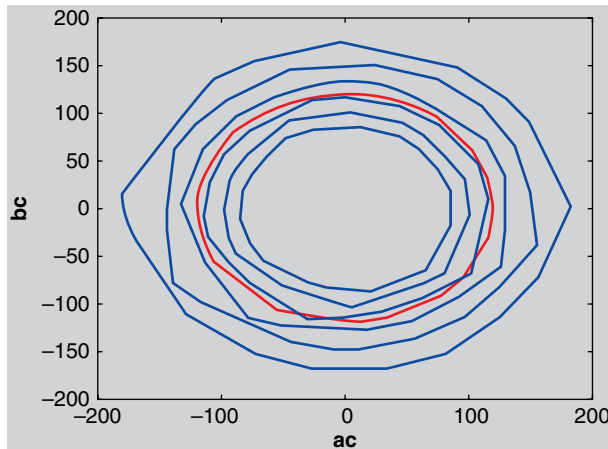


**Figure 17.4** Illustration of the creation of appearance gamuts more colorful than stimuli on the spectrum locus. The various blue contours show the boundary of the chroma gamut in CIECAM02 for various white point luminance levels relative to the display primary luminance levels. The red contour shows the perceived chroma of the spectrum locus for normal viewing conditions

despite increased luminance) and the practice that predictions of the CIECAM02 color appearance model correlated very well with observed results.

An additional, and fascinating, prediction of the Heckaman *et al.* results was that appearances equivalent to stimuli outside the spectrum locus could be produced by a properly designed display (Fairchild 2008b). Such a display would be required to have a diffuse white luminance substantially lower than that sum of the luminances of the RGB primaries (the opposite of a RGBW DLP projector). The resulting display would not only be able to produce stimuli “apparently” outside the spectrum locus of physically realizable colors, but it would be a HDR display in the sense that there would be white luminance at levels beyond diffuse white that could be used to display light sources, highlights, etc. This prediction was verified computationally with CIECAM02 (Figure 17.4) and then produced experimentally in a controlled setting. It was also possible for the authors to manipulate a slideshow in luminance through the course of a 20-minute presentation to allow the effect to be demonstrated in a darkened room. Li *et al.* (2011) showed related results on the trade-off between luminance and colorfulness in display primaries.

## 17.7 MUNSELL IN COLOR APPEARANCE SPACES

Color appearance models, scales, or spaces, can be quantitatively evaluated or inter-compared by plotting selected color samples from color order systems such as Munsell or NCS. This is a very important, but underutilized, technique for several reasons. Among them are that these color order

systems provide visual data that are often carefully collected with significant numbers of observers. These data have also been standardized, so they are available to any researchers in identical form. They are also sampled such that they systematically represent attributes of color appearance. While qualitative plots of Munsell and NCS samples are often seen, the data are ripe for more quantitative testing and comparison of models and should be used that way.

Even if the Munsell data are not perfect representations of lightness, chroma, and hue, they are a well-characterized set of reference colors available in numerical and physical forms that can be used to compare models. Wyble and Fairchild (2000) provide one example of such an inter-comparison of models based on Munsell and using a variety of visualization techniques and quantitative assessments. Figure 17.5 illustrates just one small example from that work, the lightness predictions of just four appearance models. Even with this small example, it can be easily seen that two models predict surround effects, while the other two do not, and that the lightness scales of the models vary in small, but meaningful, ways. This can be more edifying than plotting vs luminance since they all tend to look alike in that case (compressive power functions). Starting in lightness (value) takes into account the main visual effect, compressive nonlinearity, and allows easier comparison of subtle differences between the models.

## 17.8 CIE ACTIVITIES

It is certainly difficult to digest all of the above results and come up with a single answer to the question of which color appearance model is best or which should be used in a particular application. There are too many experimental variables in addition to ongoing refinement of the models to draw conclusions from the literature alone. These are some of the reasons why there are a large number of published appearance models and no international consensus on a single model for various applications. The CIE addresses these issues through the activities of its technical committees and reporterships as described below.

### TC1-34, Testing Colour-Appearance Models

CIE Technical Committee 1-34, Testing Colour-Appearance Models, was established to evaluate the performance of various models for the prediction of color appearance of object colors. TC1-34 published guidelines for coordinated research on testing color appearance models (Fairchild 1995a) that outline its plan of work with the intention of motivating researchers to perform additional model tests. In addition, TC1-34 collected various sets of data and test results and completed additional tests. Those results were

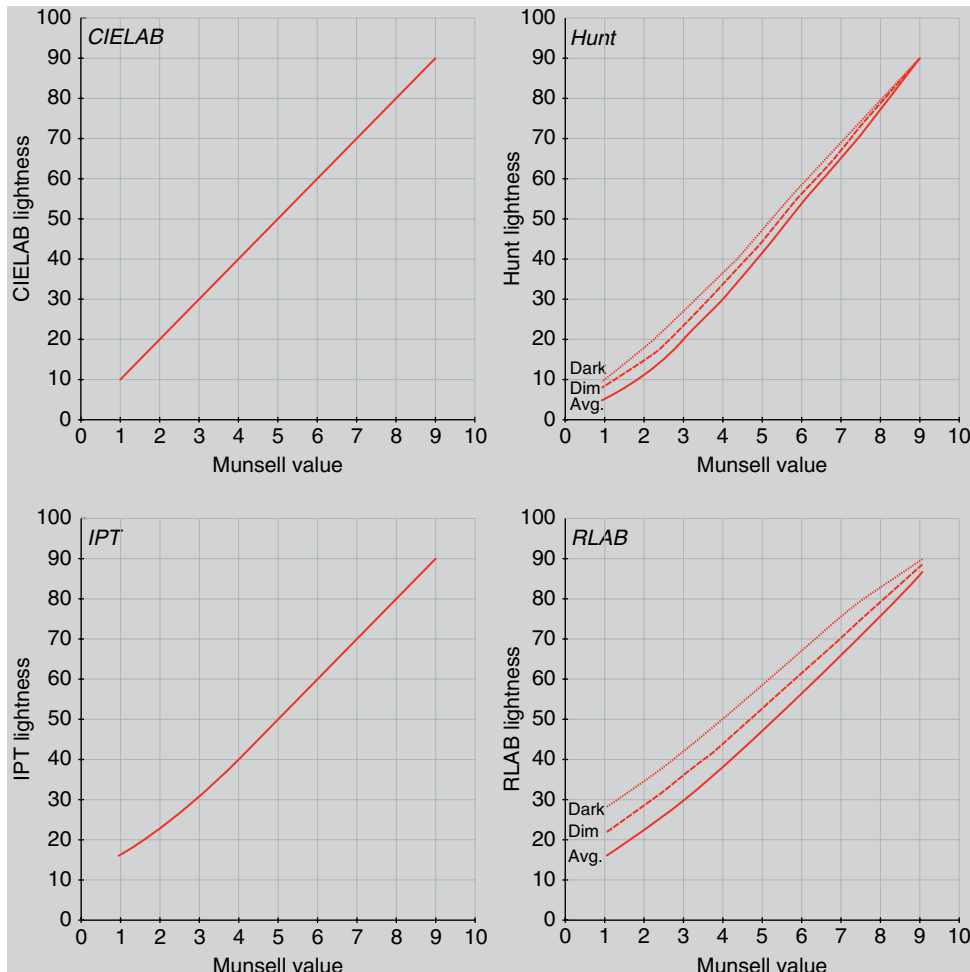


**Figure 17.5** Examples of the comparative prediction of the neutral Munsell value scale by various color appearance models. Plots on the left illustrate models with no surround dependency (CIELAB and IPT) while plots on the right show two models (Hunt and RLAB) that have dependencies on surround relative luminance

never published in a CIE technical report on the committee's progress due to disagreements within the committee on interpretation of the results. A summary of the additional TC1-34 analyses on the CSAJ, LUTCHI, and RIT experiments discussed previously follows. Ultimately, CIE TC1-34 was assigned the task of formulating a CIE color appearance model. That task was completed with the creation and publication of CIECAM97s (see Chapter 15 and CIE 1998).

The TC1-34 analyses of the CSAJ data included calculations of RMS deviations in CIELAB space for the chromatic adaptation, Stevens effect, and Hunt effect data. For the chromatic adaptation data, the Hunt, RLAB,

and CIELAB models perform similarly to one another and better than the others. They are followed, in order of performance, by the Nayatani *et al.*, LABHNU, and CIELUV models. For the Stevens effect data, the Hunt model performs best, followed by RLAB, CIELAB, LABHNU, and CIELUV, which perform identically since they predict no effect. The Nayatani *et al.* model performs worst since it over-predicts the effect. For the Hunt effect data, the Hunt model performs best, the Nayatani *et al.* next, followed by the models that do not predict any effect (RLAB, CIELAB, LABHNU, and CIELUV).

Additional analyses of the LUTCHI data contributed to CIE TC1-34 show that the Hunt model performs best, followed by RLAB, CIELAB, and then finally the Nayatani *et al.* model. The TC1-34 summary of the RIT direct model tests shows differing results for images and simple stimuli. For images, the Hunt, CIELAB, and RLAB models perform similarly and best, followed by Nayatani *et al.* and LABHNU in a tie, and then by CIELUV with the worst performance. For simple stimuli, the Hunt model performed best, the CIELUV model worst, and the others performed similarly in between those two. An overall ranking of the TC1-34 analyses results in the following ordering of model performance: Hunt, RLAB, CIELAB, Nayatani *et al.*, LABHNU, and CIELUV. Analyses of the LLAB model for all of the data have not been completed, but it performs better than the Hunt model for the LUTCHI data and is likely to also do well on the other data.

CIE TC1-34 concluded that no one or two of the published color appearance models could be recommended for general use. There were a variety of reasons for this. One of the most significant was that the models were still evolving and more tests were required to make strong conclusions. To this end, TC1-34 turned formulating a CIE color appearance model that incorporated the best features of the published models while avoiding their various pitfalls. That model, CIECAM97s, was recommended by the CIE for general use to promote uniformity of practice and further evaluation to promote the future development of an even better model. Ultimately this work led to the formulation of CIECAM02. TC1-34 was disbanded successfully after the publication of CIECAM97s.

## TC1-27, Specification of Colour Appearance for Reflective Media and Self-Luminous Display Comparisons

CIE Technical Committee 1-27 was established to evaluate the performance of various color appearance models in CRT-to-print image reproduction. TC1-27 has also published a set of guidelines for coordinated research (Alessi 1994). The various experiments of Braun *et al.* and Lo *et al.* described in Section 15.5 represent contributions to the activities of TC1-27. Additional experiments are being carried out in three or four other laboratories that will be contributed to TC1-27. This committee worked in conjunction with CIE TC1-34 with respect to the evaluation of CIECAM97s.

## TC1-33, Color Rendering

As described in Chapter 18, the CIE procedure for calculating a color rendering index for light sources is based on an obsolete color space. CIE Technical Committee 1-33 was established to formulate a new procedure for calculating a color rendering index for light sources. There are two aspects to this problem. The first is the specification of a calculation procedure and the second is the selection of a color space in which to do the calculations. A color appearance model is necessary since color rendering indices must be compared for light sources of various colors. TC1-33 developed new procedures and published a closing report (CIE 1999) but did not arrive at a new recommendation.

## TC1-52, Chromatic Adaptation Transform

TC1-52 was established to formulate a chromatic adaptation transform that could be used independent of a given color appearance model. It collected and evaluated various data sets and transforms but failed to come to a single recommendation since multiple models performed equivalently. The most logical choice, to simply use the chromatic adaptation transform in CIECAM02, could not be agreed upon by the committee. A final report of the TC1-52 analyses and results was published (CIE 2004b).

## R1-24 Colour Appearance Models

Upon closure of TC1-34, CIE Division 1 assigned a reporter on color appearance models. The task of a reporter is to keep track of developments in a technical area and make recommendations to the CIE if it appears that a new TC should be formed. This reportership was concluded since all of the relevant CIE activity on color appearance models was taking place in TC8-01 and it was reaching conclusion by publishing a new model, CIECAM02.

## TC8-01, Colour Appearance Modeling for Colour Management Applications

TC8-01 has been a very productive technical committee and ultimately created the latest CIE color appearance model, CIECAM02 (see Chapter 16 and CIE 2004a). The committee also performed a variety of model tests that are summarized in a number of papers including those by Fairchild (2001), Li *et al.* (2002), and Moroney (2002). TC8-01 has completed its activities and closed successfully.

## TC8-04, Adaptation Under Mixed Illumination Conditions

The work of TC8-04 examines techniques to estimate the state of chromatic adaptation when multiple illumination conditions exist (*e.g.*, a self-luminous display in an office environment that has illumination of a different color than the display white point). A technical report, CIE 162:2010 was published in 2010 that provides some practical guidance for appearance predictions in such situations.

## TC8-08, Testing of Spatial Colour Appearance Model

One future direction for color appearance models is more systematic and automatic modeling of the spatial properties of human vision. This is conceptually described in Chapter 20. TC8-08 was formed in 2003 to make recommendations on how to best psychophysically evaluate such models for applications such as the rendering of HDR images. The committee concluded that it was premature to perform such testing and disbanded.

## R8-05 Image Appearance

Related to spatial appearance models is the new general class of models referred to as image appearance models (Chapter 20). A reportership was established in 2003 to monitor progress in this new field and make recommendations for the formation of a TC if progress warrants CIE consideration for recommending a single model. It is not expected that these models would reach the level of a CIE recommendation for many years. It is reasonable to say that the state of image appearance models in 2003 was similar to the state of color appearance models 20 years earlier and little progress has been made in the last decade. The reportership was terminated with no technical committee formed.

## R8-06, Results of CIECAM02

With the successful closure of TC8-01, a new reportership has been established to monitor the application and testing of CIECAM02 and make recommendations for the creation of a new TC should the published results indicate need to investigate further improvements in color appearance modeling. There are no immediate indications that revisions to CIECAM02 will come as quickly as those to CIECAM97s. The mathematical limitations of CIECAM02 in some situations have resulted in the creation of TC8-11 however.

## TC8-11, CIECAM02 Mathematics

This committee was formed “to investigate the improvements of the CIECAM02 model to avoid mathematical inconsistencies.” It is working on optimizations of the CIECAM02 CAT matrix and cone nonlinearity functions to alleviate mathematical issues with negative tristimulus values and potentially propose an alternative model as described in the Chapter 16.

## TC1-75, a Comprehensive Model of Colour Appearance

The terms of reference of this committee are “to derive colour appearance models that include prediction of the appearance of coloured stimuli viewed in typical laboratory conditions: that appear as unrelated colours that are viewed under illumination down to scotopic levels that include consideration of varying size of stimulus.” Its work will focus on extensions to CIECAM02 as described in the terms of reference and in suggestions such as the CAM02-UCS.

## TC1-76, Unique Hue Data

This committee will “study and report on unique hue data, including an analysis of the scatter of those data: this to include practical viewing conditions.” Its formation is based on some recent work that suggests that the precision of unique hues, at least in terms of inter-observer variability, might be larger than previously assumed. (Kuehni *et al.* 2010, Shamey *et al.* 2010, 2011).

## 17.9 A PICTORIAL REVIEW OF COLOR APPEARANCE MODELS

No sets of equations or lists of RMS deviations or CV can truly communicate the differences among the various color appearance models. To appreciate these differences, it is useful to view images that have been calculated using the various models. Figure 17.6, Figure 17.7, and Figure 17.8 illustrate the predictions of various historical models (Fairchild and Reniff 1996). While the models included are now somewhat out of date, the images still provide useful context in comparing the various formulations. These figures cannot be generally used to indicate which models are best. They should just be considered a display of the relative performance of the various models for these types of predictions. With such a consideration in mind, the viewing conditions for these figures are not critical (although a high-luminance, D65 simulator would be ideal). Figure 17.6 illustrates the images viewed under illuminant D65 that would be predicted as matches to an original image viewed under CIE illuminant A for 14 different color



**Figure 17.6** Comparison of the predictions of various appearance models for change in chromatic adaptation from illuminant A to illuminant D65. Original image data represent reproduction of tristimulus values with no adjustment for adaptation. Original images: *Portland Head Light*, Kodak Photo Sampler PhotoCD, ©1991, Eastman Kodak; *Picnic*, Courtesy Eastman Kodak; Macbeth ColorChecker® Color Rendition Chart

models. The models include CIE XYZ to illustrate the original image, CIELAB, CIELUV, LABHNU2 (Richter 1985), von Kries, spectrally sharpened von Kries (Drew and Finlayson 1994), ATD, Nayatani *et al.*, Hunt (discounting), Hunt (no discounting), Hunt (incomplete adaptation, no Helson-Judd effect), RLAB (discounting), RLAB (partial discounting), and RLAB (no discounting).

There are several features to note in this set of images:

- The XYZ image shows a rendering of the original illuminant A image data with no adaptation model.
- The hard-copy versions of RLAB and Hunt are very similar to the von Kries model in this situation. These produce what have been found to be generally the best results in experiments completed to date (prior to CIECAM02).
- The LLAB model produces more saturated reddish hues due to the characteristics of its “cone responses” and a bluish hue shift due to its nonlinear adaptation model for the blue channel.
- CIELAB produces hue shifts (in comparison with von Kries *et al.*), particularly noticeable in the sky and grass colors, due to its “wrong von Kries” adaptation model.
- Incomplete adaptation can be noted by the yellowness of the RLAB soft-copy image, along with the intermediate level of adaptation in the RLAB slide image.
- The Hunt soft-copy image includes the Helson–Judd effect (yellow highlights and blue shadows), which can be seen even more strongly in the Nayatani *et al.* image.
- The Hunt slide image is more similar to the RLAB soft-copy image.
- The ATD model also predicts incomplete levels of adaptation due to the nature of its formulation that treats stimuli in a more absolute, rather than relative, sense.
- The spectrally sharpened von Kries transform produces highly saturated reddish hues. This is to be expected from the “color-constancy preserving” nature of sharpened responsivities.
- The CIELUV and LABHNU2 models produce unusual hue shifts due to their subtractive adaptation models. In fact, they produce predictions outside the gamut of physically realizable colors if a D65-to-A transformation is performed rather than the A-to-D65 transformation illustrated.

Figure 17.7 illustrates the changes predicted for changes in adapting luminance from  $100\text{cd/m}^2$  to  $10000\text{cd/m}^2$  with a constant D65 white point. These predictions are presented for the models with luminance dependencies (ATD, LLAB, Nayatani *et al.*, Hunt, and RLAB) in addition to a single image representing all of the other models. The original image was “gamut compressed” to allow all of the model predictions to remain within gamut. The RLAB model has very little luminance dependency and therefore produces an image very similar to the original. The Hunt and Nayatani *et al.* models produce images of lower contrast. This is to be expected according to the Hunt and Stevens effects. These low-contrast images would appear to be of higher contrast when viewed at a high luminance level. The Nayatani *et al.* model predicts a larger luminance-dependent effect than the Hunt model. The ATD model makes the opposite prediction. Since it is based on absolute rather than relative signals, the ATD model predicts that a brighter, higher contrast image will be required at the higher luminance levels. This prediction is incorrect.

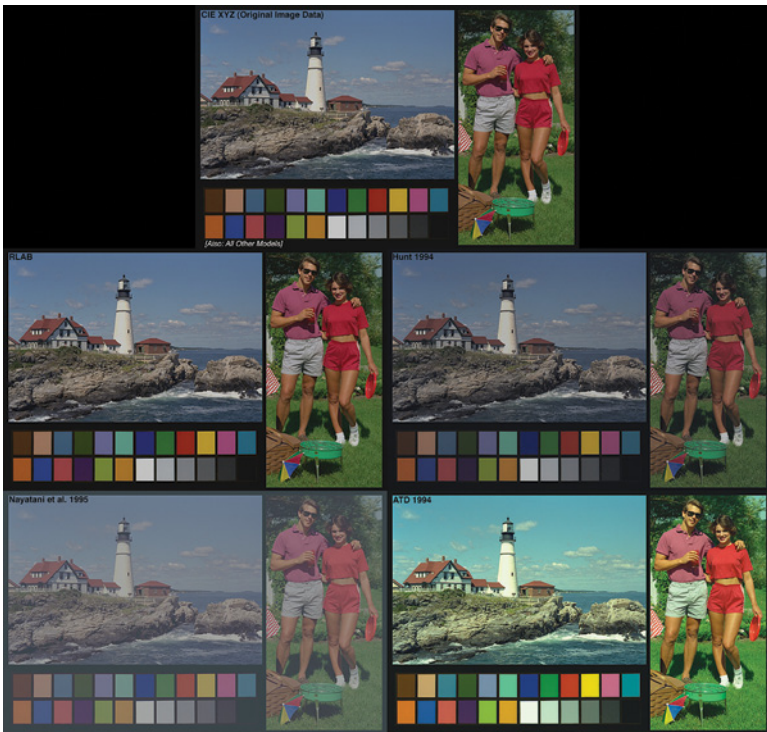


**Figure 17.7** Comparison of the predictions of various appearance models for change in luminance from illuminant D65 at 100 cd/m<sup>2</sup> to illuminant D65 at 10 000 cd/m<sup>2</sup>. Original image data represent reproduction of tristimulus values with no adjustment for luminance and therefore the predictions of all models that do not account for luminance level changes. See Figure 17.6 caption for image credits



**Figure 17.8** Comparison of the predictions of various appearance models for change in surround relative luminance from illuminant D65 with an average surround to illuminant D65 with a dark surround. Original image data represent reproduction of tristimulus values with no adjustment for surround and therefore the predictions of all models that do not account for surround changes. See Figure 17.6 caption for image credits

Figure 17.8 shows predictions for a change in surround from average to dark at a constant D65 white point for the surround-sensitive models (LLAB, Hunt, and RLAB) in addition to a single image representing all of the other models. All three models illustrate the increase in contrast required for image viewing in a dark surround. The LLAB and RLAB models have similar predictions, with the RLAB model predicting a bit stronger effect than the LLAB model. The Hunt model uses functions with additive offsets to predict the surround-dependent contrast changes. These offsets force some dark colors to have predicted corresponding colors with negative tristimulus values. Since this is physically impossible, pixels with such colors have been mapped to black. This illustrates one practical limitation of using the Hunt model for changes in surround.

# 18

# Traditional

# Colorimetric

# Applications

---

Given all of the effort put into the formulation, evaluation, and refinement of color appearance models, it is natural to wonder if they have practical application beyond the natural scientific curiosity that has driven much of the historical, and ongoing, research on color appearance phenomena. In recent decades, it has been the development of technology, and thus applications, that has really pushed the scientific investigation of color appearance and development of models. These applications can be divided into two general categories:

1. Image reproduction, which is the subject of Chapter 19.
2. The area of color measurement and specification, the subject of this chapter.

Colorimetry has steadily evolved over the past century. For many applications, simple tristimulus (XYZ) colorimetry or CIELAB-type color difference specifications are sufficient. However, there are some applications in the traditional fields of colorimetry that require further evolution. A few of these are discussed in this chapter.

## 18.1 COLOR RENDERING

*Color rendering* refers to the way in which various light sources influence, or “render,” the color appearance of objects. For example, it is possible for two light sources to be of the same color while one is a natural daylight and



**Figure 18.1** A simulation of color rendering of two white sources. The upper image represents typical color rendering under natural daylight and the lower image simulates rendering under a white made from a mixture of relatively narrow-band blue and yellow as might be found in an LED source. (Note: White LEDs with much better rendering can be made from combinations of red, green, and blue LEDs.)

the other is a fluorescent source made up of two narrow-band phosphors that happen to add together to make the same white. (Or more common today, white LED light sources are created from the combination of a blue LED and a yellow phosphor. This is still much different from a natural daylight, or incandescent light, spectrally.) While the color of the two sources will match, the appearances of objects illuminated by these two sources will differ tremendously. Figure 18.1 illustrates this situation pictorially. This phenomenon is obviously important in the engineering of artificial illumination and the choice of light sources for various installations. If illumination was specified strictly on its efficiency, or its efficacy, the appearance of objects in our environment would be quite disturbing. To aid in this

**Table 18.1** Example values of typical color rendering indices

Source	$R_a$
Tungsten halogen	100
Illuminant D65	100
Xenon	93
Daylight fluorescent	92
Metal halide	90
RGB LED	90
Triband fluorescent	85
Phosphor LED	80
Cool white fluorescent	58
Mercury vapor	45
High-pressure Sodium	25
Low-pressure Sodium	-40

application, the CIE has defined a color-rendering index as a measure of the quality with which a light source renders the colors of objects.

## Current Techniques and Recommendations

The current CIE recommended techniques for calculation of color rendering indices are described in CIE Publication 13.3 (CIE 1995a). Light sources are evaluated relative to reference illuminants, which are defined to be the CIE D-series of illuminants for CCTs greater than or equal to 5000K and Planckian radiators for CCTs less than 5000K. The reference illuminant is chosen such that it has the same CCT as the test source. Differences in color between the test source and reference illuminant are accounted for using a von Kries-type chromatic adaptation transform. The CIE technique defines a special color rendering index according to Equation 18.1.

$$R_i = 100 - \Delta E_i \quad (18.1)$$

The color difference calculation,  $\Delta E_i$ , is based on the Euclidean distance between the color of the sample under the test and reference sources in the now obsolete CIE  $U^*V^*W^*$  space. A general color rendering index,  $R_a$ , is defined as the average of the special color rendering indices for eight specified Munsell samples. Examples of general color rendering indices for various light sources are given in Table 18.1. It should be noted that the values in Table 18.1 are typical of the type of illumination, but significant variation is possible. For example, difference phosphor and LED combinations can be used in solid-state lighting systems to produce phosphor-based LEDs with a wide variety of colors and color rendering indices. Also, the color rendering index only informs us of the fidelity of color rendering for certain objects and not the observer preference for a given color rendering situation.

## Application of Color Appearance Models

The fundamental question in the specification of color rendering properties of light sources is the specification of the appearance of colored objects under different light sources. In some cases, it is necessary to compare the appearance of objects under sources of different colors. It might also be of interest to compare the rendering properties of sources at different luminance levels. To make comparisons of color appearance across changes in illumination color and luminance level, an accurate color appearance model is required. Thus, given appropriate standard references, one would be able to compare the quality of color rendering of a tungsten source with that of a daylight source and have meaningful results. Interesting work has shown that certain objects carry more weight in color rendering or color quality judgments than others, and color appearance models could aid in implementing such object-based weighting. For example, Rea *et al.* (1990) showed the importance of viewing one's own skin under the illumination in question in making reliable judgments of color rendering, and Fairchild (1992b) reported similar results for stability of chromatic adaptation.

## Future Directions

While there is certainly room for improved measures of color rendering based on an accurate color appearance model, the current status of color appearance models precludes a large change in the capabilities of an index. This situation is further exacerbated by the rapid adoption of solid-state lighting and the ability to create spectra for which the color rendering index does not correlate customer preferences. CIE Technical Committee 1-33, Colour Rendering, proposed some revised procedures for the specification of color rendering. The first step was to define a new procedure for calculation, independent of the color space used.

That procedure, using the CIELAB color space combined with an improved chromatic adaptation transform (originally the Nayatani *et al.* nonlinear transform was considered, but the CAT02 transform would be a better current solution), would be an improvement over the current color rendering index. Unwillingness to change in the lighting industry (due to optimization of current lighting systems to the original CRI standard) has made it extremely difficult for any improvements to be adopted. Currently, CIE TC1-69 is working to create a new set of procedures for assessing color rendering that are based on the Color Quality Scale (CQS) developed at the US NIST. While the CQS is certainly more sound scientifically than the current CRI, it is difficult to institute a change in the lighting industry.

With the current type of color rendering index, in which sources are only compared with a standard illuminant of the same CCT, the color appearance model is not being used for a large change in chromatic adaptation. Thus it is doubtful whether any color appearance model would be significantly better than any other, including CIELAB, for this calculation. Only when a



**Figure 18.2** A pair of images illustrating the concept of “gamut area index” in color rendering. The lower image illustrates a light source that renders objects with a much larger gamut area than the upper image. Again, both light sources are equivalent white lights in terms of their own color and luminance

more sophisticated technique for specifying color rendering across large changes in light source, color, and/or luminance level is formulated will a more complicated color appearance model be required.

Li *et al.* (2011, 2012a) have shown the advantage of using the CIECAM02 color appearance model in the computation of a color rendering index. Rea *et al.* (2008) described the utility of a “gamut area index” (GAI) in addition to a color rendering index to specify lighting quality. The GAI basically specifies the colorfulness of object rendering under a given light source (Figure 18.2). Using two metrics to evaluate the illumination provides more information and users can determine which, or which combination, is more appropriate. It seems clear that multiple metrics are needed to tackle all aspects of this problem, and these various dimensions

of information should be provided to lighting specifiers and end users to allow them to make their best choices. Given that these metrics are ultimately printed on a light-bulb box and that only the final user knows what will be illuminated, low precision is needed to address this problem, so the answer is in having multiple descriptions of the illumination quality to allow the end user to take advantage of the one that works best for their situation.

Not unrelated to color rendering questions are desires to scale the appearance of specific objects that are found, for example, in whiteness indices (Katayama and Fairchild 2010) and the appearance of soil samples (Sánchez-Marañón *et al.* 2011) which has been one long-standing use of the Munsell system (Landa and Fairchild 2005).

## 18.2 COLOR DIFFERENCES

The measurement of color differences has wide application in a variety of industries. Such measurements are required to set and maintain color tolerances for the production and sale of all colored materials. Ideally, one would be able to take a metric of color difference, such as CIELAB  $\Delta E_{ab}^*$ , and consider it as a ratio scale of perceived color differences. This would require that color differences of the same perceived magnitude have the same  $\Delta E_{ab}^*$  for all areas of color space. Another requirement would be for the perceptions of color differences to scale linearly with measured  $\Delta E_{ab}^*$ . A third desirable feature would be for  $\Delta E_{ab}^*$  values measured under one illuminant to be perceptually equal to  $\Delta E_{ab}^*$  values measured under any other illuminant such that color differences could be directly compared across different light sources. It has been well established that the CIELAB color space is not uniform for the measurement of color differences and does not meet any of the above requirements. In fact, this might not be possible in any Euclidean color space.

### Current Techniques and Recommendations

The weaknesses of the simple CIELAB  $\Delta E_{ab}^*$  formula have been addressed both within and outside CIE activities. For example, the CMC color difference formula is designed to address some of the non-uniformities in the CIELAB space in order to make color difference measurements in one region of color space equivalent to measurements in other regions of color space. CIE Technical Committee 1-29 investigated the CMC and other equations as possible refinements of the CIELAB  $\Delta E_{ab}^*$  formula. They concluded that the CMC color difference equation was more complex than warranted by the available visual data, and they created a simplified formula known as CIE  $\Delta E_{94}^*$  (CIE 1995). The  $\Delta E_{94}^*$  equations are specified in Equations 18.2 through 18.5.

$$\Delta E_{94}^* = \left[ \left( \frac{\Delta L^*}{k_L S_L} \right)^2 + \left( \frac{\Delta C_{ab}^*}{k_C S_C} \right)^2 + \left( \frac{\Delta H_{ab}^*}{k_H S_H} \right)^2 \right]^{1/2} \quad (18.2)$$

$$S_L = 1 \quad (18.3)$$

$$S_C = 1 + 0.045C_{ab}^* \quad (18.4)$$

$$S_H = 1 + 0.015C_{ab}^* \quad (18.5)$$

$C_{ab}^*$  in Equations 18.4 and 18.5 refers to the CIELAB chroma of the standard sample of the color difference pair or, alternatively, to the geometric mean of the two chroma values. Parametric factors,  $k_L$ ,  $k_C$ , and  $k_H$ , are introduced to correct for variation in perceived color difference caused by certain experimental variables such as sample size, texture, separation, etc. Under reference conditions the parametric factors are all set to 1.0. Reference conditions are defined as follows:

*Illumination:* CIE illuminant D65 Simulator

*Illuminance:* 1000 lux

*Observer:* Normal color vision

*Viewing mode:* Object

*Sample size:* Greater than 4° visual angle

*Sample separation:* Minimal, direct edge contact

*Color difference magnitude:* 0 to 5 CIELAB units

*Structure:* Visually homogeneous.

The reference conditions of the  $\Delta E_{94}^*$  equations illustrate the limitations of the CIELAB space for the specification of color appearance. These are the areas in which it might be possible for a color appearance model to make a contribution to the specification of color differences. More recently (CIE 2001) the CIE has recommended a substantially more complex, empirical color difference equation based upon the CIELAB color space, referred to as DE2000. The DE2000 equation could legitimately be considered complex, with unreasonable implied precision, for the available perceptual data. Thus, the  $\Delta E_{94}^*$  equations are often a more practical and reasonable choice.

## Application of Color Appearance Models

In the area of color difference specification, color appearance models could be used to incorporate some of the parametric effects directly into the equation. For example, an accurate color appearance model could incorporate the effects of the background and luminance level on color difference perception. A color appearance model would also make it possible to directly compare color differences measured for different viewing conditions. This has applications in the calculation of indices of metamerism, as described below. Color appearance models would also make it possible to calculate color differences between a sample viewed in one condition and a second sample viewed in another different condition. This could be useful for critical colors such as those on warning signs or corporate trademarks.

It is reasonable to expect that a color difference equation could be optimized in a color appearance space, like CIECAM02, with performance equal to, or better than, equations like  $\Delta E_{94}^*$  and DE2000. Li *et al.* (2003) have shown this to be the case and formalized their proposal as CAM02-UCS (Li *et al.* 2006), which is discussed further in Chapter 16. Oleari *et al.* (2011) have described a different approach to the problem that does not rely on the CIECAM02 model.

## Future Directions

Currently there is little activity aimed at incorporating color appearance models beyond CIELAB into practical color difference specification. Perhaps this is because of the effort already invested in fine-tuning CIELAB within various industries. Instead, research activity (which is not abundant) is aimed at further refining equations within CIELAB, such as DE2000 and  $\Delta E_{94}^*$ , and defining the influence of parametric effects such as gloss, texture, sample separation, sample size, etc. Also, the majority of effort in the formulation of color appearance models has been in the area of chromatic adaptation transforms, and little attention has been paid to color difference specification within the color appearance spaces. The notable historical exception is the formulation of the LLAB space (Luo *et al.* 1996) in which color appearance and color difference were treated simultaneously and the recent efforts by Luo *et al.* (2003) to derive similar equations in CIECAM02 that have lead to CAM02-UCS. Also, the RLAB space (Fairchild 1996) was formulated to preserve the CIELAB spacing such that CIE color difference formulas such as  $\Delta E_{94}^*$  could still be used.

Another interesting future direction for color difference specification is the incorporation of the spatial characteristics of human visual performance into the difference metric such that the relative sensitivity to color variations of various spatial frequencies is appropriately treated. Examples of this type of metric can be found in the work of Maximus *et al.* (1994), Zhang and Wandell (1996), and Johnson and Fairchild (2003). Chapter 20 discusses future directions for these ideas.

## 18.3 INDICES OF METAMERISM

*Metamerism*, the fact that two stimuli can match in color while having disparate spectral power distributions, is both a great benefit and severe detriment to a variety of industries. Techniques to quantify the degree of metamerism for various stimuli are of significant value. There are two types of metamerism to be measured:

1. Illuminant metamerism
2. Observer metamerism.

Measures of the degree of metamerism for specific stimuli are called *indices of metamerism*.

*Illuminant metamerism* is generally of most concern. It occurs when two objects match in color for one illuminant, but mismatch for a second illuminant. This happens when the spectral reflectance functions of the two stimuli differ, but those differences are unimportant with respect to the visual response functions (color matching functions) when integrated with the spectral power distribution of the first illuminant. When the illuminant is changed, these differences might become apparent to an observer. Illuminant metamerism is often a problem in industries that produce colored materials. If they produce two materials that are a metamer match to one another, they might mismatch under some practical viewing conditions. If the two materials are an identical match, meaning their spectral reflectance functions are identical, then they are not metamer and will match for any illuminant.

*Observer metamerism* is more difficult to quantify, but perhaps equally important. It is caused by the normal variations in the color responsivities of various observers. Observer metamerism is defined by two stimuli with differing spectral power distributions that match for a given observer. When these stimuli are examined by a second observer, they might no longer match. Again, stimuli that are identical spectral matches will match for any observer. Thus, illuminant metamerism becomes apparent when the illuminant is changed and observer metamerism becomes apparent when the observer is changed.

## Current Techniques and Recommendations

CIE Publication 15.2 (CIE 1986) describes a technique to calculate an index of metamerism for change in illuminant. Essentially the recommendation is to calculate the CIELAB  $\Delta E_{ab}^*$ , or any other color difference metric, for the illuminant under which the two stimuli do not match. This could be any illuminant of interest as long as the two stimuli match under the illuminant of primary interest. There is no clear recommendation on how to calculate this index of metamerism when the two stimuli are not perfect matches under the primary illuminant. In such a case, technically, there is no metamerism, but simply a pair of stimuli with an unstable color difference. Techniques for overcoming this limitation have been discussed by Fairman (1987).

CIE Publication 80 (CIE 1989) describes a technique for calculation of an index of metamerism for change in observer. Essentially, the standard colorimetric observer is replaced with a standard deviate observer and the color difference between the two stimuli is calculated for this new observer. The concept is sound, but the data on which the standard deviate observer was based had been normalized resulting in an under-prediction of the degree of observer metamerism (Alfvin and Fairchild 1997). Nimeroff *et al.* (1961) described a technique whereby a complete standard observer system, including mean and covariance color matching functions, could be specified. This concept is similar to the idea of the CIE (1989) technique, but it has never been fully implemented due to a lack of data. Some newer approaches to observer metamerism are discussed in Section 18.5.

## Application of Color Appearance Models

Color appearance models could be of some utility in the quantification of illuminant metamerism since it involves the comparison of stimuli across changes in illumination. Essentially the contribution to an index of illuminant metamerism would be the availability of a color difference metric that is consistent across a variety of illuminants. Also, an accurate color appearance model would allow the creation of a new type of metric for single stimuli. A single sample cannot be considered metameric since it does not match anything. However, it is common to talk of a single sample being metameric when its apparent color changes significantly with a change in illuminant. This is really a lack of color constancy. A good color appearance model would allow one to calculate a color difference metric between a sample under one illuminant and the same sample under a second illuminant, thus allowing the creation of an index of color constancy. This could be useful for objects that are intended to look the same color under various illumination conditions, such as those containing safety colors.

There really is little use for a color appearance model in the specification of observer metamerism beyond the potential for a better color difference metric and more accurate individual scales of appearance. The measurement of observer metamerism is an excellent example of a situation in which the problem needs to first be completely addressed at the level of basic colorimetry. In other words, the observer variability in tristimulus values must first be adequately specified before it is necessary to be concerned about the improvements that a color appearance model could make. This path should be taken as a model for all potential applications of color appearance models.

## Future Directions

There is little activity aimed at the improvement of indices of metamerism. For illuminant metamerism, effort is concentrated on the improvement of color difference metrics. For observer metamerism, there seems to be little call for a better metric, despite the flaws in the current metric (which is not widely used), but some new ideas are discussed in Section 18.5. This situation could be because it is difficult enough to address problems of illuminant metamerism to cause the difficulties associated with observer metamerism to be considered of second order at this time.

### 18.4 A GENERAL SYSTEM OF COLORIMETRY?

Consideration of some of the problems of traditional colorimetry described in this chapter leads one to wonder whether it might be possible to create a general system of colorimetry that could be used to address all of the problems of interest. Currently, colorimetry has taken a very evolutionary form of development moving from CIE XYZ tristimulus values to the CIELAB color

space, to enhancements of CIELAB for measuring color difference and color appearance. This development is useful to ensure compatibility with industrial practices that are based on previous standard procedures. However, the level of complexity is getting to the point where there might be multiple color models, each more appropriate for a different application. CIELAB and CIELUV were recommended by the CIE in 1976 to limit the number of color difference formulae being used internationally to two, rather than the ever increasing number that were being used prior to that time. That recommendation was quite successful and has resulted in CIELAB becoming essentially the only color space in use (along with a few color difference equations based on it). Perhaps a similar state of affairs is currently developing in the area of color appearance models and recent recommendations from the CIE will bring about some order. However, it is still likely that systems for color appearance and for color difference will be separate in practice. The L<sup>a</sup>L<sup>b</sup>B model (Luo *et al.* 1996) represents one interesting attempt to bring colorimetry together with one general model. Luo *et al.* (2003, 2006) have begun to carry this work forward with respect to CIECAM02 with CAM02-UCS. Perhaps this approach should be pursued, or perhaps different approaches such as those discussed in Chapters 20 and 21 should be considered.

An alternate approach is to start over from scratch, taking advantage of the progress in visual science and colorimetry over the last century, to create a new system of colorimetry that is superior for all steps in the process and can find a wide range of applications in science, technology, and industry. Color appearance models take a step in this direction by first transforming from CIE tristimulus values to cone responses and then building up color appearance correlates from there. There is also activity within the CIE (*e.g.*, TC1-36, Fundamental Chromaticity Diagram with Physiologically Significant Axes) to develop a system of colorimetry based on more accurate cone responsivities that are not necessarily tied to a CIE Standard Colorimetric Observer. It is thought that such a system would find wide use in color vision research. Boynton (1996) has reviewed the history and status of such work. Perhaps some convergence between the two activities is needed to develop a better, general system of colorimetry that could be used by everyone. Unfortunately, this paragraph is just as true for the second edition of this book in 2004 as it was when written for the first edition in 1997! And, sadly, it remains mostly true as the third edition is finished up in the waning days of 2013. However, Section 18.5 illustrates that there is some new activity in the area of observer metamerism, and it will have an intersection with newer color models proposed in Chapter 21.

## 18.5 WHAT ABOUT OBSERVER METAMERISM?

Observer metamerism is discussed in the context of general metamerism in Section 18.3. Fortunately more recent advances in technology and understanding of color vision have brought the questions of observer metamerism, along with their impact on color appearance, more to the forefront. Perhaps there is now some hope that a more general specification

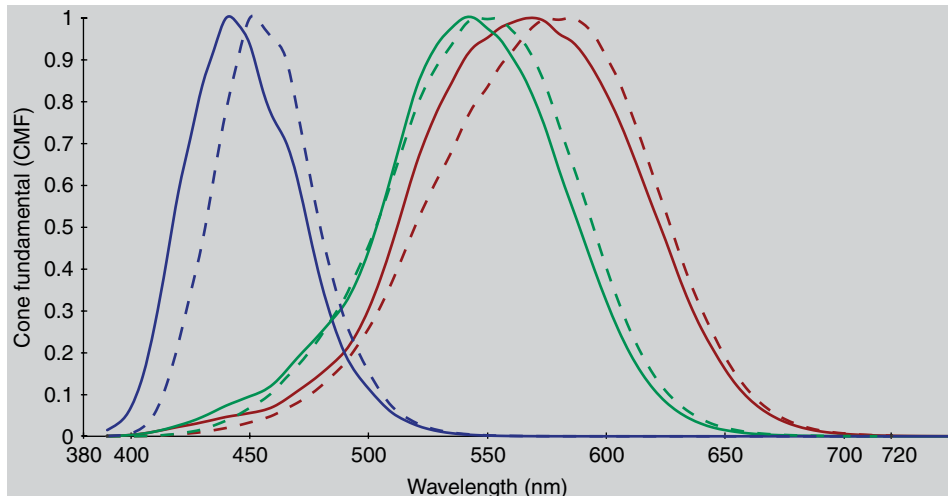


**Figure 18.3** Plots of LMS color matching functions (i.e., cone fundamentals) for two distinct observers computed using the CIE (2006) model. Solid lines represent an average observer of age 20 with a  $2^\circ$  field of view and the dashed lines represent an average observer of age 80 with a  $10^\circ$  field of view

of the variation in color matching functions across observers can be implemented for practical applications.

The CIE (2006) has published a procedure to accurately compute mean color matching functions (in the form of fundamental cone responsivities) for observers of ages from 20 to 80 and for field sizes ranging from  $1^\circ$  to  $10^\circ$ . This procedure essentially allows the computation of the color matching functions of different observers. However, it should be noted that it only computes mean functions for each age and field size, and the model has no way to incorporate individual variation that occurs at any given field size and age. Thus, this is only one step in the direction of helping to quantify individual variation in color matching functions. Nonetheless, it is a very important and useful step since the various ages and field sizes can be used as proxies for various individuals.

Figure 18.3 illustrates the cone fundamentals (color matching functions) for two extreme observers, a 20-year old with a  $2^\circ$  field size and an 80-year old with a  $10^\circ$  field size, to show what the CIE (2006) model is capable of doing. Fairchild and Wyble (2007) used the CIE (2006) model to compute the effects of various observers on image matching in a particular application. Their application was a hypothetical digital cinema theater where normal wide-band *RGB* primaries provide source material that is trying to be matched with a narrow-band *RGB* primary project (e.g., a laser projector). Figure 18.4 illustrates the visual magnitude of the problems that can be encountered with different observers in this one situation.

The CIE (2006) model is being used as a basis for creating more general models of observer variability that might help quantify and rectify the



**Figure 18.4** Examples of images that would match the center picture for various observers when the center image is presented on a broad-band display and the other four images are computed colorimetric match for a narrow-band display and various observers computed using the CIE (2006) model. The observers used were (2°, 32y) upper left, (10°, 32y) upper right, (10°, 20y) lower left, and (10°, 80y) lower right

appearance problems illustrated in Figure 18.4. Sarkar *et al.* (2010) have proposed another approach based on a relatively small number of observer categories that could be used to quantify and “calibrate” observer\_variability. This approach shows a lot of promise and could become a useful part of a general system of colorimetry. Also illustrating the impact of observer variability on color appearance is the work of Webster (2011), Webster *et al.* (2010) and Webster and Kay (2012) that combines variations in visual sensitivities with a model of chromatic adaptation to attempt to render the appearance changes due to the visual sensitivity changes.

# Device-Independent Color Imaging

---

A computer user takes a photograph, has it processed and printed, scans the print into the system, displays it on the monitor, and finally prints it on a digital printer. This user has completed at least three input-process-display cycles on this image. Even if the photograph was captured digitally, there is still significant processing between the raw signals captured and the image saved to the computer, so the number of cycles is only reduced by removing the scanner from the workflow. Despite spending large sums of money on various imaging hardware, it is extremely unlikely that the colors in the final print look anything like the original object or are even satisfactory. There are also intermediate images that might be compared to one another and the original object.

The system described above is an “open system.” This means that the user chose each of the components and put them together. Each of the imaging devices has its own intrinsic physical process for image input, processing, and/or display and they are not necessarily designed to function with each other. If each component functions in its native mode, then the results produced with an open system are nearly unpredictable. One reason for this is the open nature of the systems; there are too many possible combinations of devices to make them all work well with one another.

Allowing the devices to function in their own intrinsic color dimensions is what is known as *device-dependent color imaging*. The difficulty with device-dependent coordinates is that the *RGB* coordinates from a scanner might not mean the same thing as the *RGB* signals used to drive a monitor or printer. To solve these problems and produce reliable results with open systems, *device-independent color imaging* processes must be used. The concept of device-independent color imaging is to provide enough information along with the image color data such that the image data could, if necessary,

be described in coordinates that are not necessarily related to any particular device. Transformations are then performed to represent those colors on any particular device.

The strong technological push for reliable device-independent color imaging over the last two decades has stressed the scientific capabilities in the area of color appearance modeling since the various images are typically viewed in a wide variety of viewing conditions. While it has been recognized for some time that a color appearance model is necessary for successful device-independent color imaging, there has not been a simple solution to that problem available. The first 17 chapters of this book present some of the issues and problems that must be addressed while this chapter provides an overview of the basic concepts required to put the pieces together and build systems.

Device-independent color imaging has become the focus of many scientists and engineers over recent years. It is impossible to cover the scope of issues involved in a single chapter. Entire books dedicated to this topic have become available (Giorgianni and Madden 2008, Green 2010, Kang 1997, Morovic 2008, Reinhard *et al.* 2008, Sharma 2003). In recent years, color management systems have become more commonplace and many books aimed at advanced end users have been published (Fraser *et al.* 2003, Stone 2003). Also, Hunt's text on color reproduction (Hunt 1995) provides much necessary insight into the fundamentals of traditional and digital color reproduction. Sharma and Trussel (1997) have published a review paper on the field of digital color imaging that includes hundreds of references. The treatment in this chapter is culled from a series of earlier works (Fairchild 1994a, 1995b, 1996).

## 19.1 THE PROBLEM

The application of basic colorimetry produces significant improvement in the construction of open color imaging systems by defining the relationships between device coordinates (*e.g.*, RGB, CMYK) and the colors detected or produced by the imaging systems. However, it is important to recall that matching CIE tristimulus values across various imaging devices is only part of the story. If an image is reproduced such that it has CIE tristimulus values identical to the original, then it will match the original in appearance as long as the two are viewed under identical viewing conditions (matching those for which the tristimulus values were calculated). Since originals, reproductions, and intermediate images are rarely viewed under identical conditions, it becomes necessary to introduce color appearance models to the system in order to represent the appearance of the image at each stage of the process.

Issues in device-independent color imaging that color appearance models can be used to address include changes in white point, luminance level, surround, medium (viewing mode), *etc.* Since these parameters normally vary for different imaging modalities, the necessity for color appearance models is clear. The introduction of color appearance models allows the systems to be set up and used to preserve, or purposefully manipulate, the

appearances of image elements in a controlled manner at each step. Thus, users can view an image on an LCD display, manipulate it as they choose, and then make prints that accurately reproduce the appearance of the image on the LCD with the aid of color appearance models.

Of course, it is not always possible, or desirable, to exactly reproduce the appearance of an original image. Color appearance models can be useful in these situations as well. One problem is that different imaging devices are capable of producing different ranges of colors, known as their color gamut. A given stimulus on an LCD display produces a certain appearance. It might not be possible to produce a stimulus on a given printer that can replicate that appearance. In such cases, a color appearance model can be used to adjust the image in a perceptually meaningful way to produce the best possible result. In other cases, the viewing conditions might limit the gamut of a reproduction. For example, photographic prints of outdoor scenes are often viewed under artificial illumination at significantly lower luminance levels than the original scene. At the lower luminance level it is impossible to produce the range of luminance and chromatic contrast that is witnessed in the original scene. Thus it is common for consumer photographic prints to be produced with increased physical contrast to overcome this change in viewing conditions. Color appearance models can be used to predict such effects and guide the design of systems to address them.

Another advantage of color appearance models in device-independent color imaging is in the area of image editing. It is more intuitive for untrained users to manipulate the colors in images along perceptual dimensions such as lightness, hue, and chroma, rather than through device coordinates such as CMYK. A good color appearance model can improve the correlation between tools intended to manipulate these dimensions and the changes that users implement on their images.

## 19.2 LEVELS OF COLOR REPRODUCTION

Hunt (1970, 1995) has defined six different objectives for color reproduction.

### Spectral Color Reproduction

Spectral color reproduction involves identical reproduction of the spectral reflectance curves of the original image or objects. Two techniques that are so impractical as to be of only historical interest, the Lippman and micro-dispersion methods (Hunt 1995), managed to fulfill this difficult objective. Modern color reproduction techniques take advantage of metamerism by using *RGB* additive primaries or *CMY* subtractive primaries, thus eliminating the possibility of spectral reproduction except in cases in which the original is comprised of the same imaging materials. Recently developed, and currently developing, printing techniques that utilize six or more inks provide an opportunity for better approximations to spectral color repro-

duction that might be useful in applications such as mail-order catalogs or fine-art reproductions (in addition to expanding the output gamut).

## Colorimetric Color Reproduction

Colorimetric color reproduction is defined via metameric matches between the original and the reproduction such that they both have the same CIE XYZ tristimulus values. This will result in the reproduction of color appearances in cases for which the original and reproduction of the same size are viewed under illuminants with the same relative spectral power distribution, luminance, and surround. Hunt, however, does not make equality of luminance level a requirement for colorimetric color reproduction.

## Exact Color Reproduction

Exact color reproduction is defined as colorimetric color reproduction with the additional constraint that the luminance levels be equal for the original and the reproduction.

## Equivalent Color Reproduction

Equivalent color reproduction is defined to acknowledge situations in which the color of illumination for the original and the reproduction differ. In such cases, precise reproduction of CIE tristimulus values would result in images that were clearly incorrect since nothing has been done to account for chromatic adaptation. Equivalent color reproduction thus requires the tristimulus values and the luminances of the reproduction to be adjusted such that they produce the same appearances as found in the original. This requires the differences between the original and the reproduction viewing conditions to be incorporated using some form of color appearance or chromatic adaptation model. When there are large changes in luminance level between the original and the reproduction, it might be impossible to produce appearance matches, especially if the objective is brightness-colorfulness matching rather than lightness-chroma matching.

## Corresponding Color Reproduction

Corresponding color reproduction addresses the luminance issue by neglecting it to a degree. A corresponding color reproduction is one that is adjusted such that its tristimulus values are those required to produce appearance matches if the original and the reproduction were viewed at equal luminance levels. This eliminates the problems that arise when trying to reproduce brightly illuminated originals in dim viewing conditions and

vice versa. It can be thought of as an approximation to lightness–chroma matching if one were willing to assume (incorrectly) that lightness and chroma are constant across changes in luminance level. Since lightness and chroma are far more constant across luminance changes than brightness and colorfulness, this assumption might not be too bad, especially given practical gamut-mapping constraints.

## Preferred Color Reproduction

Preferred color reproduction is defined as reproduction in which the colors depart from equality of appearance to those in the original in order to give a more pleasing result. This might be applicable in situations such as consumer photography in which consumers prefer to have prints that reproduce colors closer to their memory colors for objects such as skin tones, vegetation, sky, bodies of water, etc. However, as Hunt (1970) points out, “the concepts of spectral, colorimetric, exact, equivalent, and corresponding color reproduction provide a framework which is a necessary preliminary to any discussion of deliberate distortions of colour reproduction.”

### 19.3 A REVISED SET OF OBJECTIVES

Hunt’s objectives for color reproduction provide a good summary of the problems encountered in color reproduction and how they can be addressed using concepts of basic and advanced colorimetry. It is interesting to note that these objectives were originally published long before issues in device-independent color imaging were commonly discussed (Hunt 1970). A slight rearrangement and simplification of Hunt’s objectives can be used to define five levels of color reproduction that provide a framework for modern color imaging systems:

#### 1. Color Reproduction,

Color reproduction refers to simple availability of devices capable of producing color graphics and images. There is usually great excitement surrounding the initial commercial availability of color devices of any given type. While this might not seem like much of an accomplishment, it is worth remembering that personal computers with reasonable color capabilities have been available for less than 20 years. The plethora of high-quality input and output devices is very recent. When these technologies are first introduced, users are excited simply by the fact that they now have color available where previously it was not. However, this “honeymoon period” quickly wears off and users begin to demand more from their color imaging devices – they want to have devices that produce and reproduce colors with some semblance of control and accuracy. This pushes open-systems technology toward the next levels of color reproduction.

**2. Pleasing Color Reproduction,**

Pleasing color reproduction refers to efforts to adjust imaging devices and algorithms such that consumers find the resulting images acceptable. Such images might not be accurate reproductions and they are probably not the preferred reproductions, but they look pleasing and are found acceptable to most consumers of the images. This level of reproduction can often be achieved through trial and error without requiring any of the concepts of device-independent color imaging. The approach to obtaining pleasing color reproduction in open systems would be similar to the approaches historically taken in closed imaging systems to achieve similar goals or, in some cases, preferred color reproduction. Pleasing color reproduction can be a reasonable final goal for a color reproduction system in which observers have no knowledge of the original scene or image and, therefore, no expectations beyond desiring a pleasing image.

**3. Colorimetric Color Reproduction,**

Colorimetric color reproduction includes calibration and characterization of imaging devices. This means that for a given device signal, the colorimetric coordinates of the image element produced (or scanned) are known with a reasonable degree of accuracy and precision. With colorimetric color reproduction, a user can put together a system in which an image is scanned, the data are converted to colorimetric coordinates (e.g., CIE XYZ), and then these coordinates are transformed into appropriate RGB signals to display on an LCD, or into CMYK signals for output to a printer. Of course, it is not necessary for the image data to actually be transformed through the device-independent color space. Instead, the full transform from one device, through the device-independent space, to the second device can be constructed and implemented for enhanced computational efficiency and minimization of quantization errors. Such a system allows the CIE tristimulus values of the original image to be accurately reproduced on any given output device. This is similar to Hunt's definition of colorimetric color reproduction. To achieve colorimetric color reproduction, devices and techniques for the colorimetric characterization and calibration of input and output devices must be readily available. A variety of such techniques and devices is available commercially, but the degree to which colorimetric color reproduction can actually be achieved by typical users is dubious. Unfortunately, the state of the art for most users is just color reproduction; colorimetric color reproduction has yet to be reliably achieved. Colorimetric color reproduction is useful only when the viewing conditions for the original and reproduced images are identical since this is the only time that tristimulus matches represent appearance matches. When the viewing conditions differ, as they usually do, one must move from colorimetric color reproduction to the next level.

**4. Color Appearance Reproduction**

Color appearance reproduction requires a color appearance model, information about the viewing conditions of the original and reproduced

images, and accurate colorimetric calibration and characterization of all the devices. For color appearance reproduction, the tristimulus values of the original image are transformed to appearance correlates, such as lightness, chroma, and hue, using information about the viewing conditions such as white point, luminance, surround, etc. Information about the viewing conditions for the image to be reproduced is then used to transform these appearance correlates into the tristimulus values necessary to produce them on the output device. Color appearance reproduction is necessary to account for the wide range of media and viewing conditions found in different imaging devices. This is similar to Hunt's equivalent color reproduction applied to lightness-chroma matches. Color appearance reproduction has yet to become a commercial reality and perhaps it cannot for typical users. However, even when reasonable color appearance reproduction does become available, there will be cases when users will desire reproductions that are not accurate appearance matches to the originals. Such cases enter the domain of color preference reproduction.

##### 5. Color Preference Reproduction.

Color preference reproduction involves purposefully manipulating the colors in a reproduction such that the result is preferable to the users over an accurate appearance reproduction. The objective is to produce the best possible reproduction for a given medium and subject. This is similar to Hunt's definition of preferred color reproduction. While the objectives of color preference reproduction are commonly considered to be culturally dependent, there have been essentially no published data that support such a conclusion (Fernandez *et al.* 2005).

Note that to achieve each level of reproduction in open systems, it is necessary to have first achieved the lower levels. To summarize, the five levels involve simply reproducing colors, reproducing pleasing colors, equality of tristimulus values, equality of appearance attributes, and manipulation of appearance attributes to "improve" the result. In closed systems, it is not necessary for technology to progress through each of the five levels. This is because the path of image data is defined and controlled throughout the whole process. For example, in color photography, the film sensitivities, dyes, processing procedures, and printing techniques are all well defined. Thus it is possible to design a photographic negative film to produce pleasing or preferred color reproduction without having the capability for colorimetric or color appearance reproduction since the processing and printing steps are well defined. A similar system exists in color television with standard camera sensitivities, signal processing, and output device setup. In open systems, an intractable number of combinations of input, processing, display, and output devices can be constructed and used together. The manufacturer of each subsystem cannot possibly anticipate all of the possible combinations of devices that might be used with it. Thus the only feasible solution is to have each device in the system develop through the five levels described

above such that colorimetric, or color appearance, data (or the information necessary for obtaining it) can be handed off from one device to the next in the process known as device-independent color imaging.

## 19.4 GENERAL SOLUTION

Figure 19.1 is a flow chart of the general process of device-independent color imaging. At the top of the diagram is the original image as represented by some input device. (Note that this “input” could come from a display device such as a CRT.) The colorimetric characterization of the input device is then used to transform the device coordinates (e.g., RGB) to colorimetric coordinates such as CIE XYZ or CIELAB, which are referred to as device-independent color spaces since the colorimetric coordinates do not depend on any specific imaging device.

The second step is to apply a chromatic adaptation and/or color appearance model to the colorimetric data with additional information on the viewing conditions of the original image in order to transform the image data into dimensions that correlate with appearance such as lightness, hue, and

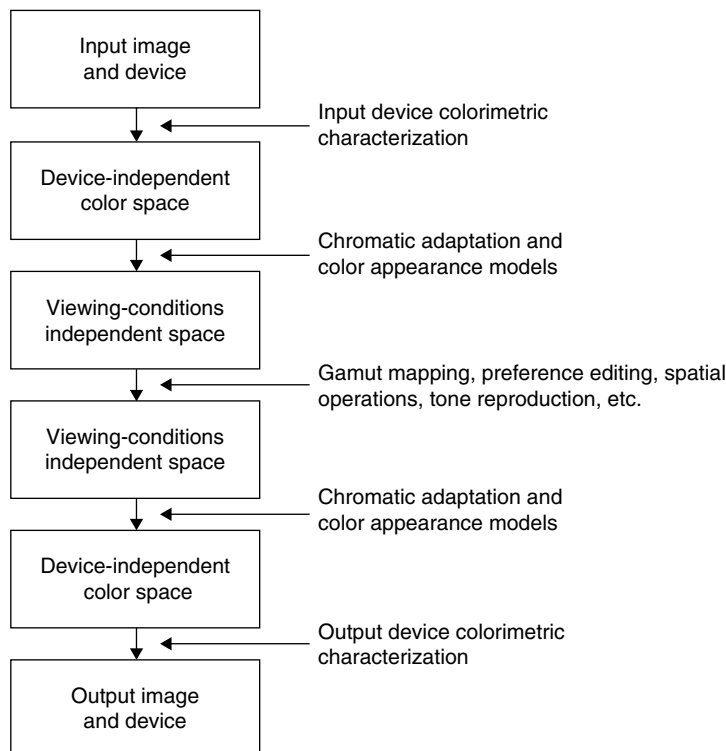


**Figure 19.1** A flow chart of the conceptual process of device-independent color imaging

chroma. These coordinates, that have accounted for the influences of the particular device and the viewing conditions, are referred to as *viewing-conditions-independent space*. At this point, the image is represented purely by its original appearance. This is the point where it is most appropriate to perform manipulations on the image colors. These manipulations might include gamut mapping, preference editing, tone reproduction adjustments, spatial scaling operations, certain forms of error diffusion, etc. At this point, the image is in its final form with respect to the appearances that are to be reproduced. Now the process must be reversed.

This highlights the utility of an analytically invertible color appearance model. The viewing conditions for the output image, along with the final image appearance data, are used in an inverted color appearance model to transform back from the viewing-conditions-independent space to a device-independent color space such as CIE XYZ tristimulus values. These values, together with the colorimetric characterization of the output device, are used to transform to the device coordinates (e.g., CMYK) necessary to produce the desired output image. The following sections provide some additional detail on each step of this process.

Note that the literal implementation of the processes of device-independent color imaging as described above requires substantial computational resources. For example, to avoid severe quantization errors, image processing is usually performed on floating-point image data with floating-point computational precision when working within the intermediate color appearance spaces. While this is acceptable for color imaging research, it is not practical in most commercial color imaging systems, particularly those that are limited to 24-bits-per-pixel color data. In such cases, the processes described above are used to construct the systems and algorithms, while implementation is left to multidimensional interpolation within eight-bits-per-channel LUTs. It is interesting to note that the computer graphics industry, as opposed to the color imaging/publishing industry, typically works with floating-point, and higher precision integer, image data. Perhaps the confluence of the two fields will solve some historical computational issues and limitations.

This general approach has been shown to work many times when carefully implemented. For example, Fairchild *et al.* (2008) were able to make different digital cameras, from different manufacturers, visually match according to psychophysical experiments when following the techniques outlined above and performing careful device characterizations. While this is strictly possible, most manufacturers do not aim for this result since they prefer to have their systems have a distinguishable characteristic “look” rather than to be indistinguishable from the competition.

## 19.5 DEVICE CALIBRATION AND CHARACTERIZATION

*Device calibration* refers to setting the imaging device to a known state. This might represent a certain white point, gain, and offset for a CRT/LCD or certain relationships between density and drive signal for a printer.

Calibration ensures that the device is producing consistent results, both from day to day and from device to device. However, device calibration can be completed with absolutely no information about the relationship between device coordinates and the colorimetric coordinates of the input or output image. Colorimetric characterization of the device is required to obtain this information. *Characterization* refers to the creation of a relationship between device coordinates and a device-independent color space – the first step in Figure 19.1.

Device calibration is usually an issue for the manufacturer, rather than the user, and the techniques depend heavily on the technology. Thus calibration will not be discussed further except to stress its importance. If consistent results are necessary from day to day or from device to device, then careful and frequent device calibration is necessary. There are tradeoffs that can be made between calibration and characterization. If careful calibration is not possible, then accuracy can be achieved through frequent characterization. If an extremely good calibration procedure is available, it might be possible to perform the colorimetric characterization just once, as long as the device is frequently calibrated.

## Three Approaches to Device Characterization

There are three main approaches to device characterization:

1. Physical modeling
2. Empirical modeling
3. Exhaustive measurement.

Of course, there are also procedures that combine aspects of one or more of these techniques. In all cases, it is typical to use the characterization to build a three-dimensional LUT that is used in conjunction with an interpolation procedure to process the vast amounts of image data that are encountered.

### Physical Modeling

Physical modeling of imaging devices involves building mathematical models that relate the colorimetric coordinates of the input or output image elements to the signals used to drive an output device or the signals originating from an input device. Such models can be derived for all types of imaging devices with varying degrees of difficulty. A physical model for a scanner would involve a step to first linearize the signals with respect to luminance, or perhaps absorbance, and then a second step to transform the signals to CIE tristimulus values. Depending on the scanner design, knowledge of the physical properties of the material being scanned might be required. This

could be avoided if the scanner were designed as a colorimeter rather than with arbitrary RGB responsivities.

A physical model for a CRT display involves a nonlinear transform to convert drive voltages to the corresponding *RGB* phosphor luminances, followed by a linear transformation to CIE *XYZ* tristimulus values. (Note that LCD displays do not intrinsically have the same physical model, but they have often been designed to mimic CRT displays.) A physical model for a hard-copy output device requires a transformation from drive signals to concentrations of dyes, pigments, or inks and then a color mixing model to predict spectral reflectances or transmittances that can then be used to calculate CIE *XYZ* tristimulus values. The advantage of physical device models is that they are robust, typically require few colorimetric measurements in order to characterize the device, and allow for easy re-characterization if some component of the imaging system is modified. The disadvantage is that the models are often quite complex to derive and can be complicated to implement. Physical models are often used for display characterization.

## Empirical Modeling

Empirical modeling of imaging devices involves collecting a fairly large set of data and then statistically fitting a relationship between device coordinates and colorimetric coordinates. Such models are often implemented to transform directly to CIELAB coordinates to avoid quantization difficulties in CIE *XYZ* tristimulus values.

Empirical models are often high-order multidimensional polynomials or, alternatively, neural network models of significant complexity. Empirical models require fewer measurements than LUT techniques, but more than physical models. Empirical models are also often poorly behaved near the edge of the device gamut, producing very large systematic errors. Since empirical models have no relationship to the physics of the imaging devices, they must be recreated each time a change is made in any component of the system. Empirical models are often used for scanner characterization.

## Exhaustive Measurement

The final class of characterization techniques involves exhaustive measurement of the output for a complete sampling of the device's gamut. (Signals for a large sampling of known input colors can be collected for scanner characterization.) Typically, something like a  $9 \times 9 \times 9$  sampling of the device drive signals is output and colorimetrically measured. This results in a total of 729 measurements. Many more measurements might be used for devices with poor image-to-image or device-to-device repeatability. The array of colorimetric data must then be nonlinearly interpolated to populate a higher

density (*e.g.*,  $33 \times 33 \times 33$ ) LUT that can be used to process image data via multidimensional interpolation. Disadvantages of such techniques include the large number of measurements that must be made, difficulties in interpolating the highly nonlinear data, the need to redo the entire process if any aspect of the device changes, and difficulty in creating the inverse solutions that are typically required. The advantage of exhaustive measurement techniques that make them popular is that they require no knowledge of the device physics. Exhaustive measurement and LUT interpolation techniques are often used for printer characterization.

## Types of Colorimetric Measurements

Different types of colorimetric measurements are required for characterization of various imaging devices.

*CRT or LCD display characterization* requires spectroradiometric or colorimetric measurements of the phosphor chromaticities in order to derive the RGB-to-XYZ transformation and relative radiometric or photometric measurements to derive the non-linear transfer functions for each channel. Berns (1996) reviews a practical procedure for the calibration and characterization of CRT displays. Berns *et al.* (1993a,b) provide further details on the measurement and characterization of CRT displays. Berns *et al.* (2003) also provide details on the measurements and techniques for LCD characterization.

*Printers and other output devices* require spectrophotometric measurements (spectral reflectance or transmittance) to characterize the device colorants or derive colorimetric coordinates for various illuminants or sources. Additional, densitometric measurements might be of value to characterize tone-transfer functions. Issues in the colorimetric characterization of binary and multilevel display devices have been discussed by a variety of authors including Jarvis *et al.* (1976), Engeldrum (1986), Gentile *et al.* (1990a), Rolleston and Balasubramanian (1993), Berns (1993b), and Haneishi *et al.* (1996).

*Scanners and digital cameras* require spectroradiometric evaluation of their channel spectral responsivities or empirical estimates of them. Spectroradiometric data on the illumination system is also required. Additionally, spectroradiometric linearity evaluation and characterization is required for the detector systems. Often, scanner data for well-characterized input targets are collected to derive relationships between scanner signals and colorimetric coordinates. The colorimetric calibration and characterization of input devices has been described by Hung (1991), Kang (1992), Engeldrum (1993), Rodriguez and Stockham (1993), and Berns and Shyu (1995).

## Flare, Metamerism, and Fluorescence

There are three additional issues regarding colorimetric measurements that are often overlooked in device characterization, but require attention: flare, metamerism, and fluorescence.

## Flare

Typically, the spectrophotometric or colorimetric measurements made to characterize a device are performed with specialized instrumentation and specially prepared samples. Such measurements are not made in the actual viewing situation for the device. Any real viewing situation includes flare. The spectral energy distribution and level of the flare must be measured and added to any real colorimetric characterization of an imaging device. Since flare is an additive mixture of light with the image, it can be treated as a simple addition of the tristimulus values of the flare to the tristimulus values of the image data. This addition might result in the need to recalculate the image white point and renormalize data appropriately. In some cases, flare might be image dependent and require a more sophisticated treatment. Alternatively, measurements of image color must be made *in situ*, using a telespectroradiometer that will include the flare of the viewing environment in the measurement.

## Metamerism

Metamerism causes difficulties in both input and output devices. For input devices, metamerism combined with non-colorimetric sensor responsivities can defeat all hope of obtaining reliable color reproduction. At the output end, it is necessary to characterize devices using spectral reflectance or transmittance functions integrated with the actually viewing spectral power distributions in order to derive colorimetric coordinates. This is necessary for reasonable accuracy even when using standardized viewing sources. For example, the colors observed under a fluorescent D50 simulator can differ dramatically from those calculated using CIE illuminant D50.

## Fluorescence

The colorimetry of fluorescent materials is a significant challenge since the energy emitted by the material is a function of the incident energy from the illuminating source. Since this is not the case for non-fluorescent materials, the light source used for spectrophotometric measurement has no impact on the colorimetric coordinates calculated for any particular illuminant. Fluorescent materials must be measured using illumination that closely simulates the illuminant to be used in colorimetric calculations in order to obtain reasonable accuracy. The best practical solution is to measure fluorescent materials in their final viewing conditions using a telespectroradiometer.

Fluorescence is an important issue in imaging applications since many substrates (*i.e.*, most paper) and many inks and dyes are fluorescent. Grum and Bartleson (1980) provide an excellent overview of the colorimetry of

fluorescent materials. Gonzalez and Fairchild (2000) examined the significance of fluorescence in the colorimetry of typical printing materials.

No matter what approach is taken to characterize an imaging device, the end result is typically used to construct a multidimensional LUT for practical implementations. This is because it is necessary to complete the many layers of nonlinear transformations and color space conversions required with computational precision significantly greater than the eight bits per channel found in most imaging devices. Such computations take prohibitive amounts of time on typical desktop imaging systems. Thus multidimensional LUT interpolation is implemented for the end-to-end transform for convenience and efficiency. The construction of multidimensional LUTs and their use through interpolation has been described by Hung (1993) and Kasson *et al.* (1993, 1995).

Multidimensional LUT interpolation is implemented in a variety of ways including proprietary software such as Adobe Photoshop® and other “color management” software that use these techniques for color space transformations. Multidimensional LUTs are also implemented in the PostScript® Level 2 (Adobe Systems Incorporated 1990) page-description language in the form of color rendering dictionaries. Another well-known open system that provides the framework for the implementation of multidimensional LUTs for device characterization is the International Color Consortium (ICC) profile format (ICC 1996; [www.color.org](http://www.color.org)) that serves as a cross-platform standard for a wide variety of system-level color management systems.

## 19.6 THE NEED FOR COLOR APPEARANCE MODELS

The process of device-independent color imaging described by Figure 19.1 illustrates the necessity of color appearance models. There are two main needs for these models: image editing and viewing-condition transformations. Image manipulations such as color preference reproduction and gamut mapping are best performed in the perceptually significant dimensions (*e.g.*, lightness, chroma, and hue) of a color appearance model. Clearly the transformation of colorimetric coordinates from one set of viewing conditions (*i.e.*, white point, luminance, surround, medium) to a second set of viewing conditions requires a color appearance model.

The only way to avoid the use of a color appearance model in device-independent color imaging is to specify a rather strong set of constraints. The original and the reproduction must be viewed in the same medium, under identical viewing conditions, with identical gamuts, and with the objective of colorimetric color reproduction. In such a constrained world, colorimetric and color-appearance reproduction are identical. Clearly, the above constraints are far too severe for all but the most specialized applications. Thus the use of color appearance models in device-independent color imaging is unavoidable if high-quality, reliable results are to be obtained in open systems.

## 19.7 DEFINITION OF VIEWING CONDITIONS

One key unresolved issue in the implementation of color appearance models in device-independent color imaging is the definition and control of viewing conditions. Even a perfect color appearance model is of little utility if the actual viewing conditions are not the same as those used in the model calculations. (The metamerism problems between CIE illuminants and their physical simulators is one self-evident example of this difficulty.)

Part of the difficulty in controlling the viewing conditions is definition of the fields. Hunt (1991b) has done the most extensive job of defining the various components of the viewing field. However, even with Hunt's extended definitions, it is difficult to decide which portions of the field should be considered the proximal field, the background, and the surround when viewing complex image displays in typical viewing conditions. For example, is the background of an image the area immediately adjacent to the image borders or should it be considered to be the areas adjacent to individual elements within the image? The latter definition might be more appropriate; however, it requires substantially more complex image-wise computations that are often completely impractical. However the particular aspects of the viewing conditions are defined, it is important that the treatment is consistent across all image transformations to avoid the introduction of bias simply due to the use of color appearance models. As a practical definition, the background for images should be defined as the area immediately around the image border with the surround defined as the remainder of the viewing environment; this definition of background, however, is different from that used by Hunt as described in Chapter 7. The definition of proximal field is unnecessary in image reproduction since the spatial relationships of the various image elements is constant in the original and the reproduction. The proximal field becomes important when it is desired to reproduce the color appearance of an image element in a completely different context (*e.g.*, logo colors, trademark colors).

Even with strict definitions of the various components of the viewing field, it is of paramount importance that the viewing conditions be carefully controlled for successful device-independent color imaging. If users are unwilling to control the viewing conditions carefully, they should expect nothing less than unpredictable color reproduction. Viewing condition parameters that must be carefully controlled for successful color appearance reproduction include:

- The spectral power distribution of the light source
- Luminance level
- Surround color and relative luminance
- Background color and relative luminance
- Image flare (if not already incorporated in the device characterization)
- Image size and viewing distance (*i.e.*, solid angle)
- Viewing geometry.

Also, observers must make critical judgments of the various images only after sufficient time has passed to allow full adaptation to the respective viewing conditions.

Braun *et al.* (1996) illustrated the importance of controlling the viewing conditions for cross-media image comparisons. They concluded that the best technique for critical judgments was *successive binocular viewing* in which the observer viewed first one image display with both eyes and then switched to the other display, allowing approximately one minute to adapt to the new viewing conditions. The arrangement was such that only one image display could be viewed at a time and the one-minute adaptation was required each time the observer changed from one display to the other. Unfortunately, the most common technique, simultaneous binocular viewing, in which the original and the reproduction (in a different medium and white point) are viewed simultaneously side-by-side produces unacceptable results. In such cases, the observer's state of chromatic adaptation cannot be reliably predicted since it depends on the relative amount of time spent viewing each image. In general, the best results will be obtained if a single, intermediate adaptation point is assumed. However, the result of such a choice will be a reproduction that matches the original when viewed side-by-side but that looks quite strange when viewed by itself.

For example, if a display has a 9300 K white point and a reproduced print is viewed under a D50 simulator, the required print to produce a simultaneously viewed match will have an overall blue cast. When this print is viewed in isolation, still under a D50 simulator, it will appear unacceptably bluish and be considered a poor match. Katoh (1995) has investigated the problems with simultaneous viewing of images in different media. However, if a successive viewing technique with sufficient adaptation time is used, an excellent neutrally balanced 9300 K CRT image will be matched by a neutrally balanced print viewed under a D50 simulator. Thus both color appearance matching and high individual-image quality can be obtained with appropriate viewing procedures.

Once the viewing conditions are appropriately defined and controlled, some computational advantage can be obtained through judicious precalculation procedures. Such procedures rely on parsing the implementation of the color appearance models into parts that need only be calculated once for each viewing condition and those that require calculation for each image element. The most efficient implementation procedure is then to precalculate the model parameters that are viewing-condition-dependent and then use this array of data for the individual appearance model calculations performed on each pixel or element of a LUT. For example, when using RLAB for a change in white point and luminance with a constant surround, the change in viewing conditions can be precalculated down to a single  $3 \times 3$  matrix transform that is applied to the CIE XYZ tristimulus values of the original in order to determine the tristimulus values of the reproduction. This is a significant computational simplification that makes it possible to allow users to interactively change the settings in a color appearance model such that they can choose the illuminant under which a given image will be viewed.

## 19.8 VIEWING-CONDITIONS-INDEPENDENT COLOR SPACE

Device-independent color spaces are well understood as representations of color based on CIE colorimetry that are not specified in terms of any particular imaging device. (Alternatively, a device-independent color space can be defined as a transform from CIE coordinates to those of some standardized device (Anderson *et al.* 1996) or attempts can be made to regularize, or convert, the illumination conditions through concepts of color appearance (Oleari *et al.* 2013).) The introduction of color appearance models to the process, as illustrated in Figure 19.1, creates the additional concept of a viewing-conditions-independent color space. The viewing-conditions-independent coordinates extend CIE colorimetry to specify the color appearance of image elements at a level that does not rely on outside constraints. Such a representation encodes the perceptual correlates (*e.g.*, lightness, chroma, and hue) of the image elements. This representation facilitates editorial adjustments to the image colors necessary for color preference reproduction and gamut mapping.

It is also worth noting that the viewing conditions themselves might introduce “perceptual gamut limits.” For example, the lightness, chroma, and hue of certain image elements viewed under a high luminance level cannot be reproduced in an image viewed at a low luminance level. In other words, certain color perceptions simply cannot be produced in certain viewing conditions.

The limitations of “perceptual gamut limits” do not in any way reduce the utility of color appearance models. In fact, they can only be reliably defined using color appearance models. It is interesting to note that the concept of viewing-conditions-independent color space has a correlate in the field of cognitive science. Davidoff (1991) presents a model of object color representation that ultimately encodes color in terms of an output lexicon, the words we use to describe color appearance. Such a representation can be thought of as a high-level color appearance model in which colors are specified by name, as people do, rather than with the mathematically necessary reduction to scales of the five requisite color appearance attributes.

## 19.9 GAMUT MAPPING

It would be misleading to suggest that all of the problems of device-independent color imaging would be solved by use of a reliable, accurate color appearance model. Even with a perfect color appearance model, the critical question of color gamut mapping would remain. The development of robust algorithms for automated gamut specification and color mappings for various devices and intents remains as perhaps the most important unresolved issue in cross-media color reproduction (Fairchild 1994a).

The gamut of a color imaging device is defined as the range of colors that can be produced by the device as specified in some appropriate three, or

more, dimensional color space. (It is important to reiterate that color gamuts must be expressed in a three-dimensional color space, since two-dimensional representations such as those often plotted on chromaticity diagrams are misleading.) The most appropriate space for the specification of a device gamut is within the coordinates of a color appearance model since the impact of viewing conditions on the perceived color gamut can be properly represented. For example, only a complete color appearance model will show that the color gamut of a printer shrinks to 0 volume as the luminance decreases! Generally, a device gamut should be represented by the lightness, chroma (or saturation), and hue dimensions within the chosen appearance model. However, in some cases, it might be more appropriate to express the gamut in terms of brightness, colorfulness, and hue. Examples of such cases include projection systems or other displays susceptible to ambient flare in which the absolute luminance level has a significant impact on the perceived color image quality.

Figure 19.2 illustrates various views of three-dimensional models of two device gamuts. These gamuts are plotted in the CIELAB color space. The wireframe model represents the gamut of a typical monitor with SMPTE phosphors and a D50 white point. The solid model represents the color gamut of a typical dye-diffusion printer under CIE illuminant D50. Note that the gamut of the CRT display exceeds that of the printer for light colors, while the gamut of the printer exceeds that of the CRT for some darker colors. This three-dimensional gamut representation should clear up some misconceptions about color gamuts. For example, Figure 19.2 illustrates the large extent to which color gamuts are not coincident and the fact that printer gamuts often extend outside the range of CRT gamuts. Typically, it is assumed that CRT gamuts are significantly larger than most printer gamuts. This is a result of examination of two-dimensional gamut boundaries in chromaticity diagrams while neglecting the third dimension of color space. Another example is given in Figure 19.3 that compares an inkjet printer gamut with a typical display gamut. This example was plotted using a color management tool available in a typical desktop operating system circa 2011.

*Gamut mapping* is the process of adjusting the colors in an image such that it can be represented on a given device (Morovic 2008). For example, it might be desired to use an LCD display to reproduce a dark, saturated cyan that is present on a print. If the LCD cannot produce the desired color, the image element must be shifted to an appropriate color that is within the LCD gamut. The opposite problem might also arise in which a device is capable of producing more saturated colors than present in the original image. If the full gamut of the output device is not utilized, users might be displeased with the results since they know that the device is capable of producing a wider range of colors. Thus, image colors might also be adjusted to fill color gamuts as well. Therefore the problem of gamut mapping can be described as gamut *compression* in regions where the desired color falls outside the device gamut and gamut *expansion* in regions where the gamut of image colors does not fully utilize the device gamut. Proper gamut expansion

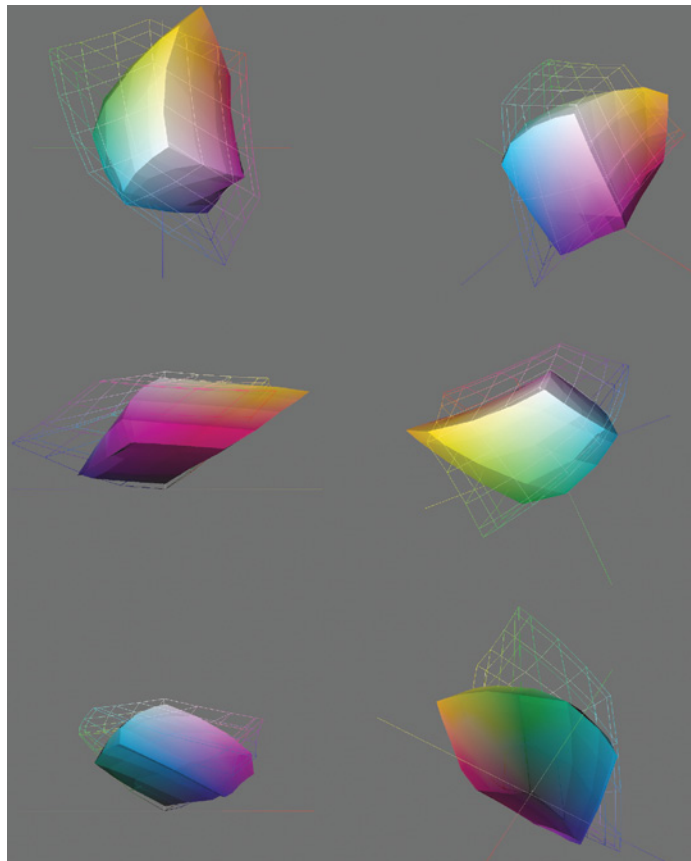


**Figure 19.2** Several views of three-dimensional representations of device gamuts in the CIELAB color space. The solid model is the gamut of a typical dye-diffusion thermal-transfer printer and the wire-frame model is the gamut of a typical CRT display

requires full knowledge of the source image's gamut and computationally expensive image-dependent processing. Thus it might not be fully implemented within practical systems for some time. This is somewhat counter to the common perception that gamut mapping is only a problem of gamut compression. Color adjustments in the opposite direction represent an equally important, and perhaps more challenging, problem. Clearly, a color appearance model is the best place to specify gamuts and perform mapping transformations since the manipulations can be carried out on perceptually meaningful dimensions.

A variety of gamut mapping techniques have been suggested, but a generalized, automated algorithm that can be used for a variety of applications has yet to be developed and probably would not be widely accepted. Lessons can be learned from the field of color photography (Evans *et al.* 1953, Hunt 1995) in which optimum reproductions are thought to be those that preserve

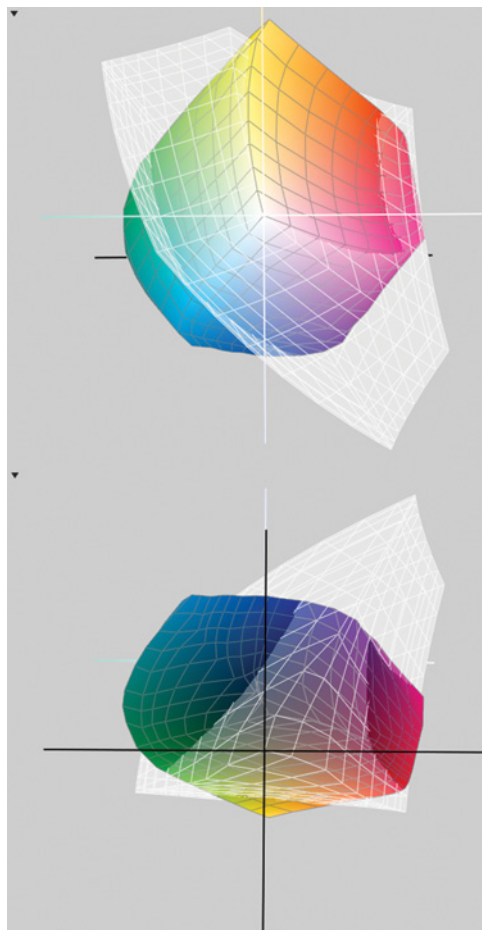


**Figure 19.3** Superimposed color gamuts in the CIELAB space. Colored contour represents a typical desktop inkjet printer and the transparent gray contour represents the sRGB gamut. Upper image shows a view from above the CIELAB space, while the lower image is a view from below. Images were made using the Apple ColorSync Utility Version 4.8.0

the hue of the original, map lightness to preserve its relative reproduction and the mean level, and map chroma such that the relationships between the relative chromas of various image elements are retained. Of course, such guidelines would be overruled by specific color preferences. Beginning with such approaches and considering other practical constraints, issues of color gamut mapping have been discussed by Stone *et al.* (1988), Gentile *et al.* (1990b), Hoshino and Berns (1993), Wolski *et al.* (1994), and Montag and Fairchild (1996, 1997).

While a general solution to the gamut-mapping problem has not been derived, some fundamental concepts can be suggested. For pictorial images, a reasonable gamut-mapping solution can be obtained by first

linearly scaling the lightnesses such that the white and black points match and the middle gray ( $L^*=50$ ) is kept constant. Next, hue is preserved as chroma is clipped to the gamut boundary for compression or linearly scaled for expansion. An alternative approach is to clip the out-of-gamut colors to the gamut boundary at a minimum distance in a uniform color space while eliminating the constant-hue constraint. Such approaches are likely to be too simplistic and do not produce the optimum results (Braun and Fairchild 1999a,b, Montag and Fairchild 1996, 1997, Wolski *et al.* 1994).

For other image types, such as business graphics, other gamut mapping strategies might be more appropriate. One such approach is to preserve the chroma of image elements while changing hue if necessary in order to retain the impact and intent of business graphic images. These differences highlight the importance of understanding the intent for an image when making a reproduction. Depending on the intended application for a given image, the optimum gamut-mapping strategy will vary. The difference between pictorial images and business graphics is readily apparent. However, even among pictorial images, different gamut-mapping strategies might be more appropriate for various applications. For example, the best strategy for a scientific or medical image will be different than that for a fine-art reproduction, which will in turn be different from that for a consumer snapshot.

## 19.10 COLOR PREFERENCES

Once the problems of color appearance and gamut mapping are solved, there will remain one last color operation, the mapping of colors to those that are preferred by observers for a given application. Thus accurate color reproduction might not be the ultimate goal, but rather a required step along the way. Color mapping for preference reproduction should be addressed simultaneously with gamut mapping since the two processes deliberately force inaccurate color reproduction and will certainly impact each other. Like gamut mapping, color preference mapping is intent-, or application-, dependent. In some applications, such as scientific and medical imaging, accurate color reproduction might be an objective that cannot be compromised. In pictorial imaging, preferred reproduction of certain object colors (*e.g.*, sky, skin, foliage) might be biased toward the idealized memory color of these objects. In abstract images, such as business graphics, preferred color reproduction might depend more upon the device capabilities or intended message than on the colors of the original image.

An additional factor in color preference reproduction is the cultural dependency of color preferences. It is well established in the color reproduction industry that preferred color reproduction systems sold into different cultures have different color capabilities and cannot be substituted between cultures without a loss in sales. While it seems likely that such cultural biases exist, they are not well documented (publicly) and their

cause is not well understood. Many such effects have achieved the level of folklore and might only exist for historical reasons. For example, certain customers might have a strong preference for certain color reproduction capabilities because they have grown accustomed to those properties and consider any change to be negative. Such biases are certainly cultural, but they are learned responses. This illustrates the point that most, if not all, cultural biases in color preference reproduction are learned in some way (this is the fundamental definition of culture). The topic of cultural biases is certainly an interesting one and worthy of additional research and exploration. Fernandez and Fairchild (2002) and Fernandez *et al.* (2005) failed to find any significant cultural biases in image preference in one recent study. They showed that individual variation in preferences were larger than any changes in the cultural averages. It would be particularly interesting to see if biases, if indeed they exist at all, could be traced historically to see if they change with advances in communication and interchange of image information.

The concept of cultural dependency in color preference reproduction sparks several interesting possibilities. However, there are also significant individual differences in color preference reproduction as well. In fact, while there might be significant differences in color preference between cultures, it is almost certainly true that the range of color preferences of individuals within any given culture exceeds the differences between the mean levels (confirmed in the Fernandez *et al.* 2005 work). One need only attempt to produce a single ideal image for two observers to understand the magnitude of such differences in preference.

Color appearance models might also enable automated techniques to identify color and object regions in images (Jetsu *et al.* 2011). With such areas identified, it might become more feasible to perform high-quality automated gamut mapping and preference adjustments.

## 19.11 INVERSE PROCESS

Thus far, the process of moving image data into the middle of the flow chart in Figure 19.1 has been described. Once all of the processing at this level is complete, the image data is conceptually in an abstract space that represents the appearances to be reproduced on the output image. At this point, the entire process must be reversed to move from the viewing-conditions-independent color space to a traditional device-independent color space, to device coordinates, and then ultimately to the reproduced image. This process highlights the importance of working in both the forward and reverse directions in order to successfully create reproductions. Clearly, the entire process is facilitated by the use of analytically invertible color appearance models and device characterizations. The main advantage is that such models allow the user to manipulate a setting on the imaging device, or change the viewing conditions, and still be able to recreate the process and produce an image in a reasonable amount of time. If the models must be

iteratively inverted or recreated through exhaustive measurements, it might be completely impractical for a user to adjust any settings in order to obtain a desired result.

## 19.12 EXAMPLE SYSTEM

The previous discussions provide an overview of the process of device-independent color imaging. It is useful to examine an illustrative example of the results that can be obtained with such processes. The impact of various color appearance models in the chain was illustrated in Chapter 17 (Figure 17.6, Figure 17.7, and Figure 17.8). Figure 19.4 illustrates the quality of color reproduction that can be obtained with high-quality device characterizations as described in the previous sections in comparison with the reproductions that would be obtained using the devices right out of the box with no additional calibration or characterization.

The example system consists of typical high-end image input, processing, display, and printing devices for the home-computer market. The images in Figure 19.4 are synthesized representations of the colors that are actually obtained at various steps in the process. While the images are synthesized representations of the results, the colors are accurate representations of the results obtained in a real system. The original image is taken to be a photographic print of a Macbeth ColorChecker® Chart (McCamy *et al.* 1976) as illustrated in the first row of Figure 19.4. The image is scanned using a 600 dpi flat-bed scanner with 10 bits per channel quantization. The second row of Figure 19.4 illustrates the accuracy of the scanned image as represented on a theoretically ideal display (*i.e.*, the display introduces no additional error). The image on the left illustrates the result obtained with no colorimetric characterization (just gamma correction), while the image on the right illustrates the accuracy obtained with a characterization technique such as that outlined by Berns and Shyu (1995).

The next step involves display on a high-resolution CRT as illustrated in the third row of Figure 19.4. The left image illustrates the result of assuming the monitor and video driver are set up to the nominally defined system gamma (*e.g.*, 1.8 for a previous Macintosh system, 1.3–1.5 for a Silicon Graphics system, 2.2–2.5 for a Windows system). It is assumed that any deviation from the nominal white point goes unnoticed due to chromatic adaptation. The image on the right illustrates the accuracy obtained with a specific characterization of the display systems using the techniques described by Berns (1996). Note that these images include both the scanner errors and the monitor errors as the full system is being constructed.

The final step is to print the image on a 600 dpi color laser printer. The image on the left illustrates the result obtained when using the default printer driver and PostScript® Printer Description (PPD) file. The image on the right illustrates the results obtained when a three-dimensional LUT is constructed using a measurement technique with a  $9 \times 9 \times 9$  sampling of the gamut. Again, these final images illustrate errors that have been

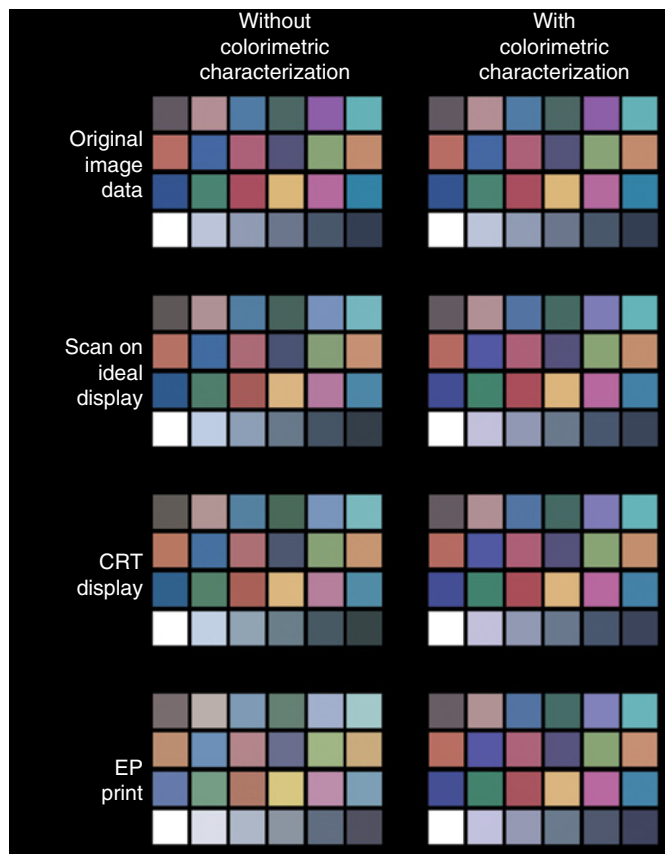


**Figure 19.4** Examples of color reproduction accuracy in a typical desktop imaging system without and with colorimetric calibration and characterization

propagated through the entire imaging system. Clearly careful colorimetric characterization of the three devices making up this system can result in significantly improved results. Unfortunately, the current state of technology does not allow typical users to achieve this level of colorimetric accuracy. However, the potential does exist. The ICC implementation described in Section 19.12 provides a framework. What remains to be implemented is the production of devices that can be accurately calibrated and characterized in the factory (and remain stable) such that typical users will not have to be concerned about calibrating and characterizing the devices themselves.

### 19.13 ICC IMPLEMENTATION

The ICC (1996) has provided a framework for a more universally implemented system to implement the process of device-independent color imaging as illustrated in Figure 19.1 through their specification of the ICC

Profile Format. The consortium consists of approximately 50 corporations and organizations involved in color reproduction software, hardware, computer systems, and operating systems. The profile format is a specification of a data structure that can be used to describe device characterizations (both models and LUTs), viewing conditions, and rendering intent. Such profiles can be used in conjunction with various imaging devices or connected with images to facilitate communication of the colorimetric history of image data. The profile format provides a structure for communication of the required data such that the profiles can be easily interchanged among different computers, operating systems, and/or software applications. While the ICC profile provides the data necessary to implement device-independent color imaging, it is up to the software and hardware developers to build software to utilize this information to complete the system. Such software is referred to as a color management system and has quickly become more and more integrated into operating systems. There is also a significant requirement for the development of profiles to accurately characterize various devices, appearance transformations, gamut-mapping transformations, and color preference mappings. The quality of a system based on ICC profiles will depend on the capabilities of the color management software and the quality of the profiles. With high-quality implementations, the ICC profile specification provides the framework and potential for excellent results.

The construction and implementation of the ICC profile format and color management systems and other compatible software is an evolving process. The current status and profile format documentation can be found at the ICC world-wide web site, [www.color.org](http://www.color.org). The ICC documents also contain information on other ongoing international standardization activities relevant to device-independent color imaging applications.

## Profile Connection Space

One important concept of the ICC specification is the profile connection space. It is often misunderstood because the exact definition and implementation of the profile connection space remains an issue of discussion and debate within ICC. The most recent ICC documentation should be referred to for an up-to-date discussion of this topic.

Essentially, the profile connection space is defined by a particular set of viewing condition parameters that are used to establish reference viewing conditions. The concept of the profile connection space is that a given input-device profile will provide the information necessary to transform device coordinates to a device-independent color specification (CIE XYZ or CIELAB) of the image data that represents the appearances of the original image data in the viewing conditions of the profile connection space (or from CIE specifications in profile connection space to device coordinates for an output-device profile). The technique for obtaining this transformation is not yet agreed upon. As an example, the original

definition of the ICC profile connection space reference viewing conditions are as follows:

Reference reproduction medium: Idealized print with  $D_{min} = 0.0$

Reference viewing environment: ANSI PH2.30 Standard Booth

Surround: Normal

Illumination color: That of CIE illuminant D50

Illuminance:  $2200 \pm 470$  lux

Colorimetry: ideal, flareless measurement

Observer: CIE 1931 Standard Colorimetric Observer (implied)

Measurement geometry: Unspecified.

As an example of using ICC profiles with the profile connection space, imagine a system with a digital camera calibrated for D65 illumination, a display with a 9300K white point, and a printer with output viewed under D50 illumination. An input profile for the digital camera would have to provide the information necessary to first transform from the camera device coordinates, say *RGB*, to CIE tristimulus values for illuminant D65 using typical device calibration and characterization techniques. The tristimulus values for illuminant D65 and the viewing conditions of image capture would then need to be transformed to corresponding tristimulus values for the profile connection space (illuminant D50, etc.) using some color appearance model. All of the information necessary to perform the transformation from device coordinates to corresponding tristimulus values in the profile connection space would have to be incorporated into the input-device profile.

The display would have an output-device profile that would include the information necessary to transform from the profile connection space to corresponding tristimulus values for the display viewing conditions (9300K white point, dim surround, etc.) and then through a device characterization to the *RGB* values required to display the desired colors. When implemented within a color management system, the two device profiles would be concatenated such that the *RGB* data from the camera is transformed directly to the *RGB* data for the display without ever existing in any of the several intermediate spaces or, indeed, even in the profile connection space.

Assuming the printer is set up and characterized for viewing conditions that match the profile connection space, the output-device profile for the printer only needs to include information for the transform from illuminant D50 CIE coordinates to the device coordinates.

An interesting “feature” of this process is that a device profile is required to provide the transformation from device coordinates to the profile connection space even for situations in which a color appearance model would normally not be required. For example, if the camera is set up for D65 illumination and the monitor is set up with a D65 white point, then it makes no sense to first transform through the appearance models to get to the D50 profile connection space and then come back out to a D65 display. Since profiles are concatenated by color management systems, this is not a problem as long as a single color appearance model is agreed upon. The ICC

is working toward this objective, but at the present time, there is no single recommended color appearance model for the construction of ICC profiles. Thus an input-device-profile builder might implement the Hunt model to get into the profile connection space, while an output-device-profile builder might implement the RLAB model to come out of the profile connection space. Since there are significant differences between the various appearance models, processed images might change dramatically in situations for which a color appearance model was not even required. The existence of CIE color appearance models might help remedy this situation. The latest ICC documentation should be examined to see how these and other issues are being addressed.

The concept of the profile connection space is completely compatible with the process described by Figure 19.1. The only addition required is a transformation out of the viewing-conditions-independent color space into a device-independent color space (CIE XYZ or CIELAB) for the viewing conditions of the profile connection space. At this point the conceptual interchange of data from one device to the other occurs. Finally, a transformation from the device-independent color space for the profile connection space

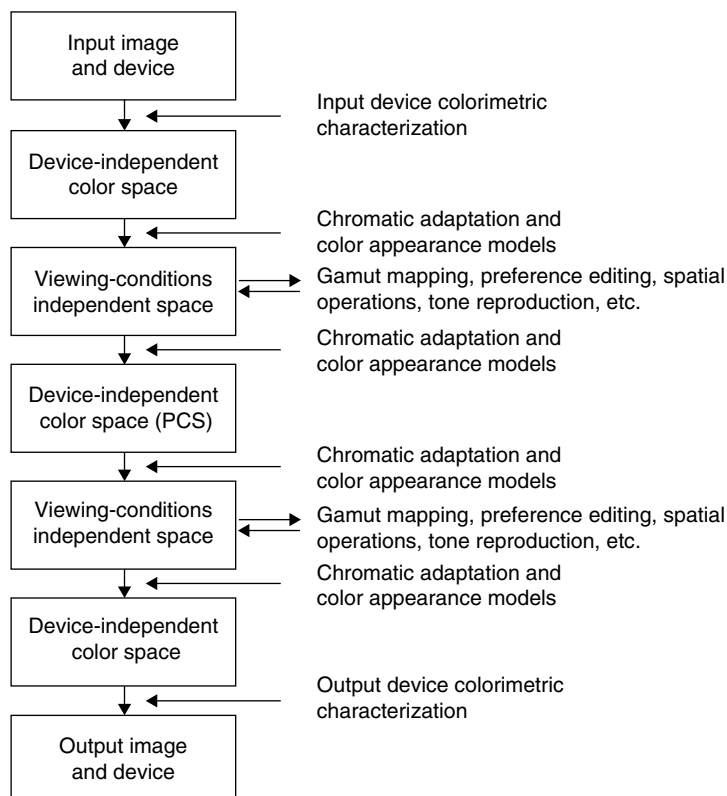


**Figure 19.5** A revision of the flow chart in Figure 19.1 to accommodate the concept of a profile connection space as described by the ICC

viewing conditions to the viewing-conditions-independent color space is made prior to adjustments for the viewing conditions of the output. This process is illustrated in Figure 19.5. The concept of the information processing is not changed. The profile connection space can be thought of as a virtual imaging device. This means that the original flow chart of Figure 19.1 is still used, but either the input device (for output situations) or the output device (for input situations) becomes the profile connection space “virtual device.”

# 20

# Image Appearance Modeling and the Future

---

Color appearance modeling has made some significant advances since the initial edition of this book. The general approach of the models presented in this book is to isolate color from other dimensions of visual performance as much as possible. It is possible, and perhaps likely, that such models have progressed about as far as they can and that further advances will require different types of models. Fairchild and Johnson (2002, 2003, 2004) have proposed a different sort of model referred to as an image appearance model. An image appearance model extends color appearance models to incorporate properties of spatial and temporal vision allowing prediction of appearance in complex stimuli and the measurement of image differences (the first step toward an image quality metric). This chapter reviews the concept of image appearance modeling and presents one such model, known as iCAM. The treatment is largely based on the Fairchild and Johnson (2004) review article. Finally, this chapter ends with some speculation on what might happen in the near future in the areas of color appearance modeling and image appearance modeling. For updates on the current status of various models and key references that appeared after publication of this book, refer to the associated website <http://www.cis.rit.edu/fairchild/CAM.html>. For updates on iCAM and related source code, refer to <http://www.cis.rit.edu/mesl/iCAM>.

## 20.1 FROM COLOR APPEARANCE TO IMAGE APPEARANCE

The history of image measurement helps set the context for the formulation and application of image appearance models, a somewhat natural evolution of color appearance, spatial vision, and temporal vision models when they are considered in a holistic sense, rather than as individual research fields. Early imaging systems were either not scientifically measured at all or measured with systems designed to specify the variables of the imaging system itself. For example, densitometers were developed for measuring photographic materials with the intent of specifying the amounts of dye or silver produced in the film. In printing, similar measurements would be made for the inks as well as measures of the dot area coverage for halftone systems. In electronic systems like television, system measurements such as signal voltages were used to colorimetrically quantify the imaging system (Hunt 1995). Vision-based measurements of imaging systems for image quality do have a long history as illustrated by the example of Schade's (1956) pioneering work. However, as imaging systems evolved in complexity and openness, the need for device-independent image measures became self-evident.

### Image Colorimetry

Electronic imaging systems, specifically the development of color television, prompted the first application of device-independent color measurements of images. Wright (1981b), in fact, points out that color television could not have been invented without colorimetry. The CIE system was used very successfully in the design and standardization of color television systems (including recent digital television systems).

Application of CIE colorimetry to imaging systems became much more prevalent with the advent of digital imaging systems and the use of computer systems to generate and proof content ultimately destined for other media. The use of CIE colorimetry to specify images across the various devices promised to solve some of the new color reproduction problems created by open, digital systems. The flexibility of digital systems also made it possible and practical to perform colorimetric transformations on image data in attempts to match the colors across disparate devices and media.

Research on imaging device calibration and characterization has spanned the range from fundamental color measurement techniques to the specification of a variety of devices including CRT, LCD, and projection displays, scanners and digital cameras, and various film recording and print media. Some of the concepts and results of this research have been summarized by Berns (1997). Such capabilities are a fundamental requirement for research and development in color and image appearance. Research on device characterization and calibration provides a means to tackle more fundamental problems in device-independent color imaging. For example, conceptual research on design and implementation of device-independent color imaging (Fairchild 1994a), gamut

mapping algorithms to deal with the reproduction of desired colors that fall outside the range that can be obtained with a given imaging device (Braun and Fairchild 2000), and computer graphics rendering of high-quality spectral images that significantly improve the potential for accurate color in rendered scenes (Johnson and Fairchild 1999). This type of research built upon and contributed to research on the development and testing of color appearance models for cross-media image reproduction.

## Color Difference Equations

Color difference research has culminated with the recently published CIEDE2000 color difference formula (Luo *et al.* 2001). At the heart of such color difference equations lies some form of uniform color space. The CIE initially recommended two such color spaces in 1976: CIELAB and CIELUV. Both spaces were initially described as interim color spaces, with the knowledge that they were far from complete. With a truly uniform color space, color differences can then be taken to be a simple measure of distance between two colors in the space, such as CIE  $\Delta E_{ab}^*$ . The CIE recognized the non-uniformity of the CIELAB color space and formulated more advanced color difference equations such as CIE DE94 and CIEDE2000. These more complicated equations are very capable of predicting perceived color differences of simple color patches. Despite these limitations, Stokes *et al.* (1992) very successfully showed that a simple color difference equation was capable of predicting color difference thresholds for images with complex, overall, color changes. They found that a mean CIELAB color difference of 2.5 units was a reasonable perceptibility threshold for complex images.

## Image Difference

The CIE color difference formulae were developed using simple color patches in controlled viewing conditions. There is no reason to believe that they are adequate for predicting color difference for spatially complex image stimuli. The S-CIELAB model (Zhang and Wandell 1996) was designed as a spatial pre-processor to the standard CIE color difference equations to account for complex color stimuli such as halftone patterns. The spatial preprocessing uses separable convolution kernels to approximate the CSFs of the human visual system. The CSF serves to remove information that is imperceptible to the visual system. For instance, when viewing halftone dots at a certain distance, the dots tend to blur and integrate into a single color. A pixel-by-pixel color difference calculation between a continuous image and a halftone image would result in very large errors, while the perceived difference might in fact be small. The spatial preprocessing would blur the halftone image so that it more closely resembles the continuous tone image.

S-CIELAB represents the first incarnation of an image difference model based upon the CIELAB color space and color difference equations.

Recently, this model has been refined and extended into a modular framework for image color difference calculations (Johnson and Fairchild 2001a,b, 2003a,b). This framework, discussed in Section 20.4, refines the CSF equations from the S-CIELAB model and adds modules for spatial frequency adaptation, spatial localization, and local and global contrast detection.

## Color Appearance

Unfortunately, fundamental CIE colorimetry does not provide a complete solution for image specification. By their very nature, the images produced or captured by various digital systems are examined in widely disparate viewing conditions, from the original captured scene, to a computer display in a dim room, to printed media under a variety of light sources to projection displays in dark rooms. Thus color appearance models were developed to extend CIE colorimetry to the prediction of color appearance (not just color matches) across changes in media and viewing conditions (not just within a single condition). Color appearance modeling research applied to digital imaging systems was very active throughout the 1990s, culminating with the recommendation of the CIECAM97s model in 1997 (Chapter 15) and its revision, CIECAM02, in 2002 (Chapter 16). The development of these models was also enabled by visual experiments performed to test the performance of published color appearance models in realistic image reproduction situations (Braun and Fairchild 1997). Such research on color appearance modeling in imaging applications naturally highlighted the areas that are not adequately addressed for spatially complex image appearance and image quality problems.

## Image Appearance and Image Quality

Color appearance models account for many changes in viewing conditions, but are mainly focused on changes in the color of the illumination (white point), the illumination level (luminance), and surround relative luminance. Such models do not directly incorporate any of the spatial or temporal properties of human vision and the perception of images. They essentially treat each pixel of an image (and each frame of a video) as completely independent stimuli.

Visual adaptation to scenes and images is not only spatially localized according to some low-pass characteristics, but also temporally localized in a similar manner. To predict the appearance of digital video sequences, particularly those of high-dynamic range, the temporal properties of light and chromatic adaptation must be considered. To predict the quality (or image differences) of video sequences, temporal filtering to remove imperceptible high-frequency temporal modulations (imperceptible “flicker”) must be added to the spatial filtering that removes imperceptible spatial artifacts (*e.g.*, noise or compression artifacts).

It is easy to illustrate that adaptation has a significant temporal low-pass characteristic. For example, if one suddenly turns on the lights in a darkened room (as upon first awakening in the morning), the increased illumination level is at first dazzling to the visual system, essentially overexposing it. After a short period of time, the visual system adapts to the new, higher level of illumination, and normal visual perception becomes possible. The same is true when going from high levels of illumination to low levels (imagine driving into a tunnel in the daytime). Fairchild and Reniff (1995) and Rinner and Gegenfurtner (2000) have made detailed measurements of the time course of chromatic adaptation. These results suggest temporal integration functions that could be used in models of moving image appearance and also illustrate one of the mechanisms for spatially low-pass adaptation stimuli due to the influence of ever-present eye movements.

There has been significant research on video quality and video quality metrics, often aimed at the creation and optimization of encoding/compression/decoding algorithms such as MPEG2 and MPEG4. By analogy, the still-image visible differences predictor of Daly (1993) is quite applicable to the prediction of the visibility of artifacts introduced into still images by JPEG image compression. The Daly model was designed to predict the probability of detecting an artifact. Instead of focusing on threshold differences in quality, the focus in developing iCAM has been on the prediction of image quality scales (e.g., scales of sharpness, contrast, graininess) for images with changes well above threshold. Such suprathreshold image differences are a different domain of image quality research based on image appearance.

Likewise, a similar situation exists in the area of video quality metrics. Metrics have been published to examine the probability of detection of artifacts in video, but there appear to be no models of video image appearance designed for rendering video and predicting the magnitudes of perceived differences in video sequences. Two well-known video image quality models, the Sarnoff JND model and the NASA digital video quality (DVQ) model, are briefly described below to contrast their capabilities with the objectives of the iCAM model.

The Sarnoff JND model is the basis of the *JNDmetrix* software package ([www.jndmetrix.com](http://www.jndmetrix.com)) and related video quality hardware. The model is briefly described in a technical report published by Sarnoff Corporation (2001) and more fully disclosed in other publications (ATIS 2001). It is based on the multiscale model of spatial vision published by Lubin (1993, 1995) with some extensions for color processing and temporal variation. The Lubin model is similar in nature to the Daly model in that it is designed to predict the probability of detection of artifacts in images. These are threshold changes in images often referred to as JNDs. The Sarnoff JND model has no mechanisms of chromatic and luminance adaptation, as are included in the iCAM model. The input to the Sarnoff model must first be normalized (which can be considered a very rudimentary form of adaptation). The temporal aspects of the Sarnoff model are also not aimed at predicting the appearance of video sequences, but rather at predicting the detectability of temporal artifacts. As such, the model only uses two frames (four fields) in its temporal

processing. Thus, while it is capable of predicting the perceptibility of relatively high-frequency temporal variation in the video (flicker), it cannot predict the visibility of low-frequency variations that would require an appearance-oriented, rather than JND-oriented, model. The Sarnoff model also is not designed for rendering video. This is not a criticism of the model formulation, but an illustration of how the objective of the Sarnoff JND model is significantly different from that of the iCAM model. While it is well-accepted in the vision science literature that JND predictions are not linearly related to suprathreshold appearance differences, it is certainly possible to use a JND model to try to predict suprathreshold image differences, and the Sarnoff JND model has been applied with some success to such data.

A similar model, the *DVQ* metric, has been published by Watson (1998) and Watson *et al.* (2001) of NASA. The *DVQ* metric is similar in concept to the Sarnoff JND model, but significantly different in implementation. Its spatial decomposition is based on the coefficients of a discrete cosine transformation (DCT) making it amenable to hardware implementation and likely making it particularly good at detecting artifacts introduced by DCT-based video compression algorithms. It also has a more robust temporal filter that should be capable of predicting a wider array of temporal artifacts. Like the Sarnoff model, the *DVQ* metric is aimed at predicting the probability of detection of threshold image differences. The *DVQ* model also includes no explicit appearance processing through spatial or temporal adaptation, or correlates of appearance attributes, and therefore also cannot be used for video rendering. Again, this is not a shortcoming, but rather a property of the design objectives for the *DVQ* model.

While color appearance modeling has been successful in facilitating device-independent color imaging and is incorporated into modern color management systems, there remains significant room for improvement and extension of capabilities. To address these issues with respect to spatial properties of vision and image perception and image quality, the concept of image appearance models has been recently introduced and implemented (Fairchild 2002a,b, Fairchild and Johnson 2002). These models combine attributes of color appearance models with attributes of spatial vision models that have been previously used for image quality metrics in an attempt to further extend the capabilities of color appearance models. Historically, color appearance models largely ignored spatial vision (*e.g.*, CIECAM97s, CIECAM02) while spatial vision models for image quality largely ignored color (Daly 1993, Lubin 1993). Some exceptions include the retinex model (Land 1964, 1986, Land and McCann 1971, McCann *et al.* 1976) and its various derivatives (Barnard and Funt 1997, Brainard and Wandell 1986, Funt *et al.* 2000). The spatial ATD model (Granger 1993) and the S-CIELAB model (Zhang and Wandell 1996) also address some of these issues to various extents. While the retinex model was never designed as a complete model of image appearance and quality, its spatially variable mechanisms of chromatic adaptation and color constancy serve some of the same purposes in image rendering and provide some of the critical groundwork for image appearance modeling.

The goal of developing an image appearance model has been to bring these research areas together to create a single model applicable to image appearance, image rendering, and image quality specifications and evaluations. One such model for still images, referred to as iCAM, is detailed in this chapter. This model was built upon previous research in uniform color spaces (Ebner and Fairchild 1998), the importance of image surround (Fairchild 1995b), algorithms for image difference and image quality measurement (Fairchild 2002b, Johnson and Fairchild 2003a), insights into observers eye movements while performing various visual imaging tasks and adaptation to natural scenes (Babcock *et al.* 2003, Webster and Mollon 1997), and an earlier model of spatial and color vision applied to color appearance problems and HDR imaging. (Pattanaik *et al.* 1998).

## Color and Image Appearance Models

A model capable of predicting perceived color difference between complex image stimuli is a useful tool, but has some limitations. Just as a color appearance model is necessary to fully describe the appearance of color stimuli, an image appearance model is necessary to describe spatially complex color stimuli. Color appearance models allow for the description of attributes such as lightness, brightness, colorfulness, chroma, and hue. Image appearance models extend upon this to also predict such attributes as sharpness, graininess, contrast, and resolution.

A uniform color space also lies in the heart of the of an image appearance model. The modular image difference framework allows for great flexibility in the choice of color spaces. Examples are the CIELAB color space, similar to S-CIELAB, the CIECAM02 color appearance model, and the IPT color space (Ebner and Fairchild 1998). Thus, the modular image difference framework can be implemented within the iCAM model as described in this chapter to create a full image appearance and image difference model. It could also be implemented in other color spaces if desired.

Models of image appearance can be used to formulate multidimensional models of image quality. For example, it is possible to take weighted sums of various appearance attributes to determine a metric of overall image quality, as described by Keelan (2002) and Engledrum (2002). Essentially, these models can augment or replace human observations to weight image attributes with overall appearances of quality. For instance, a model of quality might involve weighted sums of tonal balance, contrast, and sharpness. A step towards this type of model is illustrated in the following sections.

### 20.2 S-CIELAB

The S-CIELAB model provides an excellent example of an image appearance model, much like the CIELAB color space provides a model of the full color appearance model. S-CIELAB (Zhang and Wandell 1996) is a clear forerunner

of the concept of image appearance modeling and remains a commonly used technique for image difference computations. Its implementation has been further clarified and expanded by Johnson and Fairchild (2003b).

Simply put, S-CIELAB combines the CIELAB color space and color difference equation with a spatial filtering step that effectively blurs away any fine details that cannot be perceived (*e.g.*, halftone dots) and thus should not be represented in the color difference computation. The procedure is to first convert the image XYZ tristimulus values to opponent dimensions using the transform in equations 20.1 and 20.2. These are then spatially filtered using convolution kernels designed to represent the luminance and chromatic CSFs. The kernels are defined in Equations 20.3 and 20.4. Note that this filtering step is dependent on the image viewing distance. The filtered images are then converted back to XYZ and then CIELAB  $L^*a^*b^*$  for pixel-by-pixel computation of color differences. Statistical summaries of these image difference maps can be used to attempt to represent image differences.

$$\begin{bmatrix} O_1 \\ O_2 \\ O_3 \end{bmatrix} = \mathbf{M}_O \begin{bmatrix} X \\ Y \\ Z \end{bmatrix} \quad (20.1)$$

$$\mathbf{M}_O = \begin{bmatrix} 0.279 & 0.72 & -0.107 \\ -0.449 & 0.29 & -0.077 \\ 0.086 & -0.59 & 0.501 \end{bmatrix} \quad (20.2)$$

$$f = k \sum_i w_i E_i \quad (20.3)$$

$$E_i = k_i \exp \left[ \frac{-(x^2 + y^2)}{\sigma_i^2} \right] \quad (20.4)$$

The scale factor,  $k_i$ , is chosen such that  $E_i$  sums to 1.0. The scale factor,  $k$ , is chosen such that  $f$  sums to 1.0 for each color plane. The parameters ( $w_i$ ;  $\sigma_i$ ) for each of the chromatic planes are as follows: luminance (0.921, 0.105, -0.108; 0.0283, 0.133, 4.366), red-green (0.531, 0.330; 0.0392, 0.494), and blue-yellow (0.488, 0.371; 0.0536, 0.386).

## 20.3 THE iCAM FRAMEWORK

The iCAM framework builds upon the concept of S-CIELAB to also examine issues of spatial adaptation in addition to spatial filtering. Figure 20.1 presents a flow chart of the general framework for the iCAM image appearance model as applied to still images. For input, the model requires colorimetrically characterized data for the image (or scene) and surround in absolute luminance units. The image is specified in terms of

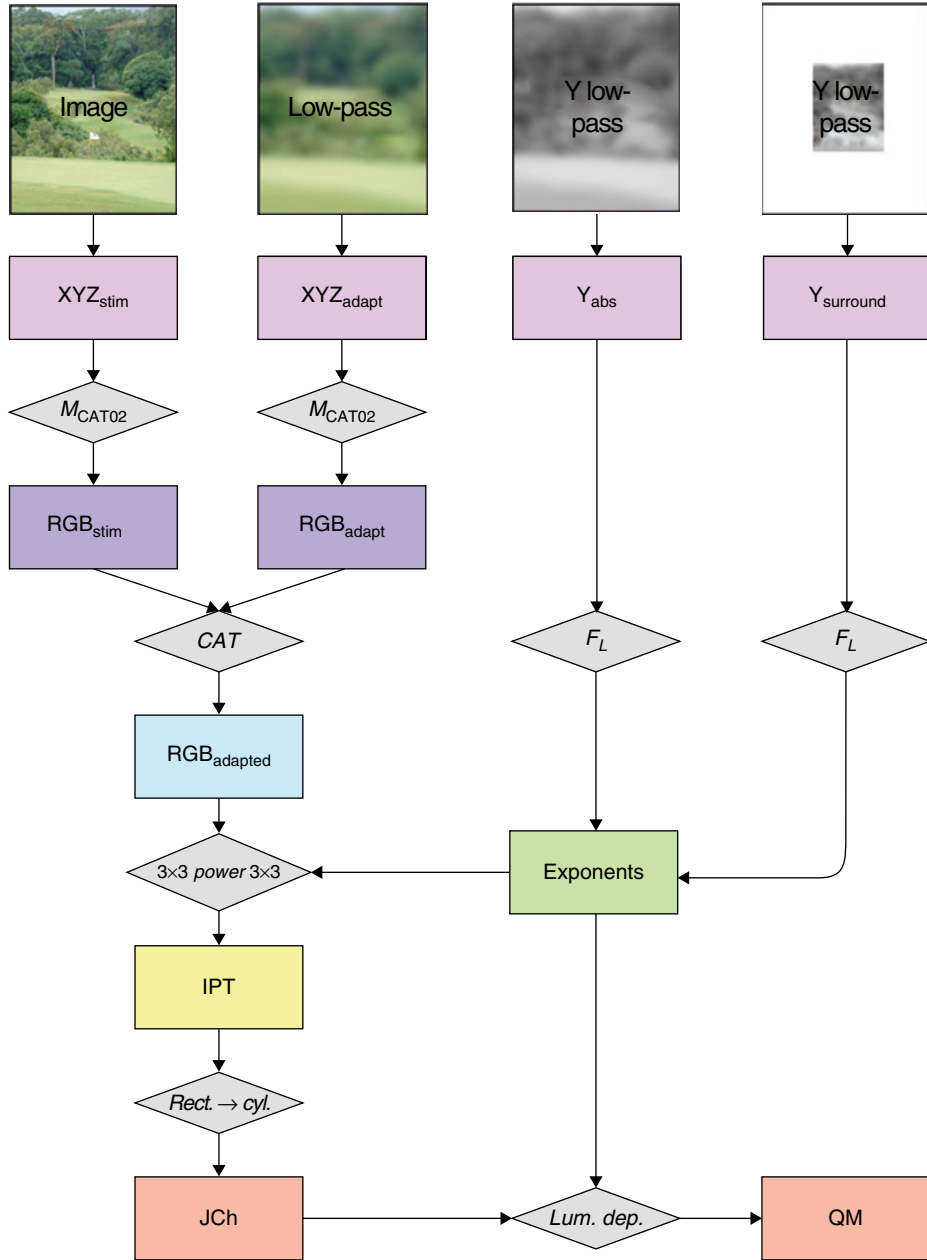


**Figure 20.1** Flowchart of the iCAM image appearance model. Inputs to the model are CIE tristimulus values,  $XYZ$ , for the stimulus image or scene and a low-pass version used as an adapting stimulus and absolute luminance information for the low-pass image and surround. Adapted signals are computed using the linear chromatic adaptation transform from CIECAM02 and then converted into an opponent space,  $IPT$ , using the luminance information to modulate a compressive nonlinearity. The rectangular  $IPT$  coordinates are then converted to cylindrical correlates of lightness,  $J$ , chroma,  $C$ , and hue,  $h$ . The lightness and chroma correlates can then be scaled by a function of the absolute luminance information to provide correlates of brightness,  $Q$ , and colorfulness,  $M$ . If desired, a saturation correlate can be computed as the ratio of chroma to lightness (or colorfulness to brightness)

relative CIE XYZ tristimulus values. The adapting stimulus is a low-pass filtered version of the CIE XYZ image that is also tagged with absolute luminance information necessary to predict the degree of chromatic adaptation. The absolute luminances (Y) of the image data are also used as a second low-pass image to control various luminance-dependent aspects of the model intended to predict the Hunt effect (increase in perceived colorfulness with luminance) and the Stevens effect (increase in perceived image contrast with luminance). Lastly, a low-pass, luminance (Y) image of significantly greater spatial extent is used to control the prediction of image contrast that is well-established to be a function of the relative luminance of the surrounding conditions (Bartleson and Breneman equations). The specific low-pass filters used for the adapting images depend on viewing distance and application. Additionally, in some image rendering circumstances it might be desirable to have different low-pass adapting images for luminance and chromatic information to avoid desaturation of the rendered images due to local chromatic adaptation. This is one example of application dependence in image appearance modeling. Local chromatic adaptation might be appropriate for image-difference or image-quality measurements but inappropriate for image-rendering situations.

The first stage of processing in iCAM is to account for chromatic adaptation. The chromatic adaptation transform embedded in CIECAM02 has been adopted in iCAM since it was well researched and established to have excellent performance with all available visual data. It is also a relatively simple chromatic adaptation model amenable to image-processing applications. The chromatic adaptation model, given in Equations 20.5 through 20.10, is a linear von Kries normalization of *RGB* image signals to the *RGB* adaptation signals derived from

$$\begin{bmatrix} R \\ G \\ B \end{bmatrix} = \mathbf{M}_{\text{CAT02}} \begin{bmatrix} X \\ Y \\ Z \end{bmatrix} \quad (20.5)$$

$$\mathbf{M}_{\text{CAT02}} = \begin{bmatrix} 0.7328 & 0.4296 & -0.1624 \\ -0.7036 & 1.6975 & 0.0061 \\ 0.0030 & 0.0136 & 0.9834 \end{bmatrix} \quad (20.6)$$

$$D = F \left[ 1 - \left( \frac{1}{3.6} \right) e^{-L_A - 42/92} \right] \quad (20.7)$$

$$R_c = \left[ \left( 100 \frac{D}{R_w} \right) + (1 - D) \right] R \quad (20.8)$$

$$G_c = \left[ \left( 100 \frac{D}{G_w} \right) + (1 - D) \right] G \quad (20.9)$$

$$B_c = \left[ \left( 100 \frac{D}{B_w} \right) + (1 - D) \right] B \quad (20.10)$$

the low-pass adaptation image at each pixel location ( $R_w G_w B_w$ ). The *RGB* signals are computed using a linear transformation from *XYZ* to *RGB* derived by CIE TC8-01 in the formulation of CIECAM02. The von Kries normalization is further modulated with a degree-of-adaptation factor,  $D$ , that can vary from 0.0 for no adaptation to 1.0 for complete chromatic adaptation. Equation 20.7 is provided in the CIECAM02 formulation, and used in iCAM, for computation of  $D$  as a function of adapting luminance,  $L_A$ , for various viewing conditions. Alternatively the  $D$  factor can be established manually. The chromatic adaptation model is used to compute corresponding colors for CIE illuminant D65 that are then used in the later stages of the iCAM model. This is accomplished by taking the adapted signals for the viewing condition,  $R_c G_c B_c$ , and then inverting Equations 20.5 through 20.10 for an illuminant D65 adapting white point and with  $D = 1.0$ . It should be noted that, while the adaptation transformation is identical to that in CIECAM02, the iCAM model is already significantly different since it uses spatially modulated image data as input rather than single color stimuli and adaptation points. One example of this is the modulation of the absolute luminance image and surround luminance image using the  $F_L$  function from CIECAM02 given in Equation 20.11. This function, slowly varying with luminance, has been

$$F_L = 0.2 \left( \frac{1}{(5L_A + 1)} \right)^4 (5L_A) + 0.1 \left( 1 - \left( \frac{1}{(5L_A + 1)} \right)^4 \right)^2 (5L_A)^{1/3} \quad (20.11)$$

established to predict a variety of luminance-dependent appearance effects in CIECAM02 and earlier models. Since the function has been established and understood, it was also adopted for the early stages of iCAM. However, the manner in which the  $F_L$  factor is used in CIECAM02 and iCAM are quite different.

The next stage of the model is to convert from *RGB* signals (roughly analogous to cone signals in the human visual system) to opponent color signals (light-dark, red-green, and yellow-blue; analogous to higher level encoding in the human visual system) that are necessary for constructing a uniform perceptual color space and correlates of various appearance attributes. In choosing this transformation, simplicity, accuracy, and applicability to image processing were the main considerations. The color space chosen was the *IPT* space previously published by Ebner and Fairchild (1998). The *IPT* space was derived specifically for image processing applications to have a relatively simple formulation and specifically to have a hue-angle component with good prediction of constant perceived hue (important in gamut-mapping applications). More recent work on perceived hue has validated the applicability of the *IPT* space. The transformation

from *RGB* to the *IPT* opponent space is far simpler than the transformations used in CIECAM02. The process, expressed in Equations 20.12 through 20.16, involves a linear transformation to a different cone-response space, application of power-function nonlinearities, and then a final linear transformation to the *IPT* opponent space (*I*, light-dark; *P*, red-green; *T*, yellow-blue).

$$\begin{bmatrix} L \\ M \\ S \end{bmatrix} = \begin{bmatrix} 0.4002 & 0.7075 & -0.0807 \\ -0.2280 & 1.1500 & 0.0612 \\ 0.0 & 0.0 & 0.9184 \end{bmatrix} \begin{bmatrix} X_{D65} \\ Y_{D65} \\ Z_{D65} \end{bmatrix} \quad (20.12)$$

$$\begin{aligned} L' &= L^{0.43}; & L \geq 0 \\ L' &= -|L|^{0.43}; & L \leq 0 \end{aligned} \quad (20.13)$$

$$\begin{aligned} M' &= M^{0.43}; & M \geq 0 \\ M' &= -|M|^{0.43}; & M \leq 0 \end{aligned} \quad (20.14)$$

$$\begin{aligned} S' &= S^{0.43}; & S \geq 0 \\ S' &= -|S|^{0.43}; & S \leq 0 \end{aligned} \quad (20.15)$$

$$\begin{bmatrix} I \\ P \\ T \end{bmatrix} = \begin{bmatrix} 0.4000 & 0.4000 & 0.2000 \\ 4.4550 & -4.8510 & 0.3960 \\ 0.8056 & 0.3572 & -1.1628 \end{bmatrix} \begin{bmatrix} L' \\ M' \\ S' \end{bmatrix} \quad (20.16)$$

The power-function nonlinearities in the *IPT* transformation are a critical aspect of the iCAM model. First, they are necessary to predict response compression that is prevalent in most human sensory systems. This response compression helps to convert from signals that are linear in physical metrics (e.g., luminance) to signals that are linear in perceptual dimensions (e.g., lightness). The CIECAM02 model uses a hyperbolic nonlinearity for this purpose. The behavior of which is that of a power function over the practical ranges of luminance levels encountered. Secondly, and a key component of iCAM, the exponents are modulated according to the luminance of the image (low-pass filtered) and the surround. This is essentially accomplished by multiplying the base exponent in the *IPT* formulation by the image-wise computed  $F_L$  factors with appropriate normalization. These modulations of the *IPT* exponents allow the iCAM model to be used for predictions of the Hunt, Stevens, and Bartleson/Breneman effects mentioned previously. They also happen to enable the tone mapping of HDR images into low-dynamic-range display systems in a visually meaningful way (see example in Figure 20.7).

For image-difference and image-quality predictions, it is also necessary to apply spatial filtering to the image data to eliminate any image variations

at spatial frequencies too high to be perceived. For example, the dots in a printed half-tone image are not visible if the viewing distance is sufficiently large. This computation is dependent on viewing distance and based on filters derived from human CSFs. Since the human contrast-sensitivity functions vary for luminance (band-pass with sensitivity to high frequencies) and chromatic (low pass) information, it is appropriate to apply these filters in an opponent space. Thus in image-quality applications of iCAM, spatial filters are applied in the *IPT* space. Since it is appropriate to apply spatial filters in a linear-signal space, they are applied in a linear version of *IPT* prior to conversion into the non-linear version of *IPT* for appearance predictions. Johnson and Fairchild (2001a,b, 2003a,b) and Fairchild and Johnson (2005) have discussed some of the important considerations for this type of filtering in image-difference applications and specified the filters used based on available visual data. Since the spatial filtering effectively blurs the image data, it is not desirable for image rendering applications in which observers might view the images more closely than the specified viewing distance. Example CSFs, derived from fits to experimental data, used to define spatial filters for image difference computations are given in Equation 20.13 for the luminance, *I*, channel and Equation 20.14 for the chromatic, *P* and *T*, channels (Johnson and Fairchild 2001a).

$$\text{csf}_{\text{lum}}(f) = a \cdot f^c \cdot e^{-b \cdot f} \quad (20.17)$$

$$\text{csf}_{\text{chrom}}(f) = a_1 \cdot e^{-b_1 \cdot f^{c_1}} + a_2 \cdot e^{-b_2 \cdot f^{c_2}} \quad (20.18)$$

The parameters, *a*, *b*, and *c*, in Equation 20.13 are set to 75, 0.2, and 0.8, respectively, for the luminance CSF applied to the *I* channel. In Equations 20.17 and 20.18, spatial frequency, *f*, is defined in terms of cycles per degree of visual angle (cpd). For the red-green chromatic CSF, applied to the *P* dimension, the parameters (*a*<sub>1</sub>, *b*<sub>1</sub>, *c*<sub>1</sub>, *a*<sub>2</sub>, *b*<sub>2</sub>, *c*<sub>2</sub>) in Equation 20.14 are set to (109.14, 0.00038, 3.424, 93.60, 0.00367, 2.168). For the blue-yellow chromatic CSF, applied to the *T* dimension, they are set to (7.033, 0.000004, 4.258, 40.69, 0.10391, 1.6487).

It is only appropriate to apply these spatial filters when the goal is to compute perceived image differences (and ultimately image quality). This is an important distinction between spatially localized adaptation (good for rendering and image quality metrics) and spatial filtering (good for image quality metrics, bad for rendering). In image quality applications, the spatial filtering is typically broken down into multiple channels for various spatial frequencies and orientations. For example, Daly (1993), Lubin (1993), and Pattanaik *et al.* (1998) describe such models. More recent results suggest that while such multiscale and multi-orientation filtering might be critical for some threshold metrics, it is often not necessary for data derived from complex images and for supra-threshold predictions of perceived image differences (Johnson and Fairchild 2001a,b, 2003a, Watson and Remirez 2000). Thus, to preserve the simplicity and ease of use of the iCAM model, single-scale spatial filtering with anisotropic filters was adopted.

Once the *IPT* coordinates are computed for the image data, a simple coordinate transformation from rectangular to cylindrical coordinates is applied to obtain image-wise predictors of lightness (*J*), chroma (*C*), and hue angle (*h*) as shown in Equations 20.19 through 20.21. Differences in these dimensions can be used to compute image difference statistics and those used to derive image quality metrics. The overall Euclidean difference in *IPT* is referred to as  $\Delta Im$  (Equation 20.24), for image difference, to distinguish it from a traditional color difference metric,  $\Delta E$ , that includes no spatial filtering. In some instances, correlates of the absolute appearance attributes of brightness (*Q*) and colorfulness (*M*) are required. These are obtained by scaling the relative attributes of lightness and chroma with the appropriate function of  $F_L$  derived from the image-wise luminance map as shown in Equations 20.22 and 20.23.

$$J = I \quad (20.19)$$

$$C = \sqrt{P^2 + T^2} \quad (20.20)$$

$$h = \tan^{-1} \left( \frac{P}{T} \right) \quad (20.21)$$

$$Q = \sqrt[4]{F_L} J \quad (20.22)$$

$$M = \sqrt[4]{F_L} C \quad (20.23)$$

$$\Delta Im = \sqrt{\Delta I^2 + \Delta P^2 + \Delta T^2} \quad (20.24)$$

For image rendering applications it is necessary to take the computed appearance correlates (*JCh*) and then render them to the viewing conditions of a given display. The display viewing conditions set the parameters for the inversion of the *IPT* model and the chromatic adaptation transform (all for an assumed spatially uniform display adaptation typical of low-dynamic-range output media). This inversion allows the appearance of original scenes or images from disparate viewing conditions to be rendered for the observer viewing a given display. One important application of such rendering is the display of HDR image data on typical displays.

## 20.4 A MODULAR IMAGE DIFFERENCE MODEL

A framework for a color image difference metric has been described by Johnson and Fairchild (2001b). That modular image difference metric is incorporated into the iCAM appearance model to address both image appearance and differences/quality within a single model. The image difference framework was designed to be modular in nature, to allow for flexibility and adaptation. The framework itself is based upon the S-CIELAB

spatial extension to the CIELAB color space. S-CIELAB merges traditional color difference equations with spatial properties of the human visual system. This was accomplished as a spatial filtering preprocessing, before a pixel-by-pixel color difference calculation.

The modular framework further extends this idea by adding several processing steps, in addition to the spatial filtering. These processing steps are contained in independent modules, so they can be tested and refined. Several modules have been defined, (Johnson and Fairchild 2003a) and include spatial filtering, adaptation, and localization, as well as local and global contrast detection. Figure 20.2 shows a general flowchart with several distinct modules. These modules and their origins are described briefly below.

## Spatial Filtering

The behavior of the human visual system in regards to spatially complex stimuli has been well studied over the years dating back to the seminal work of Campbell and Robson (1968) and Mullen (1985). Summaries of current knowledge and techniques for quantifying spatial vision can be found in several books (*e.g.*, Cooper *et al.* 2012, DeValois and DeValois 1988, Kelly 1994, Wandell 1995). The CSF describes this behavior in relation to spatial frequency. Essentially, the CSF is described in a post-retinal opponent color space, with a band-pass nature for the luminance channel and low-pass nature for the chrominance channels. S-CIELAB uses separable convolution kernels to approximate the CSF and modulate image details that are imperceptible. More complicated CSFs that include both modulation and frequency enhancement were discussed in detail by Johnson and Fairchild (2003a). Other models with similar features include the previously mentioned Lubin (1993), Daly (1993), MOM (Pattanaik *et al.* 1998), S-CIELAB (Zhang and Wandell 1996), and spatial ATD (Granger 1993) models. Other relevant discussions and models can be found in the work of Li *et al.* (1998), Taylor *et al.* (1997, 1998), and Brill's (1997) extension of the Lubin/Sarnoff model.

## Spatial Frequency Adaptation

The CSF in this framework serves to modulate spatial frequencies that are not perceptible and enhance certain frequencies that are most perceptible. Generally, CSFs are measured using simple grating stimuli with care taken to avoid spatial frequency adaptation. Spatial frequency adaptation essentially decreases sensitivity to certain frequencies based upon information present in the visual field. An early and classic description of spatial frequency adaptation was published by Blakemore and Campbell (1969). It should be noted that a multiscale, or multichannel, spatial vision model is not required to predict spatial frequency adaptation. Instead, all that is required is that the CSF functions be allowed to change shape as a function of adaptation (clearly indicating the existence of multiscale mechanisms).

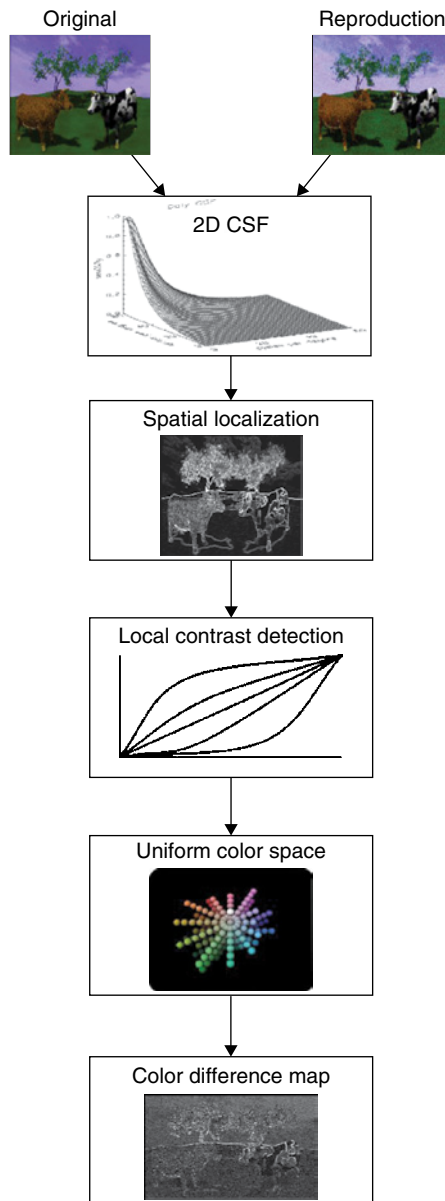


**Figure 20.2** Flowchart of a modular image difference metric

Since spatial frequency adaptation cannot be avoided in real world viewing conditions, several models of spatial frequency adaptation have been described for practical applications (Johnson and Fairchild 2001b). These models alter the nature of the CSF based upon either assumptions of the viewing conditions or based upon the information contained in the images themselves.

## Spatial Localization

The band-pass and low-pass contrast sensitivity serve to modulate high-frequency information, including high-frequency edges. The human visual system is generally acknowledged to be very adept at detecting edges. To accommodate this behavior, a module of spatial localization has been developed. This module can be as simple as an image processing edge-enhancing kernel, although that kernel must change as a function of viewing distance. Alternatively, the CSF can be modified to boost certain high-frequency information. The formulation and utility of edge-detection algorithms in vision applications has been well-described by Marr (1982).

## Local Contrast Detection

This module serves to detect local and global contrast changes between images. The utility of such processing in real visual systems has been described by Tolhurst and Heeger (1997). The current implementation is based upon the nonlinear mask-based local contrast enhancement described by Moroney (2000b). Essentially a low-pass image mask is used to generate a series of tone-reproduction curves. These curves are based upon the global contrast of the image, as well as the relationship between a single pixel and its local neighborhood.

## Color Difference Map

The output of the modular framework is a map of color differences,  $\Delta Im$ , corresponding to the perceived magnitude of error at each pixel location. This map can be very useful for determining specific causes of error or for detecting systematic errors in a color imaging system. Often it is useful to reduce the error map into a more manageable data set. This can be accomplished using image statistics, so long as care is taken. Such statistics can be image mean, max, median, or standard deviation. Different statistics might be more valuable than others depending on the application, as perhaps the mean error better describes overall difference, while the max might better describe threshold differences.

## 20.5 IMAGE APPEARANCE AND RENDERING APPLICATIONS

Figure 20.3 illustrates implementation of the iCAM framework required to complete an image rendering process necessary for HDR image tone mapping. The components essential in this process are the inversion of the IPT model for a single set of spatially constant viewing conditions (the display) and the establishment of spatial filters for the adapting stimuli used

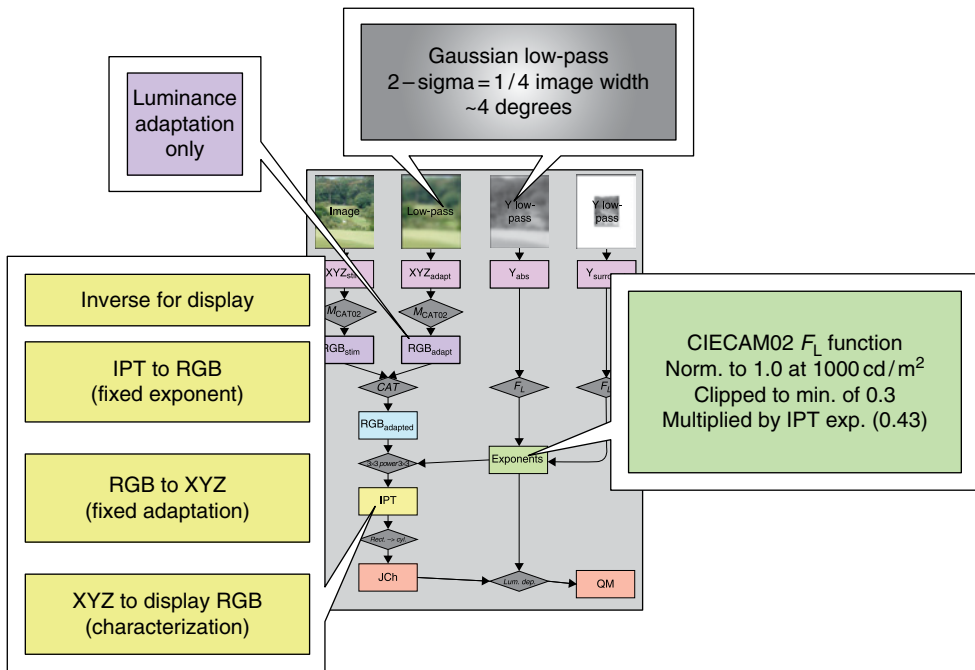


**Figure 20.3** Implementation of iCAM for tone mapping of HDR images

for local luminance adaptation and modulation of the IPT exponential nonlinearity. While the derivation of optimal model settings for HDR image rendering is still underway, quite satisfactory results have been obtained using the settings outlined in Figure 20.3. Details of this algorithm were published by Johnson and Fairchild (2003c).

The iCAM model has been successfully applied to prediction of a variety of color appearance phenomena such as chromatic adaptation (corresponding colors), color appearance scales, constant hue perceptions, simultaneous contrast, crispening, spreading, and image rendering (Fairchild and Johnson 2002).

Since iCAM uses the same chromatic adaptation transform as CIECAM02, it performs identically for situations in which only a change in state of chromatic adaptation is present (*i.e.*, change in white point only). CIE TC8-01 has worked very hard to arrive at this adaptation transform, and it is clear that no other model currently exists with better performance (although there are several with equivalent performance). Thus the chromatic adaptation performance of iCAM is as good as possible at this juncture.

The appearance scales of iCAM are identical to the *IPT* scales for the reference viewing conditions. The *IPT* space has the best available performance for constant hue contours, and thus this feature is retained in iCAM. This feature makes accurate implementation of gamut-mapping algorithms far easier in iCAM than in other appearance spaces. In addition,

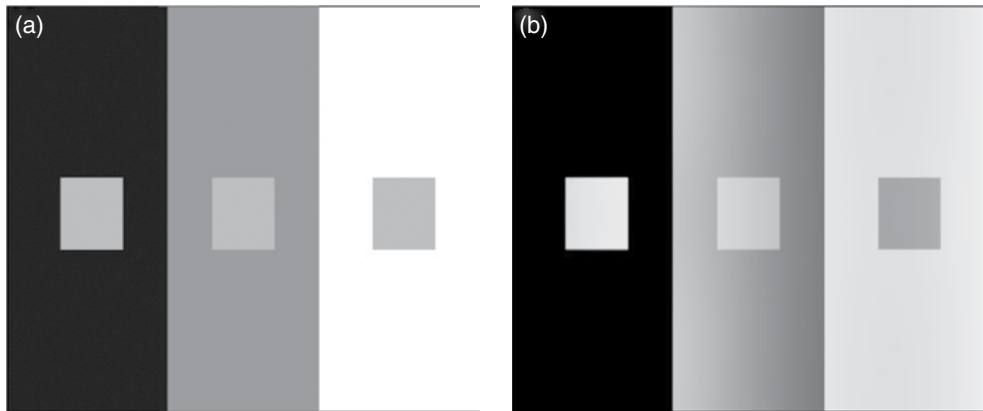


**Figure 20.4** (a) Original stimulus and (b) iCAM lightness,  $J$ , image illustrating the prediction of simultaneous contrast

the predictions of lightness and chroma in iCAM are very good and comparable with the best color appearance models in typical viewing conditions. The brightness and colorfulness scales will also perform as well as any other model for typical conditions. In more extreme viewing conditions, the performance of iCAM and other models will begin to deviate. It is in these conditions that the potential strengths of iCAM will become evident. Further visual data must be collected to evaluate the model's relative performance in such situations.

The color difference performance of iCAM will be similar to that of CIELAB since the space is very similar under the reference viewing conditions. Thus, color difference computations will be similar to those already commonly used, and the space can be easily extended to have a more accurate difference equation following the successful format of the CIE94 equations. (Following the CIEDE2000 equations in iCAM is not recommended since they are extremely complex and fitted to particular discrepancies of the CIELAB space such as poor constant-hue contours.)

Simultaneous contrast (or induction) causes a stimulus to shift in appearance away from the color of the background in terms of opponent dimensions. Figure 20.4 illustrates a stimulus that exhibits simultaneous contrast in lightness (the gray square is physically identical on all three backgrounds) and its prediction by iCAM as represented by the iCAM lightness predictor. This prediction is facilitated by the local adaptation features of iCAM.

Crispening is the phenomenon whereby the color differences between two stimuli are perceptually larger when viewed on a background that is similar to the stimuli. Figure 20.5 illustrates a stimulus that exhibits chroma crispening and its prediction by the iCAM chroma predictor. This prediction is also facilitated by the local adaptation features of iCAM.

Spreading is a spatial color appearance phenomenon in which the apparent hue of spatially complex image areas appears to fill various

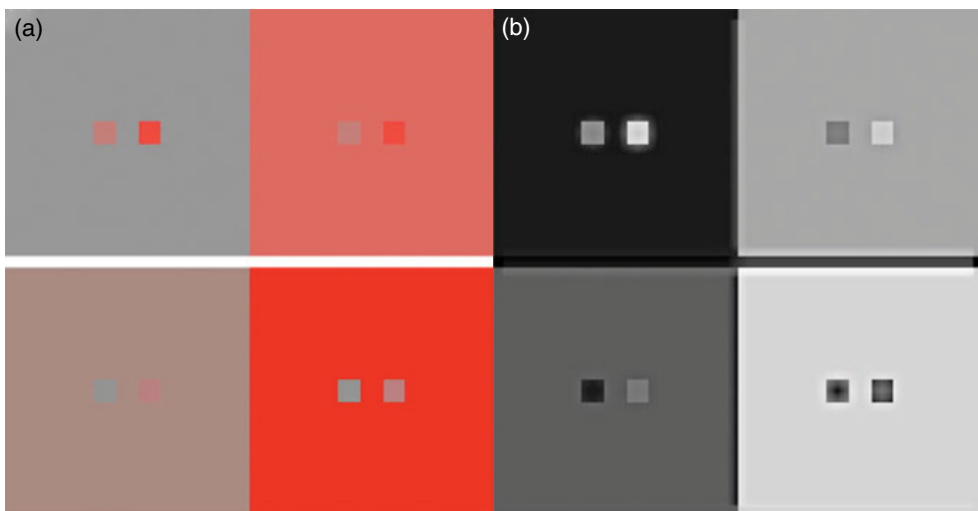


**Figure 20.5** (a) Original stimulus and (b) iCAM chroma,  $C$ , image illustrating the prediction of chroma crispening. Original image from [http://www.hpl.hp.com/personal/Nathan\\_Moroney/](http://www.hpl.hp.com/personal/Nathan_Moroney/)

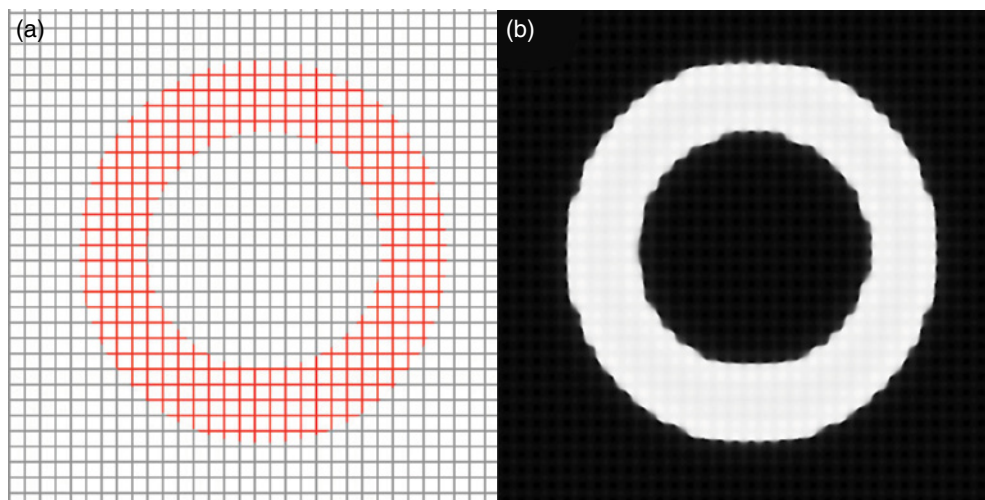


**Figure 20.6** (a) Original stimulus and (b) iCAM hue,  $h$ , image illustrating the prediction of spreading

spatially coherent regions. Figure 20.6 provides an example of spreading in which the red hue of the annular region spreads significantly from the lines to the full annulus. The iCAM prediction of spreading is illustrated through reproduction of the hue prediction. The prediction of spreading in iCAM is facilitated by spatial filtering of the stimulus image.

One of the most interesting and promising applications of iCAM is to the rendering of HDR images to low-dynamic-range display systems. HDR image data are quickly becoming more prevalent. Historically HDR images were obtained through computer graphics simulations computed with global-illumination algorithms (*e.g.*, ray tracing or radiosity algorithms) or through the calibration and registration of images obtained through multiple exposures. Real scenes, especially those with visible light sources, often have luminance ranges of up to six orders of magnitude. More recently, industrial digital imaging systems have become commercially available that can more easily capture HDR image data. It is also apparent that consumer digital cameras will soon be capable of capturing greater dynamic ranges. Unfortunately display and use of such data are difficult and will remain so since even the highest quality displays are generally limited in dynamic range to about two orders of magnitude. One approach is to interactively view the image and select areas of interest to be viewed optimally within the display dynamic range. This is only applicable to computer displays and not appropriate for pictorial imaging and printed output. Another limitation is the need for capability to work with greater than 24-bit (and often floating point) image data. It is desirable to render HDR pictorial images onto a display that can be viewed directly (no interactive manipulation) by the observer and appear similar to what the observer would perceive if the original scene was viewed. For printed images, it is not just desirable, but necessary. Pattanaik *et al.* (1998) review several such HDR rendering algorithms, and it is worth noting that several papers were presented on the topic at SIGGRAPH 2002 (Durand and Dorsey 2002, Fattal *et al.* 2002, Reinhard *et al.* 2002) illustrating continued interest. Meylan *et al.* (2007) introduced a similar approach to local adaptation with extremely localized adaptation that shows significant promise for image rendering despite perhaps not modeling the visual system so closely.

Since iCAM includes spatially localized adaptation and spatially localized contrast control, it can be applied to the problem of HDR image rendering. Since the encoding in our visual system is of a rather low dynamic range, this is essentially a replication of the image appearance processing that goes on in the human observer and is being modeled by iCAM. Figure 20.7 illustrates application of the iCAM model to HDR images obtained from Debevec ([www.debevec.org](http://www.debevec.org)). The images in the left column of Figure 20.7 are linear renderings of the original HDR data normalized to the maximum presented simply to illustrate how the range of the original data exceeds a typical 24-bit (8 bits per RGB channel) image display. For example, the memorial image data (top row) have a dynamic range covering about six orders of magnitude since the sun was behind one of the stained-glass windows. The middle column of images represents a typical image-processing solution to rendering the data. One might consider a logarithmic transformation of the data, but that would do little to change the rendering in the first column. Instead the middle column was generated interactively by finding the optimum

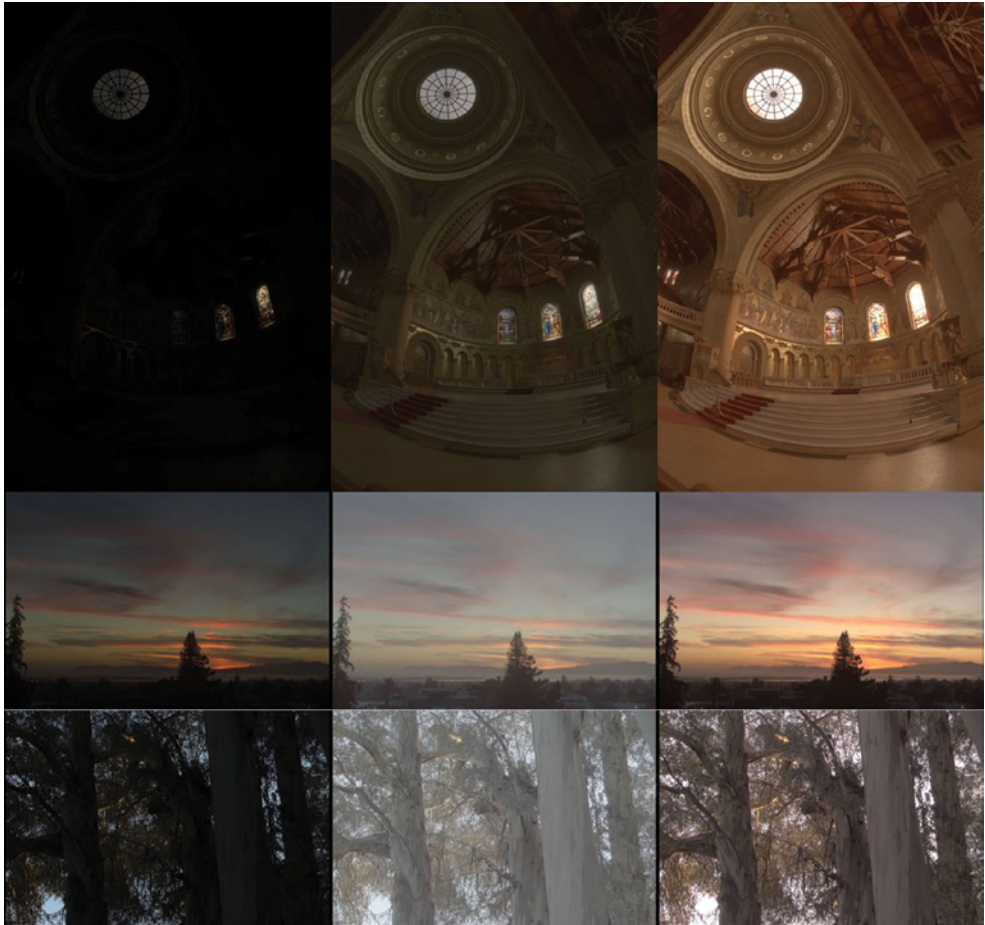


**Figure 20.7** Three HDR images from [www.debevec.org](http://www.debevec.org). The leftmost column illustrates linear rendering of the image data, the middle column illustrates manually optimized power-function transformations, and the rightmost column represents the automated output of the iCAM model implemented for HDR rendering (Figure 20.3)

power-function transformation (also sometimes referred to as gamma correction; note that the linear images in the first column are already gamma corrected). For these images, transformations with exponents, or gammas, of approximately  $1/6$  (as opposed to  $1/1.8$  to  $1/2.2$  for typical displays) were required to make the image data in the shadow areas visible. While these power-function transformations do make more of the image-data visible, they required user interaction, tend to wash out the images in a way not consistent with the visual impression of the scenes, and introduce potentially severe quantization artifacts in shadow regions. The rightmost column of images shows the output of the iCAM model with spatially localized adaptation and contrast control (as shown in Figure 20.3). These

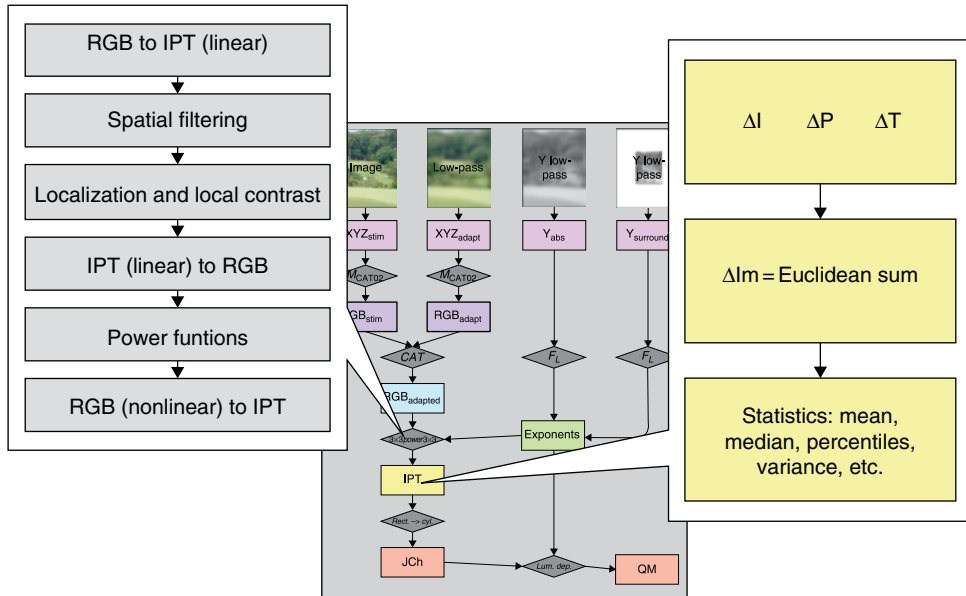


**Figure 20.8** Implementation of iCAM for image difference and image quality metrics

images both render the dynamic range of the scene to make shadow areas visible and retain the colorfulness of the scene. The resulting iCAM images are quite acceptable as reproductions of the HDR scenes (equivalent to the result of dodging and burning historically done in photographic printing). It is also noteworthy that the iCAM-rendered images were all computed with an automated algorithm (Johnson and Fairchild 2003c) mimicking human perception with no user interaction.

## 20.6 IMAGE DIFFERENCE AND QUALITY APPLICATIONS

A slightly different implementation of iCAM is required for image quality applications in order to produce image maps representing the magnitude of perceived differences between a pair of images. In these applications, viewing-distance-dependent spatial filtering is applied in a linear *IPT* space and then differences are computed in the normal nonlinear *IPT* space. Euclidean summations of these differences can be used as an overall image difference map, and then various summary statistics can be used to predict different attributes of image difference and quality. This process is outlined in Figure 20.8 and detailed in Johnson and Fairchild (2003a).

Image quality metrics can be derived from image difference metrics that are based on normal color difference formulas applied to properly spatially filtered images. This approach has been used to successfully predict various types of image quality data (Johnson and Fairchild 2001b). Figure 20.9 illustrates the prediction of perceived sharpness (Johnson and Fairchild

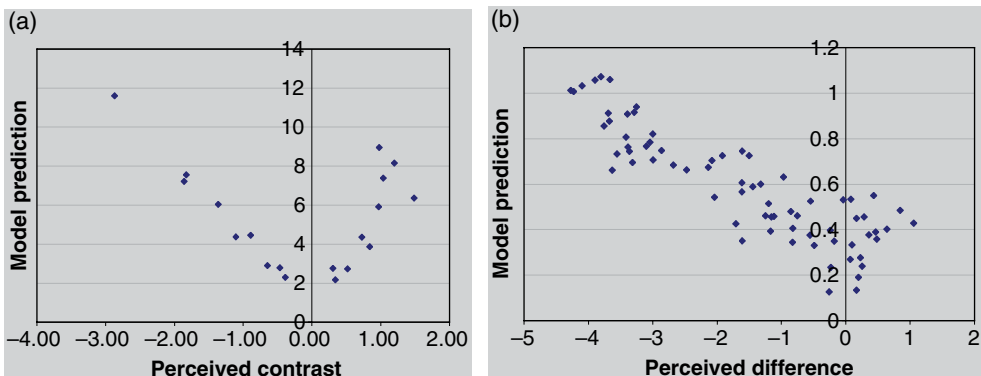


**Figure 20.9** iCAM image differences as a function of (a) perceived image contrast and (b) perceived image sharpness for a variety of image transformations. (Note: Desired predictions are V-shaped data distributions since the perceptual differences are signed and the calculated differences are unsigned.)

2000) and contrast (Calabria and Fairchild 2002) differences in images through a single summary statistic (mean image difference). This performance is equivalent to, or better than, that obtained using other color spaces optimized for the task. (Johnson and Fairchild 2001b).

The contrast results in Figure 20.9(a) were obtained by asking observers to scale perceived image contrast for a collection of images of various content subjected to a variety of transformations (Fairchild and Johnson 2003). The resulting interval scale (average data) is plotted as perceived contrast in Figure 20.9(a), and the model prediction of image difference from the original (arbitrarily selected) is compared with it. Ideally the data would follow a V-shape with two line segments of equal absolute slope on either side of the origin. The perceived contrast data are well-predicted by the iCAM image difference.

The perceived sharpness results in Figure 20.9(b) were obtained in a similar manner using a significantly larger number of image manipulations and content (Johnson and Fairchild 2003a). Observers were simply asked to scale perceived sharpness, and the results were converted to an interval scale, again with the original image as an arbitrary zero point. There is greater variability in these data, but it can be seen in Figure 20.9(b) that the results are again well-predicted by a fairly simple mean image difference metric.

More details, source code, and improvements regarding iCAM can be found at (<http://www.cis.rit.edu/mcs/iCAM>).

## 20.7 iCAM06

Kuang *et al.* (2007a,c) examined the use of iCAM and other models for accurate rendering of HDR scenes, and with another set of authors Kuang *et al.* (2007b, 2010) evaluated the reality of using HDR displays as proxies for HDR scenes. This work resulted in the development of a revised version

of iCAM, known as iCAM06, aimed mainly at HDR image rendering applications (Kuang and Fairchild 2007, Kuang *et al* 2007a).

Readers are encouraged to review the original literature, or to examine the iCAM06 website, for full details of the model formulation and implementation. The iCAM06 implementation is represented pictorially in Figure 20.10. The most significant change with respect to iCAM is that the iCAM06 implementation uses a bilateral filter implementation (Durand and Dorsey 2002) to separate a “details” layer from a “base” layer. That base layer is then tone-mapped using the low-pass adaptation function from iCAM. iCAM06 also includes ad hoc adjustments for detail contrast, colorfulness, and surround contrast effects. These are not incorporated in iCAM as separately adjustable parameters (with the exception of surround). In general, the renderings produced by iCAM06 are not considered any more accurate than iCAM, but they are often preferred because they are more colorful, contrasty, and sharper than the original images. Figure 20.11 illustrates the rendering of two HDR scenes using iCAM06 with three different settings for surround relative luminance.

iCAM06 should not be considered a replacement for the iCAM framework, but more appropriately as one specific implementation of it. More details, source code, and improvements regarding iCAM06 can be found at <http://www.cis.rit.edu/mcls/icam06/>.

## 20.8 ORTHOGONAL COLOR SPACE

One, often not discussed, attribute of image appearance and image difference modeling is that the three-color dimensions (normally opponent dimensions) should be mathematically orthogonal to one another if the spatial filtering applied is different for the three channels. If the channels are not orthogonal, then spatial filtering in one channel might well introduce chromatic (or luminance) artifacts in the other channels when an image is reconstructed. Johnson *et al* (2010) completed a series of experiments and statistical modeling of their results in order to derive an orthogonal color space that could be used for image difference modeling and differential spatial filtering. They recognized that the opponent color dimensions in many of these models are not orthogonal to one another and thus spatial filtering in one channel influences the image data in others. This is far from optimal when differential filtering across the channels is necessary, as in the human visual system.

Their experiments were based on measuring the perceptibility of noise in various color dimension (and locations in color space) with the assumption that noise would be most perceptible along a putative luminance or light-dark dimension. Principal components analyses were then used to define the luminance dimension in relationship to CIE XYZ and simultaneously define two orthogonal color dimensions. The Johnson *et al.* (2010) results depended slightly (but statistically significantly) on background relative luminance. Thus the orthogonal dimensions for all three backgrounds are presented in Equations 20.25 through 20.28.

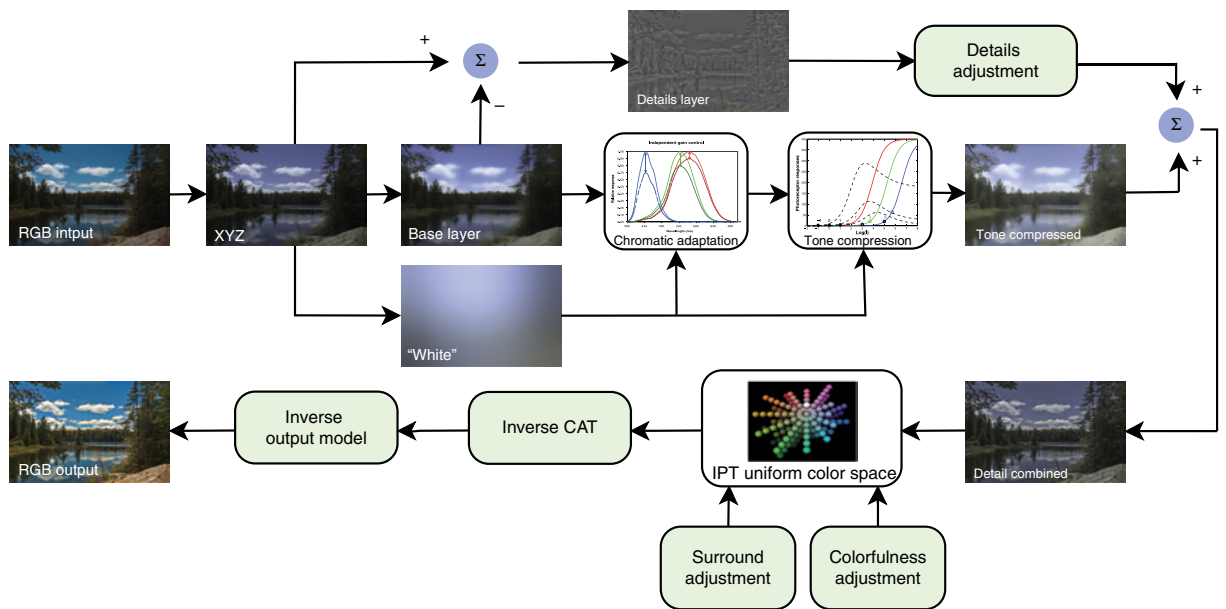


**Figure 20.10** Flow chart of the iCAM06 implementation of the iCAM framework for image color appearance modeling



**Figure 20.11** Example of HDR image rendering for different surround viewing conditions according to iCAM06. Images are rendered at lower contrast for an average surround since a dark surround will perceptually lower contrast by making dark image areas appear lighter. Images from *The HDR Photographic Survey*

$$\begin{bmatrix} V_1 \\ V_2 \\ V_3 \end{bmatrix} = \mathbf{M}_{\text{Ortho}} \begin{bmatrix} X \\ Y \\ Z \end{bmatrix} \quad (20.25)$$

$$\mathbf{M}_{\text{Ortho}(0.1)} = \begin{bmatrix} -0.0249 & -0.048 & -0.9985 \\ 0.9936 & -0.1114 & -0.0194 \\ -0.1103 & -0.9926 & 0.0505 \end{bmatrix} \quad (20.26)$$

$$\mathbf{M}_{\text{Ortho}(0.29)} = \begin{bmatrix} -0.0048 & 0.0196 & -0.9998 \\ -0.9983 & 0.0578 & -0.0059 \\ -0.0579 & -0.9981 & 0.0193 \end{bmatrix} \quad (20.27)$$

$$\mathbf{M}_{\text{Ortho}(0.65)} = \begin{bmatrix} -0.0279 & 0.0064 & -0.9996 \\ -0.9996 & -0.0018 & -0.0279 \\ 0.0016 & -1.0000 & 0.0064 \end{bmatrix} \quad (20.28)$$

The results in Equations 20.26 through 20.28 are for background relative luminances of 0.10, 0.29, and 0.65, respectively. In each case, the third dimension ( $V_3$ ) represents the dimension where noise is most perceptible (luminance), and it can be seen that it highly correlates with the CIE Y

(luminance) dimensions. Interestingly, the other two dimensions are not opponent colors dimensions, but rather correlate very highly with the CIE X and Z tristimulus values, which, by mathematical definition, carry no luminance information and are thus orthogonal to luminance. This particular result is interesting, somewhat due to the design of experiments and the analysis via principal components in tristimulus space. The results do not imply that opponent dimensions are not important in color vision modeling. However, these results should guide users to be careful when performing differential spatial filtering on chromatic channels.

## 20.9 FUTURE DIRECTIONS

The formulation, testing, and application of color appearance models have matured significantly in the years since the first edition of this book. While color appearance modeling remains an area of ongoing research, the types of models developed in the future might well follow the general concepts of image appearance modeling outlined in this chapter. Traditional color appearance models, like CIECAM02, are somewhat mature and significant advances will likely require different types of models. This section speculates on what might happen in the near future by commenting on the same areas that were discussed in the final chapter of the first edition.

### One Color Appearance Model?

Will there ever be a single color appearance model that is universally accepted and used for all applications? Absolutely not! The problem is too complex to be solved for all imaginable applications by a single model. Even the specification of color differences continues to be performed with two color spaces: CIELAB and CIELUV. While CIELAB is clearly preferable for such applications, a single color difference equation within the CIELAB space has yet to be widely accepted. There is no reason to expect the specification of a color appearance model to be any different.

The CIE activities in formulating CIECAM97s and CIECAM02 have been successful and have promoted uniformity of practice in industry and provide a significant step toward the establishment of a single, dominant technique for color appearance specification. Assuming these CIE activities continue to be well received, the use of color appearance models should become simpler and more uniform. However, there is no question that, for specific applications, other models will continue to be used and developed. Perhaps the use of color appearance models will reach a status similar to today's specification of color differences or color order systems in which a small number of techniques are dominant, with a wider variety of techniques still being used in some specific applications.

## Other Color Appearance Models

This book has concentrated on the Hunt, Nayatani *et al.*, CIELAB, RLAB, and CIE models as the key available color appearance models. These models cover the range of those that are likely to be considered for various applications in the foreseeable future. The probability of other similar color appearance models being published in the near future is low. Instead it is more likely that those involved in the above models will continue to contribute cooperatively to the development and comparative testing of the CIE model. New models will be new types of models such as iCAM or perhaps the HDR-type or color scales models described in Chapter 21. Other approaches are also being developed to explore image appearance and modeling (Reinhard *et al.* 2012).

## Ongoing Research to Test Models

Given the recent increase in interest in color appearance models and their application to practical problems, the amount of research dedicated to the evaluation of model performance has also grown. This research is being carried out by a variety of scientists in industry and academia through individual programs, product development, and the activities of various CIE Technical Committees described in Chapter 17.

Of interest in the coming years will be an evaluation of the success of color appearance models in real applications, such as device-independent color imaging through the ICC profile framework. The results of these “real world” tests will set a practical standard for color appearance modeling. It is entirely possible that a very simple level of modeling, such as a von Kries transform, will suffice if the control and specification of viewing conditions and the accuracy of device characterizations are not first improved. These are necessary prerequisites to the application of color appearance models.

An analog for the future development of color appearance models can be found in the specification of the color matching functions of the CIE 1931 Standard Colorimetric Observer. These functions were established nearly 70 years ago and have been successfully used in industry since that time. However, research on the measurement of more accurate color matching functions and the variability in those functions has continued since that time and is still ongoing. Such research has uncovered systematic errors in the CIE functions that are critical for some applications. In such applications, alternative color matching functions are often used. However, none of the discrepancies found through this research to date has been significant enough to warrant the abandonment of the 1931 recommendation that is firmly, and successfully, entrenched in a variety of industries. Perhaps a similar path will be followed in the area of color appearance models. If CIECAM02 continues to find wide

acceptance and application, research on it and the other models presented in this book will continue. If an improvement that is truly significant for practical applications is found, it will be quickly adopted. However, this might not happen until well after the other fundamental issues (*e.g.*, characterization accuracy and viewing condition control) are adequately addressed.

## Ongoing Model Development

The first edition of this book stated:

*An interesting direction that is likely to be pursued in the future is the incorporation of spatial and temporal effects into color appearance models. Some of the issues to be addressed have been discussed by Wandell (1993), Poirson and Wandell (1993, 1996), and Bäuml and Wandell (1996) (371).*

It is clear that this is coming to pass in terms of spatial and temporal models as described in the preceding sections of this chapter. Research along these lines will continue, with models being further refined, for the foreseeable future.

The first edition also speculated on the use of neural networks.

*Another approach that is being investigated for the prediction of color appearance phenomena is the use of neural network models. Courtney et al. (1995a,b) presented interesting examples of such an approach (371).*

This approach has seemed to fall out of favor in color appearance modeling and elsewhere.

# High-Dynamic-Range Color Space

---

Much of the work of color science and colorimetry is focused on the appearance of materials. This means that the dynamic range of luminance that is of interest is limited to the range of reflectances of materials under a single illumination. This luminance dynamic range is often as low as 20:1 and ranges up to only about 90:1. The same is true of most image displays when viewing flare is considered. This limitation in the dynamic range of interest necessarily results in certain, sometimes limiting, choices in the design of color spaces and metrics. For example, it is sometimes stated that CIELAB is, by design, a low-dynamic-range color space and that makes it difficult to apply in high-dynamic-range scenes.

Dynamic range, in this context, is normally defined as the ratio of the highest luminance in a scene to the lowest luminance. It should be noted that dynamic range is also sometimes expressed in terms of bits, or number of quantized levels. However, such a specification relies on an assumption of linearity and of the specification of the minimum and maximum values to be and what is coded as the maximum and minimum values. For example, a reported eight-bit dynamic range might be identical to a 255:1 dynamic range in the scene, but those eight bits might also encode only a fraction of the luminance range, an even larger range, and/or be encoded nonlinearly. Thus “bits” is not always a meaningful measure of dynamic range. Equally confusing is the term “stops” for dynamic range. A stop represents a doubling of exposure, but each exposure itself can have a dynamic range. So if each exposure is assumed to have a 255:1 dynamic range (8 bits encoded linearly), then a camera encoding 14 linear bits of luminance would have seven stops of dynamic range. (The first eight bits doubled six more times.) However, such a camera is usually reported to have a 14-stop dynamic range. All of this confusion just highlights how important it is to keep the

terms straight, and the most straightforward way to define dynamic range is as a luminance ratio. It also illustrates how colorimetry and color appearance in high-dynamic-range scenes becomes difficult.

Then the question becomes just what is “high dynamic range” or HDR. In imaging, normal scenes are encoded with 256 levels or a roughly 255:1 dynamic range. If this were a linear encoding, it would be suitable for flat scenes with no highlights, but might be insufficient to encode shadow or highlight detail. Thus, for various reasons, those 256 levels are usually encoded on a nonlinear scale approximating a power function or logarithmic, compressive response. Thus, the equivalent linear encoding is on order of 12 bits or about 4000:1. That leaves, as a practical definition, HDR as any scene or display with a luminance ratio greater than 4000:1 (and thus requiring 13 bits or more to encode in linear luminance). In reality, natural HDR scenes can have significantly greater luminance ratios due to the presence of highlights, deep shadows, light sources, *etc.* This chapter discusses some of the issues of trying to specify color appearance in HDR situations. Some insight into these difficulties can be obtained through the study of HDR imaging, *e.g.*, in the text of Reinhard *et al.* (2006).

## 21.1 LUMINANCE DYNAMIC RANGE

The range of luminances encountered in natural and man-made environments spans 14, or more, orders of magnitude from objects illuminated by starlight to direct viewing of the sun. However, some of the highest levels (*e.g.*, the sun itself) are not viewed directly for safety reasons, and the very lowest levels (*e.g.*, dark objects in the shadows under starlight) cannot normally be present at the same time as the highest luminance levels due to scattered light. Nonetheless, the human visual system is capable of functioning across this wide range of luminance levels through the mechanisms of light and dark adaptation (Chapter 1). Figure 21.1 pictorially illustrates the wide range of luminance levels the visual system is able to adapt to and perform under. To approximately calibrate these levels in terms of luminance, our visual system can function under starlight ( $0.01\text{cd/m}^2$ ), moonlight ( $0.1\text{cd/m}^2$ ), nighttime illumination ( $1\text{cd/m}^2$ ), dawn/dusk ( $10\text{cd/m}^2$ ), office lighting ( $100\text{cd/m}^2$ ), displays ( $500\text{cd/m}^2$ ), overcast daylight ( $1000\text{cd/m}^2$ ), bright daylight ( $10,000\text{cd/m}^2$ ), and direct sunlight ( $100,000\text{cd/m}^2$ ). The lowest two levels are roughly served by scotopic (rod) vision, the next two by mesopic (rod and cone) vision, and the rest by photopic (cone) vision.



**Figure 21.1** A pictorial representation of the range of luminance levels present in natural and man-made scenes

This refers to the range of vision, but not the dynamic range, which refers to the range of luminance levels encountered simultaneously within a single scene (or display). A wide variety of dynamic ranges can be encountered in natural scenes. For example, a scene with diffuse illumination and matte objects might have a very low dynamic range (*e.g.*, 20:1) while the same objects with more directional illumination might have a significantly higher dynamic range (*e.g.*, 100:1). If the scene is modified to include the geometry necessary to produce deep shadows and the surface properties necessary to produce reflected highlights, then the dynamic range is of thousands-to-one. The dynamic range of a scene can be further increased by the presence of directly visible light sources, and in such cases it is possible to find scenes with dynamic ranges as high as a million-to-one. However, it should be noted that scattering and indirect illumination into shadow areas make such very high dynamic ranges extremely rare.

An interesting artifact of exploring color in three-dimensional and HDR scenes is that some elements of the scene are almost certain to have luminance levels significantly greater than that of diffuse white (the reference point for CIELAB lightness) and that translates into computed  $L^*$  values greater than 100. This leads one to question the validity of such  $L^*$  values and the meaning of colorimetry outside the range for which it was designed. Such is the quest of the work described in the following sections.

It is worth noting that approaches other than those discussed in this chapter have been proposed. Kim *et al.* (2009) provided some discussion of the needs for color appearance modeling across wide dynamic ranges, but their focus was more on high luminance than high range in luminance. In addition, Reinhard *et al.* (2012) have begun to formalize some concepts of HDR image appearance.

## 21.2 THE HDR PHOTOGRAPHIC SURVEY

In order to study the measurement, imaging, appearance, and reproduction of HDR scenes and images, one needs a reliable set of data that can be used to test algorithms and data. The creation of such a data set of images and related data for computational and psychophysical testing was the objective of the HDR Photographic Survey (Fairchild 2007, 2008).

The survey, modeled after some of the early photographic surveys of the western USA that helped create the National Park Service and preserve other important environments, resulted in the creation of a unique collection of images, colorimetric scene data, scene appearance data, and calibration data. This collection of over 100 images, and their associated data, is freely available online (<http://www.cis.rit.edu/fairchild/HDR.html>). For most scenes, image data were collected through multiple exposures, each separated by one stop of exposure that were then assembled together into floating-point HDR images. Colorimetric data were collected in the scenes with a spot colorimeter, and appearance data were collected through visual scaling. Figure 21.2 shows an Apple Aperture window with the multiple

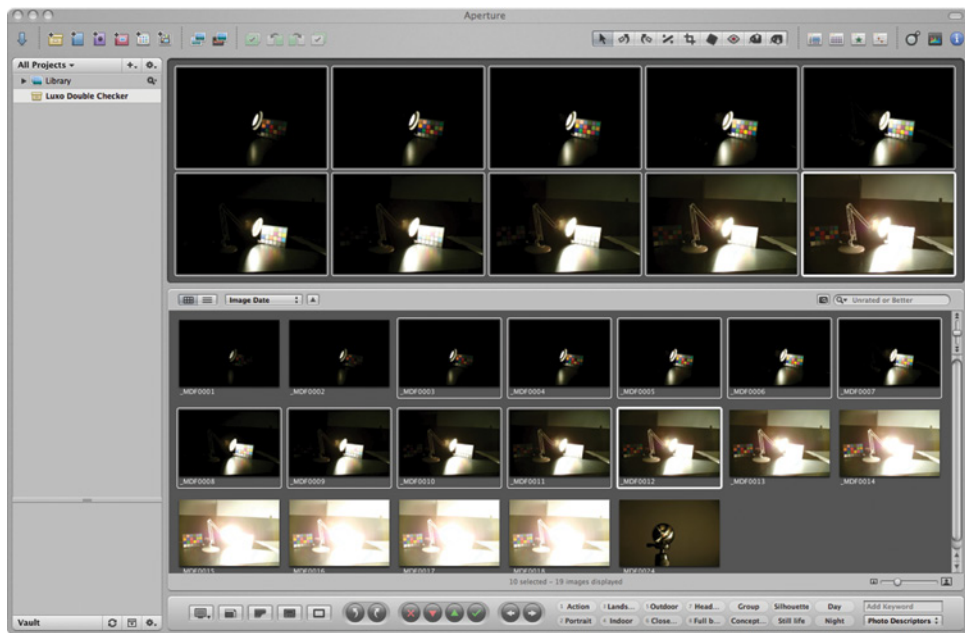


**Figure 21.2** An Apple Aperture window illustrating each of the 18 exposures, separated by one stop in exposure, captured to create an HDR image of a test scene created to have a dynamic range of roughly one million to one

exposures for a scene constructed in the laboratory to have a dynamic range of approximately one million to one. For that scene, 18 exposures were captured. Examination of the various exposures provides some enlightenment on how various details can be found at various exposure levels. It also illustrates the limiting factor of lens flare. Figure 21.3 shows one example from the project. It is an image of the Golden Gate Bridge with San Francisco in the background that was captured about 30 minutes after sunset (in late April). The upper image is a direct (linear) rendering of the HDR image created by placing the brightest lights at the maximum levels of an eight-bit imaging system and allowing the remaining luminances to fall as they might below that. The result is that most of the image is at a luminance level so low that the image is very dark. The lower image is tone mapped using a local adaptation model simulating the response of the human visual system (again with the brightest lights rendered to the maximum). The adaptation model (like that found in iCAM or iCAM06) lightens the dark areas since our visual systems would adapt to the lower luminance levels in those areas to allow us to see detail. Our visual systems do this on a local basis through the scene, thus the lower image appears very similar to the appearance of the actual scene.

Fairchild (2007) describes the technical detail behind the creation of the HDR Photographic Survey, and Fairchild (2008) provides a short book with the stories behind some of the images and renderings of the images.



**Figure 21.3** An HDR image of the Golden Gate Bridge (top) and a rendered version of that same image created using a local adaptation technique designed to mimic the response of the human visual system and the appearance to an observer standing with the camera

## 21.3 LIGHTNESS–BRIGHTNESS BEYOND DIFFUSE WHITE

In addition to having scene data for HDR studies, it is necessary to explore how humans perceive lightness and brightness for luminance levels above the adapting/diffuse white point. Chen *et al.* (2010) performed a series of experiments aimed at answering two questions: (1) how do observers perceived lightness differences above diffuse white and (2) what is the scale of perceived lightness above diffuse white? Thus, they completed both lightness scaling and difference matching experiments with rather unique adaptation and stimulus conditions (required to preserve adaptation levels) to explore these questions.

Their results were twofold. On differences, they found that the CIE DE2000 lightness weighting function worked reasonably well for lightness above diffuse white and that optimal results could be obtained with a similar

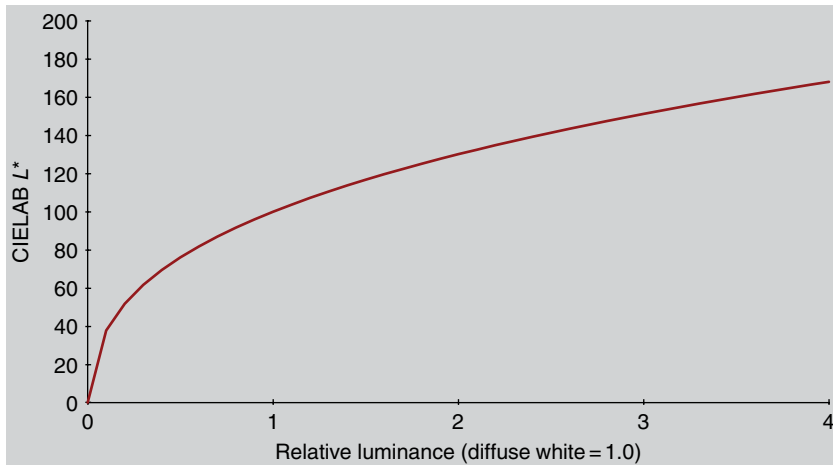


**Figure 21.4** The CIELAB  $L^*$  function extended to an input range four times the luminance of diffuse white

function using slightly different coefficients. Thus, the perception of lightness differences above diffuse white are similar in functional form to those modeled with the CIE DE2000 equations. With respect to the lightness scale itself, Chen *et al.* (2010) found that the scaled lightnesses followed the CIELAB  $L^*$  function reasonably well up to the maximum relative luminance measured of about 400 (4× diffuse white). Specific fitting to the data could produce alternative functions with better performance, but the uncertainty in the data were such that the CIELAB  $L^*$  function could be considered a reasonable fit. For reference, Figure 21.4 shows the CIELAB  $L^*$  function extended to a greater dynamic range.

## 21.4 hdr-CIELAB

Fairchild and chen (2011) took the Chen *et al.* (2010) results to extend the CIELAB color space to function across high-dynamic ranges. They replaced the cube-root nonlinearity in CIELAB with Michaelis–Menton functions (which include an offset at threshold and saturation) to reformulate CIELAB with better behavior for very low and very high luminance levels. The basic structure of such a space was proposed by Fairchild and Wyble (2010), and Fairchild and Chen (2011) provided the detailed implementation outlined below.

The new color space, referred to as hdr-CIELAB, follows the normal CIELAB formula with a new compressive nonlinearity having better performance for shadows and highlights. The fitted equation is given in Equation 21.1. The lightness function arriving from this nonlinearity is illustrated in Figure 21.5.

$$f(\omega) = 247 \frac{\omega^\epsilon}{\omega^\epsilon + 2^\epsilon} + 0.02 \quad (21.1)$$

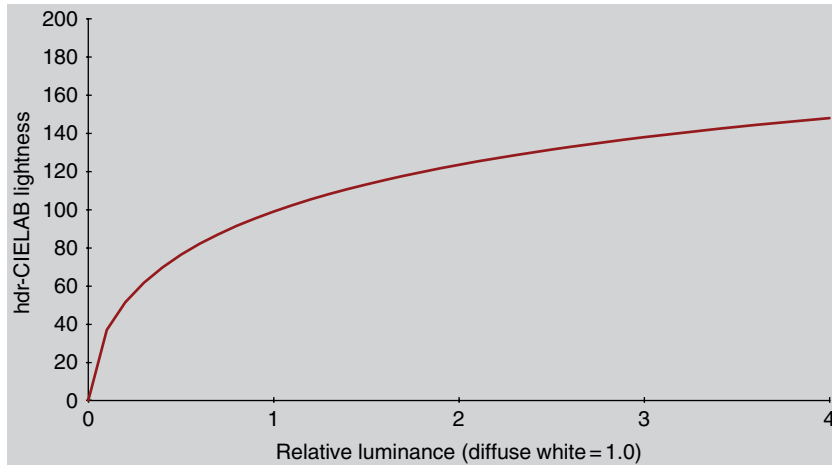


**Figure 21.5** The lightness function of the hdr-CIELAB space computed to an input range four times the luminance of diffuse white

Fairchild and Chen (2011) further allowed for the exponents to vary based on surround factors ( $sf$ ) and luminance factors ( $lf$ ) as illustrated in Equations 21.2 through 21.4. The base exponent for hdr-CIELAB is 0.58.

$$\varepsilon = \frac{0.58}{sf \cdot lf} \quad (21.2)$$

$$sf = 1.25 - 0.25 \left( \frac{Y_s}{0.184} \right); \quad (0 \leq Y_s \leq 1.0) \quad (21.3)$$

$$lf = \frac{\log(318)}{\log(Y_{abs})} \quad (21.4)$$

The hdr-CIELAB parameters are then computed the normal way.

$$L_{\text{hdr}} = f \left( \frac{Y}{Y_n} \right) \quad (21.5)$$

$$a_{\text{hdr}} = 5 \left[ f \left( \frac{X}{X_n} \right) - f \left( \frac{Y}{Y_n} \right) \right] \quad (21.6)$$

$$b_{\text{hdr}} = 2 \left[ f \left( \frac{Y}{Y_n} \right) - f \left( \frac{Z}{Z_n} \right) \right] \quad (21.7)$$

$$c_{\text{hdr}} = \sqrt{a_{\text{hdr}}^2 + b_{\text{hdr}}^2} \quad (21.8)$$

$$h_{\text{hdr}} = \tan^{-1} \left( \frac{b_{\text{hdr}}}{a_{\text{hdr}}} \right) \quad (21.9)$$

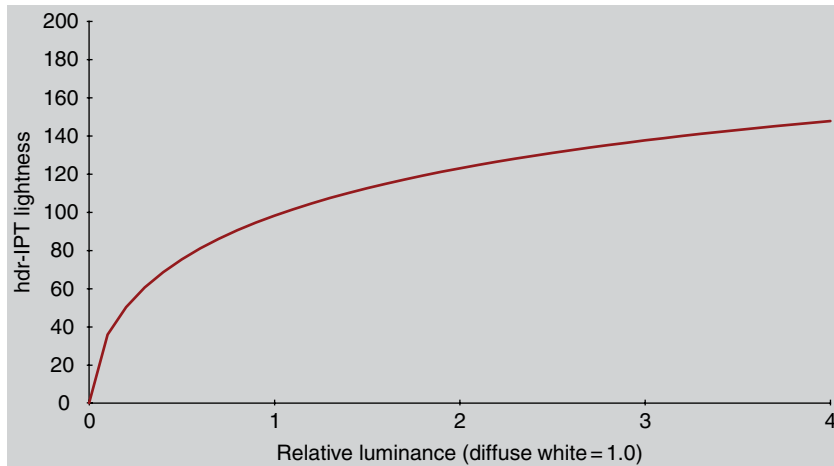


**Figure 21.6** The lightness function of the hdr-IPT space computed to an input range four times the luminance of diffuse white

## 21.5 hdr-IPT

Fairchild *et al.* (2011) took the Chen *et al.* (2010) results to extend the IPT color space to function across high-dynamic ranges. They replaced the power-function nonlinearity in IPT with Michaelis–Menton functions (which include an offset at threshold and saturation) to reformulate IPT with better behavior for very low and very high luminance levels. The basic structure of such a space was proposed by Fairchild and Wyble (2011), and Fairchild and Chen (2011) provided the detailed implementation outlined below.

The new color space, referred to as hdr-IPT, follows the normal IPT formula with a new compressive nonlinearity having better performance for shadows and highlights. The fitted equation is given in Equations 21.10. The lightness function arriving from this nonlinearity is illustrated in Figure 21.6.

$$f(\omega) = 246 \frac{\omega^\varepsilon}{\omega^\varepsilon + 2^\varepsilon} + 0.02 \quad (21.10)$$

Fairchild and Chen (2011) further allowed for the exponents to vary based on surround factors ( $sf$ ) and luminance factors ( $lf$ ) as illustrated in Equations 21.11 through 21.13. The base exponent for hdr-IPT is 0.59.

$$\varepsilon = \frac{0.59}{sf \cdot lf} \quad (21.11)$$

$$sf = 1.25 - 0.25 \left( \frac{Y_s}{0.184} \right); \quad (0 \leq Y_s \leq 1.0) \quad (21.12)$$

$$f = \frac{\log(318)}{\log(Y_{\text{abs}})} \quad (21.13)$$

The hdr-IPT parameters are then computed the normal way.

$$\begin{bmatrix} L \\ M \\ S \end{bmatrix} = \begin{bmatrix} 0.4002 & 0.7075 & -0.0807 \\ -0.2280 & 1.1500 & 0.0612 \\ 0.0 & 0.0 & 0.9184 \end{bmatrix} \begin{bmatrix} X_{\text{D65}} \\ Y_{\text{D65}} \\ Z_{\text{D65}} \end{bmatrix} \quad (21.14)$$

$$\begin{aligned} L' &= f(L); & L \geq 0 \\ L' &= -f(-L); & L < 0 \end{aligned} \quad (21.15)$$

$$\begin{aligned} M' &= f(M); & M \geq 0 \\ M' &= -f(-M); & M < 0 \end{aligned} \quad (21.16)$$

$$\begin{aligned} S' &= f(S); & S \geq 0 \\ S' &= -f(-S); & S < 0 \end{aligned} \quad (21.17)$$

$$\begin{bmatrix} I_{\text{hdr}} \\ P_{\text{hdr}} \\ T_{\text{hdr}} \end{bmatrix} = \begin{bmatrix} 0.4000 & 0.4000 & 0.2000 \\ 0.4550 & -4.8510 & 0.3960 \\ 0.8056 & 0.3572 & -1.1628 \end{bmatrix} \begin{bmatrix} L' \\ M' \\ S' \end{bmatrix} \quad (21.18)$$

$$c_{\text{hdr-IPT}} = \sqrt{P_{\text{hdr}}^2 + T_{\text{hdr}}^2} \quad (21.19)$$

$$h_{\text{hdr-IPT}} = \tan^{-1} \left( \frac{T_{\text{hdr}}}{P_{\text{hdr}}} \right) \quad (21.20)$$

## 21.6 EVANS, $G_0$ , AND BRILLIANCE

While above interesting, there remain questions about lightness for chromatic colors. For example, is lightness relative to diffuse white or something else, does chromatic lightness follow the same functions of luminance, how can the Helmholtz–Kohlrausch effect be accounted for in a simple manner, etc.?

As it turns out, much insight on this topic can be gained from the work of an historical Kodak scientist, Ralph Evans, who published on issues of appearance and color reproduction. His book, *The Perception of Color* (Evans 1974), describes the important concepts of zero-gray value and brilliance that have helped create several new ideas in color appearance modeling. Also to his credit are books such as *An Introduction to Color* (1948), *Principles of Color Photography* (Evans *et al.* 1953), and *Eye, Film, and Camera in Color Photography* (Evans 1959). He was also instrumental in the OSA Committee on Colorimetry, which produced the outstanding first edition of *The Science*

of Color (1963) that includes a chapter on perceptual and affective aspects of color that Evans clearly had a role in writing.

Evans concept of  $G_0$  (G-zero) is fairly straightforward, yet far more important for fully understanding color appearance than it seems. It is best explained with an example. Imagine you have a spot of orange light in a white background and you can control the luminance of the orange spot without affecting either its chromaticity or any aspect of the background. If the spot is reduced in luminance to near zero, it will appear black. As its luminance is increased, the spot will first appear as a darker, brown object, but it will then transition to the appearance of an orange object as it becomes brighter (lighter). However, the luminance can be increased further until it reaches a point where the spot no longer looks like an reflecting object relative to the background, but it instead starts to appear to “glow” like an orange light source. Further increases in luminance do not change the fundamental nature of the appearance any more; they simply make the spot look like a brighter orange light source.

This particular stimulus goes through a sequence from black, to brown object, to orange object, to orange light source (then to brighter orange light source) as luminance is increased. The luminance at which the transition from orange object to orange light source occurs is the  $G_0$  luminance (or luminance of zero gray content) for that particular chromaticity. It represents the luminance at which a particular stimulus transforms from object (some gray content) to illuminant (no gray content) mode of appearance, and that  $G_0$  luminance depends on the chromaticity of the stimulus and the surround, or adapting, conditions. (Note: the brown to orange transition is nothing more than a color name change since dark orange objects have a unique color name, brown.) In addition, Evans used the term “brilliance” to describe the location along the luminance scale with respect to  $G_0$ . For example, a selection of colors at  $G_0$  might all have the same brilliance. Those appearing like light sources (luminance above  $G_0$ ) would have a relatively high brilliance and those appearing like dark objects (luminance well below  $G_0$ ) would have a relatively low brilliance.

The next interesting question regards the relationship between  $G_0$  luminance for various chromaticities and the luminance of diffuse white (by definition the  $G_0$  luminance of a perceptually neutral chromaticity). If they were the same, then one could simply conclude that when a stimulus had a higher luminance than the diffuse white, it would appear to be glowing as a light source. Perhaps surprisingly, this is not even close to reality. For some, highly chromatic, stimuli the  $G_0$  luminance is significantly lower than the luminance of white. That means a stimulus can appear to be glowing at luminance levels substantially lower than that of white. What is equivalent for all these different colors at  $G_0$  is some kind of apparent brightness, perhaps brightness when the Helmholtz–Kohlrausch effect is accounted for. In other words,  $G_0$  defines the luminance of equal chromatic brightness (really, just brightness) for various chromaticities. Measuring brightness relative to  $G_0$ , instead of relative to the luminance of white, automatically adjusts for the Helmholtz–Kohlrausch effect and can truly define lightness

with a single function. The remaining difficulty is that there is no simple mathematical model of  $G_0$  yet.

The importance of Evans' concepts of  $G_0$  and brilliance are that they might well be the key missing component of color appearance models with respect to deriving a simple relationship between luminance, saturation, and lightness/brightness. Two attempts to start reconciling these differences are described in Sections 21.7 and 21.8.

## 21.7 THE NAYATANI THEORETICAL COLOR SPACE

Later in his career, Nayatani (2003, 2004) published different forms of color models that came to be known as the Nayatani theoretical (NT) color space. While in some ways the NT space could be considered an extension of the Nayatani *et al.* (Chapter 11) color appearance model, it also incorporates some new concepts based on the NCS system and Evans' concepts of  $G_0$ /brilliance. The NT color space has also been used as the basis of a color gamut mapping technique aimed at expanding colors to fill large color gamuts (Heckaman *et al.*, 2008, 2009, 2011; Fairchild, 2008a) while respecting the definitions of  $G_0$ /brilliance for both the original image content and the display color gamuts. The basic message of such an algorithm is to never expand the saturation of colors inside the  $G_0$  boundary but feel free to expand colors outside it to fill the gamut (thus making brighter lights). It also extended to a similar concept for dark colors.

The NT color space defines a medium gray as its central component. For neutral colors a scale of whiteness–blackness is defined where the middle gray is at zero on both those scales. This is similar to NCS conceptually but differs numerically. Then, for any given hue, a triangle is constructed similar to an NCS hue plane with the three corners of white, black, and maximally chromatic. As one moves through the triangle toward the brighter chromatic boundary, grayness decreases and colors look brighter and more colorful and eventually the  $G_0$  boundary is reached. Nayatani also defined a similar decrease in grayness in the direction of darker, deeper colors and proposed a  $G_0$  boundary on that side as well. A dark  $G_0$  boundary is more questionable in terms of Evans' theory, but it makes some intuitive sense as Nayatani outlined it. Another approach to incorporating  $G_0$  into a model of color appearance is given in Section 21.8.

## 21.8 A NEW KIND OF APPEARANCE SPACE

Fairchild and Heckaman (2012) proposed a new approach modeling color appearance that does not aim to create a three-dimensional color space. It is hypothesized that the desire for a three-dimensional Euclidean space might well be a limiting factor in the creation of accurate scales of color appearance (and perhaps accurate color difference metrics). This section outlines the color appearance scales proposed by Fairchild and Heckaman (2012).

Color science is not devoid of examples typically described as color spaces that are actually descriptions of color perception one dimension at a time. For example, the Munsell system, despite its common embodiments, was derived as a system of three independent perceptual dimensions: hue, value, and chroma. Similarly, Guth's ATD model of visual perception was typically described in terms of independent dimensions, although the temptation to plot some of them together for some examples proved irresistible. Likewise, color appearance models such as CIECAM02 were developed with independent predictors of the six perceptual dimensions of brightness, lightness, colorfulness, saturation, chroma, and hue. This was somewhat compromised by requests for rectangular color space dimensions which appeared as CIECAM97s evolved to CIECAM02. However, it should be noted that cylindrical representations of the appearance spaces were common even before the requests for rectangular coordinates. Lastly, the NCS system provides a useful example of hue being treated separately from whiteness–blackness and chromaticness. And while NCS whiteness–blackness and chromaticness are plotted in two-dimensional trilinear form, the dimensions are largely independent since the anchor of maximal chromaticness appropriately varies from hue to hue.

This leads to the hypothesis that perhaps color space is actually a one-dimensional space, rather than a three-dimensional space, and that Euclidean distance metrics might indeed be successful in such a space. Of course, color appearance cannot be properly described in a single one-dimensional space. Instead six of them are required. There are three fundamental appearance attributes for related colors: lightness, saturation, and hue. Combined with information about absolute luminance, colorfulness and brightness can be derived from these and are important and useful appearance attributes. Lastly, chroma can be derived from lightness and saturation if desired as an alternative relative colorfulness metric. Thus, color is rightfully and fully described with six one-dimensional appearance spaces (or scales), four of which are fundamental for related colors and two of which are derived from the fundamental scales. This chapter provides some detail of the conceptual framework of a color model made up of one-dimensional spaces and an implementation of that framework for future application and investigation. Note: One-dimensional “spaces” are more commonly referred to as “scales” in color science, thus the term “scale” is used preferentially.

A set of color appearance scales (or dimensions, or spaces) following these principles has been derived. Presented first is the general framework that could be easily adapted to different specific implementations of the concept. The first step is to apply a chromatic adaptation model to compute corresponding colors for reference viewing conditions (e.g., D65, 315cd/m<sup>2</sup>). Then the IPT model, derived specifically for accurate hue representations, is used to compute a hue angle ( $h$ ), and then a hue composition ( $H$ ) can be computed based on NCS unique hues. For the defined hue, saturation (S) is computed using the classical formula for excitation purity applied along lines of constant  $h$  in the  $u'v'$  chromaticity diagram. For that chromaticity,

the luminance for zero gray content,  $G_0$ , is defined as the reference for lightness ( $L$ ) computations that follow a power function with offset model found to perform well for HDR-brightness scaling. Saturation takes precedence over chroma since it has a more fundamental relationship to physical stimuli and other chromatic dimensions are easily derived from it (Hunt 2001). The remaining dimensions are then derived from  $L$  and  $S$  along with luminance information. Brightness ( $B$ ) is lightness ( $L$ ) scaled by a factor derived from the classic work of Stevens and Stevens that illustrated terminal brightness as a function of adapting luminance. The derived scales are colorfulness ( $C$ ), which is simply saturation ( $S$ ) scaled by brightness ( $B$ ), and chroma ( $Ch$ ) which is saturation ( $S$ ) times lightness ( $L$ ).

This type of formulation allows accurate description of color appearance for lights and objects across a variety of adaptation conditions and for low- or high-dynamic-range scenes. To the degree that each perceptual scale is accurate, differences on each of the dimensions are easily calculated, and as long as the temptation to combine those differences into a single Euclidean distance metric is resisted, quite effective results can be obtained.

The hue scale ( $h$ ) is computed as a simple hue angle using the IPT model. The required inputs for the IPT hue angle computation are the CIE tristimulus values in  $XYZ$  for the corresponding colors in CIE illuminant D65. A chromatic adaptation transform is required to obtain corresponding colors for illuminant D65 if the stimuli of interest are viewed under a different state of adaptation. The CAT02 transformation imbedded in the CIECAM02 color appearance model is recommended. If luminance information is available and impacted by the selected chromatic adaptation transformation, then transformation to a white-point luminance of 315 cd/ $m^2$  is recommended. Hue composition ( $H$ ) can be obtained by recognizing that the NCS unique hues fall, on average at hue angles of 27.4, 89.8, 162.2, 231.3 degrees for red, yellow, green, and blue, respectively. Hue composition is computed simply as percentages between these four anchor hues as done in other color appearance models.

Saturation ( $S$ ) is computed in the classical way from excitation purity at the computed IPT hue in the  $u'v'$  chromaticity diagram. A slight modification is made in the distances used in the computation however. Saturation is computed as the ratio of the distance from the white point (D65) to the stimulus in question to the distance from the white point (D65) to the spectrum locus stimulus with the same hue angle ( $h$ ) as the stimulus in question. In cases where IPT constant hue predictions fall on straight lines in the  $u'v'$  diagram, this computation is identical with the traditional excitation purity computation. In cases where constant hue contours would be curved in  $u'v'$ , there are small differences in the calculation. This is illustrated in Figure 21.7 and Equation 21.21.

$$S = \frac{\sqrt{(u' - u'_n)^2 + (V' - V'_n)^2}}{\sqrt{(u'_L - u'_n)^2 + (V'_L - V'_n)^2}} \quad (21.21)$$

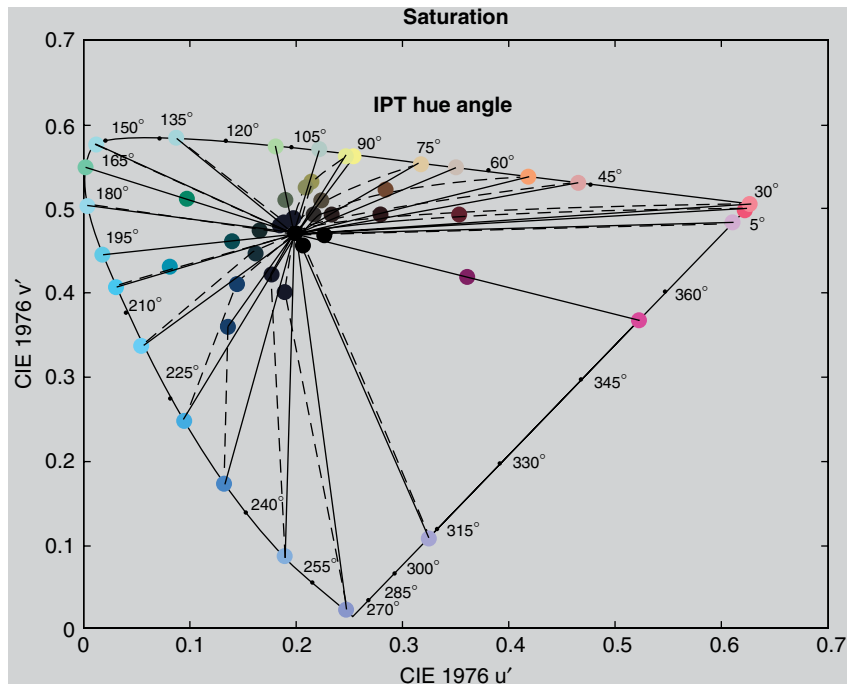


**Figure 21.7** Saturation in a  $u'v'$  chromaticity diagram annotated with IPT hue of a random sample from each of the 24 NCS Aim Hues

Maximum color saturation occurs at the locus of pure color computed in a  $u'v'$  chromaticity diagram by cascading the spectra of CIE illuminant D65 with the 2° Observer and each of the monochromatic stimuli at every integral nanometer from 300 to 830 nanometers of the visible spectrum. A LUT in  $u'v'$  as a function of IPT hue was then constructed in one-degree increments from the corresponding IPT hue values computed on the locus of pure color. Figure 21.7 illustrates samples of the resulting locus of pure color in a  $u'v'$  chromaticity diagram annotated with IPT hue angle. Saturation ( $S$ ) is then computed according to Equation 21.21.

In this computation,  $u'v'$  are the chromaticities of the stimulus,  $u'_n v'_n$  those of D65 diffuse white, and  $u'_L v'_L$  at the spectrum locus for the same hue angle from the LUT of the chromaticities of pure color in IPT hue. Figure 21.7 illustrates both a sample color randomly sampled from each of the 24 Natural Color System aim hues and the pure color at that same IPT hue. For each hue, vectors are shown as a solid line for the spectrum locus and as dotted lines for the sample color.

Lightness is computed from luminance for each color relative to the corresponding luminance at Evan's  $G_0$  (Evans 1974) from the relationships given by Nayatani (1993).  $G_0$  defines the luminance for each saturation at which stimuli of higher luminance appear self-luminous and stimuli of lower luminance appear to have gray content (or appear like object colors).

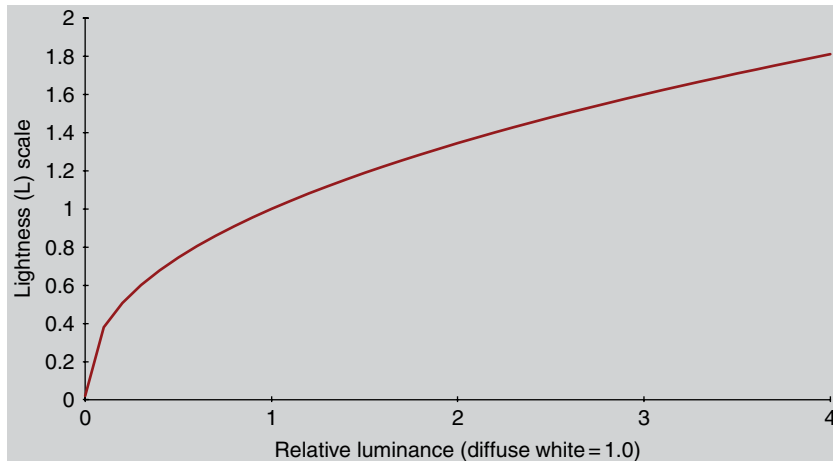


**Figure 21.8** The lightness ( $L$ ) function for a range up to four times the luminance of diffuse white and represented on a linear scale

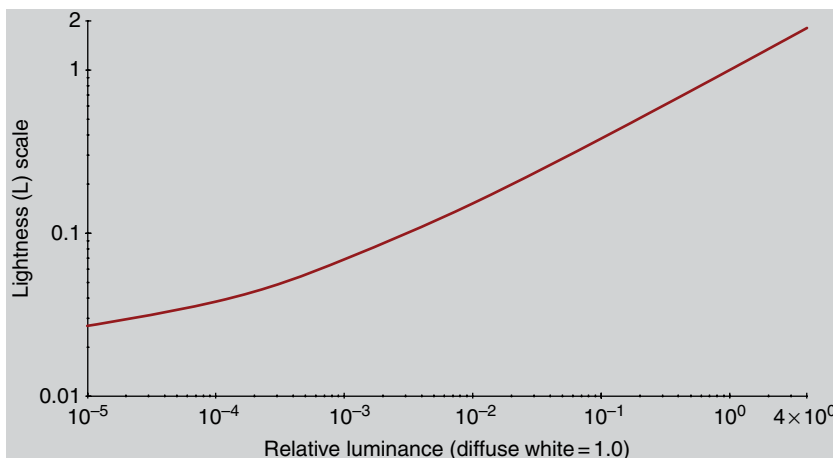


**Figure 21.9** The lightness ( $L$ ) function for a range up to four times the luminance of diffuse white and represented on a logarithmic scale

Thus the  $G_0$  luminance provides an appropriate reference for perceived lightness of object colors that accounts for the Helmholtz–Kohlrausch effect and discrepancies between photopic luminance predictions and heterochromatic brightness matches.

Chen *et al.* (2010) showed that lightness could be scaled both above and below diffuse white and that the perceptual results were well predicted by a lightness function of the form given in Equation 21.22. Equation 21.22 defines the lightness scale as a power function with an offset term, and its general form is illustrated in Figure 21.8 on a linear scale and in Figure 21.9 on a logarithmic scale.

$$L = 0.98Y_g^{1/2.3} + 0.02 \quad (21.22)$$

In Equation 21.22,  $Y_g$  is the luminance of the color relative to the luminance  $Y_{G_0}$  at  $G_0$  and its chromaticity.  $Y_{G_0}$  is given by finding relative luminance of the NCS color with minimum NCS blackness and the same chromaticities as the sample in question. The minimum value of NCS blackness is zero where grayness is said to be at  $G_0$ .

This can be determined for the value of the NCS blackness (swartz) derived from the chromaticities  $u'v'$  of the sample color, according to a method given by Heckaman and Fairchild (2008) with basis in Nayatani (1993) and the regression technique prescribed by Derefeldt and Sahlin (1986) from conversion data between NCS units of blackness and chromaticness and CIE tristimulus values taken from Bencuya (1984).

Brightness ( $Q$ ) is computed as a scaled version of lightness ( $L$ ). The scalar depends on the absolute luminance level and light adaptation to that level. This relationship has been described nicely by both Stevens and Stevens (1963) and Evans (1948) based on Marshall and Talbot (1942). In this implementation, the terminal brightness locus of Stevens and Stevens is used to define the brightness scalar. (An alternative might be to base it on the  $F_L$  function in CIECAM02 which serves a similar purpose.) The terminal brightness locus is the perceived brightness of a stimulus when an observer is adapted to the luminance of the stimulus itself. In other words, it defines how bright white appears as a function of adapting luminance. The brightness function is given by Equation 21.23.

$$Q = Q_{tbl}L \quad (21.23)$$

$Q_{tbl}$  is the terminal brightness locus where "...the level of sensation reached when the eye comes into full equilibrium with the luminance it is viewing."  $Q_{tbl}$  is computed as shown in Equation 21.24 derived from the brightness-luminance functions published by Stevens and Stevens (1963). Figure 21.10 illustrates the fitted terminal brightness locus where  $Y_w$  is the absolute luminance of diffuse white in  $\text{cd}/\text{m}^2$ .  $Q_{tbl}$  is defined to be 1.0 at an adapting luminance of  $100 \text{ cd}/\text{m}^2$ .

$$Q_{tbl} = 0.60[\log(Y_w + 1)]^{0.65} + 0.061 \quad (21.24)$$

Thus far, scales have been defined for hue ( $h$ ,  $H$ ), saturation ( $S$ ), lightness ( $L$ ), and brightness ( $Q$ ). These can be considered the most fundamental color appearance attributes for both related (HLS) and unrelated (HQS) colors. Saturation is considered a more fundamental appearance attribute than the more commonly used chroma and the rarely used colorfulness for a variety of reasons. Among these is that it is a fundamental property of materials (where chroma depends on the material and the illumination and therefore varies for three-dimensional objects made of a single material) and that it more directly relates to the physical stimulus (being constant as

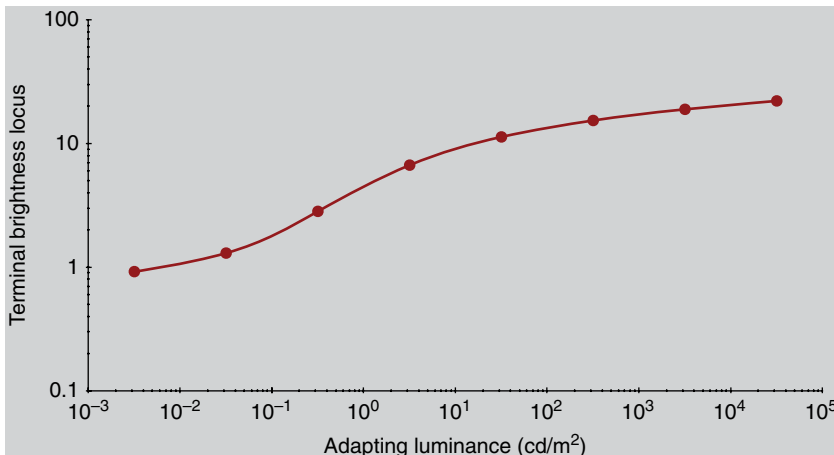


**Figure 21.10** The terminal brightness locus as a function of adapting luminance as fitted to the Stevens and Stevens results

the stimulus radiance or relative radiance is scaled). Hunt (2001) has provided an useful overview of the nature of saturation relative to other appearance attributes. That said, the final two color appearance scales of chroma and colorfulness can be useful at times and are easily derived from the scales described above. Chroma ( $C$ ) is simply defined as saturation ( $S$ ) scaled by the sample lightness ( $L$ ),  $C=LS$ . Likewise colorfulness ( $M$ ) is simply saturation ( $S$ ) scaled by brightness ( $Q$ ),  $M=QS$ .

Color differences are traditionally computed as the Euclidean distance between the coordinates of the two colors in some color space (e.g., the CIELAB  $\Delta E_{ab}^*$ ). It has long been recognized that such difference metrics do not correlate well with color difference perceptions, even when the dimensions of the color space seem to correlate well with appearance. As such, a number of weighted color difference equations (e.g., CIEDE2000) have been derived in attempts to create a more perceptually uniform color difference metric. These have met with some success, but at the expense of losing any simple relationship with the base color space.

Alternatively, users of color difference formulae are often encouraged to avoid the temptations of “mononumerosity” provided by  $\Delta E$  metrics and instead examine the individual components of color difference (e.g.,  $\Delta L^*$ ,  $\Delta C^*$ , and  $\Delta H^*$  in CIELAB). That is precisely the way color differences should be treated in a comprehensive color appearance model made up of separate one-dimensional appearance scales. In other words, since no geometrical relationship between the appearance scales is claimed or suggested, none should be assumed in the computation of color differences. Instead, only differences in the individual scales should be computed. It is likely that such differences can correlate very well with perceived color differences as either simple difference computations or with simple uni-dimensional weightings to account for differences in scales between suprathreshold appearance differences and overall appearance

scales. For tolerances to be derived for individual colors, nothing more than simple differences in the appearance scales is required (this is true of any reasonable color appearance dimensions). Such independent treatment of dimensions and their interactions can also easily be extended to appearance dimensions that are traditionally not considered part of color differences such as gloss, texture, noise, flicker, etc.

Software implementing this approach can be found at <http://www.cis.rit.edu/fairchild/CAM.html>.

## 21.9 FUTURE DIRECTIONS

To ponder future directions in a field, it is always good to look at where we stand. Our definitions of appearance dimensions (brightness, lightness, colorfulness, saturation, chroma, and hue) appear very sound and well understood. Our ability to predict these perceptions from physical measurements of stimuli still has a long way to go. Issues to resolve include accurate color matching functions with inter-observer variability, more accurate models of adaptation, more careful definition of models for appearance scales and their implementation, understanding of spatial and temporal properties of stimuli and perception, and creation of methods to combine the knowledge from all these domains and scales. While color appearance modeling has come a long way, there remains a very long way to go.

It is becoming clear that multidimensional representations of color appearance and difference almost always have significant shortcomings. Perhaps it is time to separate the dimensions and treat the separate dimensions of color appearance as distinct perceptions rather than parts of some multidimensional “color” perception. One thing is for certain, such an approach cannot hurt. Even within CIECAM02, a multiple uni-dimensional approach can be taken. These new ideas do show promise.

Ultimately, the need is for more data. Many more studies on perceptual matching, adaptation, scaling, appearance, and thresholds are needed to provide the needed data to create more accurate and precise scales of appearance. In an age where industrial research is becoming rare, this burden will fall on universities and students. The good news is there are plenty of universities with the expertise and willingness to do the research if only reliable sources of funding could be found. As is often the case, a dearth of research funding is what might be limiting this field.

### What To Do Now

Given the current status of color appearance specification, it is perfectly reasonable to ask the question: “What should I do now?” Some recommendations can be made based on the status of the models and tests as described in this book. The first point to remember is that a color appearance model should only be used if absolutely necessary. If the viewing conditions can be

arranged to eliminate the need for an appearance transform, that is the best course of action. If a complete color appearance model is required, the Hunt model is probably the best choice. If that level of complexity is not required, CIECAM02 might be a good choice. It is even possible that CIELAB might be adequate as a color appearance model in some applications. The best recommendation is to work up this chain from the simplest solution to the higher levels of complexity until the problem is solved. It is also worth noting that models should not be “mixed-and-matched” due to the significant differences between them. A single model should be used throughout a given system or process. The following listing summarizes this recommendation in order of increasing complexity and it should be noted that increasingly careful control of the viewing conditions is also required.

1. If possible, it is preferable to equate the viewing conditions such that simple tristimulus matches are also appearance matches.
2. If a white point change is necessary, CIELAB can be used as a reasonable first-order approximation of an appearance model.
3. If CIELAB is found to be inadequate, it can be enhanced by using a von Kries chromatic adaptation transform (on cone responses) to a reference viewing condition. An even better choice of adaptation transform would be a von Kries transform based on the CIECAM02  $\mathbf{M}_{\text{CAT02}}$  matrix.
4. If a more flexible adaptation model is required (*e.g.*, hard-copy to soft-copy changes) and/or there are surround changes, then the RLAB model can be used without too much added complexity. Again, the adaptation transform in RLAB could be improved by substituting the CIECAM02 adaptation transform.
5. If control of the viewing conditions and stimulus warrant a complete color appearance model, or if predictions of brightness and colorfulness are required, then the CIECAM02 model should be used.
6. If a full range of appearance phenomena and wide range of viewing conditions (*e.g.*, very high or low luminances, rod responses) must be addressed, then the Hunt model should be used.
7. True explorers could experiment with the technique of independent scales of appearance outlined in this chapter, collect more data, and then publish results to help improve upon the status quo.

*We need the tonic of wildness...At the same time that we are earnest to explore and learn all things, we require that all things be mysterious and unexplorable, that land and sea be indefinitely wild, unsurveyed and unfathomed by us because unfathomable. We can never have enough of nature* (Walden, 238).

—Henry David Thoreau

# References

---

- I. Abramov, J. Gordon, and H. Chan, Color appearance across the retina: Effects of a white surround, *J. Opt. Soc. Am. A* **9**, 195–202 (1992).
- E.H. Adelson, Perceptual organization and the perception of brightness, *Science* **2**, 2042–2044 (1993).
- Adobe Systems Incorporated, *PostScript® Language Reference Manual*, 2nd. Ed., Addison-Wesley, Reading (1990).
- J. Albers, *Interaction of Color*, Yale University Press, New Haven (1963).
- P.J. Alessi, CIE guidelines for coordinated research on evaluation of colour appearance models for reflection print and self-luminous display comparisons, *Color Res. Appl.* **19**, 48–58 (1994).
- R.L. Alfvin and M.D. Fairchild, Observer variability in metameric color matches using color reproduction media, *Color Res. Appl.* **22**, 174–188 (1997).
- D.H. Alman, R.S. Berns, G.D. Snyder, and W.A. Larson, Performance testing of color-difference metrics using a color tolerance dataset, *Color Res. Appl.* **14**, 139–151 (1989).
- M. Anderson, S. Chandrasekar, R. Motta, and M. Stokes, *Proposal for a standard color space for the internet—sRGB*, IS&T/SID 4th Color Imaging Conference, Scottsdale, 238–246 (1996).
- ANSI PH2.30-1989, *American National Standard for Graphic Arts and Photography — Color Prints, Transparencies, and Photomechanical Reproductions — Viewing Conditions*, American National Standards Institute, New York (1989).
- L.E. Arend, How much does illuminant color affect unattributed colors? *J. Opt. Soc. Am. A* **10**, 2134–2147 (1993).
- L.E. Arend and A. Reeves, Simultaneous color constancy, *J. Opt. Soc. Am. A* **3**, 1743–1751 (1986).
- L.E. Arend and R. Goldstein, Simultaneous constancy, lightness and brightness, *J. Opt. Soc. Am. A* **4**, 2281–2285 (1987).
- L.E. Arend and R. Goldstein, Lightness and brightness over spatial illumination gradients, *J. Opt. Soc. Am. A* **7**, 1929–1936 (1990).
- L.E. Arend, A. Reeves, J. Schirillo, and R. Goldstein, Simultaneous color constancy: Papers with diverse Munsell values, *J. Opt. Soc. Am. A* **8**, 661–672 (1991).
- ASTM, *Standard Terminology of Appearance*, E284–95a (1995).
- ASTM, *Standard Guide for Designing and Conducting Visual Experiments*, E1808–96 (1996).
- ATIS, *Objective perceptual video quality measurement using a JND-based full reference technique*, Alliance for Telecommunications Industry Solutions Technical Report T1.TR.PP.75-2001 (2001).

- M. Ayama, T. Nakatsue, and P.K. Kaiser, Constant hue loci of unique and binary balanced hues at 10, 100, and 1000 td, *J. Opt. Soc. Am. A* **4**, 1136–1144 (1987).
- E.S. Babbitt, *The Principles of Light and Color: The Healing Power of Color*, University Books, New Hyde Park (1967).
- J.S. Babcock, J.B. Pelz, and M.D. Fairchild, Eye tracking observers during color image evaluation tasks, *SPIE/IS&T Electronic Imaging Conference*, **5007**, Santa Clara, 218–230 (2003).
- W.G.K. Backhaus, R. Kliegl, and J.S. Werner, Eds., *Color Vision: Perspectives from Different Disciplines*, Walter de Gruyter, Berlin (1998).
- H.B. Barlow and J.D. Mollon, *The Senses*, Cambridge University Press, Cambridge (1982).
- K. Barnard and B. Funt, *Analysis and improvement of multi-scale retinex*, Proceedings of the 5th IS&T/SID Color Imaging Conference, Scottsdale, 221–226 (1997).
- C.J. Bartleson, Memory colors of familiar objects, *J. Opt. Soc. Am.* **50**, 73–77 (1960).
- C.J. Bartleson, Optimum image tone reproduction, *J. SMPTE* **84**, 613–618 (1975).
- C.J. Bartleson, Brown, *Color Res. Appl.* **1**, 181–191 (1976).
- C.J. Bartleson, A review of chromatic adaptation, *AIC Proceedings, Color* **77**, 63–96 (1978).
- C.J. Bartleson and E.J. Breneman, Brightness perception in complex fields, *J. Opt. Soc. Am.*, **57**, 953–957 (1967).
- C.J. Bartleson and F. Grum, *Optical Radiation Measurements*. Vol. 5, *Visual Measurements*, Academic, Orlando (1984).
- K.-H. Bäuml, Simultaneous color constancy: How surface color perception varies with the illuminant, *Vision Res.* **39**, 1531–1550 (1999).
- K.-H. Bäuml and B.A. Wandell, Color appearance of mixture gratings, *Vision Res.* **36**, 2849–2864 (1996).
- H.K. Bencuya, *Relations between the Natural Color System and the Munsell Color Order System*, Masters Thesis, Rensselaer Polytechnic Institute (1984).
- A. Berger-Schunn, *Practical Color Measurement*, Wiley, New York (1994).
- R.S. Berns, The mathematical development of CIE TC1-29 proposed color difference equation: CIELCH, *AIC Proceedings, Color* **93**, C19-1 (1993a).
- R.S. Berns, Spectral modeling of a dye diffusion thermal transfer printer, *J. Electron. Imaging* **2**, 359–370 (1993b).
- R.S. Berns, Methods for characterizing CRT displays, *Displays* **16**, 173–182 (1996).
- R.S. Berns, A generic approach to color modeling, *Color Res. Appl.* **22**, 318–325 (1997).
- R.S. Berns, *Billmeyer and Saltzman's Principles of Color Technology*, 3rd. Ed., John Wiley & Sons, New York (2000).
- R.S. Berns and M.J. Shyu, Colorimetric characterization of a desktop drum scanner using a spectral model, *J. Electron. Imaging* **4**, 360–372 (1995).
- R.S. Berns, R.J. Motta, and M.E. Gorzynski, CRT colorimetry. Part I: Theory and practice, *Color Res. Appl.* **18**, 299–314 (1993a).
- R.S. Berns, M.E. Gorzynski, and R.J. Motta, CRT colorimetry. Part II: Metrology, *Color Res. Appl.* **18**, 315–325 (1993b).
- R.S. Berns, S.R. Fernandez, and L. Taplin, Estimating black-level emissions of computer-controlled displays, *Color Res. Appl.* **28**, 379–383 (2003).
- K.T. Blackwell and G. Buchsbaum, The effect of spatial and chromatic parameters on chromatic induction, *Color Res. Appl.* **13**, 166–173 (1988a).
- K.T. Blackwell and G. Buchsbaum, Quantitative studies in color constancy, *J. Opt. Soc. Am. A* **5**, 1772–1780 (1988b).

- C. Blakemore and F.W. Campbell, On the existence of neurons in the human visual system selectively sensitive to the orientation and size of retinal images, *J. Physiol.* **203**, 237–260 (1969).
- B. Blakeslee and M.E. McCourt, A multiscale spatial filtering account of the White effect, simultaneous brightness contrast and grating induction, *Vision Res.* **39**, 4361–4377 (1999).
- F. Birren, *Color and Human Response*, Wiley, New York (1978).
- R.M. Boynton, *Human Color Vision*, Optical Society of America, Washington (1979).
- R.M. Boynton, History and current status of a physiologically based system of photometry and colorimetry, *J. Opt. Soc. Am. A* **13**, 1609–1621 (1996).
- D.H. Brainard and B.A. Wandell, Analysis of the retinex theory of color vision, *J. Opt. Soc. Am. A* **3**, 1651–1661 (1986).
- D.H. Brainard and B.A. Wandell, Asymmetric color matching: How color appearance depends on the illuminant, *J. Opt. Soc. Am. A* **9**, 1433–1448 (1992).
- D.H. Brainard and L.T. Maloney, Surface color perception and equivalent illumination models, *J. Vis.* **11**(5):1, 1–18 (2011).
- K.M. Braun and M.D. Fairchild, *Evaluation of five color-appearance transforms across changes in viewing conditions and media*, IS&T/SID 3rd Color Imaging Conference, Scottsdale, 93–96 (1995).
- K.M. Braun and M.D. Fairchild, Testing five color appearance models for changes in viewing conditions, *Color Res. Appl.* **21**, 165–174 (1997).
- G.J. Braun and M.D. Fairchild, Image lightness rescaling using sigmoidal contrast enhancement functions, *J. Electron. Imaging* **8**, 380–393 (1999a).
- G.J. Braun and M.D. Fairchild, *General-purpose gamut-mapping algorithms: Evaluation of contrast-preserving rescaling functions for color gamut mapping*, IS&T/SID 7th Color Imaging Conference, Scottsdale, 167–192 (1999b).
- G.J. Braun and M.D. Fairchild, General-purpose gamut-mapping algorithms: Evaluation of contrast-preserving rescaling functions for color gamut mapping, *J. Im. Sci. Tech.* **44**, 343–350 (2000a).
- K.M. Braun and M.D. Fairchild, Psychophysical generation of matching images for cross-media color reproduction, *J. Soc. Info. Disp.* **8**, 33–44 (2000b).
- K.M. Braun, M.D. Fairchild, and P.J. Alessi, Viewing environments for cross-media image comparisons, *Color Res. Appl.* **21**, 6–17 (1996).
- E.J. Breneman, Corresponding chromaticities for different states of adaptation to complex visual fields, *J. Opt. Soc. Am. A* **4**, 1115–1129 (1987).
- P. Bressan, Revisitation of the luminance conditions for the occurrence of the achromatic neon color spreading illusion, *Percept. Psychophys.* **54**, 55–64 (1993).
- H. Brettel, F. Vienot, and J.D. Mollon, Computerized simulation of color appearance for dichromats, *J. Opt. Soc. Am. A* **14**, 2647–2655 (1997).
- M.H. Brill, *Color management: New roles for color transforms*, IS&T/SID 5th Color Imaging Conference, Scottsdale, 78–82 (1997).
- M.H. Brill, Irregularity in CIECAM02 and its avoidance, *Color Res. Appl.* **31**, 142–145 (2006).
- M.H. Brill and G. West, Chromatic adaptation and color constancy: A possible dichotomy, *Color Res. Appl.* **11**, 196–227 (1986).
- M.H. Brill and S. Süsstrunk, Repairing gamut problems in CIECAM02: A progress report, *Color Res. Appl.* **33**, 424–426 (2008).
- M.H. Brill, Repairing gamut problems in CIECAM02: A progress report, *Color Res. Appl.* **33**, 424–426 (2008).
- M.H. Brill and M. Mahy, Visualization of mathematical inconsistencies in CIECAM02, *Color Res. Appl.* **37**, in press (2013).

- A.J. Calabria and M.D. Fairchild, *Herding CATs: A comparison of linear chromatic-adaptation transforms for CIECAM97s*, IS&T/SID 9th Color Imaging Conference, Scottsdale, 174–178 (2001).
- A.J. Calabria and M.D. Fairchild, *Compare and contrast: Perceived contrast of color images*, Proceedings of IS&T/SID 10th Color Imaging Conference, Scottsdale, 17–22 (2002).
- F.W. Campbell and J.G. Robson, Application of Fourier analysis to the visibility of gratings, *J. Physiol.* **197**, 551–566 (1968).
- R.C. Carter and L.D. Silverstein, Perceiving color across scale: Great and small, discrete and continuous, *J. Opt. Soc. Am. A* **29**, 1346–1355 (2012).
- L.M. Chalupa and J.S. Werner, *The Visual Neurosciences*, MIT Press, Cambridge (2004).
- P.-H. Chen, M.D. Fairchild, and R.S. Berns, *Scaling lightness perception and differences above and below diffuse white*, IS&T/SID 18th Color Imaging Conference, San Antonio, 42–48 (2010).
- M.E. Chevreul, *The Principles of Harmony and Contrast of Colors* (1839) (reprinted, Van Nostrand Reinhold, New York, 1967).
- E.-J. Chichilnisky and B.A. Wandell, Photoreceptor sensitivity changes explain color appearance shifts induced by large uniform backgrounds in dichoptic matching, *Vision Res.* **35**, 239–254 (1995).
- CIE, *Colorimetry*, CIE Publ. No. 15.2, Vienna (1986).
- CIE, *International Lighting Vocabulary*, CIE Publ. No. 17.4, Vienna (1987).
- CIE, *Special Metamerism Index: Change in Observer*, CIE Publ. No. 80, Vienna (1989).
- CIE, *CIE 1988 2° Spectral Luminous Efficiency Function for Scotopic Vision*, CIE Publ. No. 86, Vienna (1990).
- CIE, *A Method of Predicting Corresponding Colours under Different Chromatic and Illuminance Adaptations*, CIE Technical Report 109, Vienna (1994).
- CIE, *Method of Measuring and Specifying Colour Rendering Properties of Light Sources*, CIE Publ. No. 13.3, Vienna (1995a).
- CIE, *Industrial Colour-Difference Evaluation*, CIE Technical Report 116, Vienna (1995b).
- CIE, *Report to CIE Division 1 from TC1-31 Colour Notations and Colour-Order Systems* (1996a).
- CIE, *Color Standards for Image Technology*, CIE Expert Symposium '96 CIE Pub. x010, Vienna (1996b).
- CIE, *The CIE 1997 Interim Colour Appearance Model (Simple Version)*, CIECAM97s, CIE Pub. No. 131 (1998).
- CIE, *CIE Collection/Colour Rendering (TC1-33 Closing Remarks)*, CIE Pub. No. 135/2 rendering (1999).
- CIE, *Improvement to Industrial Colour Difference Evaluation*, CIE Pub. No. 142 (2001).
- CIE, *A Colour Appearance Model for Color Management Systems: CIECAM02*, CIE TC8-01 Technical Report, CIE Pub. No. 159 (2004a).
- CIE, *A Review of Chromatic Adaptation Transforms*, CIE TC1-52 Technical Report, CIE Pub. No. 160 (2004b).
- CIE, *Colorimetry*, 3rd. Ed., CIE Pub. No. 015 (2004c).
- CIE, *Fundamental Chromaticity Diagram with Physiological Axes – Part 1*, CIE Pub. 170–1 (2006).
- CIE, *CIE Supplementary System of Photometry*, CIE Pub. No. 200 (2011a).
- CIE, *ILV: International Lighting Vocabulary*, CIE Standard S 017 (2011b).
- F.J.J. Clarke, R. McDonald, and B. Rigg, Modification to the JPC 79 colour-difference formula, *J. Soc. Dyers Colour.* **100**, 128–132 (1984).
- J.B. Cohen, *Visual Color and Color Mixture: The Fundamental Color Space*, University of Illinois Press, Urbana (2001).

- B. Cooper, H. Sun, and B.B. Lee, Psychophysical and physiological responses to gratings with luminance and chromatic components of different spatial frequencies, *J. Opt. Soc. Am. A* **29**, A314–A323 (2012).
- F.W. Cornelissen and E. Brenner, On the role and nature of adaptation in chromatic induction, *Channels in the Visual Nervous System: Neurophysiology, Psychophysics and Models*, B. Blum, Ed., Freund Publishing, London, 109–123 (1991).
- F.W. Cornelissen and E. Brenner, Simultaneous colour constancy revisited: An analysis of viewing strategies, *Vision Res.* **35**, 2431–2448 (1995).
- S.M. Courtney, L.H. Finkel, and G. Buchsbaum, A multistage neural network for color constancy and color induction, *IEEE Trans. Neural Netw.* **6**, 972–985 (1995a).
- S.M. Courtney, L.H. Finkel, and G. Buchsbaum, Network simulations of retinal and cortical contributions to color constancy, *Vision Res.* **35**, 413–434 (1995b).
- K.J.W. Craik, The effect of adaptation on visual acuity, *Br. J. Psychol.* **29**, 252–266 (1939).
- B.J. Craven and D.H. Foster, An operational approach to color constancy, *Vision Res.* **32**, 1359–1366 (1992).
- S. Daly, The visible differences predictor: An algorithm for the assessment of image fidelity, in *Digital Images and Human Vision*, A. Watson, Ed., MIT Press, Cambridge, 179–206 (1993).
- J. Davidoff, *Cognition Through Color*, MIT Press, Cambridge (1991).
- P. De Weerd, R. Desimone, and L.G. Ungerleider, Perceptual filling-in: A parametric study, *Vision Res.* **38**, 2721–2734 (1998).
- P.B. Delahunt and D.H. Brainard, Control of chromatic adaptation: Signals from separate cone classes interact, *Vision Res.* **40**, 2885–2903 (2000).
- G. Derefeldt, Colour appearance systems, in *The Perception of Colour*, P. Gouras, Ed., CRC Press, Boca Raton, 218–261 (1991).
- G. Derefeldt and C. Sahlin, Transformation of NCS data into CIELAB colour space, *Color Res. Appl.* **11**, 146–152 (1986).
- R.L. DeValois and K.K. DeValois, *Spatial Vision*, Oxford University Press, Oxford (1988).
- R.L. DeValois, C.J. Smith, S.T. Kitai, and S.J. Karoly, Responses of single cells in different layers of the primate lateral geniculate nucleus to monochromatic light, *Science* **127**, 238–239 (1958).
- J.E. Dowling, *The Retina: An Approachable Part of the Brain*, Harvard University Press, Cambridge (2012).
- M.S. Drew and G.D. Finlayson, Device-independent color via spectral sharpening, IS&T/SID 2nd Color Imaging Conference, Scottsdale, 121–126 (1994).
- F. Durand and J. Dorsey, Fast bilateral filtering for the display of high-dynamic-range images, Proceedings of SIGGRAPH 2002, San Antonio, 257–266 (2002).
- M. D'Zmura and P. Lennie, Mechanisms of color constancy, *J. Opt. Soc. Am. A* **3**, 1662–1672 (1986).
- F. Ebner and M.D. Fairchild, Development and testing of a color space (IPT) with improved hue uniformity, IS&T/SID 6th Color Imaging Conference, Scottsdale, 8–13 (1998).
- A.J. Elliot and D. Niesta, Romantic red: Red enhances men's attraction to women, *J. Pers. Soc. Psychol.* **95**, 1150–1164 (2008).
- A.J. Elliot, M.A. Maier, M.J. Binser, R. Friedman, and R. Pekrun, The effect of red on avoidance behavior in achievement contexts, *Pers. Soc. Psychol. B* **35**, 365–375 (2009).
- P.G. Engeldrum, Four color reproduction theory for dot formed imaging systems, *J. Imag. Technol.* **12**, 126–131 (1986).
- P.G. Engeldrum, Color scanner colorimetric design requirements, *Proc. SPIE* **1909**, 75–83 (1993).

- P.G. Engeldrum, A framework for image quality models, *J. Imag. Sci. Tech.* **39**, 312–318 (1995).
- P.G. Engeldrum, *Psychometric Scaling: A Toolkit for Imaging Systems Development*, Imcotek Press, Winchester (2000).
- P.G. Engledrum, Extending image quality models, Proceedings of IS&T PICS Conference, 65–69 (2002).
- R.M. Evans, Visual processes and color photography, *J. Opt. Soc. Am.* **33**, 579–614 (1943).
- R.M. Evans, *An Introduction to Color*, John Wiley & Sons, New York (1948).
- R.M. Evans, *Eye, Film, and Camera in Color Photography*, John Wiley & Sons, New York (1959).
- R.M. Evans, *The Perception of Color*, John Wiley & Sons, New York (1974).
- R.M. Evans, W.T. Hanson, and W.L. Brewer, *Principles of Color Photography*, John Wiley & Sons, New York (1953).
- M.D. Fairchild, *Chromatic Adaptation and Color Appearance*, Ph.D. Dissertation, University of Rochester (1990).
- M.D. Fairchild, A model of incomplete chromatic adaptation, Proceedings of the 22nd Session of the CIE, Melbourne, 33–34 (1991a).
- M.D. Fairchild, Formulation and testing of an incomplete-chromatic-adaptation model, *Color Res. Appl.* **16**, 243–250 (1991b).
- M.D. Fairchild, Chromatic adaptation and color constancy, in *Advances in Color Vision Technical Digest*, OSA Technical Digest Series Vol. 4, Optical Society of America, Washington, DC, 112–114 (1992a).
- M.D. Fairchild, Chromatic adaptation to image displays, *TAGA* **2**, 803–824 (1992b).
- M.D. Fairchild, Chromatic adaptation in hard-copy/soft-copy comparisons, *Color Hard Copy and Graphic Arts II, Proc. SPIE* **1912**, 47–61 (1993a).
- M.D. Fairchild, Color forum: The CIE 1931 standard colorimetric observer: Mandatory retirement at age 65? *Color Res. Appl.* **18**, 129–134 (1993b).
- M.D. Fairchild, Some hidden requirements for device-independent color imaging, SID International Symposium, San Jose, 865–868 (1994a).
- M.D. Fairchild, Visual evaluation and evolution of the RLAB color space, IS&T/SID 2nd Color Imaging Conference, Scottsdale, 9–13 (1994b).
- M.D. Fairchild, Testing colour-appearance models: Guidelines for coordinated research, *Color Res. Appl.* **20**, 262–267 (1995a).
- M.D. Fairchild, Considering the surround in device-independent color imaging, *Color Res. Appl.* **20** 352–363 (1995b).
- M.D. Fairchild, Refinement of the RLAB color space, *Color Res. Appl.* **21**, 338–346 (1996).
- M.D. Fairchild, *Color Appearance Models*, Addison Wesley, Reading (1998a).
- M.D. Fairchild, The ZLAB color appearance model for practical image reproduction applications, Proceedings of the CIE Expert Symposium '97 on Colour Standards for Image Technology, CIE Pub. x014, 89–94 (1998b).
- M.D. Fairchild, A revision of CIECAM97s for practical applications, *Color Res. Appl.* **26**, 418–427 (2001).
- M.D. Fairchild, Image quality measurement and modeling for digital photography, International Congress on Imaging Science '02, Tokyo, 318–319 (2002a).
- M.D. Fairchild, Modeling color appearance, spatial vision, and image quality, in *Color Image Science: Exploiting Digital Media*, Wiley, New York, 357–370 (2002b).
- M.D. Fairchild, Spectral adaptation: A reason to use the wavenumber scale, IS&T/SID 14th Color Imaging Conference, Scottsdale, 314–319 (2006).
- M.D. Fairchild, Spectral adaptation, *Color Res. Appl.* **32**, 100–112 (2007a).

- M.D. Fairchild, *The HDR photographic survey*, IS&T/SID 15th Color Imaging Conference, Albuquerque, 233–238 (2007b).
- M.D. Fairchild, Beyond the locus of spectrally pure colors, *SPIE/IS&T Electronic Imaging, Proc.* **6807**, 680702, San Jose (2008a).
- M.D. Fairchild, *High, wide, & deep: Displayed image color appearance and perception*, SID International Symposium, Los Angeles, 780–782 (2008b).
- M.D. Fairchild, *The HDR Photographic Survey*, MDF, Honeoye Falls (2008c).
- M.D. Fairchild, Color appearance models and complex visual stimuli, *Journal of Dentistry*, **38**, s2, e25–e33 (2010).
- M.D. Fairchild, *The Color Curiosity Shop*, MDF, Honeoye Falls (2011a).
- M.D. Fairchild, Is there really such a thing as color space? Foundations of unidimensional appearance spaces, *ISCC/IS&T/SID Special Topics Meeting: Revisiting Color Spaces*, San Jose 2 (2011b).
- M.D. Fairchild and E. Pirrotta, Predicting the lightness of chromatic object colors using CIELAB, *Color Res. Appl.* **16**, 385–393 (1991).
- M.D. Fairchild and P. Lennie, Chromatic adaptation to natural and artificial illuminants, *Vision Res.* **32**, 2077–2085 (1992).
- M.D. Fairchild and R.S. Berns, Image color appearance specification through extension of CIELAB, *Color Res. Appl.* **18**, 178–190 (1993).
- M.D. Fairchild and R.L. Alfvín, *Precision of color matches and accuracy of color matching functions in cross-media color reproduction*, IS&T/SID 3rd Color Imaging Conference, Scottsdale, 18–21 (1995).
- M.D. Fairchild and L. Reniff, Time-course of chromatic adaptation for color-appearance judgements, *J. Opt. Soc. Am. A* **12**, 824–833 (1995).
- M.D. Fairchild and L. Reniff, *A pictorial review of color appearance models*, IS&T/SID 4th Color Imaging Conference, Scottsdale, 97–100 (1996).
- M.D. Fairchild and G.M. Johnson, Color appearance reproduction: Visual data and predictive modeling, *Color Res. Appl.* **24**, 121–131 (1999).
- M.D. Fairchild and G.M. Johnson, *Meet iCAM: A next-generation color appearance model*, IS&T/SID 10th Color Imaging Conference, Scottsdale, 33–38 (2002).
- M.D. Fairchild and G.M. Johnson, *Image appearance modeling*, Proceedings SPIE/IS&T Electronic Imaging Conference, **5007**, Santa Clara, 149–160 (2003).
- M.D. Fairchild and G.M. Johnson, The iCAM framework for image appearance, image differences, and image quality, *J. Electron. Imaging* **13**, 126–138 (2004).
- M.D. Fairchild and G.M. Johnson, *On the salience of novel stimuli: Adaptation and image noise*, IS&T/SID 13th Color Imaging Conference, Scottsdale, 333–338 (2005).
- M.D. Fairchild and G.M. Johnson, Measurement and modeling of adaptation to noise in images, *J. Soc. Info. Disp.* **15**, 639–647 (2007).
- M.D. Fairchild and D.R. Wyble, *Mean observer metamerism and the selection of display primaries*, IS&T/SID 15th Color Imaging Conference, Albuquerque, 151–156 (2007).
- M.D. Fairchild and D.R. Wyble, *hdr-CIELAB and hdr-IPT: Simple models for describing the color of high-dynamic-range and wide-color-gamut images*, IS&T/SID 18th Color Imaging Conference, San Antonio, 322–326 (2010).
- M.D. Fairchild and P.-H. Chen, *Brightness, lightness, and specifying color in high-dynamic-range scenes and images*, SPIE/IS&T Electronic Imaging Conference, **7867**, 786700-1–786700-14, San Francisco (2011).
- M.D. Fairchild and R.L. Heckaman, *Deriving appearance scales*, IS&T/SID 20th Color and Imaging Conference, Los Angeles, 281–286 (2012).
- M.D. Fairchild, E. Pirrotta, and T.G. Kim, Successive-Ganzfeld haploscopic viewing technique for color-appearance research, *Color Res. Appl.* **19**, 214–221 (1994).

- M.D. Fairchild, R.S. Berns, and A.A. Lester, Accurate color reproduction of CRT-displayed images as projected 35 mm slides, *J. Electron. Imaging* **5**, 87–96 (1996).
- M.D. Fairchild, D.R. Wyble, and G.M. Johnson, Matching image color from different cameras, *SPIE/IS&T Electronic Imaging Proc.* **6808**, 68080E, San Jose (2008).
- H.S. Fairman, Metameric correction using parameric decomposition, *Color Res. Appl.* **12**, 261–265 (1987).
- R. Fattal, D. Lischinski, and M. Werman, *Gradient domain high dynamic range compression*, Proceedings of SIGGRAPH 2002, San Antonio, 249–256 (2002).
- G. Fechner, *Elements of Psychophysics*. Vol. I (trans. H.E. Adler), Holt, Rinehart, and Winston, New York (1966).
- S. Fernandez and M.D. Fairchild, *Observer preferences and cultural differences in color reproduction of scenic images*, IS&T/SID 10th Color Imaging Conference, Scottsdale, 66–72 (2002).
- S. Fernandez, M.D. Fairchild, and K. Braun, Analysis of observer and cultural variability while generating preferred color reproductions of pictorial images, *J. Imag. Sci. Tech.* **49**, 96–104 (2005).
- J.A. Ferwerda, S.N. Pattanaik, P. Shirley, and D.P. Greenberg, *A model of visual adaptation for realistic image synthesis*, Proceedings of SIGGRAPH **96**, 249–258 (1996).
- G.D. Finlayson and M.S. Drew, *Positive Bradford curves through sharpening*, IS&T/SID 7th Color Imaging Conference, Scottsdale, 227–232 (1999).
- G.D. Finlayson and S. Süstrunk, *Performance of a chromatic adaptation transform based on spectral sharpening*, IS&T/SID 8th Color Imaging Conference, Scottsdale, 49–55 (2000).
- G.D. Finlayson, M.S. Drew, and B.V. Funt, Spectral sharpening: Sensor transformations for improved color constancy, *J. Opt. Soc. Am. A* **11**, 1553–1563 (1994a).
- G.D. Finlayson, M.S. Drew, and B.V. Funt, Color constancy: Generalized diagonal transforms suffice, *J. Opt. Soc. Am. A* **11**, 3011–3019 (1994b).
- D.J. Finney, *Probit Analysis*, 3rd. Ed., Cambridge University Press, Cambridge, UK (1971).
- J.D. Foley, A. van Dam, S.K. Feiner, and J.F. Hughes, *Computer Graphics: Principles and Practice*, 2nd. Ed., Addison-Wesley, Reading (1990).
- D.H. Foster and S.M.C. Nascimento, Relational colour constancy from invariant cone-excitation ratios, *Proc. R. Soc. Lond. B* **257**, 115–121 (1994).
- B. Fraser, C. Murphy, and F. Bunting, *Real World Color Management*, Peachpit Press, Berkeley (2003).
- C. Fu, C. Li, G. Cui, M.R. Luo, R.W.G. Hunt, and M.R. Pointer, An investigation of colour appearance for unrelated colours under photopic and mesopic vision, *Color Res. Appl.* **37** (4), 238–254 (2012).
- K. Fuld, J.S. Werner, and B.R. Wooten, The possible elemental nature of brown, *Vision Res.* **23**, 631–637 (1983).
- B. Funt, F. Ciurea, and J.J. McCann, *Retinex in Matlab*, Proceedings of IS&T/SID 8th Color Imaging Conference, Scottsdale, 112–121 (2000).
- K.R. Gegenfurtner and L.T. Sharpe, *Color Vision: From Genes to Perception*, Cambridge University Press, Cambridge (1999).
- R.S. Gentile, E. Walowit, and J.P. Allebach, Quantization multilevel halftoning of color images for near-original image quality, *J. Opt. Soc. Am. A* **7**, 1019–1026 (1990a).
- R.S. Gentile, E. Walowit, and J.P. Allebach, A comparison of techniques for color gamut mismatch compensation, *J. Imag. Technol.* **16**, 176–181 (1990b).
- G.A. Gescheider, *Psychophysics: Method, Theory, and Application*, 2nd. Ed., Lawrence Erlbaum Associates, Hillsdale (1985).

- K.S. Gibson and E.P.T. Tyndall, Visibility of radiant energy, *Scientific Papers of the Bureau of Standards* **10**, 131–191 (1923).
- A.L. Gilchrist, When does perceived lightness depend on perceived spatial arrangement, *Percept. Psychophys.* **28**, 527–538 (1980).
- E. Giorgianni and T. Madden, *Digital Color Management: Encoding Solutions*, 2nd. Ed., Wiley, Chichester (2008).
- S. Gonzalez and M.D. Fairchild, Evaluation of bispectral spectrophotometry for accurate colorimetry of printing materials, IS&T/SID 8th Color Imaging Conference, Scottsdale, 39–43 (2000).
- E.M. Granger, Uniform color space as a function of spatial frequency, SPIE/IS&T Electronic Imaging Conference, SPIE Vol. **1913**, San Jose, 449–457 (1993).
- E.M. Granger, ATD, appearance equivalence, and desktop publishing, SPIE, **2170**, 163–168 (1994).
- E.M. Granger, Gamut mapping for hard copy using the ATD color apace, SPIE, **2414**, 27–35 (1995).
- P. Green, *Color Management: Understanding and Using ICC Profiles*, Wiley, Chichester (2010).
- F. Grum and C.J. Bartleson, *Optical Radiation Measurements*. Vol. **2**, *Color Measurement*, Academic Press, New York (1980).
- N. Guéguen, Color and women hitchhikers' attractiveness: Gentlemen drivers preferred, *Color Res. Appl.* **37**, 76–78 (2012).
- J. Guild, The colorimetric properties of the spectrum, *Phil. Trans. Roy. Soc. A* **230**, 149–187 (1931).
- S.L. Guth, Model for color vision and light adaptation, *J. Opt. Soc. Am. A* **8**, 976–993 (1991).
- S.L. Guth, ATD model for color vision I: Background, SPIE **2170**, 149–152 (1994a).
- S.L. Guth, ATD model for color vision II: Applications, SPIE **2170**, 153–168 (1994b).
- S.L. Guth, Further applications of the ATD model for color vision, SPIE **2414**, 12–26 (1995).
- S.L. Guth, Correcting errors about ATD in Fairchild's "Color appearance models", *Color Res. Appl.* **23**, 338–339 (1998).
- S.L. Guth, The constancy myth, the vocabulary of color perception and the ATD04 model, SPIE **5292**, 1–14 (2004).
- J.C. Handley, Comparative analysis of Bradley-Terry and Thurstone-Mosteller paired comparison models for image quality assessment, IS&T PICS Conference Proceedings, Montreal, 108–112 (2001).
- H. Haneishi, T. Suzuki, N. Shimoyama, and Y. Miyake, Color digital halftoning taking colorimetric color reproduction into account, *J. Electron. Imaging* **5**, 97–106 (1996).
- A. Hard and L. Sivik, NCS-Natural Color System: A Swedish standard for color notation, *Color Res. Appl.* **6**, 129–138 (1981).
- M.M. Hayhoe and M.V. Smith, The role of spatial filtering in sensitivity regulation, *Vision Res.* **29**, 457–469 (1989).
- M.M. Hayhoe, N.I. Benimoff, and D.C. Hood, The time-course of multiplicative and subtractive adaptation processes, *Vision Res.* **27**, 1981–1996 (1987).
- R.L. Heckaman and M.D. Fairchild, Expanding display color gamut beyond the spectrum locus, *Color Res. Appl.* **31**, 475–482 (2006a).
- R.L. Heckaman and M.D. Fairchild, Effect of DLP projector white channel on perceptual gamut, *J. Soc. Info. Disp.* **14**, 755–761 (2006b).
- R.L. Heckaman and M.D. Fairchild, Brighter, more colorful colors and darker, deeper colors based on a theme of brilliance, IS&T/SID 16th Color Imaging Conference, Portland, 112–116 (2008).

- R.L. Heckaman and M.D. Fairchild,  $G_0$  and the gamut of real objects, Proceedings of AIC Color 09, Sydney (2009).
- R.L. Heckaman and M.D. Fairchild, Brighter, more colorful colors and darker, deeper colors based on a theme of brilliance, *Color Res. Appl.* **36**, 255–265 (2011).
- R.L. Heckaman, M.D. Fairchild, and D.R. Wyble, The effect of DLP projector white channel on perceptual gamut, IS&T/SID 13th Color Imaging Conference, Scottsdale, 205–210 (2005).
- H. von Helmholtz, *Handbuch der physiologischen Optick*, 1st. Ed., Voss, Hamburg (1866).
- H. Helson, Fundamental problems in color vision. I. The principle governing changes in hue, saturation, and lightness of non-selective samples in chromatic illumination, *J. Exp. Psych.* **23**, 439–477 (1938).
- H. Helson, D.B. Judd, and M.H. Warren, Object color changes from daylight to incandescent filament illumination, *Illum. Eng.* **47**, 221–233 (1952).
- E. Hering, *Outlines of a Theory of the Light Sense* (trans. L.M. Hurvich and D. Jameson, 1964), Harvard University Press, Cambridge (1920).
- T. Hoshino and R.S. Berns, Color gamut mapping techniques for color hard copy images, *Proc. SPIE*, **1909**, 152–165 (1993).
- P.-C. Hung, Colorimetric calibration for scanners and media, *Proc. SPIE* **1448**, 164–174 (1991).
- P.-C. Hung, Colorimetric calibration in electronic imaging devices using a look-up-table model and interpolations, *J. Electron. Imaging* **2**, 53–61 (1993).
- P.-C. Hung and R.S. Berns, Determination of constant hue loci for a CRT gamut and their predictions using color appearance spaces, *Color Res. Appl.* **20**, 285–295 (1995).
- R.W.G. Hunt, The effects of daylight and tungsten light-adaptation on color perception, *J. Opt. Soc. Am.* **40**, 362–371 (1950).
- R.W.G. Hunt, Light and dark adaptation and the perception of color, *J. Opt. Soc. Am.* **42**, 190–199 (1952).
- R.W.G. Hunt, Objectives in colour reproduction, *J. Phot. Sci.* **18**, 205–215 (1970).
- R.W.G. Hunt, Sky-blue pink, *Color Res. Appl.* **1**, 11–16 (1976).
- R.W.G. Hunt, The specification of colour appearance. I. Concepts and terms, *Color Res. Appl.* **2**, 55–68 (1977).
- R.W.G. Hunt, Colour terminology, *Color Res. Appl.* **3**, 79–87 (1978).
- R.W.G. Hunt, A model of colour vision for predicting colour appearance, *Color Res. Appl.* **7**, 95–112 (1982).
- R.W.G. Hunt, A model of colour vision for predicting colour appearance in various viewing conditions, *Color Res. Appl.* **12**, 297–314 (1987).
- R.W.G. Hunt, Hue shifts in unrelated and related colours, *Color Res. Appl.* **14**, 235–239 (1989).
- R.W.G. Hunt, *Measuring Colour*, 2nd. Ed., Ellis Horwood, New York (1991a).
- R.W.G. Hunt, Revised colour-appearance model for related and unrelated colours, *Color Res. Appl.* **16**, 146–165 (1991b).
- R.W.G. Hunt, Standard sources to represent daylight, *Color Res. Appl.* **17**, 293–294 (1992).
- R.W.G. Hunt, An improved predictor of colourfulness in a model of colour vision, *Color Res. Appl.* **19**, 23–26 (1994).
- R.W.G. Hunt, *The Reproduction of Colour*, 5th. Ed., Fountain Press, UK (1995).
- R.W.G. Hunt, *Measuring Color*, 3rd. Ed., Fountain Press, UK (1998).
- R.W.G. Hunt, Saturation, superfluous or superior, IS&T/SID CIC 9, Albuquerque, 1–5 (2001).

- R.W.G. Hunt, *The challenge of our known unknowns*, IS&T/SID CIC 17, Albuquerque, 238–241 (2009).
- R.W.G. Hunt and L.M. Winter, Colour adaptation in picture-viewing situations, *J. Phot. Sci.* **23**, 112–115 (1975).
- R.W.G. Hunt and M.R. Pointer, A colour-appearance transform for the CIE 1931 standard colorimetric observer, *Color Res. Appl.* **10**, 165–179 (1985).
- R.W.G. Hunt and M.R. Luo, Evaluation of a model of colour vision by magnitude scalings: Discussion of collected results, *Color Res. Appl.* **19**, 27–33 (1994).
- R.W.G. Hunt and M.R. Pointer, *Measuring Colour*, 4th. Ed., Wiley, Chichester (2011).
- D.M. Hunt, S.D. Kanwaljit, J.K. Bowmaker, and J.D. Mollon, The chemistry of John Dalton's color blindness, *Science* **267**, 984–988 (1995).
- D.M. Hunt, K.S. Dulai, J.A. Cowing, C. Julliot, J.D. Mollon, J.K. Bowmaker, W.-H. Li, and D. Hewett-Emmett, Molecular evolution of trichromacy in primates, *Vision Res.* **38**, 3299–3306 (1998).
- R.W.G. Hunt, C.J. Li, and M.R. Luo, Dynamic cone response function for models of colour appearance, *Color Res. Appl.* **28**, 82–88 (2003).
- R.S. Hunter and R.W. Harold, *The Measurement of Appearance*, 2nd. Ed., Wiley, New York (1987).
- L.M. Hurvich, *Color Vision*, Sinauer Associates, Sunderland (1981).
- L.M. Hurvich and D. Jameson, A psychophysical study of white. III. Adaptation as a variant, *J. Opt. Soc. Am.* **41**, 787–801 (1951).
- J.B. Hutchings, Food color and appearance in perspective, in *Food Color and Appearance*, 2nd. Ed., Aspen, Gaithersburg, 1–30 (1999).
- T. Indow, Multidimensional studies of Munsell color solid, *Psych. Rev.* **95**, 456–470 (1988).
- International Color Consortium, *ICC Profile Format Specification*, Version 3.3 (1996). <http://www.color.org> [accessed on 23 February 2013].
- D. Jameson and L.M. Hurvich, Some quantitative aspects of an opponent-colors theory: I. Chromatic responses and spectral saturation, *J. Opt. Soc. Am.* **45**, 546–552 (1955).
- D. Jameson and L.M. Hurvich, Essay concerning color constancy, *Ann. Rev. Psychol.* **40**, 1–22 (1989).
- J.F. Jarvis, C.N. Judice, and W.H. Ninke, A survey of techniques for the display of continuous tone images on bilevel displays, *Comp. Graphics Image Proc.* **5**, 13–40 (1976).
- T. Jetsu, U. Essiarab, V. Heikkinen, T. Jaaskelainen, and J. Parkkinen, Color classification using color vision models, *Color Res. Appl.* **36**, 266–271 (2011).
- E.W. Jin and S.K. Shevell, Color memory and color constancy, *J. Opt. Soc. Am. A* **13**, 1981–1991 (1996).
- D.J. Jobson, Z. Rahman, and G.A. Woodell, A multi-scale retinex for bridging the gap between color images and the human observation of scenes, *IEEE Trans. Im. Proc.* **6**, 956–976 (1997).
- S. Johnsen, *The Optics of Life: A Biologist's Guide to Light in Nature*, Princeton University Press, Princeton (2012).
- G.M. Johnson and M.D. Fairchild, Full-spectral color calculations in realistic image synthesis, *IEEE Comput. Graph. Appl.* **19**:4, 47–53 (1999).
- G.M. Johnson and M.D. Fairchild, *Sharpness rules*, Proceedings of IS&T/SID 8th Color Imaging Conference, Scottsdale, 24–30 (2000).
- G.M. Johnson and M.D. Fairchild, *On contrast sensitivity in an image difference model*, Proceedings of IS&T PICS Conference, 18–23 (2001a).
- G.M. Johnson and M.D. Fairchild, *Darwinism of color image difference models*, Proceedings of IS&T/SID 9th Color Imaging Conference, Scottsdale, 108–112 (2001b).

- G.M. Johnson and M.D. Fairchild, *Measuring images: Differences, quality, and appearance*, SPIE/IS&T Electronic Imaging Conference Vol. **5007**, Santa Clara, 51–60 (2003a).
- G.M. Johnson and M.D. Fairchild, A top down description of S-CIELAB and CIEDE2000, *Color Res. Appl.* **28**, 425–435 (2003b).
- G.M. Johnson and M.D. Fairchild, *Rendering HDR images*, IS&T/SID 11th Color Imaging Conference, Scottsdale, 36–41 (2003c).
- G.M. Johnson, X. Song, E.D. Montag, and M.D. Fairchild, Derivation of a color space for image color difference measurement, *Color Res. Appl.* **35**, 387–400 (2010).
- G. Jordon, S.S. Deeb, J.M. Bosten, and J.D. Mollon, The dimensionality of color vision in carriers of anomalous trichromacy, *J. Vis.* **10** (8):12, 1–19 (2010).
- D.B. Judd, Hue, saturation, and lightness of surface colors with chromatic illumination, *J. Opt. Soc. Am.* **30**, 2–32 (1940).
- D.B. Judd, Appraisal of land's work on two-primary color projections, *J. Opt. Soc. Am.* **50**, 254–268 (1960).
- P.K. Kaiser and R.M. Boynton, *Human Color Vision*, 2nd. Ed., Optical Society of America, Washington, DC (1996).
- M. Kalloniatis and C. Luu, Light and dark adaptation. <http://webvision.med.utah.edu/> [accessed on 23 February 2013] (2012).
- H. Kang, Color scanner calibration, *J. Im. Sci. Tech.* **36**, 162–170 (1992).
- H. Kang, *Color Technology for Electronic Imaging Devices*, SPIE Press, Bellingham (1997).
- J.M. Kasson, W. Plouffe, and S.I. Nin, A tetrahedral interpolation technique for color space conversion, *Proc. SPIE* **1909**, 127–138 (1993).
- J.M. Kasson, S.I. Nin, W. Plouffe, and J.L. Hafner, Performing color space conversions with three-dimensional linear interpolation, *J. Electron. Imaging* **4**, 226–250 (1995).
- I. Katayama and M.D. Fairchild, Quantitative evaluation of perceived whiteness based on a color vision model, *Color Res. Appl.* **35**, 410–418 (2010).
- N. Katoh, *Practical method for appearance match between soft copy and hard copy*, 3rd Device-Independent Color Imaging Conference SPIE Vol. **2170**, Scottsdale, 170–181 (1994).
- N. Katoh, *Appearance match between soft copy and hard copy under mixed chromatic adaptation*, IS&T/SID 3rd Color Imaging Conference, Scottsdale, 22–25 (1995).
- D. Katz, *The World of Colour*, Trubner & Co., London (1935).
- T.G. Kim, R.S. Berns, and M.D. Fairchild, *Comparing appearance models using pictorial images*, IS&T/SID 1st Color Imaging Conference, Scottsdale, 72–77 (1993).
- M.H. Kim, T. Weyrich, and J. Kautz, *Modeling human color perception under extended luminance levels*, Proceedings of SIGGRAPH 09, **28** (3), 1–9 (2009).
- B.W. Keelan, *Handbook of Image Quality: Characterization and Prediction*, Marcel Dekker, New York (2002).
- D.H. Kelly, Ed., *Visual Science and Engineering: Models and Applications*, Marcel Dekker, New York (1994).
- F.A.A. Kingdom and N. Prins, *Psychophysics: A Practical Introduction*, Academic Press, London (2010).
- J. Koenderink, *Color for the sciences*, MIT Press, Cambridge (2010).
- J.J. Koenderink and W.A. Richards, Why is snow so bright? *J. Opt. Soc. Am. A* **9**, 643–648 (1992).
- J.M. Kraft and J.S. Werner, Spectral efficiency across the life span: Flicker photometry and brightness matching, *J. Opt. Soc. Am. A* **11**, 1213–1221 (1994).
- J. von Kries, Chromatic adaptation, *Festschrift der Albrecht-Ludwig-Universität (Fribourg)* (1902) [trans. D.L. MacAdam, *Sources of Color Science*, MIT Press, Cambridge (1970)].

- J.B. Kruskal and M. Wish, *Multidimensional Scaling*, Sage Publications, Thousand Oaks (1978).
- J. Kuang and M.D. Fairchild, *iCAM06, HDR, and image appearance*, IS&T/SID 15th Color Imaging Conference, Albuquerque, 249–254 (2007).
- J. Kuang, G.M. Johnson, and M.D. Fairchild, iCAM06: A refined image appearance model for HDR image rendering, *J. Vis. Commun. Image Represent.* **18**, 406–414 (2007a).
- J. Kuang, R.L. Heckaman, and M.D. Fairchild, *Evaluation of HDR tone mapping algorithms using a high-dynamic-range display to emulate real scenes*, IS&T/SID 15th Color Imaging Conference, Albuquerque, 299–303 (2007b).
- J. Kuang, H. Yamaguchi, C. Liu, G.M. Johnson, and M.D. Fairchild, Evaluating HDR rendering algorithms, *ACM Trans. Appl. Percept.* **4** (9) (2007c).
- J. Kuang, R.L. Heckaman, and M.D. Fairchild, Evaluation of HDR tone mapping algorithms using a high-dynamic-range display to emulate real scenes, *J. Soc. Info. Disp.* **18**, 461–468 (2010).
- R.G. Kuehni, *Color Space and its Divisions: Color Order from Antiquity to the Present*, John Wiley & Sons, Hoboken (2003).
- R.G. Kuehni, *Color: An Introduction to Practice and Principles*, 2nd. Ed., John Wiley & Sons, Hoboken (2005).
- R.G. Kuehni and A. Schwarz, *Color Ordered: A Survey of Color Order Systems from Antiquity to the Present*, Oxford University Press, Oxford (2008).
- R.G. Kuehni, R. Shamey, M. Mathews and B. Keene, Perceptual prominence of Hering's chromatic primaries, *J. Opt. Soc. Am. A* **27**, 159–165 (2010).
- T. Kunkel and E. Reinhard, A neurophysiology-inspired steady-state color appearance model, *J. Opt. Soc. Am. A* **26**, 776–782 (2009).
- W.-G. Kuo, M.R. Luo, and H.E. Bez, Various chromatic-adaptation transformations tested using new colour appearance data in textiles, *Color Res. Appl.* **20**, 313–327 (1995).
- I. Kuriki and K. Uchikawa, Limitations of surface-color and apparent-color constancy, *J. Opt. Soc. Am. A* **13**, 1622–1636 (1996).
- E.H. Land, Color vision and the natural image part II, *Proc. Nat. Acad. Sci.* **45**, 636–644 (1959).
- E.H. Land, The retinex, *Amer. Sci.* **52**, 247–264 (1964).
- E.H. Land, The retinex theory of color vision, *Sci. Am.* **237**, 108–128 (1977).
- E.H. Land, Recent advances in retinex theory, *Vision Res.* **26**, 7–21 (1986).
- E.H. Land and J.J. McCann, Lightness and the retinex theory, *J. Opt. Soc. Am.* **61**, 1–11 (1971).
- E.L. Landa and M.D. Fairchild, Charting color from the eye of the beholder, *Amer. Sci.* **93**, 436–443 (2005).
- P. Lennie and M. D'Zmura, Mechanisms of color vision, *CRC Crit. Rev. Neurobiol.* **3**, 333–400 (1988).
- C.J. Li and M.R. Luo, Testing the robustness of CIECAM02, *Color Res. Appl.* **30**, 99–106 (2005).
- C. Li and M. Melgosa, A note about the abnormal hue angle change in CIELAB space, *Color Res. Appl.* **37**, in press (2013).
- B. Li, G.W. Meyer, and R.V. Klassen, *A comparison of two image quality models*, SPIE/IS&T Electronic Imaging Conference Vol. **3299**, San Jose, 98–109 (1998).
- C.J. Li, M.R. Luo, and R.W.G. Hunt, *The CAM97s2 model*, IS&T/SID 7th Color Imaging Conference, Scottsdale, 262–263 (1999).
- C.J. Li, M.R. Luo, and R.W.G. Hunt, A revision of the CIECAM97s model, *Color Res. Appl.* **25** 260–266 (2000a).

- C.J. Li, M.R. Luo, and B. Rigg, *Simplification of the CMCCAT97*, IS&T/SID 8th Color Imaging Conference, Scottsdale, 56–60 (2000b).
- C.J. Li, M.R. Luo, R.W.G. Hunt, N. Moroney, M.D. Fairchild and T. Newman, *The performance of CIECAM02*, IS&T/SID 10th Color Imaging Conference, Scottsdale, 28–32 (2002).
- C.J. Li, M.R. Luo, and G. Cui, *Colour-differences evaluation using colour appearance models*, IS&T/SID 11th Color Imaging Conference, Scottsdale, 127–131 (2003).
- C. Li, M.R. Luo, and M.R. Pointer, *Recent progress with extensions to CIECAM02*, IS&T/SID CIC 17, Albuquerque, 69–74 (2009).
- H. Li, M.D. Fairchild and A. Webster, *Appearance-based primary design for displays*, IS&T/SID 19th Color and Imaging Conference, San Jose, 139–145 (2011a).
- C. Li, M.R. Luo, G. Cui, and C.J. Li, Evaluation of the CIE colour rendering index, *Color Technol.* **127**, 129–135 (2011b).
- C. Li, M.R. Luo, and P.-L. Sun, *A new version of CIECAM02 with the HPE primaries*, IS&T 6th European Conference on Colour in Graphics, Imaging, and Vision, CGIV, Amsterdam, 151–154 (2012a).
- C. Li, M.R. Luo, and M. Melgosa, *CAT02 and HPE Triangles*, IS&T/SID 20th Color and Imaging Conference, Los Angeles, 281–286 (2012b).
- C. Li, M.R. Luo, C.J. Li, and G. Cui, The CRI-CAM02UCS colour rendering index, *Color Res. Appl.* **37**, 160–167 (2012c).
- C. Li, E. Perales, M.R. Luo, and F. Martínez-Verdú, Mathematical approach for predicting non-negative tristimulus values using the CAT02 chromatic adaptation transform, *Color Res. Appl.* **37**, 255–260 (2012d).
- C. Li, M.R. Luo, and Z. Wang, Different matrices for CIECAM02, *Color Res. Appl.* **37**, in press (2013).
- C. Liu and M.D. Fairchild, *Re-measuring and modeling perceived image contrast under different levels of surround illumination*, IS&T/SID 15th Color Imaging Conference, Albuquerque, 66–70 (2007).
- Y. Liu, J. Shigley, E. Fritsch, and S. Hemphill, Abnormal hue-angle change of the gemstone tanzanite between CIE illuminants D65 and A in CIELAB color space, *Color Res. Appl.* **20**, 245–250 (1995).
- M. Livingstone, *Vision and Art: The Biology of Seeing*, Abrams, New York (2002).
- M.-C. Lo, M.R. Luo, and P.A. Rhodes, Evaluating colour models' performance between monitor and print images, *Color Res. Appl.* **21**, 277–291 (1996).
- A.D. Logvinenko, On derivation of spectral sensitivities of the human cones from trichromatic colour matching functions, *Vision Res.* **38**, 3207–3211 (1998).
- A. Logvinenko and G. Menshikova, Trade-off between achromatic colour and perceived illumination as revealed by the use of pseudoscopic inversion of apparent depth, *Perception* **23**, 1007–1023 (1994).
- J. Long and J.T. Luke, *The New Munsell Student Color Set*, Fairchild Books, New York (2001).
- R.B. Lotto and D. Purves, The empirical basis of color perception, *Conscious. Cogn.* **11**, 609–629 (2002).
- J. Lubin, The use of psychophysical data and models in the analysis of display system performance, in *Digital Images and Human Vision*, A. Watson, Ed., MIT Press, Cambridge, 163–178 (1993).
- J. Lubin, A visual discrimination model for imaging system design and evaluation, in *Vision Models for Target Detection and Recognition*, E. Peli, Ed., World Scientific, Singapore, 245–283 (1995).
- M. Luckiesh, *Color and its Applications*, Van Nostrand, New York (1915).

- M.R. Luo, 20 years of colour appearance research at CIC, IS&T/SID 20th Color and Imaging Conference, Los Angeles, 259–263 (2012).
- M.R. Luo and J. Morovic, Two unsolved issues in colour management — colour appearance and gamut mapping, 5th International Conference on High Technology, Chiba, Japan, 136–147 (1996).
- M.R. Luo, A.A. Clarke, P.A. Rhodes, A. Schappo, S.A.R. Scrivner, and C.J. Tait, Quantifying colour appearance. Part I. LUTCHI colour appearance data, *Color Res. Appl.* **16**, 166–180 (1991a).
- M.R. Luo, A.A. Clarke, P.A. Rhodes, A. Schappo, S.A.R. Scrivner, and C.J. Tait, Quantifying colour appearance. Part II. Testing colour models performance using LUTCHI color appearance data, *Color Res. Appl.* **16**, 181–197 (1991b).
- M.R. Luo, X.W. Gao, P.A. Rhodes, H.J. Xin, A.A. Clarke, and S.A.R. Scrivner, Quantifying colour appearance. Part III. Supplementary LUTCHI color appearance data, *Color Res. Appl.* **18**, 98–113 (1993a).
- M.R. Luo, X.W. Gao, P.A. Rhodes, H.J. Xin, A.A. Clarke, and S.A.R. Scrivner, Quantifying colour appearance. Part IV. Transmissive media, *Color Res. Appl.* **18**, 191–209 (1993b).
- M.R. Luo, X.W. Gao, and S.A.R. Scrivner, Quantifying colour appearance. Part V. Simultaneous contrast, *Color Res. Appl.* **20**, 18–28 (1995).
- M.R. Luo, M.-C. Lo, and W.-G. Kuo, The LLAB(*l:c*) colour model, *Color Res. Appl.* **21**, 412–429 (1996).
- M.R. Luo, G. Cui, and B. Rigg, The development of the CIE 2000 colour difference formula, *Color Res. Appl.* **26**, 340–350 (2001).
- M.R. Luo, G. Cui, and C. Li, Uniform colour spaces based on CIECAM02 colour appearance model, *Color Res. Appl.* **31**, 320–330 (2006).
- D.L. MacAdam, Chromatic adaptation, *J. Opt. Soc. Am.* **46**, 500–513 (1956).
- D.L. MacAdam, A nonlinear hypothesis for chromatic adaptation, *Vision Res.* **1**, 9–41 (1961).
- D.L. MacAdam, Uniform color scales, *J. Opt. Soc. Am.* **64**, 1691–1702 (1974).
- D.L. MacAdam, Colorimetric data for samples of the OSA uniform color scales, *J. Opt. Soc. Am.* **68**, 121–130 (1978).
- D.L. MacAdam, Ed., *Selected Papers on Colorimetry—Fundamentals*, SPIE Milestone Series, Vol. MS 77, SPIE Press, Bellingham (1993).
- L.T. Maloney and B.A. Wandell, Color constancy: A method for recovering surface spectral reflectance, *J. Opt. Soc. Am. A* **3**, 29–33 (1986).
- K. Mancuso, W.W. Hauswirth, Q. Li, T.B. Connor, J.A. Kuchenbecker, M.C. Mauck, J. Neitz, and M. Neitz, Gene therapy for red-green colour blindness in adult primates, *Nature* **461**, 784–788 (2009).
- D. Marr, *Vision*, Freeman, New York (1982).
- W.H. Marshall and S.A. Talbot, Recent evidence for neural mechanisms in vision leading to a general theory of sensory acuity, in H. Klüver, Ed., *Biological Symposia*, **7**, The Jacques Cattell Press, 117–164 (1942).
- R. Mausfeld and R. Niederée, An inquiry into relational concepts of colour, based on incremental principles of colour coding for minimal relational stimuli, *Perception* **22**, 427–462 (1993).
- R. Mausfeld and D. Heyer, *Colour Perception: Mind and the Physical World*, Oxford University Press, Oxford (2003).
- B. Maximus, A. De Metere, and J.P. Poels, Influence of thickness variations in LCDs on color uniformity, *SID 94 Digest*, 341–344 (1994).
- J.C. Maxwell, On the theory of three primary colors, *Proc. Roy. Inst.* **3**, 370–375 (1858–1862).

- C.S. McCamy, H. Marcus, and J.G. Davidson, A color rendition chart, *J. App. Phot. Eng.* **11**, 95–99 (1976).
- J. McCann, *Color sensations in complex images*, IS&T/SID 1st Color Imaging Conference, Scottsdale, 16–23 (1993).
- J.J. McCann, S. McKee, and T. Taylor, Quantitative studies in retinex theory: A comparison between theoretical predictions and observer responses to 'Color Mondrian' experiments, *Vision Res.* **16**, 445–458 (1976).
- J.B. McCarthy, The two-color Kodachrome collection at the George Eastman House, *IMAGE: Journal of Photography and Motion Pictures of the International Museum of Photography at George Eastman House* **30** (1), 1–12 (1987).
- L. Meylan, D. Alleysson, and S. Süsstrunk, Model of retinal local adaptation for the tone mapping of color filter array images, *J. Opt. Soc. Am. A* **24**, 2807–2816 (2007).
- E.D. Montag, *Louis Leon Thurstone in Monte Carlo: Creating error bars for the method of paired comparison*, Proceedings of the SPIE/IS&T Electronic Imaging Conference Volume **5294**, 222–230 (2004).
- E.D. Montag and M.D. Fairchild, Simulated color gamut mapping using simple rendered images, *Proc. SPIE* **2658**, 316–325 (1996).
- E.D. Montag and M.D. Fairchild, Evaluation of gamut mapping techniques using simple rendered images and artificial gamut boundaries, *IEEE Trans. Im. Proc.* **6**, 977–989 (1997).
- L. Mori and T. Fuchida, Subjective evaluation of uniform color spaces used for color-rendering specification, *Color Res. Appl.* **7**, 285–293 (1982).
- L. Mori, H. Sobagaki, H. Komatsubara, and K. Ikeda, *Field trials on CIE chromatic adaptation formula*, Proceedings of the CIE 22nd Session, Melbourne, 55–58 (1991).
- N. Moroney, *A comparison of CIELAB and CIECAM97s*, Proceedings of IS&T/SID 6th Color Imaging Conference, Scottsdale, 17–21 (1998).
- N. Moroney, *Assessing hue constancy using gradients*, Proceedings of the SPIE/IS&T Electronic Imaging Conference Vol. **3963**, 294–300 (2000a).
- N. Moroney, *Local color correction using non-linear masking*, Proceedings of IS&T/SID 8th Color Imaging Conference, Scottsdale, 108–111 (2000b).
- N. Moroney, A hypothesis regarding the poor blue constancy of CIELAB, *Color Res. Appl.* **28**, 371–378 (2003).
- N. Moroney, M.D. Fairchild, R.W.G. Hunt, C.J. Li, M.R. Luo, and T. Newman, *The CIECAM02 color appearance model*, IS&T/SID 10th Color Imaging Conference, Scottsdale, 23–27 (2002).
- J. Morovic, *Color Gamut Mapping*, Wiley, Chichester (2008).
- K.T. Mullen, The contrast sensitivity of human color vision to red-green and blue-yellow chromatic gratings, *J. Physiol.* **359**, 381–400 (1985).
- A.H. Munsell, *Color and an Eye to Discern It*, AHM, Boston (1907).
- M. Murphy, *Golf in the Kingdom*, Viking, New York (1972).
- Y. Nayatani, *Relation on Helmholtz-Kohlrausch effect, purity discrimination, and G<sub>0</sub> function*, Proceedings of the 7th Congress of the International Colour Association, Vol. B, Budapest (1993).
- Y. Nayatani, Revision of chroma and hue scales of a nonlinear color-appearance model, *Color Res. Appl.* **20**, 143–155 (1995).
- Y. Nayatani, A simple estimation method for effective adaptation coefficient, *Color Res. Appl.* **22**, 259–274 (1997).
- Y. Nayatani, A modified opponent-colors theory considering chromatic strengths of various hues, *Color Res. Appl.* **28**, 284–297 (2003).

- Y. Nayatani, Proposal of an opponent-colors system based on color appearance and color-vision studies, *Color Res. Appl.* **29**, 135–150 (2004).
- Y. Nayatani, K. Takahama, and H. Sobagaki, *Estimation of adaptation effects by use of a theoretical nonlinear model*, Proceedings of the 19th CIE Session, Kyoto, 1979, CIE Publ. No. **5**, 490–494 (1980).
- Y. Nayatani, K. Takahama, and H. Sobagaki, Formulation of a nonlinear model of chromatic adaptation, *Color Res. Appl.* **6**, 161–171 (1981).
- Y. Nayatani, K. Takahama, H. Sobagaki, and J. Hirono, On exponents of a nonlinear model of chromatic adaptation, *Color Res. Appl.* **7**, 34–45 (1982).
- Y. Nayatani, K. Takahama, and H. Sobagaki, Prediction of color appearance under various adapting conditions, *Color Res. Appl.* **11**, 62–71 (1986).
- Y. Nayatani, K. Hashimoto, K. Takahama, and H. Sobagaki, A nonlinear color-appearance model using Estévez-Hunt-Pointer primaries, *Color Res. Appl.* **12**, 231–242 (1987).
- Y. Nayatani, K. Takahama, and H. Sobagaki, Field trials on color appearance of chromatic colors under various light sources, *Color Res. Appl.* **13**, 307–317 (1988).
- Y. Nayatani, K. Takahama, H. Sobagaki, and K. Hashimoto, Color-appearance model and chromatic adaptation transform, *Color Res. Appl.* **15**, 210–221 (1990a).
- Y. Nayatani, T. Mori, K. Hashimoto, K. Takahama, and H. Sobagaki, Comparison of color-appearance models, *Color Res. Appl.* **15**, 272–284 (1990b).
- Y. Nayatani, Y. Gomi, M. Kamei, H. Sobagaki, and K. Hashimoto, Perceived lightness of chromatic object colors including highly saturated colors, *Color Res. Appl.* **17**, 127–141 (1992).
- Y. Nayatani, H. Sobagaki, K. Hashimoto, and T. Yano, Lightness dependency of Chroma scales of a nonlinear color-appearance model and its latest formulation, *Color Res. Appl.* **20**, 156–167 (1995).
- M. Neitz and J. Neitz, Molecular genetics of color vision and color vision defects, *Arch. Ophthalmol.* **118**, 691–700 (2000).
- J. Neitz, J. Carroll, Y. Yamauchi, M. Neitz, and D.R. Williams, Color perception is mediated by a plastic neural mechanism that is adjustable in adults, *Neuron* **35**, 1–20 (2002).
- S.M. Newhall, Preliminary report of the O.S.A. subcommittee on the spacing of the Munsell colors, *J. Opt. Soc. Am.* **30**, 617–645 (1940).
- T. Newman and E. Pirrotta, *The darker side of colour appearance models and gamut mapping*, Proceedings of Colour Image Science, Derby, 215–223 (2000).
- D. Nickerson, History of the Munsell Color System and its scientific application, *J. Opt. Soc. Am.* **30**, 575–586 (1940).
- D. Nickerson, History of the Munsell Color System, company, and foundation, I, *Color Res. Appl.* **1**, 7–10 (1976a).
- D. Nickerson, History of the Munsell Color System and its scientific application, *Color Res. Appl.* **1**, 69–77 (1976b).
- D. Nickerson, History of the Munsell Color System, *Color Res. Appl.* **1**, 121–130 (1976c).
- T.H. Nilsson and T.M. Nelson, Delayed monochromatic hue matches indicate characteristics of visual memory, *J. Exp. Psychol. Hum. Percept. Perform.* **7**, 141–150 (1981).
- I. Nimeroff, J.R. Rosenblatt, and M.C. Dannemiller, Variability of spectral tristimulus values, *J. Res. NBS* **65**, 475–483 (1961).
- N. Ohta and A.R. Robertson, *Colorimetry: Fundamentals and Applications*, Wiley, Chichester (2005).

- C. Oleari, M. Melgosa, and R. Huertas, Generalization of color-difference formulas for any illuminant and any observer by assuming perfect color constancy in a color-vision model based on the OSA-UCS system, *J. Opt. Soc. Am. A* **28**, 2226–2234 (2011).
- C. Oleari, F. Fermi, and A. Ucakar, Digital image-color conversion between different illuminants by color-constancy actuation in a color-vision model based on the OSA-UCS system, *Color Res. Appl.* **37**, in press (2013).
- S.F. O'Neil, K.C. McDermott, Y. Mizokami, J.S. Werner, M.A. Cognale, and M.A. Webster, Tests of a functional account of the Abney effect, *J. Opt. Soc. Am. A* **29**, A165–A173 (2012).
- OSA, Psychological concepts: Perceptual and affective aspects of color, in *The Science of Color*, Optical Society of America, Washington, DC, 145–171 (1963).
- S.E. Palmer, *Vision Science: Photons to Phenomenology*, MIT Press, Cambridge (1999).
- Y.K. Park, M.R. Luo, C.J. Li, Y. Kwak, D.-S. Park, and C. Kim, Correcting veiling glare of refined CIECAM02 for mobile display, *Color Res. Appl.* **38** (1), 14–21 (2013).
- S.N. Pattanaik, J.A. Ferwerda, M.D. Fairchild, and D.P. Greenberg, *A multiscale model of adaptation and spatial vision for image display*, Proceedings of SIGGRAPH **98**, 287–298 (1998).
- S.N. Pattanaik, J. Tumblin, H. Yee, and D.P. Greenberg, *Time-dependent visual adaptation for fast realistic image display*, Proceedings of SIGGRAPH 2000, 47–54 (2000).
- H. Pauli, Proposed extension of the CIE recommendation on Uniform color spaces, color difference equations, and metric color terms, *J. Opt. Soc. Am.* **36**, 866–867 (1976).
- E. Pirrotta and M.D. Fairchild, *Directly testing chromatic-adaptation models using object colors*, Proceedings of the 23rd Session of the CIE Vol. **1**, New Delhi, 77–78 (1995).
- A.B. Poirson and B.A. Wandell, Appearance of colored patterns: Pattern-color separability, *J. Opt. Soc. Am. A* **10**, 2458–2470 (1993).
- A.B. Poirson and B.A. Wandell, Pattern-color separable pathways predict sensitivity to simple colored patterns, *Vision Res.* **36**, 515–526 (1996).
- J. Pokorny, V.C. Smith, and M. Lutze, Aging of the human lens, *Appl. Opt.* **26**, 1437–1440 (1987).
- D.M. Purdy, Spectral hue as a function of intensity, *Am. J. Psych.* **43**, 541–559 (1931).
- D. Purves and R.B. Lotto, *Why We See What We Do: An Empirical Theory of Vision*, Sinaur, Sunderland (2003).
- D. Purves, R.B. Lotto, and S. Nundy, Why we see what we do, *Amer. Sci.* **90**, 236–243 (2002).
- M.S. Rea, Toward a definition of circadian light, *J. Light Vis. Env.* **35**, 250–254 (2011).
- M.S. Rea and J.P. Freyssinier, Color rendering: A tale of two metrics, *Color Res. Appl.* **33**, 192–202 (2008).
- M.S. Rea and J.P. Freyssinier, White lighting, *Color Res. Appl.* **38** (2), 82–92 (2013).
- M.S. Rea, A.R. Robertson, and W.M. Petrusic, Colour rendering of skin under fluorescent lamp illumination, *Color Res. Appl.* **15**, 80–92 (1990).
- E. Reinhard, M. Stark, P. Shirley, and J. Ferwerda, *Gradient domain high dynamic range compression*, Proceedings of SIGGRAPH 2002, San Antonio, 267–276 (2002).

- E. Reinhard, G. Ward, S. Pattanaik, and P. Debevec, *High Dynamic Range Imaging: Acquisition, Display, and Image-Based Lighting*, Morgan Kaufmann, Amsterdam (2006).
- E. Reinhard, E.A. Khan, A.O. Aküz, and G. Johnson, *Color Imaging: Fundamentals and Applications*, AK Peters, Wellesley (2008).
- E. Reinhard, T. Pouli, T. Kunkel, B. Long, A. Ballestad, and G. Damberg, *Calibrated image appearance reproduction*, Proceedings of SIGGRAPH Asia, Singapore, Article 201 (2012).
- K. Richter, Cube-root color spaces and chromatic adaptation, *Color Res. Appl.* **5**, 7–11 (1980).
- K. Richter, *Farbempfindungsmerkmal Elementarbunton und Buntheitsabstände als Funktion von Farbart und Leuchtdichte von In- und Umfeld*, Bundesanstalt für Materialprüfung (BAM) Forschungsbericht 115, Berlin (1985).
- M. Richter and K. Witt, The story of the DIN color system, *Color Res. Appl.* **11**, 138–145 (1986).
- O. Rinner and K.R. Gegenfurtner, Time course of chromatic adaptation for color appearance discrimination, *Vision Res.* **40**, 1813–1826 (2000).
- A.R. Robertson, A new determination of lines of constant hue, *AIC Color* 69, Stockholm, 395–402 (1970).
- A.R. Robertson, The CIE 1976 color-difference formulae, *Color Res. Appl.* **2**, 7–11 (1977).
- A.R. Robertson, Historical development of CIE recommended color difference equations, *Color Res. Appl.* **15**, 167–170 (1990).
- A.R. Robertson, Figure 6-2 presented at the 1996 ISCC Annual Meeting, Orlando (1996).
- M.A. Rodriguez and T.G. Stockham, Producing colorimetric data from densitometric scans, *Proc. SPIE* **1913**, 413–418 (1993).
- R. Rolleston and R. Balasubramanian, *Accuracy of various types of Neugebauer Model*, Proceedings IS&T/SID Color Imaging Conference, Scottsdale, 32–37 (1993).
- O. Rosenthal and R.H. Phillips, *Coping with Colorblindness*, Avery, Garden City Park (1997).
- M. Sánchez-Marañón, P.A. García, R. Huertas, J. Hernández-Andrés, and M. Melgosa, Influence of natural daylight on soil color description: Assessment using a color-appearance model, *Soil Sci. Soc. Am. J.* **75**, 984–993 (2011).
- A. Sarkar, L. Blondé, P. Le Callet, F. Autrusseau, J. Stauber, and P. Morvan, *Toward reducing observer metamerism in industrial applications: Colorimetric observer categories and observer classification*, Proceedings of the IS&T/SID 18th Color Imaging Conference, San Antonio, 307–313 (2010).
- Sarnoff Corporation, *JND: A Human Vision System Model for Objective Picture Quality Measurement*, Sarnoff Technical Report, 2001. [www.jndmatrix.com](http://www.jndmatrix.com) [accessed on 23 February 2013].
- R.E. Savoie, Bezold-Brücke effect and visual nonlinearity, *J. Opt. Soc. Am.* **63**, 1253–1261 (1973).
- O.H. Schade, Optical and photoelectric analog of the eye, *J. Opt. Soc. Am.* **46**, 721–739 (1956).
- J. Schanda, Ed., *Colorimetry: Understanding the CIE System*, Wiley, Hoboken (2007).
- B.E. Schefrin and J.S. Werner, Age-related changes in the color appearance of broadband surfaces, *Color Res. Appl.* **18**, 380–389 (1993).
- J. Schirillo and S.K. Shevell, Lightness and brightness judgments of coplanar retinally noncontiguous surfaces, *J. Opt. Soc. Am. A* **10**, 2442–2452 (1993).

- J. Schirillo and L. Arend, Illumination changes at a depth edge can reduce lightness constancy, *Percept. Psychophys.* **57**, 225–230 (1995).
- J. Schirillo and S.K. Shevell, Brightness contrast from inhomogeneous surrounds, *Vision Res.* **36**, 1783–1796 (1996).
- J. Schirillo, A. Reeves, and L. Arend, Perceived lightness, but not brightness, of achromatic surfaces depends on perceived depth information, *Percept. Psychophys.* **48**, 82–90 (1990).
- I.R. Schwab, *Evolution's Witness: How Eyes Evolved*, Oxford University Press, Oxford (2012).
- T. Seim and A. Valberg, Towards a uniform colorspace: A better formula to describe the Munsell and OSA Color Scales, *Color Res. Appl.* **11**, 11–24 (1986).
- C.C. Semmelroth, Prediction of lightness and brightness on different backgrounds, *J. Opt. Soc. Am.* **60**, 1685–1689 (1970).
- R. Shamey, M. Sedito, and R.G. Kuehni, Comparison of unique hue stimuli determined by two different methods using Munsell color chips, *Color Res. Appl.* **35**, 419–424 (2010).
- R. Shamey, S. Shepherd, M. Abed, M. Chargualaf, N. Garner, N. Dippel, N. Weisner, and R.G. Kuehni, How well are color components of samples of the natural color system estimated? *J. Opt. Soc. Am. A* **28**, 1962–1969 (2011).
- G. Sharma, Ed., *Digital Color Imaging Handbook*, CRC Press, Boca Raton (2003).
- G. Sharma and H.J. Trussel, Digital color imaging, *IEEE Trans. Im. Proc.* **6**, 901–932 (1997).
- S.K. Shevell, The dual role of chromatic backgrounds in color perception, *Vision Res.* **18**, 1649–1661 (1978).
- S.K. Shevell, *Color and brightness: Contrast and context*, IS&T/SID 1st Color Imaging Conference, Scottsdale, 11–15 (1993).
- S.K. Shevell, The Verriest Lecture: Color lessons from space, time, and motion, *J. Opt. Soc. Am. A* **29**, A337–A345 (2012).
- J.M. Speigle and D.H. Brainard, Is color constancy task independent? IS&T/SID 4th Color Imaging Conference, Scottsdale, 167–172 (1996).
- L. Spillman and J.S. Werner, *Visual Perception: The Neurophysiological Foundations*, Academic Press, San Diego (1990).
- R. Stanziola, The Colorcurve System®, *Color Res. Appl.* **17**, 263–272 (1992).
- S.S. Stevens, To honor Fechner and repeal his law, *Science* **133**, 80–86 (1961).
- S.S. Stevens, *Psychophysics: Introduction to Its Perceptual, Neural, and Social Prospects*, Wiley, New York (1975).
- J.C. Stevens and S.S. Stevens, Brightness functions: Effects of adaptation, *J. Opt. Soc. Am.* **53**, 375–385 (1963).
- W.S. Stiles and J.M. Burch, N.P.L. colour-matching investigation: Final report (1958), *Optica Acta* **6**, 1–26 (1959).
- A. Stockman and L.T. Sharpe, The spectral sensitivities of the middle- and long-wavelength-sensitive cones derived from measurements in observers of known genotype, *Vision Res.* **40**, 1711–1737 (2000).
- A. Stockman, L.T. Sharpe, and C. Fach, The spectral sensitivity of the human short-wavelength sensitive cones derived from threshold and color matches, *Vision Res.* **39**, 2901–2927 (1999).
- M. Stokes, M. Fairchild, and R.S. Berns, Precision requirements for digital color reproduction, *ACM Trans. Graph.* **11**, 406–422 (1992).
- M.C. Stone, *A Field Guide to Digital Color*, A.K. Peters, Natick (2003).
- M.C. Stone, W.B. Cowan, and J.C. Beatty, Color gamut mapping and the printing of digital images, *ACM Trans. Graph.* **7**, 249–292 (1988).

- G. Svaetichin, Spectral response curves from single cones, *Acta Physiol. Scand.* **39** (Suppl. 134), 17–46 (1956).
- K. Takahama, H. Sobagaki, and Y. Nayatani, Analysis of chromatic adaptation effect by a linkage model, *J. Opt. Soc. Am.* **67**, 651–656 (1977).
- K. Takahama, H. Sobagaki, and Y. Nayatani, Formulation of a nonlinear model of chromatic adaptation for a light-gray background, *Color Res. Appl.* **9**, 106–115 (1984).
- R. Taya, W.H. Ehrenstein, and C.R. Cavonius, Varying the strength of the Munker-White effect by stereoscopic viewing, *Perception* **24**, 685–694 (1995).
- C.C. Taylor, Z. Pizlo, J.P. Allebach, and C.A. Bouman, *Image quality assessment with a Gabor pyramid model of the human visual system*, IS&T/SPIE Electronic Imaging Conference Vol. **3016**, San Jose, 58–69 (1997).
- C.C. Taylor, Z. Pizlo, and J.P. Allebach, *Perceptually relevant image fidelity*, IS&T/SPIE Electronic Imaging Conference, SPIE Vol. **3299**, San Jose, 110–118 (1998).
- H. Terstiege, Chromatic adaptation: A state-of-the-art report, *J. Col. Appear.* **1**, 19–23 (1972).
- L.L. Thurstone, A law of comparative judgment, *Psych. Review* **34**, 273–286 (1927).
- L.L. Thurstone, *The Measurement of Values*, University of Chicago Press, Chicago (1959).
- R.J.D. Tilley, *Colour and the Optical Properties of Materials*, 2nd. Ed., Wiley, Chichester (2011).
- D.J. Tolhurst and D.J. Heeger, Comparison of contrast-normalization and threshold models of the responses of simple cells in cat striate cortex, *Vis. Neurosci.* **14**, 293–309 (1997).
- W.S. Torgerson, A law of categorical judgment, in *Consumer Behavior*, L.H. Clark, Ed., New York University Press, New York, 92–93 (1954).
- W.S. Torgerson, *Theory and Methods of Scaling*, Wiley, New York (1958).
- A. Valberg, *Light Vision Color*, Wiley, Chichester (2005).
- A. Valberg and B. Lange-Malecki, “Colour constancy” in Mondrian patterns: A partial cancellation of physical chromaticity shifts by simultaneous contrast, *Vision Res.* **30**, 371–380 (1990).
- J. Vazquez-Corral, J.K. O'Regan, M. Vanrell, and G.D. Finlayson, A new spectrally sharpened sensor basis to predict color naming, unique hues, and hue cancellation, *J. Vision* **12** (6):7, 1–14 (2012).
- F. Viénot, H. Brettel, L. Ott, A.B. M'Barek, and J.D. Mollon, What do colour-blind people see? *Nature* **376**, 127–128 (1995).
- J. Walraven, Discounting the background—the missing link in the explanation of chromatic induction, *Vision Res.* **16**, 289–295 (1976).
- B.A. Wandell, Color appearance: The effects of illumination and spatial pattern, *Proc. Natl. Acad. Sci. USA* **90**, 9778–9784 (1993).
- B.A. Wandell, *Foundations of Vision*, Sinauer, Sunderland, Mass. (1995).
- A.B. Watson, Toward a perceptual video quality metric, *Human Vision and Electronic Imaging III*, SPIE Vol. **3299**, 139–147 (1998).
- A.B. Watson and C.V. Ramirez, A standard observer for spatial vision, *Investig. Ophthalmol. Vis. Sci.* **41**, S713 (2000).
- A.B. Watson, J. Hu, and J.F. McGowan, DVQ: A digital video quality metric based on human vision, *J. Electron. Imaging* **10**, 20–29 (2001).
- M.A. Webster, Adaptation and visual coding, *J. Vis.* **11** (5):3, 1–23 (2011).
- M.A. Webster and J.D. Mollon, The influence of contrast adaptation on color appearance, *Vision Res.* **34**, 1993–2020 (1994).
- M.A. Webster and J.D. Mollon, Adaptation and the color statistics of natural images, *Vision Res.* **37**, 3283–3298 (1997).

- M.A. Webster and P. Kay, Color categories and color appearance, *Cognition* **122**, 375–392 (2012).
- M.A. Webster, I. Juricevic, and K.C. McDermott, Simulations of adaptation and color appearance in observers with varying spectral sensitivity, *Ophthalmic Physiol. Opt.* **30**, 602–610 (2010).
- G.D. Webster, G.R. Urland and J. Correll, Can uniform color color aggression? Quasi-experimental evidence from professional ice hockey, *Soc. Psychol. Pers. Sci.* **3**, 274–281 (2011).
- J.S. Werner and B.E. Schefrin, Loci of achromatic points throughout the life span, *J. Opt. Soc. Am. A* **10**, 1509–1516 (1993).
- M. White, The early history of White's illusion, *Colour Design Creat.* **5** (7), 1–7 (2010).
- P. Whittle, Brightness, discriminability and the "Crispening Effect", *Vision Res.* **32**, 1493–1507 (1992).
- D.R. Williams, N. Sekiguchi, W. Haake, D. Brainard, and O. Packer, The cost of trichromacy for spatial vision, in *From Pigments to Perception* (A. Valberg and B.B. Lee, Eds.), Plenum Press, New York, 11–22 (1991).
- J.M. Wolfe, K.R. Kluender, D.M. Levi, L.M. Bartoshuk, R.S. Herz, R.L. Klatzky, S.J. Lederman, and D.M. Merfeld, *Sensation and Perception*, 3rd. Ed., Sinauer, Sunderland (2012).
- M. Wolski, J.P. Allebach, and C.A. Bouman, *Gamut mapping: Squeezing the most out of your color system*, IS&T/SID 2nd Color Imaging Conference, Scottsdale, 89–92 (1994).
- W.D. Wright, A re-determination of the trichromatic coefficients of the spectral colours, *Trans. Opt. Soc.* **30**, 141–161 (1928–1929).
- W.D. Wright, Why and how chromatic adaptation has been studied, *Color Res. Appl.* **6**, 147–152 (1981a).
- W.D. Wright, 50 years of the 1931 CIE standard observer for colorimetry, *AIC Color* **81**, Paper A3 (1981b).
- D.R. Wyble and M.D. Fairchild, Prediction of Munsell appearance scales using various color appearance models, *Color Res. Appl.* **25**, 132–144 (2000).
- G. Wyszecki, Current developments in colorimetry, *AIC Color* **73**, 21–51 (1973).
- G. Wyszecki, Color appearance, in *Handbook of Perception and Human Performance*, Wiley, New York (1986).
- G. Wyszecki and W.S. Stiles, *Color Science: Concepts and Methods, Quantitative Data and Formulae*, Wiley, New York (1982).
- K. Xiao, M.R. Luo, and C. Li, Colour size effect modeling, *Color Res. Appl.* **34**, 4–12 (2009).
- K. Xiao, M.R. Luo, and C. Li, Colour appearance of room colors, *Color Res. Appl.* **35**, 284–293 (2010).
- K. Xiao, M.R. Luo, C. Li, G. Cui, and D. Park, Investigation of colour size effect for colour appearance assessment, *Color Res. Appl.* **36**, 201–209 (2011).
- B. Xiao, B. Hurst, L. MacIntyre, and D.H. Brainard, The color constancy of three-dimensional objects, *J. Vis.* **12** (4):6, 1–15 (2012).
- X. Zhang and B.A. Wandell, A spatial extension of CIELAB for digital color image reproduction, *SID 96 Digest* (1996).

# Index

---

- Abney effect, 121–3, 241, 257, 262  
absorptance, 64–5  
achromatic color, defined, 49, 86, 88, 90, 92  
adaptation  
    chromatic *see* chromatic-adaptation  
    and chromatic induction, 117, 130, 232, 289  
    dark, 21–5, 37, 125, 128, 157–8, 161–2, 173, 400, 402  
    light, xix, 21, 23–5, 37, 79, 83, 125, 128, 132, 146, 157–9, 161–3, 173, 200, 229, 257, 259–60, 400, 402, 411, 414  
mechanisms of, 21–6, 37, 133, 157–9, 161, 163–4, 166, 169–70, 173, 181, 196, 373, 383, 400  
motion, 165, 170  
    spatial frequency, 120, 165–8, 372, 383–4  
additive mixtures, 49, 71–3, 98, 106, 109, 121, 182, 353  
additivity Grassmann's law of, 71–3, 182  
adjustment method of, 46  
advanced colorimetry, xviii, 57, 83, 345  
after images, 19–20, 159, 161, 165  
Albers, Josef, 117  
Amacrine cellsof retina, 8, 14, 37  
*aqueous humor*, 4  
art color-order systems in, 110  
*ASTM Standard Guide for Designing and Conducting Visual Experiments*, 38  
asymmetric matching, 46, 49, 174–5  
ATD color appearance model  
    adaptation model for, 191, 259–60  
    brightness equation in, 261  
    chroma equation in, 261–2  
    data for, 257–8  
    example of, 262–3  
    hue equation in, 262  
    limitations of, 257–8  
    objectives and approach of, 258  
    opponent-color dimensions in, 260–61  
perceptual correlates in, 261–2  
predictions of, 257–9  
saturation equation in, 261–2  
testing of, 325  
ATD04 model, 263–4  
axons, defined, 6, 14, 17  
  
background, defined, 145–6  
Bartleson–Breneman equations, 131–2, 222, 378  
basic colorimetry, xviii, 1, 37, 54–5, 57, 59, 68–9, 83, 97, 115, 142, 144, 337, 342, 345  
beyond diffuse white, 317, 403–4  
Bezold–Brücke hue shift, 120–23, 241, 257, 262  
bidirectional reflectance distribution functions (BRDF), 65  
bidirectional transmittance distributions functions, 65  
bilateral filter, 393  
black-body radiator, 60–61  
blackness NCS value, 105, 109, 414  
blind spot, 6, 11, 13  
Bradford–Hunt 96C color appearance model, 275  
Bradford–Hunt 96S color appearance model, 275, 676  
brain  
    visual area of, 14–15, 17–18  
    and visual signal processing, 14–16  
brightness  
    chromaticity and, 123–5, 408  
    in color appearance, 88–9, 94–6, 123–5, 218–19, 236–7, 295, 403–4  
    colorfulness reproduction, 94–6, 210, 222, 245, 254, 344  
    defined, 88–9  
    luminance and, 123–4, 127–8, 200, 403, 409–10, 414

- brilliance, 224, 407–9  
brown, xviii, xx, 64, 86, 92, 154–5, 264, 408
- cameras digital, 159, 180, 352, 366, 370, 389  
CAM02-UCS, 264, 300–302, 323, 335, 338  
CAT02, 179, 196–8, 245, 292, 299–301, 331, 411  
category scaling, 43, 50–51  
characterization  
  approaches to, 350  
  defined, 349–50  
  goals of,  
chroma  
  in color appearance, 90, 94–6, 111, 154–5, 238, 257, 304, 347, 375  
  defined, 221, 252, 415  
  equation for, 93, 221, 252, 285, 295–6  
chromatic-adaptation  
  cognitive mechanisms of, 130, 170–73  
  defined, 25–6, 158–9  
  example of, 159  
  high-level, 159, 163, 165–70  
  mechanics of, 3, 21, 25, 132, 141, 157–8, 162–3, 170–73, 177, 186, 196, 373–4  
  models, 177–98, 209, 213–17, 228, 246, 259, 289, 301, 311, 344, 348, 378–9, 410  
  applications of, 178, 378  
  CAT02 transform, 196–8, 301  
  concerns of, 94  
  equations for, 177, 183, 190  
  Fairchild's model, 192–5  
  Mac Adam's model, 187–8  
  Nayatani's model, 187–90  
  retinex theory, 186–7  
  treatises on, 171  
  von Kries model, 182–6  
photoreceptors in, 158, 163, 170  
physiology of, 159–70  
receptor gain control in, 159, 163–4  
sensory mechanisms of, 132, 170–73  
subtractive mechanisms of, 159, 163–4  
time course of, 172–3, 373  
transforms, 177–9, 181, 186, 193, 195–8, 200–202, 204, 209, 211, 215, 243, 245–6, 248, 254, 257–8, 264, 266–7, 271, 277, 282–3, 286, 288, 290–92, 297, 299, 301, 309, 313, 321, 330–31, 335, 377–8, 382, 386, 411, 417  
treatises on, 171  
chromatic color defined, 86  
chromatic contrast, 28–30, 127, 250, 343  
  contrast sensitivity functions for, 28, 381, 385  
chromatic induction, 117, 130, 145, 232, 276, 289, 295  
chromaticity and brightness, 123–5  
  diagrams of, 77–9, 109, 122–3, 178, 185, 212, 309, 338, 358, 410–12  
chromaticness NCS value, 104–5, 224, 305, 410, 414  
chromatic White effect, 118  
CIECAM02  
  color appearance model  
  adaptation model in, 290–93  
  brightness, 295  
  Cartesian coordinates, 296–7  
  chroma, 295–6  
  colorfulness, 296  
  hue, 294  
  implementation guidelines, 297–8  
  input data, 288–9  
  inverse model, 297  
  lightness, 295  
  objectives, 287–8  
  opponent dimensions, 294  
  outlook, 301–2  
  phenomena predicted, 298  
  saturation, 296  
  computational issues, 298–300  
CIECAM97s color appearance model  
  appearance correlates in, 279–80  
  chromatic adaptation in, 282–3  
  data for, 276–7  
  historical background for, 273–5  
  invertibility, 280–81  
CIE color-difference model, 201, 212, 301, 330, 334–6, 338, 371  
CIE illuminants, 59, 61–3, 83, 103, 147–8, 179, 266, 271, 304, 309, 311, 313, 315, 323, 334, 353, 355, 358, 366, 379, 411–12  
CIELAB color space  
  color differences in, 82, 106, 212, 333–4, 371, 376, 383, 396  
  coordinates of, 203, 280  
  described, 80, 201  
  example of, 375  
  lightness scale of, 43, 205  
  limitations of, 204, 243, 334  
  mapping of, 376  
  recommended usage of, 201, 371, 387  
  testing of, 245  
  uniformity of, 82, 204  
  utility of, 360  
  wrong von Kries transforms in, 201–2  
CIELAB  $\Delta E^*_{ab}$ , 81–2, 148, 245, 269, 333, 336, 415  
CIELUV, 79–81, 200–201, 210–12, 243, 309, 313, 315–16, 320, 324–5, 338, 371, 396

- CIELUV color space  
example of, 212  
testing of, 316
- CIE (2006) model, 77, 339–40
- CIE 1931 Standard Colorimetric Observer, 62, 74, 78, 103, 144, 146, 214, 226, 246, 290, 366, 397
- CIE 1964 Supplementary Standard Colorimetric Observer, 77, 83, 144
- CIE 1976 Uniform Chromaticity Scales, 79
- circadian rhythms, 14
- CMC color-difference equation, 82, 265, 268–9, 333
- CMYK device coordinates, 253, 342–3, 349
- color(s)  
adaptation to, 19, 87, 125, 132, 172, 260, 270, 416  
appearance  
cognitive aspects of, 137  
spatial influences on, 134  
appearance scales, 272, 386, 409–10, 415  
characteristics of, 87, 137  
constancy, 26–7, 140–41, 180, 186, 188, 196, 263–4, 325, 337, 374  
computational, 179–80  
constancy of, 26–7, 140–41, 180, 186, 188, 196, 263–4, 325, 337, 374  
corresponding, 49, 126, 174–9, 184–6, 188–9, 191–2, 195–7, 209, 211–12, 242, 245, 248, 259, 265, 271, 276, 282–3, 290, 304–5, 308–10, 313, 327, 344–5, 379, 386, 410–11  
defined, 86–8  
gamut, 79, 114, 224, 343, 357–8, 360–61, 409  
inconstancy index, 178–9  
matching, 3–4, 36–7, 49, 56, 68, 70–77, 148, 174, 190, 200, 264, 293, 336, 339, 397, 416  
measurement, xviii, 42, 59, 68, 75, 199–200, 370  
based on ICC Profile Format, 354, 365  
memory, 26–7, 37, 136–7, 171, 345, 361  
preferences, 347–8, 354, 357, 360–62, 365  
related, xx, 90–92, 94, 121, 125, 154–5, 176, 257, 259–60, 263, 410  
temperature, 60–61  
triangle of, 58–9, 77, 83  
tristimulus values and, 70–77, 116, 121, 155, 199, 242, 248, 258–9, 344, 347, 349  
unrelated, 91–2, 125, 154–5, 226, 241, 258, 260, 264, 302
- color appearance models applications of ATD, 190–91, 257–63, 307, 324–5, 374, 383, 410
- Bradford–Hunt models, 275–6
- CIECAM02, 79, 172, 179, 196, 198, 214, 224–5, 245, 256–7, 264, 286–302, 305–6, 312, 317, 320–23, 325, 332, 335, 338, 372, 374–5, 377–80, 386, 396–7, 410–11, 414, 416–17
- CIECAM97s, 196–7, 224, 256–7, 273–91, 293–4, 297–8, 301, 306, 309, 312, 319–20, 322, 372, 374, 396, 410
- CIELAB, 29, 43, 76, 79–83, 106, 109, 125, 147–8, 179, 200–212, 218–20, 243–4, 265, 284, 294, 307, 331, 348, 375, 401
- CIELUV, 79–81, 200–201, 210–12, 243, 309, 313, 315–16, 320, 324–5, 338, 371, 396
- color attributes and, 86, 152–3  
construction of, xix, 86, 93, 200–201, 367  
corresponding-colors data and, 174–7, 185, 189, 191–2, 195, 197, 209, 304–5, 308–10  
defined, 199–200  
developments for the future, 397  
and device-independent color imaging, 97, 275, 341–68, 370, 374, 397  
direct-model testing of, 312–16  
Hunt's, xix, 83, 97, 125–8, 132, 143, 162, 164, 172, 193, 198, 200, 213–14, 224, 228–9, 234, 236, 238–42, 275, 311–12, 417
- LLAB, 257, 264–5, 268–70, 282, 285, 309, 316, 320, 325, 327, 335, 338
- magnitude-estimation experiments and, 175, 310–12
- Nayatani's, 187, 190, 213–24, 225, 250, 265, 276, 304, 331, 397, 409
- pictorial review of, 323–7
- psychophysics and, 18, 20, 32, 38–55, 59, 68, 99, 128, 164, 190, 288
- qualitative testing of, 304–7
- research on, 318, 371–2
- RLAB, 132–3, 172, 195, 243, 254–5, 264, 275, 282, 397
- testing of, 180, 199, 251, 303–27, 371, 396
- utility of, 312, 337, 349, 355, 357
- variety of, 304
- visual system and, xix, 1, 22, 49, 58, 120, 157–60, 187, 200, 229, 241, 371, 400
- ZLAB, 276, 282–6
- color-appearance phenomena, xviii, 36–8, 54–5, 115–42, 200, 214, 241, 254–5, 275, 303, 307–8, 386, 398
- color-appearance reproduction, 346–7, 354–5

- colorcurve system, 106–7, 109  
 color-differences measurement  
   application of color appearance models to, 82, 334, 337  
   future directions for, 335, 337  
   recommendations for, 81–2, 201, 212, 336  
   techniques of, 18, 45, 330, 336, 396  
 color-differences specifications, 81–3, 212, 334–5  
 colorfulness  
   in color appearance, xix, 87, 90–96, 111, 115, 125–7, 151, 154–5, 175, 189, 199–200, 210, 214, 218, 220–22, 235–6, 238–40, 245, 252, 254–5, 257, 262, 264–5, 268–70, 280–82, 295–6, 300–301, 304, 307–8, 310–12, 316–17, 332, 344–5, 358, 375, 377–8, 382, 387, 391, 393, 410–11, 414–17  
   defined, 90, 92, 94, 111, 151, 154, 221, 252, 262, 265, 268, 344, 411, 414–15  
   varying directly with luminance, 111, 125–9, 189, 268, 304, 378, 410–11  
 colorimetric color reproduction, 344, 346, 354  
 colorimetry  
   absolute, 75  
   advanced, xviii, 57, 83, 345  
   basic, xviii, 1, 54, 57, 59, 68–9, 83, 97, 115, 142, 144, 147, 337, 342, 345  
   defined, 57–8, 62, 64–5, 67–8, 70–71, 75–7, 79–80  
   future directions in, 335, 337, 397  
   normalized, 75–6  
   origin of, 68, 77  
   relative, 59, 61–3, 67, 70, 75–6, 79, 121, 156, 182, 199  
 color-matching functions, 4, 49, 70–77, 148, 190, 200, 293, 336, 339, 397, 416  
   average, 70, 73–6  
 $2^\circ$  color-matching functions, 76–7  
 color-naming systems, 99, 112–14  
   types of, 113–14  
 color-order systems  
   applications of, 97–8, 109–10, 112  
   in art and design, 110  
   in communication, 109–11  
   in education, 109, 111  
   in evaluation of color appearance models, 108, 111  
   and imaging systems, 112  
   limitations of, 112  
   in visual experiments, 110  
 color-preference reproduction, 347–8, 354, 357, 361–2  
 color rendering  
   application of color appearance models to, 213, 321, 331–2  
   CIE technical committee on, 321, 331  
   future directions for, 331–3  
   indices for, 321, 330, 333  
   recommendations for, 321, 330  
   techniques of, 330, 332  
 color reproduction  
   defined, 94, 343–5, 347  
   enhancing accuracy of, 345–6, 353, 364  
   levels of, 343–5  
 color spaces(s)  
   CIE, 79–81  
   color differences in, 79, 82, 107, 201, 212, 268, 300, 333–4, 338, 371, 376, 383, 396, 409, 415–16  
   viewing-conditions-independent, 357  
 color vision  
   deficiencies, 19, 32–6, 54  
   gender and, 35–6  
   screening for, 36  
   historic theories of, 19, 35  
   spatial properties of, 29–30, 322  
   temporal properties of, 27–32  
 colour Standards for Image Technology, 273  
 Commission Internationale de l'Eclairage (CIE) *see also* CIE entries  
   activities of, 318–23, 333, 396  
 communication, color-order systems in, 110–11  
 computational color constancy, 141, 179–80  
 cones  
   distinguished from rods, 33  
   function of, 8, 11, 70  
   monochromatism, 33  
   incidence of, 35  
   relative abundance of, 140  
 responses, 11, 33, 76, 163, 182, 184–5, 188, 191, 200, 202, 206, 208, 215–17, 228, 232–3, 246–7, 258–9, 265–6, 271, 277–8, 282–3, 290, 295, 300, 325, 338, 380, 417  
   transformation of tristimulus values to, 182–3, 207–8  
 role in light and dark adaptation, 161–2  
 spectral responsivities of, 9–10, 14–15, 25, 76  
 types of, 9–10, 17, 20–21, 33, 35, 68–69, 76, 163, 184, 194, 218, 235  
 constant  
   hue, 101–4, 109, 111, 121–2, 204, 245, 257, 271–2, 305–6, 361, 386–7, 411  
   stimuli, method of, 46–7

- contrast  
 varying directly with luminance, 28–9  
 varying directly with surround, 393
- contrast sensitivity functions (CSFs)  
 and eye movements, 32  
 spatial, 28–9, 32  
 temporal, 29–30, 32
- cool white fluorescent lamp, and color rendering, 62, 330
- cornea  
 described, 3  
 function of, 3
- correlated color temperature (CCT), 59, 61–2, 147, 194, 227, 330–31
- corresponding colors  
 color appearance models and, 49, 78, 126, 174–9, 181, 184–6, 188–9, 191–2, 195–7, 199, 209, 211–12, 242, 245, 248, 265, 269, 271, 276, 282–3, 290, 304–5, 308–10, 313, 316, 327, 344–5, 379, 386, 410–11  
 reproduction, 344–5
- Cowan equation, 124–5
- crispening, 116–20, 145, 386–8
- CRT display, 75, 92, 113, 132, 227, 231, 254, 288, 309, 311, 313, 315–16, 351–2, 358–9  
 characterization of, 351–2
- cubo-octahedron, 107
- Dalton, John, 35–6
- dark adaptation, curve of, 21, 23–5, 37, 125, 128, 158, 161–2, 173, 400
- daylight fluorescent lamp, and color rendering, 330
- definitions, importance about being enormously careful about, 57
- design, color-order systems in, 97, 99–101, 105–7, 109–10
- deuteranomaly, 33, 35  
 incidence of, 35
- deutanopia, 32, 35  
 incidence of, 35
- Deutsches Institute für Normung (DIN), 107–9, 111
- device calibration, 349–54, 366, 370
- device characterization  
 approaches to, 350  
 defined, 349  
 goals of, 346
- device-independent color imaging  
 color appearance models and, 342–3, 354–7, 362–3, 367
- defined, 343–5, 347, 355–7, 363, 365
- device calibration and characterization in, 349–54
- example system for, 363–4  
 gamut mapping and, 345, 349, 354, 357–62, 365
- general solution to, 348–9, 360
- as goal, 346, 361
- ICC implementation of, 364–8
- inverse process, 362–3
- process of, 341–2, 347–50, 352, 354, 357–8, 362–8
- viewing conditions and, 355–7, 365
- diffuse/normal viewing geometry, 66
- digital cameras, characterization of, 349, 352, 366, 370
- DIN *see* Deutsches Institute für Normung (DIN)
- DIN color system, 109
- discounting the illuminant, 26–7, 37, 132–4, 136, 150, 172, 189, 192–3, 198, 210, 222, 228, 231, 241, 243, 245–8, 252, 254, 262, 265, 267, 269, 277, 283, 288–90, 307
- display comparisons (CIE technical committee), 320
- dynamic range, 16, 24, 76, 187, 272, 293, 372, 380, 382, 389, 391, 399–417
- education, color-order systems in, 99, 109, 111
- empirical modeling, 1, 350–51
- equivalent color reproduction, 344, 347
- exact color reproduction, 344
- eye  
 anatomy of, 2  
 optics of, 2–3
- face adaptation, 165, 169
- Fairchild, M., xviii, 29, 56, 83, 101, 125, 127, 131–2, 145–6, 148, 167, 170, 172–3, 175, 180, 192–3, 195–6, 199, 204, 219, 224, 230, 243, 245–6, 248–9, 252, 257, 271–2, 275–6, 282, 288, 290, 305, 307, 309, 312–13, 315–18, 321, 323, 331, 333, 335–6, 339, 342, 349, 354, 357, 360–62, 369–76, 379, 381–4, 386, 391–3, 401–2, 404–6, 409, 414, 416
- Fairchild's chromatic-adaptation model  
 equations of, 177, 192–5  
 predictions by, 195
- Farnsworth–Munsell 100-hue test, 36
- Fechner–Benham colors, 28
- Fechner's law, 41–2
- filling-in, 11, 13–14, 134
- film mode of appearance, 153
- flare, 146, 202, 352–3, 355, 358, 399, 402

- fluorescence, 68, 224, 352–4  
in output devices, 353
- fluorescent lamp, and color rendering, 330
- forced-choice method, 47
- fovea, 5–6, 8, 11, 32, 37, 76–7, 143
- frequency-of-seeing curve, 47
- full moon, 144
- $G_o$ , 407–9, 411–14
- gamut  
area index, 332  
color, 343, 357–8, 360, 409  
defined, 252, 357  
limits to, 357  
mapping  
defined, 357–61  
techniques for, 252, 359
- ganglion cells, 6–8, 11, 13–14, 16–17, 163
- gender, and color-vision deficiencies, 35–6
- graphical rating, 50
- Grassmann's laws, 71–4, 182
- Guth's chromatic-adaptation model  
equations of, 190–91  
predictions by, 190–92
- haploscopic matching, 126, 175, 308
- hard-copy output, 172, 351
- hdr-CIELAB, 404–6
- hdr-IPT, 406–7
- HDR Photographic Survey, The, 395,  
401–3
- Helmholtz–Kohlrausch effect, 111, 123–5,  
219, 224, 237, 241, 262, 269, 307,  
407–8, 413
- Helson–Judd effect, 129–30, 189, 214,  
222–3, 231, 240–42, 255, 269, 274,  
276, 304, 307–9, 313, 315, 324–5
- herding CATs, 196
- Hering opponent-colors theory, 19–20, 88,  
109, 171
- heterozygous females, 35
- high dynamic range (HDR), 272, 317, 322,  
372, 375, 380, 382, 385–6, 389–93,  
395, 397, 399–417
- high pressure sodium lamp, and color  
rendering, 330
- horizontal cells, of retina, 8
- hue  
in color appearance, 63  
defined, 39  
Munsell, 67–8  
NCS value, 104, 305, 409  
of nonselective samples, 129–30, 189  
varying directly with colorimetric purity,  
121–3  
varying directly with luminance, 120–21
- human visual response, quantification  
of, 68
- Hunt color appearance model  
adaptation model for, 228–33  
advantages of, 229  
brightness equations in, 236–7  
chroma equation in, 238  
colorfulness equation in, 238–9  
data for, 226–8  
example of, 225–6, 230, 240–41  
hue equations in, 234  
inversion of, 239–40  
lightness equations in, 238  
limitations of, 164, 254, 327  
objectives and approach of, 225–6  
opponent-color dimensions in, 233–4  
predictions of, 230–31  
saturation equations in, 235  
testing of, 200, 305–13, 315–16, 319–20,  
324–5, 327
- Hunt effect, xix, 125–8, 164, 192, 195, 200,  
210, 214, 220, 222, 229, 241, 255,  
269, 306–9, 319–20, 378
- Hunt, Pointer, Estevez transformation,  
192, 228
- Hunt, R.W.G., 36, 56, 83, 85–6, 97–8, 103,  
121, 124–5, 129, 131–3, 136, 147,  
157, 173, 175, 178, 189, 193, 213,  
225–7, 230, 232, 238–9, 241, 249,  
265, 274–6, 287–8, 299, 305–7,  
309–10, 312, 315, 325, 342–3, 345,  
355, 359, 370, 397, 411, 415
- iCAM06, 392–5, 402
- iCAM image appearance model, 369,  
373–82, 385–93, 397
- framework, 376–82, 385, 393–4
- future, 369–98
- image appearance and rendering, 373,  
375, 385–91
- image difference and quality, 391–2
- illuminant A, 59, 61–2, 147, 223, 308, 313,  
316, 323–5
- illuminant C, 61–2, 103
- illuminant D50, 61–3, 147–8, 309, 311,  
313, 315, 353, 358, 366
- spectral power of, 61, 63, 147–8, 353
- illuminant D65  
and color rendering, 330  
spectral power of, 59, 147, 179
- illuminant F2, 61–3, 147  
spectral power of, 61, 63, 147
- illuminant F8, 61–2, 148  
spectral power of, 61, 148
- illuminant F11, 61–2  
spectral power of, 61

- illuminants  
 CIE, 59, 61–3, 83, 103, 147–8, 179, 266, 271, 304, 309, 311, 313, 315, 323, 334, 353, 355, 358, 366, 379, 411–12
- discounting, 26–7, 37, 132–4, 136, 150, 172, 189, 192–3, 198, 210, 222, 228, 231, 241, 243, 245–8, 252, 254, 262, 265, 267, 269, 277, 283, 288–90, 307
- metamerism, 335–7
- mode of appearance, 151
- illumination  
 mode of appearance, 151  
 standard, 65
- image appearance models, 322, 370, 374–5
- image quality, 5, 38–9, 44, 96, 356, 358, 369–70, 372–5, 378, 380–82, 391
- image rendering, 374–5, 378, 381–2, 385–6, 389, 393, 395
- imaging systems, color-order systems in, 103, 112, 114
- indices of metamerism  
 application of color appearance models to, 337  
 future directions for, 337  
 recommendations for, 336  
 techniques of, 336
- interaction of color, 117
- International Color Consortium (ICC) Profile Format, 354, 365
- International Colour Association (AIC) 1997 Meeting, 275
- International Lighting Vocabulary, 86–7
- interval scale, defined, 44, 50, 79
- intrinsically photosensitive retinal ganglion cells (ipRGC), 14–15, 163
- invertibility, 108, 223, 254, 263, 270, 349, 362
- IPT color space, 271–2, 306, 375
- iris, described, 4–5
- irradiance, 59–60, 70
- Ishihara's Tests for Colour-Blindness, 36
- just-noticeable difference (JND), 41, 45, 373–4  
 experiments testing, 45
- Kodachrome, 137, 139
- LABHNU model, example of, 320
- land two-color projection, 137
- lateral geniculate nucleus (LGN), 14, 17–18, 20
- L cones  
 spectral responsivities of, 10, 36, 69, 76
- LED illumination, 62
- lens  
 described, 6  
 function of, 3
- LGN *see* Lateral geniculate nucleus (LGN)
- light adaptation  
 curve of, 24, 128  
 role of rods and cones in, 161
- lightness  
 chroma reproduction, 95  
 in color appearance, 78, 94–95, 99, 111, 115, 154–5, 175–6, 178, 181, 199–200, 214, 238–9, 245, 254, 263, 270, 307, 310, 347–8, 357, 375, 387, 410  
 defined, 89–90, 145, 204, 252, 262, 268–9, 411, 415  
 equation for, 80–81, 93, 100–101, 125, 218–19, 221, 238, 250, 252, 265, 268, 280, 285, 295, 300, 382, 404, 406, 413
- light source  
 defined, 59, 68  
 types of, 60
- limits, method of, 46–7
- linkage chromatic-adaptation model, 162, 177–98, 209, 213–15, 217, 228, 243, 246, 289, 301, 311, 344, 378–9, 410
- LLAB color appearance model  
 adaptation model for, 265, 270  
 chroma equation in, 268, 285  
 color differences in, 264–5, 268–70, 307  
 colorfulness equation in, 265  
 data for, 264–5, 270, 285, 320  
 example of, 264, 270  
 hue equations in, 265, 268  
 lightness equation in, 265, 268, 285  
 limitations of, 270  
 objectives and approach of, 264–5  
 opponent-color dimensions in, 267–8  
 perceptual correlates in, 268–9  
 predictions of, 307, 325, 327  
 saturation equation in, 268, 285  
 testing of, 264, 270
- Logit analysis, 49
- lookup tables (LUTs), 112, 239–40, 300, 349–52, 354, 356, 363, 365, 412  
 multidimensional, 349, 352, 354
- Lovibond Tintometer, 98
- luminance  
 and brightness, 45, 90–91, 111, 123–125, 127–8, 200, 219, 236, 295, 345, 377, 403, 409–10, 415  
 contrast sensitivity functions for, 28–30, 32, 376, 381  
 dynamic range, 400–401  
 varying directly with colorfulness, 127, 189, 268, 378

- varying directly with contrast, 127, 189, 378  
 varying directly with hue, 100, 105, 120–21, 125, 410  
 Luo, M. R., 175, 238, 257, 264, 269–70, 275–6, 282, 287, 299–302, 309–12, 316, 335, 338, 371  
 LUTCHI study, 310  
 LUTs *see* lookup tables (LUTs)
- MacAdam's chromatic-adaptation model, 182, 187  
 Macbeth Color Checker Chart, 112, 324, 363  
 macula, 6, 37, 73, 77  
 magnitude estimation, 42, 50–52, 128, 175, 251, 285, 304, 310, 312  
 matching techniques, 49, 176, 308, 316  
 Maxwell's color process, 19–20, 77–8, 137  
 Maxwell's triangle, 77–8  
 McCollough effect, 165  
 M cones  
   spectral responsivities of, 10, 15, 76  
 MDS *see* Multidimensional scaling (MDS)  
 measurement  
   colorimetric, 57, 59, 142, 146–7, 351–3, 366  
   exhaustive, 350–52, 363  
 melanopsin, 14, 163  
 memory color, 26–7, 37, 136–7, 171, 345, 361  
 memory matching, 49, 175–6, 186  
 mercury lamp and color rendering, 330  
 mesopic vision, 8, 400  
 metal halide lamp and color rendering, 330  
 metamer, defined, 49, 344  
 metamerism  
   indices of, 334–7  
   in input and output devices, 353  
 method of adjustment, 46  
 method of constant stimuli, 46–7  
 method of limits, 46–7  
 Michaelis-Menton function, 404, 406  
 Michelson contrast, 28  
 modeling  
   empirical, 1, 350–51  
   physical, 350–51  
 modular image difference model, 382–5  
 modulation transfer functions (MTFs), 28  
 monochromatism, 33, 35  
   incidence of, 33, 35  
 Mori experiment, 130, 304, 308  
 motion adaptation, 165, 170  
 MTFs *see* Modulation transfer functions (MTFs)
- Multidimensional scaling (MDS), 51–4  
 Munker illusion, 118  
 Munker-White illusion, 118  
 Munsell, 36, 88, 97–103, 105, 107, 109–12, 122–3, 125, 129–30, 175, 204, 206–7, 221, 244–5, 304–5, 312–13, 317–19, 330, 333, 410  
 Munsell Book of Color, 88, 99–103, 111, 125, 221, 240, 245  
 Munsell value scale, 99, 105, 204, 319
- natural color system (NCS)  
   chromaticness in, 104–5, 224, 305, 410, 414  
   hue in, 104–5, 111, 251, 305, 409–12  
 Nayatani's chromatic-adaptation model as basis for color appearance model  
   equations of, 188  
   predictions by, 188–9  
 Nayatani's color appearance model  
   adaptation model for, 215–17  
   brightness equations in, 218–19  
   chroma equations in, 221  
   colorfulness equations in, 221–2  
   data for, 189, 214–15  
   example of, 222–3, 225  
   hue equations in, 219–20  
   inversion of, 222  
   lightness equations in, 219  
   limitations of, 224  
   objectives and approach of, 213–14  
   opponent-color dimensions in, 217–18  
   predictions of, 129, 189, 222–3  
   saturation equations in, 220  
   testing of, 214, 216, 218–21, 223  
 Nayatani theoretical color space, 224, 409  
 nominal scale, defined, 43  
 normal/diffuse viewing geometry, 66–7  
 normalization constant, in colorimetry, 75  
 normalized colorimetry, 75–6  
 normal/45 viewing geometry, 67
- objects recognition of, 26–7, 158, 172  
 oblique effect, 31  
 10° observer, 77  
 observer metamerism, 84, 335–40  
 off-center ganglion cells, 16  
 on-center ganglion cells, 16  
 one-dimensional appearance scales, 50–52, 103, 415  
 one-dimensional appearance spaces, 410  
 one-dimensional scaling, 50–52  
 opponent-colors theory  
   Hering's, 19–20, 104, 109, 171  
   modern, 20–21

- opsin, 15  
 optical illusions, 133  
 Optical Society of America Uniform Color Scales (OSA UCS), 107–8  
 optic nerve, 5–7, 11, 14, 16  
 ordinal scale, defined, 43  
 orthogonal color space, 393–6  
 OSA UCS *see* Optical Society of America Uniform Color Scales (OSA UCS)  
 Ostwald system, 98, 107, 109  
 output lexicon, defined, 357
- paired comparison experiment, 51–2, 312–13, 316  
 Pantone Process Color Formula Guide, 98, 113  
 partition scaling, 50–51  
 pass-fail method, 47  
 perceptual threshold, 39–40, 42, 416  
 perfect reflecting diffuser (PRD), 67–8, 75, 291  
 photometry, 69–70, 74–5, 125  
 photopic luminous efficiency function, 74  
 photopic vision, 8–10, 69–70, 90–91, 400  
 photoreceptors *see also* Cones; Rods     energy responses of, 15  
    gain control of, 163  
 physical modeling, 350–51  
 physiological color matching functions, 4  
 pigmented epithelium, 5  
 Planckian radiator, 60–61, 330  
 pleasing color reproduction, 346–7  
 PostScript Process Color Guide, 113  
 power law, 41–3, 128  
 PRD *see* Perfect reflecting diffuser (PRD)  
 preferred color reproduction, 345, 347–8, 361  
 presbyopia, 3  
 printers characterization of, xix, 352, 366  
 Probit analysis, 48–9  
 profile connection space, 365–8  
 proportionality Grassmann's law of, 72–4, 182  
 protanomaly, 33, 35     incidence of, 33, 35  
 protanopia, 32–3, 35     incidence of, 35  
 proximal field, defined, 143, 145, 355  
 pseudoisochromatic plates, 36  
 psychometric function, 47–8  
 psychophysics     defined, 39, 97, 190  
    experimental concepts of, 54–5, 349  
    experimental design in, 38, 54–5  
    history of, 40  
    relation to color appearance modeling, 36, 99  
 PsychToolBox, 48  
 pupil in adaptation to light and dark, 161  
 Purkinje shift, 10, 70
- QUEST, 48
- radiance, 59–60, 67–8, 70, 75, 415     equation of, 60, 70, 75  
 radiator, black-body, 60–61  
 rank order experiment, 50  
 ratio estimation, 50, 52  
 ratio scale, defined, 44  
 receptive fields, 16–18, 28  
 receptor gain control, 23, 159, 163, 258  
 reflectance, 60, 64–8, 70, 75–6, 100, 106, 109–11, 130, 147, 178, 180, 186, 227, 336, 343, 351–3, 399     distribution functions of, 65, 336  
 refractive errors, 3  
 related color, xx, 90–92, 94, 121, 125, 154–5, 176, 257, 259–60, 263, 410     defined, 91–2, 154  
 relative spectral power distribution, 59–63, 75, 148, 344  
 response compression, 23, 164, 261, 278, 288, 380  
 retina     described, 5, 7–14  
    light perception in, 1, 15  
    light processing in, 3, 5–6, 15, 17, 182  
    structure of, 3, 6, 217  
 retinal, 4, 6, 8, 11–12, 14–16, 23, 31–2, 37, 60, 116, 159, 161, 163, 171, 173–5, 186, 232, 258, 383  
 retinex theory, 186–7  
 RGB, device coordinates, 342, 348, 366  
 rhodopsin, 9, 15  
 Richter, K., 108, 243, 276, 324  
 RLAB color appearance model     adaptation model for, 243, 246–8  
    chroma equation in, 252, 268  
    data for, 245–6  
    example of, 133, 254–5, 319, 356  
    hue equation in, 250–52  
    inversion of, 252–4  
    lightness equation in, 250  
    limitations of, 243, 245  
    objectives and approach of, 243–5  
    opponent-color dimensions in, 248–50  
    predictions of, 254  
    saturation equations in, 252  
    testing of, 245, 248, 252, 397  
    usefulness of, 243, 252–3, 255  
 rods     distinguished from cones, 33  
    function of, 8–9, 11, 13–14, 70

- luminous efficiency function for, 70  
 monochromatism, 33, 35  
     incidence of, 33, 35  
 role in light and dark adaptation, 162
- saturation  
     defined, 93, 211–12, 252, 268–9, 296, 415  
     equation for, 93, 212, 235, 261, 280, 296
- scales  
     types of, 43, 50  
     uses of, 44–5, 184
- scaling  
     multidimensional, 51–4  
     one-dimensional, 50–52
- scanners, characterization of, 351–2
- S-CIELAB, 371–2, 374–6, 382–3
- S cones  
     relative abundance of, 10–11  
     spectral responsivities of, 10, 14
- scotopic luminous efficiency function, 9–10, 70
- scotopic vision, 8–10, 70
- self-luminous display, xviii, 146, 172, 176, 246, 274, 298, 320, 322
- simultaneous binocular viewing, 315, 356
- simultaneous contrast  
     complexity of, 118  
     example of, 116–17  
     and shape, 134  
     vs. spreading, 119–20
- sodium lamp, and color rendering, 330
- soft-copy display, 247–8, 278
- solid state illumination, 89
- spatial CSFs, 28–9
- spatial frequency adaptation, 165–8, 372, 383–4
- spatial perception, and chromatic perception, 134
- specification of colour appearance for reflective media and self-luminous, 320
- spectral color reproduction, 343–4
- spectral luminous efficiency, 9–10, 69–70, 125
- spectral power distribution, 37, 57–64, 69, 71–3, 75, 111, 143, 147–8, 156, 179, 335–6, 344, 353, 355
- spectrophotometry, 17, 64, 66  
     CIE standards for, 66
- spectroradiometry, 17, 59–60
- spreading, 119–20, 386  
     vs. simultaneous contrast, 119–20, 386
- stage theory, 20
- staircase procedures, 48
- Stevens effect, 19, 125–9, 131, 164, 189, 200, 210, 214, 222, 229, 237, 241, 255, 269, 306–9, 313, 319–20, 325, 378
- Stevens power law, 42, 128
- stimulus  
     characteristics of, 27, 274  
     defined, 28, 45, 47–8, 71, 75, 143, 145, 214
- subtractive mixtures, 98
- successive binocular viewing, 313, 315, 356
- surface mode of appearance, 153
- surround  
     contrast and, 131–2, 307, 356, 393  
     defined, 145–6, 249, 355
- tapetum, 5
- TC1–75, a comprehensive model of colour appearance, 323
- TC8–11, CIECAM02 mathematics, 323
- TC1–33, color rendering, 321
- TC1–27, specification of color appearance for reflective media and self-luminous display comparisons, 321
- TC1–34, testing colour-appearance models, 257, 318–20  
     model preparation by, 318–19
- TC1–76, unique hue data, 323
- temporal CSFs, 29–30, 32
- testing color appearance models, 55, 303–27
- testing colour-appearance models (CIE technical committee), 199, 318, 320  
     model preparation by, 318–19
- tetrachromatic females, 35
- threshold experiments, 39, 45–8  
     types of, 46–8
- thumbnail, 5, 144
- Thurstone's law, 51
- tintometer, 98
- transmittance, 64–5, 68, 73, 75, 147, 351–3  
     distribution functions of, 65
- tri-band fluorescent lamp, and color rendering, 62, 330
- trichromatic theory, 19–20
- tristimulus values  
     measurement of, 75, 79, 199  
     transformation to cone responses, 246, 290
- XYZ, 40, 42, 74, 76, 115–16, 177, 182–3, 185, 192, 198, 200–201, 204, 206–8, 253, 258–9, 265, 276, 282–3, 288, 328, 337, 344, 349, 351, 356, 376–8, 411
- tritanomaly, 33, 35  
     incidence of, 35
- tritanopia, 32–3, 35, 235, 240  
     incidence of, 35

- troland, defined, 258–9  
Troxler fading, 32  
trumatch colorfinder, 113  
tungsten halogen lamp, and color rendering, 330–31  
two-color projections, 137–40  
two-color technicolor, 137  
  
unrelated color, 87, 91–2, 125, 154–5, 226, 241, 258, 260, 264, 275, 302, 323, 333, 414  
defined, 91–92, 154, 264  
  
viewing  
angle, 65  
conditions, definition of, 355–6  
field  
colorimetric specifications of, 146–9  
components of, 142–6, 226, 355  
configuration of, 142  
geometries, 65–6, 355  
modes of, 83, 133, 149–54, 334, 342  
viewing-conditions-independent space, 349, 357, 362, 367–8  
vision  
experiments on, 33, 190, 303  
human, 1–38, 322, 372  
visual area, 14–15, 17–18  
visual experiments, 38–40, 54, 69, 82, 92, 99, 103, 110, 222, 231, 242, 304, 313–15, 372  
types of, 39–40  
  
visual threshold, 19, 40, 261  
vitreous humor, 4, 35  
volume mode of appearance, 153  
von Kries chromatic-adaptation model  
equations of, 182, 184, 193, 248  
history of, 182  
predictions by, 185–6, 189, 196, 209, 305  
  
Ware equation, 124–5  
Weber, E.H., xix, 40–42  
Weber's law, xix, 40–42  
whiteness, NCS value, 105, 410  
[whyiscolor.org](http://whyiscolor.org), 18, 58  
Wrong von Kries transforms, 204, 206–8, 211, 245  
  
Xenon lamp, and color rendering, 330  
XYZ tristimulus values, 74, 116, 183, 200, 204, 206, 376  
  
yes–no method, 47  
  
zero gray level, 407–8, 411  
ZLAB color appearance model  
appearance correlates in, 284–5  
chromatic adaptation in, 282–3, 286  
data for, 282  
invertibility of, 285  
similarities of CIECAM97s, 282